THE ROLES OF LIPIDS IN IMMUNOMETABOLISM: THE CROSSTALK BETWEEN LIPID METABOLISMS AND INFLAMMATION

EDITED BY: Yiliang Chen, Jue Zhang and Wen Dai
PUBLISHED IN: Frontiers in Cardiovascular Medicine

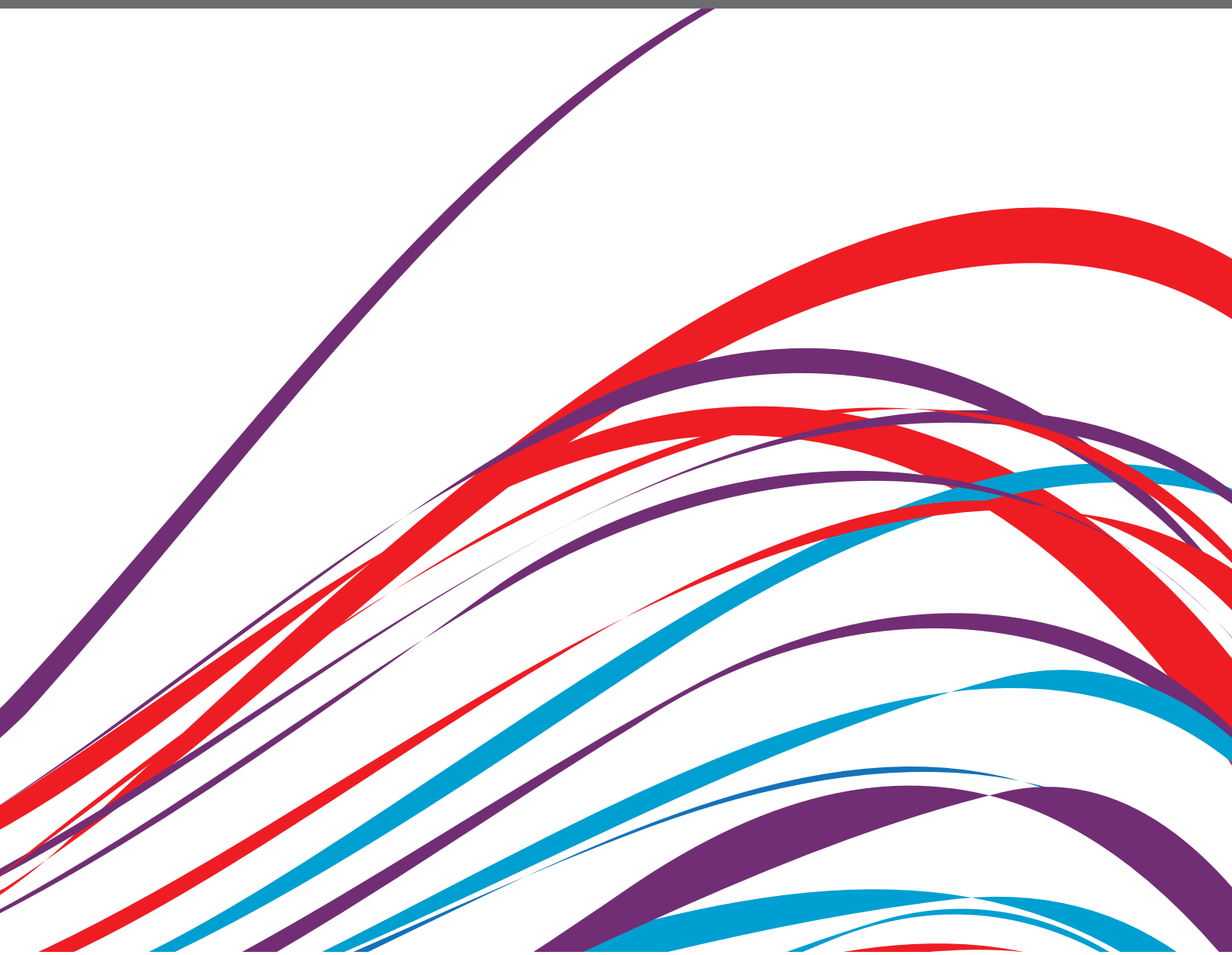

frontiers Research Topics

Frontiers eBook Copyright Statement

The copyright in the text of individual articles in this eBook is the property of their respective authors or their respective institutions or funders. The copyright in graphics and images within each article may be subject to copyright of other parties. In both cases this is subject to a license granted to Frontiers.

The compilation of articles constituting this eBook is the property of Frontiers.

Each article within this eBook, and the eBook itself, are published under the most recent version of the Creative Commons CC-BY licence. The version current at the date of publication of this eBook is CC-BY 4.0. If the CC-BY licence is updated, the licence granted by Frontiers is automatically updated to the new version.

When exercising any right under the CC-BY licence, Frontiers must be attributed as the original publisher of the article or eBook, as applicable.

Authors have the responsibility of ensuring that any graphics or other materials which are the property of others may be included in the CC-BY licence, but this should be checked before relying on the CC-BY licence to reproduce those materials. Any copyright notices relating to those materials must be complied with.

Copyright and source acknowledgement notices may not be removed and must be displayed in any copy, derivative work or partial copy which includes the elements in question.

All copyright, and all rights therein, are protected by national and international copyright laws. The above represents a summary only. For further information please read Frontiers' Conditions for Website Use and Copyright Statement, and the applicable CC-BY licence.

ISSN 1664-8714
ISBN 978-2-88976-576-8
DOI 10.3389/978-2-88976-576-8

About Frontiers

Frontiers is more than just an open-access publisher of scholarly articles: it is a pioneering approach to the world of academia, radically improving the way scholarly research is managed. The grand vision of Frontiers is a world where all people have an equal opportunity to seek, share and generate knowledge. Frontiers provides immediate and permanent online open access to all its publications, but this alone is not enough to realize our grand goals.

Frontiers Journal Series

The Frontiers Journal Series is a multi-tier and interdisciplinary set of open-access, online journals, promising a paradigm shift from the current review, selection and dissemination processes in academic publishing. All Frontiers journals are driven by researchers for researchers; therefore, they constitute a service to the scholarly community. At the same time, the Frontiers Journal Series operates on a revolutionary invention, the tiered publishing system, initially addressing specific communities of scholars, and gradually climbing up to broader public understanding, thus serving the interests of the lay society, too.

Dedication to Quality

Each Frontiers article is a landmark of the highest quality, thanks to genuinely collaborative interactions between authors and review editors, who include some of the world's best academicians. Research must be certified by peers before entering a stream of knowledge that may eventually reach the public - and shape society; therefore, Frontiers only applies the most rigorous and unbiased reviews.
Frontiers revolutionizes research publishing by freely delivering the most outstanding research, evaluated with no bias from both the academic and social point of view. By applying the most advanced information technologies, Frontiers is catapulting scholarly publishing into a new generation.

What are Frontiers Research Topics?

Frontiers Research Topics are very popular trademarks of the Frontiers Journals Series: they are collections of at least ten articles, all centered on a particular subject. With their unique mix of varied contributions from Original Research to Review Articles, Frontiers Research Topics unify the most influential researchers, the latest key findings and historical advances in a hot research area! Find out more on how to host your own Frontiers Research Topic or contribute to one as an author by contacting the Frontiers Editorial Office: frontiersin.org/about/contact

THE ROLES OF LIPIDS IN IMMUNOMETABOLISM: THE CROSSTALK BETWEEN LIPID METABOLISMS AND INFLAMMATION

Topic Editors:
Yiliang Chen, Medical College of Wisconsin, United States
Jue Zhang, Versiti Blood Research Institute, United States
Wen Dai, Versiti Blood Research Institute, United States

Citation: Chen, Y., Zhang, J., Dai, W., eds. (2022). The Roles of Lipids in Immunometabolism: The Crosstalk Between Lipid Metabolisms and Inflammation. Lausanne: Frontiers Media SA. doi: 10.3389/978-2-88976-576-8

Table of Contents

frontiers | Frontiers in Cardiovascular Medicine

EDITORIAL
published: 22 June 2022
doi: 10.3389/fcvm.2022.938535

Editorial: The Roles of Lipids in Immunometabolism: The Crosstalk Between Lipid Metabolisms and Inflammation

Jue Zhang[1], *Wen Dai*[1] *and Yiliang Chen*[1,2]*

[1] Versiti Blood Research Institute, Milwaukee, WI, United States, [2] Department of Medicine, Medical College of Wisconsin, Milwaukee, WI, United States

Keywords: lipids, immunometabolism, atherosclerosis, chronic inflammation, innate immunity metabolic syndrome, cardiovascular disease

OPEN ACCESS

Edited by:
Mary G. Sorci-Thomas,
Medical College of Wisconsin,
United States

Reviewed by:
Bishuang Cai,
Icahn School of Medicine at Mount Sinai, United States
Elda Favari,
University of Parma, Italy
Clovis Palmer,
Tulane University, United States

***Correspondence:**
Yiliang Chen
yilchen@mcw.edu

Specialty section:
This article was submitted to Lipids in Cardiovascular Disease, a section of the journal Frontiers in Cardiovascular Medicine

Received: *07 May 2022*
Accepted: *06 June 2022*
Published: *22 June 2022*

Citation:
Zhang J, Dai W and Chen Y (2022) Editorial: The Roles of Lipids in Immunometabolism: The Crosstalk Between Lipid Metabolisms and Inflammation. Front. Cardiovasc. Med. 9:938535. doi: 10.3389/fcvm.2022.938535

Editorial on the Research Topic

The Roles of Lipids in Immunometabolism: The Crosstalk Between Lipid Metabolisms and Inflammation

Mammalian cells contain a variety of lipid molecules and it was estimated that more than 1,000 lipid species can be found in one cell (1). Lipids constitute over 10% dry weight of a mammalian cell (2) and glycerophospholipids alone contribute to 20 ∼ 25% of the dry weight in brain tissues (3). The heterogeneity of the cellular lipid molecules is in agreement with their diverse functions, ranging from supporting membrane structures (e.g., phospholipids, cholesterol, and glycolipids), energy storage (e.g., triglycerides), to intracellular and intercellular signaling (e.g., lipoprotein complexes, oxysterols, phosphoinositides, and prostaglandins). An emerging research field called immunometabolism has been inspired by the observations that abnormal cellular metabolism, including lipid metabolism, is often associated with an abnormal immune response (4). Alteration in lipid metabolism in immune cells (e.g., macrophages, dendritic cells, neutrophil, B cells, and T cells, etc) and non-immune cells (e.g., endothelial cells, smooth muscle cells, platelets) often play a significant role in systemic inflammation, leading to various diseases including atherosclerosis, diabetes, obesity, and cancer [Berkowitz et al.; Khafagy and Dash, (5, 6)]. Vice versa, pro-inflammatory cytokines and signaling regulate lipid metabolism. For example, TNF-α upregulated LDL receptor (LDLR) and downregulated scavenger receptor class B type-I (SR-BI), leading to cholesterol accumulation in human arterial endothelial cells (7). In another study, TNF-α attenuated ABCA1 expression through NF-κB pathway and reduced cholesterol efflux to HDL in human intestinal cells (8). Taken together, it is clear that lipid metabolism is closely coupled with inflammation.

Despite accumulating evidence indicating a crosstalk between lipid metabolism and inflammation, underlying molecular mechanisms under physiological and pathophysiological conditions remain poorly understood. Our contributors to this Research Topic have provided their novel data and ideas through both research and review articles, addressing the fundamental question how lipids cause health issues through the immune system.

LIPOPROTEINS IN REGULATION OF THE IMMUNE SYSTEM

As hydrophobic molecules, extracellular lipids often group together in extracellular vesicles or are associated with lipid-carrying proteins, forming lipoprotein complexes such as VLDL, LDL and HDL. In human circulation, LDL are the predominant lipoproteins, which are mostly cleared by LDLR in the liver *via* receptor-mediated endocytosis (9). Consistently, knocking out of LDLR in mice leads to very high plasma LDL levels and diet-induced atherosclerosis, which becomes one of the widely used atherosclerotic animal models (10). Proprotein convertase subtilisin/kexin type 9 (PCSK9) is an enzyme promoting degradation of LDLR, and therefore regulates plasma LDL cholesterol levels. Xia et al. summarized recent progress in understanding the regulation of PCSK9 expression and function and discussed how these mechanisms influence both lipoprotein metabolism and inflammation, as PCSK9 also degrades major histocompatibility protein class I in cancer cells. Similarly, Wu et al. provided an interesting review of recent findings that PCSK9 modulates inflammation through several pathways including TLR4/NF-κB signaling, lectin-like oxidized-LDL receptor-1 (LOX-1)-mediated pro-inflammatory responses, and induction of pro-inflammatory cytokines. Altogether, PCSK9 is a typical example that lipoprotein metabolism and inflammation process are coordinated and appears to be a promising target for therapeutic intervention of the atherosclerotic cardiovascular disease (CVD).

LDL are often modified due to oxidative stress in atherosclerosis conditions, leading to accumulation of oxidized LDL (oxLDL) and acetylated LDL (acLDL) within the vascular tissues (11). These modified LDL induce many pro-inflammatory responses in various immune cells. Liao et al. reported a novel mechanism that oxLDL inhibited a microRNA, miR-491-5P in THP-1-derived macrophages. MiR-491-5P silenced expression of matrix metalloproteinase 9 (MMP-9), which facilitated the pro-inflammatory responses such as reactive oxygen species (ROS) production, expression of pro-inflammatory cytokines TNF-α, IL-1β, and IL-6. As oxLDL reduced miR-491-5P levels, MMP-9 expression was elevated along with its downstream pro-inflammatory phenotypes (Liao et al.). In another study, oxLDL bound to a macrophage surface scavenger receptor CD36 and activated an intracellular protein kinase A (PKA), which phosphorylated vimentin, a type III intermediate filament protein (Kim et al.). PKA phosphorylated vimentin at Ser72, which directed intracellular CD36 trafficking to the plasma membrane and promoted CD36-mediated oxLDL uptake as well as foam cell formation. Consistently, knocking out vimentin resulted in 57% less atherosclerotic lesion formation in *Apoe* null mice on high fat diet for 15 weeks (Kim et al.). While the pro-atherogenic role of CD36 in macrophages has been widely documented (6, 12), Rekhi et al. showed that CD36 in endothelial cells (EC) also contribute to atherosclerosis by mediating fatty acid uptake, leading to dysfunctional endothelium. The group has generated EC-specific CD36 knockout mice and crossed them with LDLR knockout mice (EC $CD36^{-/-}$/$LDLR^{-/-}$). They found that female but not male EC $CD36^{-/-}$/$LDLR^{-/-}$ mice were protected from diet-induced atherosclerosis, suggesting a sex-dependent atherogenic effect in EC CD36 (Rekhi et al.). Besides CD36, circadian genes Bmal1 expression appeared to limit oxLDL uptake and maintain EC functions in a hindlimb ischemia mouse model. Bmal1 inhibited inflammation by activating anti-inflammatory cytokine IL-10 expression and promotes angiogenesis through VEGF signaling (Xu et al.).

AcLDL is another major form of modified LDL that facilitate macrophage intracellular cholesterol accumulation and foam cell formation. Willemsen et al. have found that acLDL loading in macrophages specifically suppressed type-I interferon (IFN) signaling and IFN-β secretion. This phenotype was also observed in monocytes isolated from familial hypercholesterolemia patients by RNA sequencing analysis. Thus, this study has provided a potential connection between cellular cholesterol metabolism and inflammatory signaling in innate immune cells (Willemsen et al.). In another study, Zhao et al. revealed a crosstalk between glycolysis pathway and lipid metabolism that affected macrophage phenotype during atherogenesis. They showed that solute carrier family 37 member 2 (SLC37A2), a protein regulating glycolysis is required for alternative activation of macrophages to mediate anti-inflammatory responses. Hematopoietic cell-specific deletion of SLC37A2 in LDLR knockout mice lead to increased plasma lipid during atherogenesis as well as more atherosclerosis plaque development (Zhao et al.).

Compared to LDL and their derivatives that generally impose detrimental effects, HDL are considered beneficial to the human health and the most studied cardioprotective function of HDL is their ability to promote cholesterol efflux from peripheral cells (13). In agreement with this notion, HDL-mediated cholesterol efflux capacity (CEC) or reverse cholesterol transport (RCT) in macrophages is impaired in metabolic diseases such as atherosclerosis (14) and non-alcoholic fatty liver disease (15), both of which are associated with chronic inflammation. Moreover, impairment of CEC has been reported in autoimmune and pro-inflammatory conditions including acute phase reaction (16), rheumatoid arthritis, and systemic lupus erythematosus (17), indicating the involvement of HDL functions in regulation of the immune system. Recent evidence further indicate that systemic inflammation and autoimmune disease conditions reciprocally impact the composition and functions of HDL particles (18) as well as HDL/apoA-I plasma levels (19). Therefore, it is more and more clear that HDL is one of the major players in our immune system and more mechanistic studies are urgently needed in this field.

Al-Jarallah and Babiker reported a novel anti-hypertensive and a cardioprotective effect of HDL in spontaneously hypertensive rats after myocardial ischemia/reperfusion. Mechanistically, the effect was dependent on cardiac SR-BI, a known HDL receptor. Chronic HDL treatment protected cardiac myocytes by reducing autophagy and inflammation. Autophagy is critical for lipid metabolism in both immune and non-immune cells during atherosclerosis (20) and it is a process coupling extracellular stress signals, cellular lipid handling and

sensing, and immune cell activation (21). Therefore, the study by Al-Jarallah and Babiker on chronic HDL effects on autophagy deserves further exploration. However, while the beneficial effects of HDL on cardiovascular system are widely recognized, many questions regarding the underlying molecular mechanisms remain to be answered. For example, do HDL directly counteract LDL effects on vascular cells or immune cells through shared receptors and/or downstream effectors? Alternatively, since HDL reduce peripheral cell cholesterol levels by mediating cholesterol efflux or reverse cholesterol transport, do HDL impose beneficial effects on immune system indirectly through alleviating the cellular lipid burden? In addition, similar to LDL, HDL can be chemically modified, which appear to impair their physiological functions (22, 23). It would be highly interesting to further explore the impact of the modified HDL *in vivo* and how they alter systemic inflammation in metabolic diseases.

LIPID METABOLISM AND DYS-REGULATED INFLAMMATION IN HUMAN DISEASES

The lipid-laden macrophages in the atherosclerotic plaques are good examples of the connection between a defective lipid metabolism and abnormal inflammatory responses. Those macrophages show ectopic intracellular neutral lipid accumulation, accompanied by elevated secretion of pro-inflammatory cytokines such as IL-1β, TNF-α, MCP-1, and IL-6 (24). Thanks to the recent advancement in single cell RNA sequencing technologies combined with proteomics methods, the lipid-laden macrophages are observed in other human diseases such as cancer (25, 26), obesity (27), and non-alcoholic fatty liver disease (NAFLD) (28). *Via* genetic manipulation combined with pharmacological intervention that reduce lipid-laden macrophages, people show that those cells are actively involved in systemic inflammation during the disease development. These studies further emphasize the contributing role of abnormal lipid metabolism, especially in immune cells, in dys-regulated inflammation.

While the underlying molecular mechanisms have been widely characterized (29), Lee-Rueckert et al. summarized and broadened the view of lipid-laden macrophages beyond atherosclerosis. They discussed how the phenotypic and functional plasticity of macrophages become entangled in both atherosclerosis and cancer development. In fact, contrary to the conventional view that those macrophages simply facilitate progression in atherosclerosis and cancer, macrophage accumulation of lipid may be a response toward anti-inflammatory phenotypic switch through transcriptional reprogramming. If so, it may stimulate novel ideas targeting lipid-laden macrophages in either disease (Lee-Rueckert et al.).

Many recent studies have provided direct evidence that lipid species result in dys-regulated immune system in human. Patients with non-alcoholic fatty liver disease (NAFLD) are at increased risk of developing atherosclerosis and related CVD. Hoebinger et al. summarized and focused on the role of oxidized lipids that act as danger signals to drive pro-inflammatory processes and disease progression. Similarly, Karnati et al. used quantitative lipidomic analysis and demonstrated that altered lipid species (e.g., lysophosphatidylcholine) were associated with pro-inflammatory cytokines in the serum of human patients with Takotsubo Syndrome, an acute cardiac syndrome with increased inflammation (Karnati et al.). It should be noted here that human individual variation in many serum lipid species is high and may require a large number of samples in order to detect difference among groups. The power of this study is relatively low (262 individuals from three groups) and the data acquired here may be interpreted with caution. However, as Karnati et al. managed to show difference in lysophosphatidylchline, application of quantitative lipidomics appears to be a promising tool for a comprehensive study of serum lipid profiles. In another study, Berkowitz et al. reported that ceramide, one class of sphingolipid, plays a causative role in both type 2 diabetes and CVD. Finally, Khafagy and Dash reviewed the current knowledge of etiology and pathogenesis of inflammation in obesity-associated CVD. Animal and human data both indicate that adipose tissue, a specialized lipid storage tissue, is involved in hyperlipidemia and systemic inflammation in obesity. Based on human genetic and pharmacological studies, while anti-inflammatory treatment reduces CVD, off-target effects such as increased infection limit its broad therapeutic application, which warrants future studies on mechanistic link between lipid metabolism and systemic inflammation. It is our belief that this knowledge is critical for designing novel drugs targeting lipid metabolic enzymes because, in many disease settings, abnormal lipid metabolism may be the real driving force of inflammation.

AUTHOR CONTRIBUTIONS

YC determined the structure and drafted the editorial. JZ and WD edited and approved the final version. All authors contributed to the article and approved the submitted version.

FUNDING

This work is supported by MCW New Faculty Startup Fund and NIH grants R01HL153397 (to YC).

ACKNOWLEDGMENTS

We thank Dr. Mary Scorci-Thomas (Medical College of Wisconsin) for providing valuable advice and comments for this work.

REFERENCES

1. van Meer G, Voelker DR Feigenson GW. Membrane lipids: where they are and how they behave. *Nat Rev Mol Cell Biol.* (2008) 9:112–24. doi: 10.1038/nrm2330
2. Alberts B, Johnson A, Lewis J, Raff M, Roberts K, Walter P. *Molecular Biology of the Cell*. New York, NY: Garland Science (2002).
3. Farooqui AA, Horrocks LA Farooqui T. Glycerophospholipids in brain: their metabolism, incorporation into membranes, functions, and involvement in neurological disorders. *Chem Phys Lipids.* (2000) 106:1–29. doi: 10.1016/S0009-3084(00)00128-6
4. Mathis D, Shoelson SE. Immunometabolism: an emerging frontier. *Nat Rev Immunol.* (2011) 11:81. doi: 10.1038/nri2922
5. Beloribi-Djefaflia S, Vasseur S, Guillaumond F. Lipid metabolic reprogramming in cancer cells. *Oncogenesis.* (2016) 5:e189. doi: 10.1038/oncsis.2015.49
6. Chen Y, Zhang J, Cui W, Silverstein RL. CD36, a signaling receptor and fatty acid transporter that regulates immune cell metabolism and fate. *J Exp Med.* (2022) 219:e20211314. doi: 10.1084/jem.20211314
7. Okoro EU. TNFalpha-Induced LDL cholesterol accumulation involve elevated LDLR cell surface levels and SR-B1 downregulation in human arterial endothelial cells. *Int J Mol Sci.* (2021) 22:6236. doi: 10.21203/rs.3.rs-267515/v2
8. Field FJ, Watt K, Mathur SN. TNF-alpha decreases ABCA1 expression and attenuates HDL cholesterol efflux in the human intestinal cell line Caco-2. *J Lipid Res.* (2010) 51:1407–15. doi: 10.1194/jlr.M002410
9. Brown MS, Kovanen PT, Goldstein JL. Regulation of plasma cholesterol by lipoprotein receptors. *Science.* (1981) 212:628–35. doi: 10.1126/science.6261329
10. Ishibashi S, Goldstein JL, Brown MS, Herz J, Burns DK. Massive xanthomatosis and atherosclerosis in cholesterol-fed low density lipoprotein receptor-negative mice. *J Clin Invest.* (1994) 93:1885–93. doi: 10.1172/JCI117179
11. Alique M, Luna C, Carracedo J, Ramirez R. LDL biochemical modifications: a link between atherosclerosis and aging. *Food Nutr Res.* (2015) 59:29240. doi: 10.3402/fnr.v59.29240
12. Silverstein RL, Febbraio M. CD36, a scavenger receptor involved in immunity, metabolism, angiogenesis, and behavior. *Sci Signal.* (2009) 2:re3. doi: 10.1126/scisignal.272re3
13. Rye KA, Barter PJ. Cardioprotective functions of HDLs. *J Lipid Res.* (2014) 55:168–79. doi: 10.1194/jlr.R039297
14. Ohashi R, Mu H, Wang X, Yao Q, Chen C. Reverse cholesterol transport and cholesterol efflux in atherosclerosis. *QJM.* (2005) 98:845–56. doi: 10.1093/qjmed/hci136
15. Di Costanzo A, Ronca A, D'Erasmo L, Manfredini M, Baratta F, Pastori D, et al. HDL-Mediated cholesterol efflux and plasma loading capacities are altered in subjects with metabolically- but not genetically driven non-alcoholic fatty liver disease (NAFLD). *Biomedicines.* (2020) 8:625. doi: 10.3390/biomedicines8120625
16. Zimetti F, De Vuono S, Gomaraschi M, Adorni MP, Favari E, Ronda N, et al. Plasma cholesterol homeostasis, HDL remodeling and function during the acute phase reaction. *J Lipid Res.* (2017) 58:2051–60. doi: 10.1194/jlr.P076463
17. Ronda N, Favari E, Borghi MO, Ingegnoli F, Gerosa M, Chighizola C, et al. Impaired serum cholesterol efflux capacity in rheumatoid arthritis and systemic lupus erythematosus. *Ann Rheum Dis.* (2014) 73:609–15. doi: 10.1136/annrheumdis-2012-202914
18. Hafiane A, Favari E, Daskalopoulou SS, Vuilleumier N, Frias MA. High-density lipoprotein cholesterol efflux capacity and cardiovascular risk in autoimmune and non-autoimmune diseases. *Metabolism.* (2020) 104:154141. doi: 10.1016/j.metabol.2020.154141
19. Montecucco F, Favari E, Norata GD, Ronda N, Nofer JR, Vuilleumier N. Impact of systemic inflammation and autoimmune diseases on apoA-I and HDL plasma levels and functions. *Handb Exp Pharmacol.* (2015) 224:455–82. doi: 10.1007/978-3-319-09665-0_14
20. Robichaud S, Rasheed A, Pietrangelo A, Doyoung Kim A, Boucher DM, Emerton C, et al. Autophagy is differentially regulated in leukocyte and nonleukocyte foam cells during atherosclerosis. *Circ Res.* (2022) 130:831–47. doi: 10.1161/CIRCRESAHA.121.320047
21. Deretic V. Autophagy in inflammation, infection, and immunometabolism. *Immunity.* (2021) 54:437–53. doi: 10.1016/j.immuni.2021.01.018
22. Chadwick AC, Holme RL, Chen Y, Thomas MJ, Sorci-Thomas MG, Silverstein RL, et al. Acrolein impairs the cholesterol transport functions of high density lipoproteins. *PLoS ONE.* (2015) 10:e0123138. doi: 10.1371/journal.pone.0123138
23. Schill RL, Knaack DA, Powers HR, Chen Y, Yang M, Schill DJ, et al. Modification of HDL by reactive aldehydes alters select cardioprotective functions of HDL in macrophages. *FEBS J.* (2020) 287:695–707. doi: 10.1111/febs.15034
24. Chen Y, Yang M, Huang W, Chen W, Zhao Y, Schulte ML, et al. Mitochondrial metabolic reprogramming by CD36 signaling drives macrophage inflammatory responses. *Circ Res.* (2019) 125:1087–102. doi: 10.1161/CIRCRESAHA.119.315833
25. Katzenelenbogen Y, Sheban F, Yalin A, Yofe I, Svetlichnyy D, Jaitin DA, et al. Coupled scRNA-Seq and intracellular protein activity reveal an immunosuppressive role of TREM2 in cancer. *Cell.* (2020) 182:872–85.e19. doi: 10.1016/j.cell.2020.06.032
26. Ma X, Xiao L, Liu L, Ye L, Su P, Bi E, et al. CD36-mediated ferroptosis dampens intratumoral CD8(+) T cell effector function and impairs their antitumor ability. *Cell Metab.* (2021) 33:1001–12.e5. doi: 10.1016/j.cmet.2021.02.015
27. Jaitin DA, Adlung L, Thaiss CA, Weiner A, Li B, Descamps H, et al. Lipid-Associated macrophages control metabolic homeostasis in a Trem2-dependent manner. *Cell.* (2019) 178:686–98.e14. doi: 10.1016/j.cell.2019.05.054
28. Xiong X, Kuang H, Ansari S, Liu T, Gong J, Wang S, et al. Landscape of intercellular crosstalk in healthy and NASH liver revealed by single-cell secretome gene analysis. *Mol Cell.* (2019) 75:644–60 e5. doi: 10.1016/j.molcel.2019.07.028
29. Koelwyn GJ, Corr EM, Erbay E, Moore KJ. Regulation of macrophage immunometabolism in atherosclerosis. *Nat Immunol.* (2018) 19:526–37. doi: 10.1038/s41590-018-0113-3

Conflict of Interest: The authors declare that the research was conducted in the absence of any commercial or financial relationships that could be construed as a potential conflict of interest.

Publisher's Note: All claims expressed in this article are solely those of the authors and do not necessarily represent those of their affiliated organizations, or those of the publisher, the editors and the reviewers. Any product that may be evaluated in this article, or claim that may be made by its manufacturer, is not guaranteed or endorsed by the publisher.

Copyright © 2022 Zhang, Dai and Chen. This is an open-access article distributed under the terms of the Creative Commons Attribution License (CC BY). The use, distribution or reproduction in other forums is permitted, provided the original author(s) and the copyright owner(s) are credited and that the original publication in this journal is cited, in accordance with accepted academic practice. No use, distribution or reproduction is permitted which does not comply with these terms.

frontiers in Cardiovascular Medicine

ORIGINAL RESEARCH
published: 10 August 2021
doi: 10.3389/fcvm.2021.712903

Bmal1 Downregulation Worsens Critical Limb Ischemia by Promoting Inflammation and Impairing Angiogenesis

Lirong Xu[1,2†], Yutong Liu[2†], Qianyun Cheng[2†], Yang Shen[3], Ye Yuan[3], Xiaolang Jiang[3], Xu Li[3], Daqiao Guo[3], Junhao Jiang[3*] and Changpo Lin[3*]*

[1] Department of Pathology, School of Basic Medical Science, Shanghai University of Traditional Chinese Medicine, Shanghai, China, [2] Department of Physiology and Pathophysiology, School of Basic Medical Science, Fudan University, Shanghai, China, [3] Department of Vascular Surgery, Institute of Vascular Surgery, Zhongshan Hospital, Fudan University, Shanghai, China

OPEN ACCESS

Edited by:
Yiliang Chen, Medical College of Wisconsin, United States

Reviewed by:
Fang Li, Columbia University Irving Medical Center, United States
Xuewei Zhu, Wake Forest School of Medicine, United States

***Correspondence:**
Changpo Lin
lin.changpo@zs-hospital.sh.cn
Junhao Jiang
jhjiangau@hotmail.com
Daqiao Guo
guo.daqiao@zs-hospital.sh.cn

[†]These authors have contributed equally to this work

Specialty section:
This article was submitted to Lipids in Cardiovascular Disease, a section of the journal Frontiers in Cardiovascular Medicine

Received: *21 May 2021*
Accepted: *12 July 2021*
Published: *10 August 2021*

Citation:
Xu L, Liu Y, Cheng Q, Shen Y, Yuan Y, Jiang X, Li X, Guo D, Jiang J and Lin C (2021) Bmal1 Downregulation Worsens Critical Limb Ischemia by Promoting Inflammation and Impairing Angiogenesis. Front. Cardiovasc. Med. 8:712903. doi: 10.3389/fcvm.2021.712903

Critical limb ischemia (CLI) is the most advanced clinical stage of peripheral vascular disease with high mobility and mortality. CLI patients suffer from lower extremity rest pain, ulceration, and gangrene caused by insufficient blood and oxygen supply. Seeking for effective biomarkers and therapeutic targets is of great significance for improving the life quality of CLI patients. The circadian clock has been reported to be involved in the progression of kinds of cardiovascular diseases. Whether and how circadian genes play a role in CLI remains unknown. In this study, by collecting femoral artery and muscle specimens of CLI patients who underwent amputation, we confirmed that the circadian gene Bmal1 is downregulated in the CLI femoral artery and ischemic distal lower limb muscle. Furthermore, we verified that Bmal1 affects CLI by regulating lipid metabolism, inflammation, and angiogenesis. A hindlimb ischemia model performed in wild-type and Bmal1$^{-/-}$ mice confirmed that Bmal1 disruption would lead to impaired angiogenesis. *In vitro* experiments indicated that the decreased expression of Bmal1 would increase ox-LDL uptake and impair endothelial cell functions, including proliferation, migration, and tube formation. As for mechanisms, Bmal1 represses inflammation by inhibiting lipid uptake and by activating IL-10 transcription and promotes angiogenesis by transcriptionally regulating VEGF expression. In conclusion, we provide evidence that the circadian gene Bmal1 plays an important role in CLI by inhibiting inflammation and promoting angiogenesis. Thus, Bmal1 may be an effective biomarker and a potential therapeutic target in CLI.

Keywords: circadian clock, Bmal1, critical limb ischemia, lipids metabolism, inflammation, angiogenesis

INTRODUCTION

Critical limb ischemia (CLI) is an ischemic disease of the lower extremities caused by arterial stenosis and occlusion (1). It is a local manifestation of systemic atherosclerosis in the limbs. Its pathological progress starts with arterial intima and middle layer degenerative and proliferative changes and then leads to arterial wall thickening, hardening, and twisting, resulting in arterial lumen stenosis and even obstruction and ultimately leading to the occurrence of corresponding

ischemic symptoms at the distal end of the artery (2). There are numerous theories about the CLI etiology, including lipid deposition, inflammation, and thrombosis (2, 3). Kinds of inflammatory factors and cytokines are involved in inflammatory injury, plaque formation, plaque rupture, and final artery stenosis or occlusion (4, 5). Patients with peripheral arterial diseases often have accompanying kinds of severe comorbidities, including coronary artery disease, cerebrovascular disease, respiratory dysfunction, and end-stage renal disease (6). Thus, CLI seriously damages the health of patients, and more importantly it is strongly related to a high risk of mortality, especially due to cardiovascular events. Therefore, it is urgent to clarify the detailed pathogenesis of CLI and seek out more efficient prediction and therapy methods.

Disordered lipid metabolism has been recognized as the independent risk factor of atherosclerosis and related peripheral vascular disease (7). High levels of circulating LDL or modified LDL (i.e., ox-LDL) induce endothelial cell (EC) dysfunctions and increased adhesion molecule and proinflammatory gene expression (8–10). Accordingly, LDL and ox-LDL are the major causes of atherosclerotic lesions (10). LDL would deposit at the vascular walls, with a high serum concentration (8). ox-LDL binds to several kinds of scavenger receptors located at macrophages and ECs, including CD36, macrophage scavenger receptor 1 (MSR-1), and lectin-like oxidized low-density lipoprotein receptor 1 (LOX-1) (10). Among these, LOX-1 is the main ox-LDL receptor in ECs and mediates a host of ox-LDL-induced effects (8, 10). Once modified LDL stimulates the ECs, circulating monocytes are recruited through the activated endothelium and differentiate into macrophages (11). The activated macrophages produce inflammatory cytokines, chemokines, oxygen and nitrogen radicals, and other inflammatory molecules, ultimately leading to inflammation and tissue damage (11). The important inflammatory molecules in this process include interferon-γ, interleukin-1 (IL-1), interleukin-6 (IL-6), and tumor necrosis factor α (TNFα) (11). On the other hand, anti-inflammatory factors, including interleukin-10 (IL-10) and transforming growth factor b (TGF-β), act as protective factors in atherosclerosis. The inhibition of IL-10 (12, 13) and TGF-β (14) aggravates atherosclerosis. The balance between inflammation and anti-inflammation controls the progression of atherosclerosis and related peripheral vascular diseases. However, the role of lipid metabolism and inflammation in the progression of CLI is still unclear, and the relevant mechanism needs further investigation.

Angiogenesis occurs in response to arterial occlusion and shear force changes to restore blood flow and nutrient supply in the heart and limbs (15). This is of great significance in the treatment of ischemic diseases caused by arterial occlusion. The vascular endothelial growth factor (VEGF) plays a critical role in angiogenesis by activating target angiogenesis-related genes (15). A hypoxic environment, inflammation-related cytokines, and hormones are reported to be able to elevate the expression of VEGF (15, 16). However, the VEGF expression is attenuated in the aged and hypercholesterolemic ones. It is urgent to restore angiogenesis to cure CLI and other vascular obstruction diseases in these kinds of people (17).

The circadian clock, as a comprehensive regulation system that controls the wake–sleep cycle, body temperature, hormone secretion, etc. of an organism, plays a pivotal role in the metabolic regulation process (18). Disordered circadian rhythms would inevitably lead to severe metabolic disorders and related diseases (19–22). Studies have shown that people with circadian clock disorders are more likely to suffer from cardiovascular diseases, metabolic-related diseases, and cancer (23–26). It is reported that the occurrence of acute arterial occlusion of the limbs showed a significant circadian pattern with a peak in the early morning (27). Mice with knockout or mutant circadian clock genes are accompanied with an abnormal activity rhythm, metabolic disorders, and cardiovascular diseases (20, 22, 28). As for Bmal1, the core circadian gene, it plays a critical role in lipid metabolism, inflammation, and related cardiovascular diseases. It has been reported that plasma cholesterol ester, non-esterified fatty acids, and phospholipids are all elevated in Bmal1$^{-/-}$ mice compared with wild-type (WT) mice of the same age (22). Besides this, Bmal1 deficiency affects the cholesterol efflux to the bile. Thus, a global Bmal1 deficiency increases atherosclerosis (22). Moreover, an organ-specific knockout of Bmal1 would also lead to disordered lipid metabolism and atherosclerosis, including the liver (22), endothelial cells (29), and myeloid cells (30). Among them, mice with liver Bmal1 deficiency have accompanying increased hepatic triglyceride and cholesterol levels (22). Moreover, myeloid Bmal1 deficiency leads to proinflammatory macrophage phenotype changes and enhances monocyte recruitment to the atherosclerotic lesion, which then aggravates atherosclerosis (30). However, the role of circadian genes, especially Bmal1, in CLI needs more investigations.

This research aims to explore the relationship between the circadian gene Bmal1 and CLI. By collecting ischemic artery and the lower limb muscle of CLI patients, constructing a lower limb ischemia animal model, and conducting *in vitro* experiments in endothelial cells, we demonstrated that the disruption of Bmal1 aggravates lipid deposition and inflammation and impairs angiogenesis. Therefore, the downregulation of Bmal1 would promote the occurrence and progression of CLI. Our research may help to find effective serum markers for the early diagnosis and prevention of CLI and to develop new potential therapeutic targets.

MATERIALS AND METHODS

Patients

With the approval of the Ethical Committee of Zhongshan Hospital, three pairs of femoral artery tissues and normal artery specimens from healthy donors were collected. Nine groups of lower limb muscle were obtained from CLI patients with lower limb amputations. All patients signed the informed consent before enrollment in the study. The study was conducted in accordance with the ethical guidelines of the Declaration of Helsinki.

Animals

Bmal1$^{+/-}$ mice are introduced from the Jackson Laboratory and had been bred in the Model Animal Research Center of Nanjing

University (The GemPharmatech Company). Heterozygous mice were intercrossed to obtain homozygous Bmal1-deficient ($Bmal1^{-/-}$) mice as well as control wild-type mice. All mice were fed with a chow diet and raised in a clean room with 12-h light and 12-h dark cycles. All animal experiments were conducted strictly in accordance with the National Institutes of Health Guide for the Care and Use of Laboratory Animals and were approved by the Animal Care and Use Committee of Shanghai Medical College, Fudan University.

Cell Culture

Human umbilical vein endothelial cells (HUVECs) were obtained from ATCC. The HUVECs were grown in 1640 medium supplemented with 10% fetal bovine serum (FBS), 10 U/ml penicillin and 100 mg/ml streptomycin at 37°C with 5% CO_2.

The 293T cells were introduced from the Cell Bank Type Culture Collection of the Chinese Academy of Sciences. They were cultured in Dulbecco's modified Eagle's medium (DMEM) medium supplemented with 10% FBS, 10 U/ml penicillin, and 100 mg/ml streptomycin. The cells were cultured in a humidified CO_2 incubator at 37°C.

Oil Red O Staining

To determine the lipid deposition in the sub-endothelial femoral artery, femoral arteries from CLI patients and normal arteries are fixed with 4% paraformaldehyde and then frozen-sectioned and stained with Oil Red O.

HLI Mouse Model

At 6–8 weeks of age, the mice were anesthetized with pentobarbital sodium (50 mg/kg, i.p.) and then subjected to unilateral femoral artery ligation and resection. The blood flow in the lower limb was monitored with a laser Doppler perfusion imaging system (Perimed, Inc., Ardmore, PA) immediately after surgery (day 0) and then at days 7 and 14 post-surgery. The mice were placed on a warming pad during surgery and during laser Doppler image acquisition to maintain a constant body temperature of 37°C. Perfusion was expressed as the ratio of the left (ischemic) to right (non-ischemic) hindlimb. The right hindlimb served as an internal control for each mouse.

Small Interfering RNA, Vector, and Lentivirus Infection

The siRNAs used to silence BMAL1 expression (siBMAL1), VEGF expression (si-VEGF), and negative control siRNA (si-NC) were designed and produced by RiboBio company (Shanghai, China) which were transfected into HUVECs by Lipofectamine® 3000 (Invitrogen; Thermo Fisher Scientific, Inc.) following the manufacturer's instruction after the cell density reached 80% confluence. To perform lentiviral infection, we allowed the cells to reach 70% confluence. During the infection, the medium was replaced with fresh medium containing lentivirus (ad-BAML1 and ad-GFP), and the cells were cultured for 24 h at 37°C, the culture was changed with a fresh complete medium, and the cells were continuously cultured for another 24 h.

OX-LDL Treatment

A total of 40 μg/ml 1,1′-dioctadecyl-3,3,3′,3′-tetramethyl-indocarbocyanine perchlorate (Dil)-ox-LDL was added to the culture medium of HUVECs for 6 h. For confocal microscopy, the cells were fixed with 4% formaldehyde in room temperature for 15 min and visualized using standard rhodamine excitation: emission filters at 554:571 nm. For gene expression detection, the cells were harvested with the TRIzol reagent according to the instruction manual.

Cell Proliferation Assay

A total of 2×10^4 HUVECs were seeded on a 12-well plate (Thermo) and incubated in culture medium for 96 h at 37°C and 5% CO_2. The cells in each well were digested with trypsin and counted at 24, 48, 72, and 96 h. Each experiment was repeated three independent times.

Cell Migration Assay

The HUVECs (6×10^4) were placed into Transwell chambers (Corning Incorporated, USA) for the migration assay. The lower chambers were filled with DMEM containing 10% FBS as a chemoattractant. After maintaining at 37°C for 6–8 h, the cells that remained on the upper surface of the membrane were removed. The HUVECs on the lower surface of the membrane were fixed with 4% formaldehyde and stained with 0.1% crystal violet. The stained cells were photographed and quantified by counting in five random microscopic fields.

Tube Formation Assay

A total of 1×10^4 HUVECs were suspended in culture medium and seeded in 48-well plates that were pretreated with Matrigel matrix. The formation of the tube networks develops in 12 h at 37°C and 10% CO_2 and were visualized by a microscope and photographed at 3, 6, 8, and 12 h, and the analysis was performed with Image J. Each experiment was repeated three independent times.

Reverse Transcription-Quantitative Polymerase Chain Reaction

Total RNA was isolated from tissues and cells using the TRIzol reagent (Invitrogen; Thermo Fisher Scientific, Inc.) following the protocol of the supplier. To detect mRNA expression, total RNA was reverse-transcribed into cDNA using a ReverTra Ace® qPCR RT Kit (code no. FSQ-201, Toyobo, Japan), and real-time PCR was performed using a SYBR Green kit (Toyobo, Japan). All samples were analyzed using a Roche real-time analyzer, and the results were normalized to the glyceraldehyde-3-phosphate dehydrogenase (GAPDH) expression. The primers used are listed in **Supplementary Table 1**.

Western Blotting

Cultured cells or tissues were lysed using the RIPA lysis buffer, and total protein concentration was detected using bicinchoninic acid assay (Beyotime Institute of Biotechnology). SDS–PAGE (10%) was used to resolve equal amounts of protein. The membranes were blocked with 5% milk in PBS–Tween-20 buffer (PBST) for 1 h at room temperature prior to overnight incubation

at 4°C with primary antibodies against specific antibodies (listed in **Supplementary Table 2**). Subsequently, the membranes were peroxidase-conjugated with secondary antibodies at room temperature for 1.5 h. After three rinses with PBST, the protein bands were visualized using the ECL western blotting substrate (Bio-Rad). β-ACTIN and GAPDH were considered the loading control for normalization.

Chromatin Immunoprecipitation Assay

A total of 1×10^7 HUVEC were washed with cold phosphate-buffered saline, fixed with 1% formaldehyde for 10 min at room temperature, and then crosslinked with 125 mM glycine for 5 min at room temperature. The cells were then harvested in cell lysis buffer (50 mM HEPES, 500 mM NaCl, 1% Triton X-100, 0.1% sodium deoxycholate, 1 mM EDTA, and 0.1% SDS, pH 7.5). The cell lysates were then briefly sonicated to fragment genomic DNA. The cell lysates were then used for chromatin immunoprecipitation using anti-BMAL1 and anti-IgG antibodies. The protein A/G beads–antibody/chromatin complexes were washed with lysis buffer and wash buffer (50 mM Tris-HCl, 300 mM LiCl, 2 mM MgCl, and 0.5% NP-40, pH 7.5), and the antibody/chromatin complexes were subsequently eluted with the elution buffer (50 mM Tris-HCl, 10 mM EDTA, and 1% SDS, pH 8.0). The cross-linked protein/DNA complexes were detached at 65°C for 4 h, followed by purification of the genomic DNA. The PCR primers are shown in **Supplementary Table 1**.

Luciferase Reporter Assay

Luciferase reporter assay was conducted with the Firefly Luciferase Reporter Gene Assay Kit from Beyotime company. The primers for the luciferase reporter constructs are listed in **Supplementary Table 3**.

Statistical Analysis

Data are presented as the mean ± SEM. Statistical comparisons were conducted with unpaired Student's *t*-tests/one-way ANOVA with *post-hoc* Tukey test/two-way ANOVA with *post-hoc* Sidak test as appropriate, and $p < 0.05$ was considered statistically significant.

RESULTS

Disruption of Bmal1 Expression Is Associated With Critical Limb Ischemia

Considering the close relationship between circadian clock and cardiovascular diseases, we were wondering whether Bmal1 plays a role in critical limb ischemia. First of all, we compared the Bmal1 expression differences in femoral artery specimens from critical limb ischemia (CLI) patients and normal artery specimens from healthy donors (NA). It was shown that there is a significant decreased expression of Bmal1 in CLI femoral artery specimens compared with the normal artery (**Supplementary Figure 1A**), suggesting that Bmal1 may play a protective role in the CLI occurrence and progression. To further investigate the relationship between Bmal1 and CLI progression, we collected the proximal, middle, and distal lower limb muscle of CLI patients with different levels of ischemic severity. The demographic characteristics of these patients are shown in **Supplementary Table 4**. The mRNA (**Figure 1A**) and protein (**Figures 1B,C**) expressions of Bmal1 are both decreased in the distal lower limb muscle compared with the proximal, while there was a slight increase of BMAL1 protein expression in the middle lower limb muscle compared with the proximal. These results suggested that the decreased Bmal1 expression may promote the progression of CLI and aggravate the ischemic symptoms of the lower extremities.

Bmal1 Inhibits Inflammation by Repressing Lipid Uptake and Activating IL-10 Expression

Although CLI can be caused by vasculitis, thromboembolism, trauma, and Buerger disease, it is mostly associated with atherosclerosis (3). Atherosclerosis is a chronic disease closely related to inflammation, which is initiated by an inflammatory response resulting in elevated lipid deposition, EC dysfunction, and monocyte recruitment to the arterial intima (31). We wondered whether Bmal1 plays a role in CLI progression by affecting inflammation and lipid metabolism. First of all, we explored the expression of inflammatory factors in CLI patients. The mRNA expression of genes involved in inflammation is elevated in the femoral artery specimens of CLI patients, including pro-inflammation factors like IL-6 and TNFα and anti-inflammation factor IL-10 (**Supplementary Figure 2A**). The inflammation factor expressions were both increased in the middle and distal muscle of the lower limbs compared with the proximal lower limb muscle, while the increase in distal group is much more obvious, suggesting that inflammation is more serious in the distal lower limb (**Figure 2A**). By oil red O staining, we then verified that the sub-endothelial deposition of lipids was more pronounced in the femoral artery of CLI patients (**Figure 2B**). We then explored the mRNA expression of genes involved in lipid metabolism, including fatty acid and cholesterol uptake, transportation, and metabolism in the femoral artery and lower limb muscle of CLI patients. It was shown that low-density lipoprotein receptor and ox-LDL scavenger receptors, including CD36 and LOX-1, were elevated in CLI femoral artery (**Supplementary Figure 2B**), suggesting more lipid uptake in CLI patients. Furthermore, the above-mentioned gene expression was also increased in the distal lower limb muscles compared with the proximal ones (**Figure 2C**), indicating the association of lipid uptake with the severity of ischemia.

To further investigate the role of Bmal1 in these processes, we then explored these gene expressions in WT and Bmal1$^{-/-}$ mice lower limb muscle and found a significant increase of CD36, MSR-1, and IL-6 in Bmal1$^{-/-}$ mice (**Figure 2D**). Moreover, we measured the plasma lipid profiles in Bmal1$^{-/-}$ mice and their littermates of WT mice. It was shown that the triglyceride and LDL-C content are elevated in Bmal1$^{-/-}$ mice, while the HDL-C level is downregulated in Bmal1$^{-/-}$ mice compared with the WT mice (**Supplementary Figure 3A**). These results suggested that Bmal1 may inhibit the uptake of lipids by endothelial cells and macrophages by inhibiting ox-LDL receptors, thereby repressing inflammation and playing a protective role in the

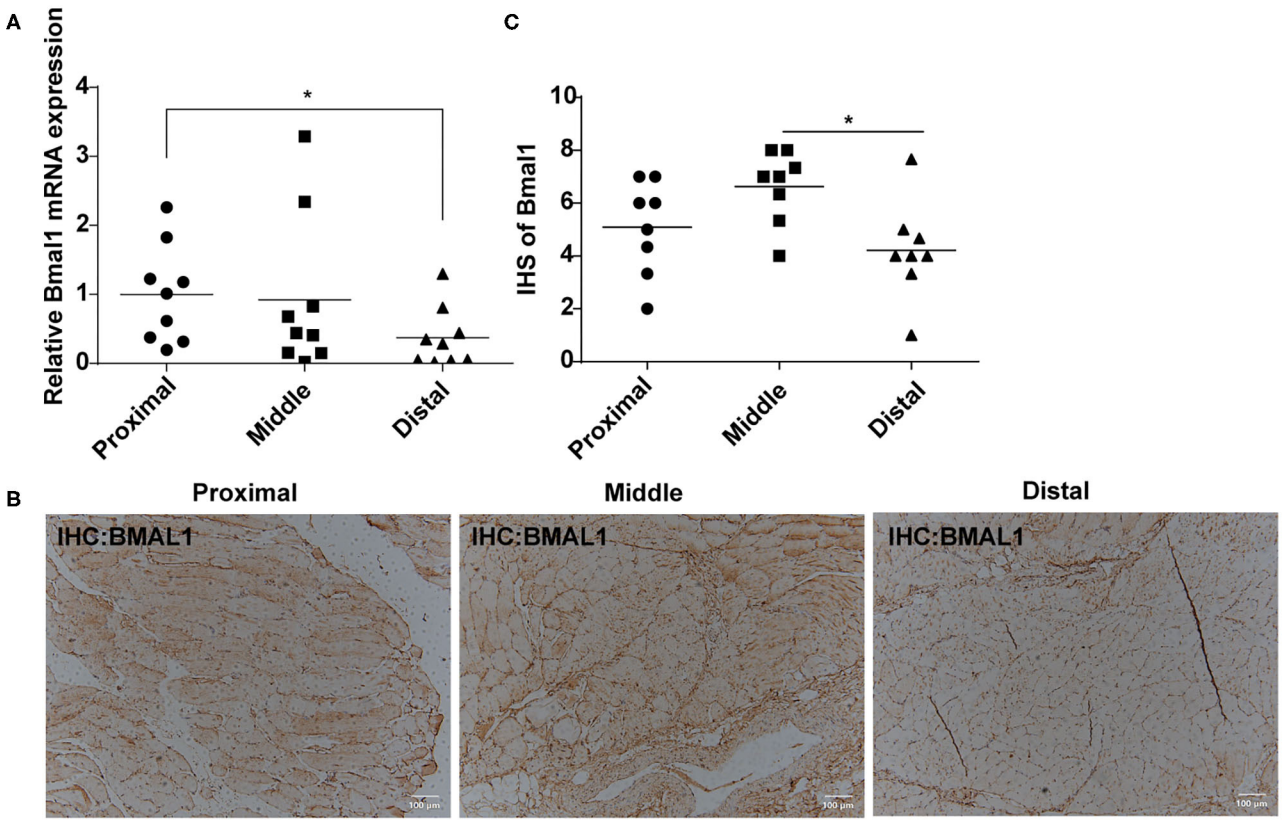

FIGURE 1 | Bmal1 expression is decreased in the distal lower limb muscle of critical limb ischemia (CLI) patients. **(A)** Relative mRNA expression of Bmal1 in the lower limb muscle of CLI patients detected by real-time PCR. Data are presented as mean ± SEM ($n = 9$, one-way ANOVA with *post-hoc* Tukey test). *$p < 0.05$ distal lower limb vs. proximal lower limb. **(B,C)** Immunohistochemistry conducted in the lower limb muscle of CLI patients with specific anti-BMAL1 antibody with a dilution of 1:100. The immunohistochemical staining results were assigned with a mean score considering the intensity of staining and the proportion of cells with a positive reaction area. Each section was independently assessed by two pathologists without prior knowledge of patient data. Data are presented as mean ± SEM ($n = 8$, one-way ANOVA with *post-hoc* Tukey test). *$p < 0.05$ distal lower limb vs. middle lower limb.

occurrence of CLI. To prove our hypothesis, we knocked down and overexpressed Bmal1 expression in HUVECs and treated the cells with Dil-labeled ox-LDL. When Dil-ox-LDL was taken up by vascular endothelial cells or macrophages, the lipoprotein is degraded by lysosomal enzymes and the Dil (fluorescent probe) accumulates in the intracellular membranes. It was shown that knocking down of Bmal1 in HUVECs caused an increase of Dil-ox-LDL uptake, while the overexpression of Bmal1 was associated with a downregulation of Dil-ox-LDL uptake (**Figure 2E**). Besides this, the mRNA expression of ox-LDL receptors, including MSR-1 and LOX-1, was consistent with the ox-LDL uptake result (**Figure 2F**). Therefore, our results demonstrated that Bmal1 inhibits inflammation in CLI by inhibiting the lipid uptake of endothelial cells.

To further demonstrate that Bmal1 regulates inflammation by affecting the lipid uptake, we changed the expression of Bmal1 together with the addition of ox-LDL. The expression alterations of the inflammatory genes verified that the addition of ox-LDL would increase the pro-inflammatory gene expression and decrease the anti-inflammatory gene expression. Besides this, the knockdown of Bmal1 would aggravate the changes, while the overexpression of Bmal1 would alleviate these changes (**Figures 3A,B**). Furthermore, we wondered whether Bmal1 can directly regulate inflammation. By overexpressing and knocking down Bmal1, we found that Bmal1 positively regulates IL-10 expression (**Figures 3C,D**). Moreover, luciferase reporter assay and chromatin immunoprecipitation (ChIP) assay indicated that Bmal1 transcriptionally regulates IL-10 expression by binding on its promoter region (**Figures 3E,F**). In conclusion, we demonstrated that Bmal1 represses inflammation in CLI by inhibiting lipid deposition and promoting the anti-inflammatory factor IL-10 expression.

Disruption of Bmal1 Impairs Angiogenesis in CLI

Angiogenesis stimulated by vascular occlusion helps restore blood and oxygen supply to the lower limbs and further alleviate symptoms. We then aimed to explore the role of Bmal1 in this process. By real-time PCR, we found that the mRNA expression of genes involved in angiogenesis is elevated in the femoral artery of CLI patients (**Supplementary Figure 4A**). We then explored the difference of angiogenesis in the proximal,

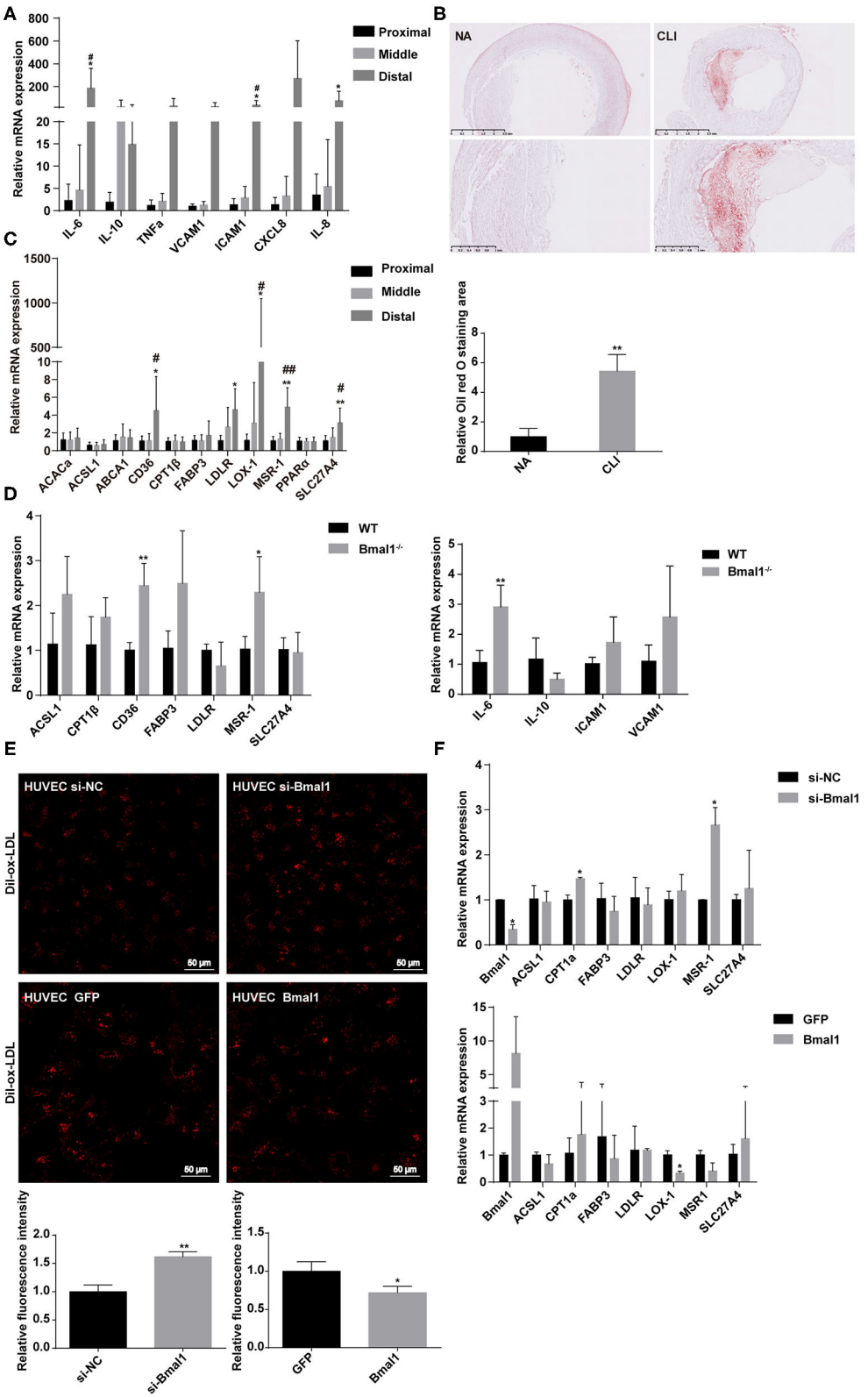

FIGURE 2 | Bmal1 inhibits lipid uptake by endothelial cells. **(A)** Relative mRNA expression of inflammation factors by real-time PCR. Data are presented as mean ± SEM ($n = 9$, one-way ANOVA with *post-hoc* Tukey test). $^{*}p < 0.05$ distal lower limb vs. proximal lower limb; $^{\#}p < 0.05$ distal lower limb vs. middle lower limb. **(B)** Oil

(Continued)

FIGURE 2 | red O staining of normal artery and femoral artery from critical limb ischemia (CLI) patients. Oil red O staining area are measured with Image J. Data are presented as mean ± SEM ($n = 3$, unpaired t-test); $^{**}p < 0.01$ CLI vs. NA. **(C)** Relative mRNA expression of genes involved in lipid metabolism in the lower limb muscle of CLI patients. Data are presented as mean ± SEM ($n = 9$, one way ANOVA with *post-hoc* Tukey test). $^{*}p < 0.05$ and $^{**}p < 0.01$, distal lower limb vs. proximal lower limb; $^{\#}p < 0.05$ and $^{\#\#}p < 0.01$, distal lower limb vs. middle lower limb. **(D)** Relative mRNA expression of genes involved in lipid metabolism and inflammation in wild-type and Bmal1$^{-/-}$ mice lower limb muscle. Data are presented as mean ± SEM ($n = 4$, unpaired t-test). $^{*}p < 0.05$ and $^{**}p < 0.01$, Bmal1$^{-/-}$ vs. WT. **(E)** Dil-ox-LDL uptake by human umbilical vein endothelial cells (HUVECs), with the expression changes of Bmal1 measured by confocal microscopy. Ox-LDL uptake is measured with the relative fluorescence intensity. Data are presented as mean ± SEM (unpaired t-test, repeated 3 independent times). $^{**}p < 0.01$ si-Bmal1 vs. si-NC and $^{*}p < 0.05$ Bmal1 vs. GFP. **(F)** Relative mRNA expression of genes involved in lipid metabolism in HUVECs with the expression changes of Bmal1. Data are presented as mean ± SEM (unpaired t-test, repeated 3 independent times). $^{*}p < 0.05$, si-Bmal1 vs. si-NC; $^{*}p < 0.05$ Bmal1 vs. GFP.

middle, and distal lower limb muscle. The immunofluorescence of CD31, an endothelial cell marker, suggested that the capillary density is much more abundant in the middle than the distal lower limb (**Figures 4A,B**). Moreover, the mRNA expression of CD31 increased significantly in the middle lower limb muscle, suggesting that angiogenesis is more announced (**Figure 4C**). However, there was no significant increase in the distal group despite of more serious ischemia (**Figure 4C**). We then wondered whether the decreased angiogenesis was related to BMAL1, CD31, and BMAL1 immunofluorescence co-staining results which showed that the BMAL1 expression was reduced in the endothelial cells in the distal lower limb muscle of CLI patients (**Supplementary Figures 5A,B**). We then detected the expression of VEGF, which is the critical factor in angiogenesis, and found that it was decreased significantly in the distal group (**Figures 4D,E**). These results indicated that decreased angiogenesis leads to serious ischemic symptoms in the distal lower limb muscle, and it is partly attributed to reduced VEGF expression.

To determine whether Bmal1 affects CLI by regulating angiogenesis, hindlimb ischemia (HLI) was surgically performed in Bmal1$^{-/-}$ mice and their littermates of WT mice. Blood flow measurements were performed at days 0, 7, and 14 after HLI. The results showed that, compared with the WT mice, the blood perfusion in the ischemic limbs of Bmal1$^{-/-}$ mice was significantly inhibited (**Figures 5A,B**). Next, immunofluorescence staining of α-SMA and CD31 was performed in ischemic muscle collected 14 days after HLI. As shown in **Figure 5C**, a lower anti-CD31-positive capillary density was observed in Bmal1$^{-/-}$ mice. Moreover, there is an obvious elevation of CD31 and α-SMA mRNA expression after HLI in WT mice, probably attributed to increased angiogenesis response after HLI (**Figure 5D**; **Supplementary Figure 6A**). However, the elevation effect was eliminated in Bmal1$^{-/-}$ mice with a significantly decreased mRNA expression of α-SMA and CD31 in both non-HLI and HLI groups (**Figure 5D**; **Supplementary Figure 6A**). Moreover, Bmal1 expression was elevated in the WT HLI group compared with WT non-HLI group (**Figures 5D,E**). These results indicated the promoting effect of Bmal1 in angiogenesis. Consistently, Bmal1 deficiency was associated with a significant decrease in the expression of angiogenic factors, including mKC (a murine functional homolog of IL-8) and VEGF (**Figures 5D,E**). Moreover, the expression changes of inflammatory factors suggested that inflammation regulation in Bmal1$^{-/-}$ mice is disordered (**Supplementary Figure 6B**). Therefore, we concluded that BMAL1 contributes to revascularization after ischemia in mice and CLI patients by promoting angiogenesis.

Bmal1 Promotes the Angiogenic Activity of HUVECs by Transcriptionally Regulating VEGF Expression

To further determine the proangiogenic role of Bmal1, assessments of human umbilical vein cell (HUVEC) proliferation, migration, and tube formation were conducted in Bmal1 knocked down or overexpressed cells. The efficiency of Bmal1 knockdown and overexpression in HUVECs was confirmed by western blotting assay (**Figure 6A**). Cell proliferation in si-Bmal1 HUVEC was significantly slower than the control group (**Figure 6B**). Consistently, an opposite result was obtained in AdBmal1 HUVEC observed by cell counting assay (**Figure 6B**). Furthermore, transwell chamber experiment was conducted to determine the migration of HUVECs. The si-Bmal1 HUVEC showed impaired cell migration, while the AdBmal1-HUVEC significantly increased cell migration (**Figure 6C**). Moreover, compared with the control group, tube formation in Bmal1 siRNA-HUVEC was significantly reduced. In AdBmal1 HUVECs, tube formation was significantly promoted (**Figure 6D**). Since Bmal1 upregulation promoted HUVEC proliferation, migration, and tube formation, it is implicated that Bmal1 is involved in angiogenesis by maintaining HUVEC functions.

To further estimate the mechanism of Bmal1 in regulating angiogenesis, we overexpressed Bmal1 in HUVEC and examined the expression of genes involved in angiogenesis. We found that there is a significant increase of VEGF expression in the Bmal1 overexpressing HUVEC (**Figure 7A**). We then knocked down Bmal1 and found an obvious downregulation of VEGF (**Figures 7B,C**). Since Bmal1 is a transcription factor, we further investigated whether VEGF was under the transcriptional regulation of Bmal1 by luciferase reporter assay. We found that Bmal1 overexpression significantly increased the luciferase activity of VEGF promoter constructs (**Figure 7D**). Thus, we generated a series of luciferase reporter constructs containing the VEGF promoter and then investigated the effect of Bmal1 overexpression on the luciferase activity of these constructs. The result suggested that Bmal1 mainly binds on the −971 to 0 region of the VEGF promoter (**Figure 7D**). Furthermore, ChIP assay verified that Bmal1 binds on the −906 to −700 and −382 to −150 regions of VEGF promoter (**Figure 7E**). Besides this, knocking down of VEGF partly dismissed the pro-angiogenesis function of Bmal1 overexpression in HUVECs (**Figures 7F,G**).

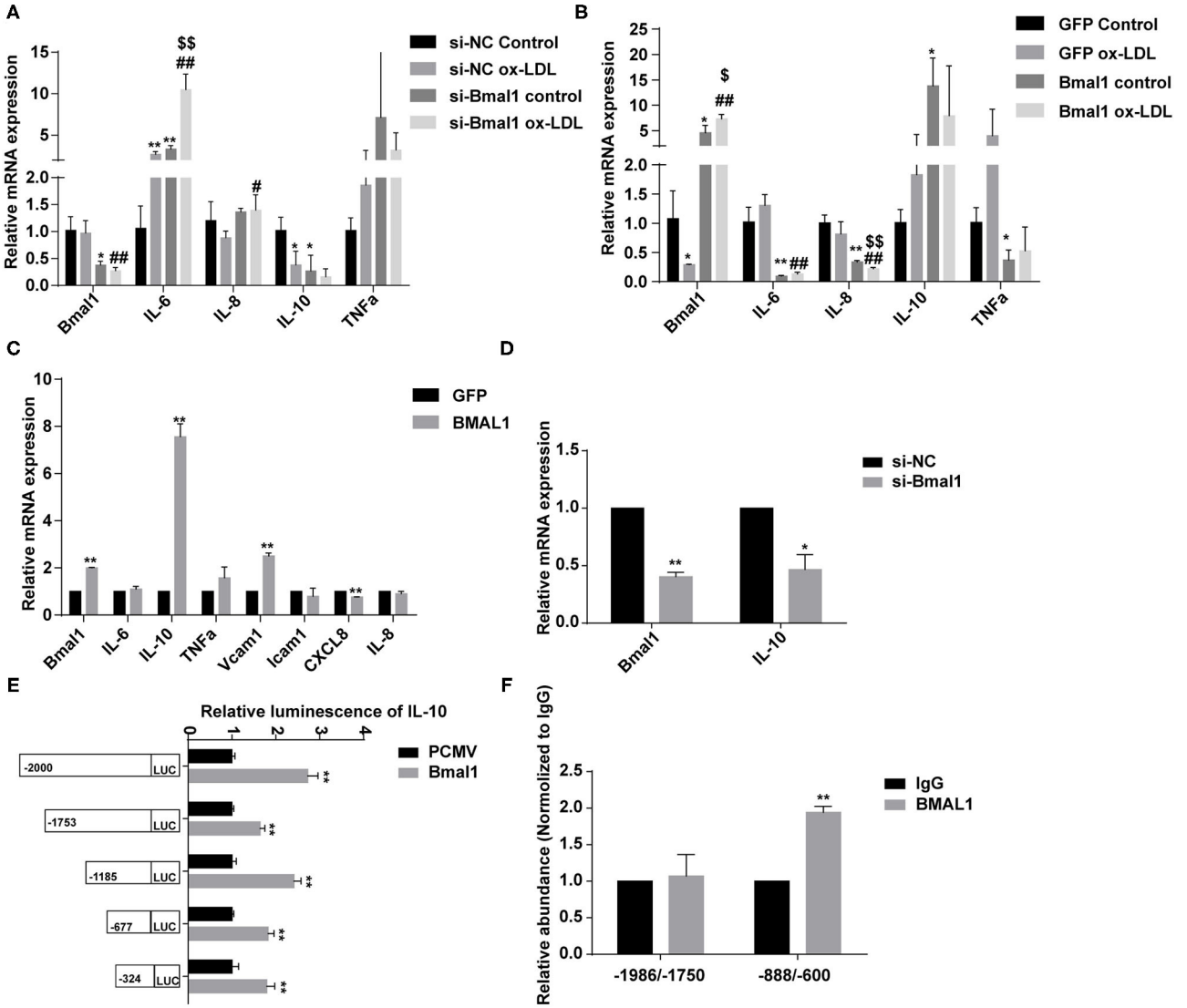

FIGURE 3 | Bmal1 represses inflammation by inhibiting the lipid uptake and transcriptionally regulating the IL-10 expression. **(A)** Relative mRNA expression of genes involved in inflammation in human umbilical vein endothelial cells (HUVECs) which had been transfected with si-NC or si-Bmal1 with or without the addition of ox-LDL. Data are presented as mean ± SEM (one-way ANOVA with *post-hoc* Tukey test). $^{*}p < 0.05$ and $^{**}p < 0.01$ vs. si-NC control; $^{\#}p < 0.05$ and $^{\#\#}p < 0.01$ vs. si-NC ox-LDL; $^{\$\$}p < 0.01$ vs. si-Bmal1 control. **(B)** Relative mRNA expression of genes involved in inflammation in HUVECs which had been transfected with adenoviruses coding for AdGFP or AdBmal1 with or without the addition of ox-LDL. Data are presented as mean ± SEM (one-way ANOVA with *post-hoc* Tukey test). $^{*}p < 0.05$ and $^{**}p < 0.01$ vs. GFP control; $^{\#\#}p < 0.01$ vs. GFP ox-LDL; $^{\$}p < 0.05$ and $^{\$\$}p < 0.01$ vs. Bmal1 control. **(C)** Relative mRNA expression of genes involved in inflammation in HUVECs which had been transfected with adenoviruses coding for AdGFP or AdBmal1. Data are presented as mean ± SEM (unpaired *t*-test). $^{**}p <$ 0.01 Bmal1 vs. GFP. **(D)** Relative mRNA expression of Bmal1 and IL-10 in HUVECs which had been transfected with Bmal1 siRNA or si-NC. Data are presented as mean ± SEM (unpaired *t*-test). $^{*}p < 0.05$ and $^{**}p < 0.01$ si-Bmal1 vs. si-NC. **(E)** Luciferase reporter constructs were created containing the truncated (−2,000, −1,753, −1,185, −677, and −324) versions of the IL-10 promoter. The luciferase reporter constructs were co-transfected with Bmal1 overexpression vector or with the control vector into HEK293T cells, and luciferase activity was evaluated 24 h later. Data are presented as mean ± SEM (unpaired *t*-test). $^{**}p < 0.01$ Bmal1 vs. PCMV. **(F)** ChIP assay conducted in HUVECs with anti-BMAL1 or IgG antibody. qRT-PCR analysis was performed with primer sequences around Bmal1-binding E-box elements in the IL-10 promoter. Data are presented as mean ± SEM (unpaired *t*-test). $^{**}p < 0.01$ BMAL1 vs. IgG. Each expreiment was repeated 3 independent times.

In conclusion, our results verified that Bmal1 promotes angiogenesis by transcriptionally regulating VEGF expression.

DISCUSSION

In this study, we found that circadian gene Bmal1 disruption aggravates critical limb ischemia by promoting lipid uptake and inflammation and impairing angiogenesis. Moreover, Bmal1 transcriptional regulation of VEGF and IL-10 is involved in this process (**Figure 8**). Thus, targeting therapy of Bmal1 in CLI patients may both promote angiogenesis to recover blood and oxygen supply and inhibit inflammation to alleviate ischemic symptoms.

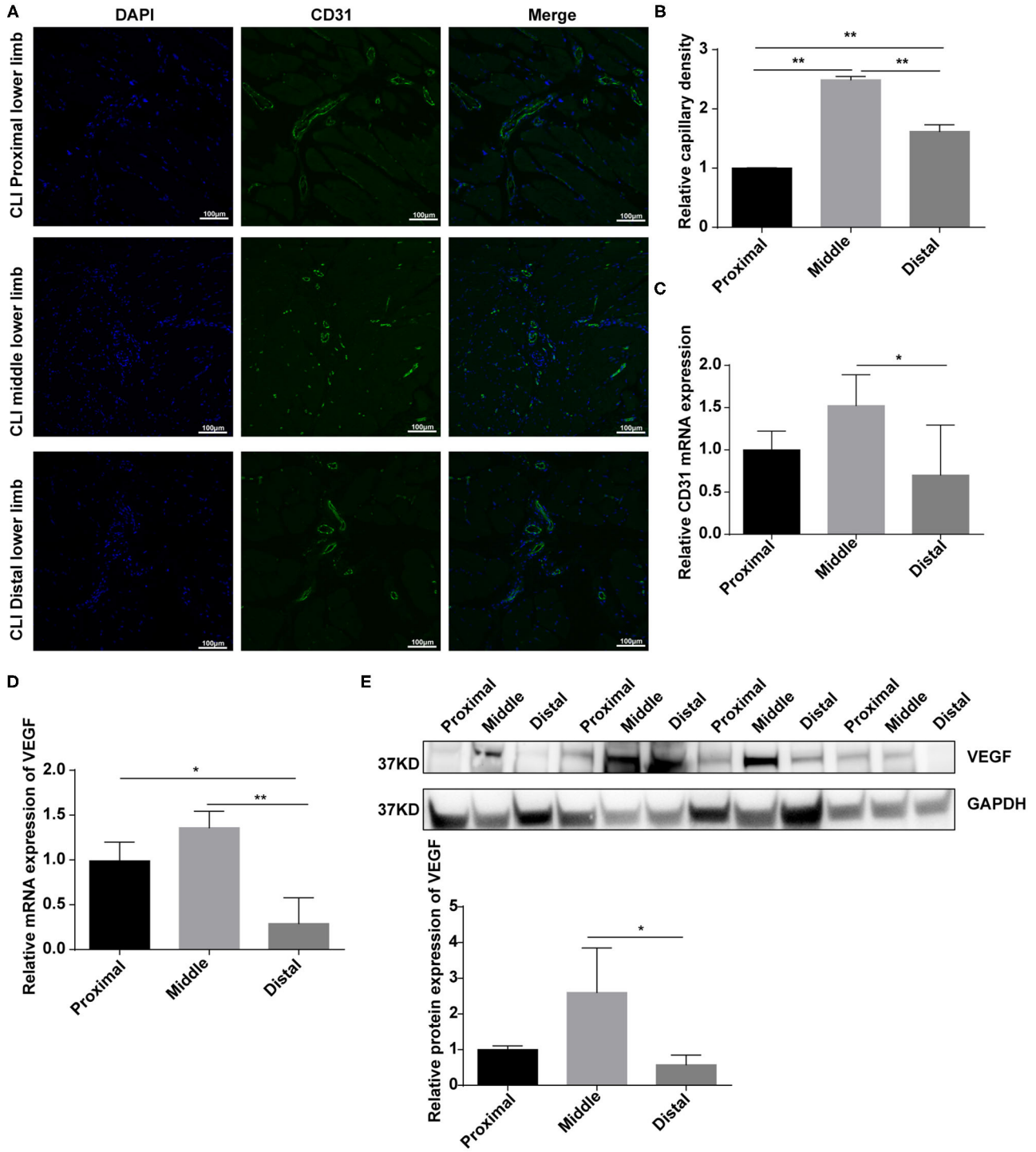

FIGURE 4 | Angiogenesis are elevated in response to vascular occlusion in the lower limb muscle of critical limb ischemia (CLI) patients. **(A,B)** Immunofluorescence conducted in the lower limb muscle of CLI patients with specific anti-CD31 antibody. Relative capillary density was determined based on immunofluorescence staining. Data are presented as mean ± SEM ($n = 9$, one-way ANOVA with *post-hoc* Tukey test). $^{**}p < 0.01$, middle lower limb vs. proximal lower limb; $^{**}p < 0.01$, distal lower limb vs. proximal lower limb; $^{**}p < 0.01$, distal lower limb vs. middle lower limb. **(C)** Relative mRNA expression of CD31 in the lower limb muscle of CLI patients by real-time PCR. Data are presented as mean ± SEM ($n = 9$, one-way ANOVA with *post-hoc* Tukey test). $^{*}p < 0.05$ middle lower limb vs. proximal lower limb; $^{*}p < 0.05$ distal lower limb vs. middle lower limb. **(D)** Relative mRNA expression of VEGF in the lower limb muscle of CLI patients by real-time PCR. Data are presented as mean ± SEM ($n = 9$, one-way ANOVA with *post-hoc* Tukey test). $^{**}p < 0.01$ distal lower limb vs. middle lower limb; $^{*}p < 0.05$ distal lower limb vs. proximal lower limb. **(E)** Relative protein expression of VEGF in the lower limb muscle of CLI patients by western blot ($n = 4$, one-way ANOVA with *post-hoc* Tukey test). Data are presented as mean ± SEM.

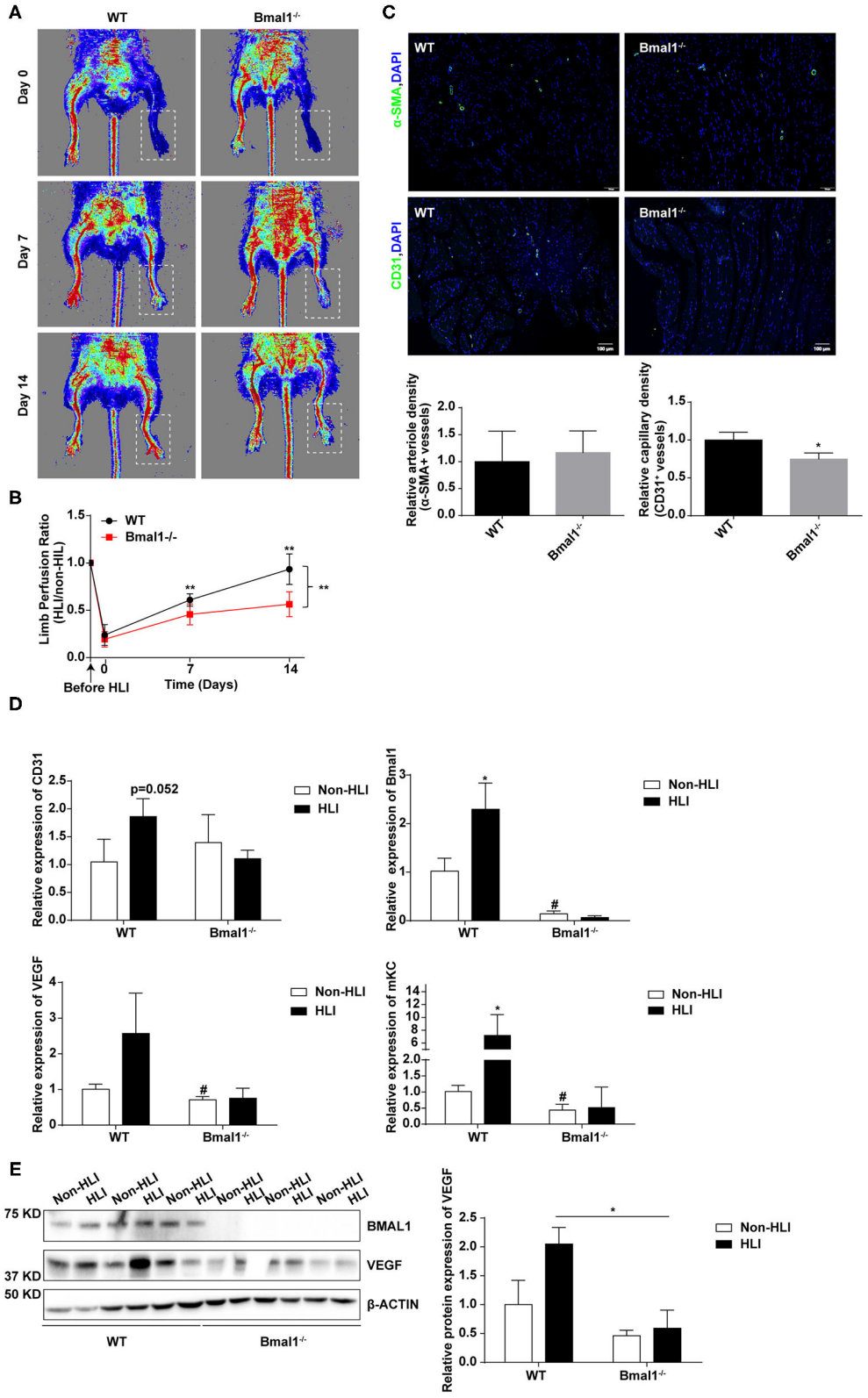

FIGURE 5 | Bmal1 promotes angiogenesis after peripheral ischemic injury. **(A)** Blood flow obtained *via* laser Doppler perfusion imaging on days 0, 7, and 14 after HLI in Bmal1$^{-/-}$ mice and WT mice. **(B)** The perfusion of the hindlimbs of mice at each time point was calculated as the ratio of measurements of the injured (HLI) and

(Continued)

FIGURE 5 | uninjured (non-HLI) limbs. $n = 4$ for Bmal1$^{-/-}$ and WT mice. Data are presented as mean ± SEM (unpaired *t*-test and two-way ANOVA with *post-hoc* Sidak test). $^{**}P < 0.01$ Bmal1$^{-/-}$ vs. WT. **(C)** At 14 days after HLI, the gastrocnemius muscle was harvested from the HLI limb of Bmal1$^{-/-}$ mice and WT mice and stained for α-smooth muscle actin (α-SMA) and CD31 expression. Data are presented as mean ± SEM ($n = 4$, unpaired *t*-test). $^{*}P < 0.05$ Bmal1$^{-/-}$ vs. WT. **(D)** mRNA levels of the CD31, Bmal1, VEGF, and murine functional IL-8 homolog keratinocyte-derived chemokine (mKC) were evaluated in HLI and non-HLI limbs *via* real-time PCR. Data are presented as mean ± SEM ($n = 4$, unpaired *t*-test). $^{*}p < 0.05$ wild-type (WT) HLI vs. WT non-HLI; $^{\#}p < 0.05$ Bmal1$^{-/-}$ non- HLI vs. WT non-HLI. **(E)** Protein expression level of BAML1 and VEGF in HLI and non-HLI limbs measured by western blot. Data are presented as mean ± SEM ($n = 3$, unpaired *t*-test). $^{*}p < 0.05$ Bmal1$^{-/-}$ HLI vs. WT HLI.

CLI is the most advanced clinical stage of peripheral arterial disease with high mobility and mortality. It is always associated with atherosclerosis (3). It has been reported that circadian genes are involved in atherosclerosis and cardiovascular diseases. Firstly, global or organ-specific knockout of Bmal1 is reported to attribute to the progression of hyperlipidemia and atherosclerosis (22, 29, 30). Besides this, other circadian genes including Clock (28), Cry (32), and Reverb (33) are all critical in atherosclerosis. However, whether and how circadian clock genes play a role in the occurrence and progression of CLI remains unclear. In this study, we found that the circadian gene Bmal1 plays an important role in CLI. Bmal1 expression in the femoral artery and distal lower limb muscle of CLI patients is decreased. Our study suggested that Bmal1 is a protective factor in CLI. We are the first to indicate the important role of circadian clock in CLI. Therefore, our research suggested that circadian rhythm disorder may be one of the pathogenic factors of CLI. Moreover, our research may provide theoretical basis for CLI treatment, including chronotherapy and gene-based therapy.

Serum lipids have a critical role in the pathogenesis of atherosclerosis and related peripheral vascular diseases. In particular, the serum LDL level is closely related to the human risk of cardiovascular diseases. LDL- and ox-LDL-mediated EC dysfunctions are thought to be the initial step of atherosclerosis (31). The upregulated expression of ox-LDL receptors in the CLI femoral artery and distal lower limb found in our research suggested that excessive lipid uptake and deposition are important factors in the formation and progression of CLI. Moreover, we found that Bmal1 inhibits ox-LDL uptake by repressing the expression of LOX-1, the main ox-LDL receptor of ECs. Thus, attenuated Bmal1 expression in CLI patients leads to increased lipid deposition and severe inflammation response. It has been reported that lipid metabolism is under the regulation of circadian clock. First of all, the concentration of circulating lipids displays a significant circadian rhythm (34), including triglyceride, cholesterol, and LDL (31). Moreover, many genes involved in lipid absorption (35) and biosynthesis (34) are under circadian clock regulation. Consistently, the circadian gene mutant mice, including Clock$^{\Delta 19}$, Bmal1$^{-/-}$, and Rev-erbα$^{-/-}$ mice, are all hyperlipidemic and prone to cardiovascular diseases (19, 22, 28, 36). The role of Bmal1 in inhibiting LOX-1, CD36, and MSR-1 as found in our research demonstrated that lipid uptake by ECs and macrophages is also under the regulation of the circadian clock. Our research supplements the role of circadian clock in lipid metabolism and cardiovascular diseases.

Emerging evidence suggested that inflammation plays an important role in the progress of CLI (4, 5). In support of this theory, it was shown that the circulating levels of cytokines (IL-6 and TNFα), adhesion molecules (VCAM-1 and ICAM-1), and selectins in patients with peripheral arterial disease are elevated (37). This is consistent with our findings that the pro-inflammatory factor expression is increased in the femoral artery of CLI patients. Moreover, we demonstrated that the expression of inflammatory factors is associated with the severity of ischemic symptoms in the lower limb muscle of CLI patients. Studies have suggested that the circadian clock is involved in the regulation of inflammation. First of all, the number of Ly6C^{hi} monocytes in peripheral blood shows a diurnal oscillation (38), indicating that the circadian clock plays a role in this process. Besides this, it has been demonstrated that Bmal1 represses the expression of Ccl2; thus, myeloid-specific Bmal1 deletion increases monocyte recruitment and worsens atherosclerosis (30). Moreover, Rev-erbα also plays a role in inflammation by regulating the expression of Ccl2 (39). In our research, we verified that circadian gene Bmal1 regulates inflammation by inhibiting lipid uptake and by directly promoting IL-10 expression. Therefore, Bmal1 may inhibit the inflammatory response by promoting the expression of the anti-inflammatory factor IL-10, thereby reducing the ischemic symptoms of CLI.

Angiogenesis occurs in response to tissue hypoxia in CLI patients, and it would lead to feeder collateral and small vessel formation. Angiogenesis plays important roles in many physiological processes, including embryonic development and reproduction (40). Stimulation of angiogenesis can be therapeutic in wound healing and peripheral arterial disease, while excessive angiogenesis may be the basis of certain diseases, including cancer (41) and atherosclerotic plaque vulnerability (42). Controlling angiogenesis is of great value in the treatment of these diseases. Targeting angiogenesis therapy in CLI has attracted great interests these years, mainly by growth factor application and stem cell therapy (1). Despite the application of VEGF (43), FGF (44), HGF (45, 46), and HIF1α (47) in CLI treatment, the effects were minimal mainly because of the formation of immature vessel walls or the activation of inflammation. Among them, only HGF showed a potential therapeutic role in CLI because of its angiogenic property while inhibiting the inflammation function (48). In our research, we found that the circadian gene Bmal1 plays an important role in angiogenesis by transcriptionally regulating VEGF expression. Besides this, it was demonstrated that Bmal1 is involved in the anti-inflammation process by inhibiting lipid uptake and activating IL-10 expression. Therefore, Bmal1 may be a potential therapeutic target in CLI treatment.

In conclusion, we demonstrated that Bmal1 downregulation worsens CLI by impairing angiogenesis and promoting inflammation. Thus, Bmal1 may be a biomarker for diagnosis and a therapeutic target in CLI patients.

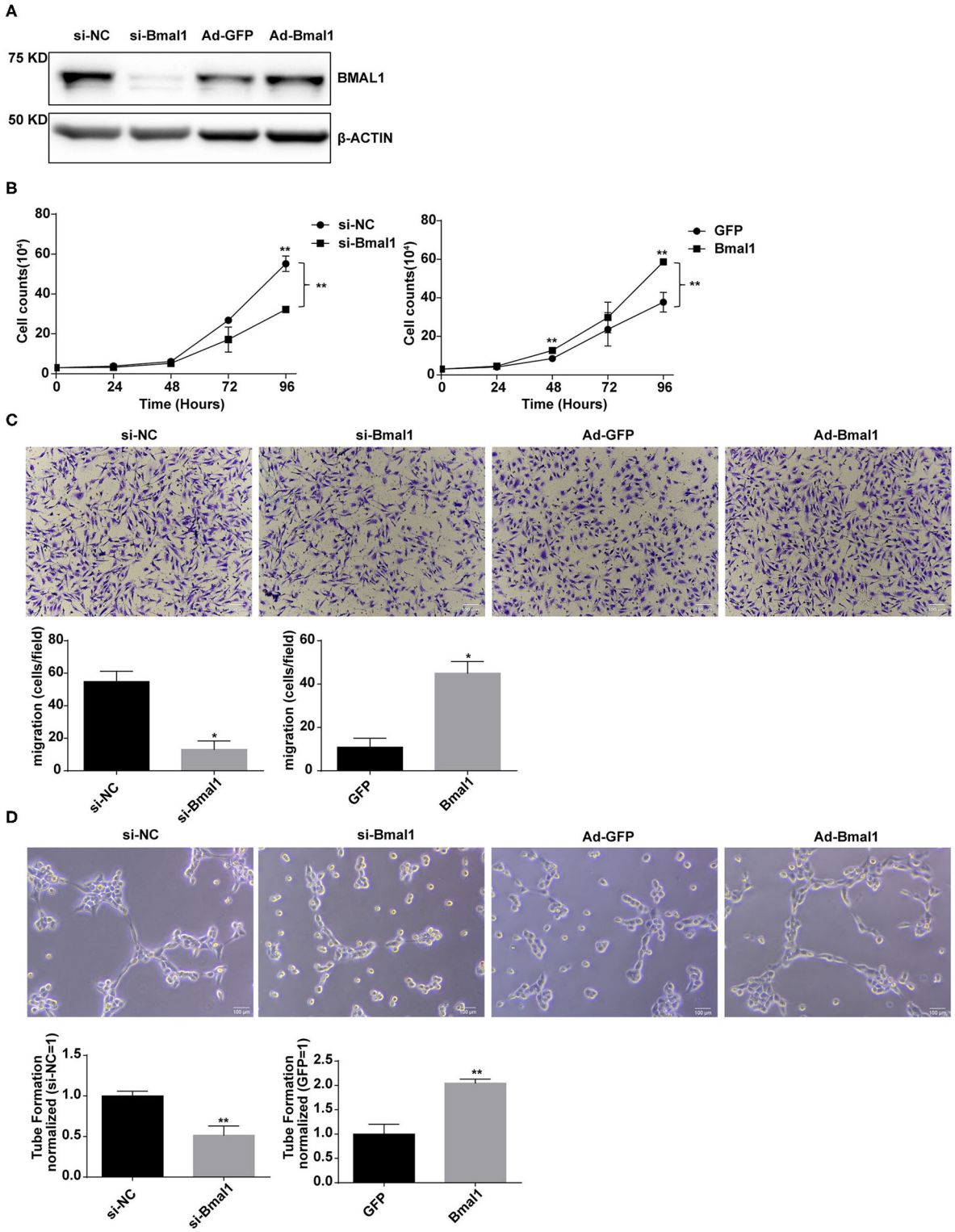

FIGURE 6 | Bmal1 promotes the proangiogenic activity of endothelial cells. **(A)** Knockdown and overexpression effect of Bmal1 in human umbilical vein endothelial cells (HUVECs). Bmal1 protein levels were evaluated *via* western blotting assay. **(B)** Cell proliferation was measured by cell counting in HUVECs. Data are presented as mean ± SEM (unpaired *t*-test and two-way ANOVA with *post-hoc* Sidak test). $^{**}p < 0.01$ si-Bmal1 vs. si-NC; $^{**}p < 0.01$ Bmal1 vs. GFP. **(C)** Cell migration measured by transwell in HUVECs. Data are presented as mean ± SEM (unpaired *t*-test). $^{*}p < 0.05$ si-Bmal1 vs. si-NC; $^{*}p < 0.05$ Bmal1 vs. GFP. **(D)** Endothelial tube formation in matrigel in HUVECs. Data are presented as mean ± SEM (unpaired *t*-test). $^{**}p < 0.01$ si-Bmal1 vs. si-NC; $^{**}p < 0.01$ Bmal1 vs. GFP. Each expreiment was repeated 3 independent times.

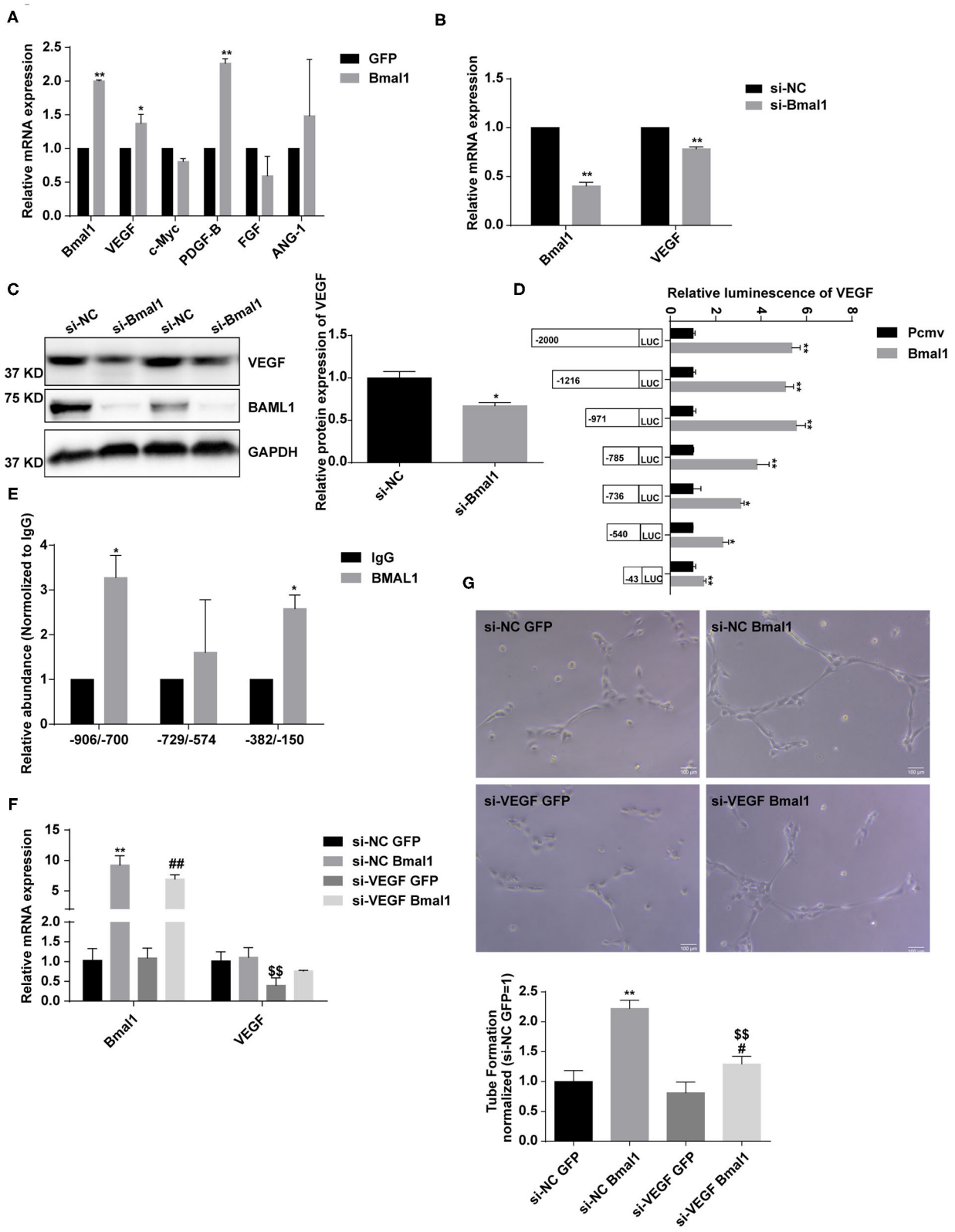

FIGURE 7 | Bmal1 promotes angiogenesis by transcriptionally regulating the vascular endothelial growth factor (VEGF) expression. **(A)** Relative mRNA expression of genes involved in angiogenesis in human umbilical vein endothelial cells (HUVECs) which had been transfected with adenoviruses coding for AdGFP or AdBmal1.

(Continued)

FIGURE 7 | Data are presented as mean ± SEM (unpaired *t*-test). $^{**}p < 0.01$ Bmal1 vs. GFP; $^{*}P < 0.05$ Bmal1 vs. GFP. **(B,C)** Relative mRNA and protein expression of Bmal1 and VEGF in HUVECs which had been transfected with Bmal1 siRNA or si-NC. Data are presented as mean ± SEM (unpaired *t*-test). $^{**}p < 0.01$ si-Bmal1 vs. si-NC; $^{*}p < 0.05$ si-Bmal1 vs. si-NC. **(D)** Luciferase reporter constructs were created containing the truncated (−2,000, −1,216, −971, −785, −736, −540, and −43) versions of the VEGF promoter. The luciferase reporter constructs were co-transfected with Bmal1 overexpression vector or with the control vector into HEK293T cells, and luciferase activity was evaluated 24 h later. Data are presented as mean ± SEM (unpaired *t*-test). $^{**}p < 0.01$ and $^{*}p < 0.05$ Bmal1 vs. PCMV. **(E)** ChIP assay conducted in HUVECs with anti-BMAL1 or IgG antibody. A qRT-PCR analysis was performed with primer sequences around Bmal1-binding E-box elements in the VEGF promoter. Data are presented as mean ± SEM (unpaired *t*-test). $^{*}p < 0.05$ BMAL1 vs. IgG. **(F)** Relative mRNA expression of Bmal1 and VEGF in HUVECs which had been transfected with/without VEGF siRNA and Bmal1/GFP. Data are presented as mean ± SEM (one-way ANOVA with *post-hoc* Tukey test). $^{**}p < 0.01$ si-NC Bmal1 vs. si-NC GFP; $^{\#\#}p < 0.01$ si-VEGF Bmal1 vs. si-VEGF GFP; $^{\$\$}p < 0.01$ si-VEGF GFP vs. si-NC GFP. **(G)** Endothelial tube formation in matrigel in HUVECs. Data are presented as mean ± SEM (one-way ANOVA with *post-hoc* Tukey test). $^{**}p < 0.01$ si-NC Bmal1 vs. si-NC GFP; $^{\#}p < 0.05$ si-VEGF Bmal1 vs. si-VEGF GFP; $^{\$\$}p < 0.01$ si-VEGF Bmal1 vs. si-NC Bmal1. Each expreiment was repeated 3 independent times.

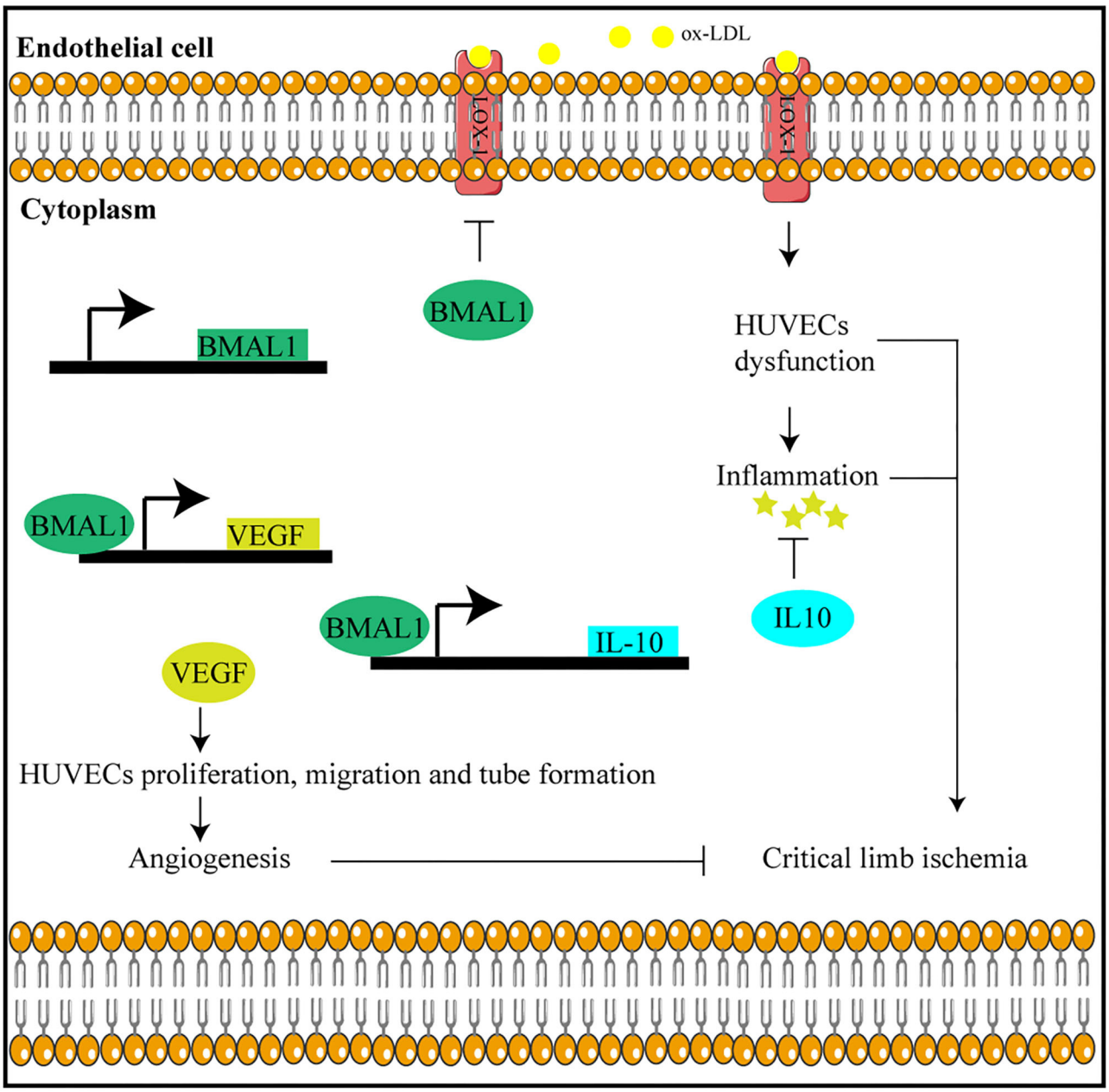

FIGURE 8 | Bmal1 plays a protective role in critical limb ischemia by inhibiting inflammation and promoting angiogenesis.

DATA AVAILABILITY STATEMENT

The original contributions presented in the study are included in the article/**Supplementary Material**, further inquiries can be directed to the corresponding author/s.

ETHICS STATEMENT

The studies involving human participants were reviewed and approved by Ethical Committee of Zhongshan Hospital. The patients/participants provided their written informed consent to participate in this study. The animal study was reviewed and approved by Animal Care and Use Committee of Shanghai Medical College, Fudan University.

AUTHOR CONTRIBUTIONS

LX, JJ, DG, and CL conceived the project. LX and CL designed the experiments and wrote and edited the manuscript. LX, QC, YL, YS, and YY performed the experiments. XL and XJ collected the specimen. All authors contributed to the article and approved the submitted version.

FUNDING

This work was supported by the Shanghai Sailing Program (grant no. 19YF1406100 to CL).

ACKNOWLEDGMENTS

We thank Dr. Jieyu Guo and Mengping Jia for their helpful discussions and sharing of reagents.

SUPPLEMENTARY MATERIAL

The Supplementary Material for this article can be found online at: https://www.frontiersin.org/articles/10.3389/fcvm.2021.712903/full#supplementary-material

REFERENCES

1. Gresele P, Busti C, Fierro T. Critical limb ischemia. *Intern Emerg Med.* (2011) 6:129–3. doi: 10.1007/s11739-011-0683-7
2. Lou X, Yu Z, Yang X, Chen J. Protective effect of rivaroxaban on arteriosclerosis obliterans in rats through modulation of the toll-like receptor 4/NF-κB signaling pathway. *Exp Ther Med.* (2019) 18:1619–3. doi: 10.3892/etm.2019.7726
3. Farber A, Eberhardt RT. The current state of critical limb ischemia: a systematic review. *JAMA Surg.* (2016) 151:1070. doi: 10.1001/jamasurg.2016.2018
4. Patel H, Yong C, Navi A, Shaw SG, Tsui JC. Toll-like receptors 2 and 6 mediate apoptosis and inflammation in ischemic skeletal myotubes. *Vasc Med.* (2019) 4:295–3. doi: 10.1177/1358863X19843180
5. Joshi D, Abraham D, Shiwen X, Baker D, Tsui J. Potential role of erythropoietin receptors and ligands in attenuating apoptosis and inflammation in critical limb ischemia. *J Vasc Surg.* (2014) 60:191–201.e2. doi: 10.1016/j.jvs.2013.06.054
6. Akagi D, Hoshina K, Akai A, Yamamoto K. Outcomes in patients with critical limb ischemia due to arteriosclerosis obliterans who did not undergo arterial reconstruction. *Int Heart J.* (2018) 59:1041–3. doi: 10.1536/ihj.17-592
7. Helkin A, Stein JJ, Lin S, Siddiqui S, Maier KG, Gahtan V. Dyslipidemia part 1—review of lipid metabolism and vascular cell physiology. *Vasc Endovasc Surg.* (2016) 2:107–3. doi: 10.1177/1538574416628654
8. Pirillo A, Norata GD, Catapano L. ALOX-1, OxLDL, and atherosclerosis. *Mediat Inflamm.* (2013) 2013:1–12. doi: 10.1155/2013/152786
9. Ishigaki Y, Katagiri H, Gao J, Yamada T, Imai J, Uno K, et al. Impact of plasma oxidized low-density lipoprotein removal on atherosclerosis. *Circulation.* (2008) 118:75–83. doi: 10.1161/CIRCULATIONAHA.107.745174
10. Di Pietro N, Formoso G, Pandolfi A. Physiology and pathophysiology of oxLDL uptake by vascular wall cells in atherosclerosis. *Vasc Pharmacol.* (2016) 84:1–7. doi: 10.1016/j.vph.2016.05.013
11. Hansson GK. Inflammation, atherosclerosis, and coronary artery disease. *N Engl J Med.* (2005) 352:1685–95. doi: 10.1056/NEJMra043430
12. Caligiuri G, Rudling M, Ollivier V, Jacob M, Michel J, Hansson GK, et al. Interleukin-10 deficiency increases atherosclerosis, thrombosis, and low-density lipoproteins in apolipoprotein E knockout mice. *Mol Med.* (2003) 9:10–7. doi: 10.1007/BF03402102
13. Pinderski LJ, Fischbein MP, Subbanagounder G, Fishbein MC, Kubo N, Cheroutre H, et al. Overexpression of interleukin-10 by activated T lymphocytes inhibits atherosclerosis in LDL receptor–deficient mice by altering lymphocyte and macrophage phenotypes. *Circ Res.* (2002) 90:1064–3. doi: 10.1161/01.RES.0000018941.10726.FA
14. Robertson L, Rudling M, Zhou X, Gorelik L, Flavell RA, Hansson GK. Disruption of TGF-β signaling in T cells accelerates atherosclerosis. *J Clin Invest.* (2003) 112:1342–3. doi: 10.1172/JCI18607
15. Hoeben A, Landuyt B, Highley MS, Wildiers H, Van Oosterom AT, De Bruijn AE. Vascular endothelial growth factor and angiogenesis. *Pharmacol Rev.* (2004) 56:549–3. doi: 10.1124/pr.56.4.3
16. Kuwahara F, Kai H, Tokuda K, Shibata R, Kusaba K. Hypoxia-inducible factor-1alpha/vascular endothelial growth factor pathway for adventitial vasa vasorum formation in hypertensive rat aorta. *Hypertension.* (2002) 39:46–50. doi: 10.1161/hy1201.097200
17. Moriya J, Minamino T. Angiogenesis, cancer, and vascular aging. *Front Cardiovasc Med.* (2017) 4:65. doi: 10.3389/fcvm.2017.00065
18. Brown SA. Circadian metabolism: from mechanisms to metabolomics and medicine. *Trends Endocrin Met.* (2016) 27:415–3. doi: 10.1016/j.tem.2016.03.015
19. Turek FW, Joshu C, Kohsaka A, Lin E, Ivanova G, McDearmon E, et al. Obesity and metabolic syndrome in circadian clock mutant mice. *Science.* (2005) 308:1043–3. doi: 10.1126/science.1108750
20. Alibhai FJ, LaMarre J, Reitz CJ, Tsimakouridze EV, Kroetsch JT, Bolz SS, et al. Disrupting the key circadian regulator CLOCK leads to age-dependent cardiovascular disease. *J Mol Cell Cardiol.* (2017) 105:24–3. doi: 10.1016/j.yjmcc.2017.01.008
21. Lefta M, Campbell KS, Feng HZ, Jin JP, Esser KA. Development of dilated cardiomyopathy in Bmal1-deficient mice. *Heart Circ Physiol.* (2012) 303:H475–85. doi: 10.1152/ajpheart.00238.2012
22. Pan X, Bradfield CA, Hussain MM. Global and hepatocyte-specific ablation of Bmal1 induces hyperlipidaemia and enhances atherosclerosis. *Nat Commun.* (2016) 7:13011. doi: 10.1038/ncomms13011
23. Haupt M, Alte D, Dorr M, Robinson DM, Felix SB, John U, et al. The relation of exposure to shift work with atherosclerosis and myocardial infarction in a general population. *Atherosclerosis.* (2008) 201:205–3. doi: 10.1016/j.atherosclerosis.2007.12.059
24. Roenneberg T, Merrow M. The circadian clock and human health. *Curr Biol.* (2016) 26:R432–43. doi: 10.1016/j.cub.2016.04.011
25. Willich SN. Circadian variation and triggering of cardiovascular events. *Vasc Med.* (1999) 4:41–3. doi: 10.1191/135886399670596924
26. Cierpka-Kmiec K, Hering D. Tachycardia: the hidden cardiovascular risk factor in uncomplicated arterial hypertension. *Cardiol J.* (2020) 27:857–67. doi: 10.5603/CJ.a2019.0021

27. Manfredini R, Gallerani M, Portaluppi F, Salmi R, Zamboni P, Fersini C. Circadian variation in the onset of acute critical limb ischemia. *Thromb Res.* (1998) 92:163–3. doi: 10.1016/S0049-3848(98)00127-3
28. Pan X, Jiang XC, Hussain MM. Impaired cholesterol metabolism and enhanced atherosclerosis in clock mutant mice. *Circulation.* (2013) 128:1758–3. doi: 10.1161/CIRCULATIONAHA.113.002885
29. Xie M, Tang Q, Nie J, Zhang C, Zhou X. BMAL1-downregulation aggravates porphyromonas gingivalis-induced atherosclerosis by encouraging oxidative stress. *Circ Res*. (2020) 126:e15–29. doi: 10.1161/CIRCRESAHA.119.315502
30. Huo M, Huang Y, Qu D, Zhang H, Wong WT, Chawla A, et al. Myeloid Bmal1 deletion increases monocyte recruitment and worsens atherosclerosis. *FASEB J.* (2017) 31:1097–3. doi: 10.1096/fj.201601030R
31. Libby P, Ridker PM, Hansson GK. Progress and challenges in translating the biology of atherosclerosis. *Nature.* (2011) 473:317–3. doi: 10.1038/nature10146
32. Yang L, Chu Y, Wang L, Wang Y, Zhao X, He W, et al. Overexpression of CRY1 protects against the development of atherosclerosis via the TLR/NF-κB pathway. *Int Immunopharmacol.* (2015) 28:525–3. doi: 10.1016/j.intimp.2015.07.001
33. Sitaula S, Billon C, Kamenecka TM, Solt LA, Burris TP. Suppression of atherosclerosis by synthetic REV-ERB agonist. *Biochem Bioph Res Commun.* (2015) 460:566–3. doi: 10.1016/j.bbrc.2015.03.070
34. Adamovich Y, Rousso-Noori L, Zwighaft Z, Neufeld-Cohen A, Golik M, Kraut-Cohen J, et al. Circadian clocks and feeding time regulate the oscillations and levels of hepatic triglycerides. *Cell Metab*. (2014) 19:319–30. doi: 10.1016/j.cmet.2013.12.016
35. Pan X, Hussain MM. Clock is important for food and circadian regulation of macronutrient absorption in mice. *J Lipid Res*. (2009) 50:1800–13. doi: 10.1194/jlr.M900085-JLR200
36. Solt LA, Wang Y, Banerjee S, Hughes T, Kojetin DJ, Lundasen T, et al. Regulation of circadian behaviour and metabolism by synthetic REV-ERB agonists. *Nature.* (2012) 485:62–3. doi: 10.1038/nature11030
37. Signorelli SS, Mazzarino MC, Pino LD, Malaponte G, Porto C, Pennisi G, et al. High circulating levels of cytokines (IL-6 and TNFa), adhesion molecules (VCAM-1 and ICAM-1) and selectins in patients with peripheral arterial disease at rest and after a treadmill test. *Vasc Med.* (2003) 8:15–3. doi: 10.1191/1358863x03vm466oa
38. Nguyen KD, Fentress SJ, Qiu Y, Yun K, Cox JS, Chawla A. Circadian gene Bmal1 regulates diurnal oscillations of Ly6C(hi) inflammatory monocytes. *Science.* (2013) 341:1483–3. doi: 10.1126/science.1240636
39. Sato S, Sakurai T, Ogasawara J, Takahashi M, Izawa T, Imaizumi K, et al. A circadian clock gene, Rev-erbalpha, modulates the inflammatory function of macrophages through the negative regulation of Ccl2 expression. *J Immunol.* (2014) 192:407–3. doi: 10.4049/jimmunol.1301982
40. Qiang M, Reiter RJ, Yundai C. Role of melatonin in controlling angiogenesis under physiological and pathological conditions. *Angiogenesis.* (2020) 23:91–104. doi: 10.1007/s10456-019-09689-7
41. Carmeliet P, Jain RK. Angiogenesis in cancer and other diseases. *Nature.* (2000) 407:249–57. doi: 10.1038/35025220
42. de Vries MR, Quax PHA. Plaque angiogenesis and its relation to inflammation and atherosclerotic plaque destabilization. *Curr Opin Lipidol.* (2016) 27:499–3. doi: 10.1097/MOL.0000000000000339
43. Kusumanto YH, Van Weel V, Mulder NH, Smit AJ, van den Dungen JJAM. Treatment with intramuscular vascular endothelial growth factor gene compared with placebo for patients with diabetes mellitus and critical limb ischemia. *Hum Gene Ther.* (2006) 17:683–91. doi: 10.1089/hum.2006.17.683
44. Belch J, Hiatt WR, Baumgartner I, Driver IV, Nikol S, Norgren L, et al. Effect of fibroblast growth factor NV1FGF on amputation and death: a randomised placebo-controlled trial of gene therapy in critical limb ischaemia. *Lancet.* (2011) 377:1929–37. doi: 10.1016/S0140-6736(11)60394-2
45. Powell RJ, Simons M, Mendelsohn FO, Daniel G, Henry TD, Minako Koga B, et al. Vascular medicine results of a double-blind, placebo-controlled study to assess the safety of intramuscular injection of hepatocyte growth factor plasmid to improve limb perfusion in patients with critical limb ischemia. *Circulation.* (2008) 9:58–65. doi: 10.1161/CIRCULATIONAHA.107.727347
46. Powell RJ, Goodney P, Mendelsohn FO, Moen EK, Annex BH. Safety and efficacy of patient specific intramuscular injection of HGF plasmid gene therapy on limb perfusion and wound healing in patients with ischemic lower extremity ulceration: results of the HGF-0205 trial. *J Vasc Surg.* (2010) 52:1525–3. doi: 10.1016/j.jvs.2010.07.044
47. Creager MA, Olin JW, Belch JJF, Moneta GL, Henry TD, Rajagopalan S, et al. Effect of hypoxia-inducible factor-1α gene therapy on walking performance in patients with intermittent claudication. *Circulation.* (2011) 124:1765–3. doi: 10.1161/CIRCULATIONAHA.110.009407
48. Kaga T, Kawano H, Sakaguchi M, Nakazawa T, Taniyama Y, Morishita R. Hepatocyte growth factor stimulated angiogenesis without inflammation: differential actions between hepatocyte growth factor, vascular endothelial growth factor and basic fibroblast growth factor. *Vasc Pharmacol.* (2012) 57:3. doi: 10.1016/j.vph.2012.02.002

Conflict of Interest: The authors declare that the research was conducted in the absence of any commercial or financial relationships that could be construed as a potential conflict of interest.

Publisher's Note: All claims expressed in this article are solely those of the authors and do not necessarily represent those of their affiliated organizations, or those of the publisher, the editors and the reviewers. Any product that may be evaluated in this article, or claim that may be made by its manufacturer, is not guaranteed or endorsed by the publisher.

Copyright © 2021 Xu, Liu, Cheng, Shen, Yuan, Jiang, Li, Guo, Jiang and Lin. This is an open-access article distributed under the terms of the Creative Commons Attribution License (CC BY). The use, distribution or reproduction in other forums is permitted, provided the original author(s) and the copyright owner(s) are credited and that the original publication in this journal is cited, in accordance with accepted academic practice. No use, distribution or reproduction is permitted which does not comply with these terms.

frontiers in Cardiovascular Medicine

ORIGINAL RESEARCH
published: 01 October 2021
doi: 10.3389/fcvm.2021.697236

Ox-LDL Aggravates the Oxidative Stress and Inflammatory Responses of THP-1 Macrophages by Reducing the Inhibition Effect of miR-491-5p on MMP-9

*Yiling Liao, Enzheng Zhu and Wanxing Zhou**

Department of Internal Cardiology Medicine, The First Affiliated Hospital/School of Clinical Medicine of Guangdong Pharmaceutical University, Guangzhou, China

OPEN ACCESS

Edited by:
Yiliang Chen,
Medical College of Wisconsin, United States

Reviewed by:
Bishuang Cai,
Icahn School of Medicine at Mount Sinai, United States
Jue Zhang,
Versiti Blood Research Institute, United States

***Correspondence:**
Wanxing Zhou
zhouwanx2015@sina.com

Specialty section:
This article was submitted to Lipids in Cardiovascular Disease, a section of the journal Frontiers in Cardiovascular Medicine

Received: *19 April 2021*
Accepted: *07 September 2021*
Published: *01 October 2021*

Citation:
Liao Y, Zhu E and Zhou W (2021) Ox-LDL Aggravates the Oxidative Stress and Inflammatory Responses of THP-1 Macrophages by Reducing the Inhibition Effect of miR-491-5p on MMP-9. Front. Cardiovasc. Med. 8:697236. doi: 10.3389/fcvm.2021.697236

Background: Oxidized low-density lipoprotein (ox-LDL) can induce oxidative stress and inflammatory responses in macrophages to facilitate the genesis and development of atherosclerosis. However, the intermediate links remain unclear. MiR-491-5P can inhibit matrix metalloproteinase 9 (MMP-9); however, it remains unclear whether ox-LDL enhances MMP-9 expression and aggravates the oxidative stress and inflammatory responses under the mediating effect of miR-491-5P.

Method: THP-1 macrophages were divided into 10 groups: blank (control), model (ox-LDL), miR-491-5P high-expression (miR-491-5P mimic), miR-491-5P control (mimic-NC), MMP-9 high-expression (MMP-9-plasmid), MMP-9 control (plasmid-NC), miR-491-5P+plasmid-NC, miR-491-5P+ MMP-9-plasmid, MMP-9 gene silencing (MMP-9-siRNA), and gene silencing control (siRNA-NC). The cells were transfected for 48 h and then treated with 50 μg/mL of ox-LDL for 24 h. MMP-9 mRNA and miR-491-5P expression levels in the cells were detected using reverse transcription-quantitative polymerase chain reaction, and the MMP-9 levels were detected with western blotting. The levels of oxidative stress factors (malondialdehyde [MDA]), reactive oxygen species (ROS), and antioxidant factors (superoxide dismutase [SOD]), and the expression levels of inflammatory factors (tumor necrosis factor [TNF-α] and interleukin-1β and−6 [IL-1β and IL-6]) in the supernatant were detected with enzyme-linked immunosorbent assay.

Results: MDA, ROS, TNF-α, IL-1β, IL-6, and MMP-9 levels were increased, SOD activity was reduced, and miR-491-5P expression was downregulated in the ox-LDL group compared to the control group. In the miR-491-5P mimic group, the MDA, ROS, TNF-α, IL-1β, IL-6, MMP-9 mRNA and protein levels were downregulated, and SOD activity was enhanced compared to the ox-LDL group. MMP-9-plasmid elevated the MDA, ROS, TNF-α, IL-1β, IL-6, MMP-9 mRNA and protein levels, and downregulated SOD activity and miR-491-5P expression. Following transfection with MMP-9-siRNA, the MMP-9-plasmid outcomes were nullified, and the resulting trends were similar to the miR-491-5p simulation group. Oxidative stress and inflammatory responses were higher

in the miR-491-5P mimic+MMP-9-plasmid co-transfection group than in the miR-491-5P mimic group.

Conclusion: Ox-LDL aggravates the oxidative stress and inflammatory responses of THP-1 macrophages by reducing the inhibition effect of miR-491-5p on MMP-9.

Keywords: ox-LDL, miR-491-5P/MMP-9 axis, THP-1 macrophages, oxidative stress, inflammatory response

INTRODUCTION

Oxidative stress and the inflammatory response play critical roles in the development of atherosclerosis (AS) (1). Low-density lipoprotein (LDL) is the primary lipoprotein involved in cholesterol-induced AS. Oxidized LDL (ox-LDL) is extremely pro-inflammatory and has pro-oxidative stress effects (2, 3). Macrophages, derived from mononuclear cells (1), can phagocytize ox-LDL to form lipid-laden foam cells, induce the generation of reactive oxygen species (ROS), secrete pro-inflammatory factors, and cause inflammation of vascular walls and their subsequent repair, leading to the genesis and development of plaques (4, 5). Matrix metalloproteinase 9 (MMP-9) is a proteolytic enzyme that can degrade the extracellular matrix (ECM) in plaque fibrous caps, weakening them and causing plaque instability (6, 7). MMP-9 is present at high expression levels in unstable plaques (8). MMP-9 exerts a positive feedback effect on many pro-inflammatory factors (9) and can aggravate the inflammatory response (10, 11), leading to the development and instability of plaques (12). Ox-LDL can induce macrophages to secrete MMP-9 (13). However, the complete bio-molecular mechanism is not comprehensively understood. MiR-491-5P is a micro-RNA (miRNA), a micromolecular non-coding RNA with a length of 20–22 nucleotides (14). It can inhibit the expression of target mRNA by binding to it, thus exerting a regulatory effect (15, 16). MiR-491-5P achieves targeted inhibition of MMP-9 expression (17). When the regulatory effect of miR-491-5P on MMP-9 is removed, MMP-9 expression is upregulated, thus increasing the incidence of atherosclerotic cerebral infarction (18). However, whether ox-LDL enhances MMP-9 expression and aggravates the oxidative stress and inflammatory responses under the mediating effect of miR-491-5P remains unclear. To address this gap in understanding, *in vitro* cell experiments were conducted and are described here.

MATERIALS AND METHODS

Cell Culture and Grouping

Human monocytes (THP-1) were purchased from the Cell Bank of the Chinese Academy of Sciences. The cells were cultured in RPMI-1640 culture medium (Gibco; Thermo Fisher Scientific, Inc.) supplemented with 10% FBS (Gibco; Thermo Fisher Scientific, Inc.). The F5 cells were incubated in a complete medium containing 100 ng/mL phorbol-12-phorbol myristate acetate (Sigma-Aldrich; Merck KGaA) for 48 h and differentiated into THP-1 macrophages as the experimental cells.

The experimental cells were divided into 10 groups: control, model (ox-LDL), miR-491-5P high-expression (miR-491-5P mimic), miR-491-5P no-load (mimic-NC), MMP-9 high-expression (MMP-9-plasmid), MMP-9 no-load (plasmid-NC), miR-491-5P+plasmid-NC, miR-491-5P+ MMP-9-plasmid, MMP-9 gene silencing (MMP-9-siRNA), and gene silencing control (siRNA-NC). Six wells were used in each group.

Cell Transfection

The oligonucleotide sequences (Gene Pharma, Shanghai, China) of miR-491-5P mimic (miR-491-5P imported) and miR-491-5P mimic-NC (miR-491-5P control), MMP-9 gene silencing (MMP-9-siRNA), gene silencing control (siRNA-NC), MMP-9 high-expression (MMP-9-plasmid), and plasmid control (plasma-NC) sequences (Santa Cruz Biotechnology) were used to establish the corresponding transfection systems. In each group, lipofectamine^{TM} 2000 transfection reagent (Invitrogen Life Technologies, CA, USA) was used to transfect the THP-1 macrophages for 48 h.

Co-Incubation of Ox-LDL and Transfected Macrophages

The differentiated THP-1 macrophages were incubated using 10, 30, 50, or 70 μg/mL ox-LDL (Sigma, USA) in an incubator (temperature: 37°C, saturated humidity: 5% CO_2) for 24 h to determine the appropriate ox-LDL concentration (19). The transfected THP-1 macrophages were then treated with 50 μg/mL of ox-LDL (Sigma) for 24 h.

Analysis of Cell Viability

The cell counting kit-8 (CCK-8) assay was used to analyze cell viability (Abcam, USA). Briefly, THP-1 cells were plated in 96-well plates and differentiated into macrophages. After exposure to 50 μg/mL ox-LDL and cell transfection, 10 μL of CCK-8 working solution was added to each well, and incubation was continued for 4 h at 37°C. The plates were detected at 450 nm using a spectrophotometer (Thermo Fisher Scientific).

Verification of THP-1 Macrophage Foaming

Oil Red O Staining

THP-1 macrophages were incubated with or without ox-LDL and transfected with miR-491-5P mimic, MMP-9-plasmid, MMP-9-siRNA, or miR-491-5P mimic+MMP-9-plasmid for 48 h before exposure to 50 μg/mL ox-LDL. After washing three times with phosphate-buffered saline (PBS), the cells were fixed with 4% paraformaldehyde for 25 min. Oil Red O solution (for cultured cells) was added and the cells were incubated for 30 min at 37°C and counterstained with Mayer Hematoxylin solution, according

to the manufacturer's protocol (G1262 Solarbio Beijing, China). After extensive washing with PBS, the cells were immediately photographed using a microscope (Olympus). After removing the staining solution, the dye retained in the cells was eluted into isopropanol and the IOD value of the Oil Red O staining was detected at 540 nm using a spectrophotometer (Thermo Fisher Scientific).

Lipid Accumulation Assay

Lipid drop (LD) accumulation was evaluated using BODIPY 493/503 (10 μg/mL; Thermo Fisher, D2148) staining. The nuclei were stained with 4′,6-diamidino-2-phenylindole (DAPI) staining solution. The average LD intensity from BODIPY 493/503 staining was quantified using Image J software (National Institutes of Health).

Reverse Transcription-Quantitative Polymerase Chain Reaction (RT-qPCR)

Total RNA was extracted from the cells using TRIzol® reagent (Invitrogen; Thermo Fisher Scientific, Inc.). Hi Script TM II Q RT Super Mix (Vazyme Biotech Co., Ltd.) was used for the reverse transcription of total RNA into cDNA. Subsequently, a SYBR Green PCR kit (Vazyme Biotech Co., Ltd.) was used for qPCR. Quantification was undertaken using the 2-ΔΔCq method (20), and the internal references were GAPDH (for mRNA) and U6 (for miRNA). The assays were repeated three times for each sample and the mean value was used. The PCR primer sequences were as follows:

MiR-491-5P forward 5′-GGAGT GGGG AACCCTTCC-3′;
reverse 5′-GTGGGGGAGGGGATTC-3′
U6 forward 5′-GCTTC GGAGCACATACT AAAA T-3′;
reverse 5′-CGCTTCACGAATTT GCGTGTCAT-3′
MMP-9 forward 5′-AGACCTGCGAGGAGATTCCAA3′;
reverse 5′-CGGAGGAGTCGAGT-3′;
GAPDH forward 5′-CTTGGGGGTA GGAAGGACTC-3′;
reverse 5′-GTA GAGAGGAGATGATGTTCT-3′.

Western Blotting Analysis

The cells were pyrolyzed using RIPA pyrolytic buffer solution (Beyotime Institute of Biotechnology, Shanghai, China), and the total protein was extracted. A BCA Protein Assay kit (Beyotime Institute of Biotechnology, Shanghai, China) was used to quantify the total protein. The equivalent amount of protein was treated for 40 min with 12% SDS-PAGE Gel SuperQuick Preparation Kit for electrophoretic separation. The separated protein was transferred to polyvinylidene difluoride membranes (Millipore Corporation) and sealed using 5% skim milk to prevent nonspecific binding. Next, the membranes were incubated with the indicated primary antibodies, including MMP-9 (1:1000, Abcam), and left overnight at 4°C. The primary antibodies were rinsed, and the membrane was incubated with secondary antibodies for 2 h; anti-GAPDH antibody (1:1000, Abcam) was used as the internal reference. After rinsing, the protein bands were assessed using an enhanced chemiluminescence reagent (WBKLS0100, Millipore, USA).

Detection of Oxidative Stress-Related Factors

A superoxide dismutase (SOD) assay kit (Cayman Chemical Company) was used to determine SOD activity, as per the manufacturer's protocol. Malondialdehyde (MDA) activity was measured using an MDA assay kit (Cayman Chemical Company), according to the manufacturer's protocol. ROS levels were analyzed using a specific kit.

Enzyme-Linked Immunosorbent Assay (ELISA)

The concentrations of inflammatory cytokines, including tumor necrosis factor α (TNF-α), interleukin-1β (IL-1β), and IL-6, were detected using ELISA kits (R & D, USA). Specific ELISA kits were used to detect the related markers, according to the manufacturer's protocols.

Statistical Analysis

Statistical analysis was performed using SPSS 26.0, followed by graphical analysis using GraphPad Prism 8.0 software (GraphPad Software Company). The normal distribution test and homogeneity test of variance were undertaken initially, and the normally distributed data were expressed as the mean ± standard deviation (SD). The least significant difference test was used to compare every two groups for homogeneity of variance. One-way analysis of variance was undertaken for multi-group comparisons; non-parametric tests were used in the case of heterogeneity of variance. $P < 0.05$ was interpreted as a statistically significant difference.

RESULTS

Ox-LDL Downregulated miR-491-5P in THP-1 Macrophages

To investigate the effect of ox-LDL on THP-1 macrophages, THP-1 macrophages were treated with ox-LDL at different concentrations (0, 10, 30, 50, and 70 μg/mL) for 24 h. Ox-LDL significantly reduced THP-1 macrophage activity and mir-491-5p expression and upregulated MMP-9 levels in a dose-dependent manner (**Figures 1A–C**). There was no significant difference between the 50 μg/mL and 70 μg/mL ox-LDL treatments; therefore, the 50 μg/mL concentration was selected for subsequent experiments.

Ox-LDL Induced Oxidative Stress and Inflammatory Response of THP-1 Macrophages by Regulating mir-491-5p and MMP-9

Subsequently, the expression levels of MMP9 and miR-491-5p in ox-LDL-induced THP-1 macrophages oxidative stress and inflammatory response were detected. The ox-LDL group had significantly higher ROS and MDA levels and lower SOD activity than the control group (**Figures 2A–C**). ELISA results showed that the ox-LDL group increased the secretory levels of TNF-α, IL-1β, and IL-6 (**Figure 2D**). RT-qPCR/western blotting

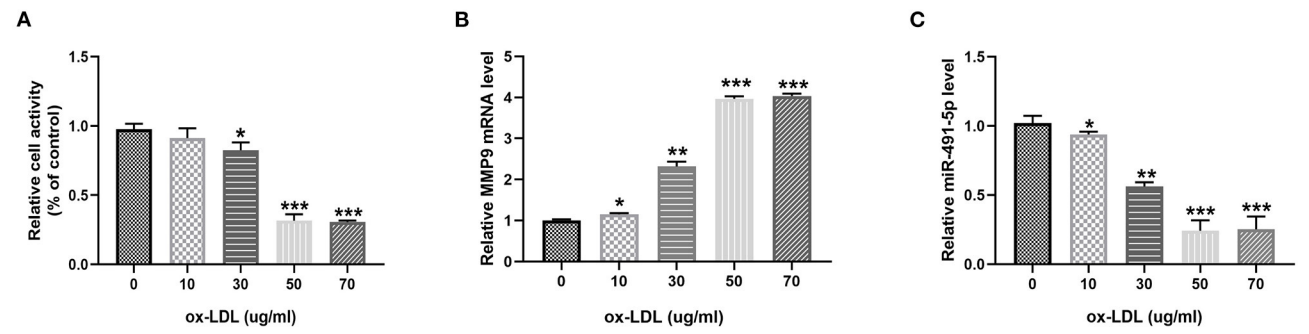

FIGURE 1 | Ox-LDL downregulated miR-491-5P and upregulated MMP-9 in THP-1 macrophages. THP-1 macrophages were induced by different concentrations (0, 10, 30, 50, and 70 μg/mL) of ox-LDL. **(A)** Cell viability was determined using CCK-8. **(B,C)** qRT-PCR analysis measured MMP-9 level and mir-491-5p level in THP-1 macrophages stimulated with different doses of ox-LDL. Data are presented as the mean ± SD, $n = 6$. $^{*}P < 0.05$, $^{**}P < 0.01$, and $^{***}P < 0.001$.

analyses showed that ox-LDL induced downregulation of miR-491-5p expression (**Figure 2E**) and upregulation of MMP-9 protein (**Figure 2F**) and mRNA (**Figure 2G**) expression in THP-1 macrophages. These results indicated that mir-491-5P and MMP-9 might mediate oxidative stress and inflammatory response induced by ox-LDL.

MMP-9 Overexpression and Knockdown Promoted and Inhibited Ox-LDL-Induced Oxidative Stress and Inflammatory Response in THP-1 Macrophages, Respectively

Next, protein and mRNA expression levels of MMP-9 in THP-1 macrophages were upregulated via gene introduction in the MMP-9-plasmid group and downregulated in the MMP9-siRNA group (**Figures 3A–D**). RT-qPCR and western blotting analyses demonstrated the ox-LDL treatment downregulated mir-491-5p (**Figure 3E**) and upregulated MMP-9 protein (**Figure 3F**) and mRNA (**Figure 3G**) expression levels. These changes were intensified by MMP-9-plasmid and suppressed by MMP-9-siRNA (**Figures 3E–G**). The MMP-9-plasmid group had higher ROS (**Figure 3H**) and MDA (**Figure 3I**) release and lower SOD activity (**Figure 3J**) than the ox-LDL group; however, the MMP-9siRNA group had significantly lower ROS and MDA release and higher SOD activity than the ox-LDL group (**Figures 3H–J**). In addition, the ox-LDL treatment markedly increased the secretory levels of TNF-α, IL-1β, and IL-6 (**Figure 3K**); however, these changes were aggravated by MMP-9-plasmid and inhibited by MMP9-siRNA. These results hinted that MMP-9 mediated ox-LDL-induced oxidative stress and inflammatory response in THP-1 macrophages.

MMP-9 Overexpression Promoted Ox-LDL-Induced THP-1 Macrophage Foaming

Meanwhile, to further investigate the effect of MMP-9 on ox-LDL-induced cell foaming, we evaluated the intracellular lipid accumulation of both MMP-9 overexpression or knockdown in THP-1 macrophages by oil red staining and fluorescence microscopy. The results showed that cytoplasmic lipid drops staining and quantitative analysis were significantly increased in the ox-LDL group, indicating THP-1 macrophage foaming (**Figures 4A,B**). The MMP-9-plasmid group had significantly aggravated THP-1 macrophage foaming (**Figure 4A**) and lipid uptake (**Figure 4B**) compared to the ox-LDL group, whereas MMP-9-siRNA significantly reduced ox-LDL-induced macrophage foaming and lipid uptake (**Figures 4A,B**). These data identified that MMP-9 not only worsened ox-LDL-induced THP-1 macrophage oxidative stress and inflammatory response but also caused cell foaming.

MiR-491-5p Inhibited Ox-LDL-Induced THP-1 Macrophages Inflammation and Oxidative Stress by Downregulating MMP-9 Expression

To further demonstrate whether the effects of mir-491-5p on inflammatory cytokines and oxidative stress induced by ox-LDL by regulating MMP-9 in THP-1 macrophage cells, experiments were carried out through the transduction of mir-491-5p mimic or mir-491-5p mimic+MMP-9 plasmid into THP-1 macrophage cells before treatment with 50 μg/mL ox-LDL. After transduction of miR-491-5p into macrophages in the miR-491-5p mimic group, miR-491-5p expression was upregulated (**Figure 5A**), and mRNA (**Figure 5B**) and protein (**Figure 5C**) expression levels of MMP-9 in THP-1 macrophages were significantly downregulated. These changes were reversed after co-transfection with the MMP9-plasmid in the miR-491-5p mimic+ MMP-9-plasmid group (**Figures 5B,C**). To investigate the role of mir-491-5P in ox-LDL-mediated damage, THP-1 macrophages transduced with mir-491-5p mimic or mimic-NC were stimulated with 50 μg/mL ox-LDL. CCK-8 analysis showed that high mir-491-5p expression increased the viability of THP-1 macrophages compared to the ox-LDL treatment alone (**Figure 5D**). MMP-9 mRNA (**Figure 5E**), protein (**Figure 5F**), ROS, MDA (**Figures 5G,H**), IL-6, IL-1β, and TNF-α (**Figure 5J**) expression levels were downregulated,

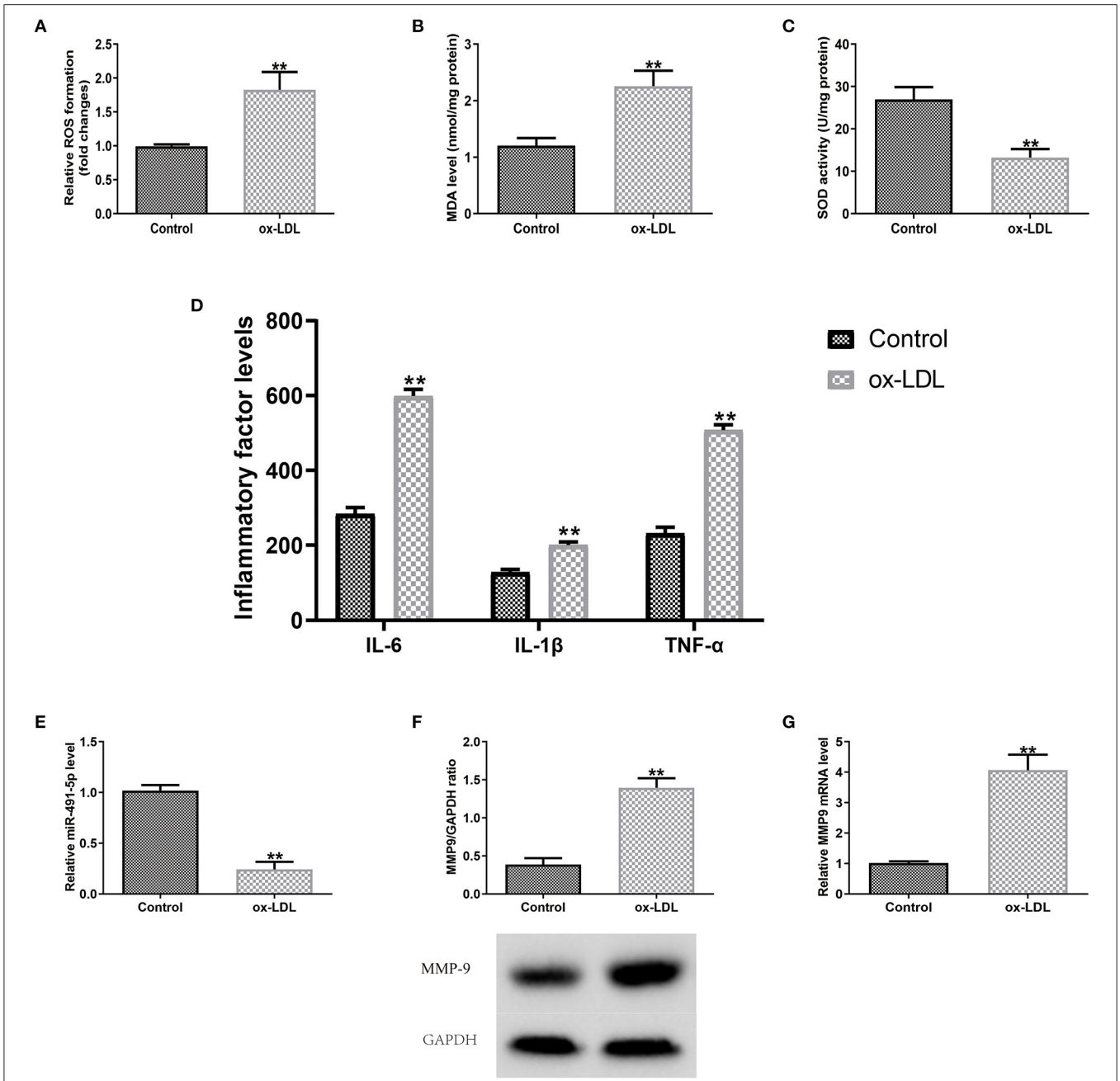

FIGURE 2 | Outcomes of ox-LDL on macrophage expression levels (miR-491-5P and MMP-9), oxidative stress and inflammatory factors. **(A–C)** ROS and MDA levels and SOD activity were measured using commercial kits. **(D)** Levels of inflammatory factors (TNF-α, IL-1β, and IL-6) were detected via ELISA. **(E–G)** MiR-491-5P, MMP-9 protein, and mRNA levels were measured with qRT-PCR, respectively. Data are presented as the mean ± SD, $n = 6$. Compared with the control group, $^{**}P < 0.01$.

and SOD activity was improved (**Figure 5I**) in the miR-491-5P mimic group compared to the ox-LDL group. In contrast, these observational indicators were reversed in the miR-491-5P mimic+MMP-9-plasmid group (**Figures 5E–J**). These results suggested that mir-491-5p inhibited ox-LDL-induced oxidative stress and inflammatory cytokines in THP-1 macrophages by inhibiting MMP-9 expression.

Mir-491-5p Attenuated Ox-LDL-Induced THP-1 Macrophages Foaming

Similarly, we observed the effect of mir-491-5p on ox-LDL-induced THP-1 macrophage foaming by oil red staining and fluorescence microscopy. Oil Red O and BODIPY 493/503 staining showed that ox-LDL induced the THP-1 macrophage foaming and increased content lipid droplets contentment

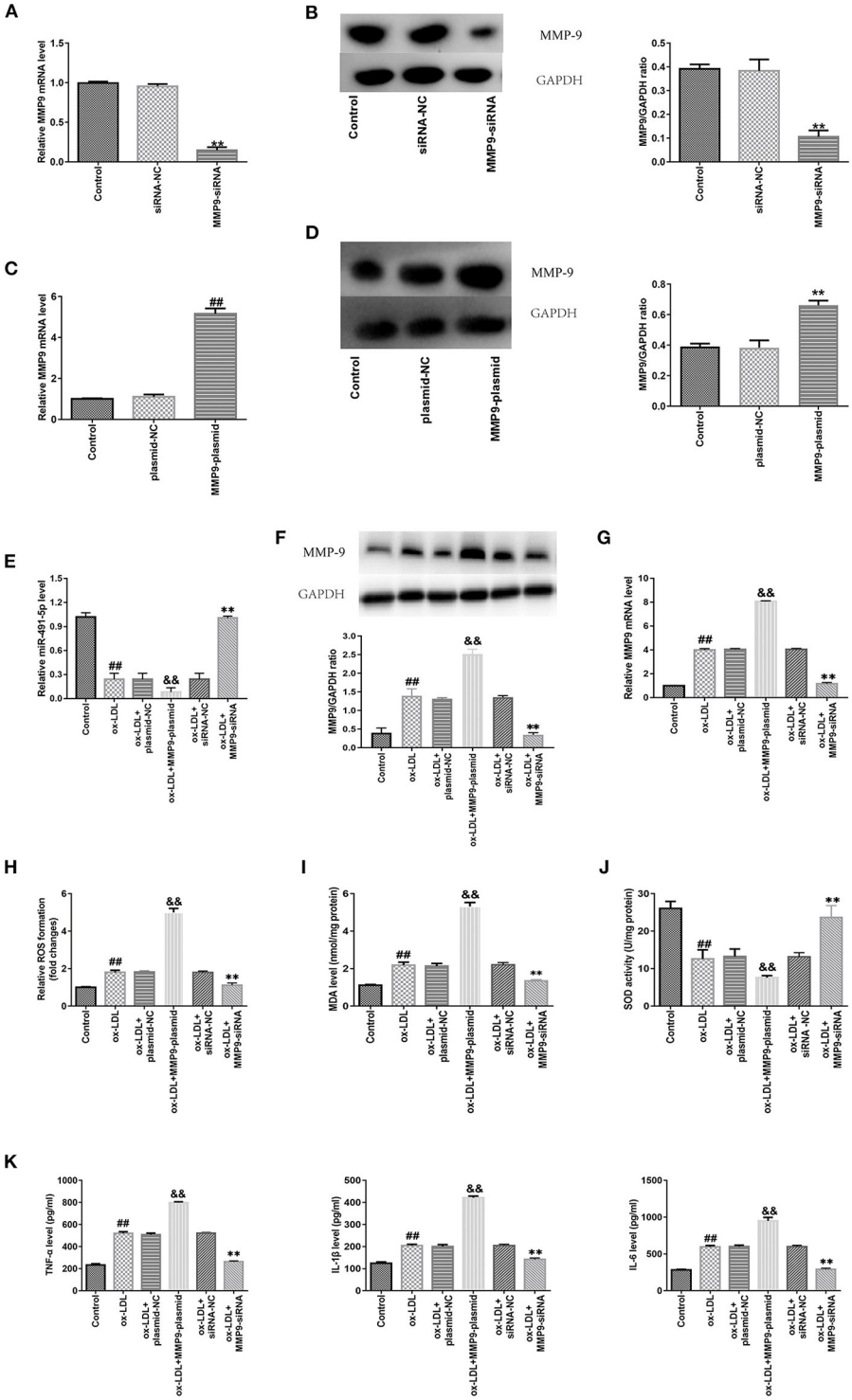

FIGURE 3 | Effect of MMP-9 on the oxidative stress and inflammatory reactions in ox-LDL-induced THP-1 macrophages. **(A–D)** THP-1 macrophages were introduced with MMP-9-siRNA and MMP-9-plasmid. Transfection efficiency of MMP-9-plasmids and MMP-9-siRNA were measured with qRT-PCR, whereas MMP-9 protein was measured with western blotting. **(E–K)** Transfected THP-1 macrophages were stimulated with 50 μg/mL ox-LDL. **(E)** MiR-491-5P expression of transfected THP-1 macrophages was determined with qRT-PCR. **(F,G)** MMP-9 protein and mRNA expression of transfected THP-1 macrophages was determined by western blotting and qRT-PCR, respectively. **(H–J)** ROS and MDA levels and SOD activity were measured using commercial kits. **(K)** Levels of inflammatory factors (TNF-α, IL-1β, and IL-6) were detected using ELISA. Data are presented as the mean ± SD, $n = 6$. Compared with the control group, $^{\#\#}P < 0.01$; compared with the plasmid-NC group, $^{\&\&}P < 0.01$; compared with the si-RNA-NC group, $^{**}P < 0.01$.

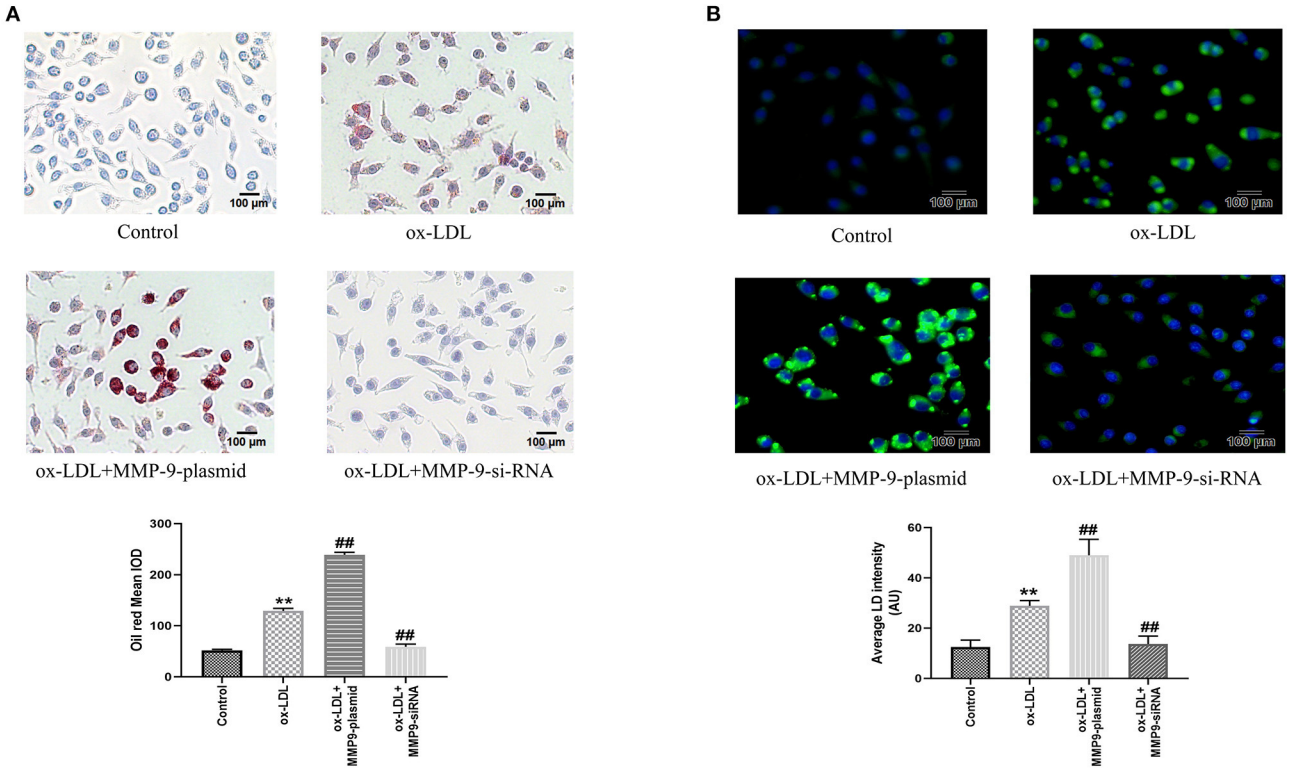

FIGURE 4 | Oil Red O and BODIPY 493/503 staining after MMP-9-plasmid and MMP-9-siRNA transfections. **(A)** THP-1 macrophage cells were transfected before incubation with ox-LDL for 24 h and stained with Oil Red O (× 200, 100 μm), the intracellular lipid droplets of the mean optical density value (mean IOD) were used to reflect the degree of cellular foam. **(B)** Lipid droplets were labeled with green fluorescence and the nuclei were labeled with DAPI (blue) (× 200, 200 μm), average LD intensity was used to quantify lipid uptake. Data are presented as the mean ± SD, $n = 6$. Compared with the control group, $^{**}P < 0.01$; compared with the ox-LDL group, $^{\#\#}p < 0.01$.

in cells (**Figures 6A,B**). The mir-491-5P mimic group had significantly lower THP-1 macrophage foaming (**Figure 6A**) and lipid uptake (**Figure 6B**) than the ox-LDL group, whereas the mir-491-5P mimic+MMP-9-plasmid significantly reversed these phenomena (**Figures 6A,B**). These results suggested that miR-491-5p inhibited ox-LDL-induced THP-1 macrophage foaming by inhibiting MMP-9 expression.

DISCUSSION

LDL is the primary lipoprotein inducing AS, and ox-LDL cannot be easily recognized and scavenged by the relevant receptors (3). The macrophages differentiated by monocytes can phagocytize ox-LDL to form lipid-laden foam cells, thus becoming a component of plaques (4, 5). Macrophage foaming and increased intracellular lipid content can be used as markers of the severity of arteriosclerosis caused by lipids. Macrophage foaming and lipid accumulation were visual after Oil Red O and BODIPY 493/503 staining, and the intracellular lipid droplets were quantitatively assessed using the mean optical density value (mean IOD) and average LD intensity, respectively. Ox-LDL can stimulate macrophages to release oxygen free radicals and inflammatory factors, resulting in local tissue necrosis and triggering and facilitating the formation of plaques (21). ROS and MDA levels reflect the lipid peroxidation degree, and SOD is an antioxidant factor (2). Upregulated expression of TNF-α, IL-1β, and IL-6 infer aggravation of the inflammatory response (12). Further, ox-LDL can stimulate macrophages to release MMP-9 and elevate MMP-9 expression level in plaques (22, 23). In the present study, after the macrophages were co-incubated with ox-LDL, the MMP-9, ROS, MDA, TNF-α, IL-1β, and IL-6 expression levels were upregulated in the model group. Simultaneously, SOD activity was reduced, and foam cell formation and lipid accumulation were increased, validating the expected effect of ox-LDL on the macrophages, consistent with previous studies (19, 24). In contrast, the miR-491-5P expression level was lowered. Further investigations illustrated that the effects of ox-LDL on macrophages were lessened in the ox-LDL + miR-491-5P mimic group after the miR-491-5P expression level was elevated via gene introduction. This phenomenon was nullified in the ox-LDL + miR-491-5Pmimic+MMP-9plasmid group with high miR-491-5P and MMP-9 expression levels. However, the MMP-9 expression level increased in the MMP-9-plasmid group, and the corresponding oxidative stress and inflammatory responses and the degree of cell foaming were enhanced. Those in the MMP-9-siRNA group with MMP-9 silencing showed the opposite

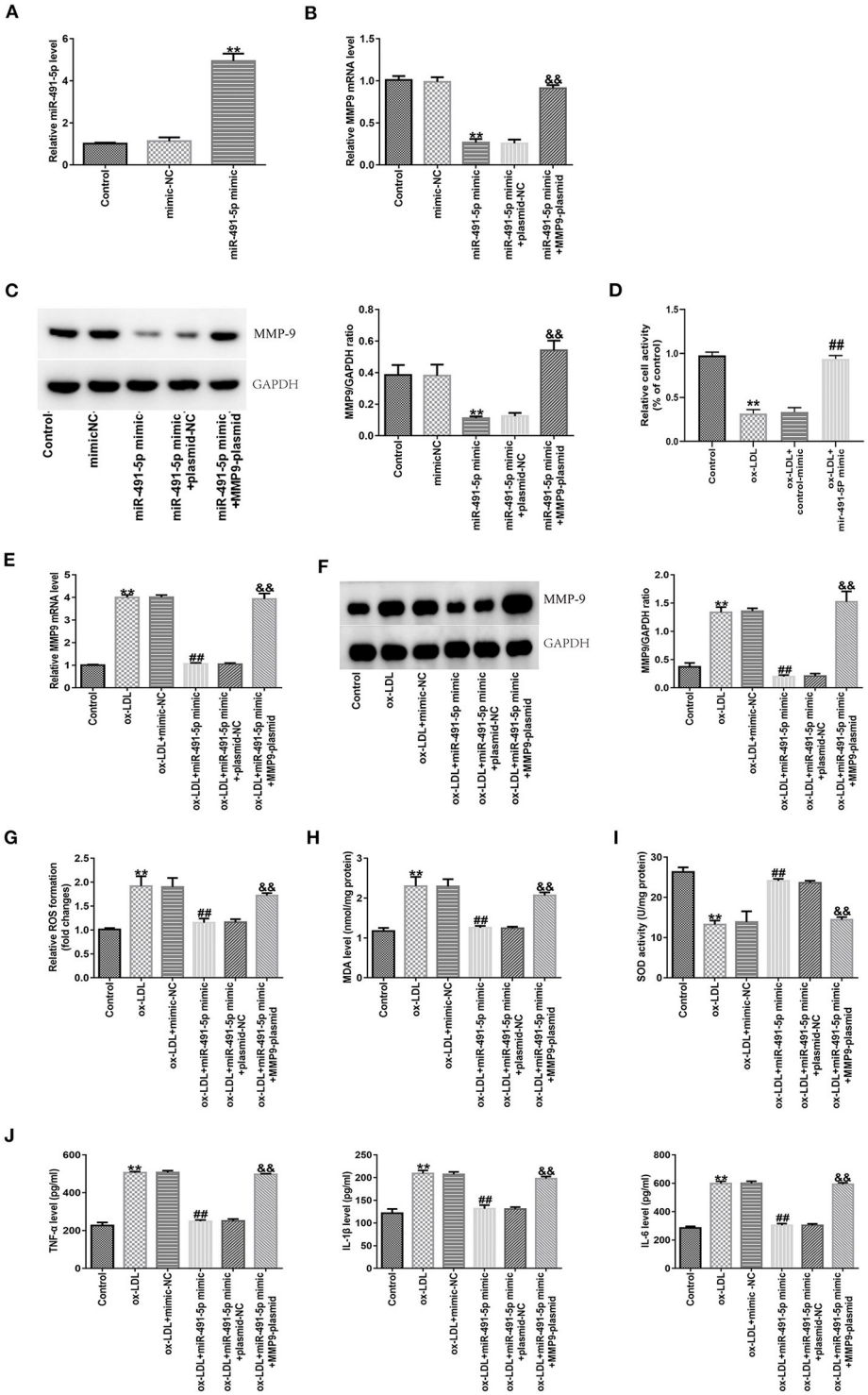

FIGURE 5 | Effect of miR-491-5p and MMP-9 on ox-LDL-induced THP-1 macrophages. **(A)** The transfection efficiency of miR-491-5P mimic was determined using qRT-PCR. **(B,C)** MMP-9 mRNA and protein levels were detected in THP-1 macrophages transduced with miR-491-5P and miR-491-5P mimic+MMP-9-plasmid. **(D–J)** Transfected THP-1 macrophages were stimulated with 50 μg/mL ox-LDL. **(D)** Cell activity after mir-491-5P mimic transfection was assessed using CCK-8. **(E,F)** MMP-9 mRNA and protein were detected in ox-LDL-induced THP-1 macrophages transduced with mir-491-5p mimic and mir-491-5p mimic +MMP-9-plasmid. **(G–I)** ROS and MDA levels and SOD activity were examined using commercial kits. **(J)** Levels of inflammatory factors (TNF-α, IL-1β, and IL-6) were measured with ELISA. Data are presented as the mean ± SD, $n = 6$. Compared with the control group, $^{**}P < 0.01$; compared with the ox-LDL+mimic-NC group, $^{\#\#}p < 0.01$; compared with the ox-LDL + miR-491-5Pmimic+plasmid-NC group, $^{\&\&}P < 0.01$.

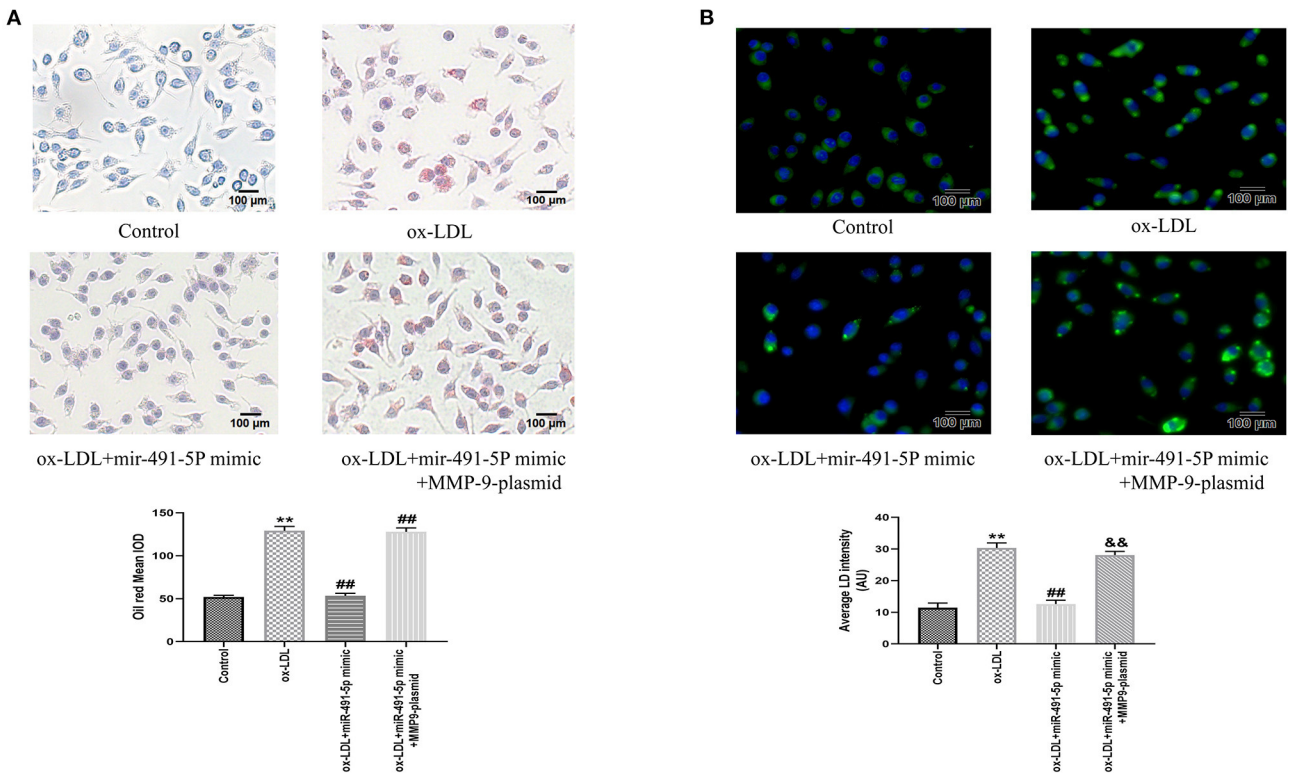

FIGURE 6 | Oil Red O and BODIPY 493/503 staining after mir-491-5P mimic and mir-491-5P mimic +MMP-9-plasmid transfections. **(A)** THP-1 macrophage cells were transfected before incubation with ox-LDL and staining with Oil Red O (× 200, 100 μm), the intracellular lipid droplets of the mean optical density value (mean IOD) were used to reflect the degree of cellular foam. **(B)** Lipid droplets were labeled with green fluorescence and the nuclei were labeled with DAPI (blue) (× 200, 100 μm), average LD intensity was used to quantify the lipid uptake. Data are presented as the mean ± SD, n = 6. Compared with the control group, $^{**}P < 0.01$; compared with the ox-LDL group, $^{\#\#}p < 0.01$; compared with the ox-LDL+mir-491-5pmimic group, $\&\&p < 0.01$.

trend, indicating that ox-LDL might aggravate the oxidative stress and inflammatory responses of THP-1 macrophages via the repression of the miR-491-5P/MMP-9 axis.

Recently, extensive research attention has focused on the biological functions of miRNA. MiR-491-5P, a type of miRNA, can regulate the expression of the MMP-9 gene by binding to the 3′UTR non-coding site of MMP-9 (25, 26). Recent *in vitro* studies have shown that miR-491-5P can inhibit the growth and migration of vascular smooth muscle cells through the targeted inhibition of MMP-9 expression (17). Furthermore, clinical studies have indicated that the binding site for miR-491-5P and MMP-9 undergoes mutation due to the gene polymorphism of MMP-9; therefore, miR-491-5P fails to bind to MMP-9, the *in vivo* MMP-9 expression level of the patient is increased, and the risk of atherosclerotic cerebral infarction is amplified (18). According to the present study, miR-491-5P repressed the ox-LDL-induced oxidative stress and inflammatory responses of THP-1 macrophages through the targeted inhibition of MMP-9, and cell foaming and lipid uptake were significantly decreased, further demonstrating the role of the miR-491-5P/MMP-9 pathway in AS attack.

However, the upstream promoter of miR-491-5P must be further clarified. Transcription factors, epigenetic modification, and the conversion of pri-miR to miRNA might play essential roles in regulating miRNA expression. Previous tumor cell studies found that the Foxi1 protein, belonging to the forkhead gene family, is a potential upstream regulator of miR-491-5p, and can bind to miR-491-5p binding sites to regulate the expression of miR-491-5p (27). Another study found that circ0001361, a circular RNA member, can specifically inhibit miR-491-5P (28) and upregulate MMP-9 to promote cell proliferation and migration. Although the existing literature indicates that the Foxi1 protein and circ0001361 are upstream of miR-491-5p, it is unclear whether the Foxi1 protein or CIRC0001361 play a role in mediating the ox-LDL-induced oxidative stress and inflammatory responses of THP-1 macrophages. If so, it remains unclear what their upstream factors are. The pathway between ox-LDL and miR-491-5p appears to be complex and requires further exploration in future studies.

As a proteolytic enzyme, MMP-9 degrades the fibers in plaque ECM. The plaques become soft, fiber caps become thin, and the plaques become unstable, increasing the probability of clinical cardiovascular events (7). Another study has shown that MMP-9 exerts a "positive feedback" regulatory effect on inflammatory factors, and its high expression can aggravate the inflammatory response (9). IL-1β and IL-8 are essential

inflammatory cytokines; MMP-9 facilitates the transformation of the inactive precursor IL-1β into active IL-1β by activating the IL-1β invertase (10) and pyrolyzes IL-8 to enhance its chemotactic activity and further aggravate the inflammatory response (11). In inflammatory diseases, MMP-9 gene silencing can also restrict ROS accumulation (29), obstruct MMP-9 activation, repress the redox reaction, and relieve neuroinflammation (30). The present study showed that high MMP-9 expression further enhanced the oxidative stress and inflammatory responses to ox-LDL. MMP-9 silencing led to the opposite outcome, further verifying the oxidative stress-promoting and pro-inflammatory effects of MMP-9. Moreover, the gene introduction downregulated the miR-491-5P expression level under high MMP-9 expression. In the MMP-9 gene silencing condition, the miR-491-5P level was upregulated, suggesting that MMP-9 might exert negative feedback on miR-491-5P. Nevertheless, the mechanism remains unclear.

Several limitations need to be considered in the present study. The *in vitro* experiment confirmed that miR-491-5P/MMP-9 mediated a possible induction mechanism of ox-LDL in AS. However, as the formation of arterial plaques could not be directly observed, this requires further verification through follow-up *in vivo* and pathophysiological studies of plaque formation. In addition, the specific mechanism underlying MMP-9 regulation by ox-LDL remains unclear.

In summary, ox-LDL was found to aggravate the oxidative stress and inflammatory reactions of THP-1 macrophages by downregulating the miR-491-5P expression level and reducing the inhibiting effect of miR-491-5P on MMP-9.

DATA AVAILABILITY STATEMENT

The original contributions presented in the study are included in the article/supplementary material, further inquiries can be directed to the corresponding author.

AUTHOR CONTRIBUTIONS

YL contributed to the conception of the study, contributed significantly to analysis and manuscript preparation, and performed the data analyses and wrote the manuscript. YL and EZ were responsible for the experiment. EZ helped perform the analysis with constructive discussions. WZ was responsible for the review and revision of the paper and supported the financial acquisition for the project leading to this publication. All authors contributed to the article and approved the submitted version.

REFERENCES

1. Tabas I, Lichtman AH. Monocyte-macrophages and T cells in atherosclerosis. *Immunity.* (2017) 47:621–34. doi: 10.1016/j.immuni.2017.09.008
2. Zhang Q, Ai Y, Dong H, Wang J, Xu L. Circulating oxidized low-density lipoprotein is a strong risk factor for the early stage of coronary heart disease. *IUBMB Life.* (2019) 71:277–82. doi: 10.1002/iub.1966
3. Tsimikas S, Witztum JL. Measuring circulating oxidized low-density lipoprotein to evaluate coronary risk. *Circulation.* (2001) 103:1930–2. doi: 10.1161/01.CIR.103.15.1930
4. Gui T, Shimokado A, Sun Y, Akasaka T, Muragaki Y. Diverse roles of macrophages in atherosclerosis: from inflammatory biology to biomarker discovery. *Mediators Inflamm.* (2012) 2012:693083. doi: 10.1155/2012/693083
5. Kockx MM, De Meyer GR, Bortier H, de Meyere N, Muhring J, Bakker A, et al. Luminal foam cell accumulation is associated with smooth muscle cell death in the intimal thickening of human saphenous vein grafts. *Circulation.* (1996) 94:1255–62. doi: 10.1161/01.CIR.94.6.1255
6. Ding S, Zhang M, Zhao Y, Chen W, Yao G, Zhang C, et al. The role of carotid plaque vulnerability and inflammation in the pathogenesis of acute ischemic stroke. *Am J Med Sci.* (2008) 336:27–31. doi: 10.1097/MAJ.0b013e3181 5b60a1
7. Brown BA, Williams H, George SJ. Evidence for the involvement of matrix-degrading metalloproteinases (MMPs) in atherosclerosis. *Prog Mol Biol Transl Sci.* (2017) 147:197–237. doi: 10.1016/bs.pmbts.2017.01.004
8. Seifert R, Kuhlmann MT, Eligehausen S, Kiefer F, Hermann S, Schäfers M. Molecular imaging of MMP activity discriminates unstable from stable plaque phenotypes in shear-stress induced murine atherosclerosis. *PLoS ONE.* (2018) 13:e0204305. doi: 10.1371/journal.pone.0204305
9. Opdenakker G, Van den Steen PE, Dubois B, Nelissen I, Van Coillie E, Masure S, et al. Gelatinase B functions as regulator and effector in leukocyte biology. *J Leukoc Biol.* (2001) 69:851–9. doi: 10.1189/jlb.69.6.851
10. Schönbeck U, Mach F, Libby P. Generation of biologically active IL-1 beta by matrix metalloproteinases: a novel caspase-1-independent pathway of IL-1 beta processing. *J Immunol.* (1998) 161:3340–6.
11. Van den Steen PE, Proost P, Wuyts A, Van Damme J, Opdenakker G. Neutrophil gelatinase B potentiates interleukin-8 tenfold by aminoterminal processing, whereas it degrades CTAP-III, PF-4, and GRO-alpha and leaves RANTES and MCP-2 intact. *Blood.* (2000) 96:2673–81. doi: 10.1182/blood.V96.8.2673
12. Zhu Y, Xian X, Wang Z, Bi Y, Chen Q, Han X, et al. Research progress on the relationship between atherosclerosis and inflammation. *Biomolecules.* (2018) 8:80. doi: 10.3390/biom8030080
13. Sigala F, Kotsinas A, Savari P, Filis K, Markantonis S, Iliodromitis EK, et al. Oxidized LDL in human carotid plaques is related to symptomatic carotid disease and lesion instability. *J Vasc Surg.* (2010) 52:704–13. doi: 10.1016/j.jvs.2010.03.047
14. Ro S, Park C, Young D, Sanders KM, Yan W. Tissue-dependent paired expression of miRNAs. *Nucleic Acids Res.* (2007) 35:5944–53. doi: 10.1093/nar/gkm641
15. Mallory AC, Vaucheret H. MicroRNAs: something important between the genes. *Curr Opin Plant Biol.* (2004) 7:120–5. doi: 10.1016/j.pbi.2004.01.006
16. Shirjang S, Mansoori B, Asghari S, Duijf PHG, Mohammadi A, Gjerstorff M, et al. MicroRNAs in cancer cell death pathways: Apoptosis and necroptosis. Free Radic Biol Med. (2019) 139:1–15. doi: 10.1016/j.freeradbiomed.2019.05.017
17. He Z, Wang Y, He Q, Chen M. microRNA-491-5p protects against atherosclerosis by targeting matrix metallopeptidase-9. *Open Med (Wars).* (2020) 15:492–500. doi: 10.1515/med-2020-0047
18. Yuan M, Zhan Q, Duan X, Song B, Zeng S, Chen X, et al. functional polymorphism at miR-491-5p binding site in the 3'-UTR of MMP-9 gene confers increased risk for atherosclerotic cerebral infarction in a Chinese population. *Atherosclerosis.* (2013) 226:447–52. doi: 10.1016/j.atherosclerosis.2012.11.026
19. Ye J, Wang C, Wang D, Yuan H. LncRBA GSA5, up-regulated by ox-LDL, aggravates inflammatory response and MMP expression in THP-1 macrophages by acting like a sponge for miR-221. *Exp Cell Res.* (2018) 369:348–55. doi: 10.1016/j.yexcr.2018.05.039
20. Livak KJ, Schmittgen TD. Analysis of relative gene expression data using real-time quantitative PCR and the 2(-Delta Delta C(T)) Method. *Methods.* (2001) 25:402–8. doi: 10.1006/meth.2001.1262
21. Zhu Z, Li J, Zhang X. Astragaloside IV protects against oxidized low-density lipoprotein (ox-LDL)-induced endothelial cell injury by reducing oxidative stress and inflammation. *Med Sci Monit.* (2019) 25:2132–40. doi: 10.12659/MSM.912894

22. Raggi P, Genest J, Giles JT, Rayner KJ, Dwivedi G, Beanlands RS, et al. Role of inflammation in the pathogenesis of atherosclerosis and therapeutic interventions. *Atherosclerosis.* (2018) 276:98–108. doi: 10.1016/j.atherosclerosis.2018.07.014
23. Khan R, Spagnoli V, Tardif JC. L'Allier PL. Novel anti-inflammatory therapies for the treatment of atherosclerosis. *Atherosclerosis.* (2015) 240:497–509. doi: 10.1016/j.atherosclerosis.2015.04.783
24. Hua Z, Ma K, Liu S, Yue Y, Cao H, Li Z. LncRNA ZEB1-AS1 facilitates ox-LDL-induced damage of HCtAEC cells and the oxidative stress and inflammatory events of THP-1 cells via miR-942/HMGB1 signaling. *Life Sci.* (2020) 247:117334. doi: 10.1016/j.lfs.2020.117334
25. Varani G. Twenty years of RNA: the discovery of microRNAs. *RNA.* (2015) 21:751–2. doi: 10.1261/rna.050237.115
26. Bu Q, Zhu Y, Chen QY Li H, Pan Y. A polymorphism in the 3'-untranslated region of the matrix metallopeptidase 9 gene is associated with susceptibility to idiopathic calcium nephrolithiasis in the Chinese population. *J Int Med Res.* (2020) 48:300060520980211. doi: 10.1177/03000605209 80211
27. Sun R, Liu Z, Tong D, Yang Y, Guo B, Wang X, et al. miR-491-5p, mediated by Foxi1, functions as a tumor suppressor by targeting Wnt3a/β-catenin signaling in the development of gastric cancer. *Cell Death Dis.* (2017) 8:e2714. doi: 10.1038/cddis.2017.134
28. Liu F, Zhang H, Xie F, Tao D, Xiao X, Huang C, et al. Hsa_circ_0001361 promotes bladder cancer invasion and metastasis through miR-491-5p/MMP9 axis. *Oncogene.* (2020) 39:1696–709. doi: 10.1038/s41388-019-1092-z
29. Zhang H, Wang ZW, Wu HB Li Z, Li LC, Hu XP, et al. Transforming growth factor-β1 induces matrix metalloproteinase-9 expression in rat vascular smooth muscle cells via ROS-dependent ERK-NF-κB pathways. *Mol Cell Biochem.* (2013) 375:11–21. doi: 10.1007/s11010-012-1512-7
30. Walter L, Canup B, Pujada A, Bui TA, Arbasi B, Laroui H, et al. Matrix metalloproteinase 9 (MMP9) limits reactive oxygen species (ROS) accumulation and DNA damage in colitis-associated cancer. *Cell Death Dis.* (2020) 11:767. doi: 10.1038/s41419-020-02959-z

Conflict of Interest: The authors declare that the research was conducted in the absence of any commercial or financial relationships that could be construed as a potential conflict of interest.

Publisher's Note: All claims expressed in this article are solely those of the authors and do not necessarily represent those of their affiliated organizations, or those of the publisher, the editors and the reviewers. Any product that may be evaluated in this article, or claim that may be made by its manufacturer, is not guaranteed or endorsed by the publisher.

Copyright © 2021 Liao, Zhu and Zhou. This is an open-access article distributed under the terms of the Creative Commons Attribution License (CC BY). The use, distribution or reproduction in other forums is permitted, provided the original author(s) and the copyright owner(s) are credited and that the original publication in this journal is cited, in accordance with accepted academic practice. No use, distribution or reproduction is permitted which does not comply with these terms.

frontiers in Cardiovascular Medicine

ORIGINAL RESEARCH
published: 12 October 2021
doi: 10.3389/fcvm.2021.721814

1-MNA Ameliorates High Fat Diet-Induced Heart Injury by Upregulating Nrf2 Expression and Inhibiting NF-κB *in vivo* and *in vitro*

*Ziguang Song[1], Xiao Zhong[1], Mingyang Li[1], Pingping Gao[1], Zhongping Ning[2], Zhiqi Sun[3] and Xiang Song[1]**

[1] Cardiovascular Center, The Fourth Affiliated Hospital, Harbin Medical University, Harbin, China, [2] Department of Cardiovascular Medicine, Shanghai University of Medicine & Health Sciences Affiliated Zhoupu Hospital, Shanghai, China, [3] Department of Cardiovascular Medicine, DaQing Oilfield General Hospital, Daqing, China

High levels of free fatty acids (FFA) are closely associated with obesity and the development of cardiovascular diseases. Recently, nicotinamide adenine dinucleotide (NAD) metabolism has emerged as a potential target for several modern diseases including diabetes. Herein, we explored the underlying mechanisms of NAD metabolism associated with the risk of cardiovascular disease. Our study found that nicotinamide N-methyltransferase (NNMT) mRNA levels were significantly increased in the hearts of FFA-bound-albumin-overloaded mice and in H9C2 cells treated with palmitic acid (PA). We studied the mechanisms underlining the anti-inflammatory and anti-oxidant activities of 1-methylnicotinamide (1-MNA), a metabolite of NNMT. We found a significantly higher level of reactive oxygen species, inflammation, apoptosis, and cell hypertrophy in PA-treated H9C2 cells and this effect was inhibited by 1-MNA treatment. *in vivo*, 1-MNA improved inflammation, apoptosis, and fibrosis damage in mice and this inhibition was associated with inhibited NF-κB activity. In conclusion, our study revealed that 1-MNA may prevent high fatty diet and PA-induced heart injury by regulating Nrf2 and NF-κB pathways.

Keywords: 1-methylnicotinamide, free fatty acids, inflammation, apoptosis, fibrosis, Nrf2, NFkB

OPEN ACCESS

Edited by:
Jue Zhang,
Versiti Blood Research Institute, United States

Reviewed by:
Minqi Huang,
Marshall University, United States
Nan Huo,
Mayo Clinic, United States

***Correspondence:**
Xiang Song
song761231@sina.com

Specialty section:
This article was submitted to Lipids in Cardiovascular Disease, a section of the journal Frontiers in Cardiovascular Medicine

Received: *07 June 2021*
Accepted: *17 September 2021*
Published: *12 October 2021*

Citation:
Song Z, Zhong X, Li M, Gao P, Ning Z, Sun Z and Song X (2021) 1-MNA Ameliorates High Fat Diet-Induced Heart Injury by Upregulating Nrf2 Expression and Inhibiting NF-κB in vivo and in vitro. Front. Cardiovasc. Med. 8:721814. doi: 10.3389/fcvm.2021.721814

INTRODUCTION

Elevated plasma free fatty acid (FFA) levels have emerged as a major link between obesity, metabolic syndrome and cardiovascular diseases. Circulating free fatty acids (FFA), mainly originating from lipolysis in the adipose tissue, has been recognized as one of the most important factors causing systemic organ damage to the heart, liver, and skeletal muscle. These adverse effects are defined lipotoxicity (1). Elevated plasma FFA levels induce chronic inflammation, cardiovascular disease, and insulin resistance (2, 3).

Increased levels of FFA promote the expression of pro-inflammatory mediators, such as TNF-α, IL-1, and IL-6. These pro-inflammatory factors further induce oxidative stress. FFA activates the NF-κB pathway (4) and may also induce cell apoptosis and damage (5). It has been reported that cellular redox is closely related to high levels of palmitic acid (PA), which generates excessive lipid-derived free radicals. Studies have shown

that a high-fat diet (HFD) results in elevated blood FFA levels and induces inflammation and oxidative stress in various organs including the heart, which subsequently leads to fibrosis, cell apoptosis, and heart injury (6, 7). Anti-inflammatory and antioxidant therapies, therefore, may have important protective and antagonistic effects on injury induced by FFA.

Nicotinamide adenine dinucleotide (NAD) is a coenzyme for redox reactions in eukaryotes and plays an important role in the occurrence and development of cell apoptosis and redox reactions (8). In mammals, key molecules of NAD metabolism regulate various physiological processes (9). For instance, 1-methylnicotinamide (1-MNA) is an effective treatment for refractory hyperproteinuria as it reduces lipid-mediated oxidative stress and cell damage (10). Under Regulation 2015/2283 of the European Parliament and Council, and the European Commission issued Regulation 2018/1123, 1-MNA chloride has been authorized as a dietary supplement.

Experimental treatment of 1-MNA has shown promise in some diseases (11). However, the protective effect of 1-MNA on FFA and HFD-induced heart injury is still unclear. In this study, we explored the anti-inflammatory and anti-oxidant activity of 1-MNA *in vitro* using the cardiomyocyte H9C2 cell line and *in vivo* using a mouse model of hyperlipidemia. Our results showed that 1-MNA mitigated PA and HFD-induced heart cardiac hypertrophy, apoptosis, and myocardial fibrosis. This effect occurred through the activation of Nrf2 and inhibition of the NF-κB pathway.

MATERIALS AND METHODS

Materials

PA and 1-MNA were purchased from Sigma-Aldrich (St. Louis, MO, USA). Stock solutions of 5 mM PA/10% BSA were prepared as follows and the stored at −20°C. Stock solutions were heated at 37°C for 20 min and 1-MNA was dissolved in DMEM and isotonic saline for *in vivo* experiments. Enhanced chemiluminescent reagent kits, Annexin V-FITC apoptosis detection kits, and TUNEL apoptosis detection kits were purchased from Beyotime (Beyotime Biotechnology, Beijing, China). Anti-fluorescence Quenching Mounting Tablets were purchased from SouthernBiotech (0100-01, Birmingham, USA).

Cell Culture and Measurement of Oxidative Stress (ROS)

The H9C2 embryonic mouse heart cell line was obtained from the Shanghai Cell Bank, Chinese Academy of Sciences and was cultured in DMEM/F12 medium (Gibco, Eggenstein, Germany) with 10% FBS, 2.25 g/L glucose, 100 U/mL penicillin, and 100 mg/mL streptomycin. The H9C2 cell was cultured at an ambient temperature of 37°C and 5% CO2 humid environment. The intracellular ROS level was measured using 2,7-dichlorodihydro fluorescein diacetate (DCFH-DA). Cells were pretreated with 1-MNA (10 mM) for 6 h, incubated with PA (500 μM) for 12 h. Then, 2 μmol/L (DCFH-DA) was added to cells at 37°C for 30 min. The fluorescence intensity was measured using a fluorescence microscope, at an excitation wavelength of 488 nm. Cells were collected and sorted by flow cytometry (Beckman Coulter) and Cell Quest software for flow cytometry.

Immunofluorescence Staining

Immunofluorescence was used to measure the cell surface area and apoptosis. To determine apoptosis, the cells were harvested cells and stained with Annexin V and propidium iodide after treatment, and then analyzed by flow cytometry using the sorting flow cytometer and Cell Quest software. For morphology examination and cell surface measurement, the cells were fixed with 4% paraformaldehyde for 20 min in a completely dark environment, washed 3 times with PBS at room temperature. Cells were permeabilized in 0.1% Triton X-100 for 10 min, washed 3 times with PBS at room temperature, and then stained with rhodamine-phalloidin at a concentration of 50 μg/mL for 30 min at room temperature. Specimens were covered with a cover slip and nail polish. The slides were washed 3 times with PBS and subjected to fluorescence microscopy.

In the immunofluorescence study to detect NF-κB, the cells were fixed and permeabilized as indicated above, and the cells were incubated with p65 antibody (1:200) at 4°C overnight, and then incubated with FITC secondary antibody (1:200) at room temperature for 2 h. After each incubation of the antibody, slides were washed 3 times with TBST, 5 min each time. The stained sections were observed under a Nikon fluorescence microscope (Nikon, Japan).

Animal Model

Eight week-old 18–22 g male C57BL/6 mice were purchased from the Animal Center of the Second Affiliated Hospital of Harbin Medical University. Thirty mice ($n = 30$) were housed in cages in a controlled environment of 22 ± 2.0°C and 50 ± 5% humidity and were maintained on 12-h light/12-h dark cycles with free access to water and food. The mice were divided into two groups. Group I mice ($n = 10$) were fed on normal diet as a control group. Group II mice ($n = 10$) were given a HFD (Hyperlipidemia model feed from Beijing Keao, China). Group III mice were given HFD and a daily gavage of 100 mg/kg/day 1-MNA solution. After eitghteen weeks, all animals were euthanized using CO_2 and the heart weights were recorded. Blood samples were collected by cardiac puncture as follows. Animals were fixed on their back and with the index finger of the operator's left hand touching the strongest apex of the heart in the third to fourth intercostal space on the left, the right hand used a syringe with a needle to puncture and collect the sample. Blood was mixed with Hank's solution and centrifuge for 15 min at 4°C to collect serum. Mouse hearts were collected under aseptic conditions and heart weights were measured. The tissues used for RNA analysis were snap-frozen and stored at −80°C. The tissues used for histology study were fixed in 10% formalin.

Abbreviations: FFA, free fatty acids; NAD, nicotinamide adenine dinucleotide; NNMT, nicotinamide N-methyltransferase; PA, palmitic acid; 1-MNA, 1-methylnicotinamide; HFD, high-fat diet; SIRT1, silent information regulator 1; SAM, S-adenosylmethionine; TG, Triglycerides; TC, Serum total cholesterol; LDL, Low-density lipoprotein.

Western Blotting Analysis

Cultured H9C2 cells or mouse heart tissues were homogenized in RIPA lysis buffer (Beyotime Biotechnology, Beijing, China). Total protein concentrations were determined using a BCA protein concentration kit (Beyotime Biotechnology, Beijing, China). Equal amounts of total protein were analyzed by western blotting. The samples were electrophoresed and electrotransferred to polyvinylidene difluoride membranes (Immobilon; Millipore, Bedford, MA, USA). The membranes were incubated with the indicated primary antibodies and horseradish peroxidase-conjugated anti-rabbit or anti-mouse secondary antibodies (Abcam, Cambridge, UK). The blots were visualized using an enhanced chemiluminescence detection system (Beyotime, Beijing, China). The density of the protein bands was quantified using a gel imaging system (BioRad, Hercules, CA). The following antibodies were used in this study: NRF2 (12721T, CST, Danvers, MA), NQO-1 (sc-376023, Santa Cruz, California, CA),HO-1 (82206S, CST, Danvers, MA), GCLC (ab53179, Abcam, Cambridge, MA), β-actin (3700s, CST, Danvers, MA). BAX (sc-7480, Santa Cruz, California, CA), BCL2 (sc-7382, Santa Cruz, California, CA), Caspase 3 (9662, CST, Danvers, MA), Cleaved Caspase 3 (9664, CST, Danvers, MA), Tgf-β (3711s, CST, Danvers, MA), SMAD3 (9523, CST, Danvers, MA), p-SMAD3 (9520s, CST, Danvers, MA), COL-1 (91144s, CST, Danvers, MA), I kappa B-alpha (sc-1643, Santa Cruz, California, CA), TNF-α (ab183218, Abcam, Cambridge, MA), MMP9 (ab283575, Abcam, Cambridge, MA), and SIRT1 (8469s, CST, Danvers, MA).

RNA Extraction and Quantitative Real-Time PCR (qRT-PCR)

Total RNA was extracted from tissues and cells using the Trizol method. The cDNA was synthesized using a high-capacity cDNA reverse transcription kit. qRT-PCR was performed on the ABI PRISM 7,500 Sequence Detection System. Primers for NNMT, TNF-α, IL-6, IL-1, TGF-β, Nrf2, heme oxygenase-1 (HO-1), glutamate-cysteine ligase (GCLC), and NADPH quinineoxidoreductase-1 (NQO-1), type 1 collagen, connective tissue growth factor (CTGF), matrix metallopeptidase 9 (MMP-9), α-myosin heavy chain (α-MyHC), brain natriuretic peptide (BNP), and β-actin were purchased from Life Technologies. The mouse housekeeping gene β-actin was used as an internal control. Relative mRNA expression levels were normalized to β-actin. The primer sequences are provided in **Supplementary Table 1**.

Histological Analysis

The heart tissues fixed in 10% formalin were dehydrated using gradient alcohol, cleared by xylene, and embedded in paraffin. The sections were cut into slices at a thickness of 7 μm using a Leica RM 2145 microtome (Leica Microsystems, Nussloch, Germany). The paraffin sections were baked in a 60°C oven for 3 h and then de-waxed with xylene 3 times for 20 min in each solution. The tissues were then dehydrated sequentially in absolute ethanol I, absolute ethanol II, 95% ethanol, 90, 80, and 70% alcohol, and finally washed in distilled water for 10 min. Tissues were treated with antigen repair buffer by microwave and washed in PBS (PH 7.4). The first and second antibodies were added successively and incubated at 4°C and 37°C for color development. The nuclear stain DAPI was applied as a counterstain. The slides were air dried and mounted with anti-fluorescence quenching mounting medium, then observed at 400 magnification under fluorescence microscope (Nikon Inc., Japan).

Measurement of Blood Lipid Levels

Blood lipid levels were determined by using total cholesterol assay kit, triglyceride assay kit and low-density lipoprotein cholesterol assay kit (Nanjing Jiancheng Institute of Bioengineering, China). Briefly, samples, as well as blank distill water and calibrator were mixed with working solution in proportion, then incubated at 37°C for 10 min. Samples were analyzed at wavelength 510 nm, light path 0.5 cm using automatic biochemical analyzer (Chemray240, Rayto, China) to measure the concentration of serum triglyceride (TG), total cholesterol (TC), and low-density lipoprotein (LDL).

Masson's Trichrome Stain

Paraffin sections were deparaffinized and hydrated in distilled water. The sections were rinsed gently with deionized water blotting the excess liquid on the slides. Weigert's iron hematoxylin staining was applied for 10 min, followed by 1% hydrochloric acid alcohol differentiation. After cleaning, Ponceau acid fuchsin solution staining was applied for 10 min, phosphomolybdic acid aqueous solution treatment for about 5 min, and aniline blue liquid counterstaining was applied for 5 min. Slides were dehydrated with anhydrous ethanol, mounted with anti-quenching mounting plate solution, and then observed under a microscope.

TUNEL Staining

The cell apoptosis were analyzed uing TUNEL apoptosis detection kits. Paraffin sections are deparaffinized and hydrated in distilled water 100 μl of 20 μg/ml Proteinase K solution were added and incubated at room temperature for 20 min. After washing, 100 μl 1× Equilibration Buffer were added and incubate at room temperature for 15 min. The tissue sections were incubated with Alexa Fluor 647-12-dUTP Labeling Mix in a wet box at 37°C for 60 min. After washing in PBS, the slides were nuclear counterstained with DAPI for 5 min and mounted with anti-fluorescence mounting solution. The slides were examined under a fluorescence microscope.

Statistical Analysis

Data are presented as the mean ± SEM. Comparison of multiple groups was performed using analysis of variance (ANOVA) with *post-test* Bonferroni-corrected *t*-test as *post hoc* test. An unpaired Student's *t*-test was used to compare two unmatched groups. Pearson's correlation coefficients were calculated to investigate the association between indicated parameters. *P*-values < 0.05 were considered statistically significant. For graphing and statistical analysis, we used GraphPad Prism (version 8, GraphPad Software Inc., San Diego, CA).

RESULTS

Elevated NNMT mRNA Levels in PA-Treated H9C2 Cells

NNMT enzyme transfers the methyl group from S-adenosylmethionine (SAM) to nicotinamide resulting in the formation of 1-MNA. To examine the possibility that NNMT is associated with PA-induced heart damage, we first investigated the mRNA expression level of NNMT in cardiomyocyte H9C2 cells. As shown in **Figure 1A**, the mRNA expression of endogenous NNMT increased 2.4-fold ($p < 0.01$) following PA treatment. 1-MNA prevented PA-induced NNMT expression by 27.4% ($p < 0.05$). This result indicated that NNMT was functionally overexpressed in H9C2 cells and in the PA overload model.

1-MNA Prevented ROS Formation and Oxidative Stress in PA-Induced H9C2 Cells

Elevated circulating FFA levels result in cardiovascular complications and oxidative stress. We measured the intracellular ROS level in H9C2 cells treated with PA or PA plus 1-MNA using 2,7-dichloro-dihydro fluorescein diacetate (DCF). As shown in **Figure 1B**, ROS production and ROS-positive DCFH-DA intensity was 241.4% increased in cells with 500 μM PA treatment than in the control group ($p < 0.01$). This increase was markedly reduced by 1-MNA treatment by 65.1% ($p < 0.001$). Next, we used qRT-PCR and western blotting to study the expression of Nrf2 after the removal of ROS by 1-MNA (**Figures 1C,D**). In cells treated with 10 mM 1-MNA, mRNA and protein levels of Nrf2 were increased 347.1% ($p < 0.01$) and 44.8% ($p < 0.05$), respectively. Next, we measured the expression of Nrf2-dependent antioxidant defense genes including HO-1, GCLC, and NQO-1. mRNA (**Figure 1C**) and protein expression (**Figure 1D**) of HO-1 and NQO-1 increased significantly after 1-MNA treatment, which similar to that observed for Nrf2. The up-regulated genes in1-MNA treatment group were1.25–12-fold increase, whereas the protein levels were increased by 0.5–1.3-fold. However, the protein expression of GCLC was almost unchanged after 1-MNA treatment. These results indicated that 1-MNA may act as an antioxidant by upregulating Nrf2 and antioxidant-related genes.

1-MNA Inhibited Apoptosis of PA-Induced H9C2 Cells

We next explored the protective effects of 1-MNA on H9C2 cells damaged by PA. Cell apoptosis were detected by Annexin V-FITC staining (**Figure 2A**). Flow cytometry analysis demonstrated that the apoptosis of PA treated H9C2 cells was significantly ameliorated under 10 mM 1-MNA treatment. The cells treated with PA showed an increase of Annexin V-FITC staining positive cells by 41% (vs. DMSO, $p < 0.01$). 1-MNA treatment reduced PA-induced, the apoptosis rate by 25.7% ($p < 0.001$). In the figure, the cell dots in the quadrant (upper left quadrant) where Annexin V-FITC staining is negative and PI staining is positive (Annexin V-/PI+) is the detection error within the allowable range. In this experiment apoptotic cells and necrotic cells were identified as apoptotic cells. We also examined the key pro-apoptotic protein expression. In response to the PA treatment, the proteins expression of cleaved caspase-3 and BAX/BCL2 were increased by 503.6% ($p < 0.0001$) and 989.1% ($p < 0.01$), respectively. This effects were reduced by 10 mM 1-MNA by 46.2% ($p < 0.001$) and 72.2% ($p < 0.01$; **Figure 2B**).

1-MNA Exerted Anti-inflammatory Effects on H9C2 Cells Induced by PA

Next we evaluated the anti-inflammatory activity of 1-MNA in H9C2 cells. To detect the expression and distribution of NF-κBp65 in H9C2 cells, we performed an immunofluorescence assay. In unstimulated cells, the majority of NF-κB resides in the cytoplasm in association with the IκB family of inhibitory molecules, which mask the nuclear localization signals of NF-κB. By PA treatment, degradation of IκB releases NF-κB to translocate to the nucleus where it binds κB enhancer elements and modulates gene expression and 1-MNA can significantly hinder this process. **Figure 3A** showed NFκB-p65 accumulated in the nucleus in PA-treated cells. We measured the mRNA expression of several inflammatory cytokines which were activated by NF-κB such as TNF-α, IL-1, and IL-6 (**Figure 3B**). PA increased the mRNA levels of TNF-α by 151.2% ($p < 0.01$), IL-1 by 228.6% ($p < 0.01$), and IL-6 1238.1% ($p < 0.01$). However, the activation of NF-κB pathway by PA was significantly inhibited in 1-MNA treated cells. 1-MNA decreased the mRNA expression of TNF-α, IL-1, and IL-6 by 48.4% ($p < 0.05$), 34.5% ($p < 0.05$) and 42% ($p < 0.05$) induced by PA.

1-MNA Attenuated PA-Induced Hypertrophy in H9C2 Cells

Cardiac hypertrophy and fibrosis are the major pathological features of chronic heart disease. We used rhodamine-phalloidin to detect the surface area of H9C2 cell ($n = 100$). As shown in **Figure 4A**, 1-MNA significantly inhibited hypertrophy in PA treated H9C2 cells by 25.1% ($p < 0.0001$). qRT-PCR analysis showed that the mRNA level of TGF-β (**Figure 4B**), a marker gene of myocardial fibrosis, was increased by 648.2% ($p < 0.01$) in the cells treated with PA. 1-MNA treatment resulted in a decrease of TGF-β by 57.5% ($p < 0.05$) induced by PA. We then examined multiple TGF-β signaling pathway related proteins. 1-MNA treatment inhibited PA-induced Col-1 (31.6% $p < 0.05$)and TGF-β (34.5% $p < 0.05$) (**Figure 4C**).

1-MNA Reduced Levels of Some Obesity Indicators in HFD-Fed Mice

The HFD-induced lipotoxicity mouse model used in this study was previously reported by Tanaka et al. (10). Mice fed with HFD or fed with HFD and 100 mg/kg/day 1-MNA for 18 weeks. At the end of the experiment, the mouse body weight, TG, TC, and LDL were measured. **Figure 5A** showed the body weight of mice fed with HFD increased 11% ($p < 0.01$). 1-MNA administration did not significantly reduce HDF caused body weight. This could be due to relatively short period of 18 weeks experiment. Mice fed HFD showed significantly increased TG (90.6% $p < 0.001$), TC (69.2% $p < 0.001$), and LDL (195.1% $p < 0.01$) (**Figures 5B–D**), while mice given 1-MNA demonstrated decreased TG (14.4%

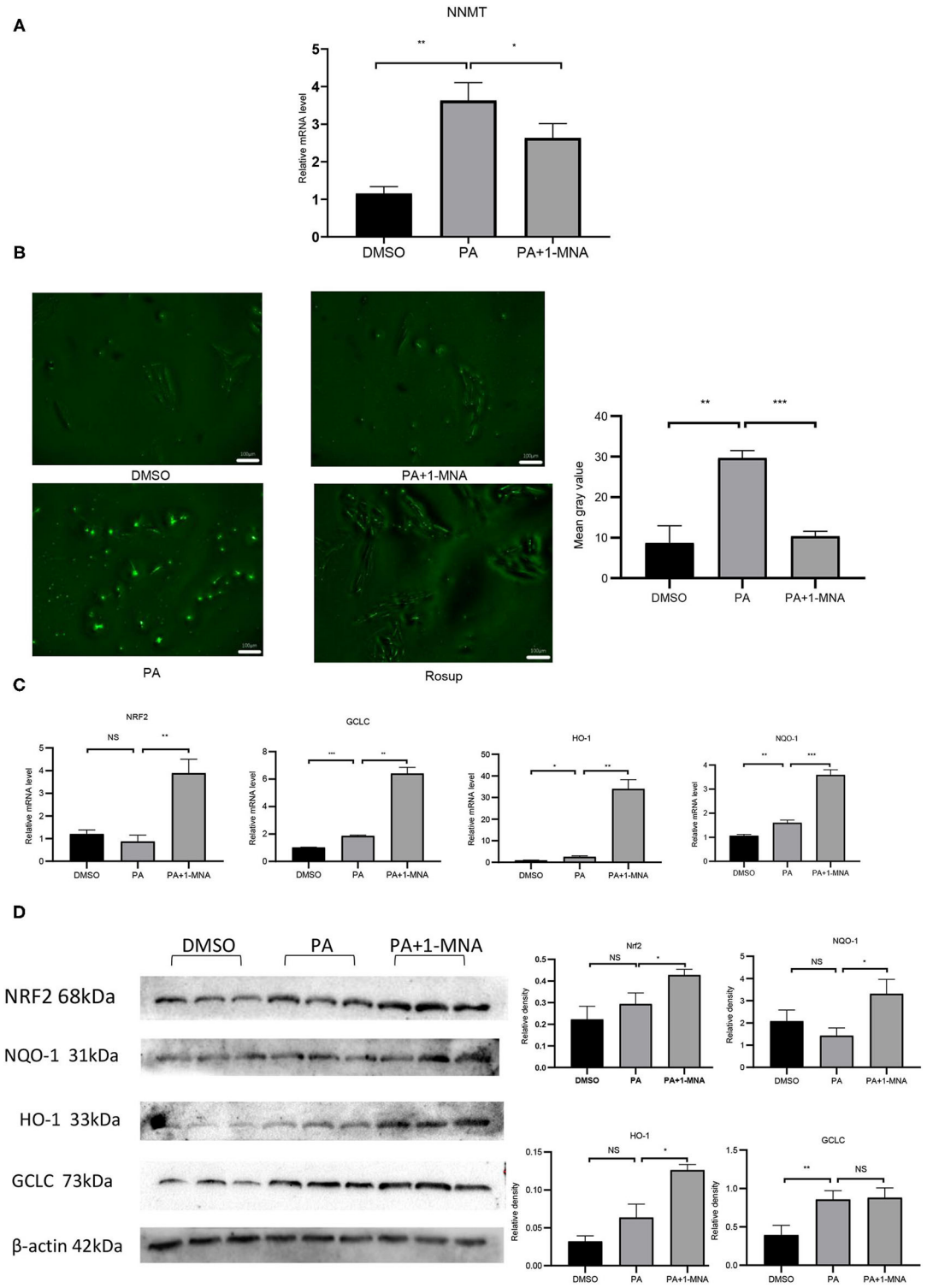

FIGURE 1 | Effects of 1-MNA on PA-induced Oxidative stress in H9C2 cells. **(A)** Real-type quantitative polymerase chain reaction analysis of mRNA expression of NNMT in the H9C2 cells.β-actin was taken as an internal control gene. Expression values are expressed as the mean ± SEM. **(B)** 1-MNA inhibits PA-induced ROS production. Immunofluorescence images of the PA group. The histogram shows the normalized intensity from three independent experiments. **(C)** qRT-PCR analysis of Nrf2, HO-1, GCLC, and NQO-1 expression. **(D)** Western blotting analysis of Nrf2, HO-1, GCLC, and NQO-1. β-actin was taken as an internal control gene. Expression is expressed as the mean ± SEM. Differences in expression were analyzed by the unpaired Student's *t*-test and one-way ANOVA ($n = 3$, NS = no significance, $^{*}P < 0.05$, $^{**}P < 0.01$, $^{***}P < 0.001$).

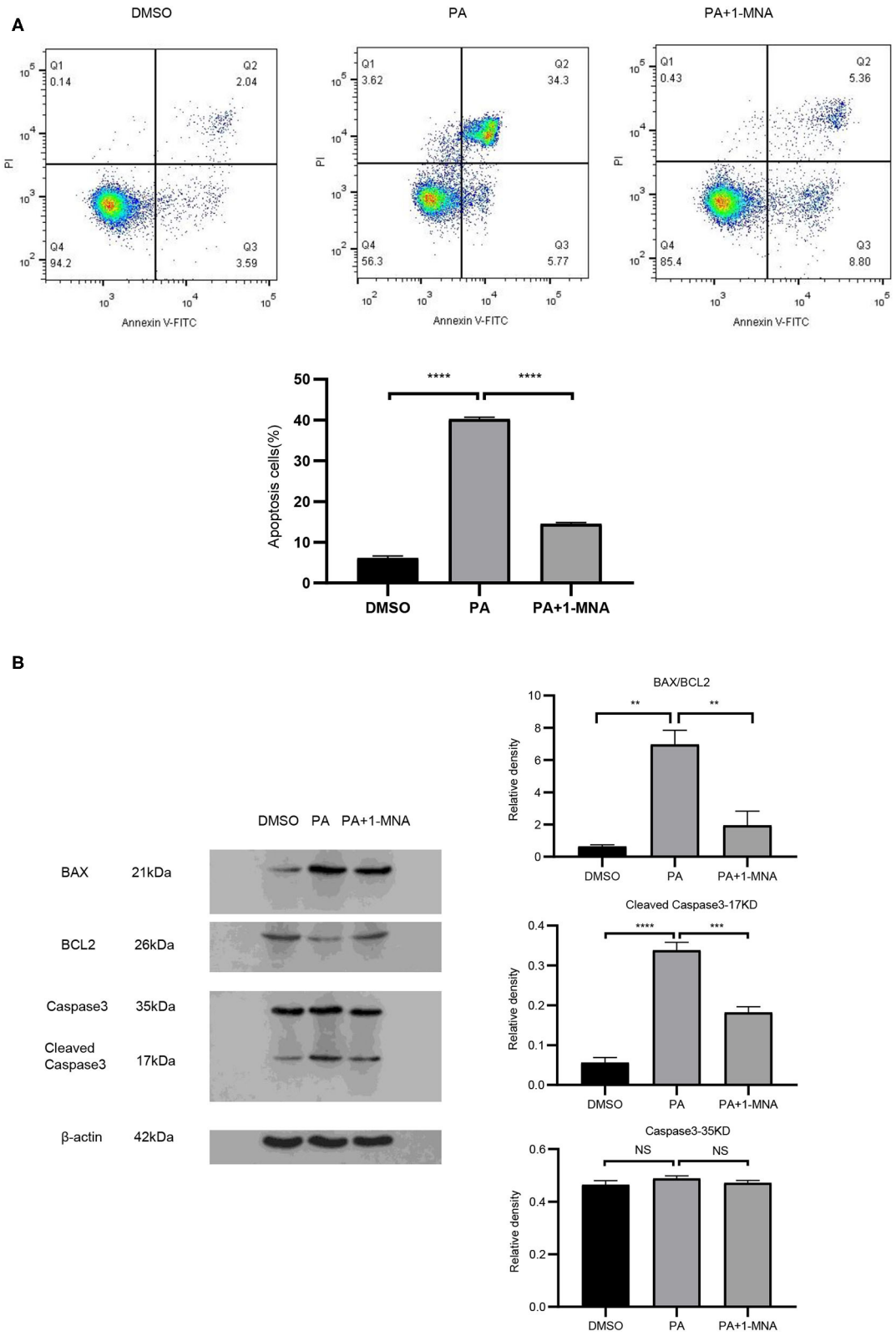

FIGURE 2 | 1-MNA inhibits apoptosis of PA-induced H9C2 cells. **(A)** Cell and nuclear images by flow cytometry analysis. Data are shown as mean ± SEM from three independent experiments. **(B)** Western blotting analysis of Caspase-3, Bax, and Bcl-2. The image of the gel shown is a representative picture. ($n = 3$, NS = no significance, $^{**}P < 0.01$, $^{***}P < 0.001$, $^{****}P < 0.0001$).

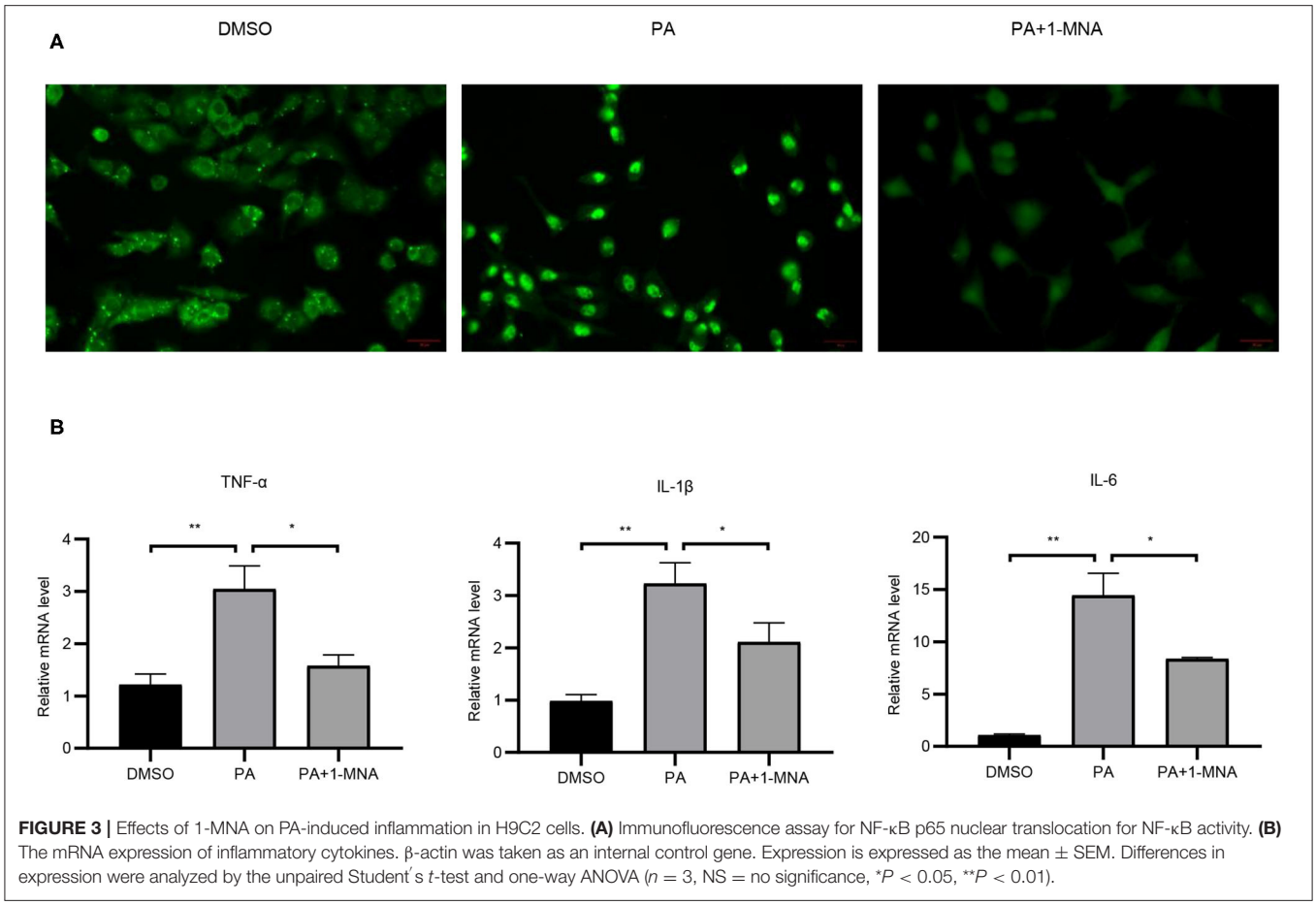

FIGURE 3 | Effects of 1-MNA on PA-induced inflammation in H9C2 cells. **(A)** Immunofluorescence assay for NF-κB p65 nuclear translocation for NF-κB activity. **(B)** The mRNA expression of inflammatory cytokines. β-actin was taken as an internal control gene. Expression is expressed as the mean ± SEM. Differences in expression were analyzed by the unpaired Student's *t*-test and one-way ANOVA ($n = 3$, NS = no significance, $^{*}P < 0.05$, $^{**}P < 0.01$).

$p < 0.05$) and LDL (35.5% $p < 0.05$) compared with HDF mice. TC also decreased but the results did not reach statistical significance (**Figure 5C**).

1-MNA Influenced Oxidative Stress and Inflammation in the HFD-Fed Mouse Heart

The IκB degradation is a key step in NF-κB activation, as it allowed NF-κBp65 to be transported from the cytoplasm to the nucleus. Next, we investigated the expression of IκB at the protein level to determine whether 1-MNA inhibited the activation of NF-κB. As shown in **Figure 6A**, protein levels of IκB-α in heart samples of mice from the HFD-fed group were reduced by 62.8% ($p < 0.05$), while IκB-α protein levels were partially restored in mice treated with 1-MNA which is a 123.6% ($p < 0.05$) increase. mRNA expression of TNF-α, IL-1β, and IL-6 (**Figure 6B**), which are closely related to the activation of NF-κB, increased 2-2.6 fold ($p < 0.05$) in HFD-fed mice as compared to the untreated control. 1-MNA inhibited the expression of inflammatory cytokines induced by HFD by 40–56.2% ($p < 0.05$). TNF-α protein levels were increased by 309.6% ($p < 0.05$) in the HFD group (**Figure 6C**), 1-MNA administration inhibited HFD-induced TNF-α expression by 50.9% ($p < 0.05$). Next, we measured the effects of 1-MNA on oxidative stress in mouse hearts. **Figure 6D** showed the increased expression of Nrf2 in HFD-fed mice heart tissue samples, reflecting a relative increase of 32.6%. 1-MNA treatment increased Nrf2 mRNA expression by 55.2% ($p < 0.05$) in comparison to the HFD group. However, the elevated protein expression was not statistically significant. There was an elevation of 294.1% ($p < 0.05$) in the HFD group and no significant change in expression after 1-MNA treatment (**Figure 6E**). Consistently, the mRNA expression of the downstream antioxidant genes, such as HO-1 and NQO-1 were decreased in HFD group, which were decreased at 60.9% ($p < 0.05$) and 32.7% ($p < 0.01$), respectively. After 1-MNA treatment, the mRNA expression of HO-1 and NQO-1 were increased 84.1% ($p < 0.05$) and 223.3% ($p < 0.01$) (**Figure 6D**). In response to the HFD treatment, the proteins expression of HO-1 and NQO-1 were increased by 180.8% ($p < 0.01$) and 232.6% ($p < 0.05$), respectively, but similarly, no significant changes were reflected in the HFD+1-MNA group (**Figure 6E**).

1-MNA Induced Anti-fibrotic Effects in the Mouse Heart

Next, we assessed the histological changes of mouse cardiac tissue. HFD-fed mice showed myocardial fiber fracture and cell morphological abnormalities. 1-MNA administration alleviated cardiac damage caused by HFD (**Figure 7A**). The tibia length will no longer change after the mouse matures and can be used

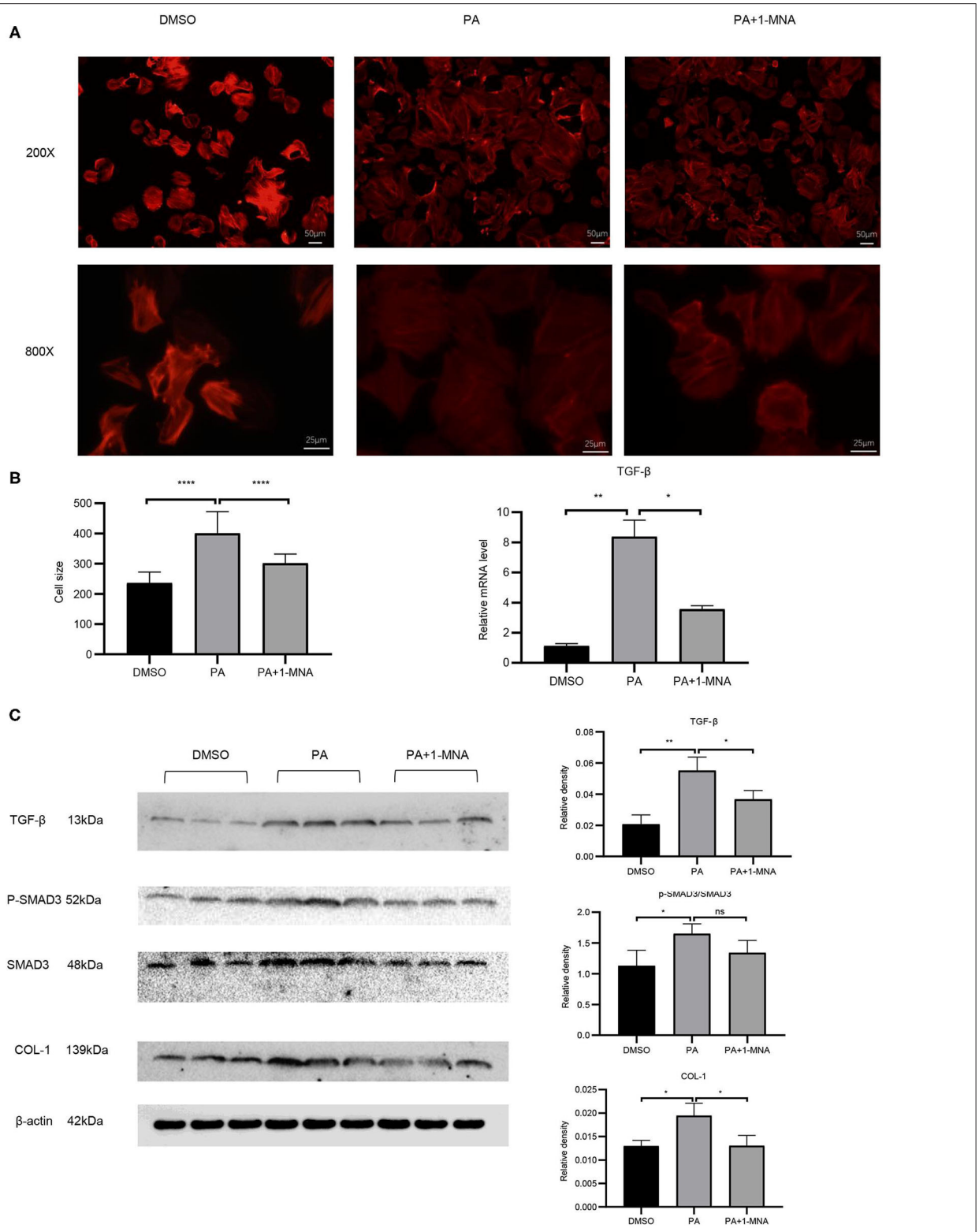

FIGURE 4 | Effects of 1-MNA on PA-induced hypertrophy and fibrosis in H9C2 cells. Representative images of H9C2 cells stained with rhodamine-phalloidin from three independent experiments. **(A)** Representative staining images are shown with the quantitative data for the cell size of 100 randomly selected cells in 3 independent experiments. **(B)** The mRNA expression of TGF-β. **(C)** Western blotting analysis of TGF-β, smad2/3, p-smad2/3, and Col-1. β-actin was taken as an internal control gene. The image of the gel shown is a representative image from three independent experiments and intensity were normalized ($n = 3$, NS = no significance, $^{*}P < 0.05$, $^{**}P < 0.01$, $^{****}P < 0.0001$).

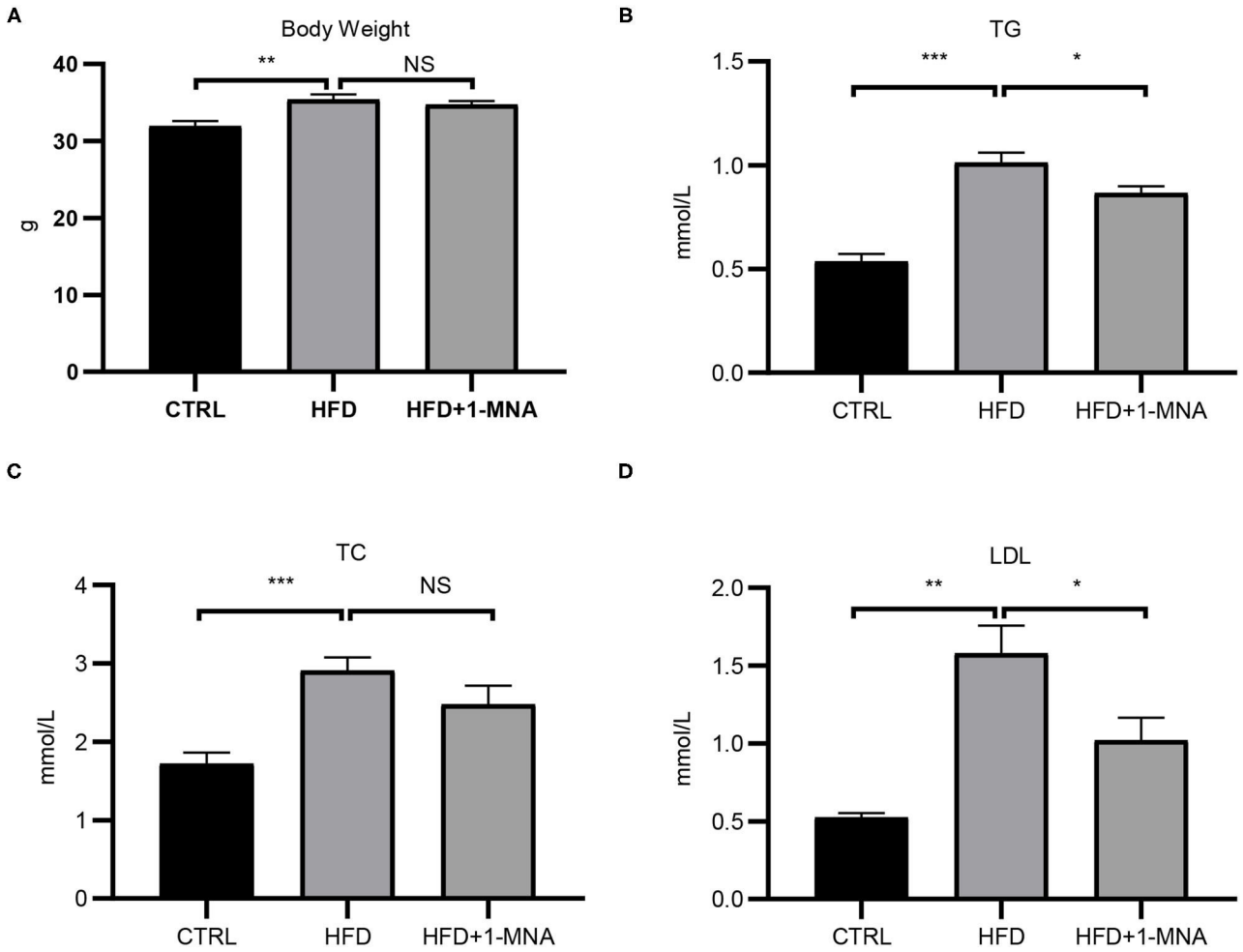

FIGURE 5 | Effects on serum TC, TG, LDL, and body weight following 1-MNA treatment. HFD induces increased **(B)** serum TG and **(D)** LDL, which are inhibited by 1-MNA treatment. **(A)** Body weight and **(C)** TC were different but not statistically significant. ($n = 3$, NS = no significance, $^{*}P < 0.05$, $^{**}P < 0.01$, $^{***}P < 0.001$).

as a quantitative comparison standard. We measured the heart weight/tibia length (HW/TL) ratio. Compared with controls, growth of HW/TL increased by 39.7% ($p < 0.0001$) on week 18 in HFD mice. After 1-MNA treatment, the HW/TL ratio was reversed by 11.7% ($p < 0.001$) (**Figure 7A**). Two cardiac hypertrophy marker genes, BNP and α-myosin heavy chain, were analyzed by real-time PCR. 1-MNA treatment reduced HFD-induced BNP(37.7% $p < 0.05$) and α-myosin heavy chain(30.8% $p < 0.05$) gene expression (**Figure 7B**). These results further indicate that 1-MNA has anti-fibrosis and hypertrophy function in the treatment of heart injury induced by hyperlipidemia. The structure change of the myocardial tissue was further examined by Masson's trichrome staining (**Figure 7C**). The results showed that the myocardial fibers in the HFD group were disordered and dissolved, the intercellular space was widened, and the deposition of collagen fibers increased. Thses morphological alteration was improved after 1-MNA treatment. The collagen volume fraction in the HFD group was significantly higher than the control group, while the 1-MNA treated mice have a lower collagen volume fraction than the HFD group.

qRT-PCR analysis showed an increase of 200.8% ($p < 0.01$) of CTGF and 147.8% ($p < 0.01$) of TGF-β expression in the HFD group (**Figure 8A**). After 1-MNA treatment, the expression of CTGF and TGF-β were downregulated 34.2 and 32.7% ($p < 0.01$) (**Figures 6A,B**), and the deposition of collagen was also ameliorated. We further detected the mRNA expression level of extracellular proteins including collagen 1 and MMP-9 in total RNA from heart tissue (**Figures 8A,B**). These two genes expression were elevated 260.2% ($p < 0.05$) and 185.1% ($p < 0.01$). The genes expression was decreased 35% ($p < 0.05$) and 79.3% ($p < 0.01$) in the HFD+1-MNA group compared to the HFD group. Similar results were observed at the protein level (**Figure 8B**), TGF-β, MMP9 and COL-1 were increased by 63.6–157.1% ($p < 0.05$) in HFD group. 1-MNA administration reduced TGF-β,MMP9 and COL-1 levels by 27.8–60.9% ($p < 0.05$) as compared to the HFD group.

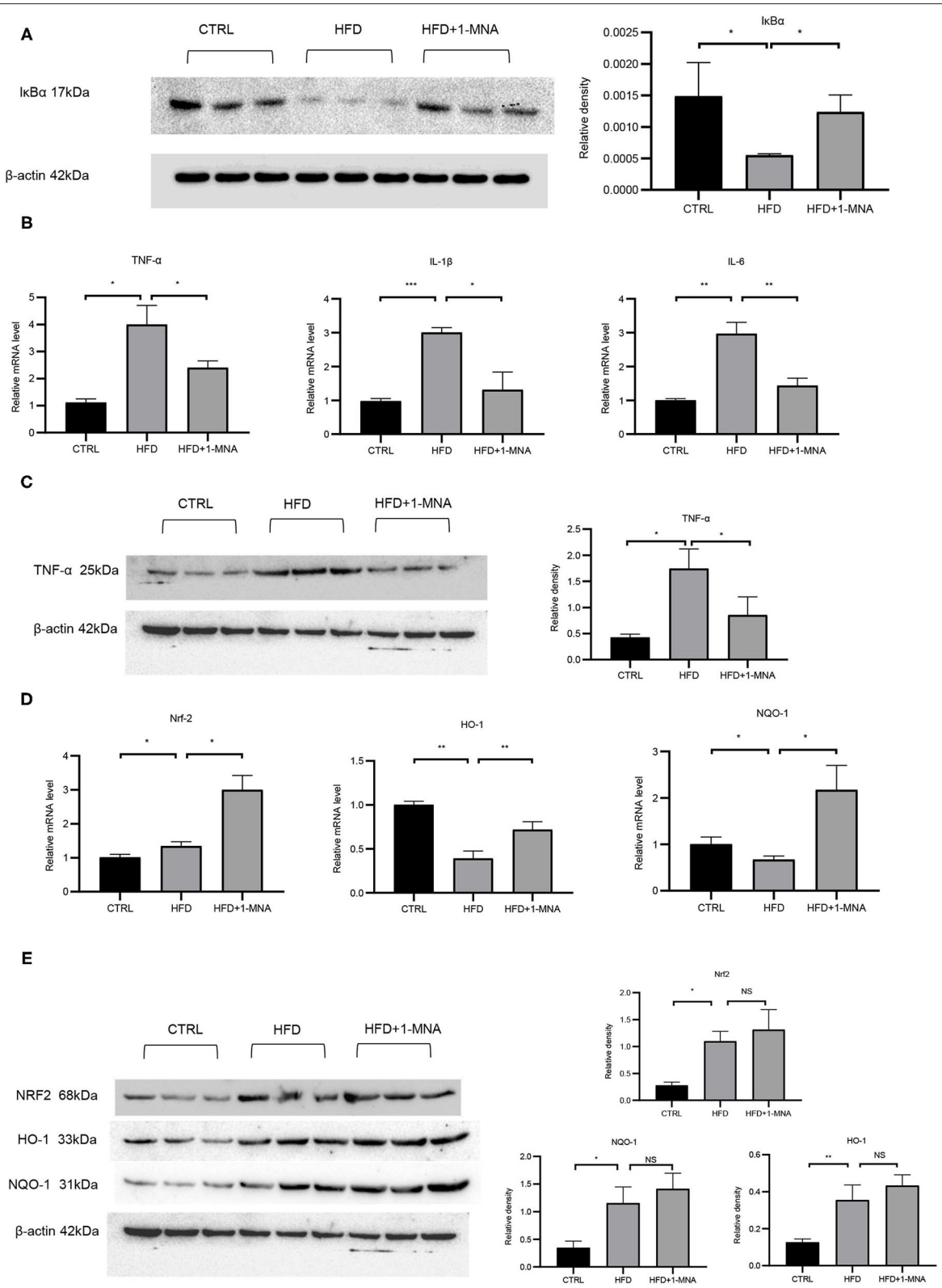

FIGURE 6 | 1-MNA administration improved the oxidative stress and inflammation of the heart induced by HFD. **(A)** Western blotting analysis of IκB expression. Quantification of protein expression shown is normalized to β-actin. **(B)** qRT-PCR analysis of oxidative stress related gene expression. **(C)** Western blotting analysis of TNF-α. β-actin was taken as an internal control gene. **(D)** qRT-PCR analysis of inflammation related gene expression. **(E)** Western blotting analysis of NRF2, HO-1, and NQO-1. β-actin was taken as an internal control gene. ($n = 3$, NS = no significance, $^{*}P < 0.05$, $^{**}P < 0.01$, $^{***}P < 0.001$).

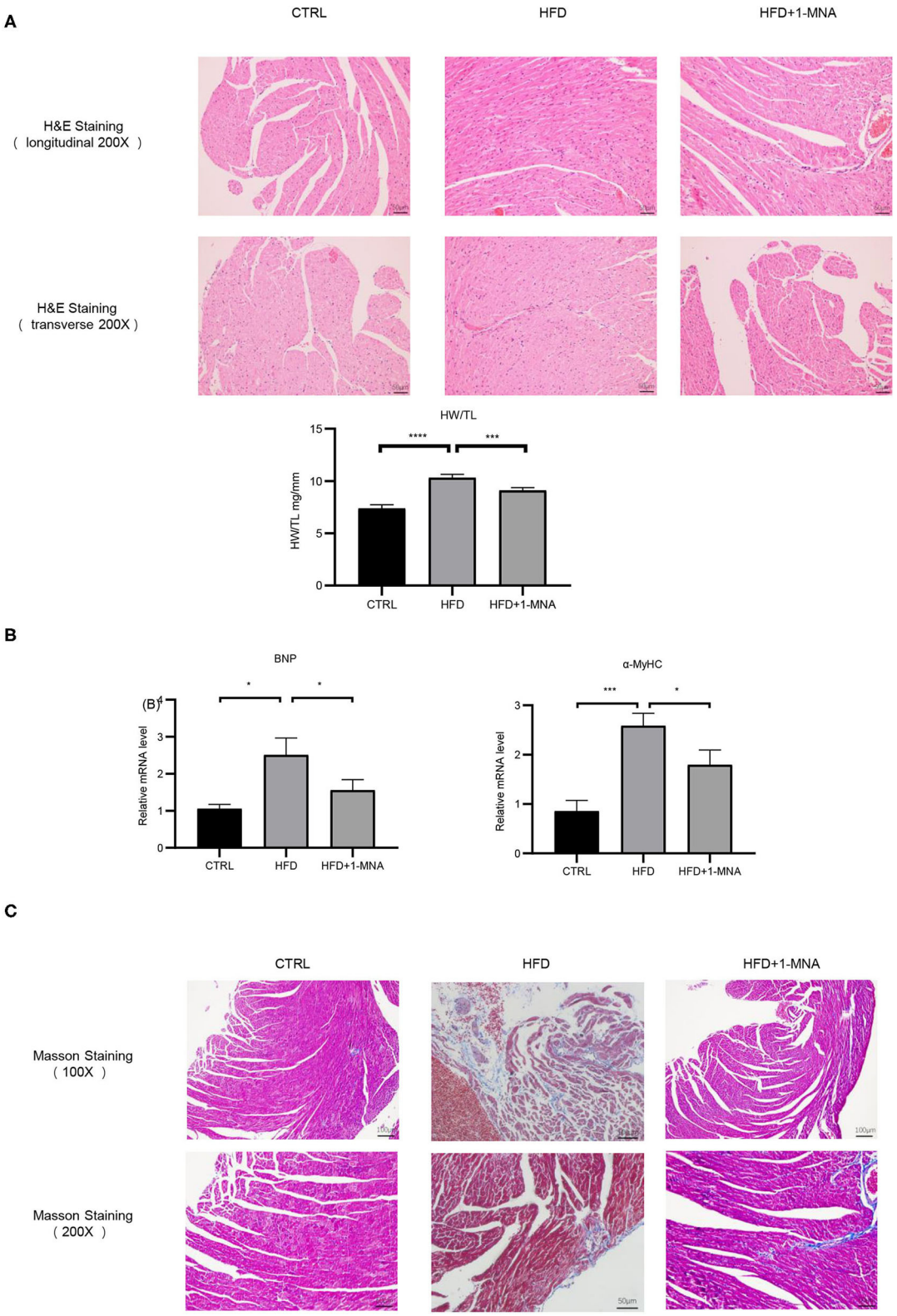

FIGURE 7 | 1-MNA amileorated HFD-induced heart injury. **(A)** Representative images from longitudinal and transverse H&E staining of heart tissues are shown. Data for the ratio of heart weight (HW) to tibia length (TL). **(B)** 1-MNA administration reduced the indicated gene expression in HFD-induced hearts. **(C)** Myocardial tissue was colored in red and collagen was colored in blue by Masson staining. Under light microscopy, the myocardial fibers of the control group were arranged neatly, with no obvious breaks or rearrangements. The size of the intercellular space was normal. ($n = 5$, $^{*}P < 0.05$, $^{***}P < 0.001$, $^{****}P < 0.0001$).

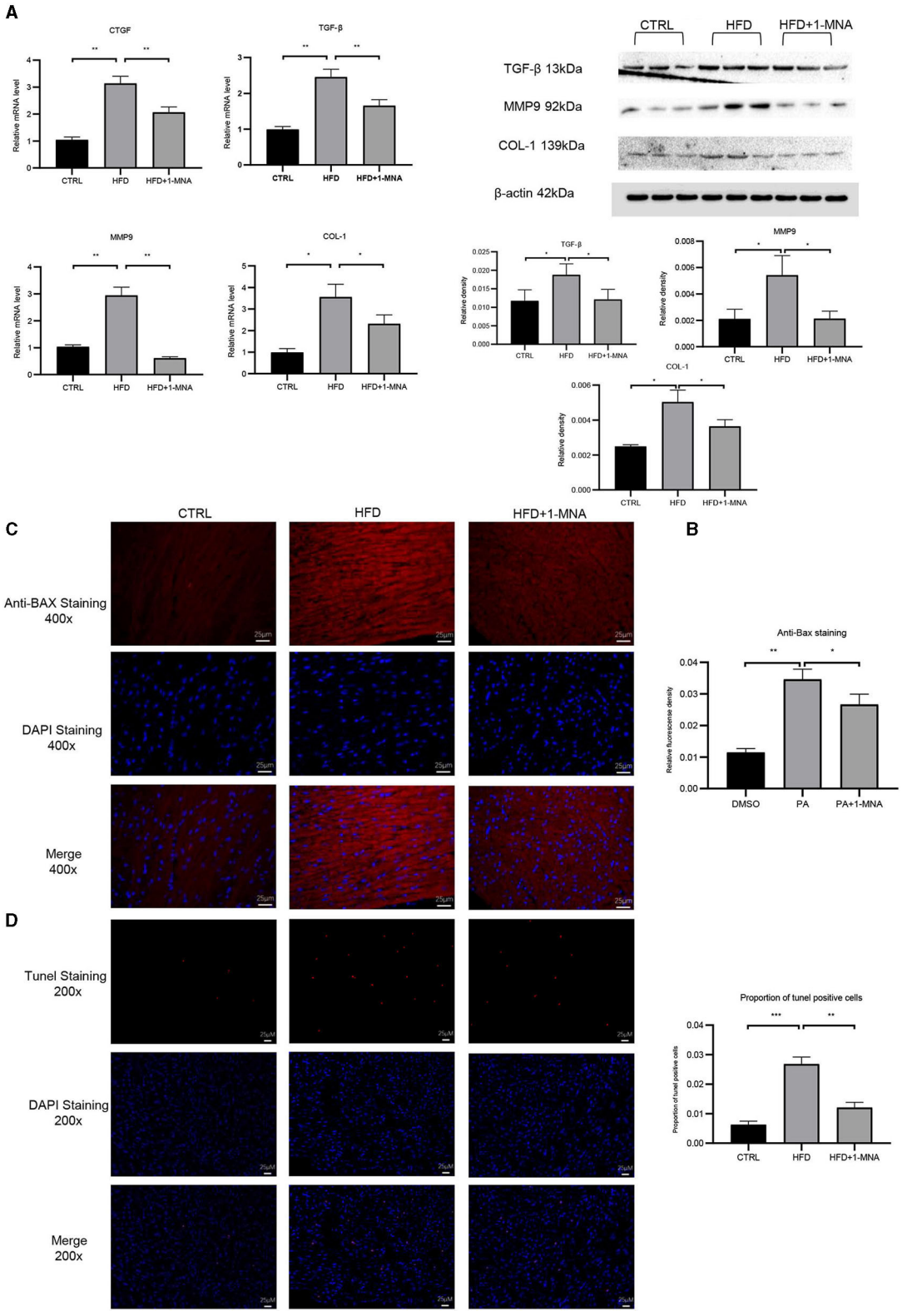

FIGURE 8 | 1-MNA administration improved the fibrosis and apoptosis of the heart induced by HFD. **(A)** Heart tissues from each group were individually processed for RNA extraction and qRT-PCR analysis. **(B)** Western blotting analysis of TGF-β, MMP9, and COL-1.1-MNA administration inhibited HFD-induced cardiomyocyte apoptosis. Images of cardiac tissue sections subject to immunohistochemical staining for Bax. **(C)** The histogram shows the relative fluorescence density of anti-Bax staining. **(D)** Images of cardiac tissue sections subject to immunohistochemical staining for Tunel. ($n = 5$, $^{*}P < 0.05$, $^{**}P < 0.01$, $^{***}P < 0.001$).

Anti-apoptotic Effects of 1-MNA in Cardiomyocytes

Finally, we investigated the anti-apoptotic effects of 1-MNA. We observed a significant increase (209.1%, $p < 0.01$) in the pro-apoptotic gene BAX in heart tissue of mice fed a HFD. 1-MNA effectively prevented HFD-induced BAX by 23.1% (**Figure 8C**). Tunel staining experiment (**Figure 8D**) showed that the number of positive cells was increased by 332.3% ($p < 0.001$) in HFD group. 1-MNA treatment significantly reduced TUNEL positive cells by 55.2%. Parallel to our *in vitro* study, administration of 1-MNA to HFD-fed mice effectively induced activation of Bax and reduced the ratio of Tunel positive cells; thus, the anti-apoptotic effects of 1-MNA may be associated with the inhibition of inflammation and oxidative stress.

DISCUSSION

Hyperlipidemia is caused by high serum levels of TC, TG, and LDL cholesterol, or low levels of circulating high-density lipoprotein cholesterol (12). Hyperlipidemia is a disorder of systemic lipid metabolism, and is one of the main risk factors for inducing atherosclerosis, fatty liver, and cardiovascular and cerebrovascular diseases (13, 14). Hyperlipidemia consists of hypertriglyceridemia, hypercholesterolemia, and mixed hyperlipidemia, in which both TG and TC are elevated. High levels of TGS and TC, are accompanied by a large amount of FFA and LDLs in the blood, are the most essential features of hyperlipidemia. Our research also confirmed this (**Figures 5B,D**). Diseases such as stroke, atherosclerosis, and coronary heart disease are closely related to hyperlipidemia (15). FFA and its metabolite TG cause cell damage, which is called lipotoxicity. Studies have shown that the leading cause of liver lipotoxicity is FFA rather than TGs. In hyperlipidemia, the increase in plasma FFA is the most important feature. It has become the main cause of obesity-related diseases such as coronary heart disease and atherosclerosis (16). According to our research,we clarified the preventive effects of 1-MNA on cardiac histopathological changes, the oxidative stress response, inflammation, and cell death pathways in the HFD mouse model and PA-treated cardiomyocytes.

Adipokines are mainly secreted by adipose tissue and can regulate glucose and lipid metabolism, inflammation, immune response, and cardiovascular function (17, 18). The relationship between obesity and cardiovascular disease has been confirmed in clinical and experimental models (19, 20). Thus, there is an urgent need to clarify the mechanism of hyperlipidemia-induced heart damage and to discover new therapeutic agents. 1-MNA, a primary metabolite of NNMT enzyme catalyzed the methylation of nicotinamide, plays an important roles in inflammatory response and immune function. We first

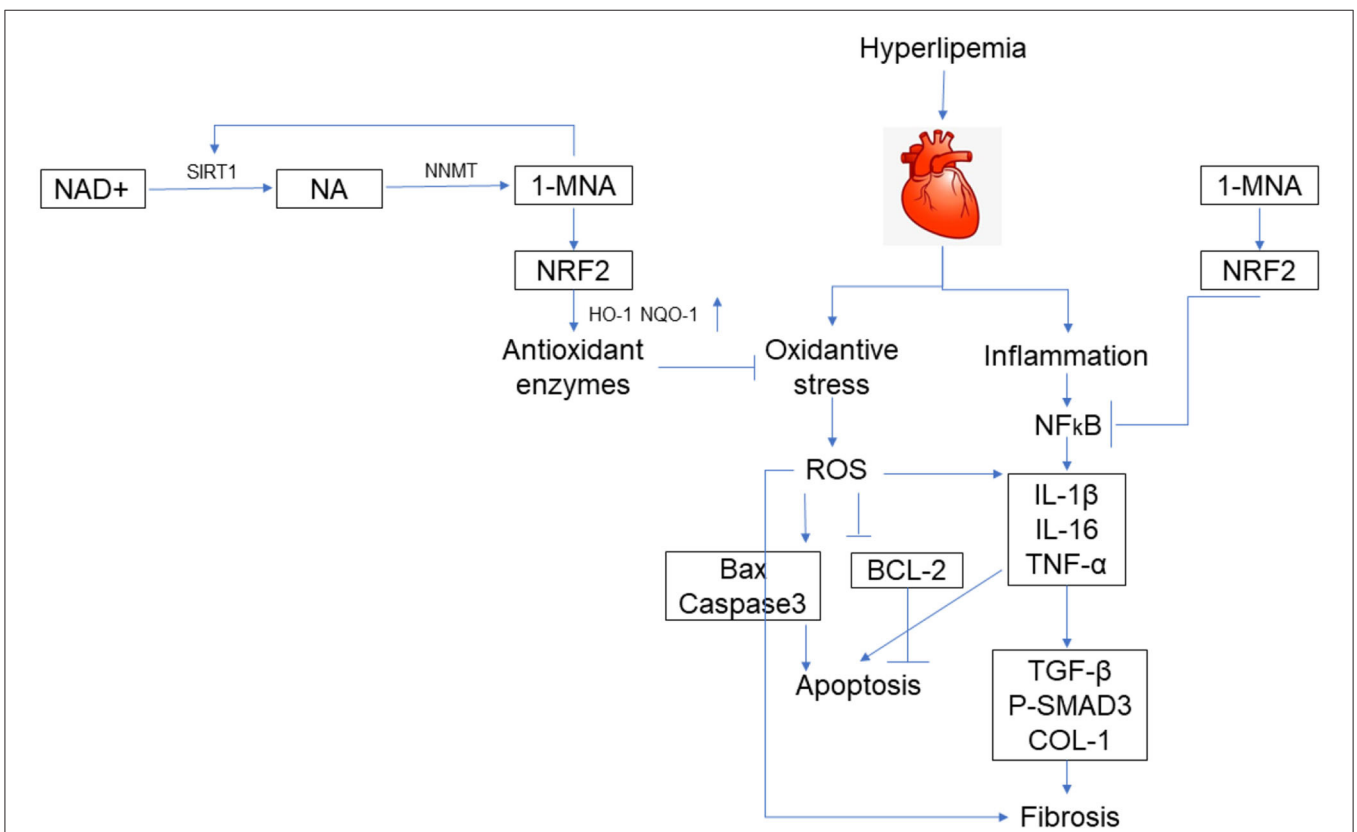

FIGURE 9 | Schematic illustration. A schematic illustration for the prevention of 1-MNA from FFA/HFD-induced injury in cardiomyocytes and hearts.

demonstrated that 1-MNA is spontaneously secreted and acts in PA-induced H9C2 cells through work such as literature review and pre-experiments (**Figure 1A**), whereby we next explored the possible antioxidant role of 1-MNA in a model of PA-induced cardiomyocyte injury.

PA is the main saturated FFA in plasma, which stimulates the production of ROS in endothelial cells and smooth muscle cells to promote the expression of inflammatory cytokines (21). In our experiments, PA treatment in H9C2 cells clearly showed an increase in ROS stress. Many studies have confirmed that Nrf2 is involved in the control of many oxidative stress-related genes (22, 23). Nrf2 activates antioxidant factors such as NQO1, HO-1, SOD, and CAT, etc., and also regulates the GSH redox system to inhibit oxidation. Our results showed that 1-MNA treatment increased the expression of Nrf2 *in vitro* (**Figures 1C,D**). Further, 1-MNA treatment also significantly increased the expression of Nrf2 downstream genes GCLC, HO-1, and NQO-1 (**Figures 1C,D**).

Although several studies (24, 25) have revealed the mechanisms involved in 1-MNA's antioxidant effects, our observations differed slightly from those of a previous report by Tanaka et al. (10), which found that 1-MNA treatment did not influence the increase in PA-induced antioxidant enzymes such as manganese superoxide dismutase and HO-1 mRNA levels. 1-MNA treatment improved PA-induced apoptosis and necrosis by inhibiting mitochondrial oxidative stress in PTCs (Proximal tubule cells), without influencing the mRNA levels of antioxidant enzymes or the intracellular concentrations of NAD or NADH. Some potential reasons for these differences include: (1) different cell types used in the studies, (2) unique cell culture conditions, and signaling molecules, (3) and the source of 1-MNA.

Recently, it has been reported that 1-MNA improves oxidative stress and cell death of proximal renal tubular cells which is caused by lipid toxicity (10). Furthermore, 1-MNA has been shown to interact with inflammatory mediators and regulate the inflammatory response in tissues (26), but the role of 1-MNA in patient heart with hyperlipidemia remains to be explored. We found significantly improved pathological indicators of HFD-induced heart damage after 1-MNA treatment. The administration of 1-MNA at 100 mg/kg/day ameliorated the characteristics of HFD-induced hyperlipidemia (**Figure 5**), indicating that one of the effects of 1-MNA on the HFD-fed mice heart is to decrease the blood lipid levels.

Chronic inflammation is closely related to obesity and it has been confirmed that obesity-related chronic inflammation is a high-risk factor for cardiovascular disease (27). Hyperlipidemia promotes the production of a variety of inflammatory molecules, which aggravate the inflammatory response. In macrophages, FFA triggers inflammation by activating Toll-like receptor 4, peroxisome proliferator receptor, and inflammatory gene expression by NF-κB (28). NF-κB is a key transcription factor that regulates inflammation, and is mainly composed of two subunits, p50 and p65. NF-κB is activated in response to cytokines, pathogens, and radiation. Our study showed that PA increases p65 translocation and NF-κB activity in cultured cardiomyocytes, while HFD reduces IκB-α levels in heart tissue of mice. Further, 1-MNA significantly inhibited PA/HFD-induced NF-κB activation, thereby reducing the expression of inflammatory cytokines such as TNF-α, IL-6, and IL-1 *in vitro* and *in vivo*. The results indicated that 1-MNA may suppress PA-induced cardiac inflammation by inhibiting NF-κB.

The occurrence and development of cardiac hypertrophy are closely related to oxidative stress. The expression of α-MyHC and BNP are considered molecular markers of cardiac hypertrophy (29), which we confirmed were upregulated in our study. Moreover, 1-MNA treatment attenuated α-MyHC- and BNP-induced cardiac hypertrophy in HFD-fed mice. Pathological cardiac hypertrophy is caused by the accumulation of collagen and the expansion of the ECM due to inflammation. As a significant feature of obesity, oxidative stress participates in the formation of fibrosis by activating TGF-β (30). We observed a wide range of fibrotic reactions in HFD-fed mice hearts, which was confirmed by the increase in mRNA expression of TGF-β, CTGF, collagen 1, and MMP-9. The antagonism of 1-MNA to fibrosis was confirmed *in vivo* and *in vitro*.

Our experiment also had many unsatisfactory problems, such as the low number of animals in some of the in *vivo* experiments. Because of some objective unavoidable factors, in the Western Blot experiment *in vivo*, only 3 mice were left for experiments. In terms of statistics, $n \geq 3$ does have a small sample size. However, combined with the cell experiments we think our experimental results still have some credibility, the small sample *t*-test is still barely usable. This is a inadequacy of this paper, and we will continue the relevant research in the future that will expand the sample size of each group to make the conclusions more convincing and will systematically explore the potential role of 1-MNA in heart disease.

In conclusion, our study confirmed that the myocardium of the HFD mouse animal model presents evidence of chronic fibrosis. TGF-β and CTGF expression in the tissue of HFD-fed mice hearts increased, which subsequently induced the expression of ECM proteins such as collagen 1. Our study showed that following 1-MNA treatment, these fibrosis indices were all downregulated, which revealed the anti-fibrotic ability of 1-MNA in HFD-fed mice hearts. High fat-induced inflammation, apoptosis, fibrosis, and hypertrophy were improved by 1-MNA both *in vivo* and *in vitro*. These effects of 1-MNA are closely dependent on its ability to increase Nrf2 expression and inhibit NF-κB activity (**Figure 9**). 1-MNA may inhibit TGF-β collateralization by activating SIRT1. Moreover, our study explored the regulatory effects of Nrf2 and NF-κB on hyperlipidemia-induced cardiac injury, through which we shed light on its protective role in cardiac hypertrophy-induced oxidative stress and PA-stimulated inflammation. Unfortunately, we did not use pathway inhibitors in the current study, and in future studies we will add inhibitors to explore the specific mechanisms by which 1-MNA acts. In conclusion these results suggest that

Nrf2, NF-κB and SIRT1 may be important targets for the treatment of myocardial injury and related diseases caused by hyperlipidemia.

DATA AVAILABILITY STATEMENT

The raw data supporting the conclusions of this article will be made available by the authors, without undue reservation.

ETHICS STATEMENT

The animal study was reviewed and approved by the Fourth Affiliated Hospital of Harbin Medical University Ethics Committee.

AUTHOR CONTRIBUTIONS

XS and ZiS designed the experiments. ZiS, PG, XZ, and ZN carried out the experiments. ZiS, ML, and ZhS provided reagents, materials, and analysis tools. ZiS wrote the manuscript. XS supervised the study and revised the manuscript. All authors reviewed the manuscript, contributed to its contents, and approved the submitted version.

FUNDING

This research was supported by the Foundation for Innovative Research Groups of the National Natural Science Foundation of China (Grant/Award Numbers: 81300248 and 81570358), 2021 Shanghai College of Health Sciences Natural Science Key Project (Grant/Award Number: SSF-21-17-01), and Discipline construction project of Pudong New District Health and Family Planning Commission of Shanghai, China (Grant/Award Numbers: PWZxq2017-01 and PWYgy2018-03).

ACKNOWLEDGMENTS

Thanks are due to Mengmeng Wang (Cancer Hospital of Harbin Medical University, China) for assistance with the experiments and to Jue Zhang (Versiti Blood Research Institute, United States) for valuable discussion.

SUPPLEMENTARY MATERIAL

The Supplementary Material for this article can be found online at: https://www.frontiersin.org/articles/10.3389/fcvm.2021.721814/full#supplementary-material

REFERENCES

1. Unger RH. Lipotoxic diseases. *Annu Rev Med.* (2002) 53:319–36. doi: 10.1146/annurev.med.53.082901.104057
2. Nakamura M, Liu T, Husain S, Zhai P, Warren JS, Hsu CP, et al. Glycogen synthase kinase-3alpha promotes fatty acid uptake and lipotoxic cardiomyopathy. *Cell Metab.* (2019) 29:1119–34 e12. doi: 10.1016/j.cmet.2019.01.005
3. Scherer T, O'Hare J, Diggs-Andrews K, Schweiger M, Cheng B, Lindtner C, et al. Brain insulin controls adipose tissue lipolysis and lipogenesis. *Cell Metab.* (2011) 13:183–94. doi: 10.1016/j.cmet.2011.01.008
4. Ajuwon KM, Spurlock ME. Palmitate activates the NF-kappaB transcription factor and induces IL-6 and TNFalpha expression in 3T3-L1 adipocytes. *J Nutr.* (2005) 135:1841–6. doi: 10.1093/jn/135.8.1841
5. Ghosh A, Gao L, Thakur A, Siu PM, Lai CWK. Role of free fatty acids in endothelial dysfunction. *J Biomed Sci.* (2017) 24:50. doi: 10.1186/s12929-017-0357-5
6. Zeng C, Zhong P, Zhao Y, Kanchana K, Zhang Y, Khan ZA, et al. Curcumin protects hearts from FFA-induced injury by activating Nrf2 and inactivating NF-kappaB both in vitro and *in vivo*. *J Mol Cell Cardiol.* (2015) 79:1–12. doi: 10.1016/j.yjmcc.2014.10.002
7. Lopaschuk GD, Ussher JR, Folmes CD, Jaswal JS, Stanley WC. Myocardial fatty acid metabolism in health and disease. *Physiol Rev.* (2010) 90:207–58. doi: 10.1152/physrev.00015.2009
8. Smyrnias I, Zhang X, Zhang M, Murray TV, Brandes RP, Schroder K, et al. Nicotinamide adenine dinucleotide phosphate oxidase-4-dependent upregulation of nuclear factor erythroid-derived 2-like 2 protects the heart during chronic pressure overload. *Hypertension.* (2015) 65:547–53. doi: 10.1161/HYPERTENSIONAHA.114.04208
9. Lin SJ, Guarente L. Nicotinamide adenine dinucleotide, a metabolic regulator of transcription, longevity and disease. *Curr Opin Cell Biol.* (2003) 15:241–6. doi: 10.1016/S0955-0674(03)00006-1
10. Tanaka Y, Kume S, Araki H, Nakazawa J, Chin-Kanasaki M, Araki S, et al. 1-Methylnicotinamide ameliorates lipotoxicity-induced oxidative stress and cell death in kidney proximal tubular cells. *Free Radic Biol Med.* (2015) 89:831–41. doi: 10.1016/j.freeradbiomed.2015.10.414
11. Mu RH, Tan YZ, Fu LL, Nazmul Islam M, Hu M, Hong H, et al. 1-Methylnicotinamide attenuates lipopolysaccharide-induced cognitive deficits via targeting neuroinflammation and neuronal apoptosis. *Int Immunopharmacol.* (2019) 77:105918. doi: 10.1016/j.intimp.2019.105918
12. Arsenault BJ, Boekholdt SM, Kastelein JJ. Lipid parameters for measuring risk of cardiovascular disease. *Nat Rev Cardiol.* (2011) 8:197–206. doi: 10.1038/nrcardio.2010.223
13. Libby P, Buring JE, Badimon L, Hansson GK, Deanfield J, Bittencourt MS, et al. Atherosclerosis. *Nat Rev Dis Primers.* (2019) 5:56. doi: 10.1038/s41572-019-0106-z
14. Anderson N, Borlak J. Molecular mechanisms and therapeutic targets in steatosis and steatohepatitis. *Pharmacol Rev.* (2008) 60:311–57. doi: 10.1124/pr.108.00001
15. Navarro–Millan I, Yang S, DuVall SL, Chen L, Baddley J, Cannon GW, et al. Association of hyperlipidaemia, inflammation and serological status and coronary heart disease among patients with rheumatoid arthritis: data from the national veterans health administration. *Ann Rheum Dis.* (2016) 75:341–7. doi: 10.1136/annrheumdis-2013-204987
16. Guida MC, Birse RT, Dall'Agnese A, Toto PC, Diop SB, Mai A, et al. Intergenerational inheritance of high fat diet-induced cardiac lipotoxicity in Drosophila. *Nat Commun.* (2019) 10:193. doi: 10.1038/s41467-018-08128-3
17. Neumann E, Junker S, Schett G, Frommer K, Muller-Ladner U. Adipokines in bone disease. *Nat Rev Rheumatol.* (2016) 12:296–302. doi: 10.1038/nrrheum.2016.49
18. Gomez R, Conde J, Scotece M, Gomez-Reino JJ, Lago F, Gualillo O. What's new in our understanding of the role of adipokines in rheumatic diseases? *Nat Rev Rheumatol.* (2011) 7:528–36. doi: 10.1038/nrrheum.2011.107
19. Ortega FB, Lavie CJ, Blair SN. Obesity and cardiovascular disease. *Circ Res.* (2016) 118:1752–70. doi: 10.1161/CIRCRESAHA.115.306883
20. Mirzaei H, Di Biase S, Longo VD. Dietary interventions, cardiovascular aging, and disease: animal models and human studies. *Circ Res.* (2016) 118:1612–25. doi: 10.1161/CIRCRESAHA.116.307473
21. Tsushima K, Bugger H, Wende AR, Soto J, Jenson GA, Tor AR, et al. Mitochondrial reactive oxygen species in lipotoxic hearts induce post-translational modifications of AKAP121, DRP1, and

OPA1 that promote mitochondrial fission. *Circ Res.* (2018) 122:58–73. doi: 10.1161/CIRCRESAHA.117.311307
22. Niture SK, Jain AK, Shelton PM, Jaiswal AK. Src subfamily kinases regulate nuclear export and degradation of transcription factor Nrf2 to switch off Nrf2-mediated antioxidant activation of cytoprotective gene expression. *J Biol Chem.* (2011) 286:28821–34. doi: 10.1074/jbc.M111.255042
23. Rubio V, Zhang J, Valverde M, Rojas E, Shi ZZ. Essential role of Nrf2 in protection against hydroquinone- and benzoquinone-induced cytotoxicity. *Toxicol In Vitro.* (2011) 25:521–9. doi: 10.1016/j.tiv.2010.10.021
24. Kuchmerovska T1, Shymanskyy I, Chlopicki S, Klimenko A. 1-methylnicotinamide (MNA) in prevention of diabetes-associated brain disorders. *Neurochem Int.* (2010) 56:221–8. doi: 10.1016/j.neuint.2009.10.004
25. Szafarz M, Kus K, Walczak M, Zakrzewska A, Niemczak M, Pernak J, et al. Pharmacokinetic Profile of 1-Methylnicotinamide nitrate in rats. *J Pharm Sci.* (2017) 106:1412–8. doi: 10.1016/j.xphs.2017.01.022
26. Hong S, Moreno-Navarrete JM, Wei X, Kikukawa Y, Tzameli I, Prasad D, et al. Nicotinamide N-methyltransferase regulates hepatic nutrient metabolism through Sirt1 protein stabilization. *Nat Med.* (2015) 21:887–94. doi: 10.1038/nm.3882
27. Koene RJ, Prizment AE, Blaes A, Konety SH. Shared risk factors in cardiovascular disease and cancer. *Circulation.* (2016) 133:1104–14. doi: 10.1161/CIRCULATIONAHA.115.020406
28. Valdearcos M, Esquinas E, Meana C, Pena L, Gil-de-Gomez L, Balsinde J, et al. Lipin-2 reduces proinflammatory signaling induced by saturated fatty acids in macrophages. *J Biol Chem.* (2012) 287:10894–904. doi: 10.1074/jbc.M112.342915
29. Camacho Londono JE, Tian Q, Hammer K, Schroder L, Camacho Londono J, Reil JC, et al. A background Ca2+ entry pathway mediated by TRPC1/TRPC4 is critical for development of pathological cardiac remodelling. *Eur Heart J.* (2015) 36:2257–66. doi: 10.1093/eurheartj/ehv250
30. Michaeloudes C, Chang PJ, Petrou M, Chung KF. Transforming growth factor-beta and nuclear factor E2-related factor 2 regulate antioxidant responses in airway smooth muscle cells: role in asthma. *Am J Respir Crit Care Med.* (2011) 184:894–903. doi: 10.1164/rccm.201011-1780OC

Conflict of Interest: The authors declare that the research was conducted in the absence of any commercial or financial relationships that could be construed as a potential conflict of interest.

Publisher's Note: All claims expressed in this article are solely those of the authors and do not necessarily represent those of their affiliated organizations, or those of the publisher, the editors and the reviewers. Any product that may be evaluated in this article, or claim that may be made by its manufacturer, is not guaranteed or endorsed by the publisher.

Copyright © 2021 Song, Zhong, Li, Gao, Ning, Sun and Song. This is an open-access article distributed under the terms of the Creative Commons Attribution License (CC BY). The use, distribution or reproduction in other forums is permitted, provided the original author(s) and the copyright owner(s) are credited and that the original publication in this journal is cited, in accordance with accepted academic practice. No use, distribution or reproduction is permitted which does not comply with these terms.

frontiers in Cardiovascular Medicine

REVIEW
published: 15 October 2021
doi: 10.3389/fcvm.2021.764038

Regulation of PCSK9 Expression and Function: Mechanisms and Therapeutic Implications

Xiao-dan Xia[1†], Zhong-sheng Peng[2†], Hong-mei Gu[3], Maggie Wang[3], Gui-qing Wang[1] and Da-wei Zhang[3*]*

[1] Department of Orthopedics, The Sixth Affiliated Hospital of Guangzhou Medical University, Qingyuan People's Hospital, Qingyuan, China, [2] School of Economics, Management and Law, University of South China, Hengyang, China, [3] Group on the Molecular and Cell Biology of Lipids, Department of Pediatrics, Faculty of Medicine and Dentistry, University of Alberta, Edmonton, AB, Canada

OPEN ACCESS

Edited by:
Yiliang Chen,
Medical College of Wisconsin,
United States

Reviewed by:
Fang Li,
Columbia University Irving Medical Center, United States
Daisy Sahoo,
Medical College of Wisconsin,
United States

***Correspondence:**
Gui-qing Wang
dzhang@ualberta.ca
Da-wei Zhang
1918635344@qq.com

[†] These authors have contributed equally to this work

Specialty section:
This article was submitted to Lipids in Cardiovascular Disease, a section of the journal Frontiers in Cardiovascular Medicine

Received: 24 August 2021
Accepted: 16 September 2021
Published: 15 October 2021

Citation:
Xia X-d, Peng Z-s, Gu H-m, Wang M, Wang G-q and Zhang D-w (2021) Regulation of PCSK9 Expression and Function: Mechanisms and Therapeutic Implications. Front. Cardiovasc. Med. 8:764038. doi: 10.3389/fcvm.2021.764038

Proprotein convertase subtilisin/kexin type 9 (PCSK9) promotes degradation of low-density lipoprotein receptor (LDLR) and plays a central role in regulating plasma levels of LDL cholesterol levels, lipoprotein(a) and triglyceride-rich lipoproteins, increasing the risk of cardiovascular disease. Additionally, PCSK9 promotes degradation of major histocompatibility protein class I and reduces intratumoral infiltration of cytotoxic T cells. Inhibition of PCSK9 increases expression of LDLR, thereby reducing plasma levels of lipoproteins and the risk of cardiovascular disease. PCSK9 inhibition also increases cell surface levels of major histocompatibility protein class I in cancer cells and suppresses tumor growth. Therefore, PCSK9 plays a vital role in the pathogenesis of cardiovascular disease and cancer, the top two causes of morbidity and mortality worldwide. Monoclonal anti-PCSK9 antibody-based therapy is currently the only available treatment that can effectively reduce plasma LDL-C levels and suppress tumor growth. However, high expenses limit their widespread use. PCSK9 promotes lysosomal degradation of its substrates, but the detailed molecular mechanism by which PCSK9 promotes degradation of its substrates is not completely understood, impeding the development of more cost-effective alternative strategies to inhibit PCSK9. Here, we review our current understanding of PCSK9 and focus on the regulation of its expression and functions.

Keywords: lipid metabolism, cardiovascular disease, atherosclerosis, cancer immunotherapy, PCSK9, LDL receptor, major histocompatibility protein class I

INTRODUCTION

Plasma low-density lipoprotein cholesterol (LDL-C) levels are positively correlated to the risk of cardiovascular disease (CVD). Statins, the currently most-prescribed lipid-lowering drug, reduce cardiovascular events by 20–40%. However, there is mounting evidence that about 50% of statin-treated patients and 80% of very high-risk patients do not achieve the recommended cholesterol values even with the highest tolerated dose. Furthermore, up to 20% of statin-treated people show statin intolerance, and about 10–12% of cases exhibit maladaptive side effects (1). Thus, there is an urgent need to develop a non-statin-based cholesterol-lowering drug.

Proprotein convertase subtilisin/kexin type 9 (PCSK9) plays a critical role in regulating plasma cholesterol homeostasis through promoting LDL receptor (LDLR)

degradation (**Figure 1**). Gain-of-function mutations in PCSK9 cause autosomal dominant hypercholesterolemia, while loss-of-function mutations are associated with reduced plasma levels of LDL-C (2–6). PCSK9 also promotes major histocompatibility protein class I (MHCI) degradation and suppresses immune attacks to tumors (7) (**Figure 1**). Therefore, PCSK9 plays a central role in the pathogenesis of CVD and cancers. In addition, it has been reported that PCSK9, especially extra-hepatic PCSK9, can recruit inflammatory cells and induce local inflammation (8, 9). Here, we summarize the latest advances in PCSK9 and focus on its role in lipid metabolism and cancer immunotherapy and the molecular mechanisms for the regulation of PCSK9 expression.

PCSK9 FUNCTION

Human and mouse PCSK9 is encoded by the *PCSK9*/*Pcsk9* gene located at chromosome 1p32.3 and 4C7, containing thirteen and twelve exons that encode a 692 and 694-amino acid PCSK9 protein, respectively (10). PCSK9 is highly conserved among mammals, including chimpanzee, monkey, camel, alpaca, rat, and mouse, with an approximate amino acid identity of 99, 96, 82, 81, 77, and 77%, respectively. The majority of identified gain-of-function and loss-of-function mutations occur in entirely conserved residues, such as gain-of-function mutations D35Y, L108R, S127R, D129G, N157K, R215H, F216L, R218S, A220T, R357H, D374Y, N425S, R468W, R496W and R499H, and loss-of-function mutations R104C, R105Q, G106R, G236S, L253F, G316C, N354I and S462P (2, 4, 11, 12). However, loss-of-function mutations R46L and R93C and gain-of-function mutations R96L, A168E, R499H, and S636R are not conserved between human and mouse or rat PCSK9. The correspondence residues of Arg46, Arg93, Arg96, Ala168, Arg499, and Ser636 in mouse/ rat PCSK9 are Pro49/Pro48, Gln93/Gln92, His99/His95, Thr211/Thr167, Trp512/Arg498, and Ser639/Ser635, respectively. Whether the difference in these residues affects PCSK9 function, however, is unclear.

PCSK9 contains a signal peptide [amino acid (aa) 1-30], a prodomain (Pro) (aa 31-152), a catalytic domain (CAT) (aa 153-425) and a Cys and His-rich C-terminal domain (CTD) (aa 426-692) (13) (**Figure 1**). The CAT contains a classical serine protease catalytic triad of Asp186, His226 and Ser386 and is highly conserved with the CAT of other proprotein convertases. PCSK9 is self-cleaved by the CAT at the FAQ152/SIPK site in the endoplasmic reticulum (ER). After autocleavage, the prodomain is associate with the CAT and masks the catalytic activity of PCSK9. This process is required for PCSK9 maturation and secretion. Compared to the other subtilisin-like serine protease family members, the CTD of PCSK9 is unique and contains multiple potential protein-protein interaction motifs (13). The CTD is positively charged and may interact with the negatively charged ligand-binding repeats of LDLR in the acidic endosomal environment, blocking recycling of the receptor (14, 15). In addition, partial deletion of the CTD markedly damages PCSK9 secretion, indicating its essential role in this process (16, 17). However, the underlying mechanism is unclear. Our recent study suggests that the CTD mediates PCSK9 secretion, possibly *via* a coat protein complex II (COPII) component Sec24 (17).

PCSK9 induces degradation of LDLR and its family members, including very low-density lipoprotein receptor (VLDLR), apolipoprotein E receptor 2 (ApoER2), and LDLR-related protein 1 (LRP1) (10, 18–20), thereby playing an essential role in lipid metabolism. However, PCSK9 at a physiological concentration can effectively degrade LDLR but not other LDLR family members in cultured cells (19, 20). Similarly, PCSK9 degrades LDLR but not LRP1 in mouse liver (21), but it can regulate visceral adipogenesis likely through promoting VLDLR degradation in mouse adipose tissues (22). Conversely, loss of functional PCSK9 in humans does not cause any known abnormality except for reduced plasma cholesterol levels (3, 6). Nevertheless, these findings indicate that PCSK9's action on its substrates is cell/tissue-type and/or species-dependent.

The CAT of PCSK9 directly binds to the epidermal growth factor precursor homology domain A (EGF-A) of LDLR on the cell surface. After endocytosis, PCSK9 remains bound to LDLR in the acidic endosome, preventing LDLR from recycling and redirecting the receptor to the lysosome for degradation (**Figure 1**) (19, 21, 23, 24). PCSK9 can also promote LDLR degradation *via* an intracellular pathway, especially when overexpressed in cultured cells (25). Of note, evolocumab and alirocumab are humanized monoclonal anti-PCSK9 antibodies targeting the catalytic domain of PCSK9. They block PCSK9 binding to LDLR on the cell surface and do not affect the intracellular pathway. On the other hand, Inclisiran is a small siRNA that targets PCSK9 mRNA and reduces its expression. It can inhibit both the intracellular and extracellular pathways. However, evolocumab, alirocumab, and Inclisiran all markedly reduce plasma LDL cholesterol levels in patients to a similar degree (26–28). Therefore, the extracellular pathway appears to be mainly responsible for the LDL-lowering effect of PCSK9 inhibition.

PCSK9 directs its substrates for lysosomal degradation (**Figure 1**), which does not require its proteolytic activity (29). Both caveolae-dependent and clathrin-mediated endocytosis have been reported to play an important role in the endocytosis of PCSK9/LDLR complex in HepG2 cells (30–32). Additionally, DeVay et al. reported that amyloid beta precursor-like protein 2 (APLP2) directly bound to PCSK9 and targeted the PCSK9/LDLR complex to lysosomes for degradation in HepG2 cells (33), while other studies showed that APLP2 did not affect PCSK9-promoted LDLR degradation in mice, HepG2, or Huh7 cells (34, 35). Differences in approaches and/or models used in these studies may cause these discrepancies. However, further studies are required to elucidate the underlying mechanism for PCSK9-promoted LDLR degradation.

PCSK9 and LDL

Plasma LDL is eliminated from circulation primarily *via* hepatic LDLR. Upon binding, the LDL-LDLR complex is internalized *via* the clathrin-coated pits and subsequently delivered to endosomes, where LDL is released from LDLR and then transported to lysosomes for degradation, while LDLR is recycled to the cell surface to clear more LDL. Mutations in LDLR cause familial hypercholesterolemia (FH), characterized by elevated plasma levels of cholesterol, particularly LDL cholesterol, and

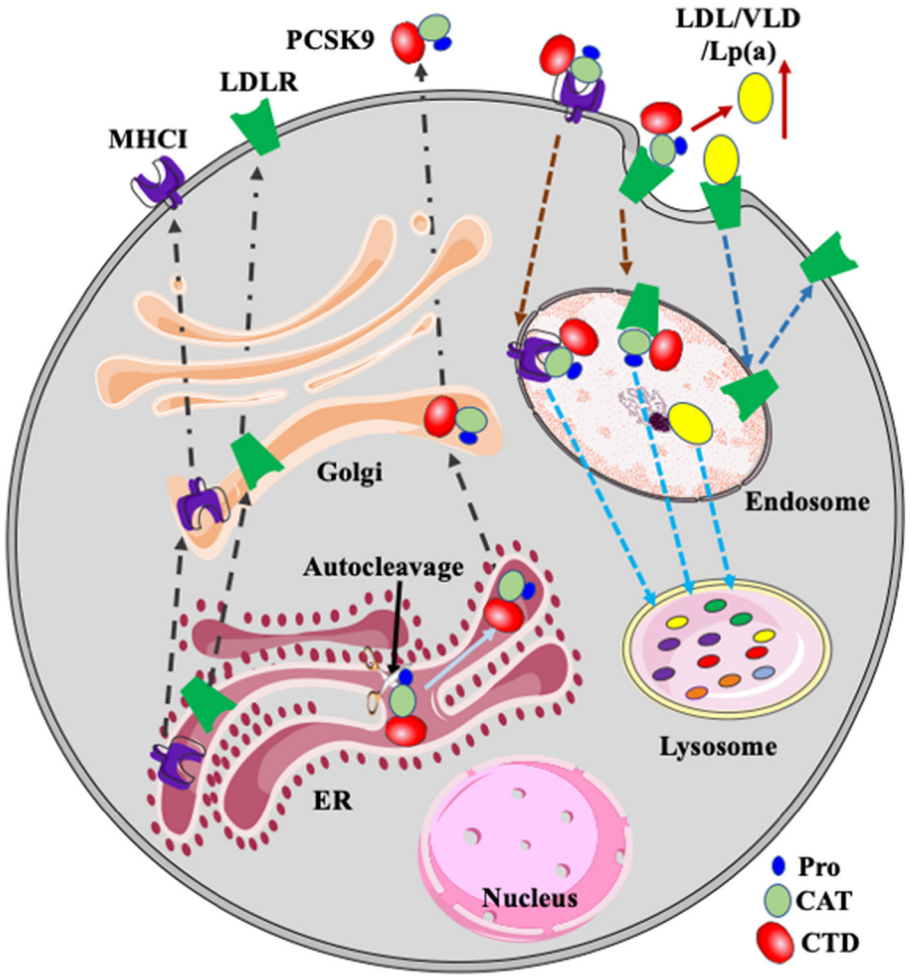

FIGURE 1 | PCSK9, LDLR, and MHCI. PCSK9 is auto-cleaved in the ER. Mature PCSK9 is transported to the Golgi and then secreted. PCSK9 binds to LDLR and MHCI on the cell surface. After, the complex is delivered to endosomes *via* endocytosis and then transported to the lysosome for degradation. LDLR binds to its ligands such as LDL, VLDL, and Lp(a) and then the receptor/ligand complex enters cells *via* receptor-mediated endocytosis and is delivered to the endosome. In the acidic endosomal environment, the ligand, such as LDL, is released from LDLR and transported to the lysosome for degradation. LDLR is recycled to plasma membrane. PCSK9-promoted degradation of LDLR increases plasma levels of LDL and Lp(a). Pro, prodomain; CAT, catalytic domain; CTD, C-terminal domain.

increased risk of CVD (36). PCSK9 promotes LDLR lysosomal degradation. Circulating PCSK9 preferentially degrades LDLR in mouse liver (37), which may be due to hepatic heparan sulfate proteoglycans (HSPG). HSPG can recruit circulating PCSK9 to hepatocytes, enhancing its action on LDLR (38). Knockout of PCSK9 increases hepatic LDLR levels, reduces plasma LDL cholesterol levels, and improves sensitivity to statin treatment in mice (37).

LDL is derived from VLDL catabolism, which is a triglyceride-enriched lipoprotein exclusively secreted by the liver. Triglycerides in VLDL are hydrolyzed by lipoprotein lipase, resulting in intermediate-density lipoprotein (IDL), which can be further metabolized to LDL (39). PCSK9 can directly interact with apoB100, the main structural lipoprotein on VLDL, and inhibit apoB100 degradation, thereby promoting its secretion. Knockout of PCSK9 reduces hepatic apoB secretion and plasma LDL cholesterol levels in $Ldlr^{-/-}/Apobec1^{-/-}$ mice (40). Conversely, gain-of-function mutant PCSK9 increases apoB100 secretion in a rat hepatoma-derived cell line, McArdle-7777 cells (41). These findings indicate that, in addition to reducing the availability of hepatic LDLR, PCSK9 may promote the production of LDL through increasing secretion of VLDL. However, hepatocytes typically produce apoB100 in abundance, and the rate-limiting step in VLDL secretion is lipidation of apoB100. Therefore, the physiological role of PCSK9-promoted VLDL secretion may not be significant *in vivo*.

PCSK9 is also expressed in extra-hepatic cells and tissues, such as the vascular smooth muscles cells (VSMCs), macrophages, endothelial cells, the pancreas, the kidneys, the intestine and the central nervous system (10). The arterial vessel has the maximal secretion of PCSK9 at the lowest level of shear stress that occurs in the aortic branching and aorta-iliac bifurcation regions of

the mouse aorta. Cultured VSMCs produce substantially more PCSK9 than endothelial cells (42). Elevated PCSK9 in VSMCs can reduce LDLR levels in VSMCs and macrophages (42, 43), which may impair LDL clearance and accelerate retention of LDL in VSMCs and macrophages in the location of arterial bifurcation. PCSK9 is also expressed in and secreted from pancreatic beta cells. However, inhibition of PCSK9 does not affect insulin secretion in the human EndoC-betaH1 beta cell line and mice even though PCSK9 promotes LDLR degradation in beta cells (44). Together, these findings indicate a cell-type-specific function of PCSK9.

PCSK9 and Triglyceride-Rich Lipoproteins

Elevated plasma levels of triglyceride-rich lipoproteins and their remnants are an independent risk factor for atherosclerosis and CVD. Hepatic LDLR binds to apoE on remnant lipoprotein particles to mediate their clearance (36). Therefore, PCSK9 can affect plasma triglyceride and remnant cholesterol levels through the LDLR pathway. Elevated plasma PCSK9 levels are positively associated with plasma TG levels in humans upon a short-term high-fructose intake (45). Treatments with PCSK9 inhibitors increase clearance of VLDL remnants in patients (46). Alirocumab, a fully human PCSK9 monoclonal antibody, reduces LDL particles by 56.3% in human patients. This reduction is partly due to an increase in the clearance rate of IDL particles, thereby decreasing the conversion of IDL to LDL (27).

PCSK9 is expressed in the intestine and can affect chylomicron metabolism. Knockout of PCSK9 in mice significantly reduces lymphatic apoB48 secretion and increases secretion of TG-rich large chylomicrons. Clearance of chylomicron remnants is also increased in *Pcsk9*$^{-/-}$ mice (47). Rashid et al. further demonstrated that PCSK9 promoted chylomicron secretion through both LDLR-dependent and -independent pathways in mice and a human enterocyte cell line, CaCo-2 cells, such as increasing the expression of apoB, microsomal triglyceride transfer protein and lipogenic genes in enterocytes (48). However, inhibition of PCSK9 by evolocumab or alirocumab does not significantly affect VLDL production or postprandial plasma levels of apoB48 and triglycerides in healthy humans or patients with hypercholesterolemia (49). Conversely, in patients with type-II diabetes mellitus, evolocumab reduces postprandial apoB48 levels even though the effect on postprandial triglyceride levels is not significant, while alirocumab can significantly reduce fasting plasma apoB48 and TG levels and postprandial TG levels (50). Plasma PCSK9 levels are also correlated with plasma apoB48-containing TG-rich lipoproteins in men with insulin resistance (51). However, the impact of PCSK9 on plasma levels of TG-rich lipoproteins, such as VLDL and chylomicrons, is much less than its effect on plasma LDL (52). This may be because VLDL and chylomicron remnants can also be effectively cleared by an LDLR-independent pathway, such as LRP1 (53). In summary, extracellular PCSK9 regulates LDLR-mediated catabolism, and intracellular PCSK9 modulates apoB secretion; the two pathways might act in a complementary fashion to regulate TG-rich lipoproteins metabolism with the extracellular pathway as the primary contributor.

PCSK9 and Lipoprotein(a)

Elevated plasma lipoprotein(a) [Lp(a)] levels are a highly prevalent risk factor for cardiovascular disease, especially for myocardial infarction, atherosclerotic stenosis and aortic valve stenosis. Lp(a) is an apoB100–containing lipoprotein particle covalently linked to the plasminogen-like glycoprotein apo(a) by a disulfide bond (54). The statin treatment and lifestyle interventions hardly affect circulating Lp(a) levels, which brings a real challenge for successfully managing elevated Lp(a) levels in patients. Conversely, PCSK9 inhibitors dramatically reduce plasma Lp(a) levels up to ∼35% in patients (54, 55). Inhibition of PCSK9 reduces the risk of coronary heart disease to a much greater degree in patients with a high plasma Lp(a) level compared to patients with a low plasma Lp(a) level (23 vs. 7%) (54). However, how PCSK9 regulates Lp(a) levels is unclear. Plasma Lp(a) levels are determined by its production and clearance. Lp(a) is removed from circulation through LDLR, SR-BI, and LRP1(54). Lp(a) levels are increased in FH patients who carry loss-of-function mutant LDLR. Overexpression of LDLR enhances Lp(a) clearance in mice. PCSK9 promotes LDLR degradation and reduces Lp(a) catabolism in HepG2 cells and primary fibroblasts (31). These findings indicate that PCSK9 can regulate plasma Lp(a) levels in a LDLR-dependent pathway. However, while statin treatment increases LDLR levels, it has no significant effect on plasma Lp(a) levels in patients. Furthermore, lymphocytes from patients with homozygous FH can effectively take up Lp(a) particles, and PCSK9 inhibitors can lower circulating Lp(a) in homozygous FH patients (56), indicating a LDLR-independent pathway. Lp(a) usually cannot compete with LDL for binding to LDLR. It has been proposed that PCSK9 inhibition can promote hepatic clearance of Lp(a) through LDLR-mediated endocytosis when plasma LDL levels are low (57). Nevertheless, although the mechanism by which PCSK9 inhibitors reduce Lp(a) levels remains to be determined, the fact that PCSK9 inhibitors provide an additional beneficial effect in lowering circulating Lp(a) may confer protection against CVD from a clinical perspective. Further work is needed to understand the role of PCSK9 in the overall metabolism of apoB-containing lipoproteins, especially for Lp(a).

PCSK9 and Cancer Cell Immunity

MHCI on the cell surface presents specific antigens to T-cell receptors (TCR) on CD8$^+$ T cells, activating CD8$^+$ T cell-mediated cell killing. After antigen presentation, MHCI enters cells *via* endocytosis and is recycled to present new antigens. On the other hand, programmed cell death protein 1 receptor (PD-1) on the cell surface interacts with its ligand programmed death-ligand 1 (PD-L1) on T cells to act as an immune checkpoint, which suppresses the immune response and prevents indiscriminate attacks (58).

During tumor development, cancer cells evolve various mechanisms to escape immune attacks, such as stimulating immune checkpoint targets and reducing tumor-specific antigen (TSA) presentation. Monoclonal anti-PD1 or PDL1 antibodies, which inhibit the PD1 pathway and promote antitumor immune response, have been approved to treat various types of cancers such as melanoma, bladder cancer, non-small cell lung cancer,

and renal cell carcinoma. On the other hand, MHCI on the cancer cell surface presents TSA to CD8+ cells, activating CD8+ cell-mediated cancer cell killing (58). Recently, Liu et al. reported that PCSK9 bound to MHCI on the cancer cell surface and redirected it to the lysosome for degradation, thereby reducing cell surface MHCI levels and TSA presentation. Knockout of PCSK9 or inhibition of circulating PCSK9 increased $CD8^+$ T cell intratumoral infiltration and enhanced antitumor activity of $CD8^+$ T cells in mice. This suppressed tumor growth of several mouse cancer cell lines, including 4T1 (breast cancer), MC38 (colon adenocarcinoma), and the PD-1 inhibitor-resistant cancer cell line, MC38R, in mice (7). In addition, knockout of PCSK9 suppressed tumor growth in $Ldlr^{-/-}$ mice, indicating a LDLR-independent mechanism. However, Yuan et al. reported that inhibition of PCSK9 attenuated MC38 tumor growth in a LDLR-dependent manner. They found that LDLR directly interacted with T-cell receptor complex (TCR) and increased its cell surface levels. Inhibition of PCSK9 increased LDLR and TCR levels in MC38 tumors, enhancing TCR signaling and $CD8^+$ T cell-dependent cancer cell killing in mice. The reason for the discrepancy is unclear. Yuan et al. did not report whether MHCI levels in MC38 tumors were affected by PCSK9, but they found that PCSK9 inhibition did not alter MHCI levels in B16F10 melanoma cells (59), indicating that PCSK9 regulates MHCI levels in a tumor/cell type-specific manner. These findings suggest that PCSK9 may control tumor growth through the LDLR and the MHCI pathway independently and/or collaboratively.

PCSK9 produced locally in vascular cells and cardiomyocytes can promote inflammation *via* the NF-κB signaling pathway (60, 61). Chronic inflammation increases the risk of cancer. PCSK9 expression is high in various cancers, such as hepatocellular carcinoma, gastricadenocarcinoma and prostate cancer cell lines (62–64). Zhang et al. reported that PCSK9 expression is positively correlated with poor prognosis. The authors found that PCSK9 suppressed apoptosis in cultured hepatoma-derived cell lines through the Bax/Bcl-2/Caspase9/3 pathway (64). Consistently, inhibition of PCSK9 by siRNA promotes apoptosis in a human lung adenocarcinoma cell line, A549 cells, *via* activation of caspase-3 and stimulation of ER stress (62). On the other hand, silencing PCSK9 by siRNA reduces radiation-induced apoptosis in prostate cancer cell lines, PC-3 and LnCap and thus enhances cell viability (65). However, the authors did not investigate the potential contribution of inflammation in these studies. Nevertheless, these studies suggest that PCSK9 plays a complex role in cancer development *via* different mechanisms. Cancer risk analysis of subjects carrying loss-of-function and gain-of-function mutations in PCSK9 will further reveal and confirm the role of PCSK9 in cancer progression.

REGULATION OF PCSK9

PCSK9 plays a critical role in regulating circulating lipid homeostasis and MHCI-dependent immune responses. The complexity of PCSK9's functions indicates that its activity is strictly regulated by various mechanisms at multiple levels.

Regulation of PCSK9 Expression

Epigenetically, binding of forkhead box O (FoxO) 3 to the promoter of PCSK9 recruits Sirt6 to deacetylate histone H3, suppressing PCSK9 expression (**Figure 2**) (66). On the other hand, histone nuclear factor P (HINFP) binds to a HINFP motif in 20 bp upstream of the sterol regulatory element motif (SRE) in PCSK9 promoter, promoting histone H4 acetylation to activate sterol regulatory element-binding protein 2 (SREBP2)-mediated upregulation of PCSK9 transcription (67). Furthermore, *PCSK9* promoter is methylated. Alcohol use disorder (AUD) causes hypomethylation in *PCSK9* promoter and consequently reduces PCSK9 expression and plasma cholesterol levels in a mouse model of AUD, which may partially contribute to the protective effect on CVD risk observed in light alcohol users (68).

At the transcriptional level, both SREBP1 and SREBP2 have been reported to bind to SRE in PCSK9 promoter and thus upregulate PCSK9 expression in cultured cells; however, PCSK9 is predominantly regulated by SREPB2 *in vivo* (69–71). Statin treatment activates the transcriptional activity of SREBP2 and thus increases the expression of LDLR and PCSK9 (71). However, Poirier et al. reported that the expression of PCSK9 in the rodent central nervous system was regulated in a SREBP2-independnet manner (72). *PCSK9* promoter also contains a binding site of the transcription factor hepatocyte nuclear factor 1 alpha (HNF1α) (70, 73). Silencing of HNF1α but not HNF1β significantly reduced PCSK9 expression. Furthermore, insulin increases the mTORC1 signaling pathway and activates PKCδ, which reduces HNF1α-mediated expression of PCSK9 and increases hepatic LDLR levels (74). Li et al. reported that HNF1α worked cooperatively with SREBP2 to activate PCSK9 transcription since mutations in the HNF1α-binding site significantly reduced SREBP2-mediated upregulation of PCSK9 transcription (73). However, the HNF1α binding site is just 28 bp upstream of the SREBP2 bindings site. Mutations in the HNF1α binding site may affect the integrity of SRE and then indirectly impair SREBP2 binding.

The HNF1α binding site in the promoter of *PCSK9* contains a consensus FoxO binding site (**Figure 2**). FoxO3 can inhibit PCSK9 expression competitively *via* inhibiting HNF1α-mediated upregulation of PCSK9 (66). In addition, Lai et al. reported that transcription factor E2F2 could bind to the *PCSK9* promoter region and upregulate its expression under a condition of feeding or high cellular cholesterol levels (75). The promoter region of PCSK9 also contains NF-Y and SP1 binding sites upstream of SRE (71). The putative NF-Y binding site appears not to affect PCSK9 expression. However, the SP1 site may mediate basal transcription of PCSK9 since it is not required for the sterol-dependent regulation of PCSK9 expression, but mutations in this site reduce PCSK9 expression (69). A variant, C-332C>A, in the SP1 binding site, increases PCSK9 expression by approximately 2.5-fold independent of lovastatin treatment (76).

Several lines of evidence demonstrate the regulation of *PCSK9* transcription by small molecules (**Figure 2**). Curcumin and the methanol extract of *Cajanus cajan* L. leaves reduce HNF1α levels and downregulate PCSK9 transcription in HepG2 cells (77, 78). Epigallocatechingallate (humans, Sprague-Dawl rats, HepG2 and Huh7 cells), ascorbic acid (mice, HepG2 and

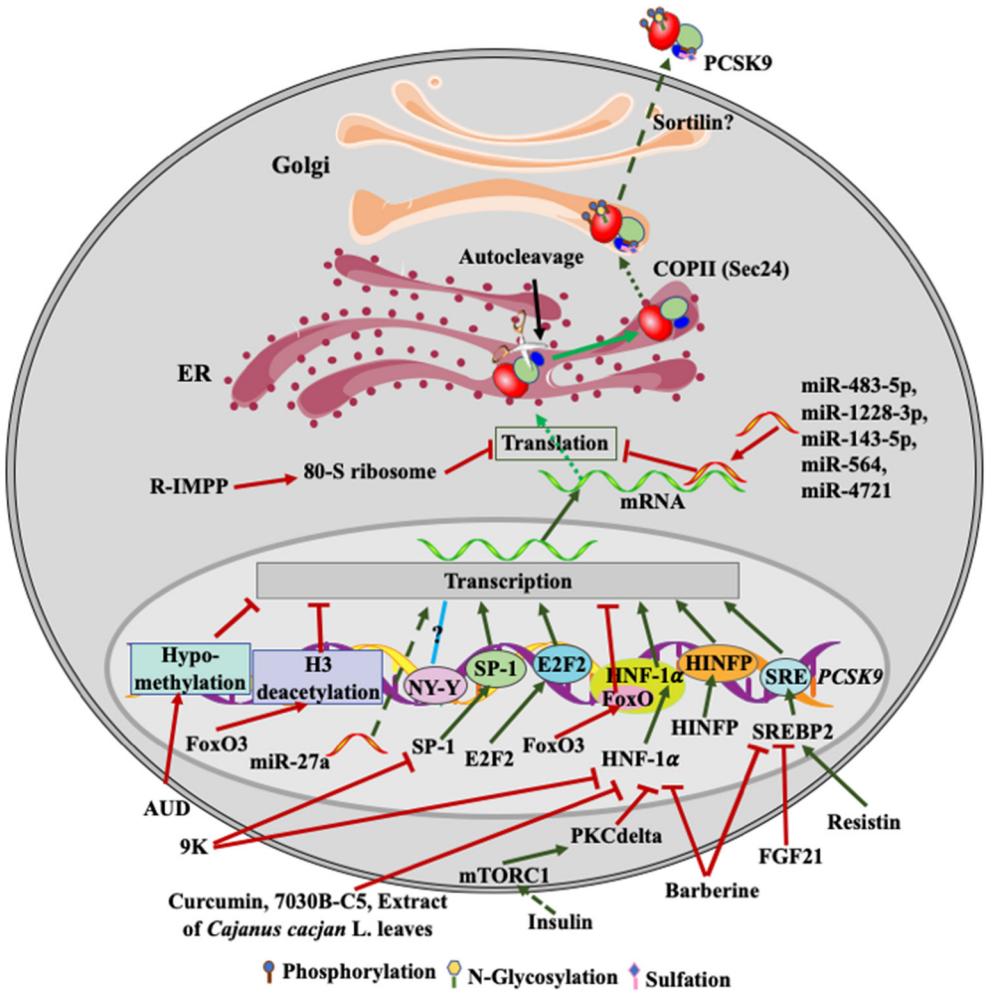

FIGURE 2 | Regulation of PCSK9 expression. Transcriptional factors, such as SREBP2, HNF-1α, SP-1and E2F2, upregulate PCSK9 transcription. FGF21 and resistin inhibit and increase SREBP2-mediated transcription of PCSK9, respectively. Barberine reduces PCSK9 expression *via* suppressing the activity of SREBP2 and HNF-1α on PCSK9 transcription. 9K suppresses PCSK9 expression through SP1 and HNF-1α, while Curcumin, 7030B-C5 inhibits HNF-1α-induced transcription of PCSK9. Alcohol use causes hypomethylation of PCSK9 promoter and then reduces PCSK9 expression. Insulin activates mTROC1 and then PKCδ to suppress PCSK9 transcription *via* HNF-1α. miR-483-5p, miR-1228-3p, miR-143-5p, miR-564, and miR-4721 bind to the 3'UTR of PCSK9 mRNA, reducing PCSK9 expression, while miR27a somehow increases PCSK9 expression. R-IMPP inhibits 80S ribosome and reduces PCSK9 expression. After autocleavage in the ER, PCSK9 is transported to the Golgi *via* classical COPII vesicles. There, PCSK9 undergoes posttranslational modifications, such as phosphorylation, glycosylation, and sulfation. Mature PCSK9 is then secreted into the extra cellular environment.

Huh7 cells), Pinostrobin (HepG2 cells), and tanshinone IIA (HepG2 cells) reduce PCSK9 expression in a FoxO3a-dependent manner, probably *via* attenuating HNF1α-mediated activation of PCSK9 expression and/or methylation in the promoter region of PCSK9 (79–82). A small molecular, 7030B-C5, also reduces PCSK9 expression in HepG2 cells and mice mainly through the FoxO1 and HNF1α pathway (83). In addition, Berberine reduces PCSK9 expression mainly through attenuating SREBP2 and HNF1α-mediated upregulation of PCSK9 transcription in HepG2 cells (73), which may account for its cholesterol-lowering effect. Conversely, a berberine derivative, 9k, downregulates PCSK9 expression *via* suppressing the transcriptional activity of HNF1α and/or SP1 in HepG2 cells (84). Fibroblast growth factor 21 inhibits the transcriptional activity of SREBP2, thereby reducing PCSK9 expression in mouse liver (85). In addition, glucagon, bile acids, fibrate, and oncostatin M have been reported to inhibit PCSK9 expression at the transcriptional levels in HepG2 cells (86–88), but the underlying mechanisms are unclear. On the other hand, resistin, a small cysteine-rich protein secreted from macrophages and adipose tissues, increases PCSK9 transcription *via* the SREBP2 pathway in HepG2 cells and primary human hepatocytes (89). Nevertheless, these findings indicate the potential of inhibiting PCSK9 transcription as an avenue to lower plasma cholesterol levels, reducing CVD risk. However, the aforementioned transcriptional factors also regulate the transcription of many other proteins that play important roles in various physiological processes. For example, inhibition of SREBP2 reduces LDLR expression, attenuating LDL

clearance. Inhibition of HNF1α activity does not affect LDLR expression. However, HNF1α can act as a tumor suppressor, and its expression is reduced in patients with liver malignancies (90). Thus, it is a big challenge to develop small molecules that can specifically modify PCSK9 expression at the transcriptional level.

Post-transcriptionally, the expression of PCSK9 is regulated by microRNAs (miRNA) (**Figure 2**). miR-483-5p targets the 3′-UTR of the PCSK9 mRNA, reduces PCSk9 expression and decreases plasma cholesterol levels in HepG2 cells and mice (91). Similarly, miR-224, miR-191, miR-222, miR-1228-3p, miR-564, miR-4721, miR-337-3p, and miR-143-5p can reduce PCSK9 expression through targeting its 3′-UTR in cultured cells, such as Huh7, HepG2 and BON-1 cells (92–94). A common variant, 1420C>G, decreases the inhibitory effect of miR-1228-3p and miR-143-5p on PCSK9 expression, reducing plasma levels of PCSK9 and LDL cholesterol (95). Similarly, Los et al. identified several variants in *PCSK9* 3′-UTR in FH patients. The variant 345C>T impairs binding of miR-4721 and miR-564 to *PCSK9* 3′-UTR and increases PCSK9 expression (93). Conversely, miR-27a upregulates PCSK9 expression, possibly through binding to the upstream of PCSK9 promoter in HepG2 cells (96). It is of note that a single miRNA often targets multiple genes as binding of miRNAs to their target genes requires seed pairing of as few as six nucleotides or even imperfect seed pairing (97). Thus, one of the key issues of miRNA-based therapies is their potential off-target effect.

Compared to miRNA, siRNAs bind to their complementary sequence in mRNA that completely matches their antisense strand, thereby specifically reducing the expression of their target genes. Phase III trials of Inclisiran, a chemically modified siRNA that targets PCSK9 mRNA, shows a promising lipid-lowering effect. Subcutaneous injection of Inclisiran reduces plasma LDL-C levels up to 50% in heterozygous FH patients without any major side-effects (26). Inclisiran, which requires twice-yearly administration, may reduce the cost of PCSK9 inhibitors compared to the current PCSK9 monoclonal antibody therapy that needs administration every 2–4 weeks. However, it is still a financial burden as a primary prevention measure for all eligible patients. In addition, siRNAs, particularly at a high dose, also exhibit miRNA-like off-target activity (98). Additionally, duplex siRNA can trigger an innate immune response in Toll-like receptors-dependent and independent mechanisms (99). Patients with Inclisiran treatment do show a slightly increased rate of mild-to-moderate bronchitis (4.3 vs. 0.7% for Inclisiran and placebo, respectively) (26). Therefore, possible long-term side effects of using siRNAs as a lifelong primary prevention strategy need to be assessed.

A small molecule, R-IMPP, can selectively target human 80S ribosome and inhibit PCSK9 translation. R-IMPP significantly reduces the protein level of PCSK9, thereby increasing LDLR levels and LDL uptake in Huh7 cells (100). However, the therapeutic potential of R-IMPP is uncertain because ribosomes are the core of protein translation machinery and not an ideal therapeutic target.

Most recently, Liu et al. reported that the blood flow rate regulated PCSK9 expression through the toll-like receptor 4-MyD88-NF-κB signaling pathway in the rabbit thoracic aorta. Low-flow state increased, whereas high-flow state reduced the mRNA and protein level of PCSK9 in vascular cells. Interestingly, they observed an opposite effect on the expression of LDLR (101), indicating that the impact of flow rate is independent of SREBP2. Interestingly, knockdown of PCSK9 suppressed, while overexpression of PCSK9 enhanced the toll-like receptor 4-NF-κB signaling pathway and inflammation in the atherosclerotic lesions of apoE$^{-/-}$ mice (60). It will be of interest to see if the increased expression of PCSK9 under the low-flow state promotes the toll-like receptor 4-NF-κB signaling pathway in the thoracic aorta.

Circulating PCSK9 is mainly produced by hepatocytes. Blood flow rate may not have a similar effect on PCSK9 expression in hepatocytes since hepatocytes, unlike aortic vascular cells, are not directly exposed to blood flow. On the other hand, blood flow rate equals blood flow divided by cross-section area. Atherosclerosis causes blood vessels to harden and to narrow, which increases blood flow rate. It would be of interest to assess whether PCSK9 expression in vascular cells near and at atherosclerotic lesion area is reduced due to the increased blood flow rate, which could lead to a beneficial outcome since vascular cell PCSK9 can promote inflammation.

Regulation of PCSK9 Secretion

Although multiple tissues express PCSK9, circulating PCSK9 is mainly secreted from the liver (102). Loss-of-function PCSK9 mutations such as G236S, S462P, and C679X reduce its secretion, while gain-of-function mutations such as E32K enhance PCSK9 secretion (17, 103). Furthermore, circulating PCSK9 is rapidly cleared from the blood with a half-life of about 5 min in mice (37), indicating that targeting PCSK9 secretion is a promising therapeutic strategy. However, the machinery system controlling PCSK9 secretion is still elusive.

PCSK9 undergoes autocleavage in the ER (104), which is essential for its maturation and secretion. However, the enzymatic activity is not required for this processing. Mutant PCSK9 that losses its catalytic activity is retained in the ER, but coexpression of prodomain with catalytic dead mutant PCSK9 rescues its secretion in HepG2 cells (29). In addition, deletion of part of the C-terminal domain of PCSK9 impairs its secretion but does not affect its autocleavage in cultured human hepatocytes, such as HepG2 and Huh7 cells (17, 105), indicating that the autocleavage is not sufficient to support PCSK9 secretion. After autocleavage, the cleaved N-terminal PRO is associated with the catalytic domain and functions as an intramolecular chaperone, guaranteeing the correct folding of the catalytic domain in the ER. This step is believed to be the rate-limiting step for PCSK9 mature and secretion (103).

PCSK9 is transported from the ER to the Golgi *via* the classical COPII vesicles. The lack of SEC24, one of COPII components, significantly reduces PCSK9 secretion in mice and cultured human hepatocytes, HepG2 and Huh7 cells (17, 106). However, PCSK9 is a secretory protein located in the ER lumen, while SEC24 is located in the cytosol. Therefore, a cargo receptor is required to bridge the interaction between PCSK9 and SEC24. Emmer et al. reported that a cargo receptor Surf4 facilitated secretion of PCSK9 that was overexpressed in HEK293 cells.

They found that Surf4 co-immunoprecipitated with PCSK9, and knockout of Surf4 significantly reduced the amount of PCSK9 detected in culture medium (107). Surf4 is a transmembrane protein that mainly resides in the ER membrane. It contains five putative transmembrane domains, an ER lumen-exposed N-terminus that binds cargo proteins within the lumen, and a cytoplasmic domain that interacts with COPII components, facilitating cargo sorting into COPII vesicles. However, we found that knockdown of Surf4 in cultured immortalized human hepatocytes, HepG2 and Huh7 cells, did not impair endogenous PCSK9 secretion (108). This discrepancy may be caused by different types of cells used in the two studies. We investigated endogenous PCSK9 secretion from cultured hepatocytes, HepG2 and Huh7 cells, while Emmer et al. studied the effect of Surf4 on secretion of PCSK9 overexpressed in HEK293 cells that do not express endogenous PCSK9. Furthermore, we found that knockdown of Surf4 in mouse liver had no significant effect on plasma and hepatic PCSK9 levels. In liver-specific Surf4 knockout mice, the levels of PCSK9 in plasma and liver homogenate were also comparable to that in the wild-type mice (109). Therefore, Surf4 is not required for endogenous PCSK9 secretion.

The C-terminal domain of PCSK9 has been implicated in its secretion. Loss-of-function mutations such as E498K and S462P located in the C-terminus of PCSK9 damage its secretion (12, 103). Deletion of the entire C-terminal PCSK9 from amino acids 456 to 692 does not impair PCSK9 secretion. Conversely, removing part of the C-terminal region (from amino acids 457 to 528 or 608 to 692) damages PCSK9 secretion (16, 17, 105). Furthermore, the deletion of part of or the entire hinge region that connects the catalytic domain and the C-terminal domain also significantly reduces PCSK9 secretion, indicating the important role of this region. SEC24 silencing significantly reduces the secretion of the wild-type but not mutant PCSK9 without the C-terminal domain, indicating that the C-terminal region of PCSK9 may be involved in SEC24-facilitated PCSK9 secretion (17). Further studies are required to elucidate how PCSK9 is sorted into COPII vesicles. Most recently, Rogers et al. reported that dynamin-related protein1 (DRP1)-mediated ER remodeling involved in PCSK9 secretion (110). Inhibition of DRP1 by mitochondrial division inhibitor 1 or knockout hepatic DRP1 markedly reduced PCSK9 secretion in HepG2 cells and mice.

After delivery to the Golgi apparatus, PCSK9 undergoes various posttranslational modifications and is then packed into secretory vesicles. The vesicles are delivered to and fused with the plasma membrane, releasing PCSK9 into the extracellular milieu. Gustafsen et al. reported that sortilin co-immunoprecipitated with PCSK9, and the two proteins were colocalized in the trans-Golgi network in HepG2 cells. Knockout of sortilin significantly reduced plasma PCSK9 levels in mice and reduced PCSK9 secretion from mouse primary hepatocytes. The author further showed that PCSK9 levels were positively correlated with sortilin levels in human serum. Thus, they concluded that sortilin interacted with PCSK9 in the trans-Golgi network, facilitating PCSK9 secretion (111). On the other hand, Butkinaree et al. reported that plasma levels of PCSK9 were comparable in sortilin

TABLE 1 | PSCK9 inhibitors.

Name	Strategy	Target	Mechanism	Status
Evolocumab	Humanized monoclonal antibody	CAT of PCSK9	Blocking PCSK9 binding to LDLR	Approved
Alirocumab	Humanized monoclonal antibody	CAT of PCSK9	Blocking PCSK9 binding to LDLR	Approved
Inclisiran	GalNAc-conjugated siRNA	mRNA of PCSK9	Inhibiting PCSK9 expression	Under review by the FDA
LIB003	Adnectin-human serum albumin fusion protein	CAT of PCSK9	Blocking PCSK9 binding to LDLR	Phase III
AT04A and AT06A	PCSK9 peptide Vaccine	Aa 153-162 of PCSK9	Blocking PCSK9 binding to LDLR	Phase I
Mimetic peptide	Mimicking the binding site of PCSCK9 on LDLR	CAT of PCSK9	Blocking PCSK9 binding to LDLR	Preclinical
DRP	Small PCSK9 inhibitor		Inhibiting interaction between PCSK9 and HSPG	Preclinical
NYX-330	Small PCSK9 inhibitor	PCSK9	Inhibition of PCSK9 binding to LDLR	Preclinical
PF-0644846	Inhibitor of ribosome	80S ribosome	Inhibition of *PCSK9* translation	Preclinical
CRISPR-Cas9	Gene editing	PCSK9 gene	Knockout/knockdown of PCSK9 expression	Preclinical
9k	Small inhibitor, berberine derivative	The HNF1α pathway	Inhibition of *PCSK9* transcription	Preclinical
7030B-C5	Small inhibitor	the FoxO1 and HNF1α pathway	Inhibition of *PCSK9* transcription	Preclinical

knockout mice and wild-type littermates, and sortilin had no effect on PCSK9-promoted LDLR degradation in HepG2 and Huh7 cells. Instead, PCSK9 induced sortilin degradation (35). The reason for this discrepancy is unclear. The mice used in the Gustafsen study were C57BL/6J background, while Butkinaree et al. did not report their mouse background. Nevertheless, these findings reveal the complexity of the molecular mechanisms of PCSK9 secretion.

Posttranslational Modifications of PCSK9

PCSK9 is predicted to be phosphorylated on serine, threonine, asparagine, and lysine residues by PhosphoSitePlus (www.phosphosite.org). Mass spectrometry analysis of plasma samples confirms this prediction. Furthermore, Dewpura et al. reported that PCSK9 was partially phosphorylated on serine residues at positions 47 and 688 by a Golgi casein kinase-like kinase in a cell-type dependent manner, with the highest phosphorylation in HepG2 cell (∼70%), followed by Huh 7 cells (∼54%), HEK293 cells (∼23%), and CHO-K1cells (none). Phosphorylation may protect PCSK9 against proteolysis and increase its stability in Huh 7 cells (112). Meanwhile, this finding also indicates that serine phosphorylation is not required for PCSK9's action on LDLR since PCSK9 purified from CHO-K1 cells is unphosphorylated and can effectively promote LDLR degradation (38). It has also been reported that PCSK9 was phosphorylated on serine residues at positions 47, 666, 668, and 688 by family with sequence similarity 20, member C (FAM20C), which increased PCSK9 secretion and enhanced its ability to promote LDLR degradation in HepG2 cells (113). However, phosphorylation at these sites was also not required for PCSK9-promoted LDLR degradation since mutant PCSK9 that lost phosphorylation at the four serine residues still could stimulate LDLR degradation. In addition, FAM20C phosphorylates serine residue in a consensus Ser-x-Glu motif present in many secreted proteins (114). Thus, it cannot be ruled out that FAM20C may indirectly affect PCSK9 secretion and function *via* phosphorylation of other proteins.

PCSK9 is N-glycosylated on asparagine residue at position 533 and sulfated on tyrosine residues (104). Detailed analysis revealed that the N-glycosylation at Asn533 and sulfation at Tyr38 were not required for PCSK9 processing, secretion and function in HepG2 and Huh 7 cells (115). Treatment of cells with tunicamycin that inhibits N-glycosylation or chlorate that inhibits tyrosine sulfation had no effect on PCSK9 expression and secretion in the human hepatocyte cell line, Huh7 cells. When overexpressed, mutant PCSK9 that lost the N-glycosylation and Tyr sulfation sites alone or together could be efficiently secreted and promote LDLR degradation in Huh7 and HepG2 cells (116). However, the secreted mutant PCSK9 appeared to promote LDLR degradation less effectively than the wild-type protein, suggesting that N-glycosylation may enhance the ability of PCSK9 to stimulate LDLR degradation.

Plasma levels of PCSK9 in subjects carrying phosphomannose mutase 2 (PMM2) variants (p.R141H and p.P69S) are significantly reduced by approximately 42% compared to the controls, which might contribute to hypolipidemia observed in these patients (116). The PMM2 variants may affect N-glycosylation of PCSK9 and its secretion *in vivo*, even though removal or inhibition of N-glycosylation in PCSK9 does not affect its secretion in cultured cells. Alternatively, these variants may impair PCSK9 secretion indirectly by affecting unknown factors that are important for PCSK9 secretion since PMM2 is required for the synthesis of GDP-mannose, a mannose donor for N-glycosylation. Analysis of secretion of N-glycosylation defective PCSK9 mutant in *Pcsk9*$^{-/-}$ mice might provide a clue for the potential role of N-glycosylation in PCSK9 secretion *in vivo*. Nevertheless, these studies indicate that posttranslational modifications, including phosphorylation, sulfation and N-glycosylation, may affect but are not required for PCSK9 processing, secretion, stability and function.

CONCLUSION AND PERSPECTIVES

PCSK9 regulates plasma cholesterol levels and tumor-specific antigen presentation primarily through promoting LDLR and MHCI degradation, respectively. Of note, the lack of PCSK9 in humans does not cause any known notable side effects (3, 6). Therefore, PCSK9 is a promising therapeutic target to reduce the risk of the top two leading causes of mortality worldwide, cardiovascular disease and cancer. Various strategies have been or are being developed to inhibit PCSK9 (117–120) (**Table 1**). Current PCSK9 inhibitors, evolocumab and alirocumab, are humanized monoclonal anti-PCSK9 antibodies. They can significantly reduce plasma LDL cholesterol levels and cardiovascular events in patients with hypercholesterolemia and suppress tumor growth in mice. Inclisiran, a chemically synthesized siRNA targeting PCSK9 mRNA, also significantly reduces plasma LDL cholesterol levels by about 30–50% with only two injections each year. However, these strategies are expensive, limiting their widespread use. Other strategies, such as CRISPR-Cas9 gene editing and PCSK9 vaccine, are only in preclinical studies or phase I clinical trials (119, 120). Therefore, there is an urgent need for further research to elucidate the underlying mechanisms for PCSK9's impact on lipid metabolism and cancer growth. For example, (1) PCSK9 binds to LDLR with a much higher affinity at the acidic endosomal environment to block LDLR recycling. Does PCSK9 bind to MHCI in a pH-dependent manner? (2) PCSK9, LDLR and MHCI do not contain a lysosomal targeting signal; how is PCSK9/LDLR and PCSK9/MHCI complex redirected from the endosome to the lysosome for degradation? (3) Circulating PCSK9 is mainly secreted from hepatocytes and then promotes LDLR and MHCI degradation. What machinery system assists PCSK9 secretion? (4) HSPG facilitates PCSK9-promoted hepatic LDLR degradation. Is there a cofactor assisting PCSK9's action on MHCI? Answering these questions is critical to the development of innovative and more cost-effective treatment options to inhibit PCSK9-promoted degradation of LDLR and MHCI.

AUTHOR CONTRIBUTIONS

X-dX and Z-sP wrote the initial draft. G-qW and D-wZ supervised the final version. H-mG participated in the discussion and the preparation of the manuscript. MW reviewed and edited the manuscript. All authors contributed to the article and approved the submitted version.

FUNDING

This study was supported by the Natural Sciences and Engineering Research Council of Canada (RGPIN-2016-06479) and Canadian Institutes of Health Research (PS 155994). X-dX and G-qW were supported by funding from Qingyuan People's Hospital.

REFERENCES

1. Fitchett DH, Hegele RA, Verma S. Cardiology patient page. Statin intolerance. *Circulation.* (2015) 131:e389–91. doi: 10.1161/CIRCULATIONAHA.114.013189
2. Abifadel M, Varret M, Rabes JP, Allard D, Ouguerram K, Devillers M, et al. Mutations in PCSK9 cause autosomal dominant hypercholesterolemia. *Nat Genet.* (2003) 34:154–6. doi: 10.1038/ng1161
3. Cohen J, Pertsemlidis A, Kotowski IK, Graham R, Garcia CK, Hobbs HH. Low LDL cholesterol in individuals of African descent resulting from frequent nonsense mutations in PCSK9. *Nat Genet.* (2005) 37:161–5. doi: 10.1038/ng1509
4. Zhao Z, Tuakli-Wosornu Y, Lagace TA, Kinch L, Grishin NV, Horton JD, et al. Molecular characterization of loss-of-function mutations in PCSK9 and identification of a compound heterozygote. *Am J Hum Genet.* (2006) 79:514–23. doi: 10.1086/507488
5. Guo S, Xia XD, Gu HM, Zhang DW. Proprotein convertase subtilisin/Kexin-Type 9 and lipid metabolism. *Adv Exp Med Biol.* (2020) 1276:137–56. doi: 10.1007/978-981-15-6082-8_9
6. Lebeau P, Platko K, Al-Hashimi AA, Byun JH, Lhotak S, Holzapfel N, et al. Loss-of-function PCSK9 mutants evade the unfolded protein response sensor GRP78 and fail to induce endoplasmic reticulum stress when retained. *J Biol Chem.* (2018) 293:7329–43. doi: 10.1074/jbc.RA117.001049
7. Liu X, Bao X, Hu M, Chang H, Jiao M, Cheng J, et al. Inhibition of PCSK9 potentiates immune checkpoint therapy for cancer. *Nature.* (2020) 588:693–8. doi: 10.1038/s41586-020-2911-7
8. Ricci C, Ruscica M, Camera M, Rossetti L, Macchi C, Colciago A,et al. PCSK9 induces a pro-inflammatory response in macrophages. *Sci Rep.* (2018) 8:2267. doi: 10.1038/s41598-018-20425-x
9. Giunzioni I, Tavori H, Covarrubias R, Major AS, Ding L, Zhang Y, et al. Local effects of human PCSK9 on the atherosclerotic lesion. *J Pathol.* (2016) 238:52–62. doi: 10.1002/path.4630
10. Seidah NG. The PCSK9 revolution and the potential of PCSK9-based therapies to reduce LDL-cholesterol. *Glob Cardiol Sci Pract.* (2017) 2017:e201702. doi: 10.21542/gcsp.2017.2
11. Guo Q, Feng X, Zhou Y. PCSK9 variants in familial hypercholesterolemia: a comprehensive synopsis. *Front Genet.* (2020) 11:1020. doi: 10.3389/fgene.2020.01020
12. Benjannet S, Hamelin J, Chretien M, Seidah NG. Loss- and gain-of-function PCSK9 variants: cleavage specificity, dominant negative effects, and low density lipoprotein receptor (LDLR) degradation. *J Biol Chem.* (2012) 287:33745–55. doi: 10.1074/jbc.M112.399725
13. Cunningham D, Danley DE, Geoghegan KF, Griffor MC, Hawkins JL, Subashi TA, et al. Structural and biophysical studies of PCSK9 and its mutants linked to familial hypercholesterolemia. *Nat Struct Mol Biol.* (2007) 14:413–9. doi: 10.1038/nsmb1235
14. Tveten K, Holla OL, Cameron J, Strom TB, Berge KE, Laerdahl JK, et al. Interaction between the ligand-binding domain of the LDL receptor and the C-terminal domain of PCSK9 is required for PCSK9 to remain bound to the LDL receptor during endosomal acidification. *Hum Mol Genet.* (2012) 21:1402–9. doi: 10.1093/hmg/ddr578
15. Yamamoto T, Lu C, Ryan RO. A two-step binding model of PCSK9 interaction with the low density lipoprotein receptor. *J Biol Chem.* (2011) 286:5464–70. doi: 10.1074/jbc.M110.199042
16. Saavedra YG, Day R, Seidah NG. The M2 module of the Cys-His-rich domain (CHRD) of PCSK9 protein is needed for the extracellular low-density lipoprotein receptor (LDLR) degradation pathway. *J Biol Chem.* (2012) 287:43492–501. doi: 10.1074/jbc.M112.394023
17. Deng SJ, Shen Y, Gu HM, Guo S, Wu SR, Zhang DW. The role of the C-terminal domain of PCSK9 and SEC24 isoforms in PCSK9 secretion. *Biochim Biophys Acta Mol Cell Biol Lipids.* (2020) 1865:158660. doi: 10.1016/j.bbalip.2020.158660
18. Rashid S, Curtis DE, Garuti R, Anderson NN, Bashmakov Y, Ho YK, et al. Decreased plasma cholesterol and hypersensitivity to statins in mice lacking Pcsk9. *Proc Natl Acad Sci USA.* (2005) 102:5374–9. doi: 10.1073/pnas.0501652102
19. Zhang DW, Lagace TA, Garuti R, Zhao Z, McDonald M, Horton JD, et al. Binding of proprotein convertase subtilisin/kexin type 9 to epidermal growth factor-like repeat A of low density lipoprotein receptor decreases receptor recycling and increases degradation. *J Biol Chem.* (2007) 282:18602–12. doi: 10.1074/jbc.M702027200
20. Gu HM, Adijiang A, Mah M, Zhang DW. Characterization of the role of EGF-A of low-density lipoprotein receptor in PCSK9 binding. *J Lipid Res.* (2013) 54:3345–57. doi: 10.1194/jlr.M041129
21. Lagace TA, Curtis DE, Garuti R, McNutt MC, Park SW, Prather HB, et al. Secreted PCSK9 decreases the number of LDL receptors in hepatocytes and in livers of parabiotic mice. *J Clin Invest.* (2006) 116:2995–3005. doi: 10.1172/JCI29383
22. Roubtsova A, Munkonda MN, Awan Z, Marcinkiewicz J, Chamberland A, Lazure C, et al. Circulating proprotein convertase subtilisin/kexin 9 (PCSK9) regulates VLDLR protein and triglyceride accumulation in visceral adipose tissue. *Arterioscler Thromb Vasc Biol.* (2011) 31:785–91. doi: 10.1161/ATVBAHA.110.220988
23. Kwon HJ, Lagace TA, McNutt MC, Horton JD, Deisenhofer J. Molecular basis for LDL receptor recognition by PCSK9. *Proc Natl Acad Sci USA.* (2008) 105:1820–5. doi: 10.1073/pnas.0712064105
24. Zhang DW, Garuti R, Tang WJ, Cohen JC, Hobbs HH. Structural requirements for PCSK9-mediated degradation of the low-density lipoprotein receptor. *Proc Natl Acad Sci USA.* (2008) 105:13045–50. doi: 10.1073/pnas.0806312105
25. Maxwell KN, Fisher EA, Breslow JL. Overexpression of PCSK9 accelerates the degradation of the LDLR in a post-endoplasmic reticulum compartment. *Proc Natl Acad Sci USA.* (2005) 102:2069–74. doi: 10.1073/pnas.0409736102
26. Wright RS, Ray KK, Raal FJ, Kallend DG, Jaros M, Koenig W,et al. Pooled patient-level analysis of inclisiran trials in patients with familial hypercholesterolemia or atherosclerosis. *J Am Coll Cardiol.* (2021) 77:1182–93. doi: 10.1016/j.jacc.2020.12.058
27. Reyes-Soffer G, Pavlyha M, Ngai C, Thomas T, Holleran S, Ramakrishnan R, et al. Effects of PCSK9 inhibition with alirocumab on lipoprotein metabolism in healthy humans. *Circulation.* (2017) 135:352–62. doi: 10.1161/CIRCULATIONAHA.116.025253
28. Bonaca MP, Nault P, Giugliano RP, Keech AC, Pineda AL, Kanevsky E, et al. Low-density lipoprotein cholesterol lowering with evolocumab and outcomes in patients with peripheral artery disease: insights from the FOURIER trial (further cardiovascular outcomes research with PCSK9 inhibition in subjects with elevated risk). *Circulation.* (2018) 137:338–50. doi: 10.1161/CIRCULATIONAHA.117.032235
29. McNutt MC, Lagace TA, Horton JD. Catalytic activity is not required for secreted PCSK9 to reduce low density lipoprotein receptors in HepG2 cells. *J Biol Chem.* (2007) 282:20799–803. doi: 10.1074/jbc.C700095200

30. Wang Y, Huang Y, Hobbs HH, Cohen JC. Molecular characterization of proprotein convertase subtilisin/kexin type 9-mediated degradation of the LDLR. *J Lipid Res.* (2012) 53:1932–43. doi: 10.1194/jlr.M028563
31. Romagnuolo R, Scipione CA, Boffa MB, Marcovina SM, Seidah NG, Koschinsky ML. Lipoprotein(a) catabolism is regulated by proprotein convertase subtilisin/kexin type 9 through the low density lipoprotein receptor. *J Biol Chem.* (2015) 290:11649–62. doi: 10.1074/jbc.M114.611988
32. Jang H-D, Lee SE, Yang J, Lee H-C, Shin D, Lee H, et al. Cyclase-associated protein 1 is a binding partner of proprotein convertase subtilisin/kexin type-9 and is required for the degradation of low-density lipoprotein receptors by proprotein convertase subtilisin/kexin type-9. *Eur Heart J.* (2020) 41:239–52. doi: 10.1093/eurheartj/ehz566
33. DeVay RM, Shelton DL, Liang H. Characterization of proprotein convertase subtilisin/kexin type 9 (PCSK9) trafficking reveals a novel lysosomal targeting mechanism via amyloid precursor-like protein 2 (APLP2). *J Biol Chem.* (2013) 288:10805–18. doi: 10.1074/jbc.M113.453373
34. Fu T, Guan Y, Xu J, Wang Y. APP, APLP2 and LRP1 interact with PCSK9 but are not required for PCSK9-mediated degradation of the LDLR in vivo. *Biochim Biophys Acta.* (2017) 1862:883–9. doi: 10.1016/j.bbalip.2017.05.002
35. Butkinaree C, Canuel M, Essalmani R, Poirier S, Benjannet S, Asselin MC, et al. Amyloid precursor-like protein 2 and sortilin do not regulate the PCSK9 convertase-mediated low density lipoprotein receptor degradation but interact with each other. *J Biol Chem.* (2015) 290:18609–20. doi: 10.1074/jbc.M115.647180
36. Goldstein JL, Brown MS. A century of cholesterol and coronaries: from plaques to genes to statins. *Cell.* (2015) 161:161–72. doi: 10.1016/j.cell.2015.01.036
37. Grefhorst A, McNutt MC, Lagace TA, Horton JD. Plasma PCSK9 preferentially reduces liver LDL receptors in mice. *J Lipid Res.* (2008) 49:1303–11. doi: 10.1194/jlr.M800027-JLR200
38. Gustafsen C, Olsen D, Vilstrup J, Lund S, Reinhardt A, Wellner N, et al. Heparan sulfate proteoglycans present PCSK9 to the LDL receptor. *Nat Commun.* (2017) 8:503. doi: 10.1038/s41467-017-00568-7
39. Wang H, Eckel RH. Lipoprotein lipase: from gene to obesity. *Am J Physiol Endocrinol Metab.* (2009) 297:E271–88. doi: 10.1152/ajpendo.90920.2008
40. Sun H, Krauss RM, Chang JT, Teng BB. PCSK9 deficiency reduces atherosclerosis, apolipoprotein B secretion, and endothelial dysfunction. *J Lipid Res.* (2018) 59:207–23. doi: 10.1194/jlr.M078360
41. Sun XM, Eden ER, Tosi I, Neuwirth CK, Wile D, Naoumova RP, et al. Evidence for effect of mutant PCSK9 on apolipoprotein B secretion as the cause of unusually severe dominant hypercholesterolaemia. *Hum Mol Genet.* (2005) 14:1161–9. doi: 10.1093/hmg/ddi128
42. Ding Z, Liu S, Wang X, Deng X, Fan Y, Sun C, et al. Hemodynamic shear stress via ROS modulates PCSK9 expression in human vascular endothelial and smooth muscle cells and along the mouse aorta. *Antioxid Redox Signal.* (2015) 22:760–71. doi: 10.1089/ars.2014.6054
43. Ferri N, Tibolla G, Pirillo A, Cipollone F, Mezzetti A, Pacia S, et al. Proprotein convertase subtilisin kexin type 9 (PCSK9) secreted by cultured smooth muscle cells reduces macrophages LDLR levels. *Atherosclerosis.* (2012) 220:381–6. doi: 10.1016/j.atherosclerosis.2011.11.026
44. Peyot ML, Roubtsova A, Lussier R, Chamberland A, Essalmani R, Murthy Madiraju SR, et al. Substantial PCSK9 inactivation in beta-cells does not modify glucose homeostasis or insulin secretion in mice. *Biochim Biophys Acta Mol Cell Biol Lipids.* (2021) 1866:158968. doi: 10.1016/j.bbalip.2021.158968
45. Cariou B, Langhi C, Le Bras M, Bortolotti M, Le KA, Theytaz F, et al. Plasma PCSK9 concentrations during an oral fat load and after short term high-fat, high-fat high-protein and high-fructose diets. *Nutr Metab.* (2013) 10:4. doi: 10.1186/1743-7075-10-4
46. Hollstein T, Vogt A, Grenkowitz T, Stojakovic T, Marz W, Laufs U, et al. Treatment with PCSK9 inhibitors reduces atherogenic VLDL remnants in a real-world study. *Vascul Pharmacol.* (2019) 116:8–15. doi: 10.1016/j.vph.2019.03.002
47. Le May C, Kourimate S, Langhi C, Chetiveaux M, Jarry A, Comera C, et al. Proprotein convertase subtilisin kexin type 9 null mice are protected from postprandial triglyceridemia. *Arterioscler Thromb Vasc Biol.* (2009) 29:684–90. doi: 10.1161/ATVBAHA.108.181586
48. Rashid S, Tavori H, Brown PE, Linton MF, He J, Giunzioni I, et al. Proprotein convertase subtilisin kexin type 9 promotes intestinal overproduction of triglyceride-rich apolipoprotein B lipoproteins through both low-density lipoprotein receptor-dependent and -independent mechanisms. *Circulation.* (2014) 130:431–41. doi: 10.1161/CIRCULATIONAHA.113.006720
49. Watts GF, Gidding SS, Mata P, Pang J, Sullivan DR, Yamashita S, et al. Familial hypercholesterolaemia: evolving knowledge for designing adaptive models of care. *Nat Rev Cardiol.* (2020) 17:360–77. doi: 10.1038/s41569-019-0325-8
50. Taskinen MR, Bjornson E, Andersson L, Kahri J, Porthan K, Matikainen N, et al. Impact of proprotein convertase subtilisin/kexin type 9 inhibition with evolocumab on the postprandial responses of triglyceride-rich lipoproteins in type II diabetic subjects. *J Clin Lipidol.* (2020) 14:77–87. doi: 10.1016/j.jacl.2019.12.003
51. Drouin-Chartier JP, Tremblay AJ, Hogue JC, Lemelin V, Lamarche B, Couture P. Plasma PCSK9 correlates with apoB-48-containing triglyceride-rich lipoprotein production in men with insulin resistance. *J Lipid Res.* (2018) 59:1501–9. doi: 10.1194/jlr.M086264
52. Taskinen MR, Bjornson E, Kahri J, Soderlund S, Matikainen N, Porthan K, et al. Effects of Evolocumab on the Postprandial Kinetics of Apo (Apolipoprotein) B100- and B48-Containing Lipoproteins in Subjects With Type 2 Diabetes. *Arterioscler Thromb Vasc Biol.* (2020) 41:962–75 doi: 10.1161/ATVBAHA.120.315446
53. Rohlmann A, Gotthardt M, Hammer RE, Herz J. Inducible inactivation of hepatic LRP gene by cre-mediated recombination confirms role of LRP in clearance of chylomicron remnants. *J Clin Invest.* (1998) 101:689–95. doi: 10.1172/JCI1240
54. O'Donoghue ML, Fazio S, Giugliano RP, Stroes ESG, Kanevsky E, Gouni-Berthold I, et al. Lipoprotein(a), PCSK9 inhibition, and cardiovascular risk. *Circulation.* (2019) 139:1483–92. doi: 10.1161/CIRCULATIONAHA.118.037184
55. Farmakis I, Doundoulakis I, Pagiantza A, Zafeiropoulos S, Antza C, Karvounis H, et al. Lipoprotein(a) reduction with proprotein convertase subtilisin/kexin type 9 inhibitors: a systematic review and meta-analysis. *J Cardiovasc Pharmacol.* (2021) 77:397–407. doi: 10.1097/FJC.0000000000000963
56. Blom DJ, Harada-Shiba M, Rubba P, Gaudet D, Kastelein JJP, Charng MJ, et al. Efficacy and safety of alirocumab in adults with homozygous familial hypercholesterolemia: the ODYSSEY HoFH trial. *J Am Coll Cardiol.* (2020) 76:131–42. doi: 10.1016/j.jacc.2020.05.027
57. Stoekenbroek RM, Lambert G, Cariou B, Hovingh GK. Inhibiting PCSK9 - biology beyond LDL control. *Nat Rev Endocrinol.* (2018) 15:52–62. doi: 10.1038/s41574-018-0110-5
58. Jhunjhunwala S, Hammer C, Delamarre L. Antigen presentation in cancer: insights into tumour immunogenicity and immune evasion. *Nat Rev Cancer.* (2021) 21:298–312. doi: 10.1038/s41568-021-00339-z
59. Yuan J, Cai T, Zheng X, Ren Y, Qi J, Lu X, et al. Potentiating CD8(+) T cell antitumor activity by inhibiting PCSK9 to promote LDLR-mediated TCR recycling and signaling. *Protein Cell.* (2021) 12:240–60. doi: 10.1007/s13238-021-00821-2
60. Tang ZH, Peng J, Ren Z, Yang J, Li TT, Li TH, et al. New role of PCSK9 in atherosclerotic inflammation promotion involving the TLR4/NF-kappaB pathway. *Atherosclerosis.* (2017) 262:113–22. doi: 10.1016/j.atherosclerosis.2017.04.023
61. Guo Y, Yan B, Tai S, Zhou S, Zheng XL. PCSK9: associated with cardiac diseases and their risk factors? *Arch Biochem Biophys.* (2021) 704:108717. doi: 10.1016/j.abb.2020.108717
62. Xu X, Cui Y, Cao L, Zhang Y, Yin Y, Hu X. PCSK9 regulates apoptosis in human lung adenocarcinoma A549 cells via endoplasmic reticulum stress and mitochondrial signaling pathways. *Exp Ther Med.* (2017) 13:1993–9. doi: 10.3892/etm.2017.4218
63. Marimuthu A, Subbannayya Y, Sahasrabuddhe NA, Balakrishnan L, Syed N, Sekhar NR, et al. SILAC-based quantitative proteomic analysis of gastric cancer secretome. *Proteomics Clin Appl.* (2013) 7:355–66. doi: 10.1002/prca.201200069
64. Zhang SZ, Zhu XD, Feng LH, Li XL, Liu XF, Sun HC, et al. PCSK9 promotes tumor growth by inhibiting tumor cell apoptosis in hepatocellular carcinoma. *Exp Hematol Oncol.* (2021) 10:25. doi: 10.1186/s40164-021-00218-1

65. Gan SS, Ye JQ, Wang L, Qu FJ, Chu CM, Tian YJ, et al. Inhibition of PCSK9 protects against radiation-induced damage of prostate cancer cells. *Onco Targets Ther.* (2017) 10:2139–46. doi: 10.2147/OTT.S129413
66. Tao R, Xiong X, DePinho RA, Deng CX, Dong XC. FoxO3 transcription factor and Sirt6 deacetylase regulate low density lipoprotein (LDL)-cholesterol homeostasis via control of the proprotein convertase subtilisin/kexin type 9 (Pcsk9) gene expression. *J Biol Chem.* (2013) 288:29252–9. doi: 10.1074/jbc.M113.481473
67. Li H, Liu J. The novel function of HINFP as a co-activator in sterol-regulated transcription of PCSK9 in HepG2 cells. *Biochem J.* (2012) 443:757–68. doi: 10.1042/BJ20111645
68. Lohoff FW, Sorcher JL, Rosen AD, Mauro KL, Fanelli RR, Momenan R, et al. Methylomic profiling and replication implicates deregulation of PCSK9 in alcohol use disorder. *Mol Psychiatry.* (2018) 23:1900–10. doi: 10.1038/mp.2017.168
69. Jeong HJ, Lee HS, Kim KS, Kim YK, Yoon D, Park SW. Sterol-dependent regulation of proprotein convertase subtilisin/kexin type 9 expression by sterol-regulatory element binding protein-2. *J Lipid Res.* (2008) 49:399–409. doi: 10.1194/jlr.M700443-JLR200
70. Dong B, Wu M, Li H, Kraemer FB, Adeli K, Seidah NG, et al. Strong induction of PCSK9 gene expression through HNF1alpha and SREBP2: mechanism for the resistance to LDL-cholesterol lowering effect of statins in dyslipidemic hamsters. *J Lipid Res.* (2010) 51:1486–95. doi: 10.1194/jlr.M003566
71. Dubuc G, Chamberland A, Wassef H, Davignon J, Seidah NG, Bernier L, et al. Statins upregulate PCSK9, the gene encoding the proprotein convertase neural apoptosis-regulated convertase-1 implicated in familial hypercholesterolemia. *Arterioscler Thromb Vasc Biol.* (2004) 24:1454–9. doi: 10.1161/01.ATV.0000134621.14315.43
72. Poirier S, Prat A, Marcinkiewicz E, Paquin J, Chitramuthu BP, Baranowski D, et al. Implication of the proprotein convertase NARC-1/PCSK9 in the development of the nervous system. *J Neurochem.* (2006) 98:838–50. doi: 10.1111/j.1471-4159.2006.03928.x
73. Li H, Dong B, Park SW, Lee HS, Chen W, Liu J. Hepatocyte nuclear factor 1alpha plays a critical role in PCSK9 gene transcription and regulation by the natural hypocholesterolemic compound berberine. *J Biol Chem.* (2009) 284:28885–95. doi: 10.1074/jbc.M109.052407
74. Ai D, Chen C, Han S, Ganda A, Murphy AJ, Haeusler R, et al. Regulation of hepatic LDL receptors by mTORC1 and PCSK9 in mice. *J Clin Invest.* (2012) 122:1262–70. doi: 10.1172/JCI61919
75. Lai Q, Giralt A, Le May C, Zhang L, Cariou B, Denechaud PD, et al. E2F1 inhibits circulating cholesterol clearance by regulating Pcsk9 expression in the liver. *JCI Insight.* (2017) 2:e89729. doi: 10.1172/jci.insight.89729
76. Blesa S, Vernia S, Garcia-Garcia AB, Martinez-Hervas S, Ivorra C, Gonzalez-Albert V, et al. A new PCSK9 gene promoter variant affects gene expression and causes autosomal dominant hypercholesterolemia. *J Clin Endocrinol Metab.* (2008) 93:3577–83. doi: 10.1210/jc.2008-0269
77. Tai MH, Chen PK, Chen PY, Wu MJ, Ho CT, Yen JH. Curcumin enhances cell-surface LDLR level and promotes LDL uptake through downregulation of PCSK9 gene expression in HepG2 cells. *Mol Nutr Food Res.* (2014) 58:2133–45. doi: 10.1002/mnfr.201400366
78. Chang HY, Wu JR, Gao WY, Lin HR, Chen PY, Chen CI, et al. The cholesterol-modulating effect of methanol extract of pigeon pea (*Cajanus cajan* (L.) Millsp.) leaves on regulating LDLR and PCSK9 expression in HepG2 cells. *Molecules.* (2019) 24:493. doi: 10.3390/molecules24030493
79. Cui CJ, Jin JL, Guo LN, Sun J, Wu NQ, Guo YL, et al. Beneficial impact of epigallocatechingallate on LDL-C through PCSK9/LDLR pathway by blocking HNF1alpha and activating FoxO3a. *J Transl Med.* (2020) 18:195. doi: 10.1186/s12967-020-02362-4
80. Wang D, Yang X, Chen Y, Gong K, Yu M, Gao Y, et al. Ascorbic acid enhances low-density lipoprotein receptor expression by suppressing proprotein convertase subtilisin/kexin 9 expression. *J Biol Chem.* (2020) 295:15870–15882. doi: 10.1074/jbc.RA120.015623
81. Gao WY, Chen PY, Chen SF, Wu MJ, Chang HY, Yen JH. Pinostrobin inhibits proprotein convertase subtilisin/kexin-type 9 (PCSK9) gene expression through the modulation of FoxO3a protein in HepG2 cells. *J Agric Food Chem.* (2018) 66:6083–93. doi: 10.1021/acs.jafc.8b02559
82. Chen HC, Chen PY, Wu MJ, Tai MH, Yen JH. Tanshinone IIA modulates low density lipoprotein uptake via down-regulation of PCSK9 gene expression in HepG2 cells. *PLoS ONE.* (2016) 11:e0162414. doi: 10.1371/journal.pone.0162414
83. Wang X, Chen X, Zhang X, Su C, Yang M, He W, et al. A small-molecule inhibitor of PCSK9 transcription ameliorates atherosclerosis through the modulation of FoxO1/3 and HNF1alpha. *EBioMedicine.* (2020) 52:102650. doi: 10.1016/j.ebiom.2020.102650
84. Fan TY, Yang YX, Zeng QX, Wang XL, Wei W, Guo XX, et al. Structure-activity relationship and biological evaluation of berberine derivatives as PCSK9 down-regulating agents. *Bioorg Chem.* (2021) 113:104994. doi: 10.1016/j.bioorg.2021.104994
85. Lin Z, Pan X, Wu F, Ye D, Zhang Y, Wang Y, et al. Fibroblast growth factor 21 prevents atherosclerosis by suppression of hepatic sterol regulatory element-binding protein-2 and induction of adiponectin in mice. *Circulation.* (2015) 131:1861–71. doi: 10.1161/CIRCULATIONAHA.115.015308
86. Langhi C, Le May C, Kourimate S, Caron S, Staels B, Krempf M, et al. Activation of the farnesoid X receptor represses PCSK9 expression in human hepatocytes. *FEBS Lett.* (2008) 582:949–55. doi: 10.1016/j.febslet.2008.02.038
87. Kourimate S, Le May C, Langhi C, Jarnoux AL, Ouguerram K, Zair Y, et al. Dual mechanisms for the fibrate-mediated repression of proprotein convertase subtilisin/kexin type 9. *J Biol Chem.* (2008) 283:9666–73. doi: 10.1074/jbc.M705831200
88. Momtazi AA, Banach M, Pirro M, Katsiki N, Sahebkar A. Regulation of PCSK9 by nutraceuticals. *Pharmacol Res.* (2017) 120:157–69. doi: 10.1016/j.phrs.2017.03.023
89. Melone M, Wilsie L, Palyha O, Strack A, Rashid S. Discovery of a new role of human resistin in hepatocyte low-density lipoprotein receptor suppression mediated in part by proprotein convertase subtilisin/kexin type 9. *J Am Coll Cardiol.* (2012) 59:1697–705. doi: 10.1016/j.jacc.2011.11.064
90. Patitucci C, Couchy G, Bagattin A, Caneque T, de Reynies A, Scoazec JY, et al. Hepatocyte nuclear factor 1alpha suppresses steatosis-associated liver cancer by inhibiting PPARgamma transcription. *J Clin Invest.* (2017) 127:1873–88. doi: 10.1172/JCI90327
91. Dong J, He M, Li J, Pessentheiner AR, Wang C, Zhang J, et al. MicroRNA-483 ameliorates hypercholesterolemia by inhibiting PCSK9 production. *JCI Insight.* (2020) 5:e143812. doi: 10.1172/jci.insight.143812
92. Naeli P, Mirzadeh Azad F, Malakootian M, Seidah NG, Mowla SJ. Post-transcriptional regulation of PCSK9 by miR-191, miR-222, and miR-224. *Front Genet.* (2017) 8:189. doi: 10.3389/fgene.2017.00189
93. Los B, Borges JB, Oliveira VF, Freitas RC, Dagli-Hernandez C, Bortolin RH, et al. Functional analysis of PCSK9 3'UTR variants and mRNA-miRNA interactions in patients with familial hypercholesterolemia. *Epigenomics.* (2021) 13:779–791. doi: 10.2217/epi-2020-0462
94. Xu X, Dong Y, Ma N, Kong W, Yu C, Gong L, et al. MiR-337-3p lowers serum LDL-C level through targeting PCSK9 in hyperlipidemic mice. *Metabolism.* (2021) 119:154768. doi: 10.1016/j.metabol.2021.154768
95. Decourt C, Janin A, Moindrot M, Chatron N, Nony S, Muntaner M, et al. PCSK9 post-transcriptional regulation: role of a 3'UTR microRNA-binding site variant in linkage disequilibrium with c.1420G. *Atherosclerosis.* (2020) 314:63–70. doi: 10.1016/j.atherosclerosis.2020.10.010
96. Alvarez ML, Khosroheidari M, Eddy E, Done SC. MicroRNA-27a decreases the level and efficiency of the LDL receptor and contributes to the dysregulation of cholesterol homeostasis. *Atherosclerosis.* (2015) 242:595–604. doi: 10.1016/j.atherosclerosis.2015.08.023
97. Broughton JP, Lovci MT, Huang JL, Yeo GW, Pasquinelli AE. Pairing beyond the seed supports MicroRNA targeting specificity. *Mol Cell.* (2016) 64:320–33. doi: 10.1016/j.molcel.2016.09.004
98. Jackson AL, Bartz SR, Schelter J, Kobayashi SV, Burchard J, Mao M, et al. Expression profiling reveals off-target gene regulation by RNAi. *Nat Biotechnol.* (2003) 21:635–7. doi: 10.1038/nbt831
99. Pecot CV, Calin GA, Coleman RL, Lopez-Berestein G, Sood AK. RNA interference in the clinic: challenges and future directions. *Nat Rev Cancer.* (2011) 11:59–67. doi: 10.1038/nrc2966
100. Petersen DN, Hawkins J, Ruangsiriluk W, Stevens KA, Maguire BA, O'Connell TN, et al. A small-molecule anti-secretagogue of PCSK9 targets the 80S ribosome to inhibit PCSK9 protein translation. *Cell Chem Biol.* (2016) 23:1362–71. doi: 10.1016/j.chembiol.2016.08.016

101. Liu S, Deng X, Zhang P, Wang X, Fan Y, Zhou S, et al. Blood flow patterns regulate PCSK9 secretion via MyD88-mediated pro-inflammatory cytokines. *Cardiovasc Res.* (2020) 116:1721–32. doi: 10.1093/cvr/cvz262
102. Zaid A, Roubtsova A, Essalmani R, Marcinkiewicz J, Chamberland A, Hamelin J, et al. Proprotein convertase subtilisin/kexin type 9 (PCSK9): hepatocyte-specific low-density lipoprotein receptor degradation and critical role in mouse liver regeneration. *Hepatology.* (2008) 48:646–54. doi: 10.1002/hep.22354
103. Chorba JS, Galvan AM, Shokat KM. Stepwise processing analyses of the single-turnover PCSK9 protease reveal its substrate sequence specificity and link clinical genotype to lipid phenotype. *J Biol Chem.* (2018) 293:1875–86. doi: 10.1074/jbc.RA117.000754
104. Benjannet S, Rhainds D, Essalmani R, Mayne J, Wickham L, Jin W, et al. NARC-1/PCSK9 and its natural mutants: zymogen cleavage and effects on the low density lipoprotein (LDL) receptor and LDL cholesterol. *J Biol Chem.* (2004) 279:48865–75. doi: 10.1074/jbc.M409699200
105. Du F, Hui Y, Zhang M, Linton MF, Fazio S, Fan D. Novel domain interaction regulates secretion of proprotein convertase subtilisin/kexin type 9 (PCSK9) protein. *J Biol Chem.* (2011) 286:43054–61. doi: 10.1074/jbc.M111.273474
106. Chen XW, Wang H, Bajaj K, Zhang P, Meng ZX, Ma D, et al. SEC24A deficiency lowers plasma cholesterol through reduced PCSK9 secretion. *Elife.* (2013) 2:e00444. doi: 10.7554/eLife.00444.017
107. Emmer BT, Hesketh GG, Kotnik E, Tang VT, Lascuna PJ, Xiang J, et al. The cargo receptor SURF4 promotes the efficient cellular secretion of PCSK9. *Elife.* (2018) 7:e38839. doi: 10.7554/eLife.38839.026
108. Shen Y, Wang B, Deng S, Zhai L, Gu HM, Alabi A, et al. Surf4 regulates expression of proprotein convertase subtilisin/kexin type 9 (PCSK9) but is not required for PCSK9 secretion in cultured human hepatocytes. *Biochim Biophys Acta Mol Cell Biol Lipids.* (2020) 1865:158555. doi: 10.1016/j.bbalip.2019.158555
109. Wang B, Shen Y, Zhai L, Xia X, Gu HM, Wang M, et al. Atherosclerosis-associated hepatic secretion of VLDL but not PCSK9 is dependent on cargo receptor protein Surf4. *J Lipid Res.* (2021) 62:100091. doi: 10.1016/j.jlr.2021.100091
110. Rogers MA, Hutcheson JD, Okui T, Goettsch C, Singh SA, Halu A, et al. Dynamin-related protein 1 inhibition reduces hepatic PCSK9 secretion. *Cardiovasc Res.* (2021) 117:2340–53. doi: 10.1093/cvr/cvab034
111. Gustafsen C, Kjolby M, Nyegaard M, Mattheisen M, Lundhede J, Buttenschon H, et al. The hypercholesterolemia-risk gene SORT1 facilitates PCSK9 secretion. *Cell Metab.* (2014) 19:310–8. doi: 10.1016/j.cmet.2013.12.006
112. Dewpura T, Raymond A, Hamelin J, Seidah NG, Mbikay M, Chretien M, et al. PCSK9 is phosphorylated by a Golgi casein kinase-like kinase ex vivo and circulates as a phosphoprotein in humans. *FEBS J.* (2008) 275:3480–93. doi: 10.1111/j.1742-4658.2008.06495.x
113. Ben Djoudi Ouadda A, Gauthier MS, Susan-Resiga D, Girard E, Essalmani R, Black M, et al. Ser-phosphorylation of PCSK9 (proprotein convertase subtilisin-kexin 9) by Fam20C (family with sequence similarity 20, member C) kinase enhances its ability to degrade the LDLR (low-density lipoprotein receptor). *Arterioscler Thromb Vasc Biol.* (2019) 39:1996–2013. doi: 10.1161/ATVBAHA.119.313247
114. Zhang H, Zhu Q, Cui J, Wang Y, Chen MJ, Guo X, et al. Structure and evolution of the Fam20 kinases. *Nat Commun.* (2018) 9:1218. doi: 10.1038/s41467-018-03615-z
115. Benjannet S, Rhainds D, Hamelin J, Nassoury N, Seidah NG. The proprotein convertase (PC) PCSK9 is inactivated by furin and/or PC5/6A: functional consequences of natural mutations and post-translational modifications. *J Biol Chem.* (2006) 281:30561–72. doi: 10.1074/jbc.M606495200
116. Chong M, Yoon G, Susan-Resiga D, Chamberland A, Cheillan D, Pare G, et al. Hypolipidaemia among patients with PMM2-CDG is associated with low circulating PCSK9 levels: a case report followed by observational and experimental studies. *J Med Genet.* (2020) 57:11–17. doi: 10.1136/jmedgenet-2019-106102
117. Catapano AL, Pirillo A, Norata GD. New pharmacological approaches to target PCSK9. *Curr Atheroscler Rep.* (2020) 22:24. doi: 10.1007/s11883-020-00847-7
118. Katzmann JL, Gouni-Berthold I, Laufs U. PCSK9 inhibition: insights from clinical trials and future prospects. *Front Physiol.* (2020) 11:595819. doi: 10.3389/fphys.2020.595819
119. Musunuru K, Chadwick AC, Mizoguchi T, Garcia SP, DeNizio JE, Reiss CW, et al. *In vivo* CRISPR base editing of PCSK9 durably lowers cholesterol in primates. *Nature.* (2021) 593:429–34. doi: 10.1038/s41586-021-03534-y
120. Zeitlinger M, Bauer M, Reindl-Schwaighofer R, Stoekenbroek RM, Lambert G, Berger-Sieczkowski E, et al. A phase I study assessing the safety, tolerability, immunogenicity, and low-density lipoprotein cholesterol-lowering activity of immunotherapeutics targeting PCSK9. *Eur J Clin Pharmacol.* (2021) 77:1473–1484. doi: 10.1007/s00228-021-03149-2

Conflict of Interest: The authors declare that the research was conducted in the absence of any commercial or financial relationships that could be construed as a potential conflict of interest.

Publisher's Note: All claims expressed in this article are solely those of the authors and do not necessarily represent those of their affiliated organizations, or those of the publisher, the editors and the reviewers. Any product that may be evaluated in this article, or claim that may be made by its manufacturer, is not guaranteed or endorsed by the publisher.

Copyright © 2021 Xia, Peng, Gu, Wang, Wang and Zhang. This is an open-access article distributed under the terms of the Creative Commons Attribution License (CC BY). The use, distribution or reproduction in other forums is permitted, provided the original author(s) and the copyright owner(s) are credited and that the original publication in this journal is cited, in accordance with accepted academic practice. No use, distribution or reproduction is permitted which does not comply with these terms.

frontiers in Cardiovascular Medicine

REVIEW
published: 25 October 2021
doi: 10.3389/fcvm.2021.768119

Obesity and Cardiovascular Disease: The Emerging Role of Inflammation

Rana Khafagy[1,2,3] *and Satya Dash*[2,3]*

[1] Department of Pharmacy, The Hospital for Sick Children, Toronto, ON, Canada, [2] Banting & Best Diabetes Centre, University of Toronto, Toronto, ON, Canada, [3] Department of Medicine, University Health Network, Toronto, ON, Canada

Obesity is a growing public health challenge across the globe. It is associated with increased morbidity and mortality. Cardiovascular disease (CVD) is the leading cause of mortality for people with obesity. Current strategies to reduce CVD are largely focused on addressing traditional risk factors such as dyslipidemia, type 2 diabetes (T2D) and hypertension. Although this approach is proven to reduce CVD, substantial residual risk remains for people with obesity. This necessitates a better understanding of the etiology of CVD in people with obesity and alternate therapeutic approaches. Reducing inflammation may be one such strategy. A wealth of animal and human data indicates that obesity is associated with adipose tissue and systemic inflammation. Inflammation is a known contributor to CVD in humans and can be successfully targeted to reduce CVD. Here we will review the etiology and pathogenesis of inflammation in obesity associated metabolic disease as well as CVD. We will review to what extent these associations are causal based on human genetic studies and pharmacological studies. The available data suggests that anti-inflammatory treatments can be used to reduce CVD, but off-target effects such as increased infection have precluded its broad therapeutic application to date. The role of anti-inflammatory therapies in improving glycaemia and metabolic parameters is less established. A number of clinical trials are currently ongoing which are evaluating anti-inflammatory agents to lower CVD. These studies will further clarify whether anti-inflammatory agents can safely reduce CVD.

Keywords: obesity, cardiovascular disease(s), inflammation, atherosclerosis, genetic pathway

OPEN ACCESS

Edited by:
Jue Zhang,
Versiti Blood Research Institute, United States

Reviewed by:
Ziyu Zhang,
Versiti Blood Research Institute, United States
Minqi Huang,
Marshall University, United States

***Correspondence:**
Satya Dash
satya.dash@uhn.ca

Specialty section:
This article was submitted to Lipids in Cardiovascular Disease, a section of the journal Frontiers in Cardiovascular Medicine

Received: *31 August 2021*
Accepted: *27 September 2021*
Published: *25 October 2021*

Citation:
Khafagy R and Dash S (2021) Obesity and Cardiovascular Disease: The Emerging Role of Inflammation. Front. Cardiovasc. Med. 8:768119. doi: 10.3389/fcvm.2021.768119

INTRODUCTION

Obesity is a chronic disease which increases mortality and morbidity and has reached epidemic proportions (1, 2). Recent data estimates that roughly 604 million adults and 108 million children worldwide are obese (3). This has led to an increase in obesity-related comorbidities including cardiovascular disease, type 2 diabetes (T2D), fatty liver disease, dementia, osteoarthritis, obstructive sleep apnea, and several cancers (3–5). Cardiovascular disease (CVD) is of particular concern due to its significant mortality, strain on healthcare systems, and loss of labor productivity (6). Despite therapeutic progress, CVD is the leading cause of mortality in people with obesity, accounting for ∼70% of deaths in people with obesity (5, 6).

The increased risk of CVD, and in particular atherosclerotic CVD (ACVD), in people with obesity is to a large extent mediated by traditional established risk factors such as insulin resistance, dyslipidemia, T2D, hypertension, and obstructive sleep apnea (OSA) (7). Despite improved treatments to target these traditional risk factors, people with obesity remain at risk of ACVD,

suggesting that additional factors play a role (7). Recent data indicates that inflammation is an important contributor to ACVD (8, 9).

Notably, obesity is associated with chronic low-grade inflammation, which is a plausible mediator of the increased CVD seen in people with obesity (10–14). Here we will review the association between inflammation, obesity and ACVD. As genetically validated therapeutic targets have increased likelihood of success, we will specifically focus on the genetic evidence for a causal association between inflammation and cardio-metabolic disease.

THE ASSOCIATION BETWEEN OBESITY AND ESTABLISHED CVD RISK FACTORS

Obesity is a chronic disease in which excess adiposity impairs health (15). It is associated with insulin resistance, dyslipidemia, T2D, hypertension, and OSA, which are established CVD risk factors (7, 14). Although conventionally defined by a body mass index (BMI; weight in kilograms divided by square of height in meters) >30, this does not uniformly stratify patients at risk of cardiometabolic disease (16, 17). In contrast, waist-to-hip ratio (WHR) is a better predictor of both metabolic disease and myocardial infarction compared to BMI (16, 17). In a recent observational study from Holland which included participants from multiple ethnic groups (African Surinamese, South Asian Surinamese, Turkish, Moroccan, Ghanaian, and Dutch Caucasian), WHR was the most reliable predictor of T2D, overall and across ethnic groups, in both men and women (18). The receiver operated curves (ROC) for WHR was 0.78 in men and 0.81 for women (18). The ROC for BMI was 0.68 and 0.74 in men and women, respectively (18). Observational data also indicates that the odds ratio for myocardial infarction significantly increased for every successive WHR quintile (1.15, 1.39, 1.9, and 2.52, respectively) (17). Risk of myocardial infarction for those in the top two quintiles of BMI was 7.7%, compared to 24.3% for the top two quintiles of WHR (17). For each 1 standard deviation increase in WHR, the odds ratio of myocardial infarction increased by 1.37, even following adjustment for BMI (17). In contrast, the odds ratio increased by 1.10 for BMI and 1.02 when adjusted for WHR (17).

OBESITY AND INSULIN RESISTANCE IN T2D

Increased WHR, a predictor of insulin resistance and T2D, is associated with increased centripetal adiposity and/or lack of femoro-gluteal adiposity (16, 19). Genetic analyses suggest that these are causal associations mediated by reduced adipose storage capacity (7, 20). Weight gain in the presence of reduced adipose storage capacity leads to ectopic lipid deposition in the liver, skeletal muscle, and pancreas and increase in visceral adipose tissue (**Figure 1**) (13, 14). The BMI threshold at which this occurs is variable and influenced by age, ethnicity, sex, and genetic factors (13, 14). Although obesity rates are higher in women, pre-menopausal women are protected from metabolic disease (21–26). Conversely, men develop metabolic disease at lower BMI (21–26).

Ectopic lipid in liver and skeletal muscle has been causally implicated in insulin resistance via lipid intermediaries such as diacylglycerol and ceramides (27, 28). Pancreatic lipid deposition likely impairs beta cell function (29). Weight loss of 5–10% can reduce ectopic lipid, thus improving insulin sensitivity and glycemica (30). Greater weight loss of ∼15% or more, either through reduced caloric intake or bariatric surgery (the most efficacious weight loss treatment), can reverse ectopic lipid deposition and potentially reverse insulin resistance and T2D (29, 31–33).

OBESITY AND INSULIN RESISTANCE IN DYSLIPIDEMIA

Patients with obesity and insulin resistance frequently have elevated triglyceride (TG), triglyceride rich lipoproteins (TRL), low high density lipoproteins (HDL), and increased small dense low density lipoproteins (LDL) (34). The increase in TG and TRL is likely mediated by compensatory hyperinsulinaemia, secondary to insulin resistance in the presence of increased lipid flux to liver and intetsine (34). Consequently, hepatic lipogenesis, and production of TRL from liver (very low-density lipoprotein secreted in the fasted and post-prandial state) and intestine (chylomicrons secreted after meals) increases (34). Increased TG/TRL results in triglyceride enriched HDL which has enhanced hepatic clearance which reduces reverse cholesterol transport and lowers HDL. Increased TRL also yields smaller dense LDL particles (13). TRL undergo lipolysis to yield remnant particles. Both TRL remnants and small dense LDL likely have atherogenic properties (13). Human genetic studies have consistently implicated TRL as a causative risk factor for CVD (35–39).

Weight loss improves dyslipidemia in patients with insulin resistance (13). Weight loss through lifestyle intervention, pharmacotherapy, and bariatric surgery have been shown to lower plasma triglycerides (TG) and increase plasma HDL but whether this translates to lower CVD is not conclusively established (40–42) Pharmacotherapy to reduce plasma TG, which does not always result in reduced TRL/TRL remnant particle number, has not consistently translated to reduced CVD (13).

OBESITY AND INSULIN RESISTANCE IN HYPERTENSION

Obesity is estimated to contribute to ∼70% of the risk for primary/essential hypertension (14, 16). Mechanical effects of visceral fat on natriuresis, leptin-mediated sympathetic nervous system activation as well as increased renin-aldosterone action likely contribute to obesity-associated hypertension (43–45).

Obesity is associated with a 2-fold increased risk in OSA and prevalence of OSA in those with obesity has been

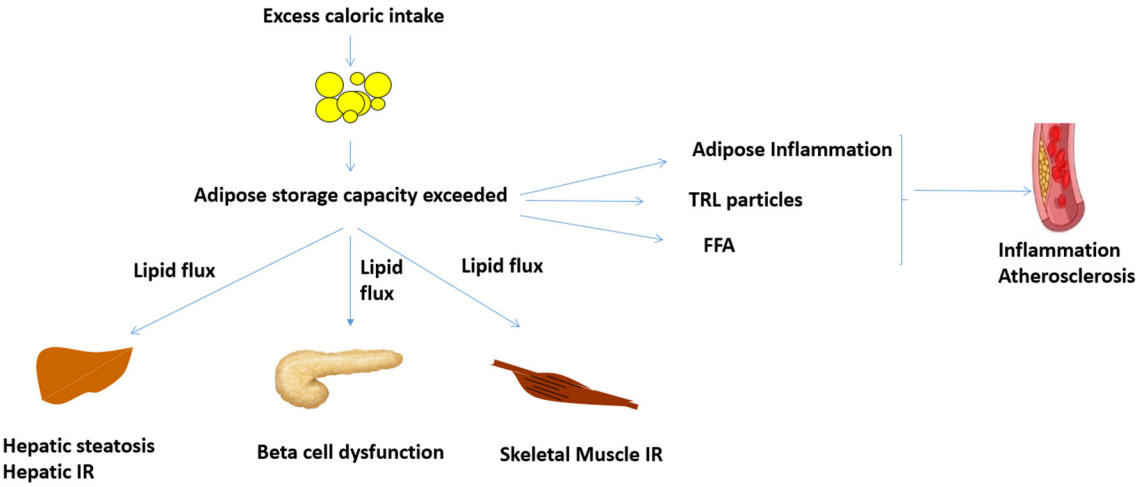

FIGURE 1 | Proposed mechanisms linking obesity, inflammation and cardiovascular disease. When adipose storage capacity is exceeded, increased lipid flux, and ectopic lipid in liver, skeletal muscle, and pancreas reduce insulin sensitivity and beta cell function. Compromised adipose storage is also associated with adipose and systemic inflammation, which can potentially potentiate atheroma development. Increased TRL and FFA, which are features of insulin resistance, may also increase inflammation and atheroma development. *FFA, free fatty acids; IR, insulin resistance; TRL, triglyceride rich lipoproteins*.

reported to be ∼45% (46, 47). Treatment of OSA with continuous positive airway pressure (CPAP) therapy induces small but significant improvement in hypertension (48). Weight loss through lifestyle changes, the medication liraglutide and bariatric surgery attenuates many of the underlying pathological processes contributing to hypertension and improves/resolves hypertension, especially early in the course of the disease before end organ damage (40, 41, 43, 49).

OBESITY, INSULIN RESISTANCE AND INFLAMMATION

As alluded to earlier, compromised adipose storage capacity in the setting of weight gain is causally associated with cardiometabolic disease. WHR is a better predictor of compromised adipose storage and cardiometabolic disease than BMI (16, 19). Compromised adipose storage is associated with adipose hyperplasia and hypertrophy and hypoxia with apoptosis (50, 51). This is associated with recruitment of inflammatory cells including macrophages, neutrophils, and lymphocytes (50). Compromised adipose storage is also associated with increased visceral adipose tissue and visceral adipose inflammation (50). Adipose tissue macrophages in insulin resistant states are polarized to a more inflammatory phenotype and secrete inflammatory cytokines including tumor necrosis factor-alpha (TNF-alpha), interleukin-1beta and interleukin-6 (**Table 1**) (50, 52). Administration of TNF-alpha in mice induces insulin resistance, while attenuation of TNF-alpha with genetic or pharmacologic manipulation protects against metabolic dysfunction (52). TNF-alpha has been shown to increase the activity of kinases such as c-Jun N-terminal kinases (JNK 1 and 2) and I kappa B Kinase (IKK), which phosphorylate insulin receptor substrate at serine residues to impair insulin action (52). Adipose inflammation is also associated with recruitment of neutrophils which release neutrophil elastase, promoting further increase in adipose tissue macrophage infiltration (52). Innate lymphoid cells, CD4+ helper T cells, cytotoxic CD8+ cells and innate-like T cells further propagate inflammation with secretion of inflammatory cytokines including, TNF-alpha and gamma-interferon (50). In animal models, gamma-interferon has been implicated in impaired insulin signaling, reduced adipogenesis, and adipose storage via JAK-STAT signaling (50). Depleting these sub-populations of lymphocytes in obesity in mouse models is associated with protection against metabolic disease (50).

Free fatty acids, which are increased in obesity and insulin resistance, can directly impact inflammation. Palmitate, which is increased in high fat fed mice, activates the NACHT, LRR, and PYD domain-containing protein 3 (NLRP3) inflammasome protein complex which secretes caspase-1 (52). This results in cleavage and secretion of active IL-1beta and Il-18 from macrophages (52, 53). In addition to insulin resistance, IL-1 beta has been implicated in impaired insulin secretion and T2D (53). Fatty acid can also promote inflammation via activating TLR4 (toll like receptor 4), which in turn can activate macrophages and TNF-alpha production (52).

IMPACT OF INFLAMMATION ON ATHEROMA DEVELOPMENT

Inflammation plays an important role in the development of an atheroma (8, 9). Blood vessels have three layers: tunica intima (facing the lumen), tunica media, and tunica adventitia. Vessel wall damage in the tunica intima layer and endothelial dysfunction are early steps in the pathogenesis of atherosclerosis (8). Under these circumstances, endothelial

TABLE 1 | Critical regulators of inflammation in obesity and CVD (50, 52).

	Impact on metabolic function	Impact on atherosclerosis
Free fatty acid	- Contributes ectopic lipid deposition and insulin resistance and type 2 diabetes	- Activates NLRP3 inflammasome and TLR4 in macrophages
IL-6	- Impairs insulin sensitivity and increases T2D risk in genetic analyses	- Secreted by macrophages to further increase inflammation in atheromas
PAI-1	- FFA increases production - Elevated levels found in individuals with abdominal fat accumulation	- Increases risk of intravascular thrombus and CVD by inhibiting tPA and contributing to fibrinolysis and atherothrombosis
TNF-alpha	- Secreted by macrophages in adipose tissue. Implicated in reduced insulin signaling in animal models	- Secreted by macrophages and inflammatory cells in atheromas to further increase inflammation - Causally implicated in CVD in Mendelian randomization analysis

FFA, free fatty acid; IL, interleukin; IR, insulin resistance; PAI-1, plasminogen activator inhibitor-1; T2D, type 2 diabetes; TG, triglycerides; TNF, tumor necrosis factor; tPA, tissue plasminogen activator; WC, waist circumference.

express adhesion molecules such as vascular cell adhesion molecule-1 (VCAM-1) and chemoattractant proteins such as of monocyte chemoattractant protein 1 (MCP-1), which recruit inflammatory cells including monocytes and lymphocytes to the endothelium and can further propagate inflammation by secretion of cytokines such as interleukin-1, interleukin-6, TNF-alpha, and colony stimulating factor 1 (8). Monocytes recruited to vessel mature into macrophages and take up cholesterol particles to form foam cells (8). The cytokine milieu promotes vascular smooth cell proliferation within the intima, which with the secretion of extracellular matrix gives further propagates atheroma development (8). Animal data indicates that vascular smooth muscle cells from the tunica media can migrate to the intima and undergo metaplasia and acquire foam cell markers (8, 9). Apoptosis and ineffective clearance of phagocytes and other inflammatory entities promotes the development of a necrotic core in the atherosclerotic lesion (8, 9). Superficial erosion of the plaque due to loss of the endothelial monolayer can result in entrapped neutrophils releasing "neutrophil extracellular traps," which further propagate inflammation and thrombus formation with healing leading to stenosis of the vessel (8, 9). Plaque rupture activates a coagulation cascade and thrombus formation with acute ischemia/infarction (8).

Obesity and associated inflammatory processes can potentially modulate these steps in atheroma development. Vessel wall damage and recruitment of inflammatory cells is likely enhanced under conditions of systemic inflammation (8). TRL, which are increased with insulin resistance, promote inflammation directly given their apolipoprotein CIII content and by delivering cholesterol to macrophages in the atheroma (8). In *in vitro* studies, TRL remnant particles upregulate the expression MCP-1, a key step in the recruitment of monocytes to vascular endothelial cells (54). It also upregulates a number of cellular adhesion molecules such as VCAM-1 (vascular cell adhesion molecule-1) and ICAM-1 (intracellular adhesion molecule-1). These processes facilitate retention of monocytes and formation of foam cells (54). TRL particles promote vascular smooth muscle cell proliferation *in vitro*, a key step in plaque progression. In animal models, insulin resistance, and associated hyperinsulinemia is associated with selective insulin resistance in the vasculature; insulin signaling via Phosphoinositide 3-kinase (PI3K) is impaired but insulin signaling via mitogen-activated protein kinase (MAPK) signaling is increased (13). The increased MAPK signaling promotes vasoconstriction due to endothelin-1 secretion, proliferation of vascular smooth muscle cells, secretion of pro-coagulant factors such as Plasminogen activator inhibitor-1 (PAI-1) and secretion of chemo-attractant proteins and cell adhesion molecules which promote recruitment of macrophages (13).

To what extent obesity associated inflammation modulates atheroma development in people with established CVD is not established. Circulating C-reactive protein, a marker of inflammation, is a predictor of CVD and is higher in people with obesity, in particular centripetal adiposity (55). Among individuals with high CRP free of CVD, those with obesity have higher CRP and higher coronary artery calcium scores and carotid artery intima thickness (55). However, this association appeared to be independent of CRP (55). Data on other inflammatory markers were unavailable—notably Mendelian randomization indicates that raised CRP *per se* does not cause CVD (56).

CLONAL HEMATOPOIESIS OF INDETERMINATE POTENTIAL

Somatic mutations in hematopoietic stem cells leads to clonal expansion of hematopoietic cells and has been implicated in various hematological malignancies (54, 57, 58). The majority of patients with clonal hematopoiesis do not develop malignancy (clonal hematopoiesis of indeterminate potential) (54, 57, 58). This is however associated with increased risk of CVD in part due to increased secretion of pro-inflammatory cytokines, including IL-6, with greater recruitment and retention of macrophages in plaques and increased vascular smooth muscle proliferation contributing to ACVD and heart failure (54, 57, 58).

GENETIC EVIDENCE FOR A POTENTIAL ROLE FOR OBESITY ASSOCIATED INFLAMMATION IN ACVD

Circulating cytokines: As alluded to above, obesity and insulin resistance are associated with increased circulating concentration of inflammatory cytokines including TNF-alpha, IL-1beta, IL-6, and Il-18 (54, 57, 58). Mendelian randomization studies assess the genetic association between a trait and a downstream outcome. Such associations are suggestive of a causal link, providing the genetic instrument does not affect an intermediary trait that can influence the downstream outcome (59). Genetically-determined

increase in TNF have been associated with ACVD, suggesting a causal link (60). However, it also protects against malignancy (60). Whether this impacts insulin resistance or T2D is not established. Genetically-determined increase in IL-6 action is associated with both increased risk for T2D and CVD, suggesting shared underlying etiology (61, 62). Data from genetic and pharmacologic studies of IL-1 receptor modulation have not been consistent. Genetically-determined IL-1 receptor antagonist was surprisingly has been associated with increased CVD; whether this is due to dual IL-1 alpha and beta reduction is not clear (62). Genetically modulated IL-1 receptor activity does not impact T2D risk (63). Notably, pharmacological IL-1beta blockade has been shown to reduce CVD in a large randomized control trial with no effect on progression of glycemia (64). Genetically-determined IL-18 is not associated with either T2D or CVD (62, 63).

CHIP: In the Women's Health Initiative study, CHIP increased with increased BMI in post-menopausal women (highest in those with BMI>30 vs. BMI 27–30 kg/m^2 compared to normal weight women) (65). This suggests obesity may be associated with increased CHIP. CHIP may also be increased in patients with T2D (66). A potential contributor to CHIP in T2D and obesity may be the adipokine leptin (67). Circulating leptin concentration is proportional to fat mass and increase/decrease with fat gain/loss (68). Leptin increases haematopoiesis and activates Janus kinase 2 (JAK2), a critical node for CHIP (66, 69). In mice, reduction in leptin via exercise-induced weight loss reduced CHIP (67).

In summary, the available evidence suggests increased circulating IL-6 and TNF-alpha, which are features of obesity associated insulin resistance, likely causally increase risk of CVD. CHIP, a more recently reported CVD risk factor, may be increased in T2D and obesity.

PHARMACOLOGICAL EVIDENCE SUPPORTING A ROLE OF INFLAMMATION IN T2D AND CVD

Recently, there has been pharmacologic evidence for the association between inflammation and CVD (**Table 2**). The JUPITER trial concluded that individuals with increased levels of the inflammatory biomarker C-reactive protein (CRP) responded to rosuvastatin pharmacotherapy and had significant decreases in major cardiovascular events, regardless of presence of dyslipidemia (71). Statins are known to lower cholesterol, as well as high-sensitivity CRP (71). Healthy adults with a high CRP treated with rosuvastatin were found to have, on average, a 47% lower risk of myocardial infarction, stroke, or death from cardiovascular causes compared to those who did not receive statin therapy (71). This confirms that CVD is an inflammatory disorder and that inflammatory markers can be utilized to stratify patients, independent of traditional risk factors such as LDL. ∼40% of patients in the trial had evidence of metabolic syndrome; to what extent centripetal adiposity/obesity modulated atherosclerosis and the response to statin treatment is not known (71).

A number of anti-inflammatory agents have been evaluated in CVD outcomes trials. These agents are not known to affect weight or metabolic disease and thus any effects are independent of weight loss and metabolic status (64, 74, 78–81). The CANTOS trial evaluated the role of IL-1 beta antagonism on the incidence of T2D and CVD. CVD decreased by ∼15% in patients with elevated hsCRP, an effect seen with and without T2D (64, 78). These finding are scientifically important as they represent the first convincing evidence that a strategy that targets a specific inflammatory pathway reduces CVD. The long term feasibility of this therapy remains to be determined given potential side effects, including sepsis, and cost (64). Intriguingly, although canakinumab reduced CVD in patients with T2D, it did not affect glycaemia in the long term (78). It did not prevent incident T2D in normoglycaemic patients and those with pre-T2D. Furthermore, the magnitude of reduction in CVD risk in patients with T2D compared to those without (78). These results suggest that IL-1b contributes to CVD risk in patients with inflammation but likely does not play a major role in the etiology of T2D.

The CALCOT trial evaluated the use of colchicine in individuals with a recent myocardial infarction (79). It concluded that low-dose colchicine resulted in a significantly lower risk of cardiovascular events compared to placebo post-myocardial infarction (79). However, there was an increase in incidence of pneumonia in the treatment group (79). These CVD benefits of colchicine were confirmed in the Low Dose Colchicine 2 (LoDoCo2) study, although there was a trend toward increased non-CVD death (82). Colchicine inhibits tubulin polymerization and microtubule generation and its role in CVD is linked to inhibition of the NLRP3 inflammasome (79). Although initial data suggested colchicine may be beneficial for improving insulin sensitivity and glycemia, this has not been subsequently confirmed (79–81).

In the CIRT study, low-dose methotrexate, an anti-inflammatory agent, did not reduce levels of interleukin-1b, interleukin-6 or CRP, nor did it result in a difference in cardiovascular events compared to placebo (74). Methotrexate inhibits dihydrofolate reductase which may not be of relevance in CVD (9, 74). Darapladib, an lp-PLA2 (Lipoprotein-associated phospholipase A2) inhibitor, and varespladib, an sPLA2 (secretory phospholipase A2) inhibitor, have not been promising either in clinical trials (9). They target phospholipase A2 which are secreted by inflammatory cells and postulated to contribute to atherosclerosis. Notably genetic studies of this pathway in humans have not consistently showed an association with CVD (9).

There is considerable interest in utilizing tocilizumab, an IL-6 receptor antagonist, for treating CVD and T2D as this is a genetically validated target as discussed above (9). However, a potential concern with IL-6 inhibition is an increase in LDL due to reduced clearance (83).

In summary, there is growing evidence that reducing inflammation can lower incident CVD but off-target effects,

TABLE 2 | Pharmacologic therapies for CVD targeting inflammatory pathway.

Drug	Trial (Author)	Mechanism	Study findings	Comments
Anakinra	VCU-ART3 Abbate et al. (70)	Decrease IL-1 receptor	CRP AUC decreased with treatment in patients with STEMI (median 67 vs. 214; $p < 0.001$)	Significantly decreased death, new onset HF or death/hospitalization for HF as well; effets short-term (rebound CRP and IL-6 upon stopping); not supported by genetic studies
Canakinumab	CANTOS Ridker et al. (64)	Decreasing IL-1b	Nonfatal MI, stroke or CV death decreased with the 150mg dose (HR 0.83; $p = 0.005$)	Independent of dyslipidemia; patients had high CRP at baseline; higher incidence of fatal infection compared to placebo; no significant impact on all-cause mortality
Colchicine	CALCOT Tardif et al. (71)	Decrease CRP, NLRP3 inflammasome inhibitor	CV death, resuscitated cardiac arrest, MI, stroke, or urgent hsopitalization for angina requiring coronary revascularization decreased with treatment (HR 0.77; $p = 0.02$)	Significant GI side effects
Darapladib	SOLID-TIMI 52 O'Donoghue et al. (72)	Decrease lp-PLA2	No significant difference in major coronary events with treatment (HR 0.99; $p = 0.78$)	Genetic studies inconsistent; lp-PLA2 did not decrease inflammatory markers
Low dose IL-2	LILACS Zhao et al. (73)	Promotes regulatory T-cells	Results pending	Effective in preclinical data; more selective T-cell regulators than Aldesleukin being developed
Methotrexate	CIRT Ridker et al. (74)	Dihydrofolate reducatase inhibitor	Nonfatal MI, stroke or CV death not significantly changed with treatment (HR 0.96; $p = 0.91$)	Treatment did not decrease inflammatory markers; pathway may not be relevant
Rosuvastatin	JUPITER Ridker et al. (71)	Decrease high-sensitivity CRP	MI, stroke or death from CV causes decreased with treatment (HR 0.56; p<0.00001)	Independent of dyslipidemia
Tocilizumab	ASSAIL-MI Broch et al. (75)	Anti-IL-6 receptor antibody	Myocardial salvage in acute STEMI larger with treatment (difference 5.6; $p = 0.04$)	No significant difference in infarct size between treatment and placebo; non-specific blocker of IL-6 signalling
Varespladib	VISTA-16 Nicholls et al. (76)	Decrease sPLA2	CV death, nonfatal MI, nonfatal stroke and unstable angina did not significantly decrease with treatment (HR 1.25; $p = 0.08$)	Trial stopped early for greater risk of MI with treatment; non-specific treatment; pathway not supported by Mendelian randomization
Xilonix	El Sayed et al. (77)	Anti-IL-1a antibody	MACE did not significantly change with treatment (9% vs. 24%; $p = 0.22$)	Limited clinical data available; did not lower CRP

AUC, area under the curve; CRP, C-reactive protein; CV, cardiovascular; GI, gastrointestinal; HF, heart failure; HR, hazard ratio; IL, interleukin; Lp-PLA2, lipoprotein-associated phospholipase A2; MACE, major adverse cardiovascular events; MI, myocardial infarction; S-PLA2, secretory phospholipase A2; STEMI, ST-segment elevation myocardial infarction.

in particular infection/sepsis, are a concern. In contrast, we do not have convincing evidence yet that anti-inflammatory therapies lead to sustained reduction in T2D and metabolic disease (72, 73, 75–77, 84).

IMPACT OF WEIGHT LOSS

Weight loss can potentially reduce inflammation and improve multiple CVD risk factors. In the LOOK-AHEAD trial, modest weight loss associated with intensive lifestyle changes was associated with improvement in cardiometabolic parameters in patients with T2D but overall no CVD benefit was seen (42). *Post-hoc* analyses suggest that those who achieved sustained weight loss of 10% or more had a reduction in CVD (85). Similarly, weight loss through pharmacotherapy improves cardiometabolic parameters, but whether this translates to benefits in major CVD outcomes is unknown (40, 86). GLP-1 receptor agonists (GLP-1RA) have beneficial cardiovascular outcomes in patients with T2D (86). The exact mechanisms have not been delineated but are likely independent of glucose lowering as not all glucose lowering drugs prevent CVD (87). Further, the effects are likely independent of blood pressure lowering and weight loss as the GLP-1RA albiglutide reduces CVD despite no significant reduction in weight or blood pressure (88). Animal models suggest that GLP-1 may have beneficial effects on vascular inflammation (89). Higher doses of GLP-1

analogs are now being used and evaluated as weight loss agents (40, 90). Whether these agents will improve cardiovascular outcomes remains to be seen. The SELECT study will evaluate the effect of 2.4 mg once weekly of semaglutide on heart disease and stroke in patients with obesity and CVD (NCT03574597).

To date, bariatric surgery remains the most efficacious weight loss treatment and improves multiple metabolic parameters, including adipose tissue and systemic inflammation (51, 70, 91, 92). Retrospective data analysis suggests that bariatric surgery is associated with reduced major adverse cardiovascular outcomes in patients with obesity both with and without T2D (70, 91–93). The extent to which this is mediated by reduced inflammation secondary to weight loss will require more detailed mechanistic studies.

EFFECT OF WEIGHT LOSS ON INFLAMMATORY MARKERS

As discussed earlier, increased WHR is likely causally associated with increased adipose and systemic inflammation. Consistent with that weight loss is associated with reduced adipose and systemic inflammation. Bariatric surgery is associated with decreases in CRP and interleukin-6 concentrations in proportion to weight less, however, TNF-alpha levels did not change (51, 94) Despite this, insulin resistance was not normalized and some adipose pathology remained post-surgery (51). Lifestyle weight loss interventions, with or without statins, have also been found to decrease CRP but whether this translates to reduced CVD is not established (95). Liraglutide treatment, which is known to reduce CVD in people with T2D, has been associated with reductions in inflammatory markers, but to what extent this is mediated by weight loss is unknown (40).

CONCLUSION

Although considerable progress has been made in reducing the burden of CVD, it remains the leading cause of mortality in people with obesity. Thus, further therapies are needed to reduce the burden of CVD. Inflammation is a key mediator of atherosclerosis and can potentially be targeted for reduction in CVD; its role in treating T2D and metabolic disease is less established. However, to date, lack of efficacy, and off-target effects have limited the broad utility of anti-inflammatory treatments. The emergence of more "omics" data will likely identify further anti-inflammatory targets. Whether this translates to reduced cardiometabolic disease remains to be seen. In the interim, we await more data from current clinical trials evaluating anti-inflammatory agents to reduce CVD. There is emerging observational data that substantial weight loss, through bariatric surgery, may reduce CVD. The extent to which this is mediated by reduction in inflammation remains to be determined.

AUTHOR CONTRIBUTIONS

RK and SD wrote the manuscript. All authors contributed to the article and approved the submitted version.

FUNDING

SD was funded by the Canadian Institute for Health Research, Diabetes Canada, Heart & Stroke Foundation of Canada and Banting & Best Diabetes Center (DH Gales Family Charitable Foundation New Investigator Award and Reuben & Helene Dennis Scholar in Diabetes).

REFERENCES

1. Centers for Disease Control and Prevention. *Adult Obesity Facts*. (2021). Available online at: https://www.cdc.gov/obesity/data/adult.html (accessed June 7, 2021)
2. Finucane MM, Stevens GA, Cowan MJ, Danaei G, Lin JK, Paciorek CJ, et al. National, regional, and global trends in body-mass index since 1980: systematic analysis of health examination surveys and epidemiological studies with 960 country-years and 9.1 million participants. *Lancet*. (2011) 377:557–67. doi: 10.1016/S0140-6736(10)62037-5
3. Afshin A, Forouzanfar MH, Reitsma MB, Sur P, Estep K, Lee A, et al. Health effects of overweight and obesity in 195 countries over 25 years. *N Engl J Med*. (2017) 377:13–27. doi: 10.1056/NEJMoa1614362
4. Flegal KM, Carroll MD, Kit BK, Ogden CL. Prevalence of obesity and trends in the distribution of body mass index among US adults, 1999-2010. *JAMA*. (2012) 307:491–7. doi: 10.1001/jama.2012.39
5. Blüher, M. Obesity: a global epidemiology and pathogenesis. *Nat Rev Endocrinol*. (2019) 15:288–98. doi: 10.1038/s41574-019-0176-8
6. World Heart Federation. *Cardiovascular Disease Infographic*. (2021). Available online at: https://world-heart-federation.org/resource/cardiovascular-disease-infographic/ (accessed July 8, 2021)
7. Lotta LA, Wittemans LBL, Zuber V, Stewart ID, Sharp SJ, Luan J, et al. Association of genetic variants related to gluteofemoral vs abdominal fat distribution with type 2 diabetes, coronary disease, and cardiovascular risk factors. *JAMA*. (2018) 320:2553–63. doi: 10.1001/jama.2018.19329
8. Libby P. The changing landscape of atherosclerosis. *Nature*. (2021) 592: 24–33. doi: 10.1038/s41586-021-03392-8
9. Zhao TX, Mallat Z. Targeting the immune system in atherosclerosis: JACC state-of-the-art review. *J Am Coll Cardiol*. (2019) 73:1691–706. doi: 10.1016/j.jacc.2018.12.083
10. Henriques F, Bedard AH, Luiz Batista Junior M. Adipose tissue inflammation and metabolic disorders. *Adipose Tissue Update*. (2019) 1−11. doi: 10.5772/intechopen.88631
11. Lopez-Candales A, Hernández Burgos PM, Hernandez-Suarez DF, Harris D. Linking chronic inflammation with cardiovascular disease: from normal aging to the metabolic syndrome. *J Nat Sci*. (2017) 3:e341. PMID: 28670620; PMCID: PMC5488800.
12. Ebron K, Andersen CJ, Aguilar D, Blesso CN, Barona J, Dugan CE, et al. A larger body mass index is associated with increased atherogenic dyslipidemia, insulin resistance, and low-grade inflammation in individuals with metabolic syndrome. *Metab Syndr Relat Disord*. (2015) 13:458–64. doi: 10.1089/met.2015.0053
13. Dash S, Leiter LA. Residual cardiovascular risk among people with diabetes. *Diabetes Obes Metab*. (2019) 21(Suppl. 1):28–38. doi: 10.1111/dom.13646
14. Sarma S, Sockalingam S, Dash S. Obesity as a multisystem disease: trends in obesity rates and obesity-related complications. *Diabetes Obes Metab*. (2021) 23(Suppl. 1):3–16. doi: 10.1111/dom.14290
15. U.S. Department of Health and Human Services. *Overweight and Obesity*. (2021). National Heart Lung and Blood Institute. Available online at: https://www.nhlbi.nih.gov/health-topics/overweight-and-obesity (accessed Aug 10, 2021).

16. Zhang C, Rexrode KM, van Dam RM, Li TY, Hu FB. Abdominal obesity and the risk of all-cause, cardiovascular, and cancer mortality: sixteen years of follow-up in US women. *Circulation.* (2008) 117:1658–67. doi: 10.1161/CIRCULATIONAHA.107.739714
17. Yusuf S, Hawken S, Ounpuu S, Bautista L, Franzosi MG, Commerford P, et al. Obesity and the risk of myocardial infarction in 27,000 participants from 52 countries: a case-control study. *Lancet*. (2005) 366:1640–9. doi: 10.1016/S0140-6736(05)67663-5
18. Zethof M, Mosterd CM, Collard D, Galenkamp H, Agyemang C, Nieuwdorp M, van Raalte DH, van den Born BH. Differences in body composition convey a similar risk of type 2 diabetes among different ethnic groups with disparate cardiometabolic risk – the HELIUS study. *Diabetes Care*. (2021) 18:dc210230. Epub ahead of print. PMID: 34006564. doi: 10.2337/dc21-0230 (accessed May 18, 2021).
19. Sharma AM, Kushner RF. A proposed clinical staging system for obesity. *Int J Obes.* (2009) 33:289–95. doi: 10.1038/ijo.2009.2
20. Lotta LA, Gulati P, Day FR, Payne F, Ongen H, van de Bunt M, et al. Integrative genomic analysis implicates limited peripheral adipose storage capacity in the pathogenesis of human insulin resistance. *Nat Genet.* (2017) 49:17–26. doi: 10.1038/ng.3714
21. Kautzky-Willer A, Harreiter J, Pacini G. Sex and gender differences in risk, pathophysiology and complications of type 2 diabetes mellitus. *Endocr Rev.* (2016) 37:278–316. doi: 10.1210/er.2015-1137
22. Taylor R, Holman RR. Normal weight individuals who develop type 2 diabetes: the personal fat threshold. *Clin Sci (Lond).* (2015) 128:405–10. doi: 10.1042/CS20140553
23. Gujral UP, Pradeepa R, Weber MB, Narayan KM, Mohan V. Type 2 diabetes in South Asians: similarities and differences with white Caucasian and other populations. *Ann N Y Acad Sci.* (2013) 1281:51–63. doi: 10.1111/j.1749-6632.2012.06838.x
24. Ma RC, Chan JC. Type 2 diabetes in East Asians: similarities and differences with populations in Europe and the United States. *Ann N Y Acad Sci.* (2013) 1281:64–91. doi: 10.1111/nyas.12098
25. Fabbrini E, Yoshino J, Yoshino M, Magkos F, Tiemann Luecking C, Samovski D, et al. Metabolically normal obese people are protected from adverse effects following weight gain. *J Clin Invest.* (2015) 125:787–95. doi: 10.1172/JCI78425
26. Stefan N. Causes, consequences, and treatment of metabolically unhealthy fat distribution. *Lancet Diabetes Endocrinol.* (2020) 8:616–27. doi: 10.1016/S2213-8587(20)30110-8
27. Petersen MC, Shulman GI. Mechanisms of insulin action and insulin resistance. *Physiol Rev.* (2018) 98:2133–223. doi: 10.1152/physrev.00063.2017
28. Xia JY, Holland WL, Kusminski CM, Sun K, Sharma AX, Pearson MJ, et al. Targeted induction of ceramide degradation leads to improved systemic metabolism and reduced hepatic steatosis. *Cell Metab.* (2015) 22:266–78. doi: 10.1016/j.cmet.2015.06.007
29. Taylor R, Al-Mrabeh A, Zhyzhneuskaya S, Peters C, Barnes AC, Aribisala BS, et al. Remission of human type 2 diabetes requires decrease in liver and pancreas fat content but is dependent upon capacity for beta cell recovery. *Cell Metab.* (2018) 28:547–56. doi: 10.1016/j.cmet.2018.07.003
30. Magkos F, Fraterrigo G, Yoshino J, Luecking C, Kirbach K, Kelly SC, et al. Effects of moderate and subsequent progressive weight loss on metabolic function and adipose tissue biology in humans with obesity. *Cell Metab.* (2016) 23:591–601. doi: 10.1016/j.cmet.2016.02.005
31. Lean MEJ, Leslie WS, Barnes AC, Brosnahan N, Thom G, McCombie L, et al. Durability of a primary care-led weight-management intervention for remission of type 2 diabetes: 2-year results of the DiRECT open-label, cluster-randomised trial. *Lancet Diabetes Endocrinol.* (2019) 7:344–55. doi: 10.1016/S2213-8587(19)30068-3
32. Yoshino M, Kayser BD, Yoshino J, Stein RI, Reeds D, Eagon JC, et al. Effects of diet vs. gastric bypass on metabolic function in diabetes. *N Engl J Med.* (2020) 383:721–32. doi: 10.1056/NEJMoa2003697
33. Aminian A, Vidal J, Salminen P, Still CD, Nor Hanipah Z, Sharma G, et al. Late relapse of diabetes after bariatric surgery: not rare, but not a failure. *Diabetes Care.* (2020) 43:534–40. doi: 10.2139/ssrn.3320174
34. Semple RK, Sleigh A, Murgatroyd PR, Adams CA, Bluck L, Jackson S, et al. Postreceptor insulin resistance contributes to human dyslipidemia and hepatic steatosis. *J Clin Invest.* (2009) 119:315–22. doi: 10.1172/JCI37432
35. Do R, Willer CJ, Schmidt EM, Sengupta S, Gao C, Peloso GM, et al. Common variants associated with plasma triglycerides and risk for coronary artery disease. *Nat Genet.* (2013) 45:1345–52. doi: 10.1038/ng.2795
36. Myocardial Infarction Genetics CARDIoGRAM Exome Consortia Investigators, Stitziel NO, Stirrups KE, Masca NG, Erdmann J, Ferrario PG, et al. Coding variation in ANGPTL4, LPL, and SVEP1 and the risk of coronary disease. *N Engl J Med.* (2016) 374:1134–44. doi: 10.1056/NEJMoa1507652
37. Jørgensen AB, Frikke-Schmidt R, Nordestgaard BG, Tybjærg-Hansen A. Loss-of-function mutations in APOC3 and risk of ischemic vascular disease. *N Engl J Med.* (2014) 371:32–41. doi: 10.1056/NEJMoa1308027
38. TG and HDL Working Group of the Exome Sequencing Project, National Heart, Lung, Blood Institute, Crosby J, Peloso GM, et al. Loss-of-function mutations in APOC3, triglycerides, and coronary disease. *N Engl J Med.* (2014) 371:22–31. doi: 10.1056/NEJMoa1307095
39. Do R, Stitziel NO, Won HH, Jørgensen AB, Duga S, Angelica Merlini P, et al. Exome sequencing identifies rare LDLR and APOA5 alleles conferring risk for myocardial infarction. *Nature.* (2015) 518:102–6. doi: 10.1038/nature13917
40. Pi-Sunyer X, Astrup A, Fujioka K, the SCALE Obesity and Prediabetes NN8022-1839 Study Group. A randomized, controlled trial of 3.0 mg of liraglutide in weight management. *N Engl J Med.* (2015) 373:11–22. doi: 10.1056/NEJMoa1411892
41. Ikramuddin S, Korner J, Lee WJ, Connett JE, Inabnet WB, Billington CJ, et al. Roux-en-Y gastric bypass vs intensive medical management for the control of type 2 diabetes, hypertension, and hyperlipidemia: the Diabetes Surgery Study randomized clinical trial. *JAMA.* (2013) 309:2240–9. doi: 10.1001/jama.2013.5835
42. Look AHEAD Research Group, Wing RR, Bolin P, Brancati FL, Bray GA, Clark JM, et al. Cardiovascular effects of intensive lifestyle intervention in type 2 diabetes. *N Engl J Med.* (2013) 369:145–54. doi: 10.1056/NEJMoa1212914
43. Hall JE, do Carmo JM, da Silva AA, Wang Z, Hall ME. Obesity-induced hypertension: interaction of neurohumoral and renal mechanisms. *Circ Res.* (2015) 116:991–1006. doi: 10.1161/CIRCRESAHA.116.305697
44. Greenfield JR, Miller JW, Keogh JM, Henning E, Satterwhite JH, Cameron GS, et al. Modulation of blood pressure by central melanocortinergic pathways. *N Engl J Med.* (2009) 360:44–52. doi: 10.1056/NEJMoa0803085
45. Gordon RD, Küchel O, Liddle GW, Island DP. Role of the sympathetic nervous system in regulating renin and aldosterone production in man. *J Clin Invest.* (1967) 46:599–605. doi: 10.1172/JCI105561
46. Schwartz AR, Patil SP, Laffan AM, Polotsky V, Schneider H, Smith PL. Obesity and obstructive sleep apnea: pathogenic mechanisms and therapeutic approaches. *Proc Am Thorac Soc.* (2008) 5:185–92. doi: 10.1513/pats.200708-137MG
47. Romero-Corral A, Caples SM, Lopez-Jimenez F, Somers VK. Interactions between obesity and obstructive sleep apnea: implications for treatment. *Chest.* (2010) 137:711–9. doi: 10.1378/chest.09-0360
48. Fava C, Dorigoni S, Dalle Vedove F, Danese E, Montagnana M, Guidi GC, et al. Effect of CPAP on blood pressure in patients with OSA/hypopnea: a systematic review and meta-analysis. *Chest.* (2014) 145:762–71. doi: 10.1378/chest.13-1115
49. Stevens VJ, Obarzanek E, Cook NR, Lee IM, Appel LJ, Smith West D, et al. Long-term weight loss changes in blood pressure: results of the Trials of Hypertension Prevention, phase II. *Ann Intern Med.* (2001) 134:1–11. doi: 10.7326/0003-4819-134-1-200101020-00007
50. Khan S, Chan YT, Revelo XS, Winter DA. The immune landscape of visceral adipose tissue during obesity and aging. *Front Endocrinol.* (2020) 11:267. doi: 10.3389/fendo.2020.00267
51. Camastra S, Vitali A, Anselmino M, Gastaldelli A, Bellini R, Berta R, et al. Muscle and adipose tissue morphology, insulin sensitivity and beta-cell function in diabetic and nondiabetic obese patients: effects of bariatric surgery. *Sci Rep.* (2017) 7:9007. doi: 10.1038/s41598-017-08444-6
52. Hotamisligil GS. Foundations of immunometabolism and implications for metabolic health and disease. *Immunity.* (2017) 47:406–20. doi: 10.1016/j.immuni.2017.08.009
53. Donath MY, Meier DT, Boni-Schnetzler M. Inflammation in the pathophysiology and therapy of cardiometabolic disease. *Endocr Rev.* (2019) 40:1080–91. doi: 10.1210/er.2019-00002
54. Fujioka Y, Ishikawa Y. Remnant lipoproteins as strong key particles to atherogenesis. *J Atheroscler Thromb.* (2009) 16:145–54. doi: 10.5551/jat.E598

55. Blaha MJ, Rivera JJ, Budoff MJ, Blankstein R, Agatston A, O'Leary DH, et al. Association between obesity, high-sensitivity C-reactive protein >/=2 mg/L, and subclinical atherosclerosis: implications of JUPITER from the Multi-Ethnic Study of Atherosclerosis. *Arterioscler Thromb Vasc Biol.* (2011) 31:1430–8. doi: 10.1161/ATVBAHA.111.223768
56. Elliott P, Chambers JC, Zhang W, Clarke R, Hopewell JC, Peden JF, et al. Genetic Loci associated with C-reactive protein levels and risk of coronary heart disease. *JAMA*. (2009) 302:37–48. doi: 10.1001/jama.2009.954
57. Low Wang CC, Hess CN, Hiatt WR, Goldfine AB. Clinical update: cardiovascular disease in diabetes mellitus: atherosclerotic cardiovascular disease and heart failure in type 2 diabetes mellitus - mechanisms, management, and clinical considerations. *Circulation.* (2016) 133:2459–502. doi: 10.1161/CIRCULATIONAHA.116.022194
58. Natarajan P, Jaiswal S, Kathiresan S. Clonal hematopoiesis: somatic mutations in blood cells and atherosclerosis. *Circ Genom Precis Med.* (2018) 11:e001926. doi: 10.1161/CIRCGEN.118.001926
59. Hemani G, Zheng J, Elsworth B, Wade KH, Haberland V, Baird D, et al. The MR-Base platform supports systematic causal inference across the human phenome. *Elife.* (2018) 7:e34408. doi: 10.7554/eLife.34408
60. Yuan S, Carter P, Bruzelius M, Vithayathil M, Kar S, Mason AM, et al. Effects of tumour necrosis factor on cardiovascular disease and cancer: a two-sample Mendelian randomization study. *EBioMedicine.* (2020) 59:102956. doi: 10.1016/j.ebiom.2020.102956
61. Bowker N, Shah RL, Sharp SJ, Luan J, Stewart ID, Wheeler E, et al. Meta-analysis investigating the role of interleukin-6 mediated inflammation in type 2 diabetes. *EBioMedicine.* (2020) 61:103062. doi: 10.1016/j.ebiom.2020.103062
62. Yuan S, Lin A, He QQ, Burgess S, Larsson SC. Circulating interleukins in relation to coronary artery disease, atrial fibrillation and ischemic stroke and its subtypes: a two-sample Mendelian randomization study. *Int J Cardiol.* (2020) 313:99–104. doi: 10.1016/j.ijcard.2020.03.053
63. Folkersen L, Gustafsson S, Wang Q, Hansen DH, Hedman ÅK, Schork A, et al. Genomic and drug target evaluation of 90 cardiovascular proteins in 30,931 individuals. *Nat Metab.* (2020) 2:1135–48. doi: 10.1038/s42255-020-00287-2
64. Ridker PM, Everett BM, Thuren T, MacFadyen JG, Chang WH, Ballantyne C, et al. Antiinflammatory therapy with canakinumab for atherosclerotic disease. *N Engl J Med*. (2017) 377:1119–31. doi: 10.1056/NEJMoa1707914
65. Haring B, Reiner AP, Liu J, Tobias DK, Whitsel E, Berger JS, et al. Healthy lifestyle and clonal hematopoiesis of indeterminate potential: results from the Women's Health Initiative. *J Am Heart Assoc.* (2021) 10:e018789. doi: 10.1161/JAHA.120.018789
66. Jaiswal S, Fontanillas P, Flannick J, Manning A, Grauman PV, Mar BG, et al. Age-related clonal hematopoiesis associated with adverse outcomes. *N Engl J Med.* (2014) 371:2488–98. doi: 10.1056/NEJMoa1408617
67. Frodermann V, Rohde D, Courties G, Severe N, Schloss MJ, Amatullah H, et al. Exercise reduces inflammatory cell production and cardiovascular inflammation via instruction of hematopoietic progenitor cells. *Nat Med.* (2019) 25:1761–71. doi: 10.1038/s41591-019-0633-x
68. Rosenbaum M, Sy M, Pavlovich K, Leibel RL, Hirsch J. Leptin reverses weight loss-induced changes in regional neural activity responses to visual food stimuli. *J Clin Invest.* (2008) 118:2583–91. doi: 10.1172/JCI35055
69. Bennett BD, Solar GP, Yuan JQ, Mathias J, Thomas GR, Matthews W. A role for leptin and its cognate receptor in hematopoiesis. *Curr Biol.* (1996) 6:1170–80. doi: 10.1016/S0960-9822(02)70684-2
70. Doumouras AG, Wong JA, Paterson JM, et al. Bariatric surgery and cardiovascular outcomes in patients with obesity and cardiovascular disease: a population-based retrospective cohort study. *Circulation.* (2021) 143:1468–80. doi: 10.1161/CIRCULATIONAHA.120.052386
71. Ridker PM, Danielson E, Fonseca FA, Genest J, Gotto AM Jr, Kastelein JJ, et al. Rosuvastatin to prevent vascular events in men and women with elevated C-reactive protein. *N Engl J Med*. (2008) 359:2195–207. doi: 10.1056/NEJMoa0807646
72. O'Donoghue ML, Braunwald E, White HD, Lukas MA, Tarka E, Steg PG, et al. Effect of darapladib on major coronary events after an acute coronary syndrome: the SOLID-TIMI 52 randomized clinical trial. *JAMA*. (2014) 312:1006–15. doi: 10.1001/jama.2014.11061
73. Zhao TX, Kostapanos M, Griffiths C, Arbon EL, Hubsch A, Kaloyirou F, et al. Low-dose interleukin-2 in patients with stable ischaemic heart disease and acute coronary syndromes (LILACS): protocol and study rationale for a randomised, double-blind, placebo-controlled, phase I/II clinical trial. *BMJ Open.* (2018) 8:e022452. doi: 10.1136/bmjopen-2018-022452
74. Ridker, PM. Low-dose methotrexate for the prevention of atherosclerotic events. *N Engl J Med.* (2019) 380:752–62. doi: 10.1056/NEJMoa1809798
75. Broch K, Anstensrud AK, Woxholt S, Sharma K, Tøllefsen IM, Bendz B, et al. Randomized trial of interleukin-6 receptor inhibition in patients with acute ST-segment elevation myocardial infarction. *J Am Coll Cardiol.* (2021) 77:1845–55. doi: 10.1016/j.jacc.2021.02.049
76. Nicholls SJ, Kastelein JJ, Schwartz GG, Bash D, Rosenson RS, Cavender MA, et al. Varespladib and cardiovascular events in patients with an acute coronary syndrome: the VISTA-16 randomized clinical trial. *JAMA*. (2014) 311:252–62. doi: 10.1001/jama.2013.282836
77. El Sayed H, Kerensky R, Stecher M, Mohanty P, Davies M. A randomized phase II study of Xilonix, a targeted therapy against interleukin 1α, for the prevention of superficial femoral artery restenosis after percutaneous revascularization. *J Vasc Surg.* (2016) 63:133–41.e1. doi: 10.1016/j.jvs.2015.08.069
78. Everett BM, Donath MY, Pradhan AD, Thuren T, Pais P, Nicolau JC, et al. Anti-inflammatory therapy with canakinumab for the prevention and management of diabetes. *J Am Coll Cardiol.* (2018) 71:2392–401. doi: 10.1016/j.jacc.2018.03.002
79. Tardif JC, Kouz S, Waters DD, Bertrand OF, Diaz R, Maggioni AP, et al. Efficacy and safety of low-dose colchicine after myocardial infarction. *N Engl J Med.* (2019) 381:2497–505. doi: 10.1056/NEJMoa1912388
80. Demidowich AP, Levine JA, Onyekaba GI, Khan SM, Chen KY, Brady SM, et al. Effects of colchicine in adults with metabolic syndrome: a pilot randomized controlled trial. *Diabetes Obes Metab.* (2019) 21:1642–51. doi: 10.1111/dom.13702
81. Wang Y, Peng X, Hu J, Luo T, Wang Z, Cheng Q, et al. Low-dose colchicine in type 2 diabetes with microalbuminuria: a double-blind randomized clinical trial. *J Diabetes.* (2021) 13:827–36. doi: 10.1111/1753-0407.13174
82. Nidorf SM, Fiolet ATL, Mosterd A, Eikelboom JW, Schut A, Opstal TSJ, et al. Colchicine in patients with chronic coronary disease. *N Engl J Med*. (2020) 383:1838–47. doi: 10.1056/NEJMoa2021372
83. Bacchiega BC, Bacchiega AB, Usnayo MJ, Bedirian R, Singh G, Pinheiro GD. Interleukin 6 inhibition and coronary artery disease in a high-risk population: a prospective community-based clinical study. *J Am Heart Assoc.* (2017) 6:e005038. doi: 10.1161/JAHA.116.005038
84. Abbate A, Trankle CR, Buckley LF, Lipinski MJ, Appleton D, Kadariya D, et al. Interleukin-1 blockade inhibits the acute inflammatory response in patients with ST-segment-elevation myocardial infarction. *J Am Heart Assoc.* (2020) 9:e014941. doi: 10.1161/JAHA.119.014941
85. Look AHEAD Research Group, Gregg EW, Jakicic JM, Blackburn G, Bloomquist P, Bray GA, et al. Association of the magnitude of weight loss and changes in physical fitness with long-term cardiovascular disease outcomes in overweight or obese people with type 2 diabetes: a post-hoc analysis of the Look AHEAD randomised clinical trial. *Lancet Diabetes Endocrinol.* (2016) 4:913–21. doi: 10.1016/S2213-8587(16)30162-0
86. Hollander P, Gupta AK, Plodkowski R, Greenway F, Bays H, Burns C, et al. Effects of naltrexone sustained-release/bupropion sustained-release combination therapy on body weight and glycemic parameters in overweight and obese patients with type 2 diabetes. *Diabetes Care*. (2013) 36:4022–9. doi: 10.2337/dc13-0234
87. Bethel MA, Patel RA, Merrill P, Lokhnygina Y, Buse JB, Mentz RJ, et al. Cardiovascular outcomes with glucagon-like peptide-1 receptor agonists in patients with type 2 diabetes: a meta-analysis. *Lancet Diabetes Endocrinol.* (2018) 6:105–13. doi: 10.1016/S2213-8587(17)30412-6
88. UK Prospective Diabetes Study (UKPDS) Group. Intensive blood-glucose control with sulphonylureas or insulin compared with conventional treatment and risk of complications in patients with type 2 diabetes (UKPDS 33). *Lancet*. (1998) 352:837–53. doi: 10.1016/S0140-6736(98)07019-6
89. Hernandez AF, Green JB, Janmohamed S, D'Agostino RB Sr, Granger CB, Jones NP, et al. Albiglutide and cardiovascular outcomes in patients with type 2 diabetes and cardiovascular disease (Harmony Outcomes): a double-blind, randomised placebo-controlled trial. *Lancet*. (2018) 392:1519–29. doi: 10.1016/S0140-6736(18)32261-X
90. Drucker DJ. The cardiovascular biology of Glucagon-like Peptide-1. *Cell Metab.* (2016) 24:15–30. doi: 10.1016/j.cmet.2016.06.009

91. O'Neil PM, Birkenfeld AL, McGowan B, Mosenzon O, Pedersen SD, Wharton S, et al. Efficacy and safety of semaglutide compared with liraglutide and placebo for weight loss in patients with obesity: a randomised, double-blind, placebo and active controlled, dose-ranging, phase 2 trial. *Lancet.* (2018) 392:637–49. doi: 10.1016/S0140-6736(18)31773-2
92. Aminian A, Zajichek A, Arterburn DE, Wolski KE, Brethauer SA, Schauer PR, et al. Association of metabolic surgery with major adverse cardiovascular outcomes in patients with type 2 diabetes and obesity. *JAMA*. (2019) 322:1271–82. doi: 10.1001/jama.2019.14231
93. Doumouras AG, Wong JA, Paterson JM, Lee Y, Sivapathasundaram B, Tarride JE, et al. Association between bariatric surgery and all-cause mortality: a population-based matched cohort study in a universal health care system. *Ann Intern Med.* (2020) 173:694-703. doi: 10.7326/M19-3925
94. Kopp HP, Kopp CW, Festa A, Krzyzanowska K, Kriwanek S, Minar E, et al. Impact of weight loss on inflammatory proteins and their association with the insulin resistance syndrome in morbidly obese patients. *Arterioscler Thromb Vasc Biol.* (2003) 23:1042–7. doi: 10.1161/01.ATV.0000073313.16135.21
95. Belalcazar LM, Haffner SM, Lang W, Hoogeveen RC, Rushing J, Schwenke DC, et al. Lifestyle intervention and/or statins for the reduction of C-reactive protein in type 2 diabetes: from the look AHEAD study. *Obesity*. (2013) 21:944–50. doi: 10.1002/oby.20431

Conflict of Interest: The authors declare that the research was conducted in the absence of any commercial or financial relationships that could be construed as a potential conflict of interest. SD has received speaker fees/consultant fees from Novonordisk and Eli Lilly.

Publisher's Note: All claims expressed in this article are solely those of the authors and do not necessarily represent those of their affiliated organizations, or those of the publisher, the editors and the reviewers. Any product that may be evaluated in this article, or claim that may be made by its manufacturer, is not guaranteed or endorsed by the publisher.

Copyright © 2021 Khafagy and Dash. This is an open-access article distributed under the terms of the Creative Commons Attribution License (CC BY). The use, distribution or reproduction in other forums is permitted, provided the original author(s) and the copyright owner(s) are credited and that the original publication in this journal is cited, in accordance with accepted academic practice. No use, distribution or reproduction is permitted which does not comply with these terms.

frontiers in Cardiovascular Medicine

ORIGINAL RESEARCH
published: 23 November 2021
doi: 10.3389/fcvm.2021.768481

Endothelial Cell CD36 Reduces Atherosclerosis and Controls Systemic Metabolism

*Umar R. Rekhi[1], Mohamed Omar[1], Maria Alexiou[1], Cole Delyea[2], Linnet Immaraj[1], Shokrollah Elahi[1] and Maria Febbraio[1]**

[1] Department of Dentistry, University of Alberta, Edmonton, AB, Canada, [2] Department of Medical Microbiology and Immunology, University of Alberta, Edmonton, AB, Canada

High-fat Western diets contribute to tissue dysregulation of fatty acid and glucose intake, resulting in obesity and insulin resistance and their sequelae, including atherosclerosis. New therapies are desperately needed to interrupt this epidemic. The significant idea driving this research is that the understudied regulation of fatty acid entry into tissues at the endothelial cell (EC) interface can provide novel therapeutic targets that will greatly modify health outcomes and advance health-related knowledge. Dysfunctional endothelium, defined as activated, pro-inflammatory, and pro-thrombotic, is critical in atherosclerosis initiation, in modulating thrombotic events that could result in myocardial infarction and stroke, and is a hallmark of insulin resistance. Dyslipidemia from high-fat diets overwhelmingly contributes to the development of dysfunctional endothelium. CD36 acts as a receptor for pathological ligands generated by high-fat diets and in fatty acid uptake, and therefore, it may additionally contribute to EC dysfunction. We created EC CD36 knockout (CD36°) mice using cre-lox technology and a cre-promoter that does not eliminate CD36 in hematopoietic cells (Tie2e cre). These mice were studied on different diets, and crossed to the low density lipoprotein receptor (LDLR) knockout for atherosclerosis assessment. Our data show that EC CD36° and EC CD36°/LDLR° mice have metabolic changes suggestive of an uncompensated role for EC CD36 in fatty acid uptake. The mice lacking expression of EC CD36 had increased glucose clearance compared with controls when fed with multiple diets. EC CD36° male mice showed increased carbohydrate utilization and decreased energy expenditure by indirect calorimetry. Female EC CD36°/LDLR° mice have reduced atherosclerosis. Taken together, these data support a significant role for EC CD36 in systemic metabolism and reveal sex-specific impact on atherosclerosis and energy substrate use.

Keywords: CD36, fatty acid transport, endothelium, atherosclerosis, metabolism

OPEN ACCESS

Edited by:
Wen Dai,
Versiti Blood Research Institute, United States

Reviewed by:
Teppei Fujikawa, University of Texas Southwestern Medical Center, United States
Elke Marsch, ScientificWriter, Netherlands

***Correspondence:**
Maria Febbraio
febbraio@ualberta.ca

Specialty section:
This article was submitted to Lipids in Cardiovascular Disease, a section of the journal Frontiers in Cardiovascular Medicine

Received: *31 August 2021*
Accepted: *20 October 2021*
Published: *23 November 2021*

Citation:
Rekhi UR, Omar M, Alexiou M, Delyea C, Immaraj L, Elahi S and Febbraio M (2021) Endothelial Cell CD36 Reduces Atherosclerosis and Controls Systemic Metabolism. Front. Cardiovasc. Med. 8:768481. doi: 10.3389/fcvm.2021.768481

INTRODUCTION

CD36 is a transmembrane glycoprotein, which was first described on platelets and later found to be expressed on an extensive range of cells and tissues including endothelial cells (ECs), monocytes/macrophages, adipocytes, hepatocytes, and muscles (1–5). CD36 plays a role in the uptake of apoptotic cells and modified lipoproteins, and in the recognition of ligands that trigger an innate immune response (6–11). It facilitates fatty acid (FA) transport into white and brown adipose tissue, heart and skeletal muscle, but the mechanism is not well-understood (12). Recent

data also suggest a role in dermal albumin transcytosis, adipocyte FA export, and in tumor growth and metastasis (13–16). Structurally, CD36 has two transmembrane domains that terminate with very short intracellular domains (17). Despite these short cytoplasmic domains, work by our lab and others has shown that CD36 signals and is involved in cellular responses related to angiogenesis, innate immunity, scavenger receptor activity, EC apoptosis, cell migration, nuclear factor kappa beta, and inflammasome activation (10, 18–30). These responses affect the development of obesity, atherosclerosis, thrombosis, insulin resistance, and inflammation.

Metabolically active tissues, including heart, skeletal muscle and brown fat, require FA to meet their energy demands. While it is true that FA can diffuse across membranes (flip/flop mechanism), it has become apparent that uptake of long-chain FA, the major FA in our diet, is mediated by transporters, and this is necessary for efficient regulated supply to tissues and to prevent inappropriate delivery (31–34). FA uptake by CD36 has been controversial, both because protein-mediated FA uptake in general was thought to be unnecessary, and because CD36 does not structurally resemble a transporter (35). Considerable work in humans and animal models, however, supports a role for CD36 in FA transport (12, 36–43). The greatest bodily FA consumer is the heart, and CD36-deficient mice and humans have been shown to have decreased cardiac FA uptake and increased glucose uptake (12, 39, 40). In isolated working heart studies, global and cardiomyocyte-specific CD36° mice were shown to have a significantly lower rate of FA oxidation and a compensatory increase in glucose oxidation (44, 45).

We and others have shown that CD36 plays a role in obesity, atherosclerosis, and insulin resistance by both uptake of ligands and promotion of inflammatory signaling pathways, with the resultant secretion of reactive oxygen species and cytokines (29, 36, 46–49). This previous work was focused on macrophages, adipocytes, heart, and skeletal muscle. While global CD36 deficiency was protective against high-fat diet-induced obesity and insulin resistance, absence of CD36 in macrophages (using a bone marrow transplant approach) was not, in spite of reduction in macrophage inflammatory pathways (47). Both global and macrophage deficiency of CD36 were found to be protective against atherosclerosis (29, 48, 49).

Initiation of atherosclerosis has been shown to be a result of changes in EC, allowing prediction of atheroprone sites in the vasculature as a function of EC inflammation and dysfunction (50–52). Hyperlipidemia exerts pro-atherogenic decreased shear stress, and increased plasma FA and modified lipoprotein ligands trigger EC pro-inflammatory pathways, leading to expression of immune cell chemoattractants and surface receptors (52–57).

We hypothesize that CD36 is a major EC receptor for pro-inflammatory atherogenic ligands, and as such will regulate EC inflammation and have a significant impact on the initiation of atherosclerosis lesions. In this report, we show evidence to support the important role of EC CD36 in regulating systemic metabolism and in the development of atherosclerosis.

MATERIALS AND METHODS

Experimental Animals and Diets

All animal procedures were prior approved by the University of Alberta Animal Care and Use Committee (AUP 0001953). To study the role of EC CD36 in metabolism and its effect on atherosclerosis, floxed (fl) *CD36* mice in the C57Bl/6j background were created by our lab by targeting exon 2 (exon 3 was included due to proximity), which contains the translation start site and first transmembrane domain, as previously described (44). These mice were then crossed to EC-specific Tie2e cre mice (58–60). Fl/fl *CD36* Tie2e cre+ mice were mated to LDLR knockout (LDLR°) mice (The Jackson Laboratory, B6.129S7-Ldlr^{tm1Her}/J, IMSR Cat# JAX:002207, RRID:IMSR_JAX:002207), a classic atherosclerosis model, to generate fl/fl *CD36*/LDLR° and fl/fl *CD36* Tie2e cre+/LDLR° mice (EC CD36°/LDLR°). The mice were genotyped as previously described (44). EC CD36°/LDLR° and fl/fl *CD36*/LDLR° mice were fed with a diet containing 42.7 kilocalorie (kcal) % carbohydrate, 42 kcal% fat, and 1.25% added cholesterol (TD 96121, Envigo) for 3, 6, and 16 weeks for atherosclerosis studies (different cohorts). This diet was used previously in CD36°/LDLR° studies to induce CD36-dependent atherosclerosis (29, 30, 61). For metabolic analyses, mice were fed with ingredient-matched diets containing 35 kcal% carbohydrate and 45 kcal% fat (D12451, Research Diets, Inc.) or 70 kcal% carbohydrate and 10 kcal% fat (D12450H, Research Diets, Inc.); the amount of sucrose is the same.

En face Aortic Morphometric Analysis

Dissection, processing, and *en face* morphometry of aortas were completed as previously described (29, 30, 49, 61). Briefly, the mice were euthanized by pentobarbital overdose (200 mg/kg, intraperitoneal) and the vasculature perfused through the heart with 10 ml phosphate buffered saline followed by 5 ml buffered formalin (Formaldefresh, Fisher Scientific). The entire aorta, from the heart, including the subclavian, right, and left carotid arteries, and extending 2–5 mm after bifurcation of the iliacs, was dissected free of fat and postfixed in buffered formalin for 24 h at 4°C and then stored in phosphate buffered saline at 4°C. Aortae were stained with oil red O (Sigma-Aldrich), which identifies neutral lipids in plaque, as per the manufacturer's instructions, to quantify lesion burden. After staining, the aortae were opened, laid flat, and digitally scanned. *En face* morphometry was performed in a blinded fashion. Briefly, three independent measurements of lesion area (red pixels) were selected and averaged for each aorta, using Adobe Photoshop software (RRID:SCR_014199). Similarly, the total aorta area was determined. The lesion area was expressed as mean percent ± S.E.M. of total aortic area.

Glucose Tolerance Testing

For glucose tolerance testing, the mice were fasted overnight and received an intraperitoneal injection of 2 mg glucose per gram of body weight. Blood was drawn from the tail vein at baseline and then 15, 30, 45, 60, and 120 min after the administration of glucose. Blood glucose was measured using

an Accu-Chek Advantage Glucometer. Area under the curve was calculated for individual curves using Graph Pad Prism software (RRID:SCR_002798).

Total Cholesterol, Free Cholesterol, and Triglyceride Assays

The mice were fasted overnight and blood was collected by cardiac puncture into ethylenediaminetetraacetic acid containing syringes. The blood was centrifuged at 3,800 × g for 5 min and plasma aliquoted and frozen at −20°C. Total and free plasma cholesterol and triglyceride concentrations were measured using colorimetric assays (Wako chemicals, Fujifilm, Japan) as per the manufacturer's instructions. The levels in samples were determined by comparison against a curve constructed from serially diluted standards.

Lipoprotein Analysis

The mice were fasted overnight and fresh plasma aliquots were used to perform fast protein liquid chromatography by the Lipidomics Core facility at the University of Alberta. The area under each peak was calculated using GraphPad Prism software (RRID:SCR_002798).

Indirect Calorimetry

Four-week-old fl/fl *CD36* and EC CD36° mice were housed and maintained in metabolic cages. Following a 24-h acclimatization period, the mice were monitored over a 12 h light:12 h dark cycle (0600–1800 light) with *ad libitum* access to food (normal chow) and water. Indirect calorimetry was performed using the Comprehensive Laboratory Animal Monitoring System (Columbus Instruments). The respiratory exchange ratio (RER), calculated as the ratio of carbon dioxide to oxygen production, was used to calculate the percent contribution of fat (RER = 0.7) and carbohydrates (RER = 1) to whole body energy metabolism. Total activity of the mice was calculated by adding *Z* counts (rearing or jumping) to total counts associated with stereotypical behavior (grooming and scratching) and ambulatory movement. Data were analyzed using the web-based tool CalR (RRID:SCR_015849) (62).

Flow Cytometry

Flow cytometry was performed on mouse blood as previously described (63). Briefly, to obtain single-cell suspensions, spleen samples were ground between sterile frosted glass slides in 7 ml of red blood cell lysis buffer (0.15 mM NH_4Cl, 10 mM KHCO3, 0.1 mM disodium ethylenediaminetetraacetic acid, pH 7.2) and then filtered through sterile nylon mesh. Whole blood, obtained by cardiac puncture, was treated with red blood cell lysis buffer twice. Cell pellets were washed and resuspended in phosphate-buffered saline containing 2 mM ethylenediaminetetraacetic acid and 0.5% bovine serum albumin. Fluorophore-conjugated antibodies with specificity to mouse cell antigens were as follows: anti-CD11b (M1/70) (BD Biosciences Cat# 550993, RRID:AB_394002), anti-CD11c (HL3) (BD Biosciences Cat# 561022, RRID:AB_2033997), anti-SiglecF (E50-2440) (BD Biosciences Cat# 552125, RRID:AB_394340), anti-Ly6G (1A8) (BD Biosciences Cat# 561236, RRID:AB_10611860), and anti-CD36 (JC63.1) (Cayman Chemical Cat# 10009870, RRID:AB_10342682). Live/dead fixable dead cell stains (ThermoFisher) were used to exclude dead cells. CD11b+/c+ cells were analyzed for CD36 expression. Paraformaldehyde-fixed cells were acquired using a Becton Dickinson (BD) LSR Fortessa flow cytometer (BD Biosciences, University of Alberta Flow Cytometry core) and analyzed with FlowJo (version 10) software (RRID:SCR_008520).

Dual-Energy X-Ray Absorptiometry

Lean and fat body mass were determined using dual-energy X-ray absorptiometry (Faxitron, model DXA UltraFocus, Hologic), as per the manufacturer's instructions. Acquisition, image processing, and analysis were performed by the associated Faxitron Vision software (Faxitron Bioptics LLC.).

Statistical Analyses

Data are presented as mean ± S.E.M. Data were assessed for normal distribution by Shapiro–Wilk test. If normally distributed, the significance was evaluated using parametric Student's *t*-test. For non-normally distributed data, the significance was evaluated using Mann-Whitney. The significance was set at $p < 0.05$. Analyses and graphs were performed using GraphPad Prism software (RRID:SCR_002798).

RESULTS

To demonstrate the specificity of cre expression, we performed flow cytometry on blood and gated on the CD11b+/c+ population. As shown in **Figure 1**, there was no loss of CD36 expression in EC CD36° samples (**Figure 1B**) compared with fl/fl *CD36* controls (**Figure 1A**). These data are in agreement with previous reports using this cre driver (58–60).

To determine the impact of the loss of EC CD36 on basal systemic metabolism, we began with young mice that were similar in weight and lean body mass as measured by dual-energy X-ray absorptiometry. The mean percent lean body mass in 4-week-old fl/fl *CD36* male mice was 92.84 ± 0.26 vs. 93.54 ± 1.27 for EC CD36° males. Female fl/fl *CD36* mice had a mean lean body mass percent of 93.41 ± 0.37 vs. 94.56 ± 0.41 for EC CD36° females. Four-week-old EC CD36° male and female mice showed similar clearance of glucose compared with sex-matched controls in glucose tolerance testing (**Figures 2A,B**). At 4-6 months of age, both male and female EC CD36° showed significantly better glucose clearance compared with controls (**Figures 2C,D**), despite the similar weight.

Indirect calorimetry of 4-week-old normal chow-fed EC CD36° and controls showed mixed carbohydrate and fat use early in the light period for both strains of male mice (**Figure 3A**, Respiratory Exchange Ratio). EC CD36° males showed generally lower levels of oxygen consumption (**Figure 3B**) and carbon dioxide production (**Figure 3C**), indicative of lower energy expenditure, compared with controls. While cumulative food intake did not differ (**Figures 3D,E**), the time of feeding did. EC CD36° male mice ate more during the light period (**Figures 3D,E**), and this was reflected in increased carbohydrate metabolism after the midpoint of the light period (**Figure 3A**).

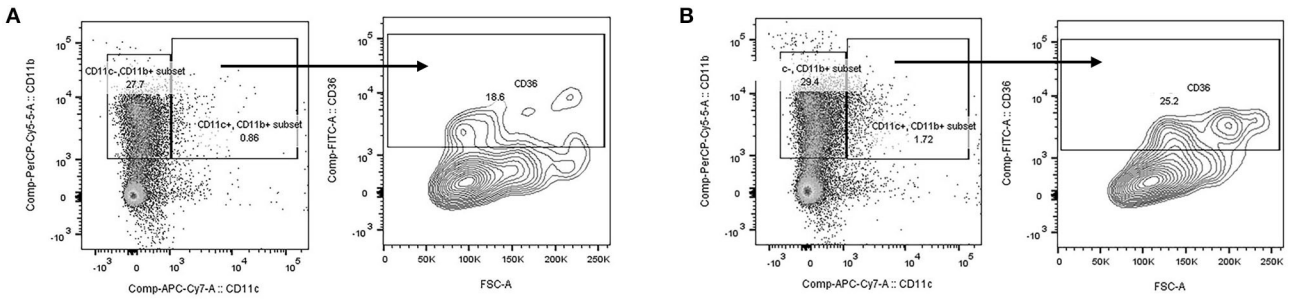

FIGURE 1 | Flow cytometry analysis of mouse blood. Blood was prepared for flow cytometry and cells gated on the CD11b+/c+ population. CD36 expression was similar in **(A)** fl/fl *CD36* and **(B)** EC CD36° samples, demonstrating no loss of expression of CD36 on the monocyte population.

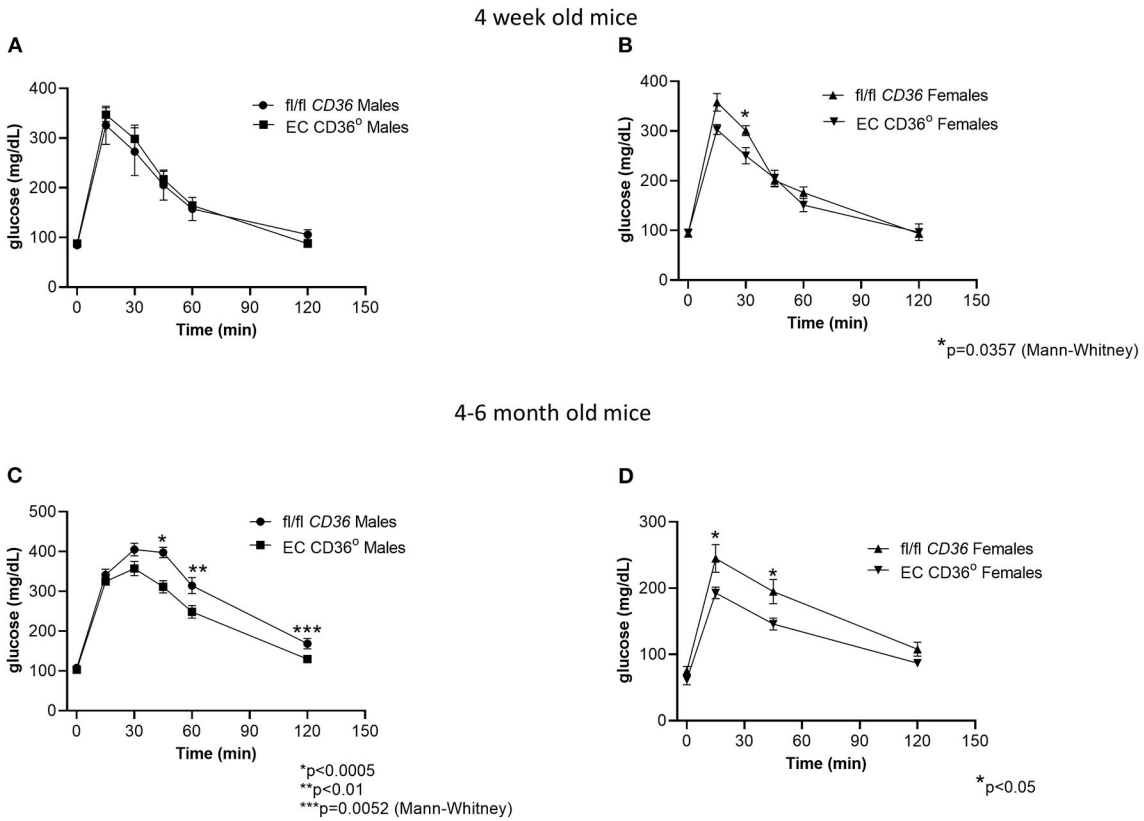

FIGURE 2 | Glucose tolerance testing of normal chow-fed EC CD36° and fl/fl *CD36* mice. **(A)** Four-week-old male mice showed no differences (fl/fl *CD36*, $n = 3$; EC CD36°, $n = 6$). **(B)** Four-week-old female mice showed a significant difference at 30 min; area under the curve (AUC) was not significant (fl/fl *CD36*, $n = 5$; EC CD36°, $n = 3$). **(C)** Four–six-month-old male mice showed significant differences at 45, 60, and 120 min (fl/fl *CD36*, $n = 13$; EC CD36°, $n = 12$). AUC was significantly different (fl/fl *CD36*: 34,817 ± 1,437; EC CD36°: 28,888 ± 1,015, $p < 0.005$). **(D)** Four-six-month-old female mice showed significant differences at 15 and 45 min ($n = 8$/group). AUC was significantly different (fl/fl *CD36*: 20,341 ± 1,491; EC CD36°: 15,713 ± 862, $p < 0.02$).

The increase in carbohydrate usage by EC CD36° males continued until late in the dark period. EC CD36° males showed noticeably less locomotor activity (**Figure 3F**). Female mice did not show any differences in any parameters measured (data not shown).

To determine the impact of the loss of EC CD36 in a diabetogenic setting, we fed the mice with ingredient-matched diets containing 35 kcal% carbohydrate and 45 kcal% fat (D12451, Research Diets, Inc.) or 70 kcal% carbohydrate and 10 kcal% fat (D12450H, Research Diets, Inc.); the extra carbohydrate is delivered in the form of starch, and the amount of sucrose between the diets is the same. At baseline, there were no differences in weight between the mice of the same sex. Weight gain was similar between the groups for both males and females

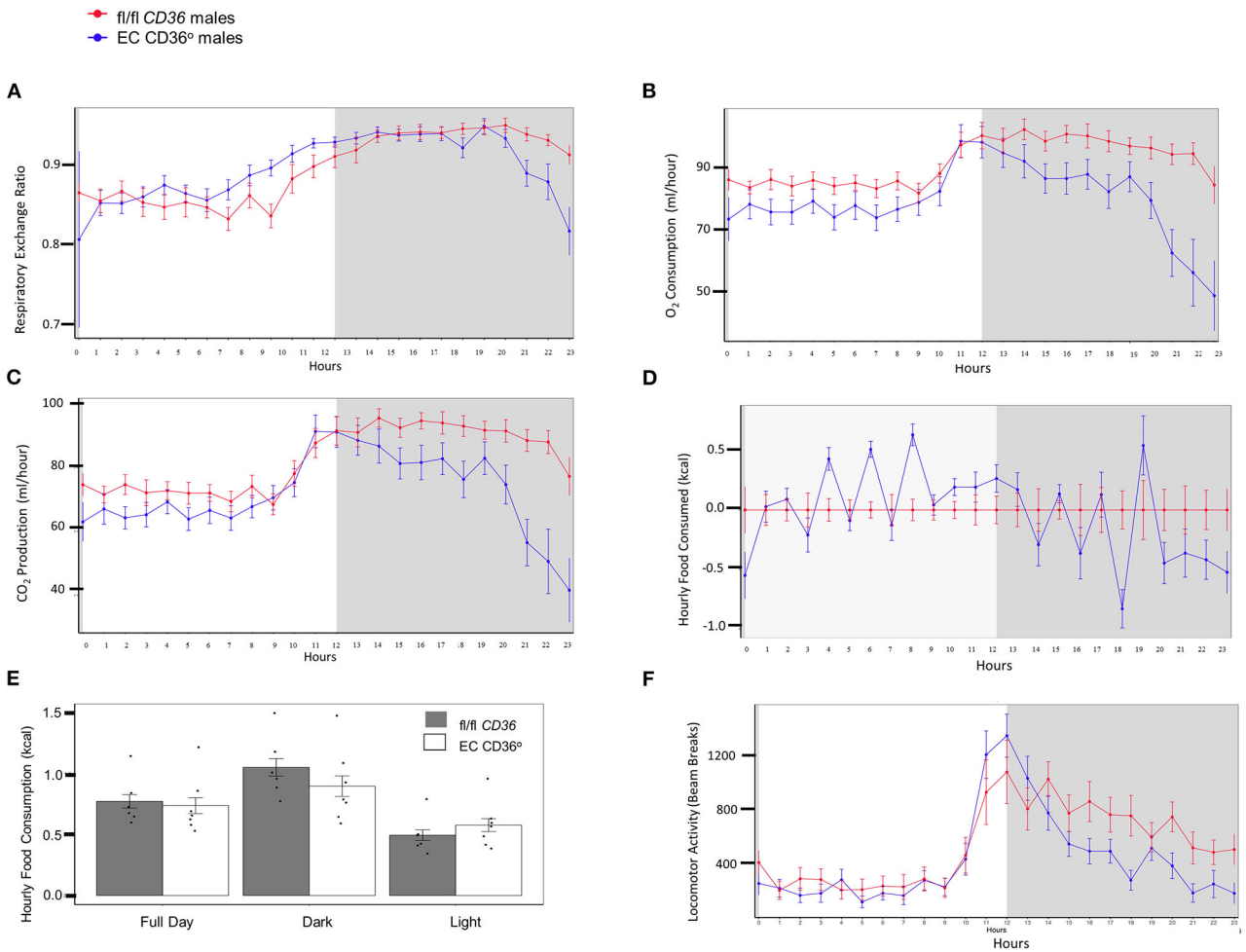

FIGURE 3 | Indirect calorimetry of 4-week-old normal chow-fed male fl/fl *CD36* ($n = 6$) and EC CD36° ($n = 7$) mice. Plots show data from a 12 h light:12 h dark cycle after a 24 h acclimation period. White panel = light phase; gray panel = dark phase. **(A)** Respiratory exchange ratio, **(B)** oxygen consumption, **(C)** CO_2 production, **(D)** food consumption, **(E)** total food consumption, and **(F)** locomotor activity.

over the 12 weeks of the diet, with transient small differences between the female groups at 6 and 9 weeks (**Figures 4A–D**). After 8 weeks of diet feeding, we compared glucose clearance by glucose tolerance testing (**Figures 5A–D**). Female EC CD36° mice showed better glucose clearance compared with controls when fed with either diet (**Figures 5B,D**); male EC CD36° mice showed improved glucose clearance compared with controls when fed with the 45 kcal% diet (**Figure 5C**). Lipoprotein analysis showed that the distribution of cholesterol was similar between the groups of both sexes when fed with either diet (**Table 1**). The distribution of triacylglycerides, however, showed differences, especially in female mice (**Table 1**). Female EC CD36° mice fed with the 10 kcal% fat diet had a greater percentage of triacylglycerides in the LDL/IDL (intermediate density lipoprotein) fraction compared with controls. Male and female EC CD36° mice fed with the 45 kcal% diet both showed a greater percentage of triaclyglycerides in the LDL/IDL fractions (**Table 1**) compared with controls. Female EC CD36° mice showed less triacylglycerides overall.

To determine the impact of the loss of EC CD36 on atherosclerosis, we crossed EC CD36° mice with the atherogenic LDLR° strain. We fed these mice a Western-style diet containing 42.7 kcal% carbohydrate, 42 kcal% fat, and 1.25% added cholesterol (TD 96121, Envigo) to promote atherosclerosis development, for 16 weeks. **Figure 6A** gives a general overview of the study timeline. *En face* morphometry of whole aortas stained with oil red O showed no difference in male mice (**Figure 6B**, $p = 0.0872$, Mann–Whitney). In contrast, female EC CD36°/LDLR° mice showed a 41% reduction in aortic lesions (**Figure 6C**). Representative aortas are shown in **Figure 6D**. Female mice showed decreased fasting glucose (**Figure 6E**). At sacrifice, there were no differences in plasma total cholesterol or weight in males or females (**Figures 6F,G**).

Glucose tolerance testing after 10 weeks of diet feeding showed female EC CD36°/LDLR° mice had swifter glucose clearance compared with controls, and both males and females had lower fasting glucose (**Figures 7A,B**). Body weights measured at the

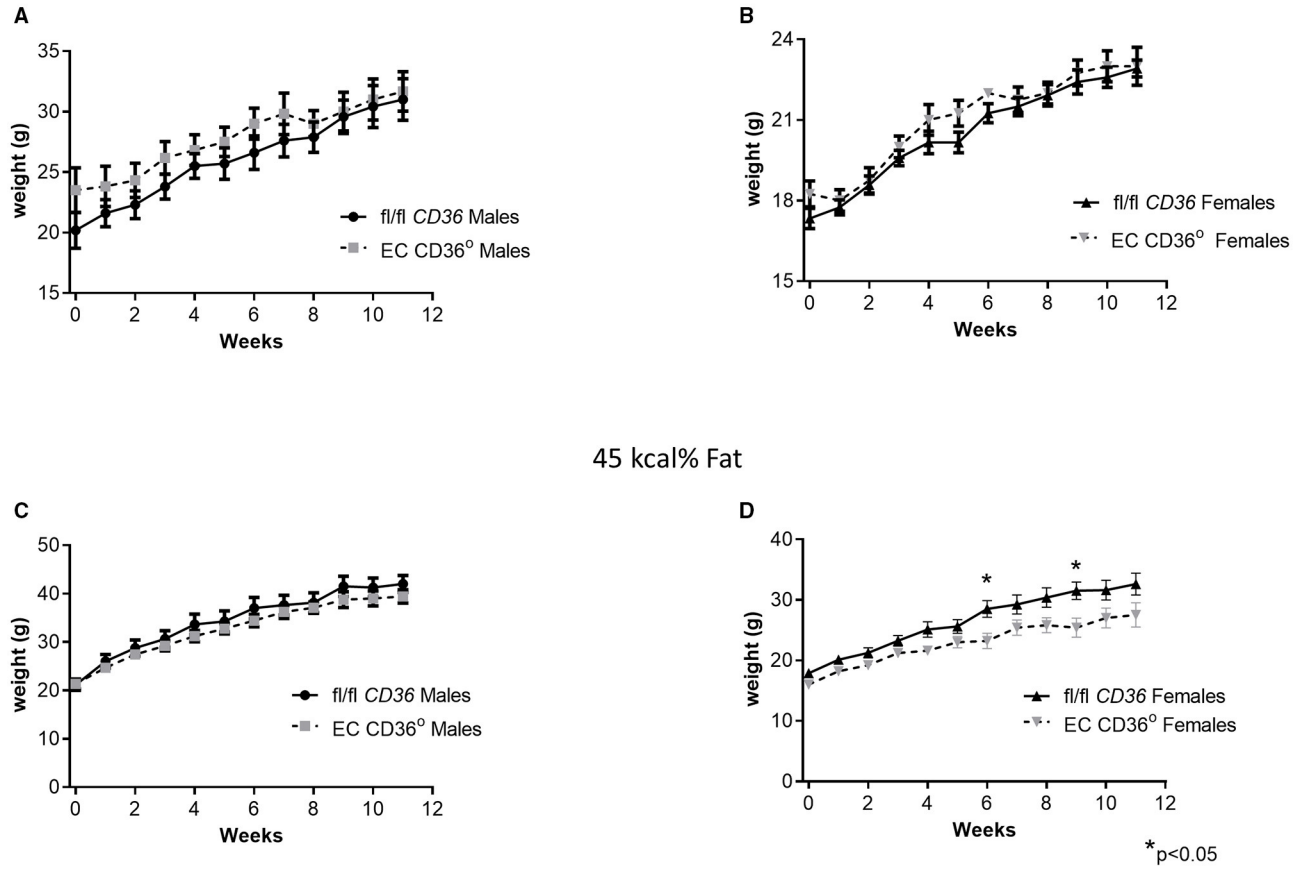

FIGURE 4 | Change in weight over time of EC CD36° and fl/fl *CD36* mice fed with ingredient-matched diets. **(A)** Male mice fed with the 10 kcal% fat diet. (fl/fl *CD36*, $n = 10$; EC CD36°, $n = 6$). **(B)** Female mice fed with the 10 kcal% fat diet (fl/fl *CD36*, $n = 12$; EC CD36°, $n = 4$). **(C)** Male mice fed with the 45 kcal% fat diet. (fl/fl *CD36*, $n = 8$; EC CD36°, $n = 9$). **(D)** Female mice fed with the 45 kcal% fat diet (fl/fl *CD36*, $n = 12$; EC CD36°, $n = 5$). There was a significant difference in weight at the 6 and 9 week time points.

time of glucose tolerance testing did not differ for females (24.4 + 0.434 g vs. 23.6 + 0.51 g, fl/fl *CD36*/LDLR° vs. EC CD36°/LDLR°, respectively), but fl/fl *CD36*/LDLR° males were significantly heavier than EC CD36°/LDLR° males (35 + 0.646 g vs. 30.71 + 1.085 g, $p<0.02$). Tracking backward, female mice were not different in terms of clearing a bolus of glucose at baseline (**Figure 8A**). After 3 weeks of high-fat, high-cholesterol diet feeding, EC CD36°/LDLR° females showed faster glucose clearance, reduced plasma total, and free cholesterol and triacylglycerides (**Figures 8B–D**) (this was a different cohort). At 8 weeks of diet feeding, EC CD36°/LDLR° females weighed less (**Figure 8E**). Lipoprotein analysis after 16 weeks showed no differences in male mice (**Table 2**). Female EC CD36°/LDLR° mice showed a greater percentage of triacylglycerides in the very low density lipoprotein (VLDL) fraction compared with controls (**Table 2**). Female EC CD36° mice showed less triacylglycerides overall and a delayed increase in plasma cholesterol.

DISCUSSION

Endothelial CD36 is recognized for its importance in angiogenesis; its role in tissue FA uptake at this interface is less studied. There is now increased awareness that ECs are a second obstacle to FA uptake into tissues (64–66). Previously considered as a passive barrier to FA diffusion, studies have shown regulation at this interface by CD36 and many of the same proteins involved in tissue FA uptake (64–69). CD36 was first implicated in the management of EC FA uptake in research on the EC-specific peroxisome proliferator activated receptor γ° mouse, which has markedly reduced EC CD36 expression and in many ways mimics the metabolic phenotype of the CD36°(70). This implies significant uncompensated metabolic control by EC. Changes in systemic metabolism may partly explain atherosclerosis protection in global CD36° mice, as obesity and insulin-resistance are strong determinants of lesion development.

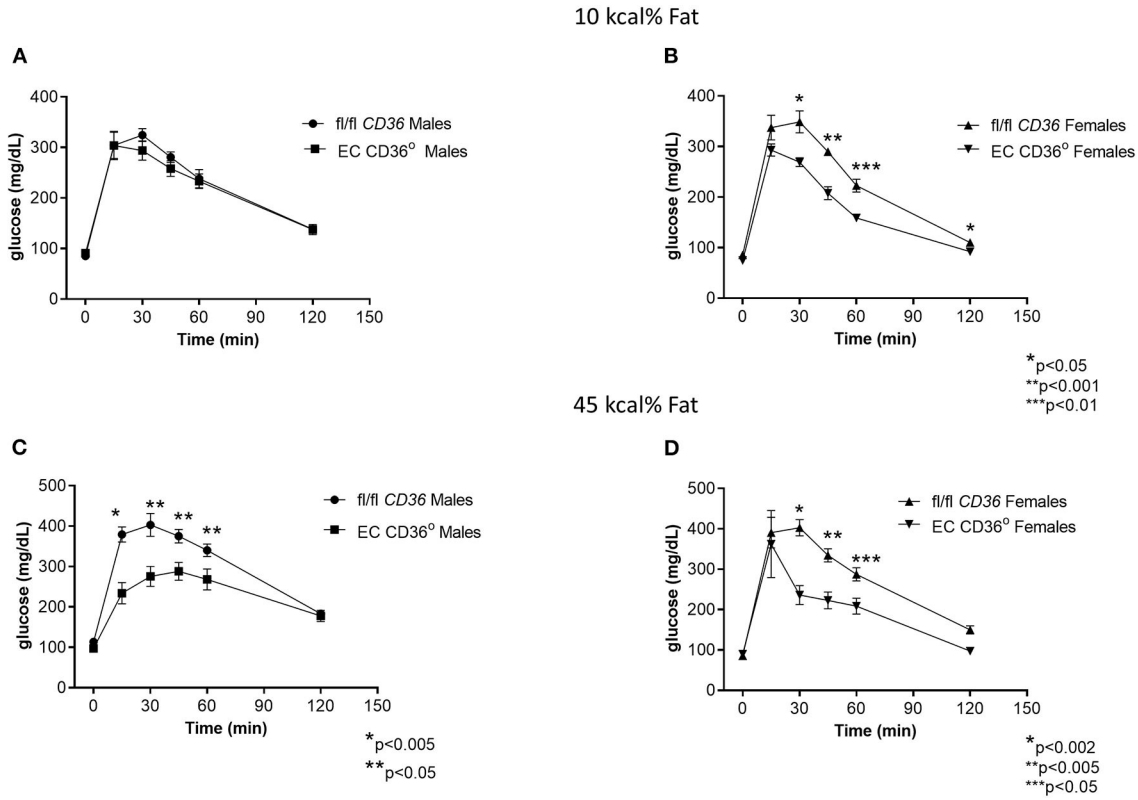

FIGURE 5 | Glucose tolerance testing of EC CD36° and fl/fl *CD36* mice after 8 weeks feeding ingredient matched diets. **(A)** Male mice fed with the 10 kcal% fat diet showed no significant differences (fl/fl *CD36*, $n = 5$; EC CD36°, $n = 6$). **(B)** Female mice fed with the 10 kcal% fat diet showed significant differences at 30, 45, 60, and 120 min. AUC was significantly different (fl/fl *CD36*: 26,939 ± 688; EC CD36°: 20,815 ± 625, $p = 0.001$) (fl/fl *CD36*, $n = 5$; EC CD36°, $n = 3$). **(C)** Male mice fed with the 45 kcal% fat diet showed significant differences at 15, 30, 45, and 60 min. AUC was significantly different (fl/fl *CD36*: 36,455 ± 1,589; EC CD36°: 28,080 ± 1,974, $p < 0.02$) (fl/fl *CD36*, $n = 5$; EC CD36°, $n = 3$). **(D)** Female mice fed with the 45 kcal% fat diet showed significant differences at 30, 45, and 60 min. AUC was significantly different (fl/fl *CD36*: 32,822 ± 1,813; EC CD36°: 23,733 ± 62,135, $p = 0.0238$, Mann–Whitney) (fl/fl *CD36*, $n = 5$; EC CD36°, $n = 3$).

TABLE 1 | Lipoprotein Analysis of Mice Fed With the 10 and 45 kcal % Fat Diets.

	fl/fl *CD36*	EC CD36°	fl/fl *CD36*	EC CD36°
10 kcal% fat	**Cholesterol (% of total)**		**Triacylglyceride (% of total)**	
Males				
VLDL	2	1	62	69
LDL/IDL	9	11	30	26
HDL	89	88	9	5
Females				
VLDL	2	2	51	41
LDL/IDL	7	11	39	48
HDL	91	87	11	11
45 kcal% fat	**Cholesterol (% of total)**		**Triacylglyceride (% of total)**	
Males				
VLDL	0.3	0.7	54	37
LDL/IDL	20	14	39	48
HDL	80	86	7	15
Females				
VLDL	0.8	0.5	27	25
LDL/IDL	11	9	46	64
HDL	88	91	27	12

Conscious of the potential confounding impact of the loss of CD36 in macrophages and other hematopoietic cells on atherosclerosis development and systemic inflammation, we created an EC CD36° using the Tie2e cre, which spares these cells (58–60). Floxed CD36 mice were previously generated utilizing C57Bl/6j embryonic stem cells to avoid background issues (44). These mice, therefore, differ in these ways from previously published EC CD36° mice, which were created using the Tek cre on a mixed genetic background (71). The development of an animal model to study EC CD36 in FA uptake and in the context of a pro-atherosclerotic environment is an important outcome of this work. Additionally, these mice will allow study of EC CD36 signaling pathways, triggered by excess dietary fat, which may also contribute to EC inflammation, plaque development, and pathological metabolic states.

A major finding of this study is that there was a strong contribution of EC CD36 to metabolic homeostasis in both male and female mice, yet there were interesting differences. At 4 weeks of age, when EC CD36° and control mice have similar lean body mass (93–95%) and fat stores, indirect calorimetry showed an increased reliance on carbohydrate metabolism and decreased locomotor activity and energy expenditure in male

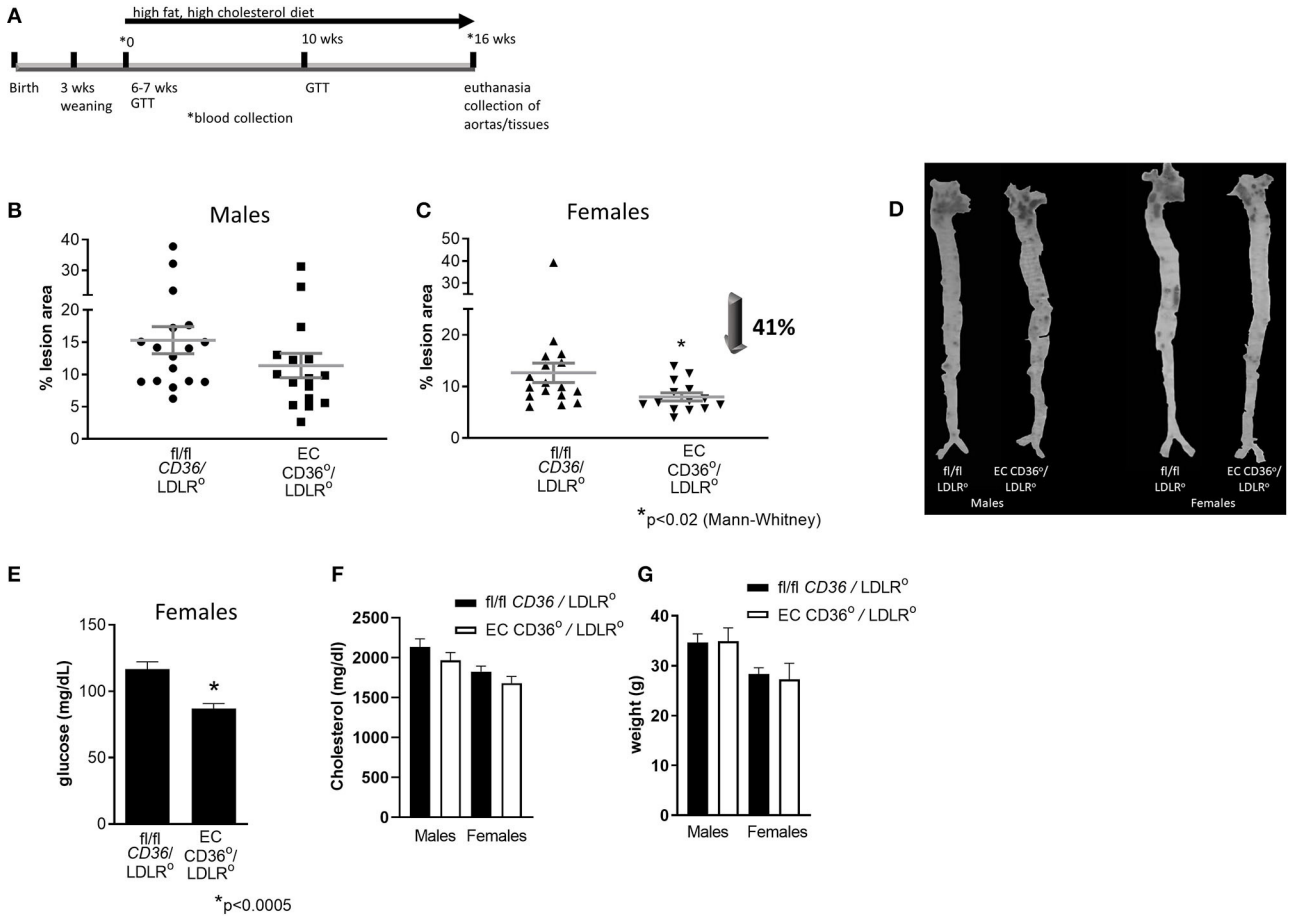

FIGURE 6 | Atherosclerosis lesion analysis. *En face* oil red O aortic lesions were quantified using Adobe Photoshop software after 16 weeks high-fat high-cholesterol diet feeding. **(A)** Timeline of atherosclerosis study. This was a longitudinal study. Mice were weaned at 3 weeks of age, and the high-fat, high-cholesterol diet was begun when the mice were 6–7 weeks of age. Just prior to the diet start (0), glucose tolerance testing (GTT) was performed and blood was collected; this and other blood collection timepoints are indicated by *. GTT was also performed after 10 weeks of diet feeding. Mice were euthanized and aortas, blood, and tissues were collected after 16 weeks of diet feeding. **(B)** Male mice showed no difference in percent atherosclerosis lesion (fl/fl *CD36*/LDLR°: 15.31 ± 2.096% vs. EC CD36°/LDLR°: 11.37 ± 1.884%) (fl/fl *CD36*/LDLR°, $n = 17$; EC CD36°/LDLR°, $n = 16$). **(C)** Female EC CD36°/LDLR° mice showed a significant 40% decrease in percent atherosclerosis lesion compared with controls (fl/fl *CD36*/LDLR°: 12.65 ± 1.896% vs. EC CD36°/LDLR°: 7.447 ± 0.897%, $p < 0.02$, Mann–Whitney) (fl/fl *CD36*/LDLR°, $n = 17$; EC CD36°/LDLR°, $n = 14$). **(D)** Representative aortas stained with oil red O. **(E)** Female EC CD36°/LDLR° mice had significantly lower fasting glucose compared with controls. **(F)** Total cholesterol showed no differences in males (fl/fl *CD36*/LDLR°: 2,132 ± 103.4 mg/dL vs. EC CD36°/LDLR°: 1,967 ± 96.42 mg/dL) or females (fl/fl *CD36*/LDLR°: 1,824 ± 68.94 mg/dL vs. EC CD36°/LDLR°: 1,680 ± 84.2 mg/dL) at endpoint. **(G)** Weights were not different at endpoint in males (fl/fl *CD36*/LDLR°: 35.51 ± 1.34 g vs. EC CD36°/LDLR°: 34.88 ± 0.673 g) or females (fl/fl *CD36*/LDLR°: 28.6 ± 0.78 g vs. EC CD36°/LDLR°: 27.27 ± 0.831 g).

mice only. Both control and EC CD36° male mice showed mixed carbohydrate and fat utilization during the early light period, based on RER. EC CD36° male mice ate more than controls in the light period, and toward the latter part, showed greater carbohydrate metabolism. During the dark phase, when mice are most active, EC CD36° male mice had decreased locomotor activity; oxygen consumption and carbon dioxide production, which are indicative of energy expenditure, were reduced in both periods compared with controls. This may reflect reduced adenosine triphosphate (ATP) generated as a result of anaerobic respiration of carbohydrates. These data suggest a systemic change in energy metabolism, with a decrease in high energy producing FA oxidation. It will be important to continue these studies in older mice to understand if these early metabolic patterns persist in both sexes, and to determine the effects of different diets.

The metabolic data in males are similar to what has been shown for the global CD36°: increased utilization of carbohydrates over fat as an energy substrate, specifically in heart and muscle (12, 36, 45, 72). Unlike global CD36° mice, the weights were similar between EC CD36° and controls. The data also reveal dichotomy between the sexes that was not observed in the global CD36°. Systemic metabolic changes resulting from reduced uptake of FA were also shown for EC CD36° made with the Tek cre, and they also showed sex-dependent differences: male mice showed a significant decrease in oleic acid uptake into heart, muscle, and brown adipose, while females had no difference in uptake in muscle (71). If

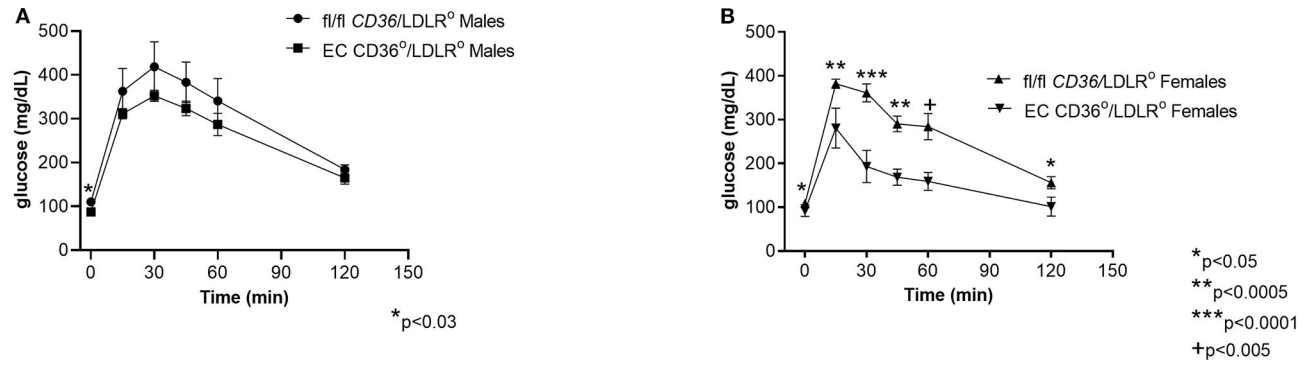

FIGURE 7 | Glucose tolerance testing of EC CD36°/LDLR° and fl/fl *CD36*/LDLR° mice after 10 weeks of high-fat high-cholesterol diet feeding. **(A)** Male EC CD36°/LDLR° mice showed a significant difference at the 0 time point. AUC was not different (fl/fl *CD36*/LDLR°, $n = 4$; EC CD36°/LDLR°, $n = 7$). **(B)** Female EC CD36°/LDLR° mice showed significant differences at all time points. AUC was significantly different (fl/fl *CD36*/LDLR°: 30,817 ± 1,142; EC CD36°/LDLR°: 19,331 ± 1,161, $p < 0.0001$) (fl/fl *CD36*/LDLR°, $n = 9$; EC CD36°/LDLR°, $n = 5$).

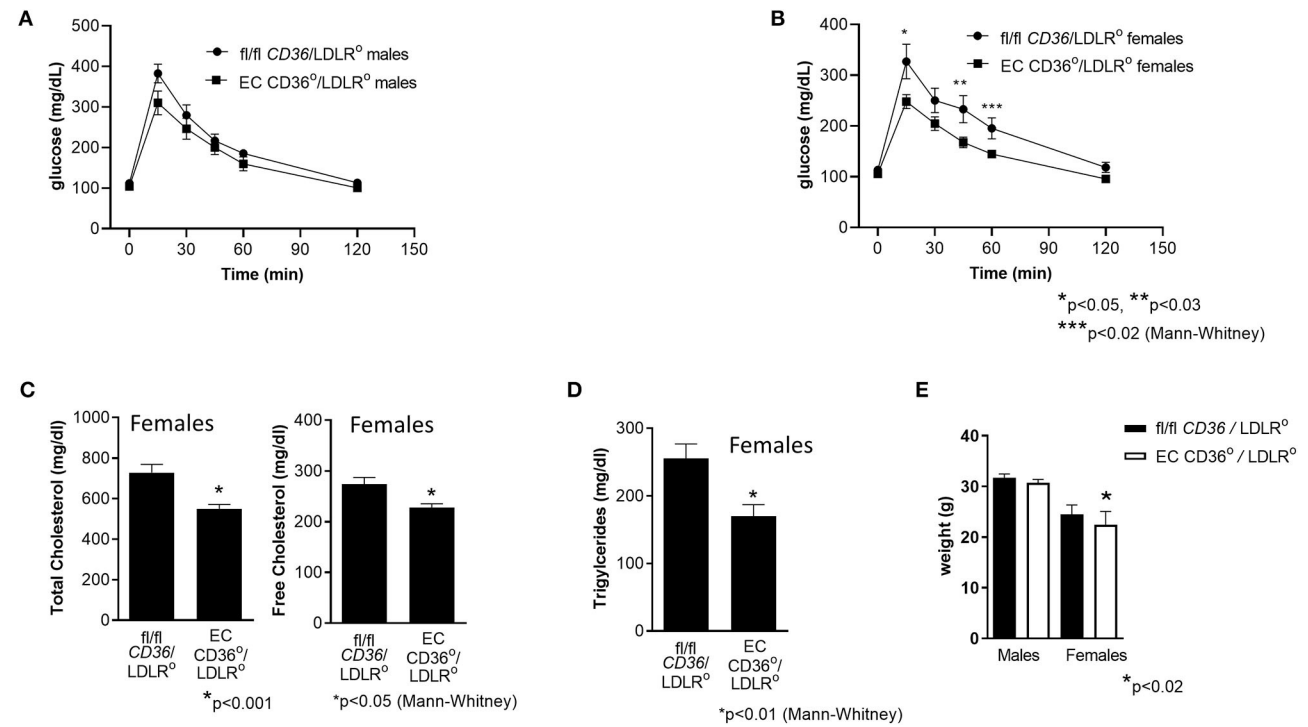

FIGURE 8 | Glucose tolerance testing, plasma cholesterol, and triacylglycerides of female EC CD36°/LDLR° and fl/fl *CD36*/LDLR° mice at baseline and after 3 weeks high-fat high-cholesterol diet feeding. **(A)** At 6–7 weeks of age, prior to initiation of the high fat high cholesterol diet, there were no differences in glucose clearance between the groups. **(B)** After 3 weeks diet feeding, female EC CD36°/LDLR° showed significant differences at 15, 45, and 60 min time points. AUC was significantly different (fl/fl *CD36*/LDLR°: 23,896 ± 1,920; EC CD36°/LDLR°: 18,409 ± 719, $p < 0.02$) (fl/fl *CD36*/LDLR°, $n = 8$; EC CD36°/LDLR°, $n = 10$). **(C)** Plasma total and free cholesterol were significantly lower in EC CD36°/LDLR° female mice after 3 weeks diet feeding (fl/fl *CD36*/LDLR°, $n = 10$; EC CD36°/LDLR°, $n = 13$). **(D)** Plasma triacylglycerides were significantly lower in EC CD36°/LDLR° female mice after 3 weeks diet feeding (fl/fl *CD36*/LDLR°, $n = 10$; EC CD36°/LDLR°, $n = 13$). **(E)** There was no difference in weights at 8 weeks in males (fl/fl *CD36*/LDLR°: 31.68 ± 0.769 g vs. EC CD36°/LDLR°: 30.17 ± 0.826 g) or females (fl/fl *CD36*/LDLR°: 24.44 ± 0.403 g vs. EC CD36°/LDLR°: 22.5 ± 0.57 g).

true of our mice, this may explain why females displayed no differences by indirect calorimetry. The data may suggest a sex difference in CD36 expression in EC subsets, or a sex difference in expression of alternative transporters. The role of estrogen *vs.* testosterone would be an important area of future study in this regard.

When fed with a low fat (4%), normal chow diet, EC CD36° mice showed faster glucose clearance at 4–5 months of age, while

TABLE 2 | Lipoprotein Analysis of Mice Fed With the HFHC Diet.

	fl/fl *CD36*/ LDLR°	EC CD36°/ LDLR°	fl/fl *CD36*/ LDLR°	EC CD36°/ LDLR°
HFHC Diet	**Cholesterol (% of total)**		**Triacylglyceride (% of total)**	
Males				
VLDL	26	26	62	64
LDL/IDL	47	48	27	29
HDL	27	26	12	7
Females				
VLDL	29	23	72	57
LDL/IDL	54	57	18	24
HDL	18	21	11	20

of similar weight. These data are similar to the findings in the global CD36° and EC CD36° made with the Tek cre (36, 71). When the mice were stressed with diets higher in fat than normal chow, weight gain did not differ compared with controls at most time points; females showed transient differences. Female EC CD36° mice continued to show faster clearance of a bolus of glucose in the context of both the 10 and 45 kcal% fat diets. Male EC CD36° mice showed swifter glucose clearance than controls when fed with the 45 kcal% fat diet. In overnutrition, macrophage pro-inflammatory signaling and other adipocyte-derived signals, along with excess FA uptake in muscle, lead to impaired insulin signaling and impaired glucose tolerance (73). Although we have not ruled out differences in insulin secretion, EC CD36° male mice may have increased glucose clearance due to an inability to efficiently utilize FA in heart and muscle and concomitant increased reliance on glucose. This may also be the case in females, if they too have decreased muscle FA uptake. Interestingly, Tek cre EC CD36° females were protected against insulin resistance, despite normal FA uptake in muscle (71). This may suggest that CD36-dependent EC inflammation contributes to systemic inflammatory pathways leading to insulin resistance. This is an important area of further study.

Distribution of cholesterol and triacylglycerides among lipoproteins was not different between male EC CD36° and control mice fed with the 10 kcal% fat diet; female EC CD36° mice showed a 23% enrichment in triacylglycerides in the LDL/IDL fraction. When fed with the 45 kcal% fat diet, both male and female EC CD36° mice showed this shift in triacylglycerides to LDL/IDL (23 and 40% increase for males and females, respectively). These data suggest a delayed ability to hydrolyze triacylglycerol from the VLDL particle. In the global CD36° mouse, increased plasma-free FA were found to inhibit the activity of lipoprotein lipase, leading to decreased VLDL hydrolysis (74). It is possible that the local free FA concentration at the EC interface rises to inhibitory levels, due to loss of EC CD36 and slower tissue uptake, preventing optimal hydrolysis. An alternative hypothesis is that EC CD36 is important in tethering the lipoprotein for lipase activity. Further experiments need to be completed to unravel the mechanism.

As shown, weight gain was similar between the groups on all diets. This was also true of the EC CD36° made with the Tek cre, which showed no difference in white adipose tissue FA uptake (71). In the global CD36° mouse, TG-rich VLDL accumulated, as a result of inefficient hydrolysis both at the EC and tissue surfaces (36). One potential reason why weight may not be affected in the EC CD36° may be that although hydrolysis is inefficient, as the lipoprotein becomes smaller in size, it can enter the subendothelial space and undergo hydrolysis at the level of the individual tissue, and FAs are then taken up by adipocytes for storage.

Activated endothelium provides the surface for initiation of atherosclerotic lesions. We were interested in how atherosclerosis would develop in the absence of EC CD36, because high-fat diets promote atherosclerosis in part through changes in shear stress and other pro-inflammatory pathways. CD36 is an important receptor for pro-atherosclerotic-modified LDL ligands, often called oxPC CD36 (75, 76). These ligands are recognized as a consequence of CD36 scavenger receptor activity. In macrophages, interaction with these ligands leads to the generation of foam cells, reactive oxygen species generation, and secretion of cytokines (46, 75, 76). While EC do not accumulate lipids to form foam cells, we considered that interaction between EC CD36 and oxPC CD36 may contribute to the initiation phase of atherosclerosis through inflammatory pathways. Lesion analysis showed a significant decrease in aortic atherosclerosis burden in EC CD36°/LDLR° female mice. These results differ from global CD36°/LDLR°, where protection against atherosclerosis was observed in both males and females (29).

Endothelial cell CD36°/LDLR° female mice showed no differences in plasma cholesterol levels compared with controls after 16 weeks of diet feeding, and only a transient small difference in weight after 6–8 weeks of diet feeding (but not at 3 or 16 weeks). EC CD36°/LDLR° mice showed decreased fasting glucose, and glucose tolerance testing showed faster glucose clearance in female EC CD36°/LDLR° mice compared with controls. This trait was apparent at the 3 week time point when female EC CD36°/LDLR° mice also showed a decrease in plasma total and free cholesterol and triacylglyceride levels. While improved glucose clearance continued to be a hallmark of EC CD36°/LDLR° female mice, differences in cholesterol and triacylglyceride levels were not found at 6 and 16 weeks of diet feeding. Lipoprotein analysis revealed that EC CD36°/LDLR° female mice had 33% more triaclylglycerides in the LDL/IDL fraction compared with controls after 16 weeks diet feeding. EC CD36°/LDLR° males were similar to controls. The atherogenic diet, although similar in kcal% fat content, differs from the 45 kcal% diet in terms of fat source (milkfat vs. lard) and sucrose amount (341 vs. 206 g/kg). Unlike in the case of the 45 kcal% diet, male EC CD36°/LDLR° mice did not show a difference in glucose tolerance testing, and this may, in part, explain the lack of atherosclerosis protection. Male mice at 4 weeks of age had systemic metabolic changes that suggested greater carbohydrate utilization, and perhaps greater capacity to resist the detrimental effects of excess FA, similar to the global CD36°. The high-fat, high-cholesterol diet, however, may have resulted in a systemic inflammatory response that was greater than in the global CD36° due to CD36 macrophage expression and interaction with CD36

ligands. Further investigation is necessary to understand the interaction of dietary components and sex/sex hormones in the metabolic and atherogenic differences uncovered.

Atherosclerosis is a chronic inflammatory disease that begins in atheroprone regions of the vasculature with activation of the endothelium due to high-fat, cholesterol-rich diets. Inflammation affects the development of obesity and dysfunctional fat, and in muscle, insulin resistance, which are contributing risk factors. EC CD36°/LDLR° female mice showed systemic metabolic differences compared with controls, and had less atherosclerosis lesion burden, but similar weight gain. The inflammatory characteristics of the EC and fat will be interesting to characterize in future studies, as well as analysis of plasma cytokines/chemokines, as these may provide greater mechanistic insight into the protection against lesion development, and the differences between the sexes.

In addition to EC CD36 affecting tissue FA uptake, beyond the scope of this study, there may also be FA effects directly on EC. A recent report by Bou Khzam et al. (77) used a knockdown approach to decrease expression of CD36 by ∼50% in mouse lung and cardiomyocyte EC; they found no difference in survival or proliferation. In studies done in the context of added FA (primarily oleic acid), they noted that knockdown of CD36 attenuated FA-induced increases in proliferation and migration in an *in vivo* scratch wound healing assay (77). Palmitic acid had opposite effects and was toxic. Oleic acid-treated, CD36 knockdown EC showed an ∼8× increase in AMP-activated protein kinase expression, indicative of EC stress, and a pro-angiogenic response (77). The effect of added oleic acid in the context of reduced but not absent CD36 could perhaps lead to an insulin-resistant state, and similar to in diabetics, inhibits vessel formation, even in the context of pro-angiogenic signals. Using the Tek cre CD36° mice, Bou Khzam et al. (77) showed impaired angiogenesis, accompanied by upregulation of other anti-angiogenic proteins. A previous study measured hindlimb ischemia in global CD36° mice: Isenberg et al. (78) found no difference in limb survival at 7 days between wild type and CD36° mice. They attributed these findings to thrombospondin-1-CD47-dependent nitric oxide antagonism, leading to inhibition of vascular remodeling in this ischemic model. Bou Khzam et al. (77) did not investigate CD47 signaling in their report. Other studies have shown CD36 to be anti-angiogenic *via* thrombospondin-1 signaling, leading to apoptosis in normal EC, or by blocking the vascular endothelial growth factor receptor 2 pathway in tumor EC (79).

How CD36 facilitates FA uptake remains controversial, with at least three different proposed mechanisms. Hamilton and coworkers suggest that CD36 does not play a direct role in the uptake of FA, and flip-flop of FA is the prevailing mechanism (32, 80). Instead, they postulate that CD36-dependent signaling effects FA esterification and incorporation into different cellular pools, and this is why loss of CD36 appears to inhibit FA uptake (35). Based on the structure of CD36, which contains a hydrophobic cleft that reaches near to if not below the lipid bylayer, others have proposed that this acts as a tunnel through which FAs are led to the cell surface, where they may flip-flop over (81, 82). Localization of CD36 to specific plasma membrane microdomains may associate it with cytoplasmic FA binding proteins or esterifying enzymes, leading to apparent unidirectional FA flow (83). Hao et al. (84) provide data in support of a third hypothesis: in the presence of FA, CD36 in adipocyte caveolae is depalmitoylated permitting endocytosis. After delivery of FA to lipid droplets, repalmitoylated CD36 is returned to the membrane surface (84). This mechanism differs from the previous two in the rate of uptake of FA. Whether this pathway extends to all cell types remains to be elucidated. While there may be no consensus in terms of mechanism, it is clear that loss of CD36 in mice and humans leads to systemic effects (11).

Overall, in this report, we show metabolic differences consistent with reduced ability to hydrolyze and uptake FA in the absence of EC CD36, leading to decreased FA oxidation and reduced energy generation. Our work supports a previous study showing EC CD36 is necessary for optimal FA uptake by heart and muscle, and demonstrating changes in glucose tolerance testing, fasting glucose, but not weight, similar to ours (71). We further show that loss of EC CD36 led to reduced aortic atherosclerosis lesion in female mice. To our knowledge, this is the first report of the impact of loss of an EC-specific FA transport protein on atherosclerosis. The data suggest a sex-dependent role for EC CD36 in lipid metabolism, with potential impact on insulin resistance and EC inflammation, driving atherogenesis. These findings support as essential role for the endothelium in controlling tissue FA uptake and for EC CD36 in atherosclerosis development.

DATA AVAILABILITY STATEMENT

The original contributions presented in the study are included in the article/supplementary material, further inquiries can be directed to the corresponding author.

ETHICS STATEMENT

The animal study was reviewed and approved by the University of Alberta Animal Care and Use Committee.

AUTHOR CONTRIBUTIONS

URR helped in the design and planning of experiments and conducted experiments, compiled and analyzed data, and helped write the manuscript. MO helped in the atherosclerosis experiments. MA assisted with animal work. CD designed and carried out the flow cytometry experiments. LI provided assistance with experiments. SE oversaw the flow cytometry experiments. MF helped in the design and planning of experiments and conducted experiments, compiled and analyzed data, and drafted the manuscript. All authors contributed to the article and approved the submitted version.

FUNDING

We gratefully acknowledge funding from the Heart and Stroke Foundation (GIA G-17-0019162, MF), Canada

Foundation for Innovation, Alberta Enterprise and Advanced Education and the Faculty of Medicine and Dentistry, University of Alberta Motyl Graduate Studentship in Cardiac Sciences (URR).

ACKNOWLEDGMENTS

Flow Cytometry Experiments were performed at the University of Alberta Faculty of Medicine and Dentistry Flow Cytometry Facility, RRID:SCR_019195, which receives financial support from the Faculty of Medicine and Dentistry and Canada Foundation for Innovation (CFI) awards to contributing investigators. Lipidomics Experiments were performed at the University of Alberta Faculty of Medicine and Dentistry Lipidomics Core, RRID:SCR_019176, which receives financial support from the Faculty of Medicine and Dentistry, and Canada Foundation for Innovation (CFI) and Natural Sciences and Engineering Research Council of Canada (NSERC) awards to contributing investigators.

REFERENCES

1. Greenwalt DE, Watt KW, Hasler T, Howard RJ, Patel S. Structural, functional, and antigenic differences between bovine heart endothelial CD36 and human platelet CD36. *J Biol Chem.* (1990) 265:16296–9. doi: 10.1016/S0021-9258(17)46221-1
2. Swerlick RA, Lee KH, Wick TM, Lawley TJ. Human dermal microvascular endothelial but not human umbilical vein endothelial cells express CD36 *in vivo* and *in vitro*. *J Immunol.* (1992) 148:78–83. Available online at: www.jimmunol.org/content/148/1/78
3. Abumrad NA, el-Maghrabi MR, Amri EZ, Lopez E, Grimaldi PA. Cloning of a rat adipocyte membrane protein implicated in binding or transport of long-chain fatty acids that is induced during preadipocyte differentiation. Homology with human CD36. *J Biol Chem.* (1993) 268:17665–8. doi: 10.1016/S0021-9258(17)46753-6
4. Van Nieuwenhoven FA, Verstijnen CP, Abumrad NA, Willemsen PH, Van Eys GJ, Van der Vusse GJ, et al. Putative membrane fatty acid translocase and cytoplasmic fatty acid- binding protein are co-expressed in rat heart and skeletal muscles. *Biochem Biophys Res Commun.* (1995) 207:747–52. doi: 10.1006/bbrc.1995.1250
5. Zhou J, Febbraio M, Wada T, Zhai Y, Kuruba R, He J, et al. Hepatic fatty acid transporter Cd36 is a common target of LXR, PXR, and PPARgamma in promoting steatosis. *Gastroenterology.* (2008) 134:556–67. doi: 10.1053/j.gastro.2007.11.037
6. Lucas M, Stuart LM, Zhang A, Hodivala-Dilke K, Febbraio M, Silverstein R, et al. Requirements for apoptotic cell contact in regulation of macrophage responses. *J Immunol.* (2006) 177:4047–54. doi: 10.4049/jimmunol.177.6.4047
7. Greenberg ME, Sun M, Zhang R, Febbraio M, Silverstein R, Hazen SL. Oxidized phosphatidylserine-CD36 interactions play an essential role in macrophage-dependent phagocytosis of apoptotic cells. *J Exp Med.* (2006) 203:2613–25. doi: 10.1084/jem.20060370
8. Endemann G, Stanton LW, Madden KS, Bryant CM, White RT, Protter AA. CD36 is a receptor for oxidized low density lipoprotein. *J Biol Chem.* (1993) 268:11811–6. doi: 10.1016/S0021-9258(19)50272-1
9. Hoebe K, Georgel P, Rutschmann S, Du X, Mudd S, Crozat K, et al. CD36 is a sensor of diacylglycerides. *Nature.* (2005) 433:523–7. doi: 10.1038/nature03253
10. Stewart CR, Stuart LM, Wilkinson K, van Gils JM, Deng J, Halle A, et al. CD36 ligands promote sterile inflammation through assembly of a Toll-like receptor 4 and 6 heterodimer. *Nat Immunol.* (2010) 11:155–61. doi: 10.1038/ni.1836
11. Silverstein RL, Febbraio M. CD36, a scavenger receptor involved in immunity, metabolism, angiogenesis, and behavior. *Sci Signal.* (2009) 2:re3. doi: 10.1126/scisignal.272re3
12. Coburn CT, Knapp FF, Jr., Febbraio M, Beets AL, Silverstein RL. Defective uptake and utilization of long chain fatty acids in muscle and adipose tissues of CD36 knockout mice. *J Biol Chem.* (2000) 275:32523–9. doi: 10.1074/jbc.M003826200
13. Raheel H, Ghaffari S, Khosraviani N, Mintsopoulos V, Auyeung D, Wang C, et al. CD36 mediates albumin transcytosis by dermal but not lung microvascular endothelial cells: role in fatty acid delivery. *Am J Physiol Lung Cell Mol Physiol.* (2019) 316:L740–L50. doi: 10.1152/ajplung.00127.2018
14. Daquinag AC, Gao Z, Fussell C, Immaraj L, Pasqualini R, Arap W, et al. Fatty acid mobilization from adipose tissue is mediated by CD36 post-translational modifications and intracellular trafficking. *JCI Insight.* (2021) 6:e147057. doi: 10.1172/jci.insight.147057
15. Feng WW, Wilkins O, Bang S, Ung M, Li J, An J, et al. CD36-mediated metabolic rewiring of breast cancer cells promotes resistance to HER2-targeted therapies. *Cell Rep.* (2019) 29:3405–20.e5. doi: 10.1016/j.celrep.2019.11.008
16. Watt MJ, Clark AK, Selth LA, Haynes VR, Lister N, Rebello R, et al. Suppressing fatty acid uptake has therapeutic effects in preclinical models of prostate cancer. *Sci Transl Med.* (2019) 11:eaau5758. doi: 10.1126/scitranslmed.aau5758
17. Gruarin P, Thorne RF, Dorahy DJ, Burns GF, Sitia R, Alessio M. CD36 is a ditopic glycoprotein with the N-terminal domain implicated in intracellular transport. *Biochem Biophys Res Commun.* (2000) 275:446–54. doi: 10.1006/bbrc.2000.3333
18. Chen K, Li W, Major J, Rahaman SO, Febbraio M, Silverstein RL. Vav guanine nucleotide exchange factors link hyperlipidemia and a prothrombotic state. *Blood.* (2011) 117:5744–50. doi: 10.1182/blood-2009-01-201970
19. Rahaman SO, Lennon DJ, Febbraio M, Podrez EA, Hazen SL, Silverstein RL. A CD36-dependent signaling cascade is necessary for macrophage foam cell formation. *Cell Metab.* (2006) 4:211–21. doi: 10.1016/j.cmet.2006.06.007
20. Rahaman SO, Swat W, Febbraio M, Silverstein RL. Vav family Rho guanine nucleotide exchange factors regulate CD36-mediated macrophage foam cell formation. *J Biol Chem.* (2011) 286:7010–7. doi: 10.1074/jbc.M110.192450
21. Chen K, Febbraio M, Li W, Silverstein RL. A specific CD36-dependent signaling pathway is required for platelet activation by oxidized low-density lipoprotein. *Circ Res.* (2008) 102:1512–9. doi: 10.1161/CIRCRESAHA.108.172064
22. Triantafilou M, Gamper FG, Lepper PM, Mouratis MA, Schumann C, Harokopakis E, et al. Lipopolysaccharides from atherosclerosis-associated bacteria antagonize TLR4, induce formation of TLR2/1/CD36 complexes in lipid rafts and trigger TLR2-induced inflammatory responses in human vascular endothelial cells. *Cell Microbiol.* (2007) 9:2030–9. doi: 10.1111/j.1462-5822.2007.00935.x
23. Stuart LM, Bell SA, Stewart CR, Silver JM, Richard J, Goss JL, et al. CD36 signals to the actin cytoskeleton and regulates microglial migration *via* a p130Cas complex. *J Biol Chem.* (2007) 282:27392–401. doi: 10.1074/jbc.M702887200
24. Cho S, Park EM, Febbraio M, Anrather J, Park L, Racchumi G, et al. The class B scavenger receptor CD36 mediates free radical production and tissue injury in cerebral ischemia. *J Neurosci.* (2005) 25:2504–12. doi: 10.1523/JNEUROSCI.0035-05.2005
25. Jimenez B, Volpert OV, Crawford SE, Febbraio M, Silverstein RL, Bouck N. Signals leading to apoptosis-dependent inhibition of neovascularization by thrombospondin-1. *Nat Med.* (2000) 6:41–8. doi: 10.1038/71517
26. Podrez EA, Byzova TV, Febbraio M, Salomon RG, Ma Y, Valiyaveettil M, et al. Platelet CD36 links hyperlipidemia, oxidant stress and a prothrombotic phenotype. *Nat Med.* (2007) 13:1086–95. doi: 10.1038/nm1626
27. Park YM, Drazba JA, Vasanji A, Egelhoff T, Febbraio M, Silverstein RL. Oxidized LDL/CD36 interaction induces loss of cell polarity

and inhibits macrophage locomotion. *Mol Biol Cell.* (2012) 23:3057–68. doi: 10.1091/mbc.e11-12-1051
28. Park YM, Febbraio M, Silverstein RL. CD36 modulates migration of mouse and human macrophages in response to oxidized LDL and may contribute to macrophage trapping in the arterial intima. *J Clin Invest.* (2009) 119:136–45. doi: 10.1172/JCI35535
29. Kennedy DJ, Kuchibhotla SD, Guy E, Park YM, Nimako G, Vanegas D, et al. Dietary cholesterol plays a role in CD36-mediated atherogenesis in LDLR-knockout mice. *Arterioscler Thromb Vasc Biol.* (2009) 29:1481–7. doi: 10.1161/ATVBAHA.109.191940
30. Brown PM, Kennedy DJ, Morton RE, Febbraio M. CD36/SR-B2-TLR2 dependent pathways enhance *Porphyromonas gingivalis* mediated atherosclerosis in the Ldlr KO mouse model. *PLoS One.* (2015) 10:e0125126. doi: 10.1371/journal.pone.0125126
31. Kamp F, Hamilton JA. How fatty acids of different chain length enter and leave cells by free diffusion. *Prostaglandins Leukot Essent Fatty Acids.* (2006) 75:149–59. doi: 10.1016/j.plefa.2006.05.003
32. Hamilton JA, Guo W, Kamp F. Mechanism of cellular uptake of long-chain fatty acids: do we need cellular proteins? *Mol Cell Biochem.* (2002) 239:17–23. doi: 10.1007/978-1-4419-9270-3_3
33. Bonen A, Benton CR, Campbell SE, Chabowski A, Clarke DC, Han XX, et al. Plasmalemmal fatty acid transport is regulated in heart and skeletal muscle by contraction, insulin and leptin, and in obesity and diabetes. *Acta Physiol Scand.* (2003) 178:347–56. doi: 10.1046/j.1365-201X.2003.01157.x
34. Glatz JF, Luiken JJ, Bonen A. Membrane fatty acid transporters as regulators of lipid metabolism: implications for metabolic disease. *Physiol Rev.* (2010) 90:367–417. doi: 10.1152/physrev.00003.2009
35. Xu S, Jay A, Brunaldi K, Huang N, Hamilton JA. CD36 enhances fatty acid uptake by increasing the rate of intracellular esterification but not transport across the plasma membrane. *Biochemistry.* (2013) 52:7254–61. doi: 10.1021/bi400914c
36. Febbraio M, Abumrad NA, Hajjar DP, Sharma K, Cheng W, Pearce SF, et al. A null mutation in murine CD36 reveals an important role in fatty acid and lipoprotein metabolism. *J Biol Chem.* (1999) 274:19055–62. doi: 10.1074/jbc.274.27.19055
37. Hajri T, Han XX, Bonen A, Abumrad NA. Defective fatty acid uptake modulates insulin responsiveness and metabolic responses to diet in CD36-null mice. *J Clin Invest.* (2002) 109:1381–9. doi: 10.1172/JCI0214596
38. Love-Gregory L, Sherva R, Sun L, Wasson J, Schappe T, Doria A, et al. Variants in the CD36 gene associate with the metabolic syndrome and high-density lipoprotein cholesterol. *Hum Mol Genet.* (2008) 17:1695–704. doi: 10.1093/hmg/ddn060
39. Fukuchi K, Nozaki S, Yoshizumi T, Hasegawa S, Uehara T, Nakagawa T, et al. Enhanced myocardial glucose use in patients with a deficiency in long- chain fatty acid transport (CD36 deficiency). *J Nucl Med.* (1999) 40:239–43.
40. Hwang EH, Taki J, Yasue S, Fujimoto M, Taniguchi M, Matsunari I, et al. Absent myocardial iodine-123-BMIPP uptake and platelet/monocyte CD36 deficiency. *J Nucl Med.* (1998) 39:1681–4.
41. Bonen A, Parolin ML, Steinberg GR, Calles-Escandon J, Tandon NN, Glatz JF, et al. Triacylglycerol accumulation in human obesity and type 2 diabetes is associated with increased rates of skeletal muscle fatty acid transport and increased sarcolemmal FAT/CD36. *FASEB J.* (2004) 18:1144–6. doi: 10.1096/fj.03-1065fje
42. Bonen A, Tandon NN, Glatz JF, Luiken JJ, Heigenhauser GJ. The fatty acid transporter FAT/CD36 is upregulated in subcutaneous and visceral adipose tissues in human obesity and type 2 diabetes. *Int J Obes (Lond).* (2006) 30:877–83. doi: 10.1038/sj.ijo.0803212
43. McFarlan JT, Yoshida Y, Jain SS, Han XX, Snook LA, Lally J, et al. *In vivo*, fatty acid translocase (CD36) critically regulates skeletal muscle fuel selection, exercise performance, and training-induced adaptation of fatty acid oxidation. *J Biol Chem.* (2012) 287:23502–16. doi: 10.1074/jbc.M111.315358
44. Nagendran J, Pulinilkunnil T, Kienesberger PC, Sung MM, Fung D, Febbraio M, et al. Cardiomyocyte-specific ablation of CD36 improves post-ischemic functional recovery. *J Mol Cell Cardiol.* (2013) 63:180–8. doi: 10.1016/j.yjmcc.2013.07.020
45. Kuang M, Febbraio M, Wagg C, Lopaschuk GD, Dyck JR. Fatty acid translocase/CD36 deficiency does not energetically or functionally compromise hearts before or after ischemia. *Circulation.* (2004) 109:1550–7. doi: 10.1161/01.CIR.0000121730.41801.12
46. Kennedy DJ, Kuchibhotla S, Westfall KM, Silverstein RL, Morton RE, Febbraio M. A CD36-dependent pathway enhances macrophage and adipose tissue inflammation and impairs insulin signalling. *Cardiovasc Res.* (2011) 89:604–13. doi: 10.1093/cvr/cvq360
47. Nicholls HT, Kowalski G, Kennedy DJ, Risis S, Zaffino LA, Watson N, et al. Hematopoietic cell-restricted deletion of CD36 reduces high-fat diet-induced macrophage infiltration and improves insulin signaling in adipose tissue. *Diabetes.* (2011) 60:1100–10. doi: 10.2337/db10-1353
48. Febbraio M, Guy E, Silverstein RL. Stem cell transplantation reveals that absence of macrophage CD36 is protective against atherosclerosis. *Arterioscler Thromb Vasc Biol.* (2004) 24:2333–8. doi: 10.1161/01.ATV.0000148007.06370.68
49. Febbraio M, Podrez EA, Smith JD, Hajjar DP, Hazen SL, Hoff HF, et al. Targeted disruption of the class B scavenger receptor CD36 protects against atherosclerotic lesion development in mice. *J Clin Invest.* (2000) 105:1049–56. doi: 10.1172/JCI9259
50. Dolan JM, Kolega J, Meng H. High wall shear stress and spatial gradients in vascular pathology: a review. *Ann Biomed Eng.* (2013) 41:1411–27. doi: 10.1007/s10439-012-0695-0
51. Wong BW, Meredith A, Lin D, McManus BM. The biological role of inflammation in atherosclerosis. *Can J Cardiol.* (2012) 28:631–41. doi: 10.1016/j.cjca.2012.06.023
52. Lacroix S, Rosiers CD, Tardif JC, Nigam A. The role of oxidative stress in postprandial endothelial dysfunction. *Nutr Res Rev.* (2012) 25:288–301. doi: 10.1017/S0954422412000182
53. Botham KM, Wheeler-Jones CP. Postprandial lipoproteins and the molecular regulation of vascular homeostasis. *Prog Lipid Res.* (2013) 52:446–64. doi: 10.1016/j.plipres.2013.06.001
54. Yin Y, Li X, Sha X, Xi H, Li YF, Shao Y, et al. Early hyperlipidemia promotes endothelial activation *via* a caspase-1-sirtuin 1 pathway. *Arterioscler Thromb Vasc Biol.* (2015) 35:804–16. doi: 10.1161/ATVBAHA.115.305282
55. Mattaliano MD, Huard C, Cao W, Hill AA, Zhong W, Martinez RV, et al. LOX-1-dependent transcriptional regulation in response to oxidized LDL treatment of human aortic endothelial cells. *Am J Physiol Cell Physiol.* (2009) 296:C1329–C37. doi: 10.1152/ajpcell.00513.2008
56. Bryan MT, Duckles H, Feng S, Hsiao ST, Kim HR, Serbanovic-Canic J, et al. Mechanoresponsive networks controlling vascular inflammation. *Arterioscler Thromb Vasc Biol.* (2014) 34:2199–205. doi: 10.1161/ATVBAHA.114.303424
57. Heo KS, Fujiwara K, Abe J. Disturbed-flow-mediated vascular reactive oxygen species induce endothelial dysfunction. *Circ J.* (2011) 75:2722–30. doi: 10.1253/circj.CJ-11-1124
58. Kano A, Wolfgang MJ, Gao Q, Jacoby J, Chai GX, Hansen W, et al. Endothelial cells require STAT3 for protection against endotoxin-induced inflammation. *J Exp Med.* (2003) 198:1517–25. doi: 10.1084/jem.20030077
59. Yu M, Zhou H, Zhao J, Xiao N, Roychowdhury S, Schmitt D, et al. MyD88-dependent interplay between myeloid and endothelial cells in the initiation and progression of obesity-associated inflammatory diseases. *J Exp Med.* (2014) 211:887–907. doi: 10.1084/jem.20131314
60. Biswas S, Gao D, Altemus JB, Rekhi UR, Chang E, Febbraio M, et al. Circulating CD36 is increased in hyperlipidemic mice: cellular sources and triggers of release. *Free Radic Biol Med.* (2021) 168:180–8. doi: 10.1016/j.freeradbiomed.2021.03.004
61. Rekhi UR, Catunda RQ, Alexiou M, Sharma M, Fong A, Febbraio M. Impact of a CD36 inhibitor on *Porphyromonas gingivalis* mediated atherosclerosis. *Arch Oral Biol.* (2021) 126:105129. doi: 10.1016/j.archoralbio.2021.105129
62. Mina AI, LeClair RA, LeClair KB, Cohen DE, Lantier L, Banks AS. CalR: a web-based analysis tool for indirect calorimetry experiments. *Cell Metab.* (2018) 28:656–66.e1. doi: 10.1016/j.cmet.2018.06.019
63. Delyea C, Bozorgmehr N, Koleva P, Dunsmore G, Shahbaz S, Huang V, et al. CD71(+) erythroid suppressor cells promote fetomaternal tolerance through arginase-2 and PDL-1. *J Immunol.* (2018) 200:4044–58. doi: 10.4049/jimmunol.1800113
64. Mehrotra D, Wu J, Papangeli I, Chun HJ. Endothelium as a gatekeeper of fatty acid transport. *Trends Endocrinol Metab.* (2014) 25:99–106. doi: 10.1016/j.tem.2013.11.001

65. Rekhi U, Piche JE, Immaraj L, Febbraio M. Neointimal hyperplasia: are fatty acid transport proteins a new therapeutic target? *Curr Opin Lipidol.* (2019) 30:377–82. doi: 10.1097/MOL.0000000000000627
66. Abumrad NA, Cabodevilla AG, Samovski D, Pietka T, Basu D, Goldberg IJ. Endothelial cell receptors in tissue li pid uptake and metabolism. *Circ Res.* (2021) 128:433–50. doi: 10.1161/CIRCRESAHA.120.318003
67. Iso T, Maeda K, Hanaoka H, Suga T, Goto K, Syamsunarno MR, et al. Capillary endothelial fatty acid binding proteins 4 and 5 play a critical role in fatty acid uptake in heart and skeletal muscle. *Arterioscler Thromb Vasc Biol.* (2013) 33:2549–57. doi: 10.1161/ATVBAHA.113.301588
68. Hagberg C, Mehlem A, Falkevall A, Muhl L, Eriksson U. Endothelial fatty acid transport: role of vascular endothelial growth factor B. *Physiology.* (2013) 28:125–34. doi: 10.1152/physiol.00042.2012
69. Mitchell RW, On NH, Del Bigio MR, Miller DW, Hatch GM. Fatty acid transport protein expression in human brain and potential role in fatty acid transport across human brain microvessel endothelial cells. *J Neurochem.* (2011) 117:735–46. doi: 10.1111/j.1471-4159.2011.07245.x
70. Kanda T, Brown JD, Orasanu G, Vogel S, Gonzalez FJ, Sartoretto J, et al. PPARγ in the endothelium regulates metabolic responses to high-fat diet in mice. *J Clin Invest.* (2009) 119:110–24. doi: 10.1172/JCI36233
71. Son NH, Basu D, Samovski D, Pietka TA, Peche VS, Willecke F, et al. Endothelial cell CD36 optimizes tissue fatty acid uptake. *J Clin Invest.* (2018) 128:4329–42. doi: 10.1172/JCI99315
72. Bonen A, Han XX, Habets DD, Febbraio M, Glatz JF, Luiken JJ. A null mutation in skeletal muscle FAT/CD36 reveals its essential role in insulin- and AICAR-stimulated fatty acid metabolism. *Am J Physiol Endocrinol Metab.* (2007) 292:E1740–E9. doi: 10.1152/ajpendo.00579.2006
73. Zatterale F, Longo M, Naderi J, Raciti GA, Desiderio A, Miele C, et al. Chronic adipose tissue inflammation linking obesity to insulin resistance and type 2 diabetes. Front Physiol. (2020) 10:1607. doi: 10.3389/fphys.2019.01607
74. Goudriaan JR, den Boer MA, Rensen PC, Febbraio M, Kuipers F, Romijn JA, et al. CD36 deficiency in mice impairs lipoprotein lipase-mediated triglyceride clearance. *J Lipid Res.* (2005) 46:2175–81. doi: 10.1194/jlr.M500112-JLR200
75. Podrez EA, Febbraio M, Sheibani N, Schmitt D, Silverstein RL, Hajjar DP, et al. Macrophage scavenger receptor CD36 is the major receptor for LDL modified by monocyte-generated reactive nitrogen species. *J Clin Invest.* (2000) 105:1095–108. doi: 10.1172/JCI8574
76. Podrez EA, Poliakov E, Shen Z, Zhang R, Deng Y, Sun M, et al. A novel family of atherogenic oxidized phospholipids promotes macrophage foam cell formation *via* the scavenger receptor CD36 and is enriched in atherosclerotic lesions. *J Biol Chem.* (2002) 277:38517–23. doi: 10.1074/jbc.M205924200
77. Bou Khzam L, Son NH, Mullick AE, Abumrad NA, Goldberg IJ. Endothelial cell CD36 deficiency prevents normal angiogenesis and vascular repair. *Am J Transl Res.* (2020) 12:7737–61.
78. Isenberg JS, Romeo MJ, Abu-Asab M, Tsokos M, Oldenborg A, Pappan L, et al. Increasing survival of ischemic tissue by targeting CD47. *Circ Res.* (2007) 100:712–20. doi: 10.1161/01.RES.0000259579.35787.4e
79. Wang J, Li Y. CD36 tango in cancer: signaling pathways and functions. *Theranostics.* (2019) 9:4893–908. doi: 10.7150/thno.36037
80. Hamilton JA, Johnson RA, Corkey B, Kamp F. Fatty acid transport: the diffusion mechanism in model and biological membranes. *J Mol Neurosci.* (2001) 16:99–108; discussion 51–7. doi: 10.1385/JMN:16:2-3:99
81. Hsieh FL, Turner L, Bolla JR, Robinson CV, Lavstsen T, Higgins MK. The structural basis for CD36 binding by the malaria parasite. *Nat Commun.* (2016) 7:12837. doi: 10.1038/ncomms12837
82. Pepino MY, Kuda O, Samovski D, Abumrad NA. Structure-function of CD36 and importance of fatty acid signal transduction in fat metabolism. *Annu Rev Nutr.* (2014) 34:281–303. doi: 10.1146/annurev-nutr-071812-161220
83. Glatz JFC, Luiken J. Dynamic role of the transmembrane glycoprotein CD36 (SR-B2) in cellular fatty acid uptake and utilization. *J Lipid Res.* (2018) 59:1084–93. doi: 10.1194/jlr.R082933
84. Hao JW, Wang J, Guo H, Zhao YY, Sun HH, Li YF, et al. CD36 facilitates fatty acid uptake by dynamic palmitoylation-regulated endocytosis. *Nat Commun.* (2020) 11:4765. doi: 10.1038/s41467-020-18565-8

Conflict of Interest: The authors declare that the research was conducted in the absence of any commercial or financial relationships that could be construed as a potential conflict of interest.

Publisher's Note: All claims expressed in this article are solely those of the authors and do not necessarily represent those of their affiliated organizations, or those of the publisher, the editors and the reviewers. Any product that may be evaluated in this article, or claim that may be made by its manufacturer, is not guaranteed or endorsed by the publisher.

Copyright © 2021 Rekhi, Omar, Alexiou, Delyea, Immaraj, Elahi and Febbraio. This is an open-access article distributed under the terms of the Creative Commons Attribution License (CC BY). The use, distribution or reproduction in other forums is permitted, provided the original author(s) and the copyright owner(s) are credited and that the original publication in this journal is cited, in accordance with accepted academic practice. No use, distribution or reproduction is permitted which does not comply with these terms.

frontiers in Cardiovascular Medicine

ORIGINAL RESEARCH
published: 02 December 2021
doi: 10.3389/fcvm.2021.763389

The Increase in Paraoxonase 1 Is Associated With Decrease in Left Ventricular Volume in Kidney Transplant Recipients

Philip W. Connelly[1,2,3]*, *Andrew T. Yan*[4], *Michelle M. Nash*[5], *Rachel M. Wald*[6], *Charmaine Lok*[7], *Lakshman Gunaratnam*[8], *Anish Kirpalani*[9] and *G. V. Ramesh Prasad*[5]

[1] Division of Endocrinology and Metabolism, Department of Medicine, St. Michael's Hospital, University of Toronto, Toronto, ON, Canada, [2] Department of Laboratory Medicine and Pathobiology, University of Toronto, Toronto, ON, Canada, [3] Keenan Research Centre for Biomedical Science of St. Michael's Hospital, Toronto, ON, Canada, [4] Division of Cardiology, St. Michael's Hospital, University of Toronto, Toronto, ON, Canada, [5] Kidney Transplant Program, St. Michael's Hospital, Toronto, ON, Canada, [6] Division of Cardiology, Toronto General Hospital, University of Toronto, Toronto, ON, Canada, [7] Division of Nephrology, Toronto General Hospital, University of Toronto, Toronto, ON, Canada, [8] Division of Nephrology, London Health Sciences Centre, Western University, London, ON, Canada, [9] Department of Medical Imaging, St. Michael's Hospital, University of Toronto, Toronto, ON, Canada

OPEN ACCESS

Edited by:
Wen Dai,
Versiti Blood Research Institute, United States

Reviewed by:
Yi He,
University of Washington, United States
Erik Josef Behringer,
Loma Linda University, United States

***Correspondence:**
Philip W. Connelly
Phil.connelly@unityhealth.to

Specialty section:
This article was submitted to Lipids in Cardiovascular Disease, a section of the journal Frontiers in Cardiovascular Medicine

Received: *23 August 2021*
Accepted: *20 October 2021*
Published: *02 December 2021*

Citation:
Connelly PW, Yan AT, Nash MM, Wald RM, Lok C, Gunaratnam L, Kirpalani A and Prasad GVR (2021) The Increase in Paraoxonase 1 Is Associated With Decrease in Left Ventricular Volume in Kidney Transplant Recipients. Front. Cardiovasc. Med. 8:763389. doi: 10.3389/fcvm.2021.763389

Background: Patients on dialysis have impaired cardiac function, in part due to increased fluid volume and ventricular stress. Restored kidney function through transplantation reduces left ventricular volume in both systole and diastole. We previously reported that the decrease in NT-proB-type natriuretic peptide (NT-proBNP) was associated with a decrease in adiponectin. Paraoxonase 1 (PON1) has been inversely associated with cardiovascular outcomes. We now report the association of changes in PON1 with changes in left ventricular volume and left ventricular mass after kidney transplantation.

Design: Patients on dialysis were assessed at baseline and 12 months after kidney transplantation ($n = 38$). A comparison group of patients on dialysis who were not expected to receive a transplant in the next 24 months were studied ($n = 43$) to determine if the change of PON1 with kidney transplantation achieved a significance greater than that due to biologic variation. Left ventricular volume and mass were determined by cardiac magnetic resonance imaging. PON1 was measured by arylesterase activity and by mass.

Results: PON1 mass and activity were not different between the groups at baseline. Both PON1 mass and activity were increased post-kidney transplantation ($p < 0.0001$ for change). The change in PON1 mass ($p = 0.0062$) and PON1 arylesterase activity ($p = 0.0254$) were inversely correlated with the change in NT-proBNP for patients receiving a kidney transplant. However, only the change in the PON1 mass, and not the change in PON1 arylesterase, was inversely correlated with the change in left ventricular volume (ml/m2.7) ($p = 0.0146$ and 0.0114 for diastolic and systolic, respectively) and with the change in hemoglobin ($p = 0.0042$).

Conclusion: Both PON1 mass and arylesterase activity are increased by kidney transplantation. The increase in PON1 mass is consistent with a novel relationship to the increase in hemoglobin and decrease in left ventricular volume and NT-proBNP seen when kidney function is restored.

Keywords: paraoxonase 1, kidney transplantation, left ventricular hypertrophy, cardiac magnetic resonance imaging, dialysis

INTRODUCTION

Patients with chronic kidney disease (CKD) are at increased risk for cardiovascular disease, including non-atherosclerotic disease characterized by left ventricular hypertrophy (LVH) (1). Among the noninvasive tools used to measure left ventricular (LV) volume and mass, cardiac magnetic resonance imaging (CMR) is particularly useful due to its accuracy and precision. We recently reported LV changes by CMR in patients with end-stage kidney disease (ESKD) in whom kidney function was partially restored in the form of a kidney transplant (KT) (2). In addition, LV changes by CMR can be correlated with cardiovascular biomarkers such as adiponectin (2). While both LV volume and adiponectin decreased with KT, change in adiponectin was not associated with change in LV volume (2). Since CMR is a useful tool to correlate cardiovascular biomarker changes with both changes in kidney function after KT and measurable changes in cardiac function, we extended our study to paraoxonase 1 (PON1).

PON1 is a 43kDa protein synthesized primarily by hepatocytes and released to high density lipoproteins (HDL). PON1 has both metal binding and lactonase properties (3). Homocysteine thiolactone has been identified as a substrate for PON1 (4). Methylation of the PON1 gene has been associated with clopidogrel resistance (5).

HDL enriched in PON1 has been associated with less vascular disease in type 1 diabetes (6). The first report that PON1 activity was reduced in patients with ESKD on hemodialysis (HD) was from Schiavon et al. (7). We observed lower PON1 in patients on standard HD and home nocturnal HD that was inversely correlated with C-reactive protein (CRP), a marker of inflammation (8). PON1 can be measured as both its activity and mass. In a cross-sectional study comparing a control group, patients on HD and patients with KT, Sztanek et al. (9) found PON1 activity was lowest for HD patients, followed by those with KT and highest in control subjects.

Most studies of patients on dialysis have measured PON1 enzymatic activity. Although reports are inconsistent, PON1 activity may be lowest for patients on dialysis, higher for patients that have received a KT, and highest for normal control subjects. This gradient in PON1 enzymatic activity is consistent with the gradient of kidney function. However, all studies have been cross-sectional in nature, with the exception of a study comparing change in arylesterase at 1, 6 and 12 months post-transplant (10). There has been no prospective determination of change in PON1 mass and activity with prospective restoration of kidney function through KT. There has also been no study that compared the change in PON1 mass or activity with change in LV indices.

METHODS

Recruitment of participants has been previously described (2, 11). Briefly, adult patients (18-75 years old) on HD or peritoneal dialysis (PD) being considered for KT were recruited at the time of their pre-KT assessment. Patients were assigned to one of 2 groups depending on their availability of a potential living kidney donor. The KT group consisted of HD or PD patients expected to receive a living donor KT within 2 months; the dialysis group consisted of patients without identified living donors and therefore not expected to receive a transplant for the next 24 months. The study sample size target of 42 subjects per group was based on detection of a 5 μg/ml change in adiponectin, with an expected attrition rate of 20%. Study assessments were performed at baseline, and either 12 months later while still on dialysis or 12 months post-KT. The predominant immunosuppressant regimen at 12 months post-KT was the combination of tacrolimus, mycophenolate and prednisone ($n = 33$), followed by tacrolimus and prednisone ($n = 3$), mycophenolate, prednisone and sirolimus ($n = 2$) and tacrolimus with mycophenolate ($n = 1$). Either basiliximab or thymoglobulin are used for induction, followed by tacrolimus 0.1 mg/kg/d adjusted to maintain a target trough level of 5–10 ng/ml. Mycophenolate is dosed at 720 mg per os twice daily, and prednisone is dosed initially at 1 mg/kg/d, tapered to 5 mg daily by 2 months post-transplant.

The methods for cardiac MRI (CMR) measurement of LV volume and LV mass have been described in detail (11). Briefly, CMR was performed with a 1.5-tesla whole-body magnetic resonance scanner (Intera: Philips Medical Systems, Best, The Netherlands) using a phased-array cardiac coil and retrospective vectorographic gating. All CMR studies were analyzed by readers blinded to the information about the patient and the time point of data acquisition. CMR data was analyzed by an experienced reader using cvi42 software (Circle Cardiovascular, Calgary, Canada). LV volumes and mass were allometrically adjusted by dividing by height in meters$^{2.7}$ (12). Adiponectin was measured using the Meso Scale Discovery human adiponectin assay (#K151BXC-2, Meso Scale Diagnostics, Rockville, Maryland) and calibrated to the Millipore enzyme-linked immunoassay (#EZHADP-61-K, Millipore, St. Charles, MO, USA). N-terminal proB-type natriuretic peptide (NT-proBNP) was measured on the Roche Cobas 6000 601e

TABLE 1 | Characteristics of study subjects by treatment group and baseline dialysis modality.

	Hemodialysis at baseline		*p*-value	Peritoneal dialysis at baseline		*p*-value
	Dialysis	Transplant		Dialysis	Transplant	
Women/Men	8/23	10/17		4/8	2/10	
Age, yrs	54.1 ± 9.6	46.3 ± 12.1	0.008	59.2 ± 13.8	47.1 ± 13.7	0.04
Baseline						
Serum Creatinine μmol/L	674 ± 229	694 ± 230	0.75	789 ± 199	926 ± 332	0.23
BMI, kg/m^2	27.2 ± 5.2	25.5 ± 4.9	0.2	25.7 ± 4.1	27.1 ± 3.6	0.39
Hemoglobin, g/L	118.7 ± 15.3^	121.5 ± 13.4*	0.46	109.3 ± 11.7	106.7 ± 17.0	0.67
Total Chol, mM	4.0 ± 1.3	4.16 ± 1.22	0.63	4.15 ± 1.04	4.21 ± 1.11	0.89
Triglycerides, mM	1.46 ± 0.85	1.93 ± 1.39	0.12	1.53 ± 0.53	2.03 ± 0.84	0.10
LDL Chol, mM	2.17 ± 1.12	2.17 ± 0.97	0.98	2.35 ± 1.0	2.38 ± 0.95	0.93
HDL Chol, mM	1.19 ± 0.33	1.13 ± 0.32	0.51	1.11 ± 0.36	0.90 ± 0.19	0.10
Albumin, g/L	41.6 ± 4.2$^{\#}$	41.7 ± 3.8§	0.91	35.8 ± 2.4	36.9 ± 3.5	0.40
CRP, mg/L	6.5 ± 10.2	3.8 ± 5.0	0.21	6.5 ± 7.3	6.0 ± 6.0	0.88
LV systolic volume, ml/m$^{2.7}$	15.9 ± 5.5	17.5 ± 6.5	0.33	15.2 ± 5.0	19.3 ± 5.8	0.08
LV diastolic volume, ml/m$^{2.7}$	39.2 ± 10.2	40.6 ± 10.7	0.63	37.0 ± 7.8	45.0 ± 9.4	0.036
LV mass index, g/m$^{2.7}$	30.8 ± 9.9	29.2 ± 8.6	0.50	28.7 ± 4.5	31.4 ± 8.2	0.32
Ln NT-proBNP, pg/ml	7.49 ± 1.55	7.23 ± 1.27	0.50	6.81 ± 1.38	7.30 ± 1.37	0.41
Adiponectin,μg/ml	23.0 ± 13.5	20.6 ± 11.0	0.47	20.4 ± 10.7	27.5 ± 10.8	0.13
PON1 μg/ml	98.2 ± 24.2	92.0 ± 22.9	0.32	80.8 ± 19	79.5 ± 26	0.89
PON1 arylesterase, U/ml	88.1 ± 19.2	82.3 ± 19.5	0.25	82.2 ± 19.5	78.4 ± 19.7	0.65
PON1 specific activity,U/μg	0.91 ± 0.16	0.91 ± 0.18	0.99	1.02 ± 0.11	1.02 ± 0.18	0.92
Month 12						
Serum creatinine μmol/L	757 ± 234	129 ± 103	< 0.0001	696 ± 177	118 ± 31	< 0.0001
BMI, kg/m^2	27.6 ± 5.7	26.7 ± 4.7	0.49	25.0 ± 3.4	28.2 ± 5.4	0.11
Hemoglobin, g/L	116.6 ± 12.1	134.3 ± 20.3	0.0003	113.1 ± 13.3	137.6 ± 18.6	0.0012
Total Chol, mM	3.98 ± 1.32	4.39 ± 1.13	0.21	3.94 ± 1.07	4.33 ± 1.17	0.40
Triglycerides, mM	1.56 ± 0.96	1.85 ± 1.38	0.34	1.54 ± 0.58	1.90 ± 0.87	0.24
LDL Chol, mM	2.08 ± 0.93	2.33 ± 0.81	0.29	2.18 ± 0.90	2.14 ± 0.72	0.90
HDL Chol, mM	1.13 ± 0.37	1.24 ± 0.39	0.29	1.05 ± 0.29	1.19 ± 0.28	0.25
Albumin, g/L	42.8 ± 3.5	43.6 ± 2.9	0.36	36.5 ± 2.75	43.5 ± 3.0	< 0.0001
CRP, mg/L	4.1 ± 3.9	3.0 ± 4.0	0.32	9.7 ± 13.3	4.8 ± 4.9	0.26
LV systolic volume, ml/m$^{2.7}$	15.5 ± 5.2	14.5 ± 4.4	0.47	15.4 ± 11.4	14.7 ± 12.8	0.72
LV diastolic volume, ml/m$^{2.7}$	39.6 ± 10.4	36.9 ± 8.1	0.29	37.3 ± 29.5	37.1 ± 34.6	0.96
LV mass index, g/m$^{2.7}$	30.2 ± 9.5	28.0 ± 6.0	0.29	28.5 ± 8.9	27.4 ± 4.5	0.70
Ln NT-proBNP, pg/ml	7.74 ± 1.53	4.81 ± 1.28	< 0.0001	7.40 ± 1.77	4.95 ± 1.25	0.0007
Adiponectin μg/ml	21.7 ± 13.4	15.1 ± 7.1	0.021	23.3 ± 17.2	18.1 ± 11.3	0.39
PON1 μg/ml	96.2 ± 21.1	106.8 ± 22.4	0.07	83.0 ± 17.1	100.3 ± 23.8	0.06
PON1 arylesterase, U/ml	88.1 ± 19.9	99.2 ± 19.5	0.038	82.5 ± 17.0	95.4 ± 26.4	0.18
PON1 specific activity, U/μg	0.93 ± 0.2	0.95 ± 0.16	0.80	1.00 ± 0.13	0.95 ± 0.19	0.46

*Baseline hemoglobin: *p = 0.006 for hemodialysis vs. peritoneal dialysis for the transplant group; ^p = 0.06 for hemodialysis vs. peritoneal dialysis for the dialysis group; Baseline albumin: $^{\#}$p = 0.0011 for hemodialysis vs. peritoneal dialysis for the transplant group; §p < 0.0001 for hemodialysis vs. peritoneal dialysis for the dialysis group.*

module (Mississauga, ON, Canada). Measurement of PON1 was an a priori secondary variable. PON1 enzyme mass was measured using serum as described (13) with the modification that 4–20% Criterion sodium dodecylsulfate polyacrylamide gels (BioRad, Mississauga, ON, Canada) were used to separate serum proteins. A serum pool was analyzed in 11 separate runs, assigned a value of 108.8 μg/ml for PON1 concentration and used as a calibrator for all gels. PON1 Q192R phenotype was determined using high and low salt conditions with phenylacetate as a substrate and with 4-(chloromethyl)phenyl acetate as described by Richter et al. (14). We also measured blood hemoglobin and serum albumin concentrations, since they are important prognostic markers for survival in ESKD that improve with KT, as well as NT-proBNP due to its known decline post-KT and correlation with LV volumes. C-reactive protein (CRP) was measured as a marker of inflammation. Statistical analysis was done using SAS version 9.4 (Cary, NC, USA). Graphs were plotted using GraphPad

Prism version 9.2. Between-group comparisons were done using unpaired *t*-test.

Since we recruited only patients with kidney failure who were kidney transplant candidates, we excluded those who were too ill to be considered for kidney transplantation. Therefore, the dialysis patients in this study represent the healthiest subgroup of dialysis patients. The dialysis patients' good baseline health may have suppressed any changes in their cardiac parameters over time, as might be seen with improved dialysis efficiency over time. We attempted to address this bias by excluding patients who were not yet on dialysis and receiving a pre-emptive kidney transplant, since those patients might be even healthier.

The study was approved by the Research Ethics Board at St. Michael's Hospital (REB 10-239) and by the ethics boards at the collaborating sites. All subjects provided written informed consent. The work described has been carried out in accordance with The Code of Ethics of the World Medical Association (Declaration of Helsinki) for experiments involving humans.

RESULTS

The baseline and 12-month characteristics of the dialysis group and transplant groups are shown in **Table 1**. Hemoglobin and albumin concentrations were significantly different between HD and PD patients at baseline. Therefore, a *post-hoc* sensitivity analysis was performed and the univariate analyses are presented separately by baseline dialysis type. Within dialysis type, baseline values for the dialysis vs. transplant subjects were not significantly different, with the exception of LV volume at diastole (ml/$m^{2.7}$) for the PD patients. Allometrically adjusted LV mass (g/$m^{2.7}$) was not different between the two groups. KT resulted in significant increases in hemoglobin concentration for both HD and PD patients, but KT significantly increased albumin concentration only in the PD patients. CRP concentration did not differ between HD and PD patients and was not significantly affected by KT.

KT increased PON1 mass for both HD and PD patients, with near-significant *p* values of 0.07 and 0.06, respectively (**Table 1**). Univariate analyses of PON1 mass and activity comparing the dialysis and KT groups is shown in **Table 2**. The data for the HD and PD subjects within group was combined for this analysis. ESKD baseline values were not significantly different between the dialysis and KT groups, but at 12 months the absolute values for PON1 activity ($p = 0.0125$) and PON1 mass ($p = 0.0119$) were significantly higher in the KT group whether analyzed as the change in activity or mass ($p < 0.0001$ for each). Notably, the standard deviation for the dialysis group and the transplant group was similar.

Table 3 provides an analysis of differences between HD and PD patients by analysis of change in cardiovascular biomarkers. The most striking impact of dialysis modality was on change in albumin, which was highly significant for PD patients ($p = 0.0005$), but not HD patients ($p = 0.34$). The change in systolic and diastolic LV volume was greater for subjects on PD and reached statistical significance despite the smaller sample size. The decrease in systolic and diastolic LV volume seen for HD patients was consistent with a beneficial, albeit smaller, effect of KT for this group. The change in PON1 activity and mass was significant for both HD and PD patients. The change in hemoglobin was also significant for both dialysis modalities, although it was greater for the PD patients. The change in HDL cholesterol was also found to be significant for both HD and PD patients. Thus, among the measured liver products, albumin was distinguished from PON1 and HDL cholesterol as being strongly affected by baseline dialysis modality.

TABLE 2 | Paraoxonase 1 mass and activity by treatment group.

	Dialysis	Transplant	p-value
n	43	38	
Baseline			
PON1 arylesterase activity, U/ml	86.4 ± 19.3	81.2 ± 19.4	0.22
PON1 mass, μg/ml	93.4 ± 24.0	88.6 ± 24.1	0.35
PON1 specific activity, U/μg	0.94 ± 0.16	0.94 ± 0.18	0.99
Month 12			
PON1 arylesterase activity, U/ml	86.6 ± 19.1	98.09 ± 21.4	0.0125
PON1 mass, μg/ml	92.5 ± 20.7	104.9 ± 22.7	0.0119
PON1 specific activity, U/μg	0.95 ± 0.18	0.95 ± 0.16	0.89
Change PON1 arylesterase, U/ml	0.15 ± 10.5	16.9 ± 13.8	<0.0001
Change PON1 mass, μg/ml	−0.84 ± 13.3	16.6 ± 15.8	<0.0001

Tables 4, **5** (and shown in **Figures 1**–**7**) provide correlation analyses for PON1 mass and activity, HDL cholesterol, adiponectin, NT-proBNP, LV systolic and diastolic volume, and LV mass for the KT group and the dialysis group, respectively. The data for the HD and PD subjects was combined for this analysis. For the KT group, the change in PON1 mass and arylesterase activity were significantly correlated ($p < 0.0001$). The change in hemoglobin was also positively correlated with change on PON1 mass ($p = 0.0042$), but not with PON1 activity ($p = 0.275$). Further, the change in PON1 mass was inversely correlated with the change in LV diastolic volume ($p = 0.0146$), systolic volume ($p = 0.0114$) and Ln NT-proBNP ($p = 0.0062$). Although the change in PON1 mass was correlated with the change in HDL cholesterol concentration ($p = 0.0562$), the change in HDL cholesterol was not significantly correlated with LV volume or mass. The change in HDL cholesterol was significantly correlated with the change in PON1 arylesterase ($p = 0.0003$) and adiponectin ($p = 0.0062$). Thus, the change in PON1 mass has a unique association with LV changes, unlike HDL cholesterol and PON1 arylesterase activity.

The median percent change in PON1 mass was −3.9 vs. 20.3% for the dialysis and KT groups, respectively. The change in PON1 mass was not correlated with the average PON1 mass ($p = 0.56$), indicating that baseline PON1 concentrations were not a determinant of the response to KT. Thus, the incremental increase in PON1 mass was similar across the PON1 concentration range. Only the change in Ln NT-proBNP was significantly different from the null ($p = 0.0487$) in the dialysis group. The correlation of PON1 mass and arylesterase activity was significant across groups ($p < 0.0001$). Consistent with these

TABLE 3 | Change in paraoxonase-1 mass and activity and relationship with hemoglobin and albumin by baseline dialysis modality.

	Hemodialysis at baseline		*p*-value	Peritoneal dialysis at baseline		*p*-value
	Dialysis	Transplant		Dialysis	Transplant	
n	$N = 28$	$N = 26$		$N = 12$	$N = 11$	
Change in albumin, g/L	1.04 ± 3.81	2.11 ± 4.41	0.34	0.67 ± 2.74	6.9 ± 4.4	0.0005
n	$N = 30$	$N = 27$		$N = 12$	$N = 11$	
Change in LV systolic volume, ml/m$^{2.7}$	−0.43 ± 4.09	−2.93 ± 5.91	0.067	0.28 ± 5.1	−4.42 ± 4.76	0.033
Change in LV diastolic volume, ml/m$^{2.7}$	0.28 ± 9.3	−3.63 ± 7.98	0.096	0.33 ± 9.2	−7.91 ± 9.45	0.046
n	$N = 31$	$N = 27$		$N = 12$	$N = 11$	
Change in PON1 activity, U/ml	0.07 ± 11.0	16.9 ± 13	< 0.0001	0.35 ± 9.46	16.9 ± 16.2	0.0065
n	$N = 31$	$N = 27$		$N = 12$	$N = 11$	
Change in PON1 mass, μg/ml	−2.01 ± 12.9	14.9 ± 16.9	< 0.0001	2.2 ± 14.6	20.8 ± 12.32	0.0036
Change PON1 specific activity, U/μg	0.019 ± 0.12	0.03 ± 0.09	0.69	−0.018 ± 0.1	−0.061 ± 0.14	0.4
n	$N = 31$	$N = 27$		$N = 12$	$N = 12$	
Change in Hemoglobin, g/L	−2.1 ± 16.8	12.8 ± 23.2	0.0066	3.8 ± 12.1	30.9 ± 29.7	0.0106
Change HDL cholesterol, mM	−0.05 ± 0.22	0.16 ± 0.29	0.0081	−0.05 ± 0.18	0.29 ± 0.3	0.0026

TABLE 4 | Pearson correlation of change in left ventricular measurements and hemoglobin with PON1, HDL cholesterol, and adiponectin for subjects receiving a kidney transplant.

Transplant group	LV diastolic volume	LV systolic volume	LVMI$^{2.7}$	Hemoglobin g/L	LnNT-proBNP pg/ml	PON1 μg/ml	PON1 units/ml	HDLC mM	Adiponectin μg/ml
LV_diastolic	1	0.846	0.7188	−0.4969	0.6074	−0.3931	−0.1294	−0.0116	0.3019
Volume, ml/m$^{2.7}$		<0.0001	<0.0001	0.0015	0.0001	0.0146	0.4387	0.9452	0.0654
	38	38	37	38	35	38	38	38	38
LV_systolic		1	0.5729	−0.5379	0.6251	−0.406	−0.3002	−0.0912	0.2039
Volume, ml/m$^{2.7}$			0.0002	0.0005	<0.0001	0.0114	0.0671	0.5859	0.2195
		38	37	38	35	38	38	38	38
LVMI, g/m$^{2.7}$			1	−0.4171	0.3962	−0.2425	−0.1157	−0.0485	0.2169
				0.0102	0.0204	0.1482	0.4962	0.7754	0.1972
			37	37	34	37	37	37	37
Hemoglobin				1	−0.385	0.4536	0.1816	0.0661	−0.2836
					0.0224	0.0042	0.2751	0.6892	0.0845
g/L				39	35	38	38	39	38
LnNT-proBNP, pg/ml					1	−0.4536	−0.3774	−0.0572	0.3865
						0.0062	0.0254	0.7442	0.0218
					35	35	35	35	35
PON1, μg/ml						1	0.7318	0.3125	−0.1513
							<0.0001	0.0562	0.3647
						38	38	38	38
PON1, units/ml							1	0.5572	0.2414
								0.0003	0.1443
							38	38	38
HDLC, mM								1	0.4363
									0.0062
								39	38
Adiponectin, μg/ml									1
									38

Values shown in the table are the Pearson correlation coefficient, the p-value, and the number of subjects. LV, left ventricular; LVMI, left ventricular mass index; LnNT-proBNP, natural log of NT-proB-type natriuretic peptide; PON1, paraoxonase 1; HDLC, high density lipoprotein cholesterol.

TABLE 5 | Pearson correlation of change in left ventricular measurements and hemoglobin with PON1, HDL cholesterol, and adiponectin for subjects on dialysis.

Dialysis group	LV diastolic volume	LV systolic volume	LVMI$^{2.7}$	Hemoglobin g/L	LnNT-proBNP pg/ml	PON1 μg/ml	PON1 units/ml	HDLC mM	Adiponectin μg/ml
LV_diastolic	1	0.8316	0.4975	−0.3676	0.5817	−0.0004	−0.3591	0.1654	0.2458
Volume, ml/m$^{2.7}$		<0.0001	0.0008	0.0166	0.0001	0.9981	0.0195	0.2951	0.1166
	42	42	42	42	39	42	42	42	42
LV_systolic		1	0.6079	−0.3469	0.6212	−0.0329	−0.27	0.0734	0.3768
Volume, ml/m$^{2.7}$			<0.0001	0.0244	<0.0001	0.8363	0.0837	0.6443	0.0139
		42	42	42	39	42	42	42	42
LVMI, g/m$^{2.7}$			1	−0.3493	0.7602	−0.127	−0.2118	−0.0151	0.461
				0.0234	<0.0001	0.423	0.1782	0.9243	0.0021
			42	42	39	42	42	42	42
Hemoglobin,				1	−0.3371	0.183	0.2703	0.2573	0.1063
					0.0334	0.2402	0.0796	0.0958	0.4975
g/L				43	40	43	43	43	43
LnNT-proBNP, pg/ml					1	−0.1542	−0.3183	−0.1224	0.3963
						0.3421	0.0453	0.4519	0.0114
					40	40	40	40	40
PON1, μg/ml						1	0.61	0.3619	0.1381
							<0.0001	0.0171	0.3771
						43	43	43	43
PON1, units/ml							1	0.4	0.1757
								0.0082	0.2597
							43	43	43
HDLC, mM								1	0.3252
									0.0333
								43	43
Adiponectin, μg/ml									1
									43

Values shown in the table are the Pearson correlation coefficient, the p-value and the number of subjects. LV, left ventricular; LVMI, left ventricular mass index; LnNT-proBNP, natural log of NT-proB-type natriuretic peptide; PON1, paraoxonase 1; HDLC, high density lipoprotein cholesterol.

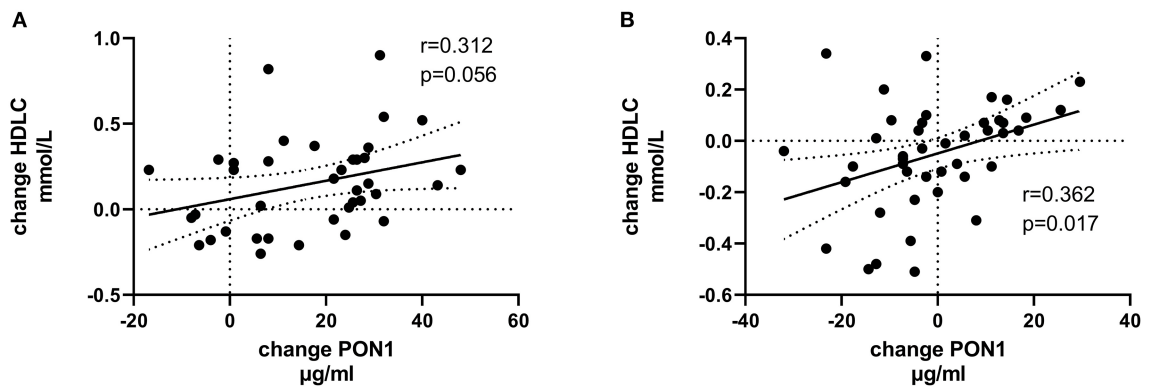

FIGURE 1 | Change in HDLC vs. change in PON1 mass. **(A)** Transplant group. **(B)** Dialysis group.

two measures having different determinants in the dialysis group (**Table 5**), PON1 arylesterase variation correlated inversely with the change in LV diastolic volume ($p = 0.019$) and with the change in Ln NT-proBNP ($p = 0.045$), whereas there was no correlation of the change in PON1 mass with these in the dialysis group ($p = 0.998, 0.342$, respectively).

PON1 Q192R phenotype frequency was not different between the dialysis and KT groups (**Supplementary Table 1**, Fishers

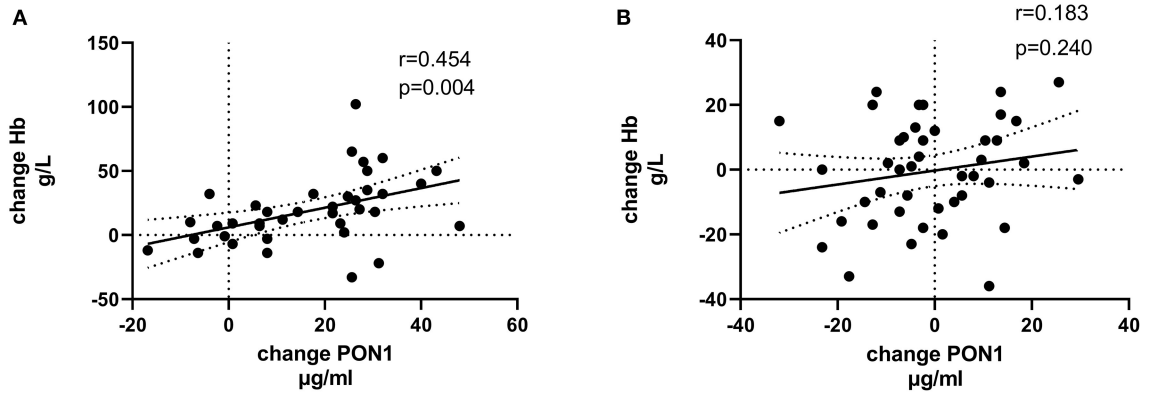

FIGURE 2 | Change in Hb vs. change in PON1 mass. **(A)** Transplant group. **(B)** Dialysis group.

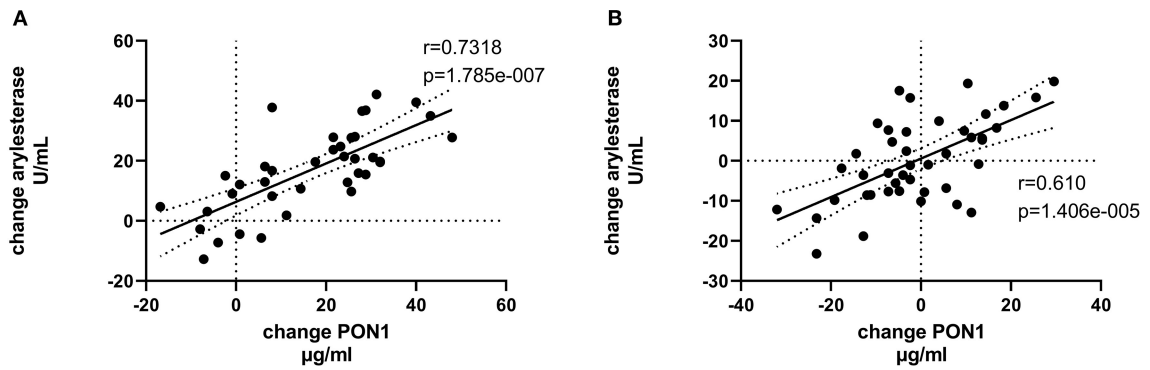

FIGURE 3 | Change in PON1 arylesterase activity vs. change in PON1 mass. **(A)** Transplant group. **(B)** Dialysis group.

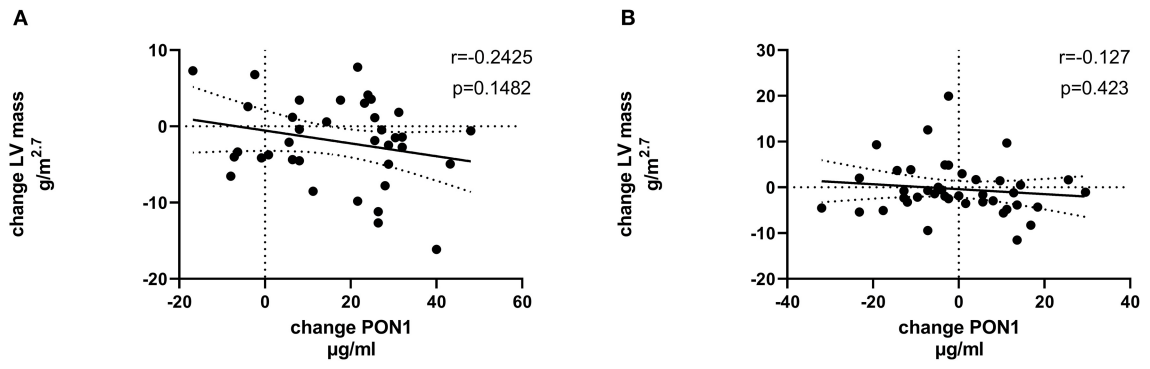

FIGURE 4 | Change in LV mass vs. change in PON1 mass. **(A)** Transplant group. **(B)** Dialysis group.

exact test $p = 0.74$). Further, PON1 Q192R phenotype was not a significant factor for the change in PON1 mass (data not shown).

DISCUSSION

We have shown for the first time that the increase in PON1 mass post-KT inversely correlates with change in LV volume and positively correlates with the change in hemoglobin. The current study also prospectively, rather than cross-sectionally, confirms that PON1 activity is higher with greater kidney function. Further, we have documented that change in PON1 mass post-KT is independent of baseline concentration or inflammation. Separating PON1 mass change from change in CRP, HDL cholesterol and albumin supports specific effects that link PON1, hemoglobin and LV volume. PON1 activity, influenced by HDL

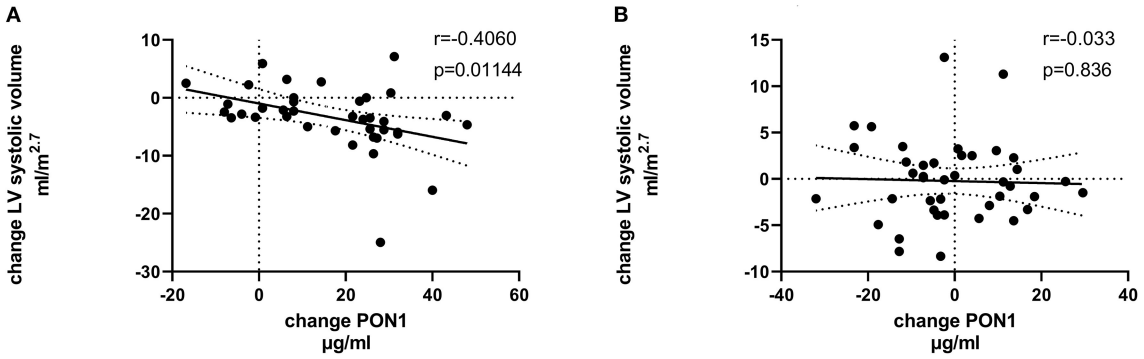

FIGURE 5 | Change in LV systolic volume vs. change in PON1 mass. **(A)** Transplant group. **(B)** Dialysis group.

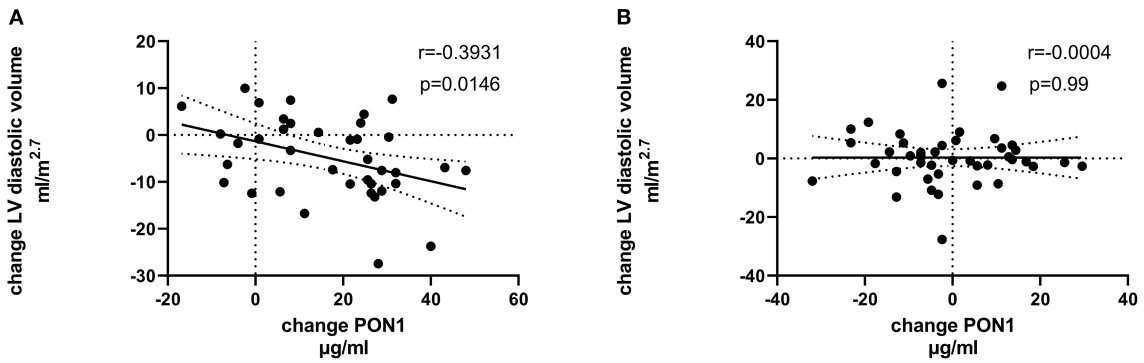

FIGURE 6 | Change in LV diastolic volume vs. change in PON1 mass. **(A)** Transplant group. **(B)** Dialysis group.

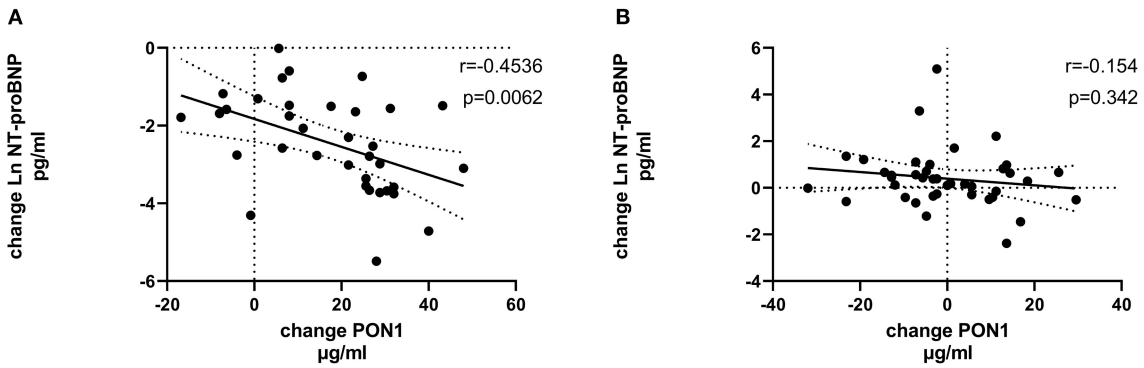

FIGURE 7 | Change in Ln NT-proBNP vs. change in PON1 mass. **(A)** Transplant group. **(B)** Dialysis group. Change was calculated as the month 12 value minus the baseline value for each variable. Values shown in the figures are the Pearson correlation coefficient and the *p*-value. LV, left ventricular; Hb, hemoglobin. LV, left ventricular; LnNT-proBNP, natural log of NT-proB-type natriuretic peptide; PON1, paraoxonase 1; HDLC, high density lipoprotein cholesterol.

cholesterol, does not uniquely share a common factor with change in hemoglobin or LV volume.

The cause-effect relationship among change in LV volume, change in hemoglobin and change in PON1 mass cannot be elucidated from the current study design. Several candidates are suggested by the current literature to explain these relationships. PON1 has been shown to be involved, as a lactonase, in the metabolic conversion of 5,6-epoxyeicosatrienoic acid (15). The epoxyeicosatrienoic acids are among the molecules that regulate response to mechano-transduction as regulators of TRPV4 (16,

17). Independently, the production of B-type natriuretic peptide, as reflected by the inverse relationship of PON1 with NT-proBNP, could indicate a link between PON1 and mechano-sensing pathways. Thus, one could speculate that PON1 mass reflects a role in response to left ventricular volume. The positive correlation of the change in PON1 mass with the change in hemoglobin could indicate that factors involved in iron metabolism regulate PON1 gene expression in concert with regulating hemoglobin concentration. This would be consistent with an increase in PON1 in response to erythropoietin therapy that has been reported in a single study (18). However, currently there is no information that would link the regulation of human PON1 gene expression and iron metabolism.

Despite a greater understanding of PON1 mass, the importance of reduced PON1 activity seen in states of reduced kidney function and partially restored kidney function remains to be established. Bhattacharyya et al. (19) reported that PON1 Q192R genotype, paraoxonase and arylesterase activities were related to cardiovascular outcomes in a cohort of subjects undergoing elective diagnostic cardiac catheterization. The lowest quartile of arylesterase activity had a 4.5-fold hazard ratio for nonfatal myocardial infarction or cerebrovascular accident. Hammadah et al. (20) reported event-free survival over 5 years for subjects with chronic heart failure from the Atlanta Cardiomyopathy Consortium. BNP was highest, and HDL cholesterol was lowest, for the lowest tertile of arylesterase activity. The lowest tertile of baseline arylesterase activity was associated with a 2.6 hazard ratio for adverse events.

PON1 has a well-recognized labile metal binding site, in addition to its enzymatic activity. This labile site requires calcium for enzyme activity, but it can also bind metals. Thus, one potential function of PON1 is in the regulation of iron, zinc and other divalent cations (21–23). Rahimi-Ardabili et al. (24) reported that zinc sulfate supplementation increased HDL cholesterol, apoAI and paraoxonase activity in patients on HD, but that this response was not specific to paraoxonase and may reflect a general effect on HDL production or clearance. This putative function of PON1 would be dependent upon its mass and would have the potential to not only be independent of the lactonase activity but inverse to such activity.

KT recipients benefit markedly from their improved kidney function compared to remaining on dialysis, experiencing improved cardiovascular outcomes (25) although outcome depends on the amount of kidney function restored (26). While reduced LV volume and increased hemoglobin are well-known effects of KT, the relationship of these improvements to improved cardiovascular outcomes remains unestablished. In this study, we have shown that PON1 mass especially, and possibly PON1 activity, may be key mediators in the pathway linking restored kidney function and improved cardiovascular outcomes. The current study generates the hypothesis that interventions selectively directed toward increasing PON1 mass and activity may help provide further insight into the mechanisms that connect the kidney and heart in patients with pathological cardiorenal syndromes, such as those with ESKD.

The study is limited by its inclusion of largely healthy patients, since those with recent (<6 months) cardiac events were also excluded. Most transplant patients received living donor transplants, which have the best outcomes with less acute tubular necrosis, acute rejection, and cardiac events. This may amplify any differences from the dialysis group. The magnitude is expected to be small since additionally, 12 months of follow-up is expected to be sufficient to overcome these challenges to the transplant, before the follow-up CMR. Fortunately, no patients in this study, transplant or dialysis, experienced cardiac events. The findings from this study cannot be generalized to deceased donor transplants, which constitute about 60% of all transplants and are subject to more complications.

DATA AVAILABILITY STATEMENT

The raw data supporting the conclusions of this article will be made available by the authors, without undue reservation.

ETHICS STATEMENT

The studies involving human participants were reviewed and approved by St. Michael's Hospital Research Ethics Board, University Health Network Research Ethics Board, and the London Health Sciences Centre Research Ethics Board. The patients/participants provided their written informed consent to participate in this study.

AUTHOR CONTRIBUTIONS

GP, PC, and AY: study conception and design and data acquisition. GP, PC, MN, RW, LG, CL, AK, and AY: data analysis and interpretation and drafting and revision of the manuscript. Each author contributed important intellectual content during manuscript drafting or revision, accepts personal accountability for the author's own contributions, and agrees to ensure that questions pertaining to the accuracy or integrity of any portion of the work are appropriately investigated and resolved. All authors contributed to the article and approved the submitted version.

FUNDING

This study was funded by the Heart and Stroke Foundation of Canada, Grant Number HSFNA7077 and the Canadian Institutes for Health Research, Grant Number 136954.

SUPPLEMENTARY MATERIAL

The Supplementary Material for this article can be found online at: https://www.frontiersin.org/articles/10.3389/fcvm.2021.763389/full#supplementary-material

REFERENCES

1. Edwards NC, Moody WE, Chue CD, Ferro CJ, Townend JN, Steeds RP. Defining the natural history of uremic cardiomyopathy in chronic kidney disease: the role of cardiovascular magnetic resonance. *JACC Cardiovasc Imaging*. (2014) 7:703–14. doi: 10.1016/j.jcmg.2013.09.025
2. Prasad GVR, Yan AT, Nash MM, Kim SJ, Wald R, Wald R, et al. Determinants of left ventricular characteristics assessed by cardiac magnetic resonance imaging and cardiovascular biomarkers related to kidney transplantation. *Can J Kidney Health Dis.* (2018) 5:205435811880997. doi: 10.1177/2054358118809974
3. Kobayashi M, Shinohara M, Sakoh C, Kataoka M, Shimizu S. Lactone-ring-cleaving enzyme: genetic analysis, novel RNA editing, and evolutionary implications. *Proc Natl Acad Sci USA*. (1998) 95:12787–92. doi: 10.1073/pnas.95.22.12787
4. Perla-Kajan J, Jakubowski H. Paraoxonase 1 and homocysteine metabolism. *Amino Acids*. (2012) 43:1405–17. doi: 10.1007/s00726-012-1321-z
5. Su J, Li J, Yu Q, Xu X, Wang J, Yang J, et al. Association of PON1 gene promoter DNA methylation with the risk of clopidogrel resistance in patients with coronary artery disease. *J Clin Lab Anal.* (2019) 33:e22867. doi: 10.1002/jcla.22867
6. Vaisar T, Kanter JE, Wimberger J, Irwin AD, Gauthier J, Wolfson E, et al. High concentration of medium-sized HDL particles and enrichment in HDL paraoxonase 1 associate with protection from vascular complications in people with long-standing Type 1 diabetes. *Diab Care.* (2020) 43:178–86. doi: 10.2337/dc19-0772
7. Schiavon R, De Fanti E, Giavarina D, Biasioli S, Cavalcanti G, Guidi G. Serum paraoxonase activity is decreased in uremic patients. *Clin Chim Acta.* (1996) 247:71–80. doi: 10.1016/0009-8981(95)06221-1
8. Kannampuzha J, Darling PB, Maguire GF, Donnelly S, McFarlane PCT, Chan CT, et al. W Paraoxonase 1 arylesterase activity and mass are reduced and inversely related to C-reactive protein in patients on either standard or home nocturnal hemodialysis. *Clin Nephrol.* (2010) 73:131–8. doi: 10.5414/CNP73131
9. Sztanek F, Seres I, Harangi M, Locsey L, Padra J, Paragh GJ, et al. Decreased paraoxonase 1 (PON1) lactonase activity in hemodialyzed and renal transplanted patients. A novel cardiovascular biomarker in end-stage renal disease. *Nephrol Dial Transplant.* (2012) 27:2866–72. doi: 10.1093/ndt/gfr753
10. Kahvecioglu S, Ersoy A, Gullulu M, Dirican M. Effects of calcineurin inhibitors on paraoxonase and arylesterase activity after a kidney transplant. *Exp Clin Transplant.* (2014) 12:334–42. doi: 10.6002/ect.2013.0110
11. Gong IY, Al-Amro B, Prasad GVR, Connelly PW, Wald RM, Wald R, et al. Cardiovascular magnetic resonance left ventricular strain in end-stage renal disease patients after kidney transplantation. *J Cardiovasc Magn Reson.* (2018) 20:83. doi: 10.1186/s12968-018-0504-5
12. de Simone G, Daniels SR, Devereux RB, Meyer RA, Roman MJ, de Divitiis O, et al. Left ventricular mass and body size in normotensive children and adults: assessment of allometric relations and impact of overweight. *J Am Coll Cardiol.* (1992) 20:1251–60. doi: 10.1016/0735-1097(92)90385-Z
13. Connelly PW, Maguire GF, Picardo CM, Teiber JF, Draganov D. Development of an immunoblot assay with infrared fluorescence to quantify paraoxonase 1 in serum and plasma. *J Lipid Res.* (2008) 49:245–50. doi: 10.1194/jlr.D700022-JLR200
14. Richter RJ, Jarvik GP, Furlong CE. Determination of paraoxonase 1 status without the use of toxic organophosphate substrates. *Circ Cardiovasc Genet.* (2008) 1:147–52. doi: 10.1161/CIRCGENETICS.108.811638
15. Eryanni-Levin S, Khatib S, Levy-Rosenzvig R, Tamir S, Szuchman-Sapir A. 5,6-delta-DHTL, a stable metabolite of arachidonic acid, is a potential substrate for paraoxonase 1. *Biochim Biophys Acta*. (2015) 1851:1118–22. doi: 10.1016/j.bbalip.2015.04.008
16. Watanabe H, Vriens J, Prenen J, Droogmans G, Voets T, Nilius B. Anandamide and arachidonic acid use epoxyeicosatrienoic acids to activate TRPV4 channels. *Nature.* (2003) 424:434–8. doi: 10.1038/nature01807
17. Vriens J, Watanabe H, Janssens A, Droogmans G, Voets T, Nilius B. Cell swelling, heat, and chemical agonists use distinct pathways for the activation of the cation channel TRPV4. *Proc Natl Acad Sci U S A*. (2004) 101:396–401. doi: 10.1073/pnas.0303329101
18. Marsillach J, Martínez-Vea A, Marcas L, Mackness B, Mackness M, Ferré N, et al. Administration of exogenous erythropoietin beta affects lipid peroxidation and serum paraoxonase-1 activity and concentration in predialysis patients with chronic renal disease and anaemia. *Clin Exp Pharmacol Physiol.* (2007) 34:347–9. doi: 10.1111/j.1440-1681.2007.04552.x
19. Bhattacharyya T, Nicholls SJ, Topol EJ, Zhang R, Yang X, Schmitt D, et al. Relationship of paraoxonase 1 (PON1) gene polymorphisms and functional activity with systemic oxidative stress and cardiovascular risk. *JAMA*. (2008) 299:1265–76. doi: 10.1001/jama.299.11.1265
20. Hammadah M, Kalogeropoulos AP, Georgiopoulou VV, Weber M, Wu Y, Hazen SL, et al. High-density lipoprotein-associated paraoxonase-1 activity for prediction of adverse outcomes in outpatients with chronic heart failure. *EurJ Hear Fail.* (2017) 19:748–55. doi: 10.1002/ejhf.777
21. Ekinci D, Beydemir S. Purification of PON1 from human serum and assessment of enzyme kinetics against metal toxicity. *Biol Trace Elem Res.* (2010) 135:112–20. doi: 10.1007/s12011-009-8500-0
22. Rovira J, Hernández-Aguilera A, Luciano-Mateo F, Cabré N, Baiges-Gaya G, Nada M, et al. Trace elements and paraoxonase-1 activity in lower extremity artery disease. *Biol Trace Elem Res.* (2018) 186:74–84. doi: 10.1007/s12011-018-1298-x
23. Luciano-Mateo F, Cabré N, Nadal M, García-Heredia A, Baiges-Gaya G, Hernández-Aguilera A, et al. Serum concentrations of trace elements and their relationships with paraoxonase-1 in morbidly obese women. *J Trace Elem Med Biol.* (2018) 48:8–15. doi: 10.1016/j.jtemb.2018.02.023
24. Rahimi-Ardabili B, Argani H, Ghorbanihaghjo A, Rashtchizadeh N, Naghavi-Behzad M, Ghorashi S, et al. Paraoxonase enzyme activity is enhanced by zinc supplementation in hemodialysis patients. *Ren Fail.* (2012) 34:1123–8. doi: 10.3109/0886022X.2012.717479
25. Meier-Kriesche HU, Schold JD, Srinivas TR, Reed A, Kaplan B. Kidney transplantation halts cardiovascular disease progression in patients with end-stage renal disease. *Am J Transplant.* (2004) 4:1662–8. doi: 10.1111/j.1600-6143.2004.00573.x
26. Meier-Kriesche HU, Baliga R, Kaplan B. Decreased renal function is a strong risk factor for cardiovascular death after renal transplantation. *Transplantation.* (2003) 75:1291–5. doi: 10.1097/01.TP.0000061602.03327.E2

Conflict of Interest: The authors declare that the research was conducted in the absence of any commercial or financial relationships that could be construed as a potential conflict of interest.

Publisher's Note: All claims expressed in this article are solely those of the authors and do not necessarily represent those of their affiliated organizations, or those of the publisher, the editors and the reviewers. Any product that may be evaluated in this article, or claim that may be made by its manufacturer, is not guaranteed or endorsed by the publisher.

Copyright © 2021 Connelly, Yan, Nash, Wald, Lok, Gunaratnam, Kirpalani and Prasad. This is an open-access article distributed under the terms of the Creative Commons Attribution License (CC BY). The use, distribution or reproduction in other forums is permitted, provided the original author(s) and the copyright owner(s) are credited and that the original publication in this journal is cited, in accordance with accepted academic practice. No use, distribution or reproduction is permitted which does not comply with these terms.

frontiers in Cardiovascular Medicine

ORIGINAL RESEARCH
published: 10 December 2021
doi: 10.3389/fcvm.2021.777098

Hematopoietic Cell-Specific SLC37A2 Deficiency Accelerates Atherosclerosis in LDL Receptor-Deficient Mice

Qingxia Zhao[1†], Zhan Wang[1†], Allison K. Meyers[2], Jennifer Madenspacher[3], Manal Zabalawi[1], Qianyi Zhang[4], Elena Boudyguina[1], Fang-Chi Hsu[5], Charles E. McCall[1,2], Cristina M. Furdui[1], John S. Parks[1], Michael B. Fessler[3] and Xuewei Zhu[1,2]*

[1] Department of Internal Medicine, Section on Molecular Medicine, Wake Forest School of Medicine, Winston-Salem, NC, United States, [2] Department of Microbiology and Immunology, Wake Forest School of Medicine, Winston-Salem, NC, United States, [3] Immunity, Inflammation and Disease Laboratory, National Institute of Environmental Health Sciences, NIH, Durham, NC, United States, [4] Department of Biology, Wake Forest University, Winston-Salem, NC, United States, [5] Department of Biostatistics and Data Science, Wake Forest School of Medicine, Winston-Salem, NC, United States

OPEN ACCESS

Edited by:
Yiliang Chen, Medical College of Wisconsin, United States

Reviewed by:
Fang Li, Columbia University Irving Medical Center, United States
Darcy Knaack, Medical College of Wisconsin, United States

***Correspondence:**
Xuewei Zhu
xwzhu@wakehealth.edu

[†]These authors have contributed equally to this work

Specialty section:
This article was submitted to Lipids in Cardiovascular Disease, a section of the journal Frontiers in Cardiovascular Medicine

Received: *14 September 2021*
Accepted: *16 November 2021*
Published: *10 December 2021*

Citation:
Zhao Q, Wang Z, Meyers AK, Madenspacher J, Zabalawi M, Zhang Q, Boudyguina E, Hsu F-C, McCall CE, Furdui CM, Parks JS, Fessler MB and Zhu X (2021) Hematopoietic Cell-Specific SLC37A2 Deficiency Accelerates Atherosclerosis in LDL Receptor-Deficient Mice. Front. Cardiovasc. Med. 8:777098. doi: 10.3389/fcvm.2021.777098

Macrophages play a central role in the pathogenesis of atherosclerosis. Our previous study demonstrated that solute carrier family 37 member 2 (SLC37A2), an endoplasmic reticulum-anchored phosphate-linked glucose-6-phosphate transporter, negatively regulates macrophage Toll-like receptor activation by fine-tuning glycolytic reprogramming *in vitro*. Whether macrophage SLC37A2 impacts *in vivo* macrophage inflammation and atherosclerosis under hyperlipidemic conditions is unknown. We generated hematopoietic cell-specific SLC37A2 knockout and control mice in C57Bl/6 Ldlr$^{-/-}$ background by bone marrow transplantation. Hematopoietic cell-specific SLC37A2 deletion in Ldlr$^{-/-}$ mice increased plasma lipid concentrations after 12-16 wks of Western diet induction, attenuated macrophage anti-inflammatory responses, and resulted in more atherosclerosis compared to Ldlr$^{-/-}$ mice transplanted with wild type bone marrow. Aortic root intimal area was inversely correlated with plasma IL-10 levels, but not total cholesterol concentrations, suggesting inflammation but not plasma cholesterol was responsible for increased atherosclerosis in bone marrow SLC37A2-deficient mice. Our *in vitro* study demonstrated that SLC37A2 deficiency impaired IL-4-induced macrophage activation, independently of glycolysis or mitochondrial respiration. Importantly, SLC37A2 deficiency impaired apoptotic cell-induced glycolysis, subsequently attenuating IL-10 production. Our study suggests that SLC37A2 expression is required to support alternative macrophage activation *in vitro* and *in vivo*. *In vivo* disruption of hematopoietic SLC37A2 accelerates atherosclerosis under hyperlipidemic pro-atherogenic conditions.

Keywords: glucose 6-phosphate transporter, macrophage inflammation, IL-10, efferocytosis, atherosclerosis

INTRODUCTION

Atherosclerosis is driven by hyperlipidemia and exacerbated by chronic low-grade inflammation (1–6). Macrophages are among the most abundant immune cells within atherosclerotic plaques (1, 5, 7–10). Inside the atherosclerotic plaque, macrophages take up modified LDL (i.e., oxidized LDL; oxLDL), forming lipid laden-macrophages or foam cells, which worsen inflammation and promote atherosclerotic plaque growth (1, 5, 7–10). As a heterogeneous cell population, macrophages can be roughly grouped into two categories based on their inflammatory activities: classically activated pro-inflammatory (M1) macrophages and alternatively activated anti-inflammatory macrophages (11). The anti-inflammatory (M2) macrophages can be subdivided into M2a, 2b, 2c, and 2d based on the stimuli and resultant transcriptional changes (11). These *in vitro* models of macrophage polarization (M1 vs. M2) are more simplified than the microenvironment that macrophages encounter in an atherosclerotic lesion (12). Nevertheless, mounting evidence suggests that macrophage plasticity or phenotypic switch impacts atherosclerotic lesion progression and regression (1, 13, 14). Uncovering the underlying mechanisms governing activation and deactivation of macrophages and their phenotypic switch provides a promising avenue to prevent and treat atherosclerosis.

Macrophages rewire intracellular metabolic pathways upon activation, which in turn modify their cellular function (15–17). Pro-inflammatory macrophages, such as lipopolysaccharide (LPS)-stimulated macrophages [M (LPS)], requires glycolysis to mount an effective inflammatory response. However, whether glycolytic reprogramming is necessary for alternative macrophage activation is still debatable and requires further investigation. Moreover, little is known about how and to what extent macrophages reprogram cellular metabolism in response to microenvironmental stimuli to promote or resolve inflammation under pro-atherogenic conditions. A positive association between glycolysis and plaque macrophage inflammation was documented as increased glucose metabolic activity in human symptomatic and unstable plaque macrophages compared with asymptomatic lesions (18). However, macrophage glycolytic rate does not always influence atherogenesis, at least based on animal studies. For example, myeloid deletion of glucose transporter 1 (GLUT1), the primary glucose transporter on the plasma membrane in macrophages, does not alter atherosclerotic plaque size or macrophage content in $Ldlr^{-/-}$ mice (19). Moreover, myeloid overexpression of GLUT1 increases glucose flux in macrophages and enhances macrophage inflammation *in vitro* but is insufficient to promote atherosclerosis (20). These findings suggest a context-dependent regulation of macrophage inflammation and disease development by cellular metabolic processes in acute vs. chronic low-grade inflammation.

Solute carrier family 37 member 2 (SLC37A2), an endoplasmic reticulum-anchored phosphate-linked glucose-6-phosphate transporter, is highly expressed in macrophages (21–23). We have recently reported that SLC37A2 plays a pivotal role in murine macrophage inflammatory activation and cellular metabolic rewiring (24). SLC37A2 deletion reprograms macrophages to a hyper-glycolytic state of energy metabolism and accelerates M (LPS) activation, partially depending on nicotinamide adenine dinucleotide (NAD^+) biosynthesis. Blockade of glycolysis or the NAD^+ salvage pathway normalizes the differential expression of pro-inflammatory cytokines between control and SLC37A2-deficient macrophages. Conversely, overexpression of SLC37A2 lowers macrophage glycolysis and significantly reduces LPS-induced pro-inflammatory cytokine expression. Our published work suggests that SLC37A2 is a negative regulator of murine macrophage pro-inflammatory activation by down-regulating glycolytic reprogramming.

Despite these findings, it remains unclear whether macrophage SLC37A2 impacts macrophage pro- or anti-inflammatory activation *in vivo* under pathologic conditions. Further, it is not known whether macrophage SLC37A2-mediated inflammation affects the pathogenesis of inflammatory diseases. Here, we found that SLC37A2 expression is necessary to maintain alternative macrophage activation *in vitro*. Our data suggest that SLC37A2 positively regulates IL-4-induced macrophage alternative activation, independent of glycolysis or mitochondrial respiration. SLC37A2 positively regulates apoptotic cell-induced macrophage alternative activation through modulation of glycolysis. Lastly, we found that disruption of hematopoietic SLC37A2 expression impairs anti-inflammatory responses and worsens hyperlipidemia-induced atherosclerosis in $Ldlr^{-/-}$ mice.

MATERIALS AND METHODS

Animals, Bone Marrow Transplantation, and Diet Feeding

Animals

Slc37a2 global knockout mice in the C57BL/6J background (T1837) were purchased from Deltagen, Inc (24). Heterozygous *Slc37a2* knockout mice were intercrossed to obtain wild type (WT) and homozygous knockout ($Slc37a2^{-/-}$) mice. $Ldlr^{-/-}$ (stock 002207) mice were purchased from Jackson Laboratories. Mice were housed in a pathogen-free facility on a 12 h light/dark cycle and received a standard laboratory diet.

BMT

7×10^6 BM cells from female donor (WT and $Slc37a2^{-/-}$) mice were injected into the retro-orbital venous plexus of irradiated male $Ldlr^{-/-}$ recipient mice. Repopulation of blood leukocytes after BMT was evaluated after 16 wks of diet feeding by determining the percentage expression of the Y-chromosome-associated sex-determining region Y gene (Sry) in genomic DNA obtained from white blood cells, as described previously (25).

Abbreviations: AC, apoptotic cells; BMDM, bone marrow-derived macrophages; BMT, bone marrow transplantation; ECAR, extracellular acidification rate; NAD^+, nicotinamide adenine dinucleotide; OCR, oxygen consumption rate; OXPHOS, oxidative phosphorylation; SLC37A2, solute carrier family 37 member 2; WD, western diet.

High-Fat Western Diet Feeding

After 5 wks of recovery from radiation, mice were switched from a standard laboratory diet to a high-fat WD containing 42% calories from fat and 0.2% cholesterol (TD. 88137, Teklad) for an additional 16 wks to induce advanced atherosclerosis.

All animal experimental protocols were approved by the Wake Forest University Animal Care and Use Committee.

Analysis of Atherosclerotic Lesions

Aortic root atherosclerosis was assessed as described before (25). Briefly, aortic root sections were stained in 0.5% Oil Red O and counterstained with hematoxylin. To measure necrosis, we drew boundary lines using NIH ImageJ software around regions free of H&E staining. We used a 3,000 μm^2 threshold to avoid counting regions that may not represent substantial areas of necrosis, as described before (25). Stained sections were photographed with an Olympus DP71 digital camera and quantified using NIH ImageJ software. Results were expressed as cross-sectional plaque area (H&E) or plaque necrosis (necrotic core), or percent of total plaque area or necrosis core. Macrophages and T cells in aortic root were stained by incubating aortic root cross-sections with the primary antibodies to CD68 (Bio-Rad) and CD3 (Abcam), followed by the biotinylated secondary antibody. The staining was visualized using the ABC reagent (ABC vector kit; Vector) and DAB substrate chromogen (Dako). Apoptotic cells in atherosclerotic lesions were stained using the Click-iT Plus TUNEL Assay kit (Thermo Fisher) according to the manufacturer's protocol. The sections were then stained with CD68 antibody (Bio-Rad), and nuclei were stained with DAPI. Only TUNEL-positive cells that co-localized with DAPI-positive nuclei were counted as apoptotic cells. Efferocytosis was determined by counting the number of macrophage-associated vs. free apoptotic cells, following established methods published before (25–29). Aortic root cross-sections were also stained with Masson's Trichrome stain to quantify collagen deposition. Areas stained blue within lesions were identified as collagen-positive using NIH ImageJ software.

Cell Culture and Treatment

Peritoneal Macrophage Culture

Peritoneal cells were harvested from mice after a 16-wk diet feeding (30, 31). Cells were plated in RPMI-1640 media containing 100 U/ml penicillin and 100 μg/ml streptomycin. After a 2 h incubation, floating cells were removed by washing with PBS, and adherent macrophages were lysed using Trizol (Invitrogen) for RNA extraction.

BMDM Culture

Mouse bone marrow was cultured in low glucose DMEM supplemented with 30% L929 cell-conditioned medium and 20% FBS for 6-7 days until the cells reached confluence. BMDMs were then reseeded in culture dishes overnight in RPMI 1640 medium containing 1% Nutridoma-SP medium (Sigma-Aldrich) before any treatment (24).

Jurkat T Cell Culture

Jurkat T cells (TIB-152, ATCC) were maintained in 10% FBS containing RPMI-1640 medium. Jurkat T cells (2×10^6/ml) were treated with 1 μM staurosporine in RPMI-1640 media containing 100 U/ml penicillin and 100 μg/ml streptomycin for 4 h to induce apoptosis.

Macrophage Stimulation

BMDMs were incubated with 20 ng/ml IL-4 or ACs (ratio of ACs to macrophages was 5:1) in 10% FBS containing for indicated times as written in the figure legends. To induce foam cell formation, BMDMs were treated with 25 or 50 μg/ml oxLDL (Athens Research & Technology) for 0-24 h. In some experiments, BMDMs were pretreated for 30 min with hexokinase inhibitor 2-deoxy-D-glucose (2-DG; 10 mM, Sigma-Aldrich), actin polymerization inhibitor cytochalasin D (10 μM, Cayman), or fatty acid β-oxidation inhibitor etomoxir (50 μM, Cayman) and subsequently treated with apoptotic cells for an additional 4 h in the presence of each inhibitor.

Cytokine Quantification

Total RNA in tissues or macrophages was extracted using Trizol (Invitrogen). cDNA preparation and real-time PCR were conducted as described previously (24, 25). Primers are listed in **Supplementary Table S1**. Concentrations of cytokines/chemokines in plasma, liver homogenate, or cell culture supernatant were measured using Bioplex assay or ELISA according to the manufacturer's instructions.

Flow Cytometry

Peripheral blood and splenocytes were stained with Gr1(Ly6C/G)-PerCP-Cy5.5 (BD Pharmingen, cat# 552093), CD115-APC (eBioscience, cat# 17-1152-82), CD11b-APC Cy7 (BD Bioscience, cat# 557657), and V450-CD45 (BD Horizon, cat# 560501) (30). Data were acquired on a BD FACS Canto II instrument (BD Biosciences) and analyzed using FACSDiva software v6.1.3 (BD Biosciences).

To examine the apoptotic rate, Jurkat T cells were stained with Annexin V-APC and PI (Thermo Fisher). To examine efferocytosis, Jurkat T cells were first stained with cell tracker green CMFDA (2 μM) at 37°C for 30 min before treated with 1 μM staurosporine for 4 h to induce apoptosis. Fluorescent labeled apoptotic Jurkat T cells were then incubated with macrophages at 37°C for 0-120 min. Macrophages were then washed with PBS for five times and incubated with accutase dissociation buffer at 37°C for 30 min. Data were acquired on a BD FACSCalibur (BD Biosciences) and analyzed using Flowjo V7.6.5 (BD Biosciences).

Glucose Tolerance Tests and Insulin Tolerance Tests

Mice were fasted overnight before intraperitoneal injection of 1 g glucose/kg body weight (BW). One wk later, the same groups of mice were used for intraperitoneal injection of 0.75 U of regular human insulin/kg BW after a 4 h fast. Blood glucose concentrations were measured at 0, 15, 30, 60, and 120 min after each injection using a Bayer Contour glucose meter kit (31).

Immunofluorescent Staining of Liver Tissues

Frozen sections of liver tissues were incubated with the primary antibodies to CD68 (Bio-Rad, 1:100 dilution) and CD206 (Cell Signaling, 1:400 dilution), followed by FITC goat anti-rat IgG (Vector, 1:200) and TexasRed conjugated goat anti-rabbit IgG (Vector, 1:200). Sections were imaged with a digital camera mounted on a fluorescent microscope (Olympus DP71), and analyzed by using ImageJ (NIH). Analysis was performed on 8 of 40 × fields/section to calculate the mean count of positively stained cells per mm^2.

Lipid Analysis

4 h-fasting plasma total cholesterol (TC), free cholesterol (FC) (Wako), and triglyceride (TG) (Roche) were determined by enzymatic analysis. Plasma was fractionated by FPLC to determine cholesterol distribution among the lipoprotein classes (32). Liver lipids were extracted with chloroform: methanol (2:1), and the extract was used for enzymatic assays (33) (cholesterol, Wako; TG, Roche), and lipids were normalized to wet liver weight. Macrophage cholesterol content was measured by gas-liquid chromatography (34) and normalized to cellular protein (34).

Seahorse Assay

2×10^5 BMDMs were plated into each well of Seahorse XF96 cell culture microplates (Agilent Technologies) and cultured overnight before treated with or without 20 ng/ml IL-4 for 6 or 24 h or ACs for 3 h. Basal and IL-4- or AC-induced changes in oxygen consumption rate (OCR) were measured with a Seahorse XF96 Extracellular Flux Analyzer (Agilent Technologies) using a Seahorse mito stress test kit. Extracellular acidification rate (ECAR) in BMDMs was recorded using a glycolysis stress test kit (Agilent Technologies). OCR and ECAR were measured under basal conditions and following the sequential addition of 10 mM glucose, 1 μM oligomycin, 1.5 μM fluoro-carbonyl cyanide phenylhydrazone (FCCP), 100 nM rotenone plus 1 μM antimycin A, or 50 mM 2DG (all the compounds were from Agilent Technologies), as described in the figure legends. After the assay, 3 μM Hoechst (Life Technologies) was added to each well to stain nuclei for cell counting. Results were collected with Wave software version 2.6 (Agilent Technologies). Data were normalized to cell numbers.

Western Blotting

BMDM protein concentration was measured using the BCA protein assay kit (Pierce). Rabbit anti-SLC37A2 polyclonal antibody was made against the peptide CTPPRHHDDPEKEQDNPEDPVNSPYSSRES (LAMPIRE Biological Lab Inc.) and used at a dilution of 1:500 (24). β-actin (Sigma-Aldrich, no. A5441; 1:5,000) was used as a loading control. Blots were developed using HRP-linked secondary antibodies. Immunoblots were visualized with the Supersignal substrate system (Pierce). Chemiluminescence was captured using the ChemiDox MP imaging system (Bio-Rad) or an LSA-3000 imaging system (Fujifilm Life Science). The experiments were repeated at least two times.

Statistics

Statistical analysis was performed using GraphPad Prism software 7 (GraphPad Software) except for the plasma lipid analysis in **Figures 1A–D**. Data are presented as the mean ± SEM unless indicated otherwise. Differences were compared with Student's *t*-test or two-way ANOVA with *post hoc* Tukey's multiple comparison test as indicated in the figure legends. In **Figures 1A–D**, the mixed-effects models were used to compare lipids variables between genotype groups at each time point. The use of random intercepts provided a source of autocorrelation between repeated measures. Genotype groups and weeks and the interaction between genotype groups and weeks were included in the model. Contrasts were used to compare lipid variables at each measured week. $P < 0.05$ was considered statistically significant.

RESULTS

Hematopoietic Cell-Specific SLC37A2 Deletion Increases Plasma Lipids in WD-Fed Ldlr$^{-/-}$ Mice

We previously showed that SLC372 is a novel regulator of macrophage inflammation by controlling glycolysis (24). In this study, we wanted to know whether mice lacking SLC37A2 in macrophages were at an increased risk of developing atherosclerosis. To do this, we generated hematopoietic SLC37A2 knockout (SLC37A2$^{\Delta hema}$) mice in Ldlr$^{-/-}$ background by BMT. The BMT efficiency was ∼90% based on the male Sry gene expression in blood leukocytes isolated from recipient mice examined after 16-wk diet feeding (**Supplementary Figures S1A,B**). Four wks of WD feeding increased plasma lipid (including plasma TC, FC, CE, and TG) concentrations in both genotypes. Interestingly, SLC37A2$^{\Delta hema}$ mice displayed significantly higher plasma cholesterol concentrations after 12 and 16 wks of diet feeding (**Figures 1A–C**). SLC37A2$^{\Delta hema}$ mice also showed significantly higher plasma TG concentration after 16 wks of diet feeding (**Figure 1D**). Furthermore, we observed significantly higher plasma VLDL and LDL cholesterol concentrations but only a marginal increase in HDL cholesterol in SLC37A2$^{\Delta hema}$ vs. WT mice after 16 wks of diet feeding (**Figure 1E**). Collectively, these results suggest a novel role for hematopoietic SLC37A2 in lipid metabolism under pro-atherogenic conditions.

Hematopoietic Cell-Specific SLC37A2 Deletion Increases Liver CE and Reduces Hepatic Macrophage Activation in WD-Fed Ldlr$^{-/-}$ Mice

Given the increased plasma lipid concentrations in high-fat WD-fed SLC37A2$^{\Delta hema}$ mice, we next measured liver lipid concentrations. Consistent with increased plasma lipid concentrations, we observed a significant increase in hepatic TC and CE, but not FC or TG in SLC37A2$^{\Delta hema}$ vs. WT mice (**Figure 2A**). The increased plasma and liver lipid concentrations in SLC37A2$^{\Delta hema}$ mice prompted us to examine the hepatic expression of genes involved in lipid

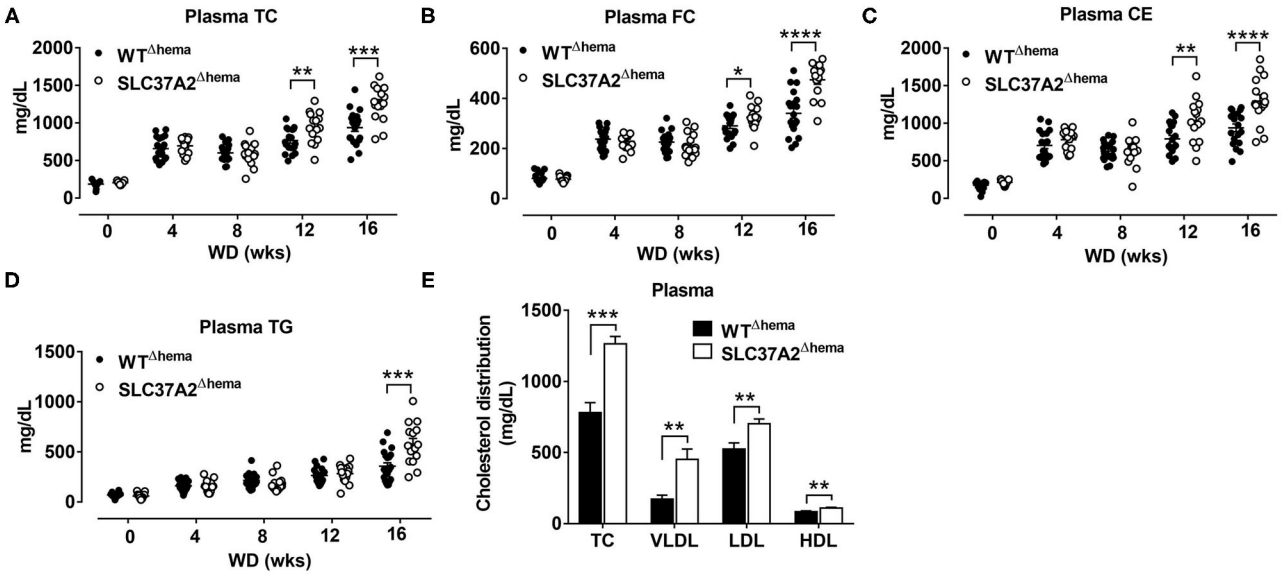

FIGURE 1 | Hematopoietic cell-specific SLC37A2 deletion increases plasma lipids in WD-fed Ldlr$^{-/-}$ mice. Hematopoietic SLC37A2 knockout (SLC37A2$^{\Delta hema}$) and control (WT$^{\Delta hema}$) Ldlr$^{-/-}$ mice were switched from a standard laboratory diet to high-fat WD for 16 wks to promote the development of advanced atherosclerosis. **(A–D)** Fasting (4 h) plasma total cholesterol (TC), free cholesterol (FC), cholesterol ester (CE), and triglyceride (TG) concentrations were measured by enzymatic assays over time (0-16 wks) (n = 12-16). **(E)** Plasma cholesterol distribution among lipoproteins after 16 wks of WD feeding was determined after fractionation of plasma by fast protein liquid chromatography (n = 6-8). Data are expressed as mean ± SEM. *P < 0.05, **P < 0.01, ***P < 0.001, ****P < 0.0001. The mixed-effects models were used to compare lipids variables between genotype groups at each time point. HDL indicates high-density lipoprotein; LDL, low-density lipoprotein; and VLDL, very-low-density lipoprotein.

metabolism in diet-fed mice. As expected, Slc37a2 transcript was significantly lower in SLC37A2$^{\Delta hema}$ mice receiving bone marrow from *Slc37a2*$^{-/-}$ mice (**Figure 2B**). We found that hepatic expression of genes responsible for *de novo* lipogenesis was similar between genotypes of mice (**Figure 2C**). However, SLC37A2$^{\Delta hema}$ liver showed decreased expression of cholesterol transporter proteins ABCA1 and SR-BI but increased expression of oxidized LDL receptor-1 (OLR1), indicating impaired cholesterol efflux but enhanced cholesterol uptake (**Figure 2C**). Furthermore, hepatic expression of the receptor for fatty acid uptake (CD36), enzymes for fatty acid oxidation (Cpt1a, Acox1, Acadl), and transcriptional factors and coactivators regulating fatty acid oxidation (PGC1α, PGC1β, PPARδ, and PPARγ) were all down-regulated in SLC37A2$^{\Delta hema}$ vs. WT liver (**Figure 2D**), suggesting an impaired fatty acid utilization in SLC37A2$^{\Delta hema}$ mouse liver at least at the transcriptional level.

Because macrophage pro-inflammation impairs reverse cholesterol transport at multiple steps (35) and alternative activation of hepatic macrophages promotes liver fatty acid oxidation and improves metabolic syndrome (36), we next examined macrophage pro- and anti-inflammatory states by measuring hepatic gene expression of macrophage markers, M1-type cytokines, and chemokines, and M2 macrophage markers. Different from our *in vitro* study, in which we observed increased pro-inflammatory cytokine production in SLC37A2$^{\Delta hema}$ macrophages in response to TLR activation (24), under pro-atherogenic conditions, hematopoietic SLC37A2 deficiency has a minor effect on the expression of genes encoding macrophage markers (**Figure 2E**) and the protein level of pro-inflammatory cytokines and chemokines (**Figures 2F,G**). Rather, we observed a slightly decreased IFN-γ and MCP-1 (**Figures 2F,G**) protein concentration in SLC37A2$^{\Delta hema}$ liver, suggesting that SLC37A2 deletion in bone marrow is not sufficient to induce a pro-inflammatory response in the liver under pro-atherogenic conditions. Despite the equivalent or slightly decreased pro-inflammatory cytokines/chemokines in SLC37A2$^{\Delta hema}$ liver, hepatic anti-inflammatory markers, including arginase 1 (Arg1), mannose receptor C-type 1 (Mrc1, also known as CD206), Ym1, and IL-10, showed significantly lower expression in SLC37A2$^{\Delta hema}$ vs. WT liver (**Figure 2H**). Consistent with the decreased transcript expression, hepatic IL-10 protein concentration showed a trend toward a decrease in SLC37A2$^{\Delta hema}$ liver, relative to control (**Figure 2I**). Moreover, the number of CD68^{+}CD206^{+} positive cells (alternatively activated macrophages) were significantly lower in SLC37A2$^{\Delta hema}$ liver than WT (**Figures 2J,K**). However, the number of CD68^{+} cells was comparable between genotypes (**Figures 2J,L**). Taken together, our results suggest that genetic deletion of SLC37A2 in bone marrow cells significantly impairs alternative activation of hepatic macrophages, associated with lower hepatic fatty acid oxidation, lower cholesterol efflux, but increased cholesterol uptake, gene expression and increased liver lipid accumulation.

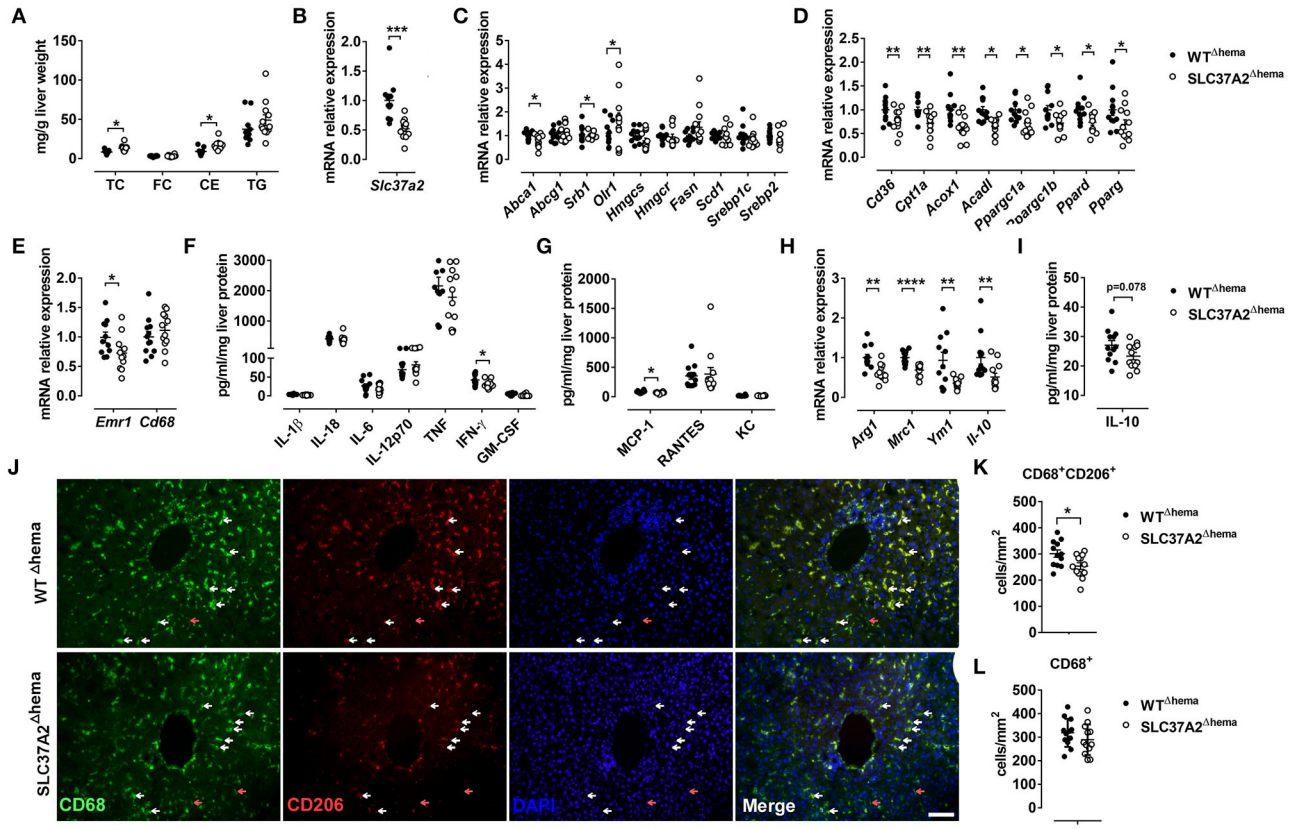

FIGURE 2 | Hematopoietic cell-specific SLC37A2 deletion increases liver cholesterol ester and reduces hepatic macrophage activation in WD-fed LDLrKO mice. Irradiated Ldlr$^{-/-}$ mice transplanted with WT or SLC37A2KO bone marrow were fed a high-fat western diet for 16 wks. **(A)** Fasting (4 h) total cholesterol (TC), free cholesterol (FC), cholesterol ester (CE), and triglyceride (TG) concentrations in the liver were measured by enzymatic assays ($n = 12$ per genotype). **(B)** Slc37a2 transcript expression in liver ($n = 12$ per genotype). **(C)** Relative transcript levels for cholesterol efflux, cholesterol uptake, cholesterol synthesis, fatty acid synthesis, and transcriptional regulators controlling these pathways in the liver ($n = 12$ per genotype). **(D)** Relative transcript levels for genes encoding key enzymes in fatty acid uptake, β-oxidation, and transcriptional regulators controlling these pathways in the liver ($n = 12$ per genotype). **(E)** Relative transcript levels for genes encoding macrophage markers in the liver ($n = 12$ per genotype). **(F,G)** Liver cytokine and chemokine protein concentrations ($n = 12$ per genotype). **(H)** Relative transcript levels for genes encoding macrophage anti-inflammatory markers in the liver ($n = 12$ per genotype). **(I)** Liver IL-10 protein concentrations ($n = 12$ per genotype). **(J)** Representative images of CD68 and CD206 double-stained liver tissues. White and red arrowheads indicate representative CD68$^+$CD206$^+$ and CD68$^+$CD206$^-$ cells, respectively. Scale bar = 100 μm. **(K)** Quantification of CD68$^+$CD206$^+$ cell number in liver tissue ($n = 12$ per genotype). **(L)** Quantification of CD68$^+$ cell number in liver tissue ($n = 12$ per genotype). Data are expressed as mean ± SEM. *$P < 0.05$, **$P < 0.01$, ***$P < 0.01$, ***$P < 0.001$, ****$P < 0.0001$, unpaired, two-tailed Student's *t*-test.

Hematopoietic Cell-Specific SLC37A2 Deletion Primarily Impairs Anti-inflammatory Responses in WD-Fed Ldlr$^{-/-}$ Mice

To determine whether hematopoietic SLC37A2 deletion affects inflammation at the systemic level, we first examined plasma concentrations of pro-inflammatory cytokines, chemokines, and anti-inflammatory cytokine using a multiplex assay. Consistent with the expression pattern of hepatic cytokines and chemokines, plasma pro-inflammatory cytokine concentrations did not differ between genotypes (**Figure 3A**). But, plasma MCP-1 concentration showed a 28.6% reduction in the SLC37A2$^{\Delta hema}$ vs. WT mice (**Figure 3B**). Strikingly, the SLC37A2$^{\Delta hema}$ mice displayed a 70% reduction of the anti-inflammatory cytokine IL-10 in plasma (**Figure 3C**) relative to their WT counterparts, suggesting hematopoietic SLC37A2 deletion impairs IL-10 production under pro-atherogenic conditions.

We next examined inflammatory cytokine expression in resident peritoneal macrophages isolated from the diet-fed mice. As expected, SLC37A2$^{\Delta hema}$ macrophages showed more than 90% reduction in transcript expression of Slc37a2, relative to WT (**Figure 3D**). Despite the indistinguishable expression of pro-inflammatory cytokines (**Figure 3E**), SLC37A2$^{\Delta hema}$ vs. WT mice showed significantly attenuated Arg1 and Mrc1 expression in resident peritoneal macrophages (**Figure 3F**) after 16-wk diet feeding. Not surprisingly, SLC37A2 deletion has little impact on the gene expression of enzymes involved in fatty acid oxidation (**Supplementary Figure S2A**) or cholesterol metabolism (**Supplementary Figure S2B**) in macrophages.

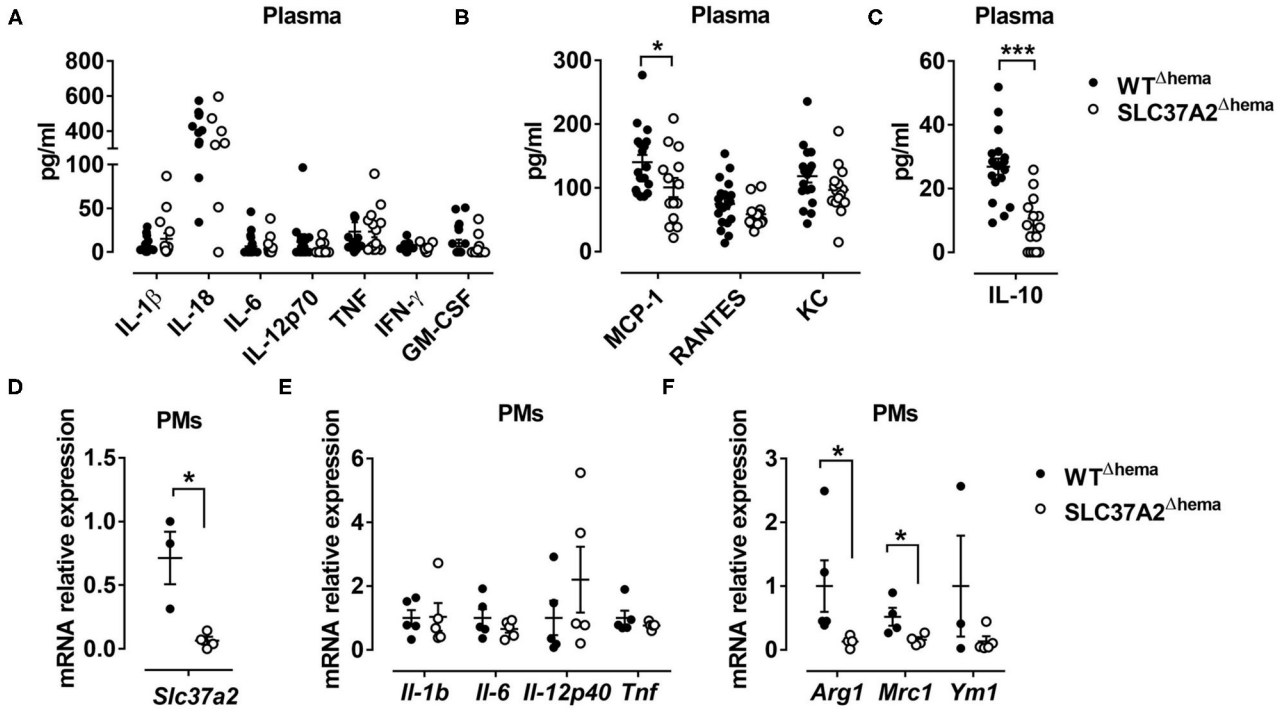

FIGURE 3 | Hematopoietic cell-specific SLC37A2 deletion primarily impairs anti-inflammatory responses in WD-fed Ldlr$^{-/-}$ mice. Hematopoietic SLC37A2 knockout (SLC37A2$^{\Delta hema}$) and control (WT$^{\Delta hema}$) Ldlr$^{-/-}$ mice were fed a high-fat western diet for 16 wks. **(A–C)** Plasma pro-inflammatory cytokine **(A)**, chemokine **(B)**, and anti-inflammatory cytokine IL-10 **(C)** concentrations were quantified by multiplex assay. **(D–F)** Relative transcript levels of Slc37a2, pro- and anti-inflammatory markers in resident peritoneal macrophages. Each symbol represents an individual mouse. Data are expressed as mean ± SEM. *$p < 0.05$; ***$p < 0.001$, unpaired, two-tailed Student's *t*-test.

Together, our results suggest that hematopoietic SLC37A2 deletion primarily impairs anti-inflammatory responses in Ldlr$^{-/-}$ mice when challenged with the WD diet.

Hematopoietic Cell-Specific SLC37A2 Deletion Has a Minor Effect on Blood Myeloid Cell Composition in WD-Fed Ldlr$^{-/-}$ Mice

We next assessed whether hematopoietic SLC37A2 deletion affects monocyte and neutrophil composition in blood as well as in the spleen. **Supplementary Figure S3A** shows our flow cytometry gating strategies. At 9-wk WD feeding, no difference was observed between genotypes regarding the frequency of blood monocytes (CD11b^{+}CD115^{+}), Gr1^{low} monocytes (CD11b^{+}CD115^{+}Gr1^{low}), Gr1^{high} monocytes (CD11b^{+}CD115^{+} Gr1^{high}), or neutrophils (CD11b^{+}CD115^{-}Gr1^{+}) (**Supplementary Figure S3B**), or the ratio of Gr1^{low} and Gr1^{high} monocytes in blood monocytes (**Supplementary Figure S3C**). After 16 wks of diet feeding, the percentage of blood neutrophils (CD11b^{+}CD115^{-}Gr1^{+}) was significantly increased in the SLC37A2$^{\Delta hema}$ mice (**Supplementary Figure S3D**). Despite the elevated plasma cholesterol and increased blood neutrophils, no difference was detected between genotypes in blood monocyte composition at 16-wk diet feeding (**Supplementary Figures S3D,E**). We did not observe any significant changes in the monocyte and neutrophil composition in the spleen between genotypes (**Supplementary Figures S3F,G**). Overall, these results suggest that hematopoietic SLC37A2 deletion has a minimal effect on blood myeloid cell composition. Note that the concentration of plasma MCP-1, a primary chemokine recruiting monocytes and macrophages from bone marrow to circulation or blood circulation to tissues, was significantly lower in the SLC37A2$^{\Delta hema}$ mice (**Figure 3B**). We reason that the unaltered blood and spleen monocytes may be the net effect of the combination of decreased plasma MCP-1 and increased plasma cholesterol in the SLC37A2$^{\Delta hema}$ mice. Taken together, our results suggest that hematopoietic SLC37A2 deletion has a minor effect on blood myeloid composition except for a slight increase in blood neutrophils after 16-wk WD feeding.

Hematopoietic Cell-Specific SLC37A2 Deficiency Promotes Atherosclerosis in WD-Fed Ldlr$^{-/-}$ Mice

Abnormal lipid metabolism and enhanced local and systemic inflammation accelerate atherosclerosis. Since we observed increased plasma lipids, especially apoB containing lipoproteins,

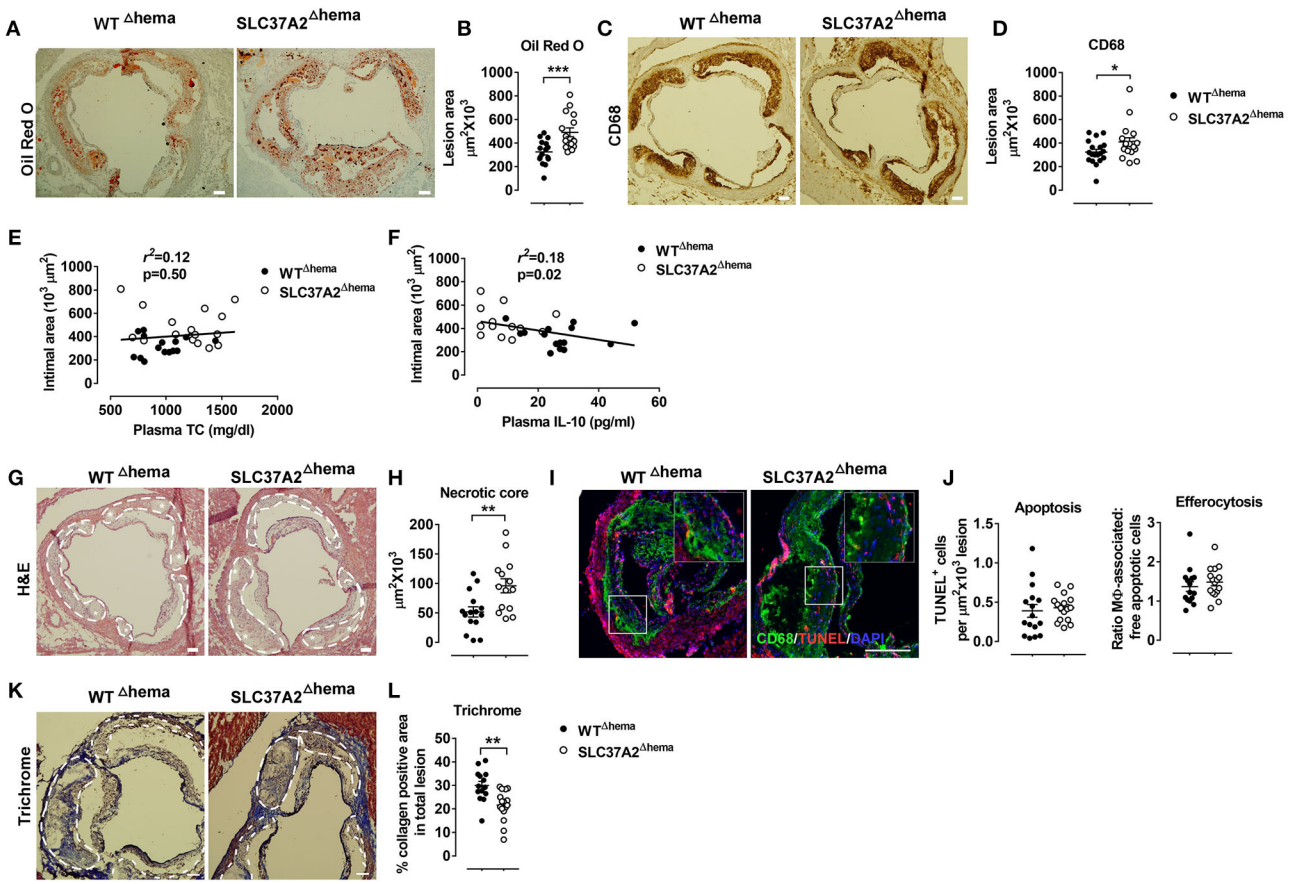

FIGURE 4 | Hematopoietic cell-specific SLC37A2 deficiency promotes atherosclerosis in WD-fed Ldlr$^{-/-}$ mice. Hematopoietic SLC37A2 knockout (SLC37A2$^{\Delta hema}$) and control (WT$^{\Delta hema}$) Ldlr$^{-/-}$ mice were fed a high-fat western diet for 16 wks (n = 12-16 mice per genotype). **(A,B)** Quantification of Oil Red O positive intimal area in the aortic root. **(C,D)** Quantification of CD68^{+} cells (macrophages) in the aortic root intimal area. **(E)** Linear regression analysis of aortic root intimal area vs. plasma total cholesterol of 16-wk diet-fed mice. Each point represents an individual animal of the denoted diet group and the correlation coefficient is shown for the entire data set. **(F)** Linear regression analysis of aortic root intimal area vs. plasma IL-10 of 16-wk diet-fed mice. Each point represents an individual animal of the denoted diet group and the correlation coefficient is shown for the entire data set. **(G,H)** Quantification of the aortic necrotic intimal area (total necrotic area) in H&E stained aortic root sections. White dash line circled lesion areas. White stars indicate the necrotic area in the plaques. **(I,J)** Quantification of apoptosis (TUNEL-positive cells) and efferocytosis (the ratio of macrophage-associated: free apoptotic cells) in aortic root sections. CD68 (green; macrophages), TUNEL (red), and DAPI (blue; nuclei) were labeled fluorescently. **(K,L)** Quantification of aortic Trichrome stain positive cells. White dash line circled lesion areas. Scale bars = 100 μm. Each symbol represents an individual mouse. Data are expressed as mean ± SEM. n = 12-16 mice per group. *$p < 0.05$; **$p < 0.01$; ***$p < 0.001$.

and decreased IL-10 in plasma, we next investigated the development of atherosclerosis in SLC37A2$^{\Delta hema}$ mice compared to controls. We found that hematopoietic SLC37A2-deficient mice showed a 51% increase in aortic root lesions stained with Oil Red O (**Figures 4A,B**), despite similar CD68 (macrophage marker) (**Figures 4C,D**), suggesting that hematopoietic SLC37A2 deletion accelerates atherosclerotic plaque formation but has no effect on macrophage content. Hematopoietic SLC37A2 deletion also did not affect T cell content in the plaque, as shown by similar CD3 (T cell marker) staining between genotypes (**Supplementary Figure S4**). We then assessed whether there is an association between plasma lipids vs. atherosclerosis or between plasma IL-10 vs. atherosclerosis in diet-fed mice by performing linear regression analysis. Despite no significant association between intimal area and plasma TC (**Figure 4E**), there was a significant inverse correlation between plasma IL-10 and intimal area (**Figure 4F**), suggesting that the attenuated anti-inflammatory response in the SLC37A2$^{\Delta hema}$ mice may be the primary driver of enhanced atherosclerosis in those mice.

IL-10 producing macrophages is responsible for the engulfment and clearance of apoptotic cells (i.e., efferocytosis) (37). Failure of efferocytosis leads to pro-inflammatory and immunogenic consequences due to secondary necrosis, exaggerating atherosclerosis (38, 39). We next examined the necrotic core formation and quantified apoptosis and efferocytosis in the plaques. Compared to WT control, SLC37A2$^{\Delta hema}$ mice had a significant increase (∼40%) in the necrotic area in aortic lesions (**Figures 4G,H**). However,

no difference was observed regarding the frequency of apoptosis or efferocytosis in lesions between genotypes at 16 wks of diet feeding (**Figures 4I,J**). Interestingly, when we stained the aortic root sections with Masson's Trichrome stain, we observed a 30% reduction in Trichrome positive staining in SLC37A2$^{\Delta hema}$ vs. WT control aortic root sections (**Figures 4K,L**), suggesting that hematopoietic SLC37A2 deficiency decreases collagen deposition, likely resulting from impaired alternative macrophage activation. As collagen formation is associated with the stability of plaques (40, 41), our data suggest that SLC37A2 deficiency in bone marrow promotes plaque instability. Together, our results indicate that hematopoietic SLC37A2 deletion worsens atherosclerosis, inversely associated with plasma IL-10 levels.

Hematopoietic Cell-Specific SLC37A2 Deletion Has Minimal Impact on Insulin Resistance and Adipose Inflammation Under Pro-atherogenic Conditions

In addition to atherosclerosis assessment, we also tested whether hematopoietic cell-specific SLC37A2 deletion influences adipose tissue inflammation and/or obesity and insulin resistance under pro-atherogenic conditions. WT and SLC37A2$^{\Delta hema}$ mice gained similar body weight over the 16 wks of diet feeding (**Supplementary Figure S5A**). Tissue (including liver, spleen, and epididymal fat) mass was comparable between genotypes (**Supplementary Figure S5B**). Both genotypic mice showed similar glucose clearance and insulin tolerance around 10-11 wks of diet feeding (**Supplementary Figures S5C,D**). As

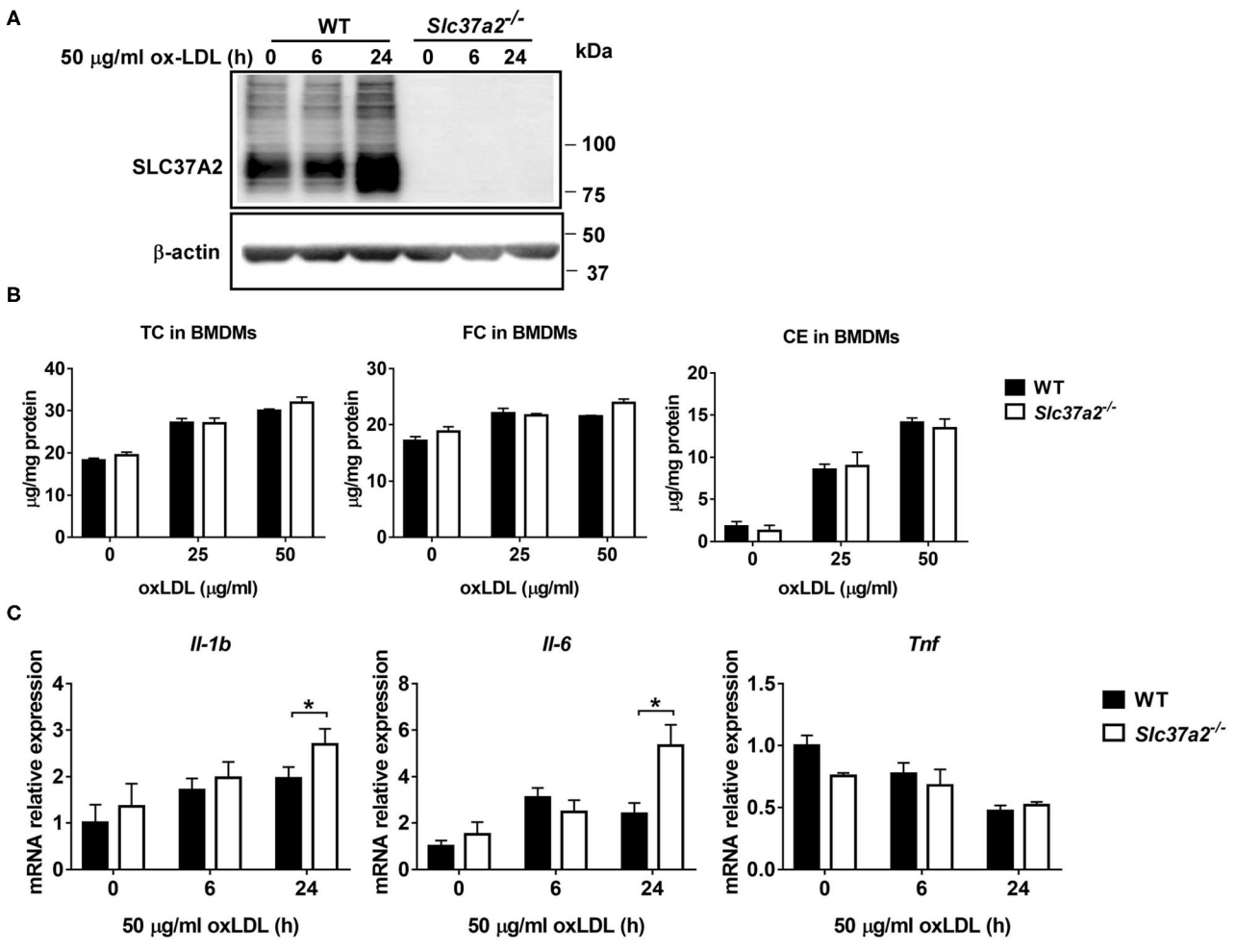

FIGURE 5 | SLC37A2 deficiency promotes oxidized LDL (OxLDL)-induced macrophage inflammation *in vitro*. **(A)** SLC37A2 protein expression analyzed by Western blotting in WT and *Slc37a2*$^{-/-}$ bone marrow-derived macrophages (BMDMs) treated with 50 μg/ml oxLDL for 0-24 h. **(B)** Quantification of cellar total cholesterol (TC), free cholesterol (FC), and cholesterol ester (CE) in WT and *Slc37a2*$^{-/-}$ BMDMs after treated with or without 25 or 50 μg/ml oxLDL for 24 h. **(C)** Relative transcript level of cytokines in WT and *Slc37a2*$^{-/-}$ BMDMs stimulated with 50 μg/ml oxLDL for 0-24 h, measured by qPCR. Data are representative of two independent experiments with three samples per group (mean ± SEM). *$p < 0.05$; unpaired, two-tailed Student's *t*-test.

expected, Slc37a2 mRNA expression was significantly reduced in the SLC37A2$^{\Delta hema}$ vs. control mouse epididymal fat. However, hematopoietic deletion of SLC37A2 did not alter adipose tissue inflammation, as quantified by qPCR analysis

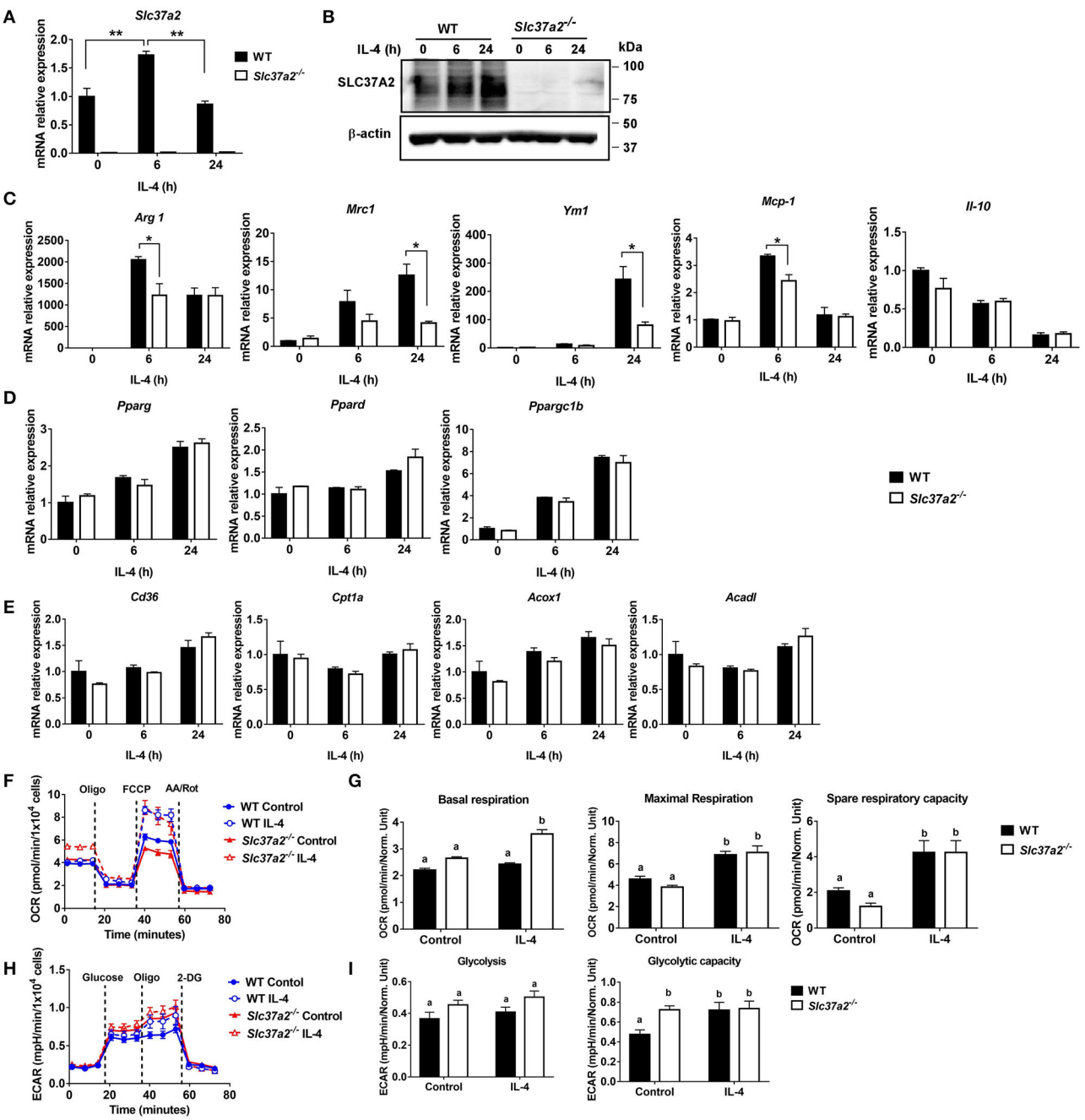

FIGURE 6 | SLC37A2 deficiency impairs IL-4-induced macrophage activation *in vitro*. **(A,B)** SLC37A2 expression in WT and *Slc37a2*$^{-/-}$ bone marrow-derived macrophages (BMDMs) stimulated with 20 ng/ml IL-4 for 0-24 h. **(A)** relative transcript expression and **(B)** protein expression of SLC37A2 measured by qPCR and western blotting, respectively. **(C)** Relative transcript level of macrophage alternative activation markers, including arginase−1 (Arg), mannose receptor, type I (Mrc1), Ym1, IL-10, and chemokine MCP-1, in WT and *Slc37a2*$^{-/-}$ BMDMs stimulated with 20 ng/ml IL-4 for 0-24 h. **(D,E)** The relative transcript level of PPARs and genes encoding transporters or enzymes involved in fatty acid uptake or β-oxidation in WT and *Slc37a2*$^{-/-}$ BMDMs stimulated with 20 ng/ml IL-4 for 0-24 h. **(F,G)** Seahorse analysis of oxygen consumption rate (OCR) in WT and *Slc37a2*$^{-/-}$ BMDMs treated with or without 20 ng/ml IL-4 for 24 h. **(H,I)** Seahorse analysis of extracellular acidification rates (ECAR) in WT and *Slc37a2*$^{-/-}$ BMDMs treated with or without 20 ng/ml IL-4 for 24 h. Data are representative of two independent experiments with three samples per group (mean ± SEM). *$p < 0.05$; **$p < 0.01$; unpaired, two-tailed Student's *t*-test **(A,C,D,E)**. Bars with different letters denote significant among groups ($p < 0.05$); two-way ANOVA with *post hoc* Tukey's multiple comparisons test **(G,I)**.

of gene expression of macrophage pro- and anti-inflammatory markers, except for increasing ccr2 (MCP-1 receptor) expression (**Supplementary Figure S5E**). These results suggest that deletion of SLC37A2 in bone marrow cells has minimal impact on WD-induced obesity, insulin resistance, and adipose tissue inflammation under pro-atherosclerotic conditions.

SLC37A2 Deficiency Promotes OxLDL-Induced Macrophage Inflammation

OxLDL promotes foam cell formation and triggers oxidative stress and pro-inflammatory responses in macrophages (42, 43), contributing to atherosclerotic plaque formation. Given that there was no significant increase in pro-inflammatory responses in SLC37A2$^{\Delta hema}$ vs. control mice after 16-wk WD feeding, we asked whether SLC37A2 deletion can affect oxLDL-induced macrophage inflammation *in vitro*. We found that oxLDL markedly increased SLC37A2 protein expression in BMDMs after 24 h stimulation (**Figure 5A**). OxLDL promoted cholesterol, particularly CE, accumulation in macrophages in a dose-dependent manner (**Figure 5B**), regardless of genotypes. However, SLC37A2 deletion does not affect cholesterol loading in macrophages (**Figure 5B**), suggesting a dispensible role for SLC37A2 in macrophage foam cell formation. Like LPS-stimulated cells, *Slc37a2*$^{-/-}$ macrophages showed increased expression of Il-1β and Il-6, but not Tnf at the transcriptional level in response to 24 h of oxLDL stimulation (**Figure 5C**), suggesting that SLC37A2 is a stress-responsive protein and increased SLC37A2 expression likely serves as a protective mechanism for resolution of stress-induced inflammation.

SLC37A2 Deficiency Impairs IL-4-Induced Macrophage Activation

IL-4 signaling activates STAT6, inducing the expression of genes involved in fatty acid metabolism and transcriptional regulation (such as transcriptional factors PPARs and PPARγ coactivator PGC1β) for reprogramming macrophage lipid metabolism (44). We found that IL-4 induced a 1.5-fold increase of Slc37a2 transcript at 6 h (**Figure 6A**) and a two-fold increase of SLC37A2 protein at 24 h of stimulation (**Figure 6B**) in WT macrophages. Consistent with our *in vivo* findings, SLC37A2-deficient macrophages showed decreased expression of M2 markers, including Arg1, Mrc1, and Ym1 (**Figure 6C**), in response to IL-4 stimulation suggesting that SLC37A2 expression is necessary for IL-4-induced macrophage [M (IL-4)] polarization. Interestingly, SLC37A2 deletion also lowered MCP-1 expression in macrophages, consistent with the lower *in vivo* MCP-1 expression in diet-fed SLC37A2$^{\Delta hema}$ vs. control mice. However, IL-4 does not induce IL-10 expression in either genotypic macrophages, suggesting that M (IL-4) is not a major source of IL-10 in macrophages. Note that WT and SLC37A2 deficient macrophages displayed similar expression levels of metabolic regulators (**Figure 6D**) and fatty acid oxidation genes (**Figure 6E**), which are primarily regulated by STAT6 signaling, suggesting that SLC37A2 deficiency does not impair the STAT6 signaling. Together, our data suggest that SLC37A2 deficiency impairs M (IL-4) polarization, independent of PPARs and PGC1 expression.

Given that mitochondrial oxidative phosphorylation (OXPHOS) supports M (IL-4) macrophage activation (45), we next examined mitochondrial respiration by measuring OCR in BMDMs treated with or without 20 ng/ml IL-4 for 6 or 24 h. As expected, 24 h IL-4 stimulation promoted mitochondrial OXPHOS in WT macrophages, as shown by increased maximal OCR and spare respiratory capacity (**Figures 6F,G**). Interestingly, *Slc37a2*$^{-/-}$ vs. WT BMDMs displayed significantly higher basal respiration after 24 h of IL-4 stimulation. However, no genotypic difference was observed in maximal respiration or spare respiratory capacity in IL-4 treated cells, suggesting a minor impact of SLC37A2 deletion on mitochondrial OXPHOS in M (IL-4) macrophages (**Figures 6F,G**). Additionally, SLC37A2 deletion has no effect on mitochondrial respiration in 6 h IL-4 treated macrophages (**Supplementary Figure S6**). Evidence suggests that glycolysis and glucose utilization are required for M (IL-4) macrophage activation (45), while another study indicates that glycolysis is dispensible as long as mitochondrial OXPHOS is intact (46). Nevertheless, SLC37A2-deficient macrophages showed slightly increased glycolytic capacity at baseline. No difference in glycolysis or glycolytic capacity was observed between genotypes after IL-4 treatment (**Figures 6H,I**). Overall, our results suggest that SLC37A2 deletion does not significantly impact glycolysis or mitochondrial OXPHOS in M (IL-4) macrophage. Thus, the attenuated M (IL-4) activation in SLC37A2-deficient macrophages is likely independent of these two cellular metabolic processes.

SLC37A2 Deficiency Impairs Apoptotic Cell-Induced Macrophage Activation

One of the striking changes in the diet-fed SLC37A2$^{\Delta hema}$ vs. control mice is the 70% reduction of plasma IL-10, a major anti-inflammatory cytokine for cellular homeostasis. Macrophages are a major type of phagocytes that can produce a large amount of IL-10 in response to apoptotic cells (47). The clearance of ACs and the suppression of inflammation by IL-10 are required to prevent chronic inflammation and reduce atherosclerosis progression. So, next, we examined apoptotic cell-induced macrophage [M (AC)] activation in WT and SLC37A2-deficient macrophages. We first incubated Jurkat T cells with 1 μM staurosporine for 4 h to induce early apoptosis (Annexin V$^+$, PI$^-$). Under this condition, 60% of Jurkat T cells underwent apoptosis (**Supplementary Figures S7A,B**). Compared to WT cells, SLC37A2-deficient macrophages showed a marked reduction in IL-10 expression at both transcriptional level (**Figure 7A**) and protein level (**Figure 7B**) in response to ACs. Engulfment of dead cells has been reported to elevate macrophage fatty acids and mitochondrial β-oxidation, which supports NAD^+ homeostasis and IL-10 production (48). To explore the possible mechanisms of the attenuated M (AC) activation in SLC37A2-deficient macrophages, we first compared the efferocytosis index between genotypes. We found SLC37A2 deletion has no effect on phagocytosis of ACs over a 2-h period (**Figure 7C**). Blockade of phagocytosis by using cytochalasin D

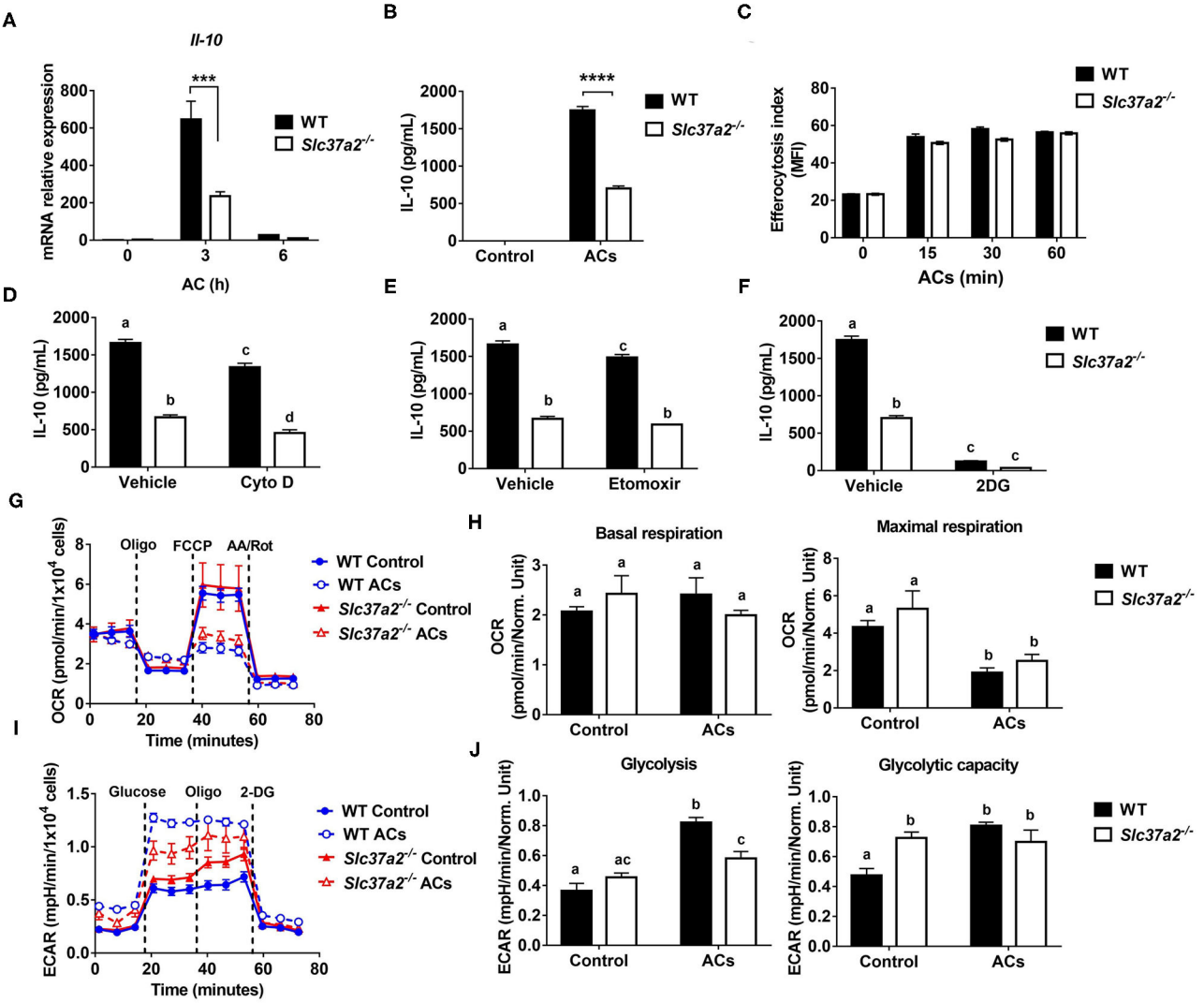

FIGURE 7 | SLC37A2 deficiency impairs apoptotic cell-induced macrophage activation *in vitro*. **(A)** IL-10 transcript expression in WT and *Slc37a2*$^{-/-}$ BMDMs stimulated with apoptotic Jurkat T cells (ACs) (macrophages: ACs = 1:5) for 0-6 h. Jurkat T cells were incubated with 1 μM staurosporine for 4 h to induce apoptosis. **(B)** IL-10 protein secretion from WT and *Slc37a2*$^{-/-}$ BMDMs stimulated with ACs (macrophages: ACs = 1:5) for 4 h. **(C)** Efferocytosis index was measured by incubating WT and *Slc37a2*$^{-/-}$ BMDMs with cell tracker green CMFDA-labeled ACs (macrophages: ACs = 1:5) for 0-120 min. After the indicated time, macrophages were washed with cold PBS 3 times and cell dissociation buffer once before being analyzed by flow cytometry. Mean fluorescence intensity (MFI) of macrophages engulfing ACs was quantified. **(D–F)** IL-10 protein secretion from WT and *Slc37a2*$^{-/-}$ BMDMs pretreated with phagocytosis inhibitor cytochalasin D (Cyto D, 10 μM), fatty acid oxidation inhibitor etomoxir (100 μM), and hexokinase inhibitor 2-deoxy-D-glucose (2-DG; 10 mM) for 30 min, followed by co-culture with ACs (macrophages: ACs = 1:5) for 4 h. **(G,H)** Seahorse analysis of oxygen consumption rate (OCR) in WT and *Slc37a2*$^{-/-}$ BMDMs treated with or without ACs (macrophages: ACs = 1:5) for 3 h. **(I,J)** Seahorse analysis of extracellular acidification rates (ECAR) in WT and *Slc37a2*$^{-/-}$ BMDMs treated with or without ACs (macrophages: ACs = 1:5) for 3 h. Data are representative of two independent experiments with 3 samples per group (mean ± SEM). ***$P < 0.001$, ****$P < 0.0001$, unpaired, two-tailed Student's *t*-test **(A–C)**. Bars with different letters denote significant among groups ($p < 0.05$); two-way ANOVA with *post hoc* Tukey's multiple comparisons test **(D–J)**.

(**Figure 7D**) or blockade of fatty acid β-oxidation by etomoxir (**Figure 7E**) slightly reduced AC-induced IL-10 production in both genotypes but did not normalize the differential expression of IL-10 between genotypes. Interestingly, blockade of glycolysis using 2-DG led to a significant reduction of IL-10 in engulfed macrophages in both mouse genotypes (**Figure 7F**), suggesting that glycolysis plays an unappreciated role in AC-induced IL-10 production. More interestingly, the blockade of glycolysis normalized the differential IL-10 secretion between genotypes. Consistent with the profound anti-inflammatory effect of efferocytosis, AC-treated macrophages produced a very low level of TNF (100 pg/ml) (**Supplementary Figures S7C–E**), likely resulting from the low-grade (7.3%) cell death induced by staurosporine (**Supplementary Figures S7A,B**). Nevertheless, AC-induced TNF production was comparable between genotypes (**Supplementary Figures S7C–E**).

Different from the drug effect on IL-10 production, cytochalasin D (**Supplementary Figure S7C**), etomoxir (**Supplementary Figure S7D**), or 2-DG (**Supplementary Figure S7E**) showed a more profound inhibitory effect on AC-induced TNF production in SLC37A2-deficient macrophages.

Next, we examined mitochondrial respiration and glycolysis by measuring OCR and ECAR, respectively. We found that ACs decreased mitochondrial OXPHOS when engulfed by macrophages regardless of genotypes, as shown by decreased maximal respiration without significant changes in basal respiration (**Figures 7G,H**). Furthermore, ACs promoted aerobic glycolysis in WT macrophages, and SLC37A2 deletion impaired AC-induced glycolysis (**Figures 7I,J**). No genotypic difference in glycolytic capacity was observed in AC-engulfed macrophages. Together, our results suggest that SLC37A2 positively regulates M (AC) activation through modulation of glycolysis and is likely independent of phagocytosis or fatty acid oxidation.

DISCUSSION

As an ER-membrane anchored G6P transporter, SLC37A2 is a critical regulator of LPS-induced inflammation in macrophages by modulation of glycolysis (24). Herein, we made novel observations that SLC37A2 expression is necessary to maintain IL-4 and apoptotic cell-induced macrophage alternative activation in a glycolysis-independent and -dependently manner, respectively. Hematopoietic expression of SLC37A2 is atheroprotective *in vivo* under pro-atherogenic conditions. Disruption of SLC37A2 significantly impairs macrophage activation induced by IL-4 or apoptotic cells. Moreover, disruption of SLC37A2 in hematopoietic cells impairs anti-inflammatory responses and worsens atherogenesis in high-fat western diet-fed $Ldlr^{-/-}$ mice. Since LPS, oxLDL, and IL-4 induce macrophage SLC37A2 protein expression, we speculate that induction of macrophage SLC37A2 expression promotes inflammation resolution and slows atherosclerosis progression.

Cellular metabolism has emerged as an essential determinant of macrophage activation in response to microenvironmental cues. Macrophage pro-inflammatory activation was long thought to primarily rely on glucose metabolism, whereas M (IL-4) macrophages switch to fatty acid oxidation and mitochondrial biogenesis to support their anti-inflammatory functions (44). However, recent studies challenged this concept and suggested that fatty acid oxidation is dispensable for M (IL-4) macrophage polarization (49, 50). Whether glycolysis plays a role in M (IL-4) activation is also under debate and requires further investigation (45). Therefore, how macrophages reprogram cellular metabolism to favor M (IL-4) polarization remains poorly defined. In our study, SLC37A2 deficiency impairs M (IL-4) polarization independent of PPARs and PGC1. Given that SLC37A2 regulates glycolysis and mitochondrial OXPHOS in LPS-treated macrophages, we hypothesized that SLC37A2 might promote M (IL-4) activation by enhancing mitochondrial respiration. Our results showed that 24 h of IL-4 stimulation significantly increased glycolysis and mitochondrial respiration in macrophages regardless of SLC37A2 expression. Despite the impaired M (IL-4) activation, SLC37A2 deletion slightly increased mitochondrial respiration and had no effect on glycolysis in M (IL-4) macrophages. These results suggest that the impaired M (IL-4) activation in SLC37A2-deficient macrophages is likely regulated by unknown mechanisms rather than rewiring the glycolytic process or altering mitochondrial respiration. Additionally, mitochondrial β-oxidation of fatty acids derived from apoptotic cells has been shown to support efferocytosis-induced IL-10 production (48). Interestingly, despite a minimal effect on phagocytosis of apoptotic cells, SLC37A2 deletion significantly impairs apoptotic cell-induced IL-10, suggesting a critical role of SLC37A2 in M (AC) activation. Importantly, our study indicates that glycolysis plays a more significant role in AC-induced IL-10 production, as evidenced by the increased ECAR in AC-treated macrophages and a greater reduction of IL-10 in 2-DG-treated macrophages relative to etomoxir-treated cells. Our results agreed with Morioka's findings that efferocytosis promotes glucose uptake, glycolysis, and lactate production (51). Unlike LPS-treated macrophages in which SLC37A2 deletion promotes glycolysis, SLC37A2-deficient macrophages showed attenuated glycolysis in response to AC stimulation. Furthermore, blockade of glycolysis, but not phagocytosis or fatty acid oxidation, normalized the differential secretion of IL-10 between genotypes. Together, our results suggest that glucose metabolism plays a central role in SLC37A2-regulated M (AC) activation.

Our *in vitro* macrophage studies suggest that SLC37A2 deletion enhances pro-inflammatory activation in both LPS- and oxLDL-treated macrophages. However, hematopoietic SLC37A2 deletion does not cause elevated pro-inflammatory responses in WD-fed $Ldlr^{-/-}$ mice. Unexpectedly, plasma MCP-1 showed a 30% reduction in $SLC37A2^{\Delta hema}$ mice. MCP-1 is one of the critical chemokines that regulate the migration and infiltration of monocytes/macrophages. A higher circulating level of MCP-1 is associated with an increased long-term risk of stroke in the general population (52). Inhibition of MCP-1 (53) decreases plaque size and limits macrophage infiltration in experimental models of atherosclerosis. As discussed above, hematopoietic SLC37A2 deletion increases lipid deposition and necrotic core formation but does not enhance macrophage ($CD68^{+}$ cells) infiltration in diet-fed $Ldlr^{-/-}$ mice. One possible explanation for the indistinguishable macrophage content between genotypes is the net effect of reducing anti-inflammatory IL-10 and pro-inflammatory MCP-1 in those knockout mice. Interestingly, IL-4 signaling induces MCP-1 expression in macrophages and other cells (54–56). We observed a significant decrease in MCP-1 expression induced by IL-4 in SLC37A2-deficient macrophages. Whether the down-regulation of MCP-1 expression results from the impaired IL-4 response in WD-diet fed $SLC37A2^{\Delta hema}$ mice requires further investigation. On the other hand, macrophage heterogeneity is more complex as activation drives a spectrum of macrophages (12). The mixed pro-inflammatory and anti-inflammatory profile in diet-fed $SLC37A2^{\Delta hema}$ mice likely reflects the complex microenviroment (for instance, atherosclerotic plaque or liver tissue) that macrophages encounter in those mice.

Alternatively-activated macrophages promote tissue remodeling and repair through collagen formation and clearance of apoptotic cells (efferocytosis). Failure of efferocytosis leads to increased apoptosis and cell death. Alternatively-activated macrophages also secrete high levels of anti-inflammatory cytokines such as IL-10 (57). IL-10 is a crucial mediator of inflammation resolution and promotes efferocytosis by a positive feedback pathway (58). Blocking IL-10 accelerates atherosclerosis (59), whereas targeting the delivery of IL-10 *via* nanoparticles attenuates atherosclerosis (60). Consistent with the impaired anti-inflammatory activation of macrophages *in vitro*, our *in vivo* study showed that SLC37A2 deficiency in bone marrow lowers plasma IL-10 level and enhances atherosclerosis in WD-fed $Ldlr^{-/-}$ mice. Moreover, we observed that plasma IL-10, but not plasma cholesterol, displays an inverse correlation with aortic plaque size in diet-fed mice. Although no significant changes in apoptosis or efferocytosis in atherosclerotic plaques were observed between genotypes, loss of SLC37A2 in bone marrow did enlarge necrotic cores and decrease collagen deposition in the diet-fed mouse plaques. This could suggest secondary necrosis of apoptotic cells may have nonetheless occurred. Because SLC37A2 expression is necessary for anti-inflammatory macrophage activation *in vitro* and *in vivo*, we speculate that the impaired anti-inflammatory responses are a major driving force of enhanced atherosclerosis in the $SLC37A2^{\Delta hema}$ mice.

Alternative activation of hepatic macrophages promotes liver fatty acid oxidation and improves metabolic syndrome (36). One interesting observation in the current study is that the $SLC37A2^{\Delta hema}$ mice displayed elevated plasma and liver cholesterol concentrations, which likely increases the risk of atherosclerosis in those animals. Consistent with the increased hepatic lipid accumulation, $SLC37A2^{\Delta hema}$ mice showed lower expression of genes encoding fatty acid oxidation enzymes and less enrichment of anti-inflammatory macrophages in the liver after 16-wk WD feeding. Our data suggest that SLC37A2 expression is necessary for alternative activation of Kupffer cells under chronic metabolic stress conditions. Therefore, disruption of SLC37A2 impairs alternative activation of Kupffer cells, leading to decreased hepatic fatty acid oxidation and increased neutral lipid accumulation in the liver under atherogenic conditions. Additionally, bone marrow SLC37A2 deletion lowers the transcript expression of genes encoding cholesterol efflux and concomitantly upregulates the expression of genes responsible for oxLDL cholesterol uptake, suggesting that hematopoietic SLC37A2 deletion may partially promote hepatic neutral lipid accumulation by disrupting cholesterol efflux/uptake in the liver. Since Kupffer cell replacement in $Slc37a2^{-/-}$ BMT mice is incomplete (61), the modest elevation of plasma and liver lipids in the $SLC37A2^{\Delta hema}$ mice may underestimate the harmful effect of SLC37A2 deletion on liver lipid homeostasis in the context of atherosclerosis.

In summary, under *in vivo* pro-atherogenic conditions, hematopoietic SLC37A2 expression is necessary for maintaining alternative macrophage activation and IL-10 production. Loss of hematopoietic cell-specific SLC37A2 impairs anti-inflammatory activities at the cell (peritoneal macrophages), tissue (liver), and systemic (plasma) levels and accelerates atherosclerosis. Our study suggests that hematopoietic SLC37A2 expression protects against atherosclerosis in mice.

Limitations of the Study

One of the limitations of the BMT model is that BM contains multiple types of immune cells. Many of them, including T cells, B cells, neutrophils, and dendritic cells, are involved in atherogenesis. Because of this, we cannot distinguish the specific contribution of macrophage SLC37A2 from other immune cells to atherosclerosis. Additionally, we only examined atherosclerosis after 16-wks diet feeding, a more advanced stage of atherosclerosis. Lastly, we only used male $Ldlr^{-/-}$ mice as recipient mice to investigate the impact of hematopoietic SLC37A2 deficiency on the pathogenesis of atherogenesis and obesity and insulin resistance induced by high-fat diet feeding. Therefore, we do not know whether there is a sex-dependent effect of hematopoietic SLC37A2 expression on the pathogenesis of atherogenesis or not.

DATA AVAILABILITY STATEMENT

The original contributions presented in the study are included in the article/**Supplementary Materials**, further inquiries can be directed to the corresponding author/s.

ETHICS STATEMENT

The animal study was reviewed and approved by Wake Forest University Animal Care and Use Committee.

AUTHOR CONTRIBUTIONS

QZhao, ZW, AKM, MZ, and QZhang performed the experiments. EB helped with mouse necropsy. JM and MBF helped with multiplex assay and manuscript writing. F-CH helped with statistical analysis. CEM, CMF, and JSP helped with manuscript writing and data discussion. XZ conceived the study and wrote the manuscript. All authors contributed to the article and approved the submitted version.

FUNDING

This study was supported by NIEHS Z01 ES102005 (MBF), NIH R01 HL119962 (JSP), NIH R35 GM126922 (CEM), NIH R01 HL132035 (XZ), and NIH T32GM127261 and NIH T32AI007401 (AKM). The study was also supported by National Center for Advancing Translational Sciences of the National Institutes of Health under Award Number UL1TR001420 (Research Assistant fund to XZ).

SUPPLEMENTARY MATERIAL

The Supplementary Material for this article can be found online at: https://www.frontiersin.org/articles/10.3389/fcvm.2021.777098/full#supplementary-material

REFERENCES

1. Amengual J, Barrett TJ. Monocytes and macrophages in atherogenesis. *Curr Opin Lipidol.* (2019) 30:401–8. doi: 10.1097/MOL.0000000000000634
2. Getz GS, Reardon CA. Atherosclerosis: cell biology and lipoproteins. *Curr Opin Lipidol.* (2020) 31:286–90. doi: 10.1097/MOL.0000000000000704
3. Bäck M, Yurdagul A, Jr., Tabas I, Öörni K, Kovanen PT. Inflammation and its resolution in atherosclerosis: mediators and therapeutic opportunities. *Nat Rev Cardiol.* (2019) 16:389–406. doi: 10.1038/s41569-019-0169-2
4. Libby P, Bornfeldt KE. How far we have come, how far we have yet to go in atherosclerosis research. *Circ Res.* (2020) 126:1107–11. doi: 10.1161/CIRCRESAHA.120.316994
5. Flynn MC, Pernes G, Lee MKS, Nagareddy PR, Murphy AJ. Monocytes, macrophages, and metabolic disease in atherosclerosis. *Front Pharmacol.* (2019) 10:666. doi: 10.3389/fphar.2019.00666
6. Remmerie A, Scott CL. Macrophages and lipid metabolism. *Cell Immunol.* (2018) 330:27–42. doi: 10.1016/j.cellimm.2018.01.020
7. Rader DJ, Puré E. Lipoproteins, macrophage function, and atherosclerosis: beyond the foam cell? *Cell Metab.* (2005) 1:223–30. doi: 10.1016/j.cmet.2005.03.005
8. Hansson GK, Libby P, Tabas I. Inflammation and plaque vulnerability. *J Intern Med.* (2015) 278:483–93. doi: 10.1111/joim.12406
9. Yvan-Charvet L, Ivanov S. Metabolic reprogramming of macrophages in atherosclerosis: is it all about cholesterol? *J Lipid Atheroscl.* (2020) 9:231–42. doi: 10.12997/jla.2020.9.2.231
10. Koelwyn GJ, Corr EM, Erbay E, Moore KJ. Regulation of macrophage immunometabolism in atherosclerosis. *Nat Immunol.* (2018) 19:526–37. doi: 10.1038/s41590-018-0113-3
11. Wang Y, Zhao M, Liu S, Guo J, Lu Y, Cheng J, et al. Macrophage-derived extracellular vesicles: diverse mediators of pathology and therapeutics in multiple diseases. *Cell Death Dis.* (2020) 11:924. doi: 10.1038/s41419-020-03127-z
12. Xue J, Schmidt SV, Sander J, Draffehn A, Krebs W, Quester I, et al. Transcriptome-based network analysis reveals a spectrum model of human macrophage activation. *Immunity.* (2014) 40:274–88. doi: 10.1016/j.immuni.2014.01.006
13. Moore KJ, Sheedy FJ, Fisher EA. Macrophages in atherosclerosis: a dynamic balance. *Nat Rev Immunol.* (2013) 13:709–21. doi: 10.1038/nri3520
14. Stremmel C, Stark K, Schulz C. Heterogeneity of macrophages in atherosclerosis. *Thromb Haemost.* (2019) 119:1237–46. doi: 10.1055/s-0039-1692665
15. O'Neill LA, Kishton RJ, Rathmell J. A guide to immunometabolism for immunologists. *Nat Rev Immunol.* (2016) 16:553–65. doi: 10.1038/nri.2016.70
16. O'Neill LA, Pearce EJ. Immunometabolism governs dendritic cell and macrophage function. *J Exp Med.* (2016) 213:15–23. doi: 10.1084/jem.20151570
17. Pearce EL, Pearce EJ. Metabolic pathways in immune cell activation and quiescence. *Immunity.* (2013) 38:633–43. doi: 10.1016/j.immuni.2013.04.005
18. Rudd JH, Warburton EA, Fryer TD, Jones HA, Clark JC, Antoun N, et al. Imaging atherosclerotic plaque inflammation with [18F]-fluorodeoxyglucose positron emission tomography. *Circulation.* (2002) 105:2708–11. doi: 10.1161/01.CIR.0000020548.60110.76
19. Freemerman AJ, Zhao L, Pingili AK, Teng B, Cozzo AJ, Fuller AM, et al. Myeloid Slc2a1-deficient murine model revealed macrophage activation and metabolic phenotype are fueled by GLUT1. *J Immunol.* (2019) 202:1265–86. doi: 10.4049/jimmunol.1800002
20. Nishizawa T, Kanter JE, Kramer F, Barnhart S, Shen X, Vivekanandan-Giri A, et al. Testing the role of myeloid cell glucose flux in inflammation and atherosclerosis. *Cell Rep.* (2014) 7:356–65. doi: 10.1016/j.celrep.2014.03.028
21. Chou JY, Sik Jun H, Mansfield BC. The SLC37 family of phosphate-linked sugar phosphate antiporters. *Mol Aspects Med.* (2013) 34:601–11. doi: 10.1016/j.mam.2012.05.010
22. Kim JY, Tillison K, Zhou S, Wu Y, Smas CM. The major facilitator superfamily member Slc37a2 is a novel macrophage- specific gene selectively expressed in obese white adipose tissue. *Am J Physiol Endocrinol Metab.* (2007) 293:E110–20. doi: 10.1152/ajpendo.00404.2006
23. Pan CJ, Chen SY, Jun HS, Lin SR, Mansfield BC, Chou JY. SLC37A1 and SLC37A2 are phosphate-linked, glucose-6-phosphate antiporters. *PLoS ONE.* (2011) 6:e23157. doi: 10.1371/journal.pone.0023157
24. Wang Z, Zhao Q, Nie Y, Yu Y, Misra BB, Zabalawi M, et al. Solute carrier family 37 member 2 (SLC37A2) negatively regulates murine macrophage inflammation by controlling glycolysis. *iScience.* (2020) 23:101125. doi: 10.1016/j.isci.2020.101125
25. Wang Z, Sequeira RC, Zabalawi M, Madenspacher J, Boudyguina E, Ou T, et al. Myeloid atg5 deletion impairs n-3 PUFA-mediated atheroprotection. *Atherosclerosis.* (2020) 295:8-17. doi: 10.1016/j.atherosclerosis.2020.01.004
26. Liao X, Sluimer JC, Wang Y, Subramanian M, Brown K, Pattison JS, et al. Macrophage autophagy plays a protective role in advanced atherosclerosis. *Cell Metab.* (2012) 15:545–53. doi: 10.1016/j.cmet.2012.01.022
27. Li S, Sun Y, Liang CP, Thorp EB, Han S, Jehle AW, et al. Defective phagocytosis of apoptotic cells by macrophages in atherosclerotic lesions of ob/ob mice and reversal by a fish oil diet. *Circ Res.* (2009) 105:1072–82. doi: 10.1161/CIRCRESAHA.109.199570
28. Thorp E, Cui D, Schrijvers DM, Kuriakose G, Tabas I. Mertk receptor mutation reduces efferocytosis efficiency and promotes apoptotic cell accumulation and plaque necrosis in atherosclerotic lesions of apoe-/- mice. *Arterioscl Thromb Vasc Biol.* (2008) 28:1421–8. doi: 10.1161/ATVBAHA.108.167197
29. Schrijvers DM, De Meyer GR, Kockx MM, Herman AG, Martinet W. Phagocytosis of apoptotic cells by macrophages is impaired in atherosclerosis. *Arterioscl Thromb Vasc Biol.* (2005) 25:1256–61. doi: 10.1161/01.ATV.0000166517.18801.a7
30. Shen L, Yang Y, Ou T, Key CC, Tong SH, Sequeira RC, et al. Dietary PUFAs attenuate NLRP3 inflammasome activation via enhancing macrophage autophagy. *J Lipid Res.* (2017) 58:1808–21. doi: 10.1194/jlr.M075879
31. Zhu X, Chung S, Bi X, Chuang CC, Brown AL, Liu M, et al. Myeloid cell-specific ABCA1 deletion does not worsen insulin resistance in HF diet-induced or genetically obese mouse models. *J Lipid Res.* (2013) 54:2708–17. doi: 10.1194/jlr.M038943
32. Bi X, Zhu X, Gao C, Shewale S, Cao Q, Liu M, et al. Myeloid cell-specific ATP-binding cassette transporter A1 deletion has minimal impact on atherogenesis in atherogenic diet-fed low-density lipoprotein receptor knockout mice. *Arterioscl Thromb Vasc Biol.* (2014) 34:1888–99. doi: 10.1161/ATVBAHA.114.303791
33. Carr TP, Andresen CJ, Rudel LL. Enzymatic determination of triglyceride, free cholesterol, and total cholesterol in tissue lipid extracts. *Clin Biochem.* (1993) 26:39–42. doi: 10.1016/0009-9120(93)90015-X
34. Zhu X, Lee JY, Timmins JM, Brown JM, Boudyguina E, Mulya A, et al. Increased cellular free cholesterol in macrophage-specific Abca1 knock-out mice enhances pro-inflammatory response of macrophages. *J Biol Chem.* (2008) 283:22930–41. doi: 10.1074/jbc.M801408200
35. McGillicuddy FC, M. de la Llera Moya, Hinkle CC, Joshi MR, Chiquoine EH, Billheimer JT, et al. Inflammation impairs reverse cholesterol transport *in vivo*. *Circulation.* (2009) 119:1135–45. doi: 10.1161/CIRCULATIONAHA.108.810721
36. Odegaard JI, Ricardo-Gonzalez RR, Red Eagle A, Vats D, Morel CR, Goforth MH, et al. Alternative M2 activation of Kupffer cells by PPARdelta ameliorates obesity-induced insulin resistance. *Cell Metab.* (2008) 7:496–507. doi: 10.1016/j.cmet.2008.04.003
37. Xu W, Roos A, Schlagwein N, Woltman AM, Daha MR, van Kooten C. IL-10-producing macrophages preferentially clear early apoptotic cells. *Blood.* (2006) 107:4930-7. doi: 10.1182/blood-2005-10-4144
38. Tabas I. Macrophage death and defective inflammation resolution in atherosclerosis. *Nat Rev Immunol.* (2010) 10:36–46. doi: 10.1038/nri2675
39. Poon IK, Lucas CD, Rossi AG, Ravichandran KS. Apoptotic cell clearance: basic biology and therapeutic potential. *Nature Rev Immunol.* (2014) 14:166–80. doi: 10.1038/nri3607
40. Deguchi JO, Aikawa E, Libby P, Vachon JR, Inada M, Krane SM, et al. Matrix metalloproteinase-13/collagenase-3 deletion promotes collagen accumulation and organization in mouse atherosclerotic plaques. *Circulation.* (2005) 112:2708–15. doi: 10.1161/CIRCULATIONAHA.105.562041
41. Rekhter MD. Collagen synthesis in atherosclerosis: too much and not enough. *Cardiovasc Res.* (1999) 41:376–84. doi: 10.1016/S0008-6363(98)00321-6

42. Libby P, Ridker PM, Hansson GK. Progress and challenges in translating the biology of atherosclerosis. *Nature.* (2011) 473:317–25. doi: 10.1038/nature10146
43. Maiolino G, Rossitto G, Caielli P, Bisogni V, Rossi GP, Calò LA. The role of oxidized low-density lipoproteins in atherosclerosis: the myths and the facts. *Mediators Inflamm.* (2013) 2013:714653. doi: 10.1155/2013/714653
44. Vats D, Mukundan L, Odegaard JI, Zhang L, Smith KL, Morel CR, et al. Oxidative metabolism and PGC-1beta attenuate macrophage-mediated inflammation. *Cell Metab.* (2006) 4:13–24. doi: 10.1016/j.cmet.2006.08.006
45. Huang SC, Smith AM, Everts B, Colonna M, Pearce EL, Schilling JD, et al. Metabolic reprogramming mediated by the mTORC2-IRF4 signaling axis is essential for macrophage alternative activation. *Immunity.* (2016) 45:817–30. doi: 10.1016/j.immuni.2016.09.016
46. Wang F, Zhang S, Vuckovic I, Jeon R, Lerman A, Folmes CD, et al. Glycolytic stimulation is not a requirement for M2 macrophage differentiation. *Cell Metab.* (2018) 28:463–75.e464. doi: 10.1016/j.cmet.2018.08.012
47. Chung EY, Liu J, Homma Y, Zhang Y, Brendolan A, Saggese M, et al. Interleukin-10 expression in macrophages during phagocytosis of apoptotic cells is mediated by homeodomain proteins Pbx1 and Prep-1. *Immunity.* (2007) 27:952–64. doi: 10.1016/j.immuni.2007.11.014
48. Zhang S, Weinberg S, DeBerge M, Gainullina A, Schipma M, Kinchen JM, et al. Efferocytosis fuels requirements of fatty acid oxidation and the electron transport chain to polarize macrophages for tissue repair. *Cell Metab.* (2019) 29:443–56.e445. doi: 10.1016/j.cmet.2018.12.004
49. Divakaruni AS, Hsieh WY, Minarrieta L, Duong TN, Kim KKO, Desousa BR, et al. Etomoxir inhibits macrophage polarization by disrupting CoA homeostasis. *Cell Metab.* (2018) 28:490–503.e497. doi: 10.1016/j.cmet.2018.06.001
50. Van den Bossche J, van der Windt GJW. Fatty acid oxidation in macrophages and T cells: time for reassessment? *Cell Metab.* (2018) 28:538-40. doi: 10.1016/j.cmet.2018.09.018
51. Morioka S, Perry JSA, Raymond MH, Medina CB, Zhu Y, Zhao L, et al. Efferocytosis induces a novel SLC program to promote glucose uptake and lactate release. *Nature.* (2018) 563:714–8. doi: 10.1038/s41586-018-0735-5
52. Georgakis MK, Malik R, Björkbacka H, Pana TA, Demissie S, Ayers C, et al. Circulating monocyte chemoattractant protein-1 and risk of stroke: meta-analysis of population-based studies involving 17 180 individuals. *Circ Res.* (2019) 125:773–82. doi: 10.1161/CIRCRESAHA.119.315380
53. Gu L, Okada Y, Clinton SK, Gerard C, Sukhova GK, Libby P, et al. Absence of monocyte chemoattractant protein-1 reduces atherosclerosis in low density lipoprotein receptor-deficient mice. *Mol Cell.* (1998) 2:275–81. doi: 10.1016/S1097-2765(00)80139-2
54. Rollins BJ, Pober JS. Interleukin-4 induces the synthesis and secretion of MCP-1/JE by human endothelial cells. *Am J Pathol.* (1991) 138:1315–9.
55. Kikuchi H, Hanazawa S, Takeshita A, Nakada Y, Yamashita Y, Kitano S. Interleukin-4 acts as a potent stimulator for expression of monocyte chemoattractant JE/MCP-1 in mouse peritoneal macrophages. *Biochem Biophys Res Commun.* (1994) 203:562–9. doi: 10.1006/bbrc.1994.2219
56. Ovsiy I, Riabov V, Manousaridis I, Michel J, Moganti K, Yin S, et al. IL-4 driven transcription factor FoxQ1 is expressed by monocytes in atopic dermatitis and stimulates monocyte migration. *Sci Rep.* (2017) 7:16847. doi: 10.1038/s41598-017-17307-z
57. Saraiva M, Vieira P, O'Garra A. Biology and therapeutic potential of interleukin-10. *J Exp Med.* (2020) 217:jem.20190418. doi: 10.1084/jem.20190418
58. Ogden CA, Pound JD, Batth BK, Owens S, Johannessen I, Wood K, et al. Enhanced apoptotic cell clearance capacity and B cell survival factor production by IL-10-activated macrophages: implications for Burkitt's lymphoma. *J Immunol.* (2005) 174:3015–23. doi: 10.4049/jimmunol.174.5.3015
59. Caligiuri G, Rudling M, Ollivier V, Jacob MP, Michel JB, Hansson GK, et al. Interleukin-10 deficiency increases atherosclerosis, thrombosis, and low-density lipoproteins in apolipoprotein E knockout mice. *Mol Med.* (2003) 9:10–7. doi: 10.1007/BF03402102
60. Kamaly N, Fredman G, Fojas JJ, Subramanian M, Choi WI, Zepeda K, et al. Targeted interleukin-10 nanotherapeutics developed with a microfluidic chip enhance resolution of inflammation in advanced atherosclerosis. *ACS Nano.* (2016) 10:5280–92. doi: 10.1021/acsnano.6b01114
61. Kennedy DW, Abkowitz JL. Kinetics of central nervous system microglial and macrophage engraftment: analysis using a transgenic bone marrow transplantation model. *Blood.* (1997) 90:986–93. doi: 10.1182/blood.V90.3.986

Conflict of Interest: The authors declare that the research was conducted in the absence of any commercial or financial relationships that could be construed as a potential conflict of interest.

Publisher's Note: All claims expressed in this article are solely those of the authors and do not necessarily represent those of their affiliated organizations, or those of the publisher, the editors and the reviewers. Any product that may be evaluated in this article, or claim that may be made by its manufacturer, is not guaranteed or endorsed by the publisher.

Copyright © 2021 Zhao, Wang, Meyers, Madenspacher, Zabalawi, Zhang, Boudyguina, Hsu, McCall, Furdui, Parks, Fessler and Zhu. This is an open-access article distributed under the terms of the Creative Commons Attribution License (CC BY). The use, distribution or reproduction in other forums is permitted, provided the original author(s) and the copyright owner(s) are credited and that the original publication in this journal is cited, in accordance with accepted academic practice. No use, distribution or reproduction is permitted which does not comply with these terms.

frontiers in Cardiovascular Medicine

REVIEW
published: 10 January 2022
doi: 10.3389/fcvm.2021.824481

Oxidized Lipids: Common Immunogenic Drivers of Non-Alcoholic Fatty Liver Disease and Atherosclerosis

Constanze Hoebinger[1], *Dragana Rajcic*[1] *and Tim Hendrikx*[1,2]*

[1] *Department of Laboratory Medicine, Klinisches Institut für Labormedizin (KILM), Medical University Vienna, Vienna, Austria,* [2] *Department of Molecular Genetics, School of Nutrition and Translational Research in Metabolism (NUTRIM), Maastricht University, Maastricht, Netherlands*

The prevalence of non-alcoholic fatty liver disease (NAFLD), ranging from simple steatosis to inflammatory steatohepatitis (NASH) and cirrhosis, continues to rise, making it one of the major chronic liver diseases and indications for liver transplantation worldwide. The pathological processes underlying NAFLD not only affect the liver but are also likely to have systemic effects. In fact, growing evidence indicates that patients with NAFLD are at increased risk for developing atherosclerosis. Indeed, cardiovascular complications are the leading cause of mortality in NAFLD patients. Here, we aim to address common pathophysiological molecular pathways involved in chronic fatty liver disease and atherosclerosis. In particular, we focus on the role of oxidized lipids and the formation of oxidation-specific epitopes, which are important targets of host immunity. Acting as metabolic danger signals, they drive pro-inflammatory processes and thus contribute to disease progression. Finally, we summarize encouraging studies indicating that oxidized lipids are promising immunological targets to improve intervention strategies for NAFLD and potentially limit the risk of developing atherosclerosis.

Keywords: NAFLD (non-alcoholic fatty liver disease), oxidized lipids, foamy macrophages, immunoglobulins, atherosclerosis, NASH (non-alcoholic steatohepatitis)

OPEN ACCESS

Edited by:
Jue Zhang,
Versiti Blood Research Institute, United States

Reviewed by:
Shunxing Rong, University of Texas Southwestern Medical Center, United States
Papasani Subbaiah, University of Illinois at Chicago, United States

***Correspondence:**
Tim Hendrikx
tim.hendrikx@meduniwien.ac.at

Specialty section:
This article was submitted to Lipids in Cardiovascular Disease, a section of the journal Frontiers in Cardiovascular Medicine

Received: *29 November 2021*
Accepted: *15 December 2021*
Published: *10 January 2022*

Citation:
Hoebinger C, Rajcic D and Hendrikx T (2022) Oxidized Lipids: Common Immunogenic Drivers of Non-Alcoholic Fatty Liver Disease and Atherosclerosis. Front. Cardiovasc. Med. 8:824481. doi: 10.3389/fcvm.2021.824481

INTRODUCTION

A sedentary lifestyle and excess caloric intake combined with reduced energy expenditure not only lead to overweight and obesity but also an increase in the prevalence of metabolic syndrome and various lipid-mediated diseases such as non-alcoholic fatty liver disease (NAFLD) (1, 2). As the liver is the most metabolic organ in the human body, increased circulatory lipid levels result in their accumulation in the liver, known as steatosis (fat accumulation in >5% of hepatocytes) (3, 4). While simple steatosis is still reversible by lifestyle modifications, the NAFLD spectrum also includes more progressive non-alcoholic steatohepatitis (NASH), characterized by inflammation, hepatocyte damage, and fibrosis (5). Importantly, the presence of NASH further increases the risk of developing an end-stage liver disease such as cirrhosis or hepatocellular carcinoma, ultimately requiring liver transplantation (4). By affecting ∼25% of individuals, both adults and children, NAFLD has become the leading cause of chronic liver disease worldwide (6, 7). Considering that the prevalence is expected to rise further (7), NAFLD can be regarded as significant health and economic burden worldwide, resulting in a reduced quality of life (8).

While NAFLD primarily affects liver structure and function, leading to morbidity and mortality from liver failure, cardiovascular disease (CVD) is the most common cause of death in early NAFLD patients (9, 10). Moreover, there is increasing evidence that NAFLD is a risk factor for developing cardiovascular complications such as atherosclerosis (11). Atherosclerosis can be broadly described as a progressive chronic inflammatory disease of the large and medium-sized arteries that share metabolic patterns with NAFLD (12, 13). More precisely, atherosclerosis is characterized by the thickening and hardening of the arterial walls, mainly caused by developing complex lesions and accumulation of lipids and fibrous elements known as atheromatous plaques narrowing the arterial lumen (14, 15). Subsequently, plaque rupture and thrombosis can lead to acute clinical complications, such as heart attacks, strokes, unstable angina, arrhythmia, or sudden cardiac death, making CVD the primary cause of morbidity and mortality in Western countries (16).

Since atherosclerosis and NAFLD co-occur in patients with the metabolic syndrome, obesity, type 2 diabetes mellitus and insulin resistance, it is difficult to decipher the exact cause-effect relationship that leads to an increased risk of CVD in patients with NAFLD (17). Recent studies in children suffering from fatty liver disease support that NAFLD may cause CVD (18–20). Nevertheless, while growing evidence indicates that NAFLD can be considered a risk factor for atherosclerosis, the underlying disease mechanisms by which NAFLD contributes to CVD are not entirely understood. In this review, we will focus on the immunomodulatory effects of oxidized lipids and provide evidence for their involvement as common metabolic triggers for disease progression during NAFLD and atherosclerosis. In addition, we will discuss how targeting oxidized lipids *via* immunization strategies can be explored to improve interventions and potentially prevent the risk for CVD.

DYSLIPIDEMIA AND THE FORMATION OF OXIDATION-SPECIFIC EPITOPES

The defining hallmark of NAFLD is the accumulation of lipids containing triglycerides, cholesterol esters, and other lipid species in the liver. The increased hepatic triglyceride content, which determines the histological appearance of a steatotic liver, is a consequence of increased calorie intake, enhanced free fatty acids (FFA) influx from lipolysis of peripheral adipose tissue, elevated triglyceride synthesis by hepatic *de novo* lipogenesis, and reduced lipid export from the liver *via* very-low-density lipoprotein (VLDL) particles (21, 22). In parallel with deregulated hepatic lipid metabolism, NAFLD is associated with systemic dyslipidemia, as manifested by elevated triglyceride and cholesterol levels, lowered high-density lipoproteins (HDL), and increased low-density lipoprotein (LDL) particles in circulation (23–25). Similarly, elevated cholesterol, high LDL, and low HDL serum levels are described as risk factors for the onset of CVD (26), where the accumulation of LDL particles in arterial walls is a crucial process in the development of atherosclerosis (27). Thus, despite the strong correlation with dyslipidemia, it has become clear that disturbances in lipid metabolism and increased LDL levels cannot merely explain the local pro-inflammatory tissue environment, of which its presence seems to be a crucial factor enhancing disease progression.

Dyslipidemia that goes beyond the body's coping mechanisms can lead to lipotoxicity, an essential mechanism associated with NAFLD and atherosclerosis (28, 29). During NAFLD, lipotoxicity occurs when the massive influx of FFAs into hepatocytes peaks at a point where the liver can no longer use or store the FFAs or export them as triglycerides. Subsequently, a chain of intracellular responses is activated, leading to lipotoxic stress in mitochondria and the endoplasmic reticulum, ultimately resulting in hepatocyte cell death and the release of pro-inflammatory cytokines and extracellular vesicles (28, 30–33). In turn, this leads to the activation of resident Kupffer cells and the recruitment of infiltrating monocytes and neutrophils to the liver, which contribute to inflammation *via* the release of cytokines, chemokines, nitric oxide, and reactive oxygen species (ROS) (4). In a similar process, lipid retention in atherosclerotic plaques induces local inflammation characterized by the influx of circulating monocytes that differentiate into macrophages that release pro-inflammatory stimuli and ROS (4, 34). Although ROS are products of normal cell metabolism and serve as signal molecules as in redox signal pathways (35), continued oxidative stress, characterized by high ROS exposure in combination with reduced levels or scavenging capacity of antioxidants, will harm different vital macromolecules such as proteins, nucleic acids (DNA/ RNA), and lipids (36).

Especially phospholipids, as building blocks of cells, and lipoproteins, are popular targets of ROS as part of a process called lipid peroxidation, which occurs *via* both enzymatic and non-enzymatic mechanisms (37, 38). Whereas, the enzymatic process of lipid peroxidation covers the activation of myeloperoxidases, lipoxygenases, cyclooxygenases, and cytochrome p450 (38, 39), the non-enzymatic process requires free radicals. Therefore, it can only be activated indirectly *via* nicotinamide adenine dinucleotide phosphate (NADPH) oxidases and nitric oxide synthases (40). Both processes result in lipid hydroperoxide molecules, which are then degraded. Notably, a large variety of secondary products are formed during the degradation process of lipid peroxidation, including

Abbreviations: 4-HNE, 4-Hydroxynonenal; BSA, Bovine serum albumin; CD36, Cluster of differentiation 36; CEP, ω-(2-Carboxyethyl) pyrrole; CFH, Complement factor H; CRP, C-reactive protein; CVD, Cardiovascular disease; DAMP, Damage-associated molecular pattern; FFA, Free fatty acid; HDL, High-density lipoprotein; IgG, Immunoglobulin type G; IgM, Immunoglobulin type M; IL, Interleukin; LDL, Low-density lipoprotein; LDLR, Low-density lipoprotein receptor; MAA, Malondialdehyde-acetaldehyde; MDA, Malondialdehyde; NADPH, Nicotinamide adenine dinucleotide phosphate; NAFLD, Non-alcoholic fatty liver disease; NAS, NAFLD activity score; NASH, Non-alcoholic steatohepatitis; OSE, Oxidation-specific epitope; OxLDL, Oxidized LDL; OxPL, Oxidized phospholipids; PAMP, Pathogen-associated molecular pattern; PC-OxPL, Phosphocholine-containing OxPL; ROS, Reactive oxygen species; SR, Scavenger receptor; TBAR, 2-Thiobarbituric acid reaction; TLR, Toll-like receptor; TREM2, Triggering receptor expressed on myeloid cells 2; VLDL, Very low-density lipoprotein.

malondialdehyde (MDA), malondialdehyde-acetaldehyde (MAA), 4-hydroxynonenal (4-HNE), and the remaining core aldehyde of oxidized phospholipids (OxPL) (41–43). These oxidized lipids and their degradation products can hamper the normal function of proteins and lipids and therefore modify them (44). Further, some of these lipid derivatives, such as highly reactive aldehydes, can alter their self-molecules and form so-called oxidation-specific epitopes (OSEs), which comprise protein adducts with degradation products of lipid peroxidation, such as MDA and phosphocholine-containing OxPL (PC-OxPL) (34, 45). If removal of these products, primarily carried by dying cells, extracellular vesicles, and damaged lipoproteins such as oxidized LDL (OxLDL), is insufficient, sterile inflammation is triggered, and oxidative damage is exacerbated (37, 46, 47).

Mounting evidence indicates increased levels of oxidized lipids and elevated presence of various OSEs during the progression from simple steatosis to NASH (46, 48–50) as well as in atherosclerosis and CVD (47). Of the different types of OSEs that can be formed during lipid peroxidation, MDA and 4-HNE are prototypical markers of oxidative stress that can be measured, for example, by the commonly used 2-thiobarbituric acid reaction (TBAR) assay (37). While the presence of 4-HNE is associated with different stages of fatty liver disease (51) and mitochondrial 4-HNE adducts are increased in NASH (52), 4-HNE is also found in atherosclerotic lesions in humans and animal models of disease (34). Furthermore, MDA epitopes are increased in patients, mice, and rats suffering from NAFLD and NASH (53–58). In addition to elevated systemic MDA concentrations, we previously demonstrated that MDA adducts accumulate in the liver during human NASH and in hypercholesterolemic $Ldlr^{-/-}$ mice with steatohepatitis (46, 59). Similarly, atherosclerotic lesions were shown to contain MDA epitopes (46), and elevated serum MDA-LDL levels are associated with the progression of carotid atherosclerosis (60). Recently, OxPLs, which are found to be present in atherosclerotic lesions in humans and mice (61), have also been described to be elevated in circulation and livers of patients and mice with NASH (48). Since it has been demonstrated that only modified LDL and not native LDL has a major influence on the development of atherosclerotic plaques (27), the presence of oxidized lipids and various types of OSEs may represent an essential link between NAFLD and atherosclerosis (34, 62). While systemic dyslipidemia might be responsible for the generation of high levels of OSE and modified LDL, thereby leading to both fatty liver disease and CVD, another possibility is that hepatic lipid accumulation increases oxidative stress and OSEs in the liver, prior to their release into circulation and thus subsequently promoting atherosclerosis development. As lipid peroxidation and consequently the accumulation of altered self-molecules involves interference with structural and functional properties of the physiological state, immunological mechanisms are taking place to protect the body from potential detrimental consequences. In the following section, we provide an overview of existing immune recognition and the pattern recognition receptors (PRRs) responsible for the uptake and/or binding of oxidized lipoproteins and OSEs (63).

IMMUNE RECOGNITION OF OXIDATION-SPECIFIC EPITOPES

Since OSEs identify and label altered proteins and lipids that have been damaged by oxidative stress, cellular debris, and apoptotic cells, recognition mechanisms to provide effective clearance are required (34, 64, 65). Consequently, oxidized lipids and OSEs are recognized by various PRRs on different components of the immune system that mediate their removal to maintain homeostasis in situations of increased oxidative stress. As such, OSEs play an essential role in tissue repair and reconstruction (66). However, during pathological conditions in which OSEs accumulate, they can act as damage-associated molecular patterns (DAMPs), ultimately resulting in chronic inflammation (66). Previous characterization of various OSEs suggested that both cellular and soluble PRRs can recognize OSEs, which we will discuss in light of their involvement in NAFLD and atherosclerosis.

Cellular Immune Response: Macrophages Orchestrate Inflammation

A variety of cell surface receptors present on innate immune cells recognize OSEs and act as sensors of oxidative stress (67). Here, we will focus on cellular PRRs expressed on macrophages, as they have been shown to play a pivotal role in initiating and sustaining the inflammatory process upon binding and subsequent phagocytosis of oxidatively altered molecules, including oxidized lipoproteins (68, 69).

Toll-like receptors (TLRs) represent a group of classic cellular PRRs of innate immunity capable of binding different pathogen-associated molecular patterns (PAMPs), including bacterial and viral components, as well as DAMPs such as OSEs. For example, oxidized cholesterol esters (OxCE) and OxPL on the surface of extracellular vesicles are ligands for TLR4 (68, 70), while OxPLs have also been reported to stimulate macrophages in a TLR2-dependent mechanism (71). Furthermore, there is evidence that hydro(pero)xylated phospholipids can be considered endogenous TLR4-activating danger signals, and thus TLR4 may act as a sensor for oxidative stress (70). In addition, certain TLRs have been found to respond to OxPL, OxLDL, and other OSEs as part of a multimeric complex with other PRRs (34). As such, it has been shown that the transmission of PC-OxPL-mediated inflammatory signaling requires the formation of a heterotrimer of TLR4-TLR6 and cluster of differentiation 36 (CD36), a scavenger receptor (72, 73). Similarly, ω-(2-Carboxyethyl) pyrrole (CEP) signaling necessitates the cooperation between TLR2 and CD36 (34). Importantly, once ligands bind to TLRs, they activate nuclear factor NF-κB, which stimulates cytokine production and macrophage proliferation (74). Thus, some OSEs represent endogenous ligands recognized by members of the TLR family that can trigger inflammatory responses either with or without cooperation *via* another class of PRRs expressed on macrophages, namely scavenger receptors.

Scavenger receptors comprise another prototypical class of different surface receptors that recognize and internalize OSEs

(67). Similar to TLRs, scavenger receptors bind oxidized and non-native LDL particles and contribute to the activation of macrophages in the context of inflammation (67, 75). There are many different types of scavenger receptors, including CD36, scavenger receptor type A1 (SR-A1), SR-A2, SR-B1, CD68, and lectin-like oxidized LDL receptor 1 (LOX1) (67). Of these, SR-A1, SR-A2, and CD36 have shown to be primarily responsible for the uptake of OxLDL, as *in vitro* assays have shown that macrophages deficient in these receptors exhibit 75–90% decreased binding and degradation of OxLDL (76). In addition, PC-OxPs have been found to bind to CD36, whereas PC from non-oxidized phospholipids does not serve as a ligand (77). Moreover, CEP-modified proteins are recognized by CD36 (78) and MDA epitopes are shown to be recognized by SR-A1 and SR-A2 (79, 80).

Interestingly, receptor-mediated uptake of oxidized lipids by macrophages has been found to play a central role in the chronic inflammatory responses present during both NAFLD and atherosclerosis. In both conditions, excess uptake of oxidized lipoproteins causes a transformation of local macrophages into bloated, lipid-rich foam cells, resulting in the activation of a cascade of pro-inflammatory events (81–84) (**Figure 1**). Under normal conditions, once internalized, lipids are transported into the lysosomal compartment for degradation by lysosomal enzymes such as cathepsins (85, 86). In contrast to native or acetylated LDL, OxLDL is poorly degraded, leading to disabled intracellular trafficking and lysosomal accumulation of oxidized lipids. Consequently, under pathological conditions characterized by the increased presence of modified lipoproteins and OxLDL, lysosomes turn dysfunctional, and cholesterol crystals are formed, resulting in NLPR3 inflammasome activation, which contributes to inflammation *via* the maturation and release of IL-1β and IL-18 (76, 87, 88). Furthermore, foamy macrophages express more CD36 and SR-A1, the primary receptors mediating OxLDL uptake, and might, in turn, take up even more oxidized lipids, thereby further amplifying inflammation (76). Studies by others and us showed that NLPR3 inflammasome activation contributes to liver disease and atherosclerosis in various murine models, indicating the involvement of this process in both entities (88–91). Moreover, we showed that hematopoietic deficiency of CD36 and SR-A1 reduces foam cell formation and hepatic inflammatory responses during NASH in mice (81, 82). In line, macrophage CD36 and SR-A1/2 contribute significantly to atherosclerotic lesion formation (92, 93). Further, it was demonstrated that $Ldlr^{-/-}$ $ApoB^{100/100}$ mice fed a Western diet showed a decrease in atherosclerosis when either SR-A or CD36 was silenced in bone marrow cells using lentivirus vectors encoding shRNA against them (94). Mechanistically, we previously demonstrated that MDA-induced cytokine secretion depends on CD36 and SR-A1. Bone marrow-derived macrophages from mice lacking either of these receptors secrete less CXCL1 upon MDA stimulation, suggesting the involvement of MDA-mediated pro-inflammatory signaling in macrophages in both disease pathologies (46).

In addition to the common findings concerning the contribution of SR-mediated uptake of oxidized lipoproteins during NAFLD and atherosclerosis, multiple studies indicate that TLR-mediated immune recognition also contributes to disease progression. Indeed, NASH has been shown to improve in TLR4 knockout mice receiving a methionine- and choline-deficient (MCD) diet (95), and $Ldlr^{-/-}$ mice receiving an atherogenic diet were found protected from triglyceride accumulation in the liver in the absence of TLR4 (96). The contribution of TLR4 to the progression of atherosclerosis is supported by two studies showing that TLR4-deficient $ApoE^{-/-}$ mice have lower aortic lipid accumulation (70–80% reduction) and reduced levels of aortic atherosclerosis compared to the control mice (97, 98). In line, a case-control study of 183 patients showed that a single nucleotide polymorphism in *Tlr4* leads to impaired signaling and is associated with reduced plaque formation and a decrease in acute coronary events (99). Moreover, *Tlr4* expression is higher in macrophages in atherosclerotic plaques of $ApoE^{-/-}$ mice on an atherogenic diet and in humans (100), suggesting that TLR4 represents a pathophysiological link between oxidized lipids, inflammation, and atherosclerosis. Although most of the available studies focus on the role of TLR4 in NASH and atherosclerosis, it has also been shown that TLR2 deficiency in $Ldlr^{-/-}$ mice leads to a reduction in atherogenesis, while administration of TLR2 agonists results in increased atherosclerosis in mice (101). Concerning fatty liver disease, it was demonstrated that administration of an anti-TLR2

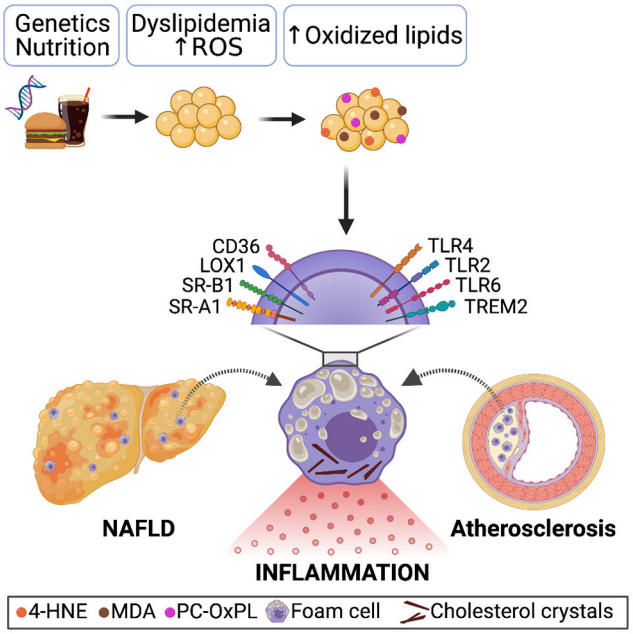

FIGURE 1 | Genetics, sedentary lifestyle and/or unhealthy nutrition causes systemic dyslipidemia characterized by increased LDL levels. Due to oxidative stress and ROS production, oxidation-specific epitopes present on oxidized lipids, dying cells, and microvesicles accumulate. Receptor-mediated recognition and uptake of oxidized lipoproteins by macrophages in the steatotic liver and atherosclerotic plaque results in a foamy appearance, lysosomal dysfunction, and cholesterol crystals formation, causing pro-inflammatory signaling and thereby enhancing disease progression.

antibody ameliorates liver injury, inflammation, steatosis, and fibrosis in rats with obesity (102). Taken together, these studies indicate that TLR signaling contributes to the inflammatory responses observed in NAFLD and atherosclerosis.

More recently, using single-cell RNA sequencing technology, multiple studies in lipid-mediated disorders including NASH and atherosclerosis demonstrate the occurrence of a specialized type of macrophages characterized by high expression of the triggering receptor expressed on myeloid cells 2 (*Trem2*). Whereas, humans and mice with NASH or cirrhosis have increased hepatic expression of *Trem2* that correlates positively with AST and ALT levels (103, 104), more *Trem2*-expressing macrophages are also found in atherosclerotic plaques (105). Interestingly, TREM2 has been shown to bind and recognize (apo-) lipoproteins, including ApoE, LDL, and MDA-LDL particles (106), suggesting TREM2 might also recognize OSEs, thereby potentially contributing to inflammatory responses and disease progression. Functional studies assessing the role of TREM2 in NAFLD and atherosclerosis are still required since this receptor might also be involved in a common lipid-induced mechanistic pathway.

Taken together, there are overarching mechanisms regulating the uptake of OSEs and OxLDL *via* PRRs on macrophages. As a result, macrophages and hepatic Kupffer cells turn into foam cells, become activated, and secrete pro-inflammatory factors in response to elevated oxidized lipids, thereby contributing to the development of NAFLD and atherosclerosis in a similar process, representing part of a shared etiology. In the next section, we will focus on soluble factors recognizing OSEs and their involvement in steatohepatitis and atherosclerosis.

Humoral Immune Response: B Cells Enter the Stage

Besides recognizing OSEs by cell surface receptors, soluble receptors capable of binding OSEs are described, such as C-reactive protein (CRP) and proteins of the complement system (62, 107). CRP, an acute-phase protein produced in the liver, was found to recognize PC-OxPL on OxLDL and apoptotic cells, indicating CRP's responsiveness to OSEs (108). Since CRP levels are a known marker of systemic inflammation, CRP in circulation might indirectly also be considered a reflection of tissue injury, oxidative stress, and/or ongoing lipid peroxidation and OSE levels. As a regulator of complement activity, an essential machinery for clearance of metabolic waste and dead cells, complement factor H (CFH) was identified to recognize and bind MDA epitopes. Moreover, genetic variants of one of the MDA-binding sites of CFH were shown to influence the capacity of CFH to bind MDA (109). Since MDA has pro-inflammatory effects during NASH, reduced CFH might contribute to the harmful effects of lipid peroxidation products in fatty liver disease progression. Nevertheless, the functional role of CFH-mediated OSE recognition and its consequences for NAFLD and CVD has not yet been fully described.

Insights from others and us give prominence to B cell-derived antibodies or immunoglobulins targeting OSEs in NAFLD and CVD (59, 107, 110–112). Antibodies exist in different isotypes (IgM, IgG, IgA, IgE, IgD) that implement key functions in defending the body against pathogens and are also responsible for maintaining homeostasis by eliminating metabolic waste (113). Owing to their broad specificity for pathogens and their ability to recognize highly conserved structures such as self-antigens, they provide another group of soluble factors able to detect OSEs residing on oxidized lipoproteins, apoptotic cells, and extracellular vesicles (64, 114). Studies in mice and humans have shown that various OSEs, including PC-OxPL, MDA, and 4-HNE adducts, are prominent targets of natural antibodies, which are pre-existing germline-encoded antibodies, predominantly of the IgM type, that are present without external antigens. In fact, several OSEs are bound by up to 30% of all natural IgM found in the plasma of both wild-type and gnotobiotic mice (64, 114), indicating their relevance for homeostasis and immune defense. In addition to innate natural IgM antibodies, produced and secreted by B1 cells, adaptive IgG isotypes secreted by B-2 cells are capable of recognizing and binding various OSEs such as MDA (115).

Interestingly, consistent observations concerning systemic levels of antibodies binding OxLDL and OSE are described between NAFLD and atherosclerosis. First of all, in line with the negative association between IgM levels in circulation and the severity of atherosclerosis and CVD in general (107), we have shown that NAFLD patients have lower serum IgM titers toward various OSEs including MDA and MAA compared to healthy controls (59). While liver disease data upon IgM deficiency is still lacking, a lack of secreted IgM antibodies resulted in increased atherosclerotic plaques in $Ldlr^{-/-}$ mice after Western-type diet (112). In addition, we previously demonstrated that an increase in B1-derived natural IgM with specificity for OxLDL in $Ldlr^{-/-}$ mice deficient for sialic acid-binding immunoglobulin-like lectin G (Siglec-G) protects against atherosclerosis and steatohepatitis after atherogenic diet, further supporting the protective role of IgM antibodies (110). By recognizing and neutralizing OSEs, IgM can limit OxLDL-induced foam cell formation, as well as pro-inflammatory macrophage responses, and generally contribute to reduced inflammation (115). More studies pointing out the protective properties of increased anti-OxLDL IgM levels are described in the section about immunotherapy.

Besides altered IgM antibody levels, ∼40% of adults (49) and 60% of children have elevated IgG titers in circulation when diagnosed with NAFLD (116). Particularly, anti-OSE IgGs produced by B-2 lymphocytes have been shown to correlate with the onset of steatohepatitis and are considered as an independent predictor of fibrosis in NAFLD patients (49, 116, 117). These observations are in line with those in atherosclerosis, where higher IgG levels are associated with more severe atherosclerosis in humans and mice (118–120). Furthermore, a meta-analysis even suggests that systemic IgG antibody titers are a potential predictor of future atherosclerosis-related cardiovascular events since a positive correlation between IgG levels and events was found (121). However, the functional significance and contribution of IgG are still unclear as studies in humans and animal models indicate that anti-OSE IgG may also have atheroprotective properties (107, 122, 123). Given these diverse and partly inconsistent findings, the role of IgG in

atherosclerosis has not been fully elucidated, which has been discussed in detail by Sage et al. (124). Nevertheless, in mice, anti-CD20 antibody-mediated depletion of B cells reduces the development of atherosclerosis (125), and ameliorates NASH progression (126). Importantly, anti-CD20 treatment preserves the production of anti-OxLDL IgM antibodies, while IgG targeting OxLDL are greatly diminished (125). In addition, TACI-Ig mice, characterized by a depletion of B2 cells, were found to have milder steatohepatitis and less progression of fibrosis (117), further supporting a more pro-inflammatory effect of anti-OSE IgG antibodies.

To summarize, altered anti-OSE IgM and IgG titers are associated with NAFLD and fibrotic NASH, consistent with findings in atherosclerosis (50, 59, 107, 127), suggesting another pathophysiological pathway in common between NAFLD and atherosclerotic CVD. While IgG-producing B-2 cells may promote pro-inflammatory mechanisms (50), natural IgM secreted by B1 cells seems to have protective properties (50). As such, antibodies recognizing OSEs provide an attractive target for B cell-mediated immunotherapeutic approaches to improve therapeutic strategies and/or prevent cardiovascular complications during NAFLD. Besides targeting B cells as done using anti-CD20 administration, immunization approaches to enhance immunity against OSEs have been investigated, which we will summarize in the next section.

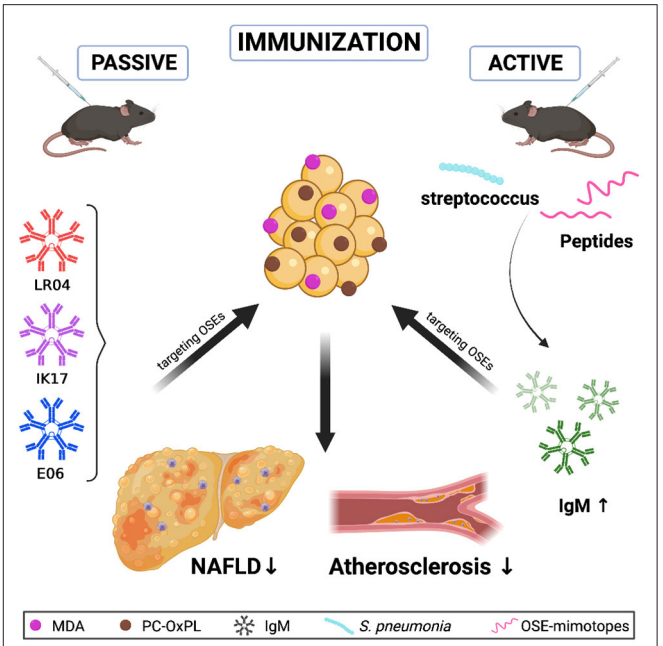

FIGURE 2 | In mice, passive immunization strategies with OSE-recognizing IgM antibodies LR04, IK17, and E06, or boosting IgM antibody titers toward oxidized lipids in active immunization approaches, such as with heat-inactivated *S. pneumococci* or specific peptides, can induce protection against NAFLD progression and reduce atherosclerotic plaque burden.

TARGETING OXIDIZED LIPIDS AS IMMUNOTHERAPEUTIC APPROACH

As neither lifestyle modification nor currently existing pharmacotherapy is sufficient to reduce liver fibrosis and inflammation, NAFLD is becoming a global burden on the healthcare system and poses an urgent need for developing therapeutic interventions (128). Although several drugs and combination therapies are under investigation, no truly effective treatment has yet been identified (129, 130). However, regarding oxidative stress, nutrients and antioxidants such as vitamin E have beneficial effects on NAFLD (131) by lowering the NAFLD activity score (NAS) and reducing inflammation (132, 133). Consistent with these findings, a recent study has demonstrated that vitamin E is negatively correlated with serum MDA in women suffering from NAFLD (54). In addition, similar outcomes also indicate a protective role of vitamin E in atherosclerosis (134, 135). Nevertheless, since we currently lack complete understanding of the metabolic pathways affected and controlled by oxidative stress, more studies are needed to design an adequate therapeutic trial to assess antioxidants to combat atherogenesis (136, 137). Growing evidence shows that directly addressing OSEs yields a high potential for reducing the inflammatory response in NAFLD and atherosclerosis, thereby representing a promising avenue for treating both diseases (48, 63, 138). Here, we will provide an overview of current data on intervention approaches addressing OSEs through immunization strategies. Simplified, enhancing protective B cell antibody responses *via* immunization can be divided into two separate classes: passive immunization in which antibodies that directly target, bind, and inactivate an antigen are infused; and active immunization, wherein an antigen is used in a vaccination protocol to boost antibody titers and as such, provide long-term immunity (**Figure 2**).

Passive Immunization

As described above, data from others and us support that anti-OSE IgM antibodies act protective against liver disease and atherosclerosis, and as such, are a viable tool to prevent disease (59, 83, 110, 127, 139). Besides our findings using *Siglec-G*$^{-/-}$ mice that have increased anti-OSE IgM levels, we showed that intravenous administration of LR04, a monoclonal IgM specifically targeting MDA, neutralizes endogenously produced MDA epitopes, leading to a decrease in liver inflammation in *Ldlr*$^{-/-}$ mice after a Western-type diet (46). Similarly, intravenous injection and intraperitoneal infusion of the human antibody IK17, directed to MDA-like epitopes, significantly reduced atherosclerosis progression by 30–50% (140, 141). Moreover, antibodies E06 and T15, which target PC epitopes on OxPL were found to protect against atherosclerosis by blocking lipid uptake by macrophages, preventing inflammation, and promoting the clearance of apoptotic cells (141). Expression of the single-chain variable fragment of E06 in *Ldlr*$^{-/-}$ mice was shown to be sufficient to suppress the development of atherosclerosis at multiple disease stages (139). These mice were also protected against various aspects of NASH, including steatosis, inflammation, fibrosis, hepatocyte cell death, and

progression to hepatocellular carcinoma, further supporting the causal role of OxPL in the pathogenesis of NASH (49).

Besides evaluating the potential beneficial effect of IgM antibodies on disease outcome, certain studies focused on using IgG antibodies. For example, administration of the human IgG antibody 2D03 directed against MDA-modified ApoB exhibited atheroprotective immune responses against OxLDL (123). More recently, a study revealed the protective function against the development of atherosclerotic plaques using autoantibodies against the ApoB100 peptide p210 in *ApoE*$^{-/-}$ mice, which was accomplished by injecting IgG2b against p210. These results in *ApoE*$^{-/-}$ mice support previous human studies, which showed an inverse association between apoB100 native p210 IgG and plaques in coronary or carotid arteries (142).

Active Immunization

Besides passive immunization approaches, several studies assessed the potential beneficial effect of enhanced immunity toward various epitopes of OxLDL using these as antigens. In one of the first studies applying active immunization, injection of homologous MDA-LDL into *Ldlr*$^{-/-}$ rabbits induced higher anti-MDA antibody titers and significantly reduced the extent of atherosclerotic lesions in the aortic tree of immunized animals (143). Consistent with this, *Ldlr*$^{-/-}$ mice injected with MDA-modified LDL showed smaller atherosclerotic lesion size after an atherogenic diet, although this was independent of changes in anti-OSE IgM levels (144). In relation to fatty liver disease, a study in which C57BL/6 mice were injected with MDA conjugated to bovine serum albumin (MDA-BSA) reported increased severity of NASH in immunized mice after MCD diet. The authors attributed this to the fact that MDA-BSA injection enhanced IgG responses and increased hepatic T cell infiltration, which may ultimately lead to increased inflammation (145). Importantly, immunization with MDA-BSA adducts did not influence IgM antibody levels toward MDA-derived antigens, potentially lacking protective capacities. On the other hand, studies that immunized *Ldlr*$^{-/-}$ mice with heat-inactivated *S. pneumonia*, which significantly induced PC-OxPL recognizing IgM titers due to molecular mimicry, showed that mice immunized were protected against diet-induced steatohepatitis and atherosclerosis after Western-type diet (83, 146), supporting the idea that raising IgM titers toward OxLDL has beneficial effects.

In addition to using various OSEs as antigens, several experimental studies assessed whether administration of stable peptides could be applied for immunization. One of these peptides is the p210-PADRE, which has already been mentioned in the section on passive immunization. Besides direct infusion of IgG antibodies, ApoE$^{-/-}$ mice were immunized with the p210-PADRE peptide, which induced a specific IgG1 response against p210, thereby preventing MDA-LDL accumulation in lesions and reducing atherosclerotic plaque formation in the aorta (142). Moreover, immunization with OxLDL- and MDA-modified ApoB100 peptides were described to have an atheroprotective effect associated with an increase in IgG and IgM antibodies specific for the antigen used (142, 147). Interestingly, two small immunogenic peptides, linear P1 and circular P2, were identified that immunologically mimic MDA-type epitopes (148). Since we have shown the critical role for endogenous MDA in NASH and P2-BSA immunization raised IgM antibody levels toward MDA, these mimotopes are a promising tool to induce immunity against this relevant antigen to reduce/prevent NAFLD progression (46). Although most of the above-mentioned immunization approaches have been reported to be successful for atherosclerosis, more studies focusing on liver disease are required to further confirm that the treatment principles of increased anti-OSE IgM to reduce atherosclerosis also apply to NASH.

OUTLOOK

Growing evidence indicates a significant association between the clinical patterns of NAFLD and atherosclerosis. Common molecular mechanistic pathways seem to play a central role in disease progression, and NAFLD might even be considered a risk factor for developing CVD.

Just as receptor-mediated uptake of oxidized lipids leads to macrophages' foamy appearance and pro-inflammatory processes is one consistent observation in the liver during NAFLD and the vessel wall during atherosclerosis, other mechanistic patterns might be similarly occurring in both pathologies (81–84). Besides, in both NAFLD and atherosclerosis, B-1-derived IgM antibodies seem to have a protective role, while IgG produced by B2 cells seems to promote inflammation (115). Therefore, studies assessing both conditions might significantly enhance our understanding of their interrelationship and potentially lead to the identification of novel targets to improve treatment strategies. In particular, the *Ldlr*$^{-/-}$ mice on a high-fat, high-cholesterol diet is a suitable model to study the underlying pathways occurring in fatty liver disease and linked atherosclerosis (149). We have previously shown that these mice develop steatotic livers with increased inflammation and oxidative stress already after 2 weeks of diet, while atherosclerotic plaques develop after 6–8 weeks of dietary intervention (46). Moreover, *Ldlr*$^{-/-}$ mice present a human-like lipid profile, which is essential to facilitate translational studies regarding lipid-mediated diseases (150). In addition, since CVD is still the primary cause of death in patients with early NAFLD (9, 10), assessing liver disease in human cardiovascular study cohorts and vice versa could further enhance our understanding and potentially identify patients with advanced disease stage and/or increased risk for cardiovascular events. In this review, we focused on the potential immunotherapeutic approach by enhancing immunity toward OSEs and oxidized lipids. Since similar observations for systemic anti-OSE antibody titers are described, one might hypothesize that results from immunization studies, which mostly come from work in the field of atherosclerosis, can be translated and tested to prevent NAFLD progression. Nevertheless, further studies are needed to understand the role of OSEs and OSE-reactive immunity in maintaining homeostasis and controlling inflammatory responses to design translational studies and eventually offer novel treatment strategies for patients.

AUTHOR CONTRIBUTIONS

CH and TH wrote and edited the manuscript. TH composed the figures. DR helped with figure composition. All authors contributed to the article and approved the submitted version.

FUNDING

TH was funded by a Veni (NWO; 91619012), MLDS Right-On-Time grant (MLDS; 19-28), and Zukunftskollegs grant (FWF; ZK81B).

REFERENCES

1. Mozaffarian D. Dietary and policy priorities for cardiovascular disease, diabetes, and obesity: a comprehensive review. *Circulation*. (2016) 133:187–225. doi: 10.1161/CIRCULATIONAHA.115.018585
2. Lemieux I, Després J-P. Metabolic syndrome: past, present and future. *Nutrients*. (2020) 12:3501. doi: 10.3390/nu12113501
3. Sayiner M, Koenig A, Henry L, Younossi ZM. Epidemiology of nonalcoholic fatty liver disease and nonalcoholic steatohepatitis in the United States and the rest of the world. *Clin Liver Dis*. (2016) 20:205–14. doi: 10.1016/j.cld.2015.10.001
4. Friedman SL, Neuschwander-Tetri BA, Rinella M, Sanyal AJ. Mechanisms of NAFLD development and therapeutic strategies. *Nat Med*. (2018) 24:908–22. doi: 10.1038/s41591-018-0104-9
5. Marengo A, Jouness RIK, Bugianesi E. Progression and natural history of nonalcoholic fatty liver disease in adults. *Clin Liver Dis*. (2016) 20:313–24. doi: 10.1016/j.cld.2015.10.010
6. Younossi ZM, Koenig AB, Abdelatif D, Fazel Y, Henry L, Wymer M. Global epidemiology of nonalcoholic fatty liver disease—meta-analytic assessment of prevalence, incidence, and outcomes. *Hepatology*. (2016) 64:73–84. doi: 10.1002/hep.28431
7. Younossi Z, Anstee QM, Marietti M, Hardy T, Henry L, Eslam M. Global burden of NAFLD and NASH: trends, predictions, risk factors and prevention. *Nat Rev Gastroenterol Hepatol*. (2018) 15:11–20. doi: 10.1038/nrgastro.2017.109
8. Mantovani A, Scorletti E, Mosca A, Alisi A, Byrne CD, Targher G. Complications, morbidity and mortality of nonalcoholic fatty liver disease. *Metabolism*. (2020) 111:154170. doi: 10.1016/j.metabol.2020.154170
9. Tang K, Lin J, Ji X, Lin T, Sun D, Zheng X. Non-alcoholic fatty liver disease with reduced myocardial FDG uptake is associated with coronary atherosclerosis. *J Nucl Cardiol*. (2021) 28:610–20. doi: 10.1007/s12350-019-01736-6
10. Targher G, Byrne CD, Tilg H. NAFLD and increased risk of cardiovascular disease: clinical associations, pathophysiological mechanisms and pharmacological implications. *Gut*. (2020) 69:1691–705. doi: 10.1136/gutjnl-2020-320622
11. Arai T, Atsukawa M, Tsubota A, Kato K, Abe H, Ono H. Liver fibrosis is associated with carotid atherosclerosis in patients with liver biopsy-proven nonalcoholic fatty liver disease. *Sci Rep*. (2021) 11:15938. doi: 10.1038/s41598-021-95581-8
12. Kapuria D, Takyar VK, Etzion O, Surana P, O'Keefe JH, Koh C. Association of hepatic steatosis with subclinical atherosclerosis: systematic review and meta-analysis. *Hepatol Commun*. (2018) 2:873–83. doi: 10.1002/hep4.1199
13. Getz GS, Reardon CA. Natural killer T cells in atherosclerosis. *Nat Rev Cardiol. Mai.* (2017) 14:304–14. doi: 10.1038/nrcardio.2017.2
14. Glass CK, Witztum JL. Atherosclerosis. The road ahead. *Cell*. (2001) 104:503–16. doi: 10.1016/S0092-8674(01)00238-0
15. Ross R. Atherosclerosis–an inflammatory disease. *N Engl J Med*. (1999) 340:115–26. doi: 10.1056/NEJM199901143400207
16. Konkoth A, Saraswat R, Dubrou C, Sabatier F, Leroyer AS, Lacroix R. Multifaceted role of extracellular vesicles in atherosclerosis. *Atherosclerosis*. (2021) 319:121–31. doi: 10.1016/j.atherosclerosis.2020.11.006
17. Paik JM, Henry L, Avila LD, Younossi E, Racila A, Younossi ZM. Mortality related to nonalcoholic fatty liver disease is increasing in the United States. *Hepatol Commun*. (2019) 3:1459–71. doi: 10.1002/hep4.1419
18. Conjeevaram Selvakumar PK, Kabbany MN, Alkhouri N. Nonalcoholic fatty liver disease in children: not a small matter. *Paediatr Drugs*. (2018) 20:315–29. doi: 10.1007/s40272-018-0292-2
19. Castillo-Leon E, Connelly MA, Konomi JV, Caltharp S, Cleeton R, Vos MB. Increased atherogenic lipoprotein profile in children with non-alcoholic steatohepatitis. *Pediatr Obes*. (2020) 15:e12648. doi: 10.1111/ijpo.12648
20. Mann JP, Raponi M, Nobili V. Clinical implications of understanding the association between oxidative stress and pediatric NAFLD. *Expert Rev Gastroenterol Hepatol*. (2017) 11:371–82. doi: 10.1080/17474124.2017.1291340
21. Mendez-Sanchez N, Cruz-Ramon VC, Ramirez-Perez OL, Hwang JP, Barranco-Fragoso B, Cordova-Gallardo J. New aspects of lipotoxicity in nonalcoholic steatohepatitis. *Int J Mol Sci*. (2018) 19:2034. doi: 10.3390/ijms19072034
22. Lambert JE, Ramos-Roman MA, Browning JD, Parks EJ. Increased *de novo* lipogenesis is a distinct characteristic of individuals with nonalcoholic fatty liver disease. *Gastroenterology*. (2014) 146:726–35. doi: 10.1053/j.gastro.2013.11.049
23. Zhang Q-Q, Lu L-G. Nonalcoholic fatty liver disease: dyslipidemia, risk for cardiovascular complications, and treatment strategy. *J Clin Transl Hepatol*. (2015) 3:78–84. doi: 10.14218/JCTH.2014.00037
24. Chatrath H, Vuppalanchi R, Chalasani N. Dyslipidemia in patients with nonalcoholic fatty liver disease. *Semin Liver Dis*. (2012) 32:22–9. doi: 10.1055/s-0032-1306423
25. Ho C-M, Ho S-L, Jeng Y-M, Lai Y-S, Chen Y-H, Lu S-C. Accumulation of free cholesterol and oxidized low-density lipoprotein is associated with portal inflammation and fibrosis in nonalcoholic fatty liver disease. *J Inflamm*. (2019) 16:7. doi: 10.1186/s12950-019-0211-5
26. Stols-Gonçalves D, Hovingh GK, Nieuwdorp M, Holleboom AG. NAFLD and atherosclerosis: two sides of the same dysmetabolic coin? *Trends Endocrinol Metab*. (2019) 30:891–902. doi: 10.1016/j.tem.2019.08.008
27. Zakiev ER, Sukhorukov VN, Melnichenko AA, Sobenin IA, Ivanova EA, Orekhov AN. Lipid composition of circulating multiple-modified low density lipoprotein. *Lipids Health Dis*. (2016) 15:134. doi: 10.1186/s12944-016-0308-2
28. Engin AB. What is lipotoxicity? *Adv Exp Med Biol*. (2017) 960:197–220. doi: 10.1007/978-3-319-48382-5_8
29. Symons JD, Abel ED. Lipotoxicity contributes to endothelial dysfunction : a focus on the contribution from ceramide. *Rev Endocr Metab Disord*. (2013) 14:59–68. doi: 10.1007/s11154-012-9235-3
30. Rada P, González-Rodríguez Á, García-Monzón C, Valverde ÁM. Understanding lipotoxicity in NAFLD pathogenesis: is CD36 a key driver? *Cell Death Dis*. (2020) 11:1–15. doi: 10.1038/s41419-020-03003-w
31. García-Monzón C, Lo Iacono O, Mayoral R, González-Rodríguez Á, Miquilena-Colina ME, Lozano-Rodríguez T, et al. Hepatic insulin resistance is associated with increased apoptosis fibrogenesis in nonalcoholic steatohepatitis chronic hepatitis C. *J Hepatol*. (2011) 54:142–52. doi: 10.1016/j.jhep.2010.06.021
32. Bellanti F, Villani R, Facciorusso A, Vendemiale G, Serviddio G. Lipid oxidation products in the pathogenesis of non-alcoholic steatohepatitis. *Free Radical Biol Med*. (2017) 111:173–85. doi: 10.1016/j.freeradbiomed.2017.01.023
33. Alkhouri N, Eng K, Lopez R, Nobili V. Non-high-density lipoprotein cholesterol (non-HDL-C) levels in children with nonalcoholic fatty liver disease (NAFLD). *Springerplus*. (2014) 3:407. doi: 10.1186/2193-1801-3-407
34. Binder CJ, Papac-Milicevic N, Witztum JL. Innate sensing of oxidation-specific epitopes in health and disease. *Nat Rev Immunol*. (2016) 16:485–97. doi: 10.1038/nri.2016.63
35. Chen Z, Tian R, She Z, Cai J, Li H. Role of oxidative stress in the pathogenesis of nonalcoholic fatty liver disease. *Free Radical Biol Med*. (2020) 152:116–41. doi: 10.1016/j.freeradbiomed.2020.02.025

36. Ore A, Akinloye OA. Oxidative stress and antioxidant biomarkers in clinical and experimental models of non-alcoholic fatty liver disease. *Medicina*. (2019) 55:26. doi: 10.3390/medicina55020026
37. Esterbauer H, Schaur RJ, Zollner H. Chemistry and biochemistry of 4-hydroxynonenal, malonaldehyde and related aldehydes. *Free Radic Biol Med*. (1991) 11:81–128. doi: 10.1016/0891-5849(91)90192-6
38. Bochkov VN, Oskolkova OV, Birukov KG, Levonen A-L, Binder CJ, Stöckl J. Generation and biological activities of oxidized phospholipids. *Antioxid Redox Signal*. (2010) 12:1009–59. doi: 10.1089/ars.2009.2597
39. Niki E, Yoshida Y, Saito Y, Noguchi N. Lipid peroxidation: mechanisms, inhibition, and biological effects. *Biochem Biophys Res Commun*. (2005) 338:668–76. doi: 10.1016/j.bbrc.2005.08.072
40. O'Donnell VB, Murphy RC. New families of bioactive oxidized phospholipids generated by immune cells: identification and signaling actions. *Blood*. (2012) 120:1985–92. doi: 10.1182/blood-2012-04-402826
41. Salomon RG. Structural identification and cardiovascular activities of oxidized phospholipids. *Circ Res*. (2012) 111:930–46. doi: 10.1161/CIRCRESAHA.112.275388
42. Yin H, Xu L, Porter NA. Free radical lipid peroxidation: mechanisms and analysis. *Chem Rev*. (2011) 111:5944–72. doi: 10.1021/cr200084z
43. Pratt DA, Tallman KA, Porter NA. Free radical oxidation of polyunsaturated lipids: new mechanistic insights and the development of peroxyl radical clocks. *Acc Chem Res*. (2011) 44:458–67. doi: 10.1021/ar200024c
44. Bartolini Gritti B, Binder CJ. Oxidation-specific epitopes are major targets of innate immunity in atherothrombosis. *Hamostaseologie*. (2016) 36:89–96. doi: 10.5482/HAMO-14-11-0069
45. Chou M-Y, Hartvigsen K, Hansen LF, Fogelstrand L, Shaw PX, Boullier A. Oxidation-specific epitopes are important targets of innate immunity. *J Intern Med*. (2008) 263:479–88. doi: 10.1111/j.1365-2796.2008.01968.x
46. Busch CJ-L, Hendrikx T, Weismann D, Jäckel S, Walenbergh SMA, Rendeiro AF. Malondialdehyde epitopes are sterile mediators of hepatic inflammation in hypercholesterolemic mice. *Hepatology*. (2017) 65:1181–95. doi: 10.1002/hep.28970
47. Leibundgut G, Witztum JL, Tsimikas S. Oxidation-specific epitopes and immunological responses: translational biotheranostic implications for atherosclerosis. *Curr Opin Pharmacol*. (2013) 13:168–79. doi: 10.1016/j.coph.2013.02.005
48. Sun X, Seidman JS, Zhao P, Troutman TD, Spann NJ, Que X. Neutralization of oxidized phospholipids ameliorates non-alcoholic steatohepatitis. *Cell Metab*. (2020) 31:189–206.e8. doi: 10.1016/j.cmet.2019.10.014
49. Albano E, Mottaran E, Vidali M, Reale E, Saksena S, Occhino G. Immune response towards lipid peroxidation products as a predictor of progression of non-alcoholic fatty liver disease to advanced fibrosis. *Gut*. (2005) 54:987–93. doi: 10.1136/gut.2004.057968
50. Sutti S, Albano E. Adaptive immunity: an emerging player in the progression of NAFLD. *Nat Rev Gastroenterol Hepatol*. (2020) 17:81–92. doi: 10.1038/s41575-019-0210-2
51. Seki S, Kitada T, Yamada T, Sakaguchi H, Nakatani K, Wakasa K. *In situ* detection of lipid peroxidation and oxidative DNA damage in non-alcoholic fatty liver diseases. *J Hepatol*. (2002) 37:56–62. doi: 10.1016/S0168-8278(02)00073-9
52. Serviddio G, Bellanti F, Tamborra R, Rollo T, Capitanio N, Romano AD. Uncoupling protein-2 (UCP2) induces mitochondrial proton leak and increases susceptibility of non-alcoholic steatohepatitis (NASH) liver to ischaemia–reperfusion injury. *Gut*. (2008) 57:957–65. doi: 10.1136/gut.2007.147496
53. Köroglu E, Canbakan B, Atay K, Hatemi I, Tuncer M, Dobrucali A. Role of oxidative stress and insulin resistance in disease severity of non-alcoholic fatty liver disease. *Turk J Gastroenterol*. (2016) 27:361–6. doi: 10.5152/tjg.2016.16106
54. Zelber-Sagi S, Ivancovsky-Wajcman D, Fliss-Isakov N, Hahn M, Webb M, Shibolet O. Serum malondialdehyde is associated with non-alcoholic fatty liver and related liver damage differentially in men and women. *Antioxidants*. (2020) 9:578. doi: 10.3390/antiox9070578
55. Yesilova Z, Yaman H, Oktenli C, Ozcan A, Uygun A, Cakir E. Systemic markers of lipid peroxidation and antioxidants in patients with nonalcoholic Fatty liver disease. *Am J Gastroenterol*. (2005) 100:850–5. doi: 10.1111/j.1572-0241.2005.41500.x
56. Schröder T, Kucharczyk D, Bär F, Pagel R, Derer S, Jendrek ST. Mitochondrial gene polymorphisms alter hepatic cellular energy metabolism and aggravate diet-induced non-alcoholic steatohepatitis. *Mol Metab*. (2016) 5:283–95. doi: 10.1016/j.molmet.2016.01.010
57. Elshazly SM. Ameliorative effect of nicorandil on high fat diet induced non-alcoholic fatty liver disease in rats. *Euro J Pharmacol*. (2015) 748:123–32. doi: 10.1016/j.ejphar.2014.12.017
58. Song L, Qu D, Zhang Q, jiang J, Zhou H, Jiang R. Phytosterol esters attenuate hepatic steatosis in rats with non-alcoholic fatty liver disease rats fed a high-fat diet. *Sci Rep*. (2017) 7:41604. doi: 10.1038/srep41604
59. Hendrikx T, Watzenböck ML, Walenbergh SMA, Amir S, Gruber S, Kozma MO. Low levels of IgM antibodies recognizing oxidation-specific epitopes are associated with human non-alcoholic fatty liver disease. *BMC Med*. (2016) 14:107. doi: 10.1186/s12916-016-0652-0
60. Tanaga K, Bujo H, Inoue M, Mikami K, Kotani K, Takahashi K, et al. Increased circulating malondialdehyde-modified LDL levels in patients with coronary artery diseases their association with peak sizes of LDL particles. *ATVB*. (2002) 22:662–6. doi: 10.1161/01.ATV.0000012351.63938.84
61. Lee S, Birukov KG, Romanoski CE, Springstead JR, Lusis AJ, Berliner JA. Role of phospholipid oxidation products in atherosclerosis. *Circul Res*. (2012) 111:778–99. doi: 10.1161/CIRCRESAHA.111.256859
62. Hendrikx T, Binder CJ. Oxidation-specific epitopes in non-alcoholic fatty liver disease. *Front Endocrinol*. (2020) 11:607011. doi: 10.3389/fendo.2020.607011
63. Papac Milicevic N, Busch CJ-L, Binder CJ. Malondialdehyde epitopes as targets of immunity and the implications for atherosclerosis. *Adv Immunol*. (2016) 131:1–59. doi: 10.1016/bs.ai.2016.02.001
64. Chou M-Y, Fogelstrand L, Hartvigsen K, Hansen LF, Woelkers D, Shaw PX. Oxidation-specific epitopes are dominant targets of innate natural antibodies in mice and humans. *J Clin Invest*. (2009) 119:1335–49. doi: 10.1172/JCI36800
65. Nicolai O, Pötschke C, Raafat D, van der Linde J, Quosdorf S, Laqua A. Oxidation-specific epitopes (OSEs) dominate the B cell response in murine polymicrobial sepsis. *Front Immunol*. (2020) 11:1570. doi: 10.3389/fimmu.2020.01570
66. Chen GY, Nuñez G. Sterile inflammation: sensing and reacting to damage. *Nat Rev Immunol*. (2010) 10:826–37. doi: 10.1038/nri2873
67. Greaves DR, Gordon S. The macrophage scavenger receptor at 30 years of age: current knowledge and future challenges. *J Lipid Res*. (2009) 50(Suppl):S282–6. doi: 10.1194/jlr.R800066-JLR200
68. Miller YI, Choi S-H, Wiesner P, Fang L, Harkewicz R, Hartvigsen K. Oxidation-specific epitopes are danger associated molecular patterns recognized by pattern recognition receptors of innate immunity. *Circ Res*. (2011) 108:235–48. doi: 10.1161/CIRCRESAHA.110.223875
69. Weismann D, Binder CJ. The innate immune response to products of phospholipid peroxidation. *Biochim Biophys Acta*. (2012) 1818:2465–75. doi: 10.1016/j.bbamem.2012.01.018
70. Manček-Keber M, Frank-Bertoncelj M, Hafner-Bratkovič I, Smole A, Zorko M, Pirher N. Toll-like receptor 4 senses oxidative stress mediated by the oxidation of phospholipids in extracellular vesicles. *Sci Signal*. (2015) 8:ra60. doi: 10.1126/scisignal.2005860
71. Kadl A, Sharma PR, Chen W, Agrawal R, Meher AK, Rudraiah S. Oxidized phospholipid-induced inflammation is mediated by Toll-like receptor 2. *Free Radic Biol Med*. (2011) 51:1903–9. doi: 10.1016/j.freeradbiomed.2011.08.026
72. Stewart CR, Stuart LM, Wilkinson K, van Gils JM, Deng J, Halle A. CD36 ligands promote sterile inflammation through assembly of a Toll-like receptor 4 and 6 heterodimer. *Nat Immunol*. (2010) 11:155–61. doi: 10.1038/ni.1836
73. Seimon TA, Nadolski MJ, Liao X, Magallon J, Nguyen M, Feric NT. Atherogenic lipids and lipoproteins trigger CD36-TLR2-dependent apoptosis in macrophages undergoing endoplasmic reticulum stress. *Cell Metab*. (2010) 12:467–82. doi: 10.1016/j.cmet.2010.09.010
74. Kazankov K, Jørgensen SMD, Thomsen KL, Møller HJ, Vilstrup H, George J. The role of macrophages in nonalcoholic fatty liver disease and nonalcoholic steatohepatitis. *Nat Rev Gastroenterol Hepatol*. (2019) 16:145–59. doi: 10.1038/s41575-018-0082-x
75. Kragh Petersen S, Bilkei-Gorzo O, Govaere O, Härtlova A. Macrophages and scavenger receptors in obesity-associated non-alcoholic liver fatty

disease (NAFLD). *Scand J Immunol*. (2020) 92:e12971. doi: 10.1111/sji.12971
76. Kunjathoor VV, Febbraio M, Podrez EA, Moore KJ, Andersson L, Koehn S. Scavenger receptors class A-I/II and CD36 are the principal receptors responsible for the uptake of modified low density lipoprotein leading to lipid loading in macrophages. *J Biol Chem*. (2002) 277:49982–8. doi: 10.1074/jbc.M209649200
77. Boullier A, Friedman P, Harkewicz R, Hartvigsen K, Green SR, Almazan F. Phosphocholine as a pattern recognition ligand for CD36. *J Lipid Res*. (2005) 46:969–76. doi: 10.1194/jlr.M400496-JLR200
78. Kim Y-W, Yakubenko VP, West XZ, Gugiu GB, Renganathan K, Biswas S. Receptor-mediated mechanism controlling tissue levels of bioactive lipid oxidation products. *Circ Res*. (2015) 117:321–32. doi: 10.1161/CIRCRESAHA.117.305925
79. Duryee MJ, Freeman TL, Willis MS, Hunter CD, Hamilton BC, Suzuki H. Scavenger receptors on sinusoidal liver endothelial cells are involved in the uptake of aldehyde-modified proteins. *Mol Pharmacol*. (2005) 68:1423–30. doi: 10.1124/mol.105.016121
80. Shechter I, Fogelman AM, Haberland ME, Seager J, Hokom M, Edwards PA. The metabolism of native and malondialdehyde-altered low density lipoproteins by human monocyte-macrophages. *J Lipid Res*. (1981) 22:63–71. doi: 10.1016/S0022-2275(20)34741-6
81. Bieghs V, Verheyen F, van Gorp PJ, Hendrikx T, Wouters K, Lütjohann D. Internalization of modified lipids by CD36 and SR-A leads to hepatic inflammation and lysosomal cholesterol storage in kupffer cells. *PLoS ONE*. (2012) 7:e34378. doi: 10.1371/journal.pone.0034378
82. Bieghs V, Wouters K, van Gorp PJ, Gijbels MJJ, de Winther MPJ, Binder CJ. Role of scavenger receptor A and CD36 in diet-induced nonalcoholic steatohepatitis in hyperlipidemic mice. *Gastroenterology*. (2010) 138:2477–86, (2486) e1-3. doi: 10.1053/j.gastro.2010.02.051
83. Bieghs V, Gorp PJ van, Walenbergh SMA, Gijbels MJ, Verheyen F, Buurman WA. Specific immunization strategies against oxidized low-density lipoprotein: a novel way to reduce nonalcoholic steatohepatitis in mice. *Hepatology*. (2012) 56:894–903. doi: 10.1002/hep.25660
84. Mushenkova NV, Bezsonov EE, Orekhova VA, Popkova TV, Starodubova AV, Orekhov AN. Recognition of oxidized lipids by macrophages and its role in atherosclerosis development. *Biomedicines*. (2021) 9:915. doi: 10.3390/biomedicines9080915
85. Yadati T, Houben T, Bitorina A, Oligschlaeger Y, Gijbels MJ, Mohren R. Inhibition of extracellular cathepsin D reduces hepatic lipid accumulation and leads to mild changes in inflammationin NASH mice. *Front Immunol*. (2021) 12:2846. doi: 10.3389/fimmu.2021.675535
86. Zhao CF, Herrington DM. The function of cathepsins B, D, and X in atherosclerosis. *Am J Cardiovasc Dis*. (2016) 6:163–70.
87. Rajamäki K, Lappalainen J, Oörni K, Välimäki E, Matikainen S, Kovanen PT. Cholesterol crystals activate the NLRP3 inflammasome in human macrophages: a novel link between cholesterol metabolism and inflammation. *PLoS ONE*. (2010) 5:e11765. doi: 10.1371/journal.pone.0011765
88. Duewell P, Kono H, Rayner KJ, Sirois CM, Vladimer G, Bauernfeind FG. NLRP3 inflamasomes are required for atherogenesis and activated by cholesterol crystals that form early in disease. *Nature*. (2010) 464:1357–61. doi: 10.1038/nature08938
89. Mridha AR, Wree A, Robertson AAB, Yeh MM, Johnson CD, Rooyen DMV. NLRP3 inflammasome blockade reduces liver inflammation and fibrosis in experimental NASH in mice. *J Hepatol*. (2017) 66:1037–46. doi: 10.1016/j.jhep.2017.01.022
90. Hendrikx T, Bieghs V, Walenbergh SMA, van Gorp PJ, Verheyen F, Jeurissen MLJ. Macrophage specific caspase-1/11 deficiency protects against cholesterol crystallization and hepatic inflammation in hyperlipidemic mice. *PLoS ONE*. (2013) 8:e78792. doi: 10.1371/journal.pone.0078792
91. Hendrikx T, Jeurissen MLJ, van Gorp PJ, Gijbels MJ, Walenbergh SMA, Houben T, et al. Bone marrow-specific caspase-1/11 deficiency inhibits atherosclerosis development in Ldlr(-/-) mice. *FEBS J*. (2015) 282:2327–38. doi: 10.1111/febs.13279
92. Febbraio M, Podrez EA, Smith JD, Hajjar DP, Hazen SL, Hoff HF. Targeted disruption of the class B scavenger receptor CD36 protects against atherosclerotic lesion development in mice. *J Clin Invest*. (2000) 105:1049–56. doi: 10.1172/JCI9259
93. Babaev VR, Gleaves LA, Carter KJ, Suzuki H, Kodama T, Fazio S, et al. Reduced atherosclerotic lesions in mice deficient for total or macrophage-specific expression of scavenger receptor-A. *Arterioscler Thromb Vasc Biol*. (2000) 20:2593–9. doi: 10.1161/01.ATV.20.12.2593
94. Mäkinen PI, Lappalainen JP, Heinonen SE, Leppänen P, Lähteenvuo MT, Aarnio JV. Silencing of either SR-A or CD36 reduces atherosclerosis in hyperlipidaemic mice and reveals reciprocal upregulation of these receptors. *Cardiovasc Res*. (2010) 88:530–8. doi: 10.1093/cvr/cvq235
95. Csak T, Velayudham A, Hritz I, Petrasek J, Levin I, Lippai D. Deficiency in myeloid differentiation factor-2 and toll-like receptor 4 expression attenuates nonalcoholic steatohepatitis and fibrosis in mice. *Am J Physiol Gastrointest Liver Physiol*. (2011) 300:G433–41. doi: 10.1152/ajpgi.00163.2009
96. Ferreira DF, Fiamoncini J, Prist IH, Ariga SK, de Souza HP, de Lima TM. Novel role of TLR4 in NAFLD development: modulation of metabolic enzymes expression. *Biochim Biophys Acta Mol Cell Biol Lipids*. (2015) 1851:1353–9. doi: 10.1016/j.bbalip.2015.07.002
97. Higashimori M, Tatro JB, Moore KJ, Mendelsohn ME, Galper JB, Beasley D. Role of toll-like receptor 4 in intimal foam cell accumulation in apolipoprotein E-deficient mice. *Arterioscler Thromb Vasc Biol*. (2011) 31:50–7. doi: 10.1161/ATVBAHA.110.210971
98. Michelsen KS, Wong MH, Shah PK, Zhang W, Yano J, Doherty TM, et al. Lack of Toll-like receptor 4 or myeloid differentiation factor 88 reduces atherosclerosis alters plaque phenotype in mice deficient in apolipoprotein E. *Proc Natl Acad Sci USA*. (2004) 101:10679–84. doi: 10.1073/pnas.0403249101
99. Ameziane N, Beillat T, Verpillat P, Chollet-Martin S, Aumont M-C, Seknadji P. Association of the toll-like receptor 4 gene Asp299Gly polymorphism with acute coronary events. *Arterioscl Thromb Vasc Biol*. (2003) 23:e61–4. doi: 10.1161/01.ATV.0000101191.92392.1D
100. Xu XH, Shah PK, Faure E, Equils O, Thomas L, Fishbein MC, et al. Toll-like receptor-4 is expressed by macrophages in murine human lipid-rich atherosclerotic plaques upregulated by oxidized LDL. *Circulation*. (2001) 104:3103–8. doi: 10.1161/hc5001.100631
101. Mullick AE, Tobias PS, Curtiss LK. Modulation of atherosclerosis in mice by Toll-like receptor 2. *J Clin Invest*. (2005) 115:3149–56. doi: 10.1172/JCI25482
102. Wu L, Sun J, Liu L, Du X, Liu Y, Yan X. Anti-toll-like receptor 2 antibody ameliorates hepatic injury, inflammation, fibrosis and steatosis in obesity-related metabolic disorder rats via regulating MAPK and NF-κB pathways. *Int Immunopharmacol*. (2020) 82:106368. doi: 10.1016/j.intimp.2020.106368
103. Xiong X, Kuang H, Ansari S, Liu T, Gong J, Wang S. Landscape of intercellular crosstalk in healthy and NASH liver revealed by single-cell secretome gene analysis. *Mol Cell*. (2019) 75:644–60.e5. doi: 10.1016/j.molcel.2019.07.028
104. Ramachandran P, Dobie R, Wilson-Kanamori JR, Dora EF, Henderson BEP, Luu NT. Resolving the fibrotic niche of human liver cirrhosis at single-cell level. *Nature*. (2019) 575:512–8. doi: 10.1038/s41586-019-1631-3
105. Cochain C, Vafadarnejad E, Arampatzi P, Pelisek J, Winkels H, Ley K. Single-Cell RNA-Seq reveals the transcriptional landscape and heterogeneity of aortic macrophages in murine atherosclerosis. *Circul Res*. (2018) 122:1661–74. doi: 10.1161/CIRCRESAHA.117.312509
106. Yeh FL, Wang Y, Tom I, Gonzalez LC, Sheng M. TREM2 binds to apolipoproteins, including APOE and CLU/APOJ, and thereby facilitates uptake of amyloid-beta by microglia. *Neuron*. (2016) 91:328–40. doi: 10.1016/j.neuron.2016.06.015
107. Tsiantoulas D, Diehl CJ, Witztum JL, Binder CJ. B cells and humoral immunity in atherosclerosis. *Circ Res*. (2014) 114:1743–56. doi: 10.1161/CIRCRESAHA.113.301145
108. Chang M-K, Binder CJ, Torzewski M, Witztum JL. C-reactive protein binds to both oxidized LDL and apoptotic cells through recognition of a common ligand: phosphorylcholine of oxidized phospholipids. *Proc Natl Acad Sci USA*. (2002) 99:13043–8. doi: 10.1073/pnas.192399699
109. Weismann D, Hartvigsen K, Lauer N, Bennett KL, Scholl HPN, Charbel Issa P. Complement factor H binds malondialdehyde epitopes and protects from oxidative stress. *Nature*. (2011) 478:76–81. doi: 10.1038/nature10449
110. Gruber S, Hendrikx T, Tsiantoulas D, Ozsvar-Kozma M, Göderle L, Mallat Z. Sialic acid-binding immunoglobulin-like lectin G promotes atherosclerosis

and liver inflammation by suppressing the protective functions of B-1 cells. *Cell Rep*. (2016) 14:2348–61. doi: 10.1016/j.celrep.2016.02.027
111. Caligiuri G, Nicoletti A, Poirier B, Hansson GK. Protective immunity against atherosclerosis carried by B cells of hypercholesterolemic mice. *J Clin Invest*. (2002) 109:745–53. doi: 10.1172/JCI7272
112. Lewis MJ, Malik TH, Ehrenstein MR, Boyle JJ, Botto M, Haskard DO. Immunoglobulin M is required for protection against atherosclerosis in low-density lipoprotein receptor-deficient mice. *Circulation*. (2009) 120:417–26. doi: 10.1161/CIRCULATIONAHA.109.868158
113. Tsiantoulas D, Perkmann T, Afonyushkin T, Mangold A, Prohaska TA, Papac-Milicevic N. Circulating microparticles carry oxidation-specific epitopes and are recognized by natural IgM antibodies 1. *J Lipid Res*. (2015) 56:440–8. doi: 10.1194/jlr.P054569
114. Chang MK, Bergmark C, Laurila A, Hörkkö S, Han KH, Friedman P. Monoclonal antibodies against oxidized low-density lipoprotein bind to apoptotic cells and inhibit their phagocytosis by elicited macrophages: evidence that oxidation-specific epitopes mediate macrophage recognition. *Proc Natl Acad Sci USA*. (1999) 96:6353–8. doi: 10.1073/pnas.96.11.6353
115. Tsiantoulas D, Sage AP, Mallat Z, Binder CJ. Targeting B cells in atherosclerosis: closing the gap from bench to bedside. *Arterioscler Thromb Vasc Biol*. (2015) 35:296–302. doi: 10.1161/ATVBAHA.114.303569
116. Nobili V, Parola M, Alisi A, Marra F, Piemonte F, Mombello C. Oxidative stress parameters in paediatric non-alcoholic fatty liver disease. *Int J Mol Med*. (2010) 26:471–6. doi: 10.3892/ijmm_00000487
117. Bruzzì S, Sutti S, Giudici G, Burlone ME, Ramavath NN, Toscani A. B2-Lymphocyte responses to oxidative stress-derived antigens contribute to the evolution of nonalcoholic fatty liver disease (NAFLD). *Free Radic Biol Med*. (2018) 124:249–59. doi: 10.1016/j.freeradbiomed.2018.06.015
118. Mayr M, Kiechl S, Tsimikas S, Miller E, Sheldon J, Willeit J. Oxidized low-density lipoprotein autoantibodies, chronic infections, and carotid atherosclerosis in a population-based study. *J Am Coll Cardiol*. (2006) 47:2436–43. doi: 10.1016/j.jacc.2006.03.024
119. Lappalainen J, Lindstedt KA, Oksjoki R, Kovanen PT. OxLDL-IgG immune complexes induce expression and secretion of proatherogenic cytokines by cultured human mast cells. *Atherosclerosis*. (2011) 214:357–63. doi: 10.1016/j.atherosclerosis.2010.11.024
120. Centa M, Jin H, Hofste L, Hellberg S, Busch A, Baumgartner R. Germinal center–derived antibodies promote atherosclerosis plaque size and stability. *Circulation*. (2019) 139:2466–82. doi: 10.1161/CIRCULATIONAHA.118.038534
121. Iseme RA, McEvoy M, Kelly B, Agnew L, Walker FR, Handley T. A role for autoantibodies in atherogenesis. *Cardiovasc Res*. (2017) 113:1102–12. doi: 10.1093/cvr/cvx112
122. Nilsson J. Can antibodies protect us against cardiovascular disease? *EBioMedicine*. (2016) 9:29–30. doi: 10.1016/j.ebiom.2016.06.039
123. Schiopu A, Bengtsson J, Söderberg I, Janciauskiene S, Lindgren S, Ares MPS. Recombinant human antibodies against aldehyde-modified apolipoprotein B-100 peptide sequences inhibit atherosclerosis. *Circulation*. (2004) 110:2047–52. doi: 10.1161/01.CIR.0000143162.56057.B5
124. Sage AP, Tsiantoulas D, Binder CJ, Mallat Z. The role of B cells in atherosclerosis. *Nat Rev Cardiol*. (2019) 16:180–96. doi: 10.1038/s41569-018-0106-9
125. Ait-Oufella H, Herbin O, Bouaziz J-D, Binder CJ, Uyttenhove C, Laurans L. B cell depletion reduces the development of atherosclerosis in mice. *J Exp Med*. (2010) 207:1579–87. doi: 10.1084/jem.20100155
126. Barrow F, Khan S, Fredrickson G, Wang H, Dietsche K, Parthiban P. Microbiota-driven activation of intrahepatic B cells aggravates NASH through innate and adaptive signaling. *Hepatology*. (2021) 74:704–22. doi: 10.1002/hep.31755
127. Wolf D, Ley K. Immunity and inflammation in atherosclerosis. *Circul Res*. (2019) 124:315–27. doi: 10.1161/CIRCRESAHA.118.313591
128. Vilar-Gomez E, Martinez-Perez Y, Calzadilla-Bertot L, Torres-Gonzalez A, Gra-Oramas B, Gonzalez-Fabian L. Weight loss through lifestyle modification significantly reduces features of nonalcoholic steatohepatitis. *Gastroenterology*. (2015) 149:367–78.e5; quiz e14–5. doi: 10.1053/j.gastro.2015.04.005
129. Francque S, Vonghia L. Pharmacological treatment for non-alcoholic fatty liver disease. *Adv Ther*. (2019) 36:1052–74. doi: 10.1007/s12325-019-00898-6
130. Neuschwander-Tetri BA. Therapeutic landscape for NAFLD in 2020. *Gastroenterology*. (2020) 158:1984–98.e3. doi: 10.1053/j.gastro.2020.01.051
131. Sanyal AJ, Friedman SL, McCullough AJ, Dimick-Santos L, American Association for the Study of Liver Diseases, United States Food Drug Administration. Challenges opportunities in drug biomarker development for nonalcoholic steatohepatitis: findings recommendations from an American Association for the Study of Liver Diseases-U.S. Food and Drug Administration joint workshop. *Hepatology*. (2015) 61:1392–405. doi: 10.1002/hep.27678
132. Younossi ZM, Ratziu V, Loomba R, Rinella M, Anstee QM, Goodman Z. Obeticholic acid for the treatment of non-alcoholic steatohepatitis: interim analysis from a multicentre, randomised, placebo-controlled phase 3 trial. *Lancet*. (2019) 394:2184–96. doi: 10.1016/S0140-6736(19)33041-7
133. Lavine JE, Schwimmer JB, Van Natta ML, Molleston JP, Murray KF, Rosenthal P. Effect of vitamin E or metformin for treatment of nonalcoholic fatty liver disease in children and adolescents: the TONIC randomized controlled trial. *JAMA*. (2011) 305:1659–68. doi: 10.1001/jama.2011.520
134. Chan AC. Vitamin E and atherosclerosis. *J Nutr*. (1998) 128:1593–6. doi: 10.1093/jn/128.10.1593
135. Su M, Wang D, Chang W, Liu L, Cui M, Xu T. Preparation of vitamin E-containing high-density lipoprotein and its protective efficacy on macrophages. *ASSAY Drug Dev Technol*. (2018) 16:107–14. doi: 10.1089/adt.2017.831
136. Wang W, Kang PM. Oxidative stress and antioxidant treatments in cardiovascular diseases. *Antioxidants*. (2020) 9:1292. doi: 10.3390/antiox9121292
137. Steinberg D, Witztum JL. Oxidized low-density lipoprotein and atherosclerosis. *Arterioscler Thromb Vasc Biol*. (2010) 30:2311–6. doi: 10.1161/ATVBAHA.108.179697
138. Hartley A, Haskard D, Khamis R. Oxidized LDL and anti-oxidized LDL antibodies in atherosclerosis – novel insights and future directions in diagnosis and therapy. *Trends Cardiovasc Med*. (2019) 29:22–6. doi: 10.1016/j.tcm.2018.05.010
139. Tsiantoulas D, Bot I, Ozsvar-Kozma M, Göderle L, Perkmann T, Hartvigsen K. Increased plasma IgE accelerate atherosclerosis in secreted IgM deficiency. *Circul Res*. (2017) 120:78–84. doi: 10.1161/CIRCRESAHA.116.309606
140. Shaw PX, Hörkkö S, Tsimikas S, Chang M-K, Palinski W, Silverman GJ. Human-derived anti-oxidized LDL autoantibody blocks uptake of oxidized LDL by macrophages and localizes to atherosclerotic lesions *in vivo*. *Arterioscler Thromb Vasc Biol*. (2001) 21:1333–9. doi: 10.1161/hq0801.093587
141. Tsimikas S, Miyanohara A, Hartvigsen K, Merki E, Shaw PX, Chou M-Y. Human oxidation-specific antibodies reduce foam cell formation and atherosclerosis progression. *J Am Coll Cardiol*. (2011) 58:1715–27. doi: 10.1016/j.jacc.2011.07.017
142. Dunér P, Mattisson IY, Fogelstrand P, Glise L, Ruiz S, Farina C. Antibodies against apoB100 peptide 210 inhibit atherosclerosis in apoE-/- mice. *Sci Rep*. (2021) 11:9022. doi: 10.1038/s41598-021-88430-1
143. Palinski W, Miller E, Witztum JL. Immunization of low density lipoprotein (LDL) receptor-deficient rabbits with homologous malondialdehyde-modified LDL reduces atherogenesis. *Proc Natl Acad Sci USA*. (1995) 92:821–5. doi: 10.1073/pnas.92.3.821
144. Freigang S, Hörkkö S, Miller E, Witztum JL, Palinski W. Immunization of LDL receptor-deficient mice with homologous malondialdehyde-modified and native LDL reduces progression of atherosclerosis by mechanisms other than induction of high titers of antibodies to oxidative neoepitopes. *Arterioscler Thromb Vasc Biol*. (1998) 18:1972–82. doi: 10.1161/01.ATV.18.12.1972
145. Sutti S, Jindal A, Locatelli I, Vacchiano M, Gigliotti L, Bozzola C, et al. Adaptive immune responses triggered by oxidative stress contribute to hepatic inflammation in NASH. *Hepatology*. (2014) 59:886–97. doi: 10.1002/hep.26749
146. Binder CJ, Hörkkö S, Dewan A, Chang M-K, Kieu EP, Goodyear CS, et al. Pneumococcal vaccination decreases atherosclerotic lesion formation: molecular mimicry between Streptococcus pneumoniae oxidized LDL. *Nat Med*. (2003) 9:736–43. doi: 10.1038/nm876

147. Tse K, Gonen A, Sidney J, Ouyang H, Witztum J, Sette A. Atheroprotective vaccination with MHC-II restricted peptides from ApoB-100. *Front Immunol.* (2013) 4:493. doi: 10.3389/fimmu.2013.00493
148. Amir S, Hartvigsen K, Gonen A, Leibundgut G, Que X, Jensen-Jarolim E. Peptide mimotopes of malondialdehyde epitopes for clinical applications in cardiovascular disease. *J Lipid Res.* (2012) 53:1316–26. doi: 10.1194/jlr.M025445
149. van den Hoek AM, Verschuren L, Worms N, van Nieuwkoop A, de Ruiter C, Attema J. A translational mouse model for NASH with advanced fibrosis and atherosclerosis expressing key pathways of human pathology. *Cells*. (2020) 9:2014. doi: 10.3390/cells9092014
150. Bieghs V, Van Gorp PJ, Wouters K, Hendrikx T, Gijbels MJ, van Bilsen M. LDL receptor knock-out mice are a physiological model particularly vulnerable to study the onset of inflammation in non-alcoholic fatty liver disease. *PLoS ONE.* (2012) 7:e30668. doi: 10.1371/journal.pone.0030668

Conflict of Interest: The authors declare that the research was conducted in the absence of any commercial or financial relationships that could be construed as a potential conflict of interest.

Publisher's Note: All claims expressed in this article are solely those of the authors and do not necessarily represent those of their affiliated organizations, or those of the publisher, the editors and the reviewers. Any product that may be evaluated in this article, or claim that may be made by its manufacturer, is not guaranteed or endorsed by the publisher.

Copyright © 2022 Hoebinger, Rajcic and Hendrikx. This is an open-access article distributed under the terms of the Creative Commons Attribution License (CC BY). The use, distribution or reproduction in other forums is permitted, provided the original author(s) and the copyright owner(s) are credited and that the original publication in this journal is cited, in accordance with accepted academic practice. No use, distribution or reproduction is permitted which does not comply with these terms.

frontiers in Cardiovascular Medicine

REVIEW
published: 14 January 2022
doi: 10.3389/fcvm.2021.785124

Sphingolipid Profiling: A Promising Tool for Stratifying the Metabolic Syndrome-Associated Risk

Loni Berkowitz[1], Fernanda Cabrera-Reyes[2], Cristian Salazar[1], Carol D. Ryff[3], Christopher Coe[3] and Attilio Rigotti[1]*

[1] Department of Nutrition, Diabetes and Metabolism & Center of Molecular Nutrition and Chronic Diseases, School of Medicine, Pontificia Universidad Católica de Chile, Santiago, Chile, [2] Department of Gastroenterology, School of Medicine, Pontificia Universidad Católica de Chile, Santiago, Chile, [3] Institute on Aging, University of Wisconsin-Madison, Madison, WI, United States

Metabolic syndrome (MetS) is a multicomponent risk condition that reflects the clustering of individual cardiometabolic risk factors related to abdominal obesity and insulin resistance. MetS increases the risk for cardiovascular diseases (CVD) and type 2 diabetes mellitus (T2DM). However, there still is not total clinical consensus about the definition of MetS, and its pathophysiology seems to be heterogeneous. Moreover, it remains unclear whether MetS is a single syndrome or a set of diverse clinical conditions conferring different metabolic and cardiovascular risks. Indeed, traditional biomarkers alone do not explain well such heterogeneity or the risk of associated diseases. There is thus a need to identify additional biomarkers that may contribute to a better understanding of MetS, along with more accurate prognosis of its various chronic disease risks. To fulfill this need, omics technologies may offer new insights into associations between sphingolipids and cardiometabolic diseases. Particularly, ceramides –the most widely studied sphingolipid class– have been shown to play a causative role in both T2DM and CVD. However, the involvement of simple glycosphingolipids remains controversial. This review focuses on the current understanding of MetS heterogeneity and discuss recent findings to address how sphingolipid profiling can be applied to better characterize MetS-associated risks.

Keywords: sphingolipids, cardiovascular risk (CVD), ceramides, metabolic syndrome, type 2 diabetes

OPEN ACCESS

Edited by:
Yiliang Chen,
Medical College of Wisconsin, United States

Reviewed by:
Matthieu Ruiz,
Université de Montréal, Canada
Leigh Goedeke,
Yale University, United States

****Correspondence:***
Loni Berkowitz
loniberko@gmail.com

Specialty section:
This article was submitted to Lipids in Cardiovascular Disease, a section of the journal Frontiers in Cardiovascular Medicine

Received: *28 September 2021*
Accepted: *21 December 2021*
Published: *14 January 2022*

Citation:
Berkowitz L, Cabrera-Reyes F, Salazar C, Ryff CD, Coe C and Rigotti A (2022) Sphingolipid Profiling: A Promising Tool for Stratifying the Metabolic Syndrome-Associated Risk. Front. Cardiovasc. Med. 8:785124. doi: 10.3389/fcvm.2021.785124

INTRODUCTION

Cardiovascular diseases (CVD) are currently a major cause of morbidity and mortality with major overall economic healthcare burden worldwide (1). Among these conditions, CVD of atherosclerotic origin (ASCVD) stands out because of its high prevalence and the significant acute ischemic complications and chronic consequences. Many risk factors for ASCVD are well-established, including family history, obesity, blood hypertension, dyslipidemia, type 2 diabetes (T2DM), and proinflammatory pathophysiology (2). In particular, metabolic syndrome (MetS) – a well-known clustering of risk factors (3)– doubles the risk for CVD and increases five-fold the chance for T2DM (4). Indeed, 13.3 to 44% of excess CVD mortality in the US is explained by MetS or MetS-related CVD (5). Furthermore, MetS is associated with increased risk of a number of common cancers (6) and neurodegenerative disorders (7) and is also an important risk factor influencing progression and prognosis of COVID-19 (8).

Based on NHANES reports, the overall prevalence of MetS in US adults was 34.7% in 2016, increasing with age and reaching 48.6% among those aged at least 60 years. Remarkably, over 2011–2016, MetS prevalence increased significantly among those aged 20 to 39 years from 16.2 to 21.3% (9). Thus, prevention, early diagnosis, and appropriate risk stratification of MetS constitute a major health priority challenge. However, besides the many components and clinical implications of MetS, there is no agreement upon clinical definition of MetS. Moreover, the pathophysiology of MetS is not consensual (10), and traditional biomarkers alone do not explain its heterogeneity or the specific risk of associated chronic diseases.

In search for new biomarkers, and in line with the refinement of new omics technologies, several studies have focused on bioactive sphingolipids (SPLs) (11). SPLs have emerged as signaling molecules that regulate many metabolic functions, and ample evidence highlights their role in the regulation of inflammatory responses (12). A substantial body of literature shows that ceramides, a major key class of this lipid family, may have a causative role in diabetes and ASCVD (13). However, the involvement of more simple glycosphingolipids (e.g., hexosylceramides and lactosylceramides) is still controversial.

This review focuses on the current understanding of MetS heterogeneity as well as recent findings that address how sphingolipid profiling may provide additional and valuable information to better characterize MetS-associated risk.

Emerging Cardiovascular Risk Factors, Including Sphingolipid Biomarkers

There are now many clinical guidelines for evaluation and management of ASCVD risk. The most common factors included in current risk calculators are age, sex, total cholesterol and HDL cholesterol (HDL-c) levels, blood pressure, diabetes, and smoking (14). Some guidelines also add in LDL cholesterol (LDL-c) levels, obesity, and high sensitivity C-reactive protein (15). However, there continue to be deficiencies in modeling risk as well as differences in the impact of each component (14). Indeed, estimations indicate that traditional risk algorithms may miss up to 20% of future CVD events (16).

The pursuit of better strategies for risk prognosis is under continuous evolution. For instance, although plasma LDL-c levels have been considered a primary etiopathogenic factor for development of ASCVD, currently the concentration of non-HDL-c is considered a better predictor of future CVD events (14, 17). Similarly, apolipoprotein B (Apo B) –the structural protein present in all atherogenic lipoproteins– and lipoprotein(a) have also been proposed as emerging cardiovascular risk factors. On the other hand, the recognition of ASCVD as an active process of vascular damage –rather than passive cholesterol infiltration of blood vessels– has highlighted inflammatory and procoagulant mechanisms and biomarkers. In this context, several proinflammatory and prothrombotic molecules (i.e., C-reactive protein, fibrinogen, IL-6, sICAM, etc.) are being assessed to add predictive power to existing CVD risk models (18, 19).

Currently, some of the most promising CVD risk prediction approaches are panels of multiple circulating biomarkers. In fact, omics technologies have provided new insights into the association between a wide variety of novel plasma molecules and cardiometabolic disorders (20). Particularly, based on the technological advances in lipidomics, researchers have identified nontraditional and less abundant lipids as possible biomarkers of early stage cardiometabolic dysfunction as well as cardiometabolic risk (21, 22). Indeed, multiple studies have identified non-traditional lipid species or lipidomic profiles related to subclinical atherosclerosis (23), future cardiovascular events (24–27), and CVD mortality (28). Most of them improved prediction of CVD beyond the sensitivity of traditional cardiovascular risk factors.

Moreover, longitudinal lipidomic phenotypes seem better predictor of future risk of ASCVD in healthy adults. One study showed that numerous non-cholesterol lipids, especially sphingolipid, phospholipid, diacylglycerol, and triglyceride species, deserved more consideration in CVD risk stratification in patients with low-risk cholesterol profiles (29). Similarly, two additional classes of circulating lipids (e.g., dihydroceramides and lysophosphatydilinositol) may serve as novel biomarkers to identify individuals at high-risk of diabetes prior to disease onset (30). In this context, a substantial body of evidence shows that some species of ceramides, a key class of the sphingolipid family, may play a causative role and be relevant for risk prediction of various cardiometabolic disorders, including CVD and diabetes (31–33). These observations have increased the pathophysiological interest and diagnostic potential of sphingolipids in MetS, a condition where the risk of CVD and diabetes converge, but with a highly heterogeneous pathobiology.

MetS Controversies in Definition and Chronic Disease Risk Association

MetS is a multicomponent condition that reflects the clustering of individual cardiometabolic risk factors related to abdominal obesity and insulin resistance. There are various definitions–based on shared elements–that somewhat have been agreed upon by different international organizations and expert groups.

A number of the most commonly used definitions are those proposed by the World Health Organization (WHO), the European Group for the Study of Insulin Resistance (EGIR), the National Cholesterol Education Program Adult Treatment Panel III (NCEP:ATPIII), the American Association of Clinical Endocrinology (AACE) and the International Diabetes Federation (IDF) (34). Most organizations recommend a harmonized definition for MetS based on the presence of any 3 of the following 5 risk factors: abdominal obesity, low HDL-c levels, high triglycerides levels, high blood pressure, and hyperglycemia (35). This delineation is congruent with the criteria outlined by the NCEP-ATPIII, one of the most popular definitions of MetS. The IDF definition has the same criteria but considers abdominal obesity as a requirement for MetS diagnosis. Conversely, AACE, WHO, and EGIR definitions regard insulin resistance as central to the pathophysiology of MetS and thus must be present for diagnosis (34).

The need to define MetS more precisely stems from the importance of correctly identifying individuals at high risk

for ASCVD vs. other chronic diseases. Several epidemiological studies have confirmed the increased risk of ASCVD in individuals with MetS, regardless of the diagnostic criteria used (36–38). However, there continues to be an ongoing controversy about whether MetS is in fact a homogeneous clinical condition, disorder, or disease (39), and whether it requires recognition as a specific syndrome. Moreover, the predictive value of MetS has been questioned because its detection may not provide additional information than its individual components (40). On the other hand, even though MetS has been associated with higher odds of cardiovascular events and T2DM, it remains unclear whether MetS is a single syndrome or a constellation of different attributes or traits conveying a divergent range of metabolic vs. cardiovascular risk (39). Using a continuous MetS severity scale, a study confirmed that a more severe presentation of this syndrome quadruples the risk of coronary events (41). But there are likely to be differences in the associated risk depending on the presence of specific MetS components as well other factors that remain to be defined. For instance, the combination of central obesity, elevated blood pressure, and hyperglycemia conferred the greatest risk for CVD and mortality in the Framingham Offspring Study (42). However, there is a lack of biomarkers that allow a more accurate prediction of a patient's risk progressing to one of the various pathologies associated with MetS (i.e., T2DM, CVD, Alzheimer's disease, cancer).

Traditional serum lipid biomarkers of cardiovascular health include low triglycerides as well as high HDL-c and low LDL-c (2). However, patients with MetS show several lipid abnormalities beyond high LDL-c, elevated triglycerides, or low HDL-c, such as high levels of modified LDL particles (43). In fact, traditional lipid measures alone do not fully explain the complexity of the altered lipid metabolism associated with MetS or its related high cardiovascular risk (CVR) (43). Moreover, currently used risk prediction calculators and available therapies are insufficient and a significant amount of undefined residual CVR remains undetected and untreated (44). In this context, biomarkers beyond those included in the existing definitions of MetS, such as endothelial dysfunction, prothrombotic tendency, and proinflammatory state, may be essential determinants of future CVR in MetS patients (45). However, these risk biomarkers would not provide information regarding the underlying metabolic status, and the risk of other pathologies such as T2DM. As described below, profiling of circulating sphingolipids could contribute to a better pathophysiological understanding of MetS, with more accurate prognosis of cardiovascular vs. diabetic risks.

Sphingolipids

Sphingolipids (SPL) are a highly diverse group of biomolecules that are not just structural components of cell membranes, but also participate in intra- and extracellular signaling. SPL are found in a wide variety of organisms and are as a matter of fact involved in many aspects of cell structure, recognition, metabolism, and regulation (46).

SPL comprise a complex family of compounds structurally defined by a backbone called "sphingoid" base, mostly represented by sphingosine, which is amide-linked with long- or very-long-chain fatty acids to form ceramides (**Figure 1**). Ceramides can be further derivatized –by addition of a headgroup– to form more complex SPL classes, such as sphingomyelin, simple glycosphingolipids (e.g., glucosylceramides, galactosylceramides and lactosylceramides), and more complex glycosphingolipids with a few to dozens of sugar residues, called gangliosides (46). Within each SPL class, there are many species components defined by structural and chemical features (i.e., carbon chain length, double bonds) of the attached fatty acid.

At a cellular level, SPL are found mainly in the plasma membrane, where they interact with cholesterol forming membrane microdomains known as "lipid rafts", which regulate signal transduction and cell recognition. In circulation, >500 species of plasma SPLs are transported in the different classes of lipoproteins (i.e., VLDL, LDL, HDL) or associated with albumin (47, 48). Lipoprotein-associated SPL can be incorporated into these lipid particles before they are secreted from cells (49), transferred from one lipoprotein to another, or modified within them (47). Consequently, changes in circulating lipoprotein levels may affect circulating sphingolipid levels (48, 50–53).

SPL Profile and Metabolic Complexity

SPL metabolism can be thought of as a discrete set of three metabolically connected pathways: (a) *de novo* synthesis coming from saturated fatty acids, (b) salvage of sphingosine, and (c) breakdown of complex SPLs (46), all of which converge into ceramides (**Figure 1**). In *de novo* synthesis, an acyl-CoA condensates with serine, which –by addition of another fatty acid– subsequently gives rise to dihydrosphingosine. Then, sequential enzymatic reactions lead to the generation of dihydroceramide, the reduced precursor of ceramides. Some dihydroceramides are not transformed further and they *per se* participate in signaling pathways while another fraction is oxidized into ceramides (46, 54). Afterwards, ceramides can be modified by incorporation of a polar group, such as phosphocholine, originating sphingomyelin, or sugars, giving rise to a wide range of glycosphingolipids (a.k.a. glycoceramides).

Many glycosyltransferases are involved in the synthesis of glycosphingolipids, starting with the addition of glucose or galactose, leading to the so-called hexosylceramides. Within these, glucosylceramide is the major form, and it may be subsequently modified by lactosylceramide synthase, which adds galactose giving rise to lactosylceramide (46, 55). Hexosylceramides and lactosylceramides are simple β-glycosphingolipids that can be further glycosylated, generating more complex glycosphingolipids (e.g., gangliosides), or remain as such leading to their biological activities (56).

SPL metabolism is interconnected with pathways involved in oxygen biology, immune response, glycolysis, amino acid metabolism, and metabolism of other lipids (46). Hence, there are multiple factors that potentially modify the SPL profile. For example, increases in reactive oxygen species (57) or a hypoxic state (58) predispose to accumulation of dihydroceramides. On the other hand, high levels of circulating saturated fatty acids stimulate a dose-dependent synthesis of ceramides (13, 59), which accounts for the accumulation of ceramides in overnutrition or dyslipidemia (50). Similarly, proinflammatory

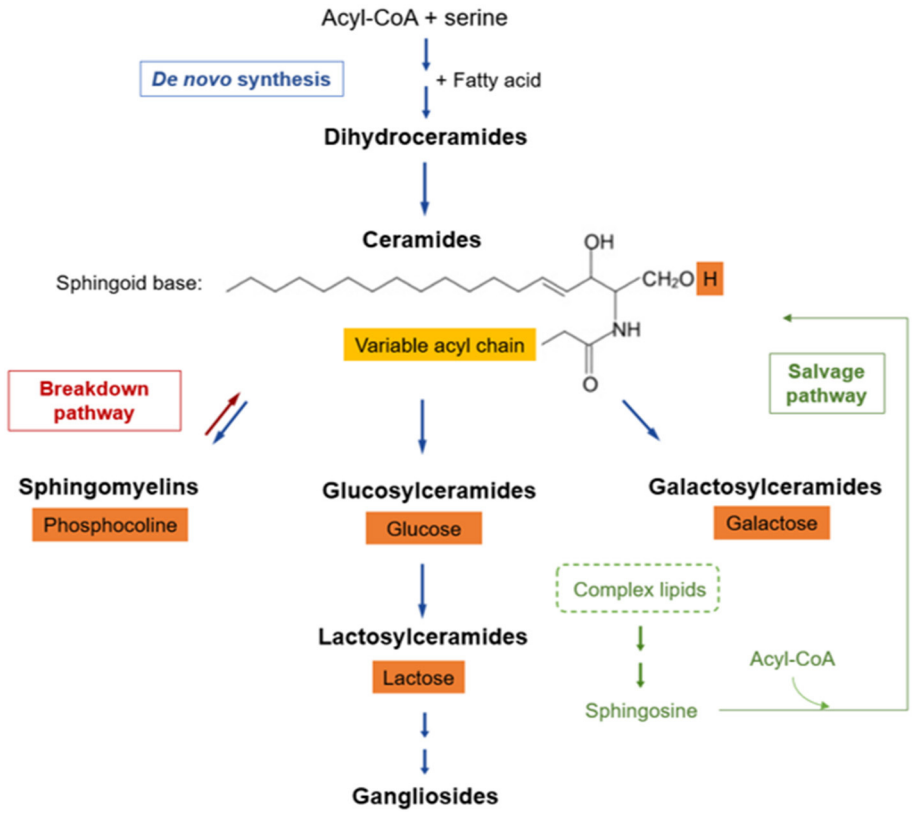

FIGURE 1 | Sphingolipid metabolic pathway. SPLs have three major metabolic pathways, all of which converge into ceramides: (a) *de novo* synthesis coming from saturated fatty acids, (b) breakdown pathway in which sphingomyelin loses its phosphocholine headgroup, and (c) salvage pathway that allows sphingosine recycling from complex SPLs. The fatty acid (light orange box) defines SPL species, whereas the headgroup (dark orange boxes) defines the SPL class.

cytokines, such as TNF-α, can stimulate the hydrolysis of sphingomyelin to ceramide (60), while bacterial antigens (e.g., LPS) promote the synthesis of some glycosphingolipids (61). Both LPS and saturated fatty acids also activate the toll-like receptor 4 (TLR4) and induce the transcription of genes associated with SPL synthesis (61). More distant modulating factors, such as lower psychological well-being, which is linked with an unhealthy lifestyle, has also been associated with higher levels of ceramides (62). Taken together, these findings show that SPL circulate in a dynamic balance that is likely to be altered under various physiological and disease conditions.

Biological Functions of SPLs Related With Cardiometabolic Diseases

Bioactive lipids are functionally defined as those lipid species whose levels respond to the action of specific stimuli and then regulate distinctive downstream effectors and targets. The most studied bioactive SPLs are ceramides. However, several additional SPL species are being evaluated as potential bioactive lipids (55). Thus, a major challenge is to keep up with the rapid growth in knowledge about the sphingolipidome (i.e., the ensemble of all SPL in living organisms) as well as its physiological and pathogenic impact.

The range of functions currently attributed to bioactive SPLs is wide and includes many aspects of cell biology and body physiology, such as cell growth and cell cycle, cell senescence and death, inflammation, immune response, cell adhesion and migration, angiogenesis, metabolism, and autophagy (55). Considering this wide variety of functions, SPLs have been implicated in several pathological disorders, including obesity, T2DM, atherosclerosis and CVD (11, 63, 64) (**Table 1**). However, many of the underlying mechanisms involved remain unclear and vary depending on the specific class, or even species, of SPL. For instance, ceramides elicit metabolic dysfunction by several mechanisms. They inhibit protein kinase B (Akt/PKB) via protein phosphatase 2 (PP2A) and protein kinase C zeta (PKCz) intermediaries, which mediate a wide range of downstream effects, including insulin resistance (55, 67, 68, 93). In addition, ceramide acts as a second messenger in activating the apoptotic cascade in many cell types, including β cells in pancreatic islets (33, 94). Ceramide overload also induces endoplasmic reticulum stress, inhibits mitochondrial fatty acid β-oxidation, and activates the NLRP3 inflammasome (13), pathophysiological processes associated with obesity.

On the other hand, glycosphingolipids fulfill most of their functions by structuring glycosphingolipid-enriched microdomains in cell membranes. Of particular importance is

TABLE 1 | Association between sphingolipid classes and cardiometabolic disorders.

Sphingolipid class	Relationship with	Proposed mechanisms	Most studied SPL species	Supporting evidence
	Obesity			
Ceramides	↑	Visceral obesity promotes the SPL biosynthetic pathway, increasing circulating ceramides.	Cer-C16 and Cer-C18	*In vitro* and animal models (61, 65, 66), cross-sectional studies (21)
HexCer/LacCer	↓ or =	Unclear. Upregulation of salvage pathway	Sphingosine-based HexCer and Hex2Cer species	*In vitro* (49), cross-sectional studies (21)
	Dyslipidemia			
Ceramides	↑c-LDL, ↑TGs, ↓c-HDL	Bidirectional. Higher levels of ApoB-containing lipoproteins increase ceramide circulation. Ceramide depletion could accelerate the catabolism of ApoB-containing lipoproteins.	-	*In vitro* (48), animal models (50), cross-sectional studies (21, 51), prospective studies (52)
HexCer/LacCer	↓c-LDL, ↓TGs, ↑c-HDL	Unclear. Upregulation of salvage pathway		*In vitro* (53), cross-sectional studies (21)
	Dysglycemia			
Ceramides	↑	Ceramide accumulation would alter glucose metabolism, by inhibition of Akt/PKB, inducing insulin resistance, and by stimulation of β cells apoptosis in pancreatic islets, increasing the risk of diabetes.	Cer-C18 and C20	*In vitro* (67–69), animal models (70–72), cross-sectional studies (73), prospective studies (21, 64)
HexCer/LacCer	↓	Increased synthesis of hexosylceramides at expense of ceramides would enhance insulin sensitivity by ceramide reduction, and by immunomodulatory actions.		*In vitro* (69), animal models (74, 75), cross-sectional studies (21), prospective studies (74–76)
GM3	↑	GM3 would cause insulin resistance, by reduction of insulin receptor presentation on fat cell surface due to changes in composition of lipid rafts.		*In vitro* and *in vivo* (77)
	Cardiovascular disease			
Ceramides	↑	Ceramides increase CV risk, by increasing transport, retention, and aggregation of ceramide-enriched LDL within the vascular wall; apoptosis of cells lining the vascular wall, and reduction of vasorelaxation and fibrinolysis.	Cer-C16, C18 and C24: 1 and their ratio over Cer-C24	*In vitro* (14, 78), animal models (79, 80), and prospective studies (81–84)
HexCer	↑	GluCer regulate downstream signaling of LPS/TLR4, increasing secretion of proinflammatory cytokines.		*In vitro* (85, 86)
LacCer	↑	LacCer increase CV risk: lead to oxidative stress environment and upregulate adhesion molecules on vascular endothelial cells and monocytes.		*In vitro* (87–90), animal models (91), prospective studies (22, 24)
GM3	↑	GM3 would increase foam cell formation		*In vitro* (92)

The arrows symbolize the relationships between blood SPL levels and MetS-associated conditions. An upward arrow indicates a positive association and a downward arrow indicates a negative association.

the assembly of these glycosphingolipids with signal transducers and other membrane proteins to form functional signaling units (95). For example, studies showed that GM3, a complex ganglioside, reduced insulin receptor presentation on the cell surface of adipocytes by modifying the composition of lipid rafts (77). However, this alteration in insulin signaling does not occur with simpler glycosphingolipids or in other types of cells, where the effect could even be favorable (69).

In the same line, glycosphingolipids are important determinants of a functional immune system. Glycosphingolipid repertoires present in the plasma membrane of immune cells impact membrane organization, molecular signaling, cell differentiation, and trans-interaction between biomolecules located in adjacent cell surfaces (96). Glycosphingolipid-enriched plasma membrane microdomains mediate immunological and inflammatory reactions, including superoxide generation, chemotaxis, and non-opsonic phagocytosis (97). In addition, lactosylceramides activate cytosolic phospholipase A2 (cPLA2), which cleaves arachidonic acid from phosphatidylcholine to generate eicosanoids and prostaglandins, two essential inflammatory intermediaries (87, 98). As detailed below, the role of glycosphingolipids in inflammation and immune response has been directly related to the development and progression of ASCVD.

All these findings have increased interest in verifying the usefulness of measuring plasma SPL levels as new biomarkers.

However, these analyses have been hampered by the complexity and diverse functions of this lipid family. Therefore, it remains a significant need to better define sphingolipidome profiles under normal and pathological conditions to further understand how absolute levels of different SPLs and, eventually, the relative ratio between them regulate cell function/body physiology and are associated with the origin and progression of chronic diseases. In fact, we must establish more precisely the relevance of SPL profiles to risk stratification and prognosis of MetS, where all the metabolic disorders mentioned above converge.

SPLs as Potential Mediators of Inflammation in Cardiometabolic Diseases

Studies *in vitro*, Cultured Cells, and Animal Models

Given their role in metabolic and inflammatory processes, there is an emerging interest in elucidating the association of SPLs and ASCVD. Ceramides have been shown to be relevant for understanding the pathophysiology of the atherothrombotic process and exert several specific actions during plaque formation and ischemic complications (79, 80) (**Table 1**). For example, generation of ceramide by sphingomyelin-breakdown induction was found to be sufficient in activating the aggregation of lipoproteins *in vitro* (99, 100). In fact, aggregated LDL particles obtained from atherosclerotic lesions have 10- to 50-fold higher levels of ceramides than plasma LDL particles (101). Ceramide was also implicated in transcytosis of oxidized LDL across endothelial cells, thus leading to the transport and retention of atherogenic lipoproteins within the vascular wall (102). Likewise, the acute induction of ceramide synthesis by monocytes increased adhesion of these proatherogenic lipoproteins to rat aortic endothelium and uptake of oxidized LDL *in vitro* (103). Moreover, ceramides have been shown to induce apoptosis of cells lining the vascular wall, a process implicated in plaque rupture during acute ischemic complications of atherothrombotic disease (78). Finally, ceramides impair endothelium-dependent vasorelaxation and fibrinolysis *in vitro* (13) further increasing the risk for atherothrombotic events. In parallel, several studies using cell and animal models have also shown that ceramides impair glucose metabolism in different cell types and organs, including pancreas, skeletal muscle, and adipose tissue (33, 70–72, 104, 105), increasing T2DM risk (64)–a prime risk factor for ASCVD.

In contrast to unglycosylated ceramides, the involvement of glycosphingolipids in cardiometabolic diseases is more controversial. Specifically, simple –rather than complex– glycosphingolipids seem to have a protective role against metabolic disorders (**Table 1**). For example, administration of simple β-glycosphingolipids showed remarkable beneficial effects on glucose intolerance and hepatic steatosis in mice (74), rats (75), and *Psammomys obesus* (76). This effect was attributed to the immunomodulatory role of this β-glycosphingolipid on immune cells involved in these disorders (74–76). As well, induction of glucosylceramide synthesis in myotubes enhanced insulin signaling (69).

In contrast, elevated levels of lactosylceramide –which were accompanied with decreased respiration and calcium retention capacity in mitochondria– have been reported in heart tissue of streptozotocin-induced type 1 diabetes mouse model (106). These metabolic changes may impair immune cell function (107). In addition, lactosylceramides lead to oxidative stress environment in human aortic smooth muscle cells by activating NADPH oxidase and generating reactive oxygen species (108). Therefore, despite the beneficial effects that these glycosphingolipids may have on glucose metabolism, lactosylceramides would contribute to mitochondrial dysfunction, oxidative stress, and inflammatory response in diabetes.

In addition, the involvement of lactosylceramides and hexosylceramides on ASCVD has been reported in several models (**Table 1**). For example, atherogenic apoE knockout mice exhibit increased serum concentrations of glycosphingolipids and accumulation of specific glycosphingolipids in atherosclerosis-prone regions of the aorta (91, 109). In keeping with this finding, using cell lines and mouse models, several immune mechanisms–as follows–have been proposed to account for a direct proatherogenic effect of specific glycosphingolipids. A recent study reported that macrophages accumulated ceramides and glucosylceramide in response to inflammatory activation with IFN-γ and LPS (110). Interestingly, glucosylceramide present in plasma membrane microdomains regulate LPS/TLR4 orientation, affecting downstream signaling proteins of this complex and the production of proinflammatory cytokines, as IL-6 and TNF-α (85, 86). On the other hand, lactosylceramide induced smooth muscle cell proliferation *in vitro* (88) while ganglioside GM3 markedly accelerated LDL uptake by macrophages, leading to generation of lipid-laden foam cells (92). On the other hand, *in vitro* studies, evaluating the pro-inflammatory role of β-glycosphingolipids, suggested that lactosylceramides may upregulate adhesion molecules on vascular endothelial cells and monocytes as well as activate neutrophils, contributing to atheromatous plaque inflammation (87, 89, 90). Moreover, a murine model showed that lactosylceramide is enriched in plasma membrane microdomains of neutrophils and involved in cell migration and phagocytosis (97). Indeed, inhibition of glycosphingolipid synthesis helped to preserve cardiac function in an animal model of diet-induced ASCVD (111).

On the other hand, peripheral monocytes isolated from healthy humans exhibited enhanced migration when incubated with exogenous lactosylceramide (112). Specifically, lactosylceramides increased the expression of ICAM-1 in human endothelial cells, through NADPH oxidase activation and ROS generation (113). Similarly, lactosylceramides induced the expression of CD11/CD18 in human neutrophils and monocytes, facilitating their adhesion to the endothelium and entry into the intimal space (87, 98). All these lactosylceramide-associated processes would contribute to inflammation and development of atherosclerosis. Finally, glycosphingolipids can also modulate the adaptative immune response in ASCVD. IFN-α, a proinflammatory cytokine found in atherosclerotic plaques, upregulated lactosylceramide and glucosylceramide production in mouse B cells (114). These lipid classes are a fundamental component of glycosphingolipid-enriched microdomains

involved in activation and proliferation of B and T lymphocytes, which modulate and regulate amplification of an inflammatory response (96).

Human Clinical and Epidemiological Studies

More recently, several studies in humans have shown an association between ceramides and cardiometabolic diseases. High levels of plasma ceramides were detected in patients with T2DM (33), arterial hypertension (115), and atherosclerosis (116). Furthermore, accumulation of ceramides in atheromatous plaques seems to stimulate apoptosis of vascular cells, destabilizing the plaque, and thus favoring acute ischemic events (14, 78). In agreement with this perspective, multiple studies have confirmed the association between ceramides and cardiovascular events, even after adjusting for all other well-known risk factors (81–84).

Among the ceramide species studied in humans, whereas Cer-C18 and C20 have been the most associated with T2DM, Cer-C16, C18 and C24:1 as well as their ratio over Cer-C24 have been the species mainly correlated with CVD (11, 73) (**Table 1**). Based on this type of evidence, a blood ceramide-based diagnostic CVR test (Ceramide Risk Score) was commercialized in 2016 (117). However, one limitation when interpreting the results from this test is that ceramides may be raised in response to different inflammatory states, which are not necessarily indicative of ASCVD (117). Moreover, basal SPL levels also evince considerable variation across different racial and ethnic populations (118). Therefore, more basic and clinical research is still required to further characterize SPL profiles before they can be employed as a diagnostic test with high sensitivity and specificity in routine medical practice.

As mentioned above, the relationship between glycosphingolipids and abnormal cardiometabolic processes remain controversial, but as this article explains, it seems dependent on the pathophysiological context. For example, three recent studies–based on different methodologies and populations–found a negative correlation between hexosylceramide levels and clinical and biochemical features of obesity and diabetes (21, 119, 120). Furthermore, a negative association between simple β-glycosphingolipids and the diagnosis of T2DM was found during follow-up (21). Interestingly, these observations have not been limited to only a few molecular forms, but to multiple species of hexosylceramides and lactosylceramides (21, 119, 120). In sum, emerging evidence seems to indicate that low circulating levels of simple β-glycosphingolipids and high levels of ceramides (i.e., high ceramide/simple β-glycosphingolipids ratio) would be consistently associated with glucometabolic disorders.

Conversely, in the last years, two large prospective cohort-based studies of lipidomic profiles positively associated both ceramides and simple β-glycosphingolipids with future cardiovascular events and cardiovascular death, even in patients with T2DM and after adjusting for traditional risk factors (22, 24). Similarly, levels of lactosylceramides, glucosylceramides, and dihydroceramides were directly correlated with levels of macrophages, IL-6, and macrophage inflammatory protein-1β in human carotid plaques (89). Moreover, a strong link between pulse wave velocity and arterial stiffness, as preclinical atherosclerotic biomarkers, with plasma lactosylceramide levels was found in overweight middle-aged subjects who had fasting hyperglycemia (121). Therefore, despite the relationship with better glucose metabolism, all these studies suggest a potential pro-atherogenic role of simple β-glycosphingolipids, consistent with the aforementioned *in vitro* studies.

SPLs and MetS Associated-Risk Stratification

Several lipidomic studies have in fact identified novel biomarkers linked to metabolic syndrome or its components (122–124). However, most of them are cross-sectional studies or consider MetS as a single disorder. To our knowledge, only one study evaluated lipid species associated with longitudinal changes in MetS components (125). Whereas lysophosphatidylcholine species were correlated with lower BMI and glycemia, two sphingomyelin species were associated with an increased blood glucose levels during follow-up. However, it remains unclear if these lipid signatures could indeed predict the future risk of diseases associated to MetS.

As mentioned above, there is a variable, and even divergent, relationship between different sphingolipid classes and cardiometabolic conditions such as dyslipidemia, insulin resistance, obesity, and atherosclerosis (**Figure 2**). Thus, it seems appropriate to hypothesize that further sphingolipid profile characterization may contribute to a better understanding of a complex clinical condition such as MetS, in which different cardiometabolic alterations converge and progress heterogeneously. However, it should be noted that although various studies relate sphingolipids with specific cardiometabolic alterations, much of its potential as biomarkers is based primarily on cohort association studies. For example, several lipid profiling studies have reported that circulating dihydroceramides were strong prognostic indicators of future glucometabolic dysfunction (126, 127). Even so, dihydroceramides would not be causative, but most likely would serve as markers of increased flux of fatty acids due to insulin resistance through the ceramide biosynthetic pathway (70).

Regarding specific components of the MetS definition, the associations of sphingolipids with obesity and insulin resistance have been well characterized in humans and animal models (13, 65, 66). Overnutrition and visceral obesity promote SPLs synthesis and turnover, which in turn remodels SPLs profiles and their topological distribution within and between cell membranes, thus defining organelle structure and function (33, 54, 125). In this context, ceramide accumulation in tissues may be impairing many metabolic processes that underlie diabetes and diabetic complications, according to the mechanisms already described (13). Interestingly, Chaurasia et al. demonstrated that inhibition of the enzymatic transformation of dihydroceramides to ceramides in obese mice resolved hepatic steatosis and insulin resistance,

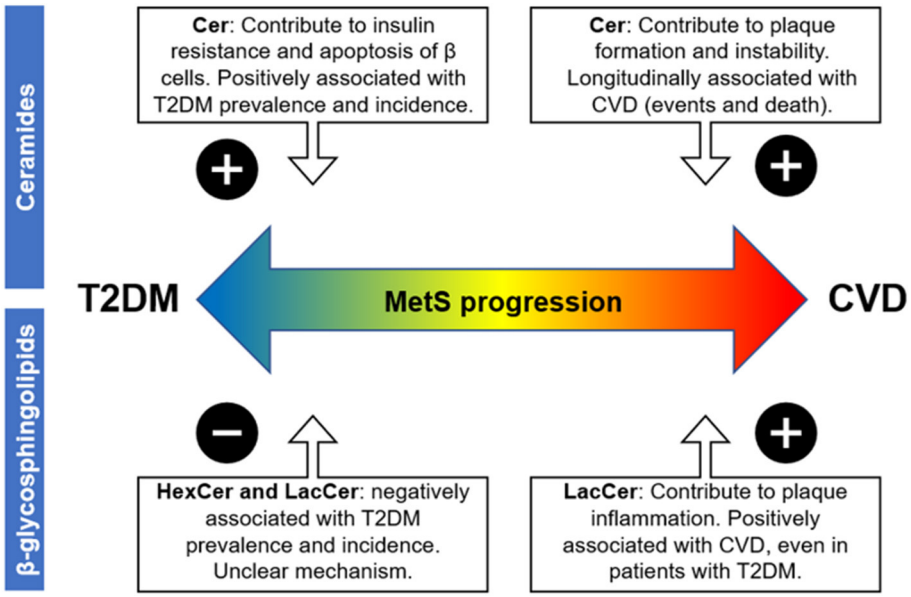

FIGURE 2 | Possible impact of blood sphingolipid profile on MetS-associated cardiovascular vs. metabolic risk based on cross-sectional and longitudinal association studies. Abbreviations are as follows: metabolic syndrome (MetS), atherosclerotic cardiovascular disease (ASCVD), and type 2 diabetes mellitus (T2DM). The "plus sign" denotes a positive association between the respective disease progression and the sphingolipid class, while the minus sign denotes a negative association.

suggesting that ceramide actions could not be recapitulated by dihydroceramides (70).

On the other hand, hexosylceramides and lactosylceramides have an immunomodulatory role, and their overall effect would depend on the overall pathophysiological context. Regarding metabolic risk, several studies have consistently shown an inverse relationship between plasma levels of simple β-glycosphingolipids and the prevalence and incidence of diabetes, using different methodologies and based on various population cohort (21, 119, 120). Although the mechanism is not clear, administration of these glycosphingolipids improved glucose intolerance in different animal models of diabetes (74, 75), suggesting a causal role. Therefore, in patients with MetS and overweight, high circulating levels of ceramides would increase the risk of diabetes, whereas this risk could be counterbalanced by the concentrations of simple glycosphingolipids.

Conversely, both ceramides and simple β-glycosphingolipids have been positively associated with ASCVD, as mentioned above. Increased levels of ceramides were related to aggregation of LDL particles in atherosclerotic lesions, induction of apoptosis of cells lining the vascular wall, and platelet activation and aggregation (100, 102, 103). On the other hand, lactosylceramides may upregulate adhesion molecules on monocytes and vascular endothelial cells as well as activate neutrophils, contributing to plaque inflammation and instability (98). In fact, human studies show that both ceramides and simple β-glycosphingolipids are associated with the occurrence of cardiovascular events and cardiovascular death, even in patients with T2DM (22). Therefore, despite the beneficial effects that simple β-glycosphingolipids may have on glucose metabolism and intolerance, both ceramides and simple β-glycosphingolipids may contribute to cardiovascular risk in patients with MetS. Interestingly, a recent study showed that statin therapy did not significantly lower circulating concentrations of these two sphingolipids (128). Therefore, high levels of ceramides and glycosphingolipids could account for a fraction of the residual cardiometabolic risk in statin-treated MetS patients.

Based on all this background, SPL profiling may provide novel and relevant insights into the burden of cardio vs. metabolic risk in patients with MetS. Although abdominal obesity seems to increase all classes of sphingolipids, a blood profile characterized by high levels of ceramides and low levels of simple β-glycosphingolipids in MetS patients may implicate a higher risk of T2DM (**Figure 2**), based on the evidence discussed here. On the other hand, a profile characterized by high levels of both ceramides and simple β-glycosphingolipids during MetS could indicate a more inflammatory and pro-atherogenic state, and therefore, a higher risk of ASCVD (**Figure 2**).

Importantly, careful consideration of experimental procedures and control variables is required during characterization of sphingolipidomes. Some differences can be observed depending on the analytic technique used, the origin of the sample (e.g., serum vs. plasma), and the feeding condition of the subject (e.g., fasting vs. non fasting) (20, 129). Furthermore, it is also necessary to evaluate the representativeness of these biomarkers among different subpopulations, since it could vary by racial, sex or age groups (130, 131). For example, there are ethnic and racial differences in the prevalence of MetS and its components (132). In general, African-Americans have lower prevalence of MetS when compared to whites, but suffer disproportionately from higher cardiovascular mortality and T2DM (132). Thus, further research is needed to explore the potential applications of SPL profiling to improve MetS-associated risk prediction in this population.

CONCLUSION

Stratification and better risk prediction of MetS constitutes a health priority and challenge. Traditional biomarkers alone do not explain its heterogeneity or the specific future risk of associated diseases. Moreover, even though MetS has previously been linked with higher odds of cardiovascular events, little is known about specific clusters of MetS components and their associated-risk differences for development of ASCVD vs. T2DM.

The evidence discussed in this review suggests that sphingolipid profiling appears as a promising tool for MetS-associated risk stratification. Evaluation of simple β-glycosphingolipids, in addition to more commonly assessed ceramide species, may provide relevant insights into the burden of dysmetabolic state vs. inflammatory state in patients with MetS. Based on this information, the sphingolipid profile –as an additional laboratory test– may have the potential to greatly improve the ability to distinguish MetS patients at risk of suffering a cardiovascular event in the short/medium term from those patients more likely to develop diabetes in the future. We are currently carrying out prospective cohort studies that will be critical to evaluate whether different SPL profiles allow a better classification of MetS patients based on their clinical progression.

AUTHOR CONTRIBUTIONS

LB and AR: conceptualization. LB, FC-R, CS, and AR: writing—original draft preparation. LB, FC-R, CS, CR, CC, and AR: writing—review and editing. All authors contributed to the article and approved the submitted version.

FUNDING

Preparation of this manuscript was supported by the National Fund of Scientific and Technological Development (Postdoctoral FONDECYT Grant #3210391 and regular FONDECYT Grant #1201607) from the Government of Chile and by the National Institute on Aging (Grant #P01 AG020166).

REFERENCES

1. World Health O. Noncommunicable diseases. (2016) Available online at: https://www.who.int/news-room/fact-sheets/detail/noncommunicable-diseases
2. Benjamin EJ, Virani SS, Callaway CW, Chamberlain AM, Chang AR, Cheng S, et al. Heart disease and stroke statistics −2018 update: a report from the american heart association. *Circulation.* (2018) 137:e67–e492. doi: 10.1161/CIR.0000000000000558
3. Grundy SM, Brewer HB, Cleeman JI, Smith SC, Lenfant C, American Heart A, et al. Definition of metabolic syndrome: Report of the National Heart, Lung, and Blood Institute/American Heart Association conference on scientific issues related to definition. *Circulation.* (2004) 109:433–8. doi: 10.1161/01.CIR.0000111245.75752.C6
4. Alberti KGMM, Eckel RH, Grundy SM, Zimmet PZ, Cleeman JI, Donato KA, et al. Harmonizing the metabolic syndrome: a joint interim statement of the International Diabetes Federation Task Force on Epidemiology and Prevention; National Heart, Lung, and Blood Institute; American Heart Association; World Heart Federation; International Atherosclerosis Society; and International Association for the Study of Obesity. *Circulation.* (2009) 120:1640–5. doi: 10.1161/CIRCULATIONAHA.109.192644
5. Liu L, Miura K, Fujiyoshi A, Kadota A, Miyagawa N, Nakamura Y, et al. Impact of metabolic syndrome on the risk of cardiovascular disease mortality in the United States and in Japan. *Am J Cardiol.* (2014) 113:84–9. doi: 10.1016/j.amjcard.2013.08.042
6. Esposito K, Chiodini P, Colao A, Lenzi A, Giugliano D. Metabolic syndrome and risk of cancer: A systematic review and meta-analysis. *Diabetes Care.* (2012) 35:2402–11. doi: 10.2337/dc12-0336
7. Borshchev YY, Uspensky YP, Galagudza MM. Pathogenetic pathways of cognitive dysfunction and dementia in metabolic syndrome. *Elsevier Inc.* (2019). doi: 10.1016/j.lfs.2019.116932
8. Costa FF, Rosário WR, Ribeiro Farias AC, de Souza RG, Duarte Gondim RS, Barroso WA. Metabolic syndrome and COVID-19: An update on the associated comorbidities and proposed therapies. *Elsevier Ltd.* (2020) p. 809–814. doi: 10.1016/j.dsx.2020.06.016
9. Hirode G, Wong RJ. Trends in the prevalence of metabolic syndrome in the United States, 2011-2016. *JAMA.* (2020) 323:2526–8. doi: 10.1001/jama.2020.4501
10. Bovolini A, Garcia J, Andrade MA, Duarte JA. Metabolic syndrome pathophysiology and predisposing factors. *Int J Sports Med.* (2020) 42:199–214. doi: 10.1055/a-1263-0898
11. Kurz J, Parnham MJ, Geisslinger G, Schiffmann S. Ceramides as novel disease biomarkers. *Trends Mol Med.* (2019) 25:20–32. doi: 10.1016/j.molmed.2018.10.009
12. Albi E, Alessenko A, Grösch S. Sphingolipids in Inflammation. *Mediators of inflammation.* (2018) (2018). doi: 10.1155/2018/7464702
13. Chaurasia B, Summers SA. Ceramides - lipotoxic inducers of metabolic disorders. *Trends Endocrinol Metab.* (2015) 26:538–50. doi: 10.1016/j.tem.2015.07.006
14. Goff DC, Lloyd-Jones DM, Bennett G, Coady S, D'Agostino RB, Gibbons R, et al. 2013 ACC/AHA guideline on the assessment of cardiovascular risk: a report of the American College of Cardiology/American Heart Association Task Force on Practice Guidelines. *J Am Coll Cardiol.* (2014) 63:2935–59. doi: 10.1016/j.jacc.2013.11.005
15. Hippisley-Cox J, Coupland C, Vinogradova Y, Robson J, Minhas R, Sheikh A et al. Predicting cardiovascular risk in England and Wales: prospective derivation and validation of QRISK2. *BMJ.* (2008) 336:1475–82. doi: 10.1136/bmj.39609.449676.25
16. MacNamara J, Eapen DJ, Quyyumi A, Sperling L. Novel biomarkers for cardiovascular risk assessment: current status and future directions. *Future Cardiol.* (2015) 11:597–613. doi: 10.2217/fca.15.39
17. Mora S, Buring JE, Ridker PM. Discordance of low-density lipoprotein (LDL) cholesterol with alternative LDL-related measures and future coronary events. *Circulation.* (2014) 129:553–61. doi: 10.1161/CIRCULATIONAHA.113.005873
18. Tzoulaki I, Murray GD, Lee AJ, Rumley A, Lowe GDO, Fowkes FGR. C-reactive protein, interleukin-6, and soluble adhesion molecules as predictors of progressive peripheral atherosclerosis in the general population: Edinburgh artery study. *Circulation.* (2005) 112:976–83. doi: 10.1161/CIRCULATIONAHA.104.513085
19. Amar J, Fauvel J, Drouet L, Ruidavets JB, Perret B, Chamontin B, et al. Interleukin 6 is associated with subclinical atherosclerosis: a link with soluble intercellular adhesion molecule 1. *J Hypertens.* (2006) 24:1083–8. doi: 10.1097/01.hjh.0000226198.44181.0c
20. Hinterwirth H, Stegemann C, Mayr M. Lipidomics: quest for molecular lipid biomarkers in cardiovascular disease. *Circ Cardiovasc Genet.* (2014) 7:941–54. doi: 10.1161/CIRCGENETICS.114.000550
21. Chew WS, Torta F, Ji S, Choi H, Begum H, Sim X, et al. Large-scale lipidomics identifies associations between plasma sphingolipids and T2DM incidence. *JCI Insight.* (2019) 4. doi: 10.1172/jci.insight.126925
22. Alshehry ZH, Mundra PA, Barlow CK, Mellett NA, Wong G, McConville MJ, et al. Plasma lipidomic profiles improve on traditional risk factors for the

prediction of cardiovascular events in type 2 diabetes mellitus. *Circulation.* (2016) 134:1637–50. doi: 10.1161/CIRCULATIONAHA.116.023233
23. Hoong JSY, Chew WS, Torta F, Ji S, Choi H, Begum H, et al. Plasma sphingolipids and subclinical atherosclerosis – novel associations uncovered by a large-scale lipidomic analysis (P18-129-19). *Curr Dev Nutr.* (2019) 3. doi: 10.1093/cdn/nzz039.P18-129-19
24. Poss AM, Maschek JA, Cox JE, Hauner BJ, Hopkins PN, Hunt SC, et al. Machine learning reveals serum sphingolipids as cholesterol-independent biomarkers of coronary artery disease. *J Clin Invest.* (2020) 130:1363–76. doi: 10.1172/JCI131838
25. Ottosson F, Emami Khoonsari P, Gerl MJ, Simons K, Melander O, Fernandez C, et al. plasma lipid signature predicts incident coronary artery disease. *Int J Cardiol.* (2021) 331:249–54. doi: 10.1016/j.ijcard.2021.01.059
26. Stegemann C, Pechlaner R, Willeit P, Langley SR, Mangino M, Mayr U, et al. Lipidomics profiling and risk of cardiovascular disease in the prospective population-based Bruneck study. *Circulation.* (2014) 129:1821–31. doi: 10.1161/CIRCULATIONAHA.113.002500
27. Zhang W, Gong L, Yang S, Lv Y, Han F, Liu H, Liu L. Lipidomics Profile Changes of Type 2 Diabetes Mellitus with Acute Myocardial Infarction. *Dis Markers*. (2019). 2019. doi: 10.1155/2019/7614715
28. Gencer B, Morrow DA, Braunwald E, Goodrich EL, Hilvo M, Kauhanen D, et al. Plasma ceramide and phospholipid-based risk score and the risk of cardiovascular death in patients after acute coronary syndrome. *Eur J Prev Cardiol.* (2020). doi: 10.1093/eurjpc/zwaa143
29. Sock-Hwee T, Jing Yi C, Bo B, Ong CC, Yang X, Teo L, et al. Circadian and longitudinal lipidomic phenotypes are associated with presymptomatic coronary artery disease in healthy subjects with low-intermediate risk cholesterol profiles | circulation. *Circulation.* (2018) 138:A15581.
30. Mousa A, Naderpoor N, Mellett N, Wilson K, Plebanski M, Meikle PJ, et al. Lipidomic profiling reveals early-stage metabolic dysfunction in overweight or obese humans. *Biochim Biophys Acta Mol Cell Biol Lipids.* (2019) 1864:335–43. doi: 10.1016/j.bbalip.2018.12.014
31. Chaurasia B, Summers SA. Ceramides – lipotoxic inducers of metabolic disorders. *Trends Endocrinol Metab.* (2018) 29:66–7. doi: 10.1016/j.tem.2017.09.005
32. Sokolowska E, Blachnio-Zabielska A. The role of ceramides in insulin resistance. *Front Endocrinol.* (2019) 10:577–577. doi: 10.3389/fendo.2019.00577
33. Yaribeygi H, Bo S, Ruscica M, Sahebkar A. Ceramides and diabetes mellitus: an update on the potential molecular relationships. *Diabetic Med.* (2020) 37:11–9. doi: 10.1111/dme.13943
34. Huang PL, A. comprehensive definition for metabolic syndrome. *Dis Model Mech.* (2009) 2:231–7. doi: 10.1242/dmm.001180
35. Grundy SM. Metabolic syndrome update. *Trends Cardiovasc Med.* (2016) 26:364–73. doi: 10.1016/j.tcm.2015.10.004
36. Hunt KJ, Rg R, Williams K, Haffner SM, Stern MP. National Cholesterol Education Program vs. World Health Organization metabolic syndrome in relation to all-cause and cardiovascular mortality in the San Antonio Heart Study. *Circulation.* (2004) 110:1251–7. doi: 10.1161/01.CIR.0000140762.04598.F9
37. Isomaa B, Almgren P, Tuomi T, Forsén B, Lahti K, Nissén M, et al. Cardiovascular morbidity and mortality associated with the metabolic syndrome. *Diabetes Care.* (2001) 24:683–9. doi: 10.2337/diacare.24.4.683
38. Lakka HM, Laaksonen DE, Lakka TA, Niskanen LK, Kumpusalo E, Tuomilehto J, et al. The metabolic syndrome and total and cardiovascular disease mortality in middle-aged men. *JAMA.* (2002) 288:2709–16. doi: 10.1001/jama.288.21.2709
39. Scuteri A, Laurent S, Cucca F, Cockcroft J, Cunha PG, Mañas LR, et al. Metabolic syndrome across Europe: different clusters of risk factors. *Eur J Prev Cardiol.* (2015) 22:486–91. doi: 10.1177/2047487314525529
40. Gami AS, Witt BJ, Howard DE, Erwin PJ, Gami LA, Somers VK, et al. Metabolic syndrome and risk of incident cardiovascular events and death. A systematic review and meta-analysis of longitudinal studies. *J Am Coll Cardiol.* (2007) 49:403–14. doi: 10.1016/j.jacc.2006.09.032
41. DeBoer MD, Gurka MJ, Golden SH, Musani SK, Sims M, Vishnu A, et al. Independent Associations Between Metabolic Syndrome Severity and Future Coronary Heart Disease by Sex and Race. *J Am Coll Cardiol.* (2017) 69:1204–5. doi: 10.1016/j.jacc.2016.10.088
42. Franco OH, Massaro JM, Civil J, Cobain MR, O'Malley B, D'Agostino RB. Trajectories of entering the metabolic syndrome: the framingham heart study. *Circulation.* (2009) 120:1943–50. doi: 10.1161/CIRCULATIONAHA.109.855817
43. Paredes S, Fonseca L, Ribeiro L, Ramos H, Oliveira JC, Palma I. Novel and traditional lipid profiles in Metabolic Syndrome reveal a high atherogenicity. *Sci Rep.* (2019) 9:11792–11792. doi: 10.1038/s41598-019-48120-5
44. Cho KI Yu J, Hayashi T, Han SH, Koh KK. Strategies to overcome residual risk during statins era. *Circulation J.* (2019). doi: 10.1253/circj.CJ-19-0624
45. Grandl G, Wolfrum C. Hemostasis, endothelial stress, inflammation, and the metabolic syndrome. *Semin Immunopathol.* (2018) 40:215–24. doi: 10.1007/s00281-017-0666-5
46. Merrill AH. Sphingolipid and glycosphingolipid metabolic pathways in the era of sphingolipidomics. *Chem Rev.* (2011) 111:6387–422. doi: 10.1021/cr2002917
47. Iqbal J, Walsh MT, Hammad SM, Hussain MM. Sphingolipids and lipoproteins in health and metabolic disorders. *Trends Endocrinol Metab.* (2017) 28:506–18. doi: 10.1016/j.tem.2017.03.005
48. Merrill AH Jr, Lingrell S, Wang E, Nikolova-Karakashian M, Vales TR, Vance DE. Sphingolipid biosynthesis *de novo* by rat hepatocytes in culture. Ceramide and sphingomyelin are associated with, but not required for, very low density lipoprotein secretion. *J Biol Chem.* (1995) 270:13834–41. doi: 10.1074/jbc.270.23.13834
49. Iqbal J, Walsh MT, Hammad SM, Cuchel M, Tarugi P, Hegele RA, et al. Microsomal triglyceride transfer protein transfers and determines plasma concentrations of ceramide and sphingomyelin but not glycosylceramide. *J Biol Chem.* (2015) 290:25863–75. doi: 10.1074/jbc.M115.659110
50. Kasumov T, Li L, Li M, Gulshan K, Kirwan JP, Liu X, et al. Ceramide as a mediator of non-alcoholic Fatty liver disease and associated atherosclerosis. *PLoS ONE.* (2015). 10:e0126910. doi: 10.1371/journal.pone.0126910
51. Heneghan HM, Huang H, Kashyap SR, Gornik HL, McCullough AJ, Schauer PR, et al. Reduced cardiovascular risk after bariatric surgery is linked to plasma ceramides, apolipoprotein-B100, and ApoB100/A1 ratio. *Surg Obes Relat Dis.* (2013) 9:100–7. doi: 10.1016/j.soard.2011.11.018
52. Ng TW, Ooi EM, Watts GF, Chan DC, Meikle PJ, Barrett PH. Association of plasma ceramides and sphingomyelin with VLDL apoB-100 fractional catabolic rate before and after rosuvastatin treatment. *J Clin Endocrinol Metab.* (2015) 100:2497–501. doi: 10.1210/jc.2014-4348
53. Wallner S, Grandl M, Liebisch G, Peer M, Orsó E, Sigrüner A, et al. oxLDL and eLDL induced membrane microdomains in human macrophages. *PLoS ONE.* (2016) 11:e0166798. doi: 10.1371/journal.pone.0166798
54. Castillo RI, Rojo LE, Henriquez-Henriquez M, Silva H, Maturana A, Villar MJ, et al. From molecules to the clinic: linking schizophrenia and metabolic syndrome through sphingolipids metabolism. *Front Neurosci.* (2016) 10:488–488. doi: 10.3389/fnins.2016.00488
55. Hannun YA, Obeid LM. Sphingolipids and their metabolism in physiology and disease. Nature reviews. *Molecular Cell Biology.* (2018) 19:175–91. doi: 10.1038/nrm.2017.107
56. Yoshizaki F, Nakayama H, Iwahara C, Takamori K, Ogawa H, Iwabuchi K. Role of glycosphingolipid-enriched microdomains in innate immunity: microdomain-dependent phagocytic cell functions. *Biochim Biophys Acta.* (2008) 1780:383–92. doi: 10.1016/j.bbagen.2007.11.004
57. Gagliostro V, Casas J, Caretti A, Abad JL, Tagliavacca L, Ghidoni R, et al. Dihydroceramide delays cell cycle G1/S transition via activation of ER stress and induction of autophagy. *Int J Biochem Cell Biol.* (2012) 44:2135–43. doi: 10.1016/j.biocel.2012.08.025
58. Rao P, Ande A, Sinha N, Kumar A, Kumar S. Effects of cigarette smoke condensate on oxidative stress, apoptotic cell death, and hiv replication in human monocytic cells. *PLoS ONE.* (2016) 11:e0155791. doi: 10.1371/journal.pone.0155791
59. Reginato A, Veras ACC, Baqueiro MDN, Panzarin C, Siqueira BP, Milanski M, et al. The role of fatty acids in ceramide pathways and their influence on hypothalamic regulation of energy balance: a systematic review. *Int J Mol Sci.* (2021) 22. doi: 10.3390/ijms22105357
60. Schütze S, Potthoff K, Machleidt T, Berkovic D, Wiegmann K, Krönke M, et al. activates NF-κB by phosphatidylcholine-specific phospholipase C-induced "Acidic" sphingomyelin breakdown. *Cell.* (1992) 71:765–76. doi: 10.1016/0092-8674(92)90553-O

61. Holland WL, Bikman BT, Wang L-P, Yuguang G, Sargent KM, Bulchand S, et al. Lipid-induced insulin resistance mediated by the proinflammatory receptor TLR4 requires saturated fatty acid-induced ceramide biosynthesis in mice. *J Clin Invest.* (2011) 121:1858–70. doi: 10.1172/JCI43378
62. Berkowitz L, Henríquez MP, Salazar C, Rojas E, Echeverría G, Love GD, et al. Association between serum sphingolipids and eudaimonic well-being in white U.S. adults. Sci Rep. (2021) 11:13139. doi: 10.1038/s41598-021-92576-3
63. Cowart LA. Sphingolipids: players in the pathology of metabolic disease. *Trends Endocrinol Metab.* (2009) 20:34–42. doi: 10.1016/j.tem.2008.09.004
64. Fretts AM, Jensen PN, Hoofnagle A, McKnight B, Howard BV, Umans J, et al. Plasma ceramide species are associated with diabetes risk in participants of the strong heart study. *J Nutr.* (2020) 150:1214–22. doi: 10.1093/jn/nxz259
65. Raichur S, Brunner B, Bielohuby M, Hansen G, Pfenninger A, Wang B, Bruning JC, Larsen PJ, Tennagels N. The role of C16:0 ceramide in the development of obesity and type 2 diabetes: CerS6 inhibition as a novel therapeutic approach. *Mol Metab.* (2019) 21:36–50.
66. Newgard CB, An J, Bain JR, Muehlbauer MJ, Stevens RD, Lien LF, et al. A branched-chain amino acid-related metabolic signature that differentiates obese and lean humans and contributes to insulin resistance. *Cell Metab.* (2009) 9:311–26.
67. Powell DJ, Hajduch E, Kular G, Hundal HS. Ceramide disables 3-phosphoinositide binding to the pleckstrin homology domain of protein kinase B (PKB)/Akt by a PKCzeta-dependent mechanism. *Mol Cell Biol.* (2003) 23:7794–808. doi: 10.1128/MCB.23.21.7794-7808.2003
68. Stratford S, Hoehn KL, Liu F, Summers SA. Regulation of insulin action by ceramide: dual mechanisms linking ceramide accumulation to the inhibition of Akt/protein kinase B. J Biol Chem. (2004) 279:36608–15. doi: 10.1074/jbc.M406499200
69. Chavez JA, Siddique MM, Wang ST, Ching J, Shayman JA, Summers SA. Ceramides and glucosylceramides are independent antagonists of insulin signaling. *J Biol Chem.* (2014) 289:723–34. doi: 10.1074/jbc.M113.522847
70. Chaurasia B, Tippetts T, Monibas R, Liu J, Li Y, Wang L, et al. Targeting a ceramide double bond improves insulin resistance and hepatic steatosis. *Science (New York, NY).* (2019). 365(6451). doi: 10.1126/science.aav3722
71. Yki-Järvinen H. Ceramides: a cause of insulin resistance in nonalcoholic fatty liver disease in both murine models and humans. *Hepatology.* (2020) 71:1499–501. doi: 10.1002/hep.31095
72. Holland WL, Brozinick JT, Wang LP, Hawkins ED, Sargent KM, Liu Y, et al. Inhibition of ceramide synthesis ameliorates glucocorticoid-, saturated-fat-, and obesity-induced insulin resistance. *Cell Metab.* (2007) 5:167–79. doi: 10.1016/j.cmet.2007.01.002
73. Razak Hady H, Błachnio-Zabielska AU, Szczerbiński Ł, Zabielski P, Imierska M, Dadan J, Kretowski AJ. Ceramide Content in Liver Increases Along with Insulin Resistance in Obese Patients. *J Clin Med.* (2019) 8. doi: 10.3390/jcm8122197
74. Margalit M, Shalev Z, Pappo O, Sklair-Levy M, Alper R, Gomori M, et al. Glucocerebroside ameliorates the metabolic syndrome in OB/OB mice. *J Pharmacol Exp Ther.* (2006) 319:105–10. doi: 10.1124/jpet.106.104950
75. Zigmond E, Zangen SW, Pappo O, Sklair-Levy M, Lalazar G, Zolotaryova L, et al. β-Glycosphingolipids improve glucose intolerance and hepatic steatosis of the Cohen diabetic rat. *Am J Physiol Endocrinol Metab.* (2009) 296:E72–8. doi: 10.1152/ajpendo.90634.2008
76. Zigmond E, Tayer-Shifman O, Lalazar G, Ben Ya'acov A, Zangen S, Shasha D, et al. Beta-glycosphingolipids ameliorated non-alcoholic steatohepatitis in the Psammomys obesus model. Journal of Inflammation Research. (2014) 151. doi: 10.2147/JIR.S50508
77. Tagami S, Inokuchi Ji J-i, Kabayama K, Yoshimura H, Kitamura F, Uemura S, et al. Ganglioside GM3 participates in the pathological conditions of insulin resistance. *J Biol Chem.* (2002) 277:3085–92. doi: 10.1074/jbc.M103705200
78. Mallat Z, Tedgui A. Current perspective on the role of apoptosis in atherothrombotic disease. *Circ Res.* (2001) 88:998–1003. doi: 10.1161/hh1001.090571
79. Kobayashi K, Nagata E, Sasaki K, Harada-Shiba M, Kojo S, Kikuzaki H. Increase in secretory sphingomyelinase activity and specific ceramides in the aorta of apolipoprotein E knockout mice during aging. *Biol Pharm Bull.* (2013) 36:1192–6. doi: 10.1248/bpb.b13-00180
80. Ishimaru K, Yoshioka K, Kano K, Kurano M, Saigusa D, Aoki J, et al. Sphingosine kinase-2 prevents macrophage cholesterol accumulation and atherosclerosis by stimulating autophagic lipid degradation. *Sci Rep.* (2019) 9:18329. doi: 10.1038/s41598-019-54877-6
81. Laaksonen R, Ekroos K, Sysi-Aho M, Hilvo M, Vihervaara T, Kauhanen D, et al. Plasma ceramides predict cardiovascular death in patients with stable coronary artery disease and acute coronary syndromes beyond LDL-cholesterol. *Eur Heart J.* (2016) 37:1967–76. doi: 10.1093/eurheartj/ehw148
82. Meeusen JW, Donato LJ, Bryant SC, Baudhuin LM, Berger PB, Jaffe AS. Plasma ceramides a novel predictor of major adverse cardiovascular events after coronary angiography. *Arterioscler Thromb Vasc Biol.* (2018) 38:1933–9. doi: 10.1161/ATVBAHA.118.311199
83. Cheng JM, Suoniemi M, Kardys I, Vihervaara T, de Boer SPM, Akkerhuis KM, et al. Plasma concentrations of molecular lipid species in relation to coronary plaque characteristics and cardiovascular outcome: Results of the ATHEROREMO-IVUS study. *Atherosclerosis.* (2015) 243:560–6. doi: 10.1016/j.atherosclerosis.2015.10.022
84. Wang DD, Toledo E, Hruby A, Rosner BA, Willett WC, Sun Q, et al. Plasma ceramides, mediterranean diet, and incident cardiovascular disease in the PREDIMED trial (prevención con dieta mediterránea). *Circulation.* (2017) 135:2028–40. doi: 10.1161/CIRCULATIONAHA.116.024261
85. Lu YC, Yeh WC, Ohashi PS. LPS/TLR4 signal transduction pathway. *Cytokine.* (2008) 42:145–151. doi: 10.1016/j.cyto.2008.01.006
86. Mobarak E, Håversen L, Manna M, Rutberg M, Levin M, Perkins R, et al. Glucosylceramide modifies the LPS-induced inflammatory response in macrophages and the orientation of the LPS/TLR4 complex *in silico*. *Sci Rep.* (2018) 8:13600. doi: 10.1038/s41598-018-31926-0
87. Arai T, Bhunia AK, Chatterjee S, Bulkley GB. Lactosylceramide stimulates human neutrophils to upregulate Mac-1 adhere to endothelium, and generate reactive oxygen metabolites *in vitro*. *Circ Res.* (1998) 82:540–7. doi: 10.1161/01.RES.82.5.540
88. Chatterjee S. Oxidized low density lipoproteins and lactosylceramide both stimulate the expression of proliferating cell nuclear antigen and the proliferation of aortic smooth muscle cells. *Indian Journal of Biochemistry and Biophysics.* (1997) 34:56–60.
89. Edsfeldt A, Dunér P, Stahlman M, Mollet IG, Asciutto G, Grufman H, et al. Sphingolipids contribute to human atherosclerotic plaque inflammation. *Arterioscler Thromb Vasc Biol.* (2016) 36:1132–40. doi: 10.1161/ATVBAHA.116.305675
90. Gong N, Wei H, Chowdhury SH, Chatterjee S. Lactosylceramide recruits PKCalpha/epsilon and phospholipase A2 to stimulate PECAM-1 expression in human monocytes and adhesion to endothelial cells. *Proc Natl Acad Sci U S A.* (2004) 101:6490–5. doi: 10.1073/pnas.0308684101
91. Chatterjee S, Bedja D, Mishra S, Amuzie C, Avolio A, Kass DA, et al. Inhibition of glycosphingolipid synthesis ameliorates atherosclerosis and arterial stiffness in apolipoprotein E-/- mice and rabbits fed a high-fat and -cholesterol diet. *Circulation.* (2014) 129:2403–13. doi: 10.1161/CIRCULATIONAHA.113.007559
92. Prokazova NV, Mikhailenko IA, Bergelson LD. Ganglioside GM3 stimulates the uptake and processing of low density lipoproteins by macrophages. *Biochem Biophys Res Commun.* (1991) 177:582–7. doi: 10.1016/0006-291X(91)92023-D
93. Stith JL, Velazquez FN, Obeid LM. Advances in determining signaling mechanisms of ceramide and role in disease. *J Lipid Res.* (2019) 60:913–8. doi: 10.1194/jlr.S092874
94. Haimovitz-Friedman A, Kolesnick RN, Fuks Z. Ceramide signaling in apoptosis. *Br Med Bull.* (1997) 53:539–53. doi: 10.1093/oxfordjournals.bmb.a011629
95. Hakomori S. Structure, organization, and function of glycosphingolipids in membrane. *Curr Opin Hematol.* (2003) 10:16–24. doi: 10.1097/00062752-200301000-00004
96. Zhang T, Waard AAd, Wuhrer M, Spaapen RM. The role of glycosphingolipids in immune cell functions. *Front Immunol.* (2019) 10:90. doi: 10.3389/fimmu.2019.00090
97. Iwabuchi K. Involvement of glycosphingolipid-enriched lipid rafts in inflammatory responses. *Front Biosci. (Landmark edition).* (2015) 20:325–34. doi: 10.2741/4312
98. Chatterjee S, Balram A, Li W. Convergence: Lactosylceramide-Centric Signaling Pathways Induce Inflammation, Oxidative Stress, and Other Phenotypic Outcomes. Int J Mol Sci. (2021) 22. doi: 10.3390/ijms22041816

99. Walters MJ, Wrenn SP. Effect of Sphingomyelinase-mediated generation of ceramide on aggregation of low-density lipoprotein. *Langmuir.* (2008) 24:9642–7. doi: 10.1021/la800714w
100. Walters MJ, Wrenn SP. Mechanistic roles of lipoprotein lipase and sphingomyelinase in low density lipoprotein aggregation. *J Colloid Interface Sci.* (2011) 363:268–74. doi: 10.1016/j.jcis.2011.07.072
101. Schissel SL, Tweedie-Hardman J, Rapp JH, Graham G, Williams KJ, Tabas I. Rabbit aorta and human atherosclerotic lesions hydrolyze the sphingomyelin of retained low-density lipoprotein: Proposed role for arterial-wall sphingomyelinase in subendothelial retention and aggregation of atherogenic lipoproteins. *J Clin Invest.* (1996) 98:1455–64. doi: 10.1172/JCI118934
102. Li W, Yang X, Xing S, Bian F, Yao W, Bai X, et al. Endogenous ceramide contributes to the transcytosis of oxldl across endothelial cells and promotes its subendothelial retention in vascular wall. *Oxid Med Cell Longev*. (2014) 2014. doi: 10.1155/2014/823071
103. Gao D, Pararasa C, Dunston CR, Bailey CJ, Griffiths HR. Palmitate promotes monocyte atherogenicity via *de novo* ceramide synthesis. *Free Radic Biol Med.* (2012) 53:796–806. doi: 10.1016/j.freeradbiomed.2012.05.026
104. Chaurasia B, Kaddai VA, Lancaster GI, Henstridge DC, Sriram S, Galam DL, et al. Adipocyte Ceramides Regulate Subcutaneous Adipose Browning, Inflammation, and Metabolism. *Cell Metab*. (2016) 24:820–34. doi: 10.1016/j.cmet.2016.10.002
105. Summers SA, Chaurasia B, Holland WL. Metabolic Messengers: ceramides. Nat Metab. (2019) 1:1051–8. doi: 10.1038/s42255-019-0134-8
106. Novgorodov SA, Riley CL, Yu J, Keffler JA, Clarke CJ, Van Laer AO, Baicu CF, et al. Lactosylceramide contributes to mitochondrial dysfunction in diabetes. *J Lipid Res.* (2016) 57:546–62. doi: 10.1194/jlr.M060061
107. Rambold AS, Pearce EL. Mitochondrial dynamics at the interface of immune cell metabolism and function. *Trends Immunol*. (2018) 39:6–18. doi: 10.1016/j.it.2017.08.006
108. Bhunia AK, Han H, Snowden A, Chatterjee S. Redox-regulated signaling by lactosylceramide in the proliferation of human aortic smooth muscle cells. *J Biol Chem.* (1997) 272:15642–9. doi: 10.1074/jbc.272.25.15642
109. Garner B, Priestman DA, Stocker R, Harvey DJ, Butters TD, Platt FM. Increased glycosphingolipid levels in serum and aortae of apolipoprotein E gene knockout mice. *J Lipid Res.* (2002) 43:205–14. doi: 10.1016/S0022-2275(20)30162-0
110. Castoldi A, Monteiro LB, van Teijlingen Bakker N, Sanin DE, Rana N, Corrado M, et al. Triacylglycerol synthesis enhances macrophage inflammatory function. *Nat Commun*. (2020). 11:4107. doi: 10.1038/s41467-020-17881-3
111. Mishra S, Bedja D, Amuzie C, Avolio A, Chatterjee S. Prevention of cardiac hypertrophy by the use of a glycosphingolipid synthesis inhibitor in ApoE-/- mice. *Biochem Biophys Res Commun*. (2015) 46:159–64. doi: 10.1016/j.bbrc.2015.07.159
112. Fiorelli S, Anesi A, Porro B, Cosentino N, Werba JP, Di Minno A, et al. Lipidomics analysis of monocytes from patients with acute myocardial infarction reveals lactosylceramide as a new player in monocyte migration. *Faseb j.* (2021). 35:e21494. doi: 10.1096/fj.202001872RRR
113. Bhunia AK, Arai T, Bulkley G, Chatterjee S. Lactosylceramide mediates tumor necrosis factor-alpha-induced intercellular adhesion molecule-1 (ICAM-1) expression and the adhesion of neutrophil in human umbilical vein endothelial cells. *J Biol Chem.* (1998) 273:34349–57. doi: 10.1074/jbc.273.51.34349
114. Tan AH, Sanny A, Ng SW, Ho YS, Basri N, Lee AP, et al. Excessive interferon-α signaling in autoimmunity alters glycosphingolipid processing in B cells. *J Autoimmun.* (2018) 89:53–62. doi: 10.1016/j.jaut.2017.11.004
115. Spijkers LJA, van den Akker RFP, Janssen BJA, Debets JJ, De Mey JGR, Stroes ESG, et al. Hypertension is associated with marked alterations in sphingolipid biology: a potential role for ceramide. *PLoS ONE.* (2011) 6:e21817–e21817. doi: 10.1371/journal.pone.0021817
116. Guyton JR, Klemp KF. Development of the Lipid-Rich Core in Human Atherosclerosis. *Arterioscler Thromb Vasc Biol.* (1996) 16:4–11. doi: 10.1161/01.ATV.16.1.4
117. Nicholls M. Plasma ceramides and cardiac risk. *Eur Heart J.* (2017) 38:1359–60. doi: 10.1093/eurheartj/ehx205
118. Buie JNJ, Hammad SM, Nietert PJ, Magwood G, Adams RJ, Bonilha L, et al. Differences in plasma levels of long chain and very long chain ceramides between African Americans and whites: An observational study. *PLoS ONE.* (2019) 14:e0216213–e0216213. doi: 10.1371/journal.pone.0216213
119. Huynh K, Barlow CK, Jayawardana KS, Weir JM, Mellett NA, Cinel M, et al. High-Throughput Plasma Lipidomics: Detailed Mapping of the Associations with Cardiometabolic Risk Factors. *Cell Chemical Biology*. (2019) 26:71–84.e4. doi: 10.1016/j.chembiol.2018.10.008
120. Lemaitre RN Yu C, Hoofnagle A, Hari N, Jensen PN, Fretts AM, et al. Circulating sphingolipids, insulin, HOMA-IR, and HOMA-B: the strong heart family study. *Diabetes.* (2018) 67:1663–72. doi: 10.2337/db17-1449
121. Kim M, Jung S, Lee SH, Lee JH. Association between arterial stiffness and serum L-octanoylcarnitine and lactosylceramide in overweight middle-aged subjects: 3-year follow-up study. *PLoS ONE*. (2015) 10:e0119519. doi: 10.1371/journal.pone.0119519
122. Meikle PJ, Christopher MJ. Lipidomics is providing new insight into the metabolic syndrome and its sequelae. *Curr Opin Lipidol*. (2011) 22:210–5. doi: 10.1097/MOL.0b013e3283453dbe
123. Ramakrishanan N, Denna T, Devaraj S, Adams-Huet B, Jialal I. Exploratory lipidomics in patients with nascent Metabolic Syndrome. *J Diabetes Complications.* (2018) 32:791–4. doi: 10.1016/j.jdiacomp.2018.05.014
124. Gong Ll, Yang S, Zhang W, Han Ff, Lv Yl, Xuan Ll, et al. Discovery of metabolite profiles of metabolic syndrome using untargeted and targeted LC–MS based lipidomics approach. *J Pharm Biomed Anal.* (2020). 177:112848-112848. doi: 10.1016/j.jpba.2019.112848
125. Yin X, Willinger CM, Keefe J, Liu J, Fernández-Ortiz A, Ibáñez B, et al. Lipidomic profiling identifies signatures of metabolic risk. *EBioMedicine.* (2020) 51:102520–102520. doi: 10.1016/j.ebiom.2019.10.046
126. Luukkonen PK, Zhou Y, Sädevirta S, Leivonen M, Arola J, Orešič M, et al. Hepatic ceramides dissociate steatosis and insulin resistance in patients with non-alcoholic fatty liver disease. *J Hepatol.* (2016) 64:1167–75. doi: 10.1016/j.jhep.2016.01.002
127. Wigger L, Cruciani-Guglielmacci C, Nicolas A, Denom J, Fernandez N, Fumeron F, et al. Plasma Dihydroceramides Are Diabetes Susceptibility Biomarker Candidates in Mice and Humans. *Cell Rep.* (2017) 18:2269–79. doi: 10.1016/j.celrep.2017.02.019
128. Chapman MJ, Orsoni A, Tan R, Mellett NA, Nguyen A, Robillard P, et al. LDL subclass lipidomics in atherogenic dyslipidemia: effect of statin therapy on bioactive lipids and dense LDL. *J Lipid Res*. (2020) 61. doi: 10.1194/jlr.P119000543
129. Hyötyläinen T, Orešič M. Optimizing the lipidomics workflow for clinical studies–practical considerations. *Anal Bioanal Chem*. (2015) 407:4973–93.
130. Osei K, Gaillard T. Disparities in cardiovascular disease and type 2 diabetes risk factors in blacks and whites: dissecting racial paradox of metabolic syndrome. Front Endocrinol. (2017) 8:204. doi: 10.3389/fendo.2017.00204
131. Torretta E, Barbacini P, Al-Daghri NM, Gelfi C. Sphingolipids in obesity and correlated co-morbidities: the contribution of gender, age and environment. *Int J Mol Sci*. (2019) 20:5901. doi: 10.3390/ijms20235901
132. Gaillard TR. The metabolic syndrome and its components in African-American women: emerging trends and implications. *Front Endocrinol (Lausanne).* (2017) 8:383. doi: 10.3389/fendo.2017.00383

Conflict of Interest: The authors declare that the research was conducted in the absence of any commercial or financial relationships that could be construed as a potential conflict of interest.

Publisher's Note: All claims expressed in this article are solely those of the authors and do not necessarily represent those of their affiliated organizations, or those of the publisher, the editors and the reviewers. Any product that may be evaluated in this article, or claim that may be made by its manufacturer, is not guaranteed or endorsed by the publisher.

Copyright © 2022 Berkowitz, Cabrera-Reyes, Salazar, Ryff, Coe and Rigotti. This is an open-access article distributed under the terms of the Creative Commons Attribution License (CC BY). The use, distribution or reproduction in other forums is permitted, provided the original author(s) and the copyright owner(s) are credited and that the original publication in this journal is cited, in accordance with accepted academic practice. No use, distribution or reproduction is permitted which does not comply with these terms.

frontiers in Cardiovascular Medicine

ORIGINAL RESEARCH
published: 10 February 2022
doi: 10.3389/fcvm.2022.829877

Monocyte and Macrophage Lipid Accumulation Results in Down-Regulated Type-I Interferon Responses

Lisa Willemsen[1†], Hung-Jen Chen[1†], Cindy P. A. A. van Roomen[1], Guillermo R. Griffith[1], Ricky Siebeler[1], Annette E. Neele[1], Jeffrey Kroon[2], Marten A. Hoeksema[1‡] and Menno P. J. de Winther[1‡]*

[1] Department of Medical Biochemistry, Experimental Vascular Biology, Amsterdam Cardiovascular Sciences, Amsterdam Infection and Immunity, University of Amsterdam, Amsterdam, Netherlands, [2] Department of Experimental Vascular Medicine, Amsterdam Cardiovascular Sciences, University of Amsterdam, Amsterdam, Netherlands

OPEN ACCESS

Edited by:
Wen Dai,
Versiti Blood Research Institute, United States

Reviewed by:
Hanrui Zhang,
Columbia University, United States
Xiaobo Wang,
Columbia University, United States

***Correspondence:**
Menno P. J. de Winther
m.dewinther@amsterdamumc.nl

[†]These authors have contributed equally to this work and share first authorship
[‡]These authors have contributed equally to this work and share last authorship

Specialty section:
This article was submitted to Lipids in Cardiovascular Disease, a section of the journal Frontiers in Cardiovascular Medicine

Received: *06 December 2021*
Accepted: *18 January 2022*
Published: *10 February 2022*

Citation:
Willemsen L, Chen H-J, van Roomen CPAA, Griffith GR, Siebeler R, Neele AE, Kroon J, Hoeksema MA and de Winther MPJ (2022) Monocyte and Macrophage Lipid Accumulation Results in Down-Regulated Type-I Interferon Responses. Front. Cardiovasc. Med. 9:829877. doi: 10.3389/fcvm.2022.829877

Macrophages are critical components of atherosclerotic lesions and their pro- and anti-inflammatory responses influence atherogenesis. Type-I interferons (IFNs) are cytokines that play an essential role in antiviral responses and inflammatory activation and have been shown to promote atherosclerosis. Although the impact of type-I IFNs on macrophage foam cell formation is well-documented, the effect of lipid accumulation in monocytes and macrophages on type-I IFN responses remains unknown. Here we examined IFN stimulated (ISG) and non-ISG inflammatory gene expression in mouse and human macrophages that were loaded with acetylated LDL (acLDL), as a model for foam cell formation. We found that acLDL loading in mouse and human macrophages specifically suppressed expression of ISGs and IFN-β secretion, but not other pro-inflammatory genes. The down regulation of ISGs could be rescued by exogenous IFN-β supplementation. Activation of the cholesterol-sensing nuclear liver X receptor (LXR) recapitulated the cholesterol-initiated type-I IFN suppression. Additional analyses of murine *in vitro* and *in vivo* generated foam cells confirmed the suppressed IFN signaling pathways and suggest that this phenotype is mediated *via* down regulation of interferon regulatory factor binding at gene promoters. Finally, RNA-seq analysis of monocytes of familial hypercholesterolemia (FH) patients also showed type-I IFN suppression which was restored by lipid-lowering therapy and not present in monocytes of healthy donors. Taken together, we define type-I IFN suppression as an athero-protective characteristic of foamy macrophages. These data provide new insights into the mechanisms that control inflammatory responses in hyperlipidaemic settings and can support future therapeutic approaches focusing on reprogramming of macrophages to reduce atherosclerotic plaque progression and improve stability.

Keywords: atherosclerosis, macrophage, monocyte, foam cell formation, cholesterol, inflammation, interferon response, immunometabolism

INTRODUCTION

Cardiovascular disease remains the leading cause of death globally with atherosclerosis as the major underlying cause (1, 2). Atherosclerosis is initiated by endothelial dysfunction caused by conventional risk factors such as hypercholesterolemia, high blood pressure, smoking, a lack of exercise, and an unhealthy diet (3–7). Familial hypercholesterolemia (FH) patients have elevated levels of serum low density lipoprotein (LDL) that have been associated with premature atherosclerosis (1, 3–5). Lifelong LDL cholesterol-lowering treatment effectively reduces cardiovascular events in FH patients.

In atherogenesis, LDL is modified within the arterial wall triggering endothelial and immune cell activation and subsequent recruitment of immune cells like monocytes (8). When monocytes enter the arterial intima, they differentiate into macrophages (9). The complex atherosclerotic microenvironment drives the formation of multiple macrophage subsets, including inflammatory and foamy macrophages (10–14). The various functions that macrophages can acquire are essential for atherosclerotic plaque development, stability and clinical outcome (9, 15, 16).

Macrophages can take up excessive amounts of modified LDL [e.g., oxidized (oxLDL) and acetylated LDL (acLDL)] using scavenging receptors causing macrophage foam cell formation (17). Lipid accumulation in foamy macrophages activate nuclear receptors, including the liver X receptor (LXR) (18). LXRs stimulate lipid efflux *via* upregulation of the lipid ATP-binding cassette transporters ABCA1 and ABCG1, but are also important for macrophage survival and immune responses (19, 20). LXR activation antagonizes NF-κB signaling and its deficiency decreases control of intracellular bacterial growth in macrophages (21).

Under homeostatic conditions, immune cells maintain low-levels of IFN-β in an autocrine fashion that is required for a rapid response to environmental cues, e.g., the production of other type-I IFNs (IFN-α/β) and its downstream signaling pathways (22). Therefore, in response to intra-and extracellular stimulation of pattern recognition receptors (PRR) with foreign substances, immune cells are capable of producing large amounts of type-I IFNs. Once secreted, type-I IFNs bind to their receptors (IFNAR1/2) on nearby cells and thereby leading to the phosphorylation and nuclear translocation of transcription factors such as Signal Transducer and Activator of Transcription (STATs) and IFN regulatory factors (IRFs) (23, 24). IRFs and STATs can form complexes and bind to DNA sequences containing IFN-sensitive response element (ISRE) triggering a diverse group of IFN-stimulated genes (ISGs) with various functions (25). Of note, IRF7 is itself an ISG, but also can bind to the promoter region of *IFNB1* and *IFNA* and thereby serves as one of the key regulators of type-I IFN autocrine feedback loop (26–28).

Studies have investigated the effect of IFN-α/β and its downstream signaling on lipid metabolism in monocytes and macrophages. While evidence suggested that IFN stimulation reduced cholesterol synthesis in macrophages (29), many studies showed type-I IFN exposure triggered cholesterol uptake (30, 31), lipid accumulation (32) and foam cell formation (30, 33). Furthermore, in a mouse model for atherosclerosis, IFN-β treatment accelerated lesion formation whereas myeloid-specific IFNAR1 deletion resulted in a more favorable atherosclerotic phenotype (34), suggesting a pro-atherogenic feature of type-I IFNs. However, the role of lipid exposure and metabolism on the type-I IFN response is still unknown. By defining this mechanistic link, macrophage subsets may be amended toward desired phenotypes using clinical therapeutic agents. In this way, reprogramming of macrophages can be applied to reduce atherosclerotic plaque progression and improve stability.

In this study, we demonstrate that lipid-loaded foamy macrophages of mice and men show perturbated type-I IFN responses caused by defective IFN-β production. This suppressed IFN response can be rescued by exogenous IFN-β treatment. Furthermore, we demonstrate that monocytes of untreated FH patients also show a deactivated IFN signature. In these FH patients, lipid-lowering treatment restored the type-I IFN response. These findings are of considerable interest for the understanding of regulation of macrophages in the context of lipid-related diseases, like atherosclerosis and FH, and viral infections.

MATERIALS AND METHODS

Mice

Ldlr$^{-/-}$ mice (on a C57Bl/6 background) were housed at the Animal Research Institute Amsterdam UMC (ARIA). All mice experiments were conducted after approval of the Committee for Animal Welfare (University of Amsterdam).

Bone Marrow-Derived Macrophages

Bone marrow cells were isolated from the hind limbs of C57Bl/6 mice and cultured in RPMI-1640 medium, with 10% heat inactivated fetal bovine serum (FBS), penicillin (100 U/ml), streptomycin (100 μg/ml), 2 mML-glutamine (all purchased from ThermoFisher), and 15% L929-conditioned medium containing M-CSF. Bone marrow-derived macrophages (BMDMs) were generated by culturing the cells for 7 days. Next, BMDMs were loaded overnight with 50 μg/mL human acetylated LDL (KyvoBio) to induce macrophage foam cell formation, and were the next day stimulated with 10 ng/mL lipopolysaccharide (LPS from *Escherichia coli*; O111:B4; Sigma) or 50 ng/mL rmIFN-β (R&D Systems 8234-MB) as indicated (for 6 or 24 h). For serial dilution experiment, rmIFN-β was applied with the concentration as indicated in the figure. When indicated, BMDMs were stimulated with 2 μM LXR-agonist GW3965 (Sigma) for 17 h.

IFN-β ELISA

Non-foamy and acLDL-loaded BMDMs prepared as described above, followed by LPS stimulation for 6 h. Supernatant were collected and the IFN-β concentration was measured using the mouse IFN-beta DuoSet enzyme-linked immunosorbent assay (ELISA) kit (R&D Systems) according to manufacturer's protocol with no additional dilution.

Human Monocyte-Derived Macrophages

Buffy coats of healthy anonymous blood donors were obtained from Sanquin blood bank in Amsterdam, the Netherlands. All the subjects provided written informed consent. Human monocyte-derived macrophages (hMDMs) were prepared as previously described (35). In short, $CD14^+$ monocytes were isolated with Lymphoprep™ (Axis-Shield) followed by MACS CD14 magnetic beads (Miltenyi) purification. The resulting monocytes were seeded at a density of 0.8 million cells/well on 24-well tissue culture plates (Greiner) and differentiated to macrophages with 50 ng/mL human M-CSF (Miltenyi) for 6 days in Iscove's Modified Dulbecco's Medium (life technology) containing 10% heat-inactivated fetal bovine serum (Gibco), 1% penicillin/streptomycin solution (Gibco) and 1% L-glutamine solution (Gibco). After differentiation, hMDMs were loaded 18 h with 50 μg/mL human acetylated LDL (Invitrogen) followed by 50 ng/mL IFN-β (R&D) stimulation or remained untreated.

Gene Expression Analysis by qPCR

Total RNA was isolated using the GeneJET RNA Purification kit (Thermo). cDNA synthesis was then performed using the iScript cDNA synthesis kit (Biorad), followed by quantitative real-time PCR with Sybr Green Fast Mix. qPCR was performed on a Viia7 Real-time PCR system (Applied Biosystems). The delta-delta Ct ($2^{-\Delta\Delta Ct}$) method was used to calculate the relative fold change of qPCR data using the housekeeping genes: *HPRT1* and *RACK1* for human, and *Actb*, *Gapdh*, and *Ptgs1* for mouse data. Primer sequences are shown in **Supplementary Table 3**.

RNA Sequencing and Bioinformatics for BMDMs

RNA was isolated from BMDMs using the RNeasy Mini Kit (QIAGEN) with DNase treatment. 700 ng RNA was used for Illumina library construction. RNA amplification, cDNA generation, and adaptor ligation were performed using the KAPA mRNA HyperPrep Kit (Roche) following the manufacturer's instructions. Samples were pooled, diluted to 10 nM, and sequenced single-end on an Illumina HiSeq 4,000 system (Illumina) to a depth of ± 20 million reads with a length of 50 base pairs. Reads were aligned to the mouse genome mm10 by STAR 2.5.2b with default settings (36). BAM files were indexed and filtered on MAPQ >15 with v1.3.1 SAMtools (37). Raw tag counts and reads per kilobase million (RPKM) per gene were summed using HOMER2's analyzeRepeats.pl script with default settings and the -noadj or -rpkm options for raw counts and RPKM reporting (38). Differential expression was assessed using the DESeq2 Bioconductor package in an R 3.6.3 environment (39).

Familial Hypercholesterolemic Patients and Healthy Subjects

The study population, design, and further processing of these human study subjects and their samples have been extensively described (40). Briefly, untreated FH patients who indicated to start lipid-lowering therapy (statin, PCSK9 antibody, and/or ezetimibe) according to their treating physician were included. The healthy controls were age, sex, and body mass index (BMI) matched with the FH patients. After inclusion, FH patients fasted for at least 9 h before blood samples were drawn for lipid measurements and monocyte isolation. This was repeated after 12 weeks of lipid-lowering therapy. The healthy controls underwent these procedures once. All participants provided written informed consent. The study protocol was approved by the ethics committee of the Amsterdam UMC and was conducted according to the principles of the Declaration of Helsinki.

RNA Sequencing and Bioinformatics for Human Monocytes

Monocytes were isolated as described above. Monocytes were lysed using TriPure (Sigma Aldrich) and stored at −80°C until further processing. For RNA isolation, 0.2 mL chloroform was added per mL of TriPure. Next, samples were spinned at 12,000 g for 15' at 4°C. Subsequently, the aqueous phase was added to 450 μl isopropanol containing GlycoBlue. Next, tubes were shaken vigorously, chilled for 30 min at −20°C and centrifuged at 12,000 g for 10' at 4°C. RNA pellets were washed twice with 75% ethanol and pellets were air-dried at RT and resuspended in nuclease-free H_2O. RNA-seq libraries were prepared, including rRNA depletion, by using the NEBNext Ultra II Directional RNA Library Prep Kit for Illumina according to manufacturer's instructions. Poly-A containing transcripts were sequenced on an Illumina Novaseq 6,000 instrument to a depth of ± 20 million reads by GenomeScan. Reads were aligned to the human reference genome (hg38) using a short-read aligner based on Burrows-Wheeler Transform with default settings (41). Binary alignment map (BAM) files were sorted on coordinates and indexed with the samtools v1.3 package (37). Normalized read count values were calculated. Differential expression was assessed using the DESeq2 Bioconductor package in an R V.3.6.3 programming environment with gene expression called differential with a false discovery rate (FDR) <0.05 and a median read count >1 in at least one group (39). Presented normalized counts were tested using one-way analysis of variance (ANOVA) followed by Bonferroni's comparisons test.

Genome-Wide Transcriptomic Data Analysis

Upstream regulator analysis and regulatory network analysis were performed on Ingenuity Pathway Analysis (Ingenuity System Inc., USA). Pathway overrepresentation analysis was conducted on Meta scape platform [http://metascape.org; (42)]. Known transcription factor motif analysis on gene subsets was performed by using HOMER (v4.11) with the following setting: findMotis.pl "genelist" -start−200 -end 100 -len 8, 10, 12 (38).

Data Availability

Public transcriptomic data sets used in the current study are available in the Gene Expression Omnibus (GEO): (1) GSE118656: acLDL-loaded BMDMs (43) (2) GSE42061: peritoneal macrophages derived from wildtype or *Apoe*$^{-/-}$ mouse (44), and (3) GSE6054: Monocytes from familial hypercholesterolemia patients (45). RNA-seq data of the BMDMs treated with the LXR-agonist GW3965 or DMSO are deposited in the Gene Expression Omnibus (GEO) under the

accession number: GSE193118. RNA-seq data of the monocytes from familial hypercholesterolemia patients and healthy subjects are deposited in GEO under the accession number: GSE192709 (processed data) and EGA (raw data).

Statistical Analysis

Except genome-wide transcriptomic data, statistical analyses were performed using GraphPad Prism 9.1.0 (GraphPad Software). For single comparison tests, paired or unpaired *t*-tests were applied based on the experiment design. For multiple comparison tests, one-way, two-way analysis of variance (ANOVA) or multiple *t*-tests were conducted on the basis of the addressed question.

RESULTS

Macrophage Foam Cell Formation Leads to Decreased Expression of IFN-β and Its Targets

To determine the effect of macrophage foam cell formation on type-I IFN responses, murine bone marrow cells were differentiated to macrophages (BMDMs) and subsequently treated with acLDL or left untreated as control. Foamy and non-foamy macrophages were subsequently stimulated with IFN-β or kept untreated for 6 h (**Figure 1A**). Macrophage foam cell formation resulted in a significant upregulation of the cholesterol efflux transporter genes *Abca1* and *Abcg1,* compared to non-foamy macrophages, indicating proper foam cell formation (46); (**Figure 1B**). Interestingly, we found that macrophage lipid loading significantly suppressed the transcription of *Ifnb1* (**Figure 1C**), as well as several members of its downstream ISGs, including IFN-induced protein with tetratricopeptide repeats 1 (*Ifit1*), *Ifit3*, *Isg15*, MX dynamin like GTPase 1 (*Mx1*), C-X-C motif chemokine ligand 10 (*Cxcl10*), *Ccl5* and *Cxcl9* (**Figure 1D**; **Supplementary Figure 1A**). Remarkably, most of these differences disappeared after subsequent stimulation with exogenous IFN-β suggesting that foam cells remained responsive to IFN-β, while some differences persisted (**Supplementary Figure 1A**). This cholesterol loading-induced immunomodulation seemed to be IFN-specific since other pro-inflammatory genes, such as *Tnf*, *Cd86*, and *Il6* were not affected (**Figure 1E**). Furthermore, IFN-responsive transcription factors, *Stat1*, *Stat2*, and *Irf7* show the same regulation pattern as the ISGs (**Supplementary Figure 1B**). To test whether IFN-β secretion was down regulated by foam cell formation, we stimulated macrophages with LPS and found IFN-β secretion to be significantly decreased after acLDL-loading compared to controls (**Figure 1F**). This indicates that macrophage foam cell formation hampers the endogenous IFN pathways.

Exogenous IFN-β Treatment Rescues the Cholesterol-Initiated Type-I IFN Suppression

To determine whether the suppression of ISGs was solely caused by the reduced IFN-β production in the context of lipid loading, we tested whether the expression of the ISGs changed when different doses of exogenous IFN-β were applied on foam cells and control macrophages. A concentration range (from 1.5 pg/mL to 50 ng/mL) of IFN-β was administered to acLDL-loaded and untreated mouse BMDMs. In line with our previous observations, acLDL loading increased the expression of *Abca1* and *Abcg1* (**Supplementary Figure 2A**), and many ISGs including *Ifit1*, *Ifit3*, *Isg15*, *Mx1*, *Cxcl10, Stat1*, *Stat2,* and *Irf7* were suppressed by acLDL loading which suppression was rescued by exogenous IFN-β treatment (**Figure 2A**). Moreover, a strong dose-dependent effect of IFN-β on the ISGs was observed, although a few ISGs (*Cxcl9* and *Ccl5*) were not rescued by IFN-β administration (**Supplementary Figure 2B**) whereas the non-ISG pro-inflammatory cytokine *Il6* again showed no differences with or without acLDL loading (**Supplementary Figure 2C**). Previous studies have shown that macrophages maintain constitutive production of low levels of type-I IFNs for rapid response to pathogen activation (22). Our data suggest that lipid-loading disrupts this basal macrophage type-I IFN autocrine/paracrine loop through suppressing the homeostatic production of IFNs.

Stimulation of the Cholesterol-Sensing Nuclear Receptor LXR Recapitulates the Cholesterol-Initiated Type-I IFN Suppression

Liver X receptors (LXRs) are cholesterol-sensing transcription factors regulating lipid metabolism and transport, also impacting on inflammatory signaling in macrophages (19). LXR activation is a classical transcriptional response upon lipid loading (18). To determine whether the cholesterol-initiated type-I IFN suppression might be mediated *via* LXR, a synthetic LXR agonist (GW3965) was administered to BMDMs. Interestingly, LXR activation led to a clear suppression of ISGs, a signature that resembles that of lipid-laden macrophages (**Figure 2B**). This indicates that the lipid-driven type-I IFN suppression may be mediated through LXR activation.

Lipid-Loading Affects the Expression of ISGs Associated With IRF Promoter Motifs

To further explore the underlying mechanism of the lipid-induced IFN suppression, we analyzed the transcriptome of acLDL-treated and untreated BMDMs using a publicly available dataset (GSE118656) (43). In line with our data, we found decreased ISG expression (*Ifit2*, *Isg15*, *Cxcl10*, *Oas1a*, *Irf7*, and *Stat1*) in acLDL-loaded macrophages (**Figure 3A**). Pathway analysis of significantly down regulated genes showed that the responses to IFNs and viral infections were the most affected biological processes (**Figure 3B**), while lipid metabolism was a top hit in the upregulated genes (**Supplementary Figure 3A**). Furthermore, upstream regulator analysis identified IFNs (IFN-α and IFN-γ), type-I IFN receptor (Ifnar), and the transcription factors STAT1, IRF3, and IRF7 as the most inhibited upstream regulators in acLDL-loaded macrophages (**Figure 3C**, green bars). IRF3 and IRF7 are the key transcription factors that mediate the transcription of type-I IFNs (15, 47, 48). The

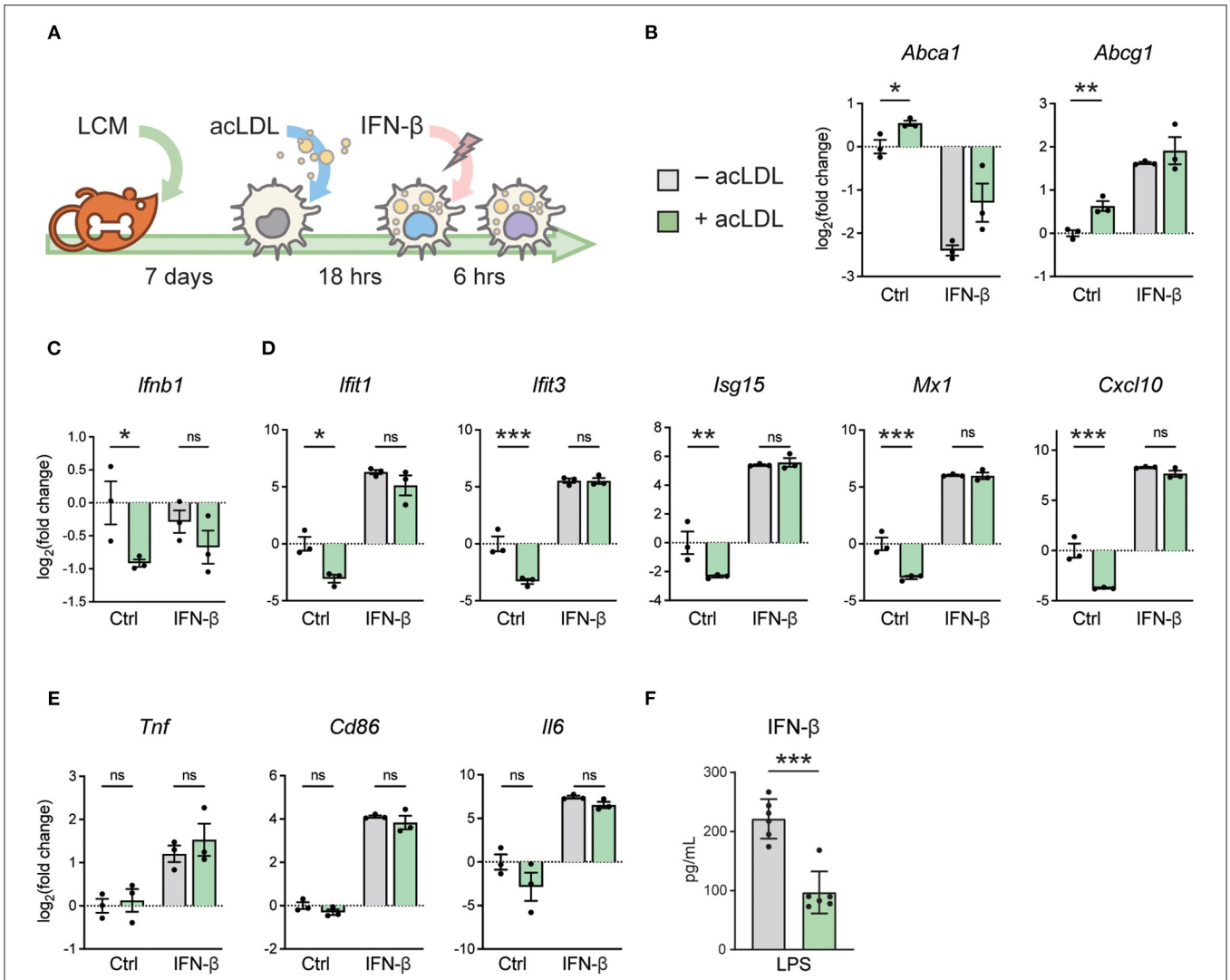

FIGURE 1 | acLDL exposure suppresses type-I IFN gene programs in BMDMs. **(A)** Schematic plot showing the protocol of generating foamy BMDMs with 16-h (50 μg/mL) acLDL exposure. Subsequently, these foamy macrophages were treated with (50 ng/mL) or without IFN-β for 6 h and mRNA expression of type-I interferon genes was determined. **(B)** mRNA expression of the cholesterol efflux transporters *Abca1* and *Abcg1* was measured as a control for lipid loading using qPCR. **(C)** *Ifnb1* mRNA expression of unstimulated, acLDL, and/or IFN-β stimulated BMDMs measured by qPCR. **(D)** *Ifit1*, *Ifit3*, *Isg15*, *Mx1,* and *Cxcl10* mRNA expression of unstimulated, acLDL and/or IFN-β stimulated BMDMs measured by qPCR. **(E)** *Tnf*, *Cd86,* and *Il6* mRNA expression of unstimulated, acLDL and/or IFN-β stimulated BMDMs. **(F)** IFN-β production in supernatant of foamy and non-foamy BMDMs that were stimulated with LPS for 6 h. ns, not significant, $^{*}P < 0.05$, $^{**}P < 0.01$, $^{***}P < 0.001$. **(B–E)** $n = 3$ and **(F)** $n = 6$ biological replicates per group.

importance of IRFs in the lipid-driven type-I IFN suppression was confirmed by a constructed regulatory network of the foamy BMDMs transcriptome (**Supplementary Figure 3C**). Moreover, the anti-inflammatory macrophage-associated upstream regulators SIRT1 (49, 50), SOCS1 (51), and IL-10 receptor (IL10R) (52–54) were activated in the foamy BMDMs (**Figure 3C**, orange bars). Furthermore, studies have shown that these regulatory factors suppress IFN responses (49, 51, 52, 54), confirming the suppressive role of cholesterol accumulation to type-I IFN suppression. Further focusing on the transcriptional control, motif enrichment analysis of down regulated genes in acLDL-loaded BMDMs showed a clear enrichment of genes harboring IRFs and IFN-sensitive response element (ISRE) motifs in the promoter regions (**Figure 3D**). These data suggest that the type-I IFN suppression induced by lipid loading, is likely mediated *via* suppression of the upstream IRFs.

Foamy Peritoneal Macrophages Show a Similar Reduction in ISG Expression

Next, to investigate whether lipid loading affects the macrophage IFN response *in vivo* as well, we analyzed microarray data of foamy macrophages from mice in published datasets (GSE42061) (44). Macrophage foam cell formation increased the expression of *Abca1* and *Abcg1* in peritoneal macrophages from *Apoe*$^{-/-}$

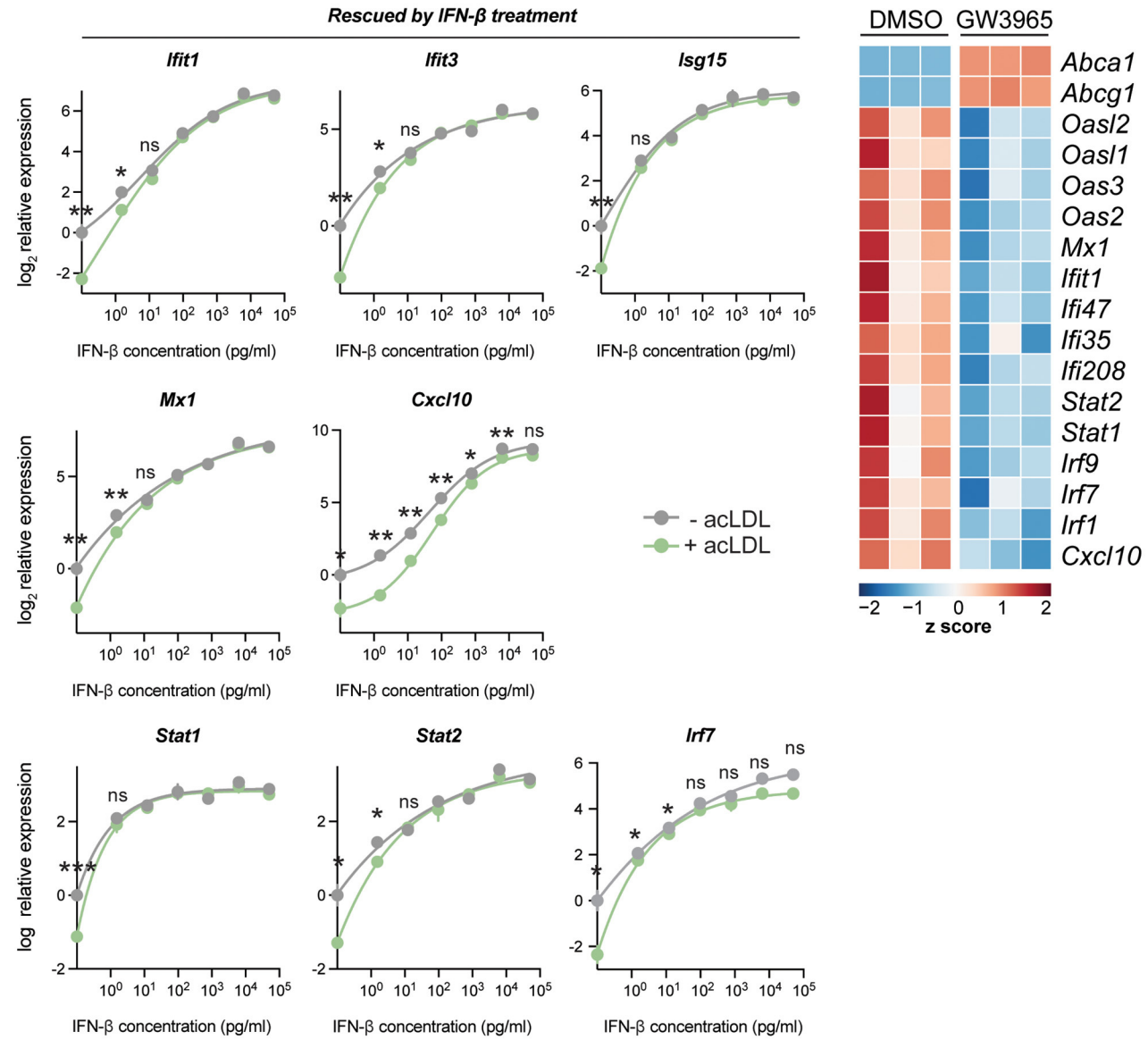

FIGURE 2 | IFN-β exposure reverses acLDL-suppressed type-I interferon response in BMDMs. **(A)** mRNA expression of type-I interferon stimulated genes in BMDMs after a total of 24 h of acLDL exposure combined with different concentrations (1.5 pg/mL to 50 ng/mL) of IFN-β for 6 h of stimulation. The transcriptional suppression of *Cxcl10, Isg15, Ifit1, Ifit3, Stat1, Stat2,* and *Mx1* that was induced by acLDL loading was reversed after IFN-β exposure. **(B)** Heatmap indicating the row z score of the cholesterol loading-responsive genes *Abca1* and *Abcg1*, and genes the type-I interferon response of BMDMs treated with LXR agonist (GW3965) or DMSO for 17 h. **(A,B)** $n = 3$ biological replicates per group. ns, not significant, $^{*}P < 0.05$, $^{**}P < 0.01$.

compared to WT mice (**Figure 3E**). In line with our *in vitro* data, we observed suppression of ISGs in foam cells from *Apoe*$^{-/-}$ mice (**Figure 3E**). Pathway analysis of the down-regulated genes showed suppressed IFN response in the peritoneal macrophages (PMs) derived from hypercholesterolemic mice (**Figure 3F**). Upstream regulator analysis (**Figure 3G**) and motif (**Figure 3H**) analysis indicated lipid-suppressed IFN-signaling *via* IRFs in macrophages. Furthermore, the regulatory network of PMs derived from hypercholesterolemia mice (**Supplementary Figure 3C**) enclosed IRFs, including IRF3 and IRF7, that were highly connected to IFN-β and the affected biological processes. Taken together, our analyses revealed that cholesterol accumulation in macrophages dampens the IFN response, both *in vitro* and *in vivo*, which is likely through suppressing IRF expression and the subsequent type-I IFN production.

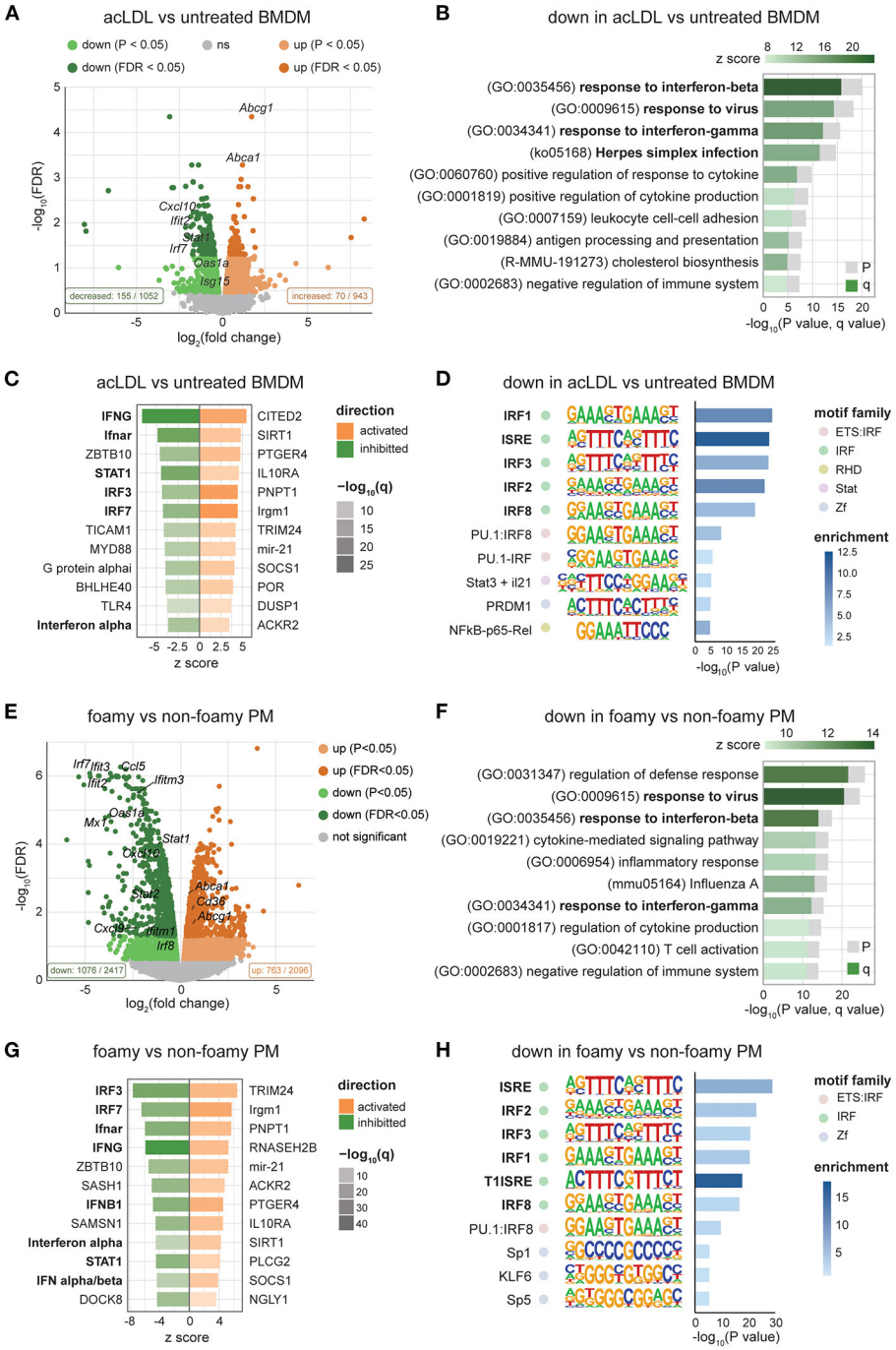

FIGURE 3 | Transcriptomic analysis shows suppressed IFN signaling in foamy macrophages in different mouse models. **(A)** Volcano plot of RNA-seq data showing the log_2FC and -log_{10}(FDR) of acLDL-treated macrophages with downregulated genes in green and upregulated genes in orange. **(B)** Pathway enrichment analysis of significantly downregulated genes (FDR<0.05) in acLDL-loaded macrophages. **(C)** Upstream regulators predicted by the Ingenuity Pathway Analysis (IPA) software of acLDL-loaded vs. untreated macrophages. **(D)** Motif enrichment analysis showed an enrichment of interferon-related motifs among the down-regulated genes in acLDL-loaded macrophages. **(E)** Volcano plot of RNA-seq data showing the log_2FC and -log_{10} (FDR) of peritoneal macrophages (PMs) derived from *Apoe*$^{-/-}$ compared to WT, with downregulated genes in green and upregulated genes in orange. **(F)** Pathway enrichment analysis of significantly downregulated genes (FDR <0.05) in *Apoe*$^{-/-}$ PMs. **(G)** Upstream regulators predicted by the IPA software of *Apoe*$^{-/-}$ vs. WT PMs. **(H)** Motif enrichment analysis showed an enrichment of interferon-related motifs among the down-regulated genes in *Apoe*$^{-/-}$ PMs. **(A–D)** raw data obtained from GSE118656 and **(E–H)** GSE42061.

Cholesterol-Loading in Human Macrophages Suppresses Type-I IFN Response

To translate our findings to human, we applied the same lipid loading strategy using acLDL in hMDMs followed by IFN-β treatment (**Figure 4A**). Cholesterol loading was associated with an expected increased expression of the cholesterol efflux transporters *ABCA1* and *ABCG1* (**Figure 4B**). As we observed in mouse macrophages, cholesterol loading in hMDMs caused a reduced expression of ISGs, including *IFIT1*, *MX1*, *CXCL9,* and *CXCL10* (**Figure 4C**). Genes upstream of ISGs, including *IFNB1* (**Supplementary Figure 4A**) and IFN regulatory factors *IRF3*, *IRF7*, and *IRF8* (**Supplementary Figure 4B**) were also suppressed, supporting the concept of perturbated IFN-autocrine loop by cholesterol accumulation in human macrophages. In line with the mouse data, we did not observe this effect in non-ISG inflammatory genes such as *IL1B*, *IL6*, *CXCL8*, and *TNF*, confirming an IFN signaling-specific effect (**Supplementary Figure 4C**). This indicates that cholesterol loading also hampers the type-I IFN responses in human macrophages.

Lipid Accumulation in Monocytes of Hypercholesterolemia Patients Results in Type-I IFN Suppression Which Is Reversed After Lipid-Lowering Treatment

We have previously shown that peripheral monocytes from FH patients accumulate lipids (55). To determine whether the suppressed IFN signature is also observed in monocytes of FH patients, we performed RNA-seq of peripheral monocytes derived from FH patients before and after lipid-lowering treatment by ezetimibe, statins, and/or PCSK9 antibodies, as well as age and gender-matched healthy donors (**Supplementary Tables 1**, **2**). Indeed, serum LDL-C levels in untreated FH patients were significantly higher than samples obtained after treatment and from healthy donors (**Figure 4D**). RNA-seq analysis confirmed an elevated expression of *ABCA1* and *ABCG1*, whereas ISGs including *IFIT1*, *IFIT3*, *OASL,* and *CXCL10* were suppressed in untreated FH monocytes compared to monocytes from healthy donors (FDR <0.05, **Figure 4E**). Interestingly, the suppressed gene expression of ISGs was restored after lipid-lowering treatment. To confirm these findings in monocytes from another FH patient cohort, we analyzed a publicly available dataset containing expression data of monocytes from FH patients and healthy donors (GSE60514) (45). Differential gene expression analysis showed that many ISGs were down regulated in monocytes derived from FH patients compared to healthy donors (**Supplementary Figure 4D**). Upstream regulator analysis on the differentially regulated genes confirmed inhibition of type-I IFNs, IRFs, and STAT1 (**Figure 4F**). In line with this, motif enrichment analysis identified ISRE as the most enriched promoter motif among the down regulated genes in FH patients (**Figure 4G**). Regulatory network analysis of the differentially expressed genes in monocytes from FH patients revealed STAT1 and IRF7 to be the central modulators of this network (**Figure 4H**). Thus, as observed in macrophages (mouse BMDMs, PMs and hMDMs), lipid accumulation in monocytes of FH patients also results in a deactivated type-I IFN response which can be restored by lipid-lowering therapy.

DISCUSSION

In the current study, we demonstrate that the expression of IFN-β and ISGs are affected by lipid-loading. We show that cholesterol accumulation *in vitro* and *in vivo* suppresses the type-I IFN response in both monocytes and macrophages. This cholesterol loading-induced immunomodulation is also observed by LXR activation and specifically affecting ISGs, but not other pro-inflammatory genes. By applying exogenous IFN-β to macrophages, we showed that the cholesterol-induced decreased ISG expression can be largely restored. Analysis of transcriptional profiles of FH monocytes confirmed this phenotype which was restored by lipid-lowering treatment in FH patients. Moreover, these analyses implicated a profound role of IRFs in the down regulation of type-I IFNs and the subsequent responses.

It has become increasingly clear that foam cell formation suppresses macrophage proinflammatory activation. Studies have shown that foamy peritoneal macrophages are less activated by TLR-ligand stimulation as a result of the accumulation of the LXR ligand desmosterol and suppressed activation of the pentose phosphate pathway (56, 57). Moreover, experiments comparing foamy vs. non-foamy plaque macrophages show that foamy macrophages in atherosclerotic lesions lack clear inflammatory characteristics (11, 13) and have identified LXR as a key transcriptional regulator in these cells (11). Here we show that foam cell formation specifically suppresses ISGs in macrophages, resembling an LXR-activated phenotype. In line with our results, desmosterol depletion in macrophages of atherosclerotic lesions increased the expression of ISGs and promoted the progression of atherosclerosis (58). Type-I IFNs have been shown to have a role in the resolution of inflammation by stimulation of IL-10 production as well as optimal macrophage activation and pro-inflammatory responses (23, 48). Moreover, type-I IFNs are mediators of many different human inflammatory and immune disorders and have also been implicated in atherosclerosis (15, 59). Blockade of type-I IFN signaling in macrophages suppressed atherogenesis, while IFN-β treatment accelerated atherosclerosis through the induction of the chemokine CCL5 which leads to increased monocyte recruitment to plaques (34). Altogether, this suggests that the cholesterol-induced down regulation of type-I IFN pathways is an anti-inflammatory, athero-protective characteristic of foamy macrophages.

Our main finding is that foam cells have reduced *Ifnb1* expression and IFN-β secretion resulting in a suppression of IFN-β-dependent ISG expression. The latter could be overcome by supplying exogenous IFN-β and suggests that at basal conditions there is type I IFN production by *in vitro* macrophages. Although we could not measure the low concentrations of IFN-β secreted by unstimulated macrophages, the rescue of ISG expression by low concentrations of IFN-beta (lower than measurable in our ELISA) does suggest autocrine/paracrine effects of type I IFN.

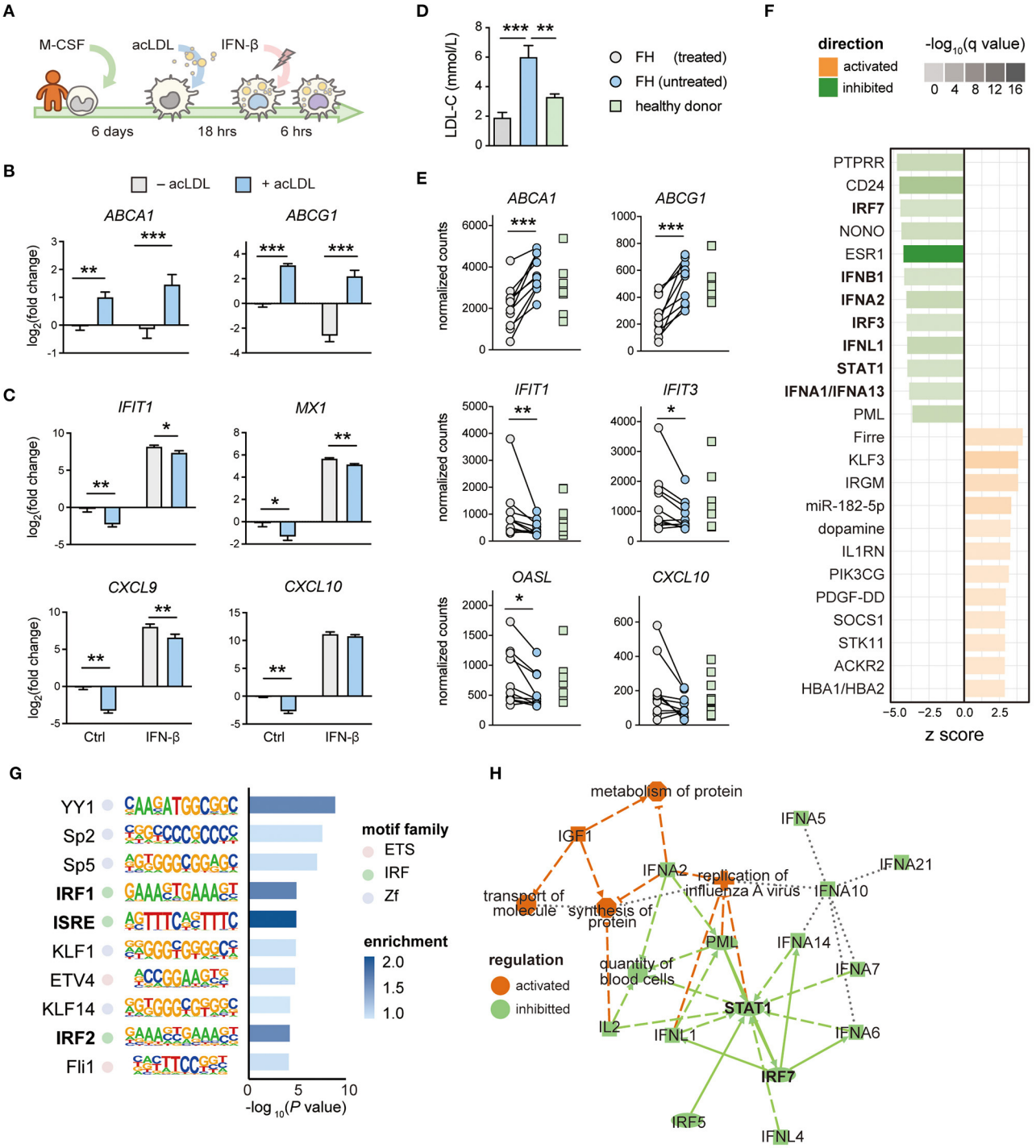

FIGURE 4 | The IFN response is perturbated by lipid accumulation in human macrophages and monocytes from hypercholesterolemia patients. **(A)** Protocol of generating human monocyte-derived (foamy) macrophages (hMDM). Monocytes were differentiated with M-CSF for 6 days followed by 16-h (50 μg/mL) acLDL exposure. Next, the generated foamy hMDM were treated with (50 ng/mL) or without IFN-β for 6 h. **(B)** Cholesterol efflux transporter *ABCA1* and *ABCG1* were transcriptionally up-regulated by acLDL loading in foamy hMDM. **(C)** Interferon stimulated genes (*IFIT1*, *MX1*, *CXCL9,* and *CXCL10*) were transcriptionally downregulated in acLDL-loaded foamy hMDM **(B,C)** $n = 5$ biological replicates, data are represented as mean ± SEM, *FDR <0.05, **FDR <0.01, ***FDR <0.001). **(D)** serum LDL-cholesterol (LDL-C) levels of treated/untreated familial hypercholesterolemia (FH) patients ($n = 10$) and healthy donors (HD, $n = 9$). **(E)** Gene expression of interferon stimulated genes (*IFIT1*, *IFIT3*, *OASL,* and *CXCL10*) from monocytes derived from treated/untreated FH patients and healthy donors. **(F)** Ingenuity Pathway Analysis revealed inhibition of interferon-related upstream regulators, such as IFNs, IRFs, and STAT1, in monocytes derived from FH patients. **(G)** Motif analysis showed an enrichment of the interferon-sensitive response element (ISRE) motif in the promoter region among the downregulated genes in FH monocytes. **(H)** Regulatory network analysis of differentially regulated genes showed an inhibition of highly interconnected IFN signatures. **(F–H)** raw data obtained from GSE6054.

Some ISGs, like *Ccl5* and *Cxcl9,* however, could not be rescued by IFN-β supplementation, which suggests that some IFN targets are regulated in a different manner and may for example utilize different IRFs to regulate gene expression. Future research should investigate whether blocking basal IFN-β production prevents autocrine/paracrine signaling of IFN-β and also leads to suppression of IFN-β-dependent ISG expression.

It has been described that type-I IFNs, including IFN-β, trigger both pro- and anti-inflammatory gene programs (60, 61). We observed this dual characteristic also after acLDL and IFN-β exposure. More specifically, IFN-β treatment suppressed the expression of certain proinflammatory genes (*IL1B* and *CXCL8*), while simultaneously the expression of other proinflammatory genes (*IL6* and *TNF*) was induced. acLDL treatment inhibited the transcription of ISGs, but induced the transcription of *IL1B* and *CXCL8*. This nicely confirms that inflammatory signaling pathways in macrophages can be differentially regulated through numerous interconnected modulatory processes. The cholesterol-mediated type-I IFN suppressive actions may contribute to the cholesterol-induced proinflammatory genes, which are suppressed by IFN, or *vice versa*.

IRFs are important immune orchestrators and not only trigger the transcription of ISGs upon IFN stimulation (23, 48, 62), but are also required for the production of type-I IFNs (63, 64) by recognizing the ISRE at these genes' promoter region (62, 65). IRF3 and IRF7 are highly homologous and are the key transcription factors for type-I IFN expression (63, 64, 66) directly binding to promoter regions (67) of genes encoding both IFN-α and IFN-β (63). In both mouse and human macrophages, cholesterol loading decreased the expression of *IRF3* and *IRF7* suggesting a central role in the suppressed IFN-β production. Interestingly, Chen et al. showed a negative feedback loop between LXR and IRF3 that is activated through LXR stimulation by oxLDL loading or GW3965 treatment of macrophages (68). Furthermore, it has been described that LXR can interact with STAT1 preventing STAT1 to bind to ISGs (69). Taken together, our results suggest a crosstalk between IFNs and cholesterol metabolism forming a feedback loop which might be mediated *via* IRF3 and/or IRF7.

The crosstalk between lipid metabolism and the IFN response could also contribute to the pathogenesis of infections. In the recent pandemic of coronavirus disease 2019 (COVID-19) caused by severe acute respiratory syndrome coronavirus 2 (SARS-CoV-2), disease morbidity and mortality are linked to reduced type-I IFN activities (70–72). Interestingly, *ex vivo* SARS-CoV-2 exposure of peripheral monocytes derived from healthy donors resulted in lipid droplet accumulation (73). Although data is lacking whether FH patients have an increased risk for severe COVID19, a meta-analysis suggested the potential favorable effect of lipid-lowering therapy (e.g., statins) on disease outcome (74). Other studies have indicated that PCSK9 inhibits *IFNB1* expression, and contributes to dampened antiviral cellular responses in Dengue fever patients, which could be abrogated by a PCSK9 inhibitor (75, 76). Because of the IFN enhancing effects of the PCSK9 inhibitor, the PCSK9 inhibitor was proposed as potential therapeutic for the treatment of COVID-19 (77, 78). Our results are in line with this hypothesis and show that lipid-lowering treatment in FH patients rescues the dampened IFN-responses in circulating monocytes. Targeting lipid-metabolism in monocytes using lipid-lowering treatment might thus be beneficial to promote anti-viral defense.

Future studies should investigate the mechanistic link between cholesterol exposure and the subsequent immune response modulations, including the type-I IFN response, in order to integrate these findings in the development of new therapeutic approaches for the treatment of e.g., cardiovascular and infectious disease.

DATA AVAILABILITY STATEMENT

The datasets presented in this study can be found in online repositories. The names of the repository/repositories and accession number(s) can be found below: RNA-seq data of the BMDMs treated with the LXR-agonist GW3965 or DMSO are deposited in the Gene Expression Omnibus (GEO) under the accession number: GSE193118. RNA-seq data of the monocytes from familial hypercholesterolemia patients and healthy subjects are deposited in GEO under the accession number: GSE192709 (processed data) and EGA (raw data).

ETHICS STATEMENT

The studies involving human participants were reviewed and approved by the Amsterdam UMC and was conducted according to the principles of the Declaration of Helsinki. The patients/participants provided their written informed consent to participate in this study. The animal study was reviewed and approved by the Committee for Animal Welfare (University of Amsterdam).

AUTHOR CONTRIBUTIONS

LW, H-JC, MH, and MW designed the research or gave critical input to the design. LW and H-JC performed the majority of experiments with contributions from CR and AN (BMDM experiments), GG (human macrophage experiments), RS (IFN-β ELISA), JK (FH monocytes). LW and H-JC analysed the data and generated graphical representation. LW and H-JC wrote the manuscript and JK, MH, and MW gave critical feedback. MH and MW supervised the study. All authors contributed to the article and approved the submitted version.

FUNDING

This work was supported by the European Union (EU) Horizon 2020 program EPIMAC (SEP-210163258). AN was supported by Amsterdam Cardiovascular Sciences (ACS) and the Netherlands Heart Foundation (Dekker grant 2020T029). JK received a VENI grant from ZonMW (91619098) and a Senior Scientist Dekker grant from the Netherlands Heart Foundation (03-004-2021T045). MH was supported by a Marie Sklodowska Curie Action individual fellowship (MSCA-IF-EF 895411). MW was

supported by Amsterdam UMC, Amsterdam Cardiovascular Sciences, the Netherlands Heart Foundation (CVON GENIUS and GENIUSII 2017-20), Spark-Holding BV (2015B002 and 2019B016), Fondation Leducq (Transatlantic Network Grant No. 16CVD01), and ZonMW (open competition 09120011910025).

ACKNOWLEDGMENTS

We are grateful to all authors and participants of the studies utilized in this work for sharing their transcriptomic data. We would like to thank Dr. M.C.S. Boshuizen for her insights and expertise.

SUPPLEMENTARY MATERIAL

The Supplementary Material for this article can be found online at: https://www.frontiersin.org/articles/10.3389/fcvm.2022.829877/full#supplementary-material

Supplementary Figure 1 | acLDL exposure suppresses interferon-responsive genes and transcription factors in BMDMs. mRNA expression of **(A)** *Cxcl9* and *Ccl5* and **(B)** *Stat1*, *Stat2*, and *Irf7* in unstimulated, acLDL and/or IFN-β (50 ng/mL) stimulated BMDMs measured by qPCR. $^{*}P < 0.05$, $^{**}P < 0.01$, $^{***}P < 0.001$. **(A,B)** $n = 3$ biological replicates per group.

Supplementary Figure 2 | Transcriptional analysis on BMDMs stimulated with different concentration of IFN-β **(A)** mRNA expression of the cholesterol efflux transporters *Abca1* and *Abcg1* in BMDMs after a total of 24 h of acLDL exposure combined with different concentrations (1.5 pg/mL to 50 ng/mL) of IFN-β for 6 h of stimulation. **(B)** the transcriptional inhibition of *Cxcl9* and *Ccl5* that was induced by acLDL loading was unaffected after IFN-β exposure. **(C)** mRNA expression of pro-inflammatory cytokine *Il6* was unaffected by acLDL but induced by IFN-β in a dose-dependent manner. **(A–C)** $n = 3$ biological replicates per group.

Supplementary Figure 3 | Transcriptomic analysis identifies IRFs as important regulators of the suppressed IFN response in foamy macrophages *in vitro* and *in vivo*. **(A)** Pathway enrichment analysis of significantly upregulated genes (FDR <0.05) and **(B)** IPA regulatory network analysis of transcriptional profile in acLDL-loaded macrophages. **(C)** IPA regulatory network analysis of the transcriptional profile of foamy PMs. **(A,B)** GSE118656. **(C)** GSE42061.

Supplementary Figure 4 | The transcription of IFN-independent pro-inflammatory cytokines and chemokines was induced or unaffected by lipid-loading in human macrophages. **(A)** Type-I Interferon (*IFNB1*) and **(B)** interferon regulatory factors (*IRF3*, *IRF7*, and *IRF8*) were transcriptionally downregulated in acLDL-loaded foamy hMDM. **(C)** Gene expression of the non-interferon stimulated genes, *IL1B* and *CXCL8,* was induced in human monocyte-derived macrophages upon lipid loading, but suppressed by IFN-β treatment. Gene expression of *IL6* and *TNF* remained unaltered after acLDL loading ($n = 5$ biological replicates, data are represented as mean ± SEM. **FDR0.01, ***FDR <0.001). **(D)** Volcano plot depicting up- (orange) and down- (green) regulated genes of monocytes derived from familial hypercholesterolemia patients compared to these of healthy donors.

Supplementary Table 1 | Baseline characteristics FH patients and healthy controls.

Supplementary Table 2 | LDL-C lowering effect per individual FH patient.

REFERENCES

1. Defesche JC, Gidding SS, Harada-Shiba M, Hegele RA, Santos RD, Wierzbicki AS. Familial hypercholesterolaemia. *Nat Rev Dis Primers.* (2017) 3:17093. doi: 10.1038/nrdp.2017.93
2. Roth GA, Naghavi M, Murray CJL. Global, regional, and national age-sex-specific mortality for 282 causes of death in 195 countries and territories, 1980–2017: a systematic analysis for the global burden of disease study 2017. *Lancet.* (2018) 392:1736–88.
3. Berenson GS, Srinivasan SR, Bao W, Newman 3rd WP, Tracy RE, Wattigney WA. Association between multiple cardiovascular risk factors and atherosclerosis in children and young adults. Bogalusa heart study. *N Engl J Med.* (1998) 338:1650–6. doi: 10.1056/NEJM199806043382302
4. Crouse JR, Toole JF, McKinney WM, Dignan MB, Howard G, Kahl FR, et al. Risk factors for extracranial carotid artery atherosclerosis. *Stroke.* (1987) 18:990–6. doi: 10.1161/01.STR.18.6.990
5. Fruchart JC, Nierman MC, Stroes ES, Kastelein JJ, Duriez P. New risk factors for atherosclerosis and patient risk assessment. *Circulation.* (2004) 109:Iii15–19. doi: 10.1161/01.CIR.0000131513.33892.5b
6. Glasser SP, Selwyn AP, Ganz P. Atherosclerosis: risk factors and the vascular endothelium. *Am Heart J.* (1996) 131:379–84. doi: 10.1016/S0002-8703(96)90370-1
7. Vogel RA. Coronary risk factors, endothelial function, and atherosclerosis: a review. *Clin Cardiol.* (1997) 20:426–32. doi: 10.1002/clc.4960200505
8. Borén J, Chapman MJ, Krauss RM, Packard CJ, Bentzon JF, Binder CJ, et al. Low-density lipoproteins cause atherosclerotic cardiovascular disease: pathophysiological, genetic, and therapeutic insights: a consensus statement from the European atherosclerosis society consensus panel. *Eur Heart J.* (2020) 41:2313–30. doi: 10.1093/eurheartj/ehz962
9. Moore KJ, Sheedy FJ, Fisher EA. Macrophages in atherosclerosis: a dynamic balance. *Nat Rev Immunol.* (2013) 13:709–21. doi: 10.1038/nri3520
10. Cochain C, Vafadarnejad E, Arampatzi P, Pelisek J, Winkels H, Ley K, et al. Single-cell RNA-Seq reveals the transcriptional landscape and heterogeneity of aortic macrophages in murine atherosclerosis. *Circ Res.* (2018) 122:1661–74. doi: 10.1161/CIRCRESAHA.117.312509
11. Depuydt MAC, Prange KHM, Slenders L, Örd T, Elbersen D, Boltjes A, et al. Microanatomy of the human atherosclerotic plaque by single-cell transcriptomics. *Circ Res.* (2020) 127:1437–55. doi: 10.1161/CIRCRESAHA.120.316770
12. Fernandez DM, Rahman AH, Fernandez NF, Chudnovskiy A, Amir ED, Amadori L, et al. Single-cell immune landscape of human atherosclerotic plaques. *Nat Med.* (2019) 25:1576–88. doi: 10.1038/s41591-019-0590-4
13. Kim K, Shim D, Lee JS, Zaitsev K, Williams JW, Kim W, et al. Transcriptome analysis reveals nonfoamy rather than foamy plaque macrophages are proinflammatory in atherosclerotic murine models. *Circ Res.* (2018) 123:1127–42. doi: 10.1161/CIRCRESAHA.118.312804
14. Winkels H, Ehinger E, Vassallo M, Buscher K, Dinh HQ, Kobiyama K, et al. Atlas of the immune cell repertoire in mouse atherosclerosis defined by single-cell RNA-sequencing and mass cytometry. *Circ Res.* (2018) 122:1675–88. doi: 10.1161/CIRCRESAHA.117.312513
15. Chen H-J, Tas SW, de Winther MPJ. Type-I interferons in atherosclerosis. *J Exp Med.* (2020) 217:e20190459. doi: 10.1084/jem.20190459
16. Willemsen L, de Winther MPJ. Macrophage subsets in atherosclerosis as defined by single-cell technologies. *J Pathol.* (2020) 250:705–14. doi: 10.1002/path.5392
17. Kunjathoor VV, Febbraio M, Podrez EA, Moore KJ, Andersson L, Koehn S, et al. Scavenger receptors class A-I/II and CD36 are the principal receptors responsible for the uptake of modified low density lipoprotein leading to lipid loading in macrophages. *J Biol Chem.* (2002) 277:49982–88. doi: 10.1074/jbc.M209649200
18. Castrillo A, Tontonoz P. Nuclear receptors in macrophage biology: at the crossroads of lipid metabolism and inflammation. *Annu Rev Cell Dev Biol.* (2004) 20:455–80. doi: 10.1146/annurev.cellbio.20.012103.134432
19. Im SS, Osborne TF. Liver x receptors in atherosclerosis and inflammation. *Circ Res.* (2011) 108:996–1001. doi: 10.1161/CIRCRESAHA.110.226878
20. Joseph SB, Bradley MN, Castrillo A, Bruhn KW, Mak PA, Pei L, et al. LXR-dependent gene expression is important for macrophage survival and the innate immune response. *Cell.* (2004) 119:299–309. doi: 10.1016/j.cell.2004.09.032

21. Leopold Wager CM, Arnett E, Schlesinger LS. Macrophage nuclear receptors: emerging key players in infectious diseases. *PLoS Pathog.* (2019) 15:e1007585. doi: 10.1371/journal.ppat.1007585
22. Gough DJ, Messina NL, Clarke CJP, Johnstone RW, Levy DE. Constitutive type I interferon modulates homeostatic balance through tonic signaling. *Immunity.* (2012) 36:166–74. doi: 10.1016/j.immuni.2012.01.011
23. Ivashkiv LB, Donlin LT. Regulation of type I interferon responses. *Nat Rev Immunol.* (2014) 14:36–49. doi: 10.1038/nri3581
24. Zanin N, Viaris de Lesegno C, Lamaze C, Blouin CM. Interferon receptor trafficking and signaling: Journey to the cross roads. *Front Immunol.* (2021) 11:615603. doi: 10.3389/fimmu.2020.615603
25. van Boxel-Dezaire AH, Rani MR, Stark GR. Complex modulation of cell type-specific signaling in response to type I interferons. *Immunity.* (2006) 25:361–72. doi: 10.1016/j.immuni.2006.08.014
26. Hata N, Sato M, Takaoka A, Asagiri M, Tanaka N, Taniguchi T. Constitutive IFN-alpha/beta signal for efficient IFN-alpha/beta gene induction by virus. *Biochem Biophys Res Commun.* (2001) 285:518–25. doi: 10.1006/bbrc.2001.5159
27. Sato M, Suemori H, Hata N, Asagiri M, Ogasawara K, Nakao K, et al. Distinct and essential roles of transcription factors IRF-3 and IRF-7 in response to viruses for IFN-alpha/beta gene induction. *Immunity.* (2000) 13:539–48. doi: 10.1016/S1074-7613(00)00053-4
28. Wittling MC, Cahalan SR, Levenson EA, Rabin RL. Shared and unique features of human interferon-beta and interferon-alpha subtypes. *Front Immunol.* (2021) 11:605673. doi: 10.3389/fimmu.2020.605673
29. Blanc M, Hsieh WY, Robertson KA, Watterson S, Shui G, Lacaze P, et al. Host defense against viral infection involves interferon mediated down-regulation of sterol biosynthesis. *PLoS Biol.* (2011) 9:e1000598. doi: 10.1371/journal.pbio.1000598
30. Li J, Fu Q, Cui H, Qu B, Pan W, Shen N, et al. Interferon-α priming promotes lipid uptake and macrophage-derived foam cell formation: a novel link between interferon-α and atherosclerosis in lupus. *Arthr Rheumatism.* (2011) 63:492–502. doi: 10.1002/art.30165
31. Pulliam L, Calosing C, Sun B, Grunfeld C, Rempel H. Monocyte activation from interferon-α in hiv infection increases acetylated LDL uptake and ROS production. *J Interferon Cytokine Res.* (2014) 34:822–8. doi: 10.1089/jir.2013.0152
32. Wang Z, Wang S, Wang Z, Yun T, Wang C, Wang H. Tofacitinib ameliorates atherosclerosis and reduces foam cell formation in apoE deficient mice. *Biochem Biophys Res Commun.* (2017) 490:194–201. doi: 10.1016/j.bbrc.2017.06.020
33. Boshuizen MC, Hoeksema MA, Neele AE, van der Velden S, Hamers AA, Van den Bossche J, et al. Interferon-β promotes macrophage foam cell formation by altering both cholesterol influx and efflux mechanisms. *Cytokine.* (2016) 77:220–6. doi: 10.1016/j.cyto.2015.09.016
34. Goossens P, Gijbels MJ, Zernecke A, Eijgelaar W, Vergouwe MN, van der Made I, et al. Myeloid type I interferon signaling promotes atherosclerosis by stimulating macrophage recruitment to lesions. *Cell Metab.* (2010) 12:142–53. doi: 10.1016/j.cmet.2010.06.008
35. Chen H-J, Li Yim AYF, Griffith GR, de Jonge WJ, Mannens MAM, Ferrero E, et al. Meta-analysis of in vitro-differentiated macrophages identifies transcriptomic signatures that classify disease macrophages *in vivo*. *Front Immunol.* (2019) 10:2887–7. doi: 10.3389/fimmu.2019.02887
36. Dobin A, Davis CA, Schlesinger F, Drenkow J, Zaleski C, Jha S, et al. STAR: ultrafast universal RNA-seq aligner. *Bioinformatics.* (2013) 29:15–21. doi: 10.1093/bioinformatics/bts635
37. Li H, Handsaker B, Wysoker A, Fennell T, Ruan J, Homer N, et al. The sequence alignment/map format and SAMtools. *Bioinformatics.* (2009) 25:2078–9. doi: 10.1093/bioinformatics/btp352
38. Heinz S, Benner C, Spann N, Bertolino E, Lin YC, Laslo P, et al. Simple combinations of lineage-determining transcription factors prime cis-regulatory elements required for macrophage and B cell identities. *Mol Cell.* (2010) 38:576–89. doi: 10.1016/j.molcel.2010.05.004
39. Love MI, Huber W, Anders S. Moderated estimation of fold change and dispersion for RNA-seq data with DESeq2. *Genome Biol.* (2014) 15:550. doi: 10.1186/s13059-014-0550-8
40. Stiekema LCA, Willemsen L, Kaiser Y, Prange KHM, Wareham NJ, Boekholdt SM, et al. Impact of cholesterol on proinflammatory monocyte production by the bone marrow. *Eur Heart J.* (2021) 42:4309–20. doi: 10.1093/eurheartj/ehab465
41. Langmead B, Salzberg SL. Fast gapped-read alignment with Bowtie 2. *Nat Methods.* (2012) 9:357–9. doi: 10.1038/nmeth.1923
42. Zhou Y, Zhou B, Pache L, Chang M, Khodabakhshi AH, Tanaseichuk O, et al. Metascape provides a biologist-oriented resource for the analysis of systems-level datasets. *Nat Commun.* (2019) 10:1523. doi: 10.1038/s41467-019-09234-6
43. Liebergall SR, Angdisen J, Chan SH, Chang Y, Osborne TF, Koeppel AF, et al. Inflammation triggers liver x receptor-dependent lipogenesis. *Mol Cell Biol.* (2020) 40:e00364–19. doi: 10.1128/MCB.00364-19
44. Lei L, Li H, Yan F, Xiao Y. Hyperlipidemia impaired innate immune response to periodontal pathogen porphyromonas gingivalis in apolipoprotein E knockout mice. *PLoS ONE.* (2013) 8:e71849. doi: 10.1371/journal.pone.0071849
45. Mosig S, Rennert K, Buttner P, Krause S, Lutjohann D, Soufi M, et al. Monocytes of patients with familial hypercholesterolemia show alterations in cholesterol metabolism. *BMC Med Genomics.* (2008) 1:60. doi: 10.1186/1755-8794-1-60
46. Chistiakov DA, Melnichenko AA, Myasoedova VA, Grechko AV, Orekhov AN. Mechanisms of foam cell formation in atherosclerosis. *J Mol Med.* (2017) 95:1153–65. doi: 10.1007/s00109-017-1575-8
47. Jefferies CA. Regulating IRFs in IFN driven disease. *Front Immunol.* (2019) 10:325. doi: 10.3389/fimmu.2019.00325
48. McNab F, Mayer-Barber K, Sher A, Wack A, O'Garra A. Type I interferons in infectious disease. *Nat Rev Immunol.* (2015) 15:87–103. doi: 10.1038/nri3787
49. Jia Y, Han S, Li J, Wang H, Liu J, Li N, et al. IRF8 is the target of SIRT1 for the inflammation response in macrophages. *Innate Immunity.* (2016) 23:188–95. doi: 10.1177/1753425916683751
50. Yoshizaki T, Schenk S, Imamura T, Babendure JL, Sonoda N, Bae EJ, et al. SIRT1 inhibits inflammatory pathways in macrophages and modulates insulin sensitivity. *Am J Physiol Endocrinol Metabolism.* (2009) 298:E419–28. doi: 10.1152/ajpendo.00417.2009
51. Whyte CS, Bishop ET, Rückerl D, Gaspar-Pereira S, Barker RN, Allen JE, et al. Suppressor of cytokine signaling (SOCS)1 is a key determinant of differential macrophage activation and function. *J Leukoc Biol.* (2011) 90:845–54. doi: 10.1189/jlb.1110644
52. Donnelly RP, Dickensheets H, Finbloom DS. The interleukin-10 signal transduction pathway and regulation of gene expression in mononuclear phagocytes. *J Interferon Cytokine Res.* (1999) 19:563–73. doi: 10.1089/107999099313695
53. Joss A, Akdis M, Faith A, Blaser K, Akdis CA. IL-10 directly acts on T cells by specifically altering the CD28 co-stimulation pathway. *Eur J Immunol.* (2000) 30:1683–90. doi: 10.1002/1521-4141(200006)30:6<1683::AID-IMMU1683>3.0.CO;2-A
54. Smith LK, Boukhaled GM, Condotta SA, Mazouz S, Guthmiller JJ, Vijay R, et al. Interleukin-10 directly inhibits CD8(+) T cell function by enhancing N-glycan branching to decrease antigen sensitivity. *Immunity.* (2018) 48:299–312.e295. doi: 10.1016/j.immuni.2018.01.006
55. Bernelot Moens SJ, Neele AE, Kroon J, van der Valk FM, Van den Bossche J, Hoeksema MA, et al. PCSK9 monoclonal antibodies reverse the pro-inflammatory profile of monocytes in familial hypercholesterolaemia. *Euro Heart J.* (2017) 38:1584–93. doi: 10.1093/eurheartj/ehx002
56. Baardman J, Verberk SGS, Prange KHM, van Weeghel M, van der Velden S, Ryan DG, et al. A defective pentose phosphate pathway reduces inflammatory macrophage responses during hypercholesterolemia. *Cell Rep.* (2018) 25:2044–52.e2045. doi: 10.1016/j.celrep.2018.10.092
57. Spann NJ, Garmire LX, McDonald JG, Myers DS, Milne SB, Shibata N, et al. Regulated accumulation of desmosterol integrates macrophage lipid metabolism and inflammatory responses. *Cell.* (2012) 151:138–52. doi: 10.1016/j.cell.2012.06.054
58. Zhang X, McDonald JG, Aryal B, Canfrán-Duque A, Goldberg EL, Araldi E, et al. Desmosterol suppresses macrophage inflammasome activation and protects against vascular inflammation and atherosclerosis. *Proc Natl Acad Sci USA.* (2021) 118:e2107682118. doi: 10.1073/pnas.2107682118
59. López de Padilla CM, Niewold TB. The type I interferons: basic concepts and clinical relevance in immune-mediated inflammatory diseases. *Gene.* (2016) 576:14–21. doi: 10.1016/j.gene.2015.09.058

60. Benveniste EN, Qin H. Type I interferons as anti-inflammatory mediators. *Sci STKE.* (2007) 2007:pe70. doi: 10.1126/stke.4162007pe70
61. Bolívar S, Anfossi R, Humeres C, Vivar R, Boza P, Muñoz C, et al. IFN-β plays both pro- and anti-inflammatory roles in the rat cardiac fibroblast through differential stat protein activation. *Front Pharmacol.* (2018) 9:1368. doi: 10.3389/fphar.2018.01368
62. Levy DE, Kessler DS, Pine R, Reich N, Darnell Jr JE. Interferon-induced nuclear factors that bind a shared promoter element correlate with positive and negative transcriptional control. *Genes Dev.* (1988) 2:383–93. doi: 10.1101/gad.2.4.383
63. Honda K, Takaoka A, Taniguchi T. Type I inteferon gene induction by the interferon regulatory factor family of transcription factors. *Immunity.* (2006) 25:349–60. doi: 10.1016/j.immuni.2006.08.009
64. Honda K, Yanai H, Negishi H, Asagiri M, Sato M, Mizutani T, et al. IRF-7 is the master regulator of type-I interferon-dependent immune responses. *Nature.* (2005) 434:772–7. doi: 10.1038/nature03464
65. Au-Yeung N, Mandhana R, Horvath CM. Transcriptional regulation by STAT1 and STAT2 in the interferon JAK-STAT pathway. *JAK STAT.* (2013) 2:e23931. doi: 10.4161/jkst.23931
66. Barnes BJ, Field AE, Pitha-Rowe PM. Virus-induced heterodimer formation between IRF-5 and IRF-7 modulates assembly of the IFNA enhanceosome in vivo and transcriptional activity of IFNA genes. *J Biol Chem.* (2003) 278:16630–41. doi: 10.1074/jbc.M212609200
67. Ning S, Pagano JS, Barber GN. IRF7: activation, regulation, modification and function. *Genes Immunity.* (2011) 12:399–414. doi: 10.1038/gene.2011.21
68. Chen S, Sorrentino R, Shimada K, Bulut Y, Doherty TM, Crother TR, et al. Chlamydia pneumoniae-induced foam cell formation requires MyD88-dependent and -independent signaling and is reciprocally modulated by liver X receptor activation. *J Immunol.* (2008) 181:7186. doi: 10.4049/jimmunol.181.10.7186
69. Lee JH, Park SM, Kim OS, Lee CS, Woo JH, Park SJ, et al. Differential SUMOylation of LXRalpha and LXRbeta mediates transrepression of STAT1 inflammatory signaling in IFN-gamma-stimulated brain astrocytes. *Mol Cell.* (2009) 35:806–17. doi: 10.1016/j.molcel.2009.07.021
70. Bastard P, Zhang Q, Cobat A, Jouanguy E, Zhang SY, Abel L, et al. Insufficient type I IFN immunity underlies life-threatening COVID-19 pneumonia. *C R Biol.* (2021) 344:19–25. doi: 10.5802/crbiol.36
71. Lei X, Dong X, Ma R, Wang W, Xiao X, Tian Z, et al. Activation and evasion of type I interferon responses by SARS-CoV-2. *Nat Commun.* (2020) 11:3810. doi: 10.1038/s41467-020-17665-9
72. Zhang Q, Bastard P, Liu Z, Le Pen J, Moncada-Velez M, Chen J, et al. Inborn errors of type I IFN immunity in patients with life-threatening COVID-19. *Science.* (2020) 370:eabd4570. doi: 10.1126/science.abd4570
73. Dias SSG, Soares VC, Ferreira AC, Sacramento CQ, Fintelman-Rodrigues N, Temerozo JR, et al. Lipid droplets fuel SARS-CoV-2 replication and production of inflammatory mediators. *PLoS Pathog.* (2020) 16:e1009127. doi: 10.1371/journal.ppat.1009127
74. Kow CS, Hasan SS. Meta-analysis of effect of statins in patients with COVID-19. *Am J Cardiol.* (2020) 134:153–5. doi: 10.1016/j.amjcard.2020.08.004
75. Gan ESHC, Tan DHT, Le TT, Huynh B, Wills NG, Seidah EE, et al. Dengue virus induces PCSK9 expression to alter antiviral responses and disease outcomes. *J Clin Invest.* (2020) 130:5223–34. doi: 10.1172/JCI137536
76. Li Z, Liu Q. Proprotein convertase subtilisin/kexin type 9 inhibits interferon β expression through interacting with ATF-2. *FEBS Lett.* (2018) 592:2323–33. doi: 10.1002/1873-3468.13152
77. Scicali R, Di Pino A, Piro S, Rabuazzo AM, Purrello F. May statins and PCSK9 inhibitors be protective from COVID-19 in familial hypercholesterolemia subjects? *Nutr Metab Cardiovasc Dis.* (2020) 30:1068–9. doi: 10.1016/j.numecd.2020.05.003
78. Vuorio A, Kovanen PT. PCSK9 inhibitors for COVID-19: an opportunity to enhance the antiviral action of interferon in patients with hypercholesterolaemia. *J Int Med.* (2021) 289:749–51. doi: 10.1111/joim.13210

Conflict of Interest: The authors declare that the research was conducted in the absence of any commercial or financial relationships that could be construed as a potential conflict of interest.

Publisher's Note: All claims expressed in this article are solely those of the authors and do not necessarily represent those of their affiliated organizations, or those of the publisher, the editors and the reviewers. Any product that may be evaluated in this article, or claim that may be made by its manufacturer, is not guaranteed or endorsed by the publisher.

Copyright © 2022 Willemsen, Chen, van Roomen, Griffith, Siebeler, Neele, Kroon, Hoeksema and de Winther. This is an open-access article distributed under the terms of the Creative Commons Attribution License (CC BY). The use, distribution or reproduction in other forums is permitted, provided the original author(s) and the copyright owner(s) are credited and that the original publication in this journal is cited, in accordance with accepted academic practice. No use, distribution or reproduction is permitted which does not comply with these terms.

frontiers in Cardiovascular Medicine

MINI REVIEW
published: 14 February 2022
doi: 10.3389/fcvm.2022.777822

Lipid-Laden Macrophages and Inflammation in Atherosclerosis and Cancer: An Integrative View

Miriam Lee-Rueckert[1], *Jani Lappalainen*[1], *Petri T. Kovanen*[1*†] *and Joan Carles Escola-Gil*[2*†]

[1] Wihuri Research Institute, Helsinki, Finland, [2] Institut d'Investigacions Biomèdiques (IIB) Sant Pau and CIBER de Diabetes y Enfermedades Metabólicas Asociadas, Barcelona, Spain

Atherosclerotic arterial plaques and malignant solid tumors contain macrophages, which participate in anaerobic metabolism, acidosis, and inflammatory processes inherent in the development of either disease. The tissue-resident macrophage populations originate from precursor cells derived from the yolk sac and from circulating bone marrow-derived monocytes. In the tissues, they differentiate into varying functional phenotypes in response to local microenvironmental stimulation. Broadly categorized, the macrophages are activated to polarize into proinflammatory M1 and anti-inflammatory M2 phenotypes; yet, noticeable plasticity allows them to dynamically shift between several distinct functional subtypes. In atherosclerosis, low-density lipoprotein (LDL)-derived cholesterol accumulates within macrophages as cytoplasmic lipid droplets thereby generating macrophage foam cells, which are involved in all steps of atherosclerosis. The conversion of macrophages into foam cells may suppress the expression of given proinflammatory genes and thereby initiate their transcriptional reprogramming toward an anti-inflammatory phenotype. In this particular sense, foam cell formation can be considered anti-atherogenic. The tumor-associated macrophages (TAMs) may become polarized into anti-tumoral M1 and pro-tumoral M2 phenotypes. Mechanistically, the TAMs can regulate the survival and proliferation of the surrounding cancer cells and participate in various aspects of tumor formation, progression, and metastasis. The TAMs may accumulate lipids, but their type and their specific roles in tumorigenesis are still poorly understood. Here, we discuss how the phenotypic and functional plasticity of macrophages allows their multifunctional response to the distinct microenvironments in developing atherosclerotic lesions and in developing malignant tumors. We also discuss how the inflammatory reactions of the macrophages may influence the development of atherosclerotic plaques and malignant tumors, and highlight the potential therapeutic effects of targeting lipid-laden macrophages in either disease.

Keywords: atherosclerosis, cancer, inflammation, LDL, macrophages

OPEN ACCESS

Edited by:
Wen Dai,
Versiti Blood Research Institute, United States

Reviewed by:
Xiaobo Wang,
Columbia University, United States
Linzhang Huang,
Fudan University, China
Elda Favari,
University of Parma, Italy
Scott M. Gordon,
University of Kentucky, United States
Michihisa Umetani,
University of Houston, United States

***Correspondence:**
Petri T. Kovanen
petri.kovanen@wri.fi
Joan Carles Escola-Gil
jescola@santpau.cat

† These authors share last authorship

Specialty section:
This article was submitted to Lipids in Cardiovascular Disease, a section of the journal Frontiers in Cardiovascular Medicine

Received: *15 September 2021*
Accepted: *18 January 2022*
Published: *14 February 2022*

Citation:
Lee-Rueckert M, Lappalainen J, Kovanen PT and Escola-Gil JC (2022) Lipid-Laden Macrophages and Inflammation in Atherosclerosis and Cancer: An Integrative View. Front. Cardiovasc. Med. 9:777822. doi: 10.3389/fcvm.2022.777822

INTRODUCTION

Macrophages are a heterogeneous group of effector cells with essential roles in metabolism and host defense in tissues. They are innate immune cells capable of recognizing and clearing dead cells and pathogens, orchestrating inflammatory and healing processes that occur in response to injury. Through a wide variety of functions, macrophages play a central role in organ development

and body homeostasis both in health and disease (1). With the exception of the brain and the intestine, macrophages in other organs originate from 2 sources: the embryonic yolk sac and the bone marrow. Moreover, each organ has its own particular composition of embryonically derived and adult-derived macrophage subsets, and each organ dictates the degree to which circulating monocytes replace resident macrophages after birth (2). Under homeostatic conditions, the embryonically derived and the adult-derived macrophages co-exist but it remains unclear whether macrophages of distinct origins have overlapping or distinct functional imprints within the same tissue. Yet, it is known that whereas macrophages in a specific tissue are mainly seeded during embryonic development, infiltration of monocyte-derived macrophages progressively occurs after birth and, particularly, in response to local inflammatory cues (3). Such extravasation of circulating monocytes across the blood vessel wall, as it occurs in immunoinflammatory diseases like atherosclerosis and cancer, is a multistep event facilitated by several families of endothelial junctional cell adhesion molecules such as intercellular adhesion molecule (ICAM)-1, vascular cell adhesion molecule (VCAM)-1, selectins, and integrins. The complex role of the adhesion molecules facilitating the immune cells trafficking across the endothelium is beyond the scope of this work, and the reader is referred to excellent reviews revisiting this field in the context of atherosclerosis and cancer (4, 5).

Because macrophages generated from recruited blood monocytes can partially replace embryonically derived macrophages with variable kinetics, the ontogeny of tissue-resident macrophages is flexible rather than static (6). The lack of specific markers to discriminate and selectively target macrophages originated from different sources and living in distinct biological microenvironments has represented a technical limitation to functional studies related to macrophage ontogeny. In the following sections, we provide detailed information about the ontogeny of arterial and tumoral macrophages. Because the characterization of the macrophage ontogeny in the various organ tissues is still in its infancy and for simplicity's sake, in further sections of this review we will refer to the entire population of macrophages residing in an atherosclerotic plaque or a tumor as "tissue-resident macrophages" regardless their origins. Thus, they comprise the ones embryonically derived and seeded during the early embryonic stage, those derived from monocytes recruited from circulation at post-natal stages, as well as the multiple generations of macrophages successively derived from them. The role of the extracellular environment within a given tissue is critical for macrophage differentiation and specialization, thereby, irrespective of their ontogeny, tissue-resident macrophages display a high degree of phenotypic and functional plasticity in different tissues and exert multifaceted roles in diseases such as atherosclerosis, cancer, Alzheimer's disease, multiple sclerosis, and diabetes (7). Notably, tissue macrophages can also become lipid-laden cells which, then, exert diverse functions in each disease context (8). A current topic of research is how accumulation of various macrophage subsets and their lipid-laden forms are capable to influence the specific courses of an atherosclerotic lesion and a tumor.

Tissue-resident macrophages can be functionally polarized in response to a cocktail of growth factors and cytokines present in their microenvironment (9). Two distinct phenotypes: the M1 (proinflammatory) classically activated or the M2 (anti-inflammatory) alternatively activated macrophages, have been generated and defined in experimental cell cultures in which the macrophages' responses were evaluated after incubation with interferon gamma and lipopolysaccharide or with interleukin (IL)-4 and IL-13, respectively (9). M1 macrophages are key players in the defense against bacterial infections and rely on glycolysis to meet the rapid energy consumption and cope with a hypoxic tissue microenvironment, while M2 macrophages are rather involved in tissue repair and wound healing and use fatty acid oxidation to fuel their longer-term functions (10). Despite providing a useful framework, this dichotomous classification of macrophages only represents the opposite ends of a wide spectrum of macrophage phenotypes and is an oversimplification of the macrophage diversity occurring in response to different microenvironments *in vivo*. The granulocyte-macrophage colony-stimulating factor (GM-CSF) and the macrophage colony-stimulating factor (M-CSF), widely used to differentiate cultured human monocytes into macrophages, also, respectively, polarize the cells toward M1- and M2-like phenotypes (11), which reflects the complexity of the macrophage nomenclature, also when identifying the heterogeneous subtypes generated *in vitro*.

The remarkable functional plasticity of macrophages in response to microenvironmental stimuli triggering diverse polarization states also involves global changes in the macrophage transcriptome. Such functional plasticity can also modify their evolutionary role from host protection (originally against bacterial infections) into host damage. Prime examples of such possible transformation of macrophages from a friend into a foe are their roles as pathogenic promoters of atherosclerosis and cancer. Importantly, whereas atherosclerosis development directly involves the accumulation of lipids in macrophages, the role of lipid-loaded macrophages in cancer is still poorly understood. Despite intrinsic differences between atherosclerosis and cancer, monocyte accumulation and chronic inflammation are common features. Thereby, early studies on the role of monocytes in atherosclerosis have provided insights into cancer, and vice versa (12), a concept that can be now extended to the monocyte-derived macrophages and the lipid-loaded foam cells generated from them. Moreover, macrophages play critical physiopathological roles in either disease by inducing the formation, growth, and rupture of an atherosclerotic plaque, as well as the initiation, growth, and metastasis of a malignant tumor (**Table 1**).

Excitingly, the modern single-cell omics technologies have revealed enormous cellular heterogeneity of macrophages and other immune/inflammatory cells in advanced atherosclerotic lesions (30–32). The use of these tools has now enabled to perform more detailed transcriptional analyses of macrophages in the atherosclerotic plaques and also in certain solid tumors. In this sense, atherosclerosis and cancer also show resemblance

TABLE 1 | Effects of macrophages during the various developmental stages of atherosclerotic plaques and malignant solid tumors.

Disease stage	Atherosclerotic plaques	Malignant solid tumors
Initiation	The first inflammatory cells to invade an atherosclerotic lesion (as blood monocytes) (13) The major cellular component of inflammatory cell population in atherosclerotic lesions. *Via* uptake of modified-LDL, macrophages become cholesterol-loaded macrophage foam cells, the hallmarks of atherosclerotic lesions (13, 14) Activated intimal macrophages promote local inflammation (14)	Accessory cells in the malignant tumor, which are involved in tumor growth and progression (15) Secretion of chemokines and cytokines that promote development of tumors, such as IL-6, IL-8, and IL-10 (16) Activated TAMs promote local inflammation (15, 16)
Progression	Proteolytic remodeling of the extracellular matrix of the plaque (17, 18) Apoptosis of macrophage foam cells increases plaque size and growth of the atherosclerotic plaque with formation of a necrotic lipid core (19) Thinning of the fibrous cap by expression of MMPs with ensuing formation of the rupture-prone "vulnerable" plaque (17, 18) Promotion of angiogenesis in hypoxic areas of advanced atherosclerotic lesions (20)	Proteolytic remodeling of the extracellular matrix of the tumor (21) Promotion of the proliferation of tumor cells directly by secretion of growth factors, which contributes to the growth of the malignant tumor (21–24) Immune regulation by inhibition of antitumoral responses of T cell-mediated cytotoxicity (15, 16) Facilitation of the motility and intravasation of tumor cells with ensuing promotion of their metastatic spreading (15) Induction of therapeutic resistance (25) Stimulation of endothelial cell proliferation and promotion of neovascularization of the tumor tissue (21)
Regression	Lesional macrophage may egress from the plaque during plaque regression (26, 27)	Anti-tumor immunity response by phagocytosing cancer cells (16, 28, 29)

Note that the phenotype of macrophages residing within an atherosclerotic plaque or a tumor will influence both disease progression or regression depending on how they respond to specific microenvironment signals via polarized and functional programs. These signals include the cocktails of cytokines and growth factors present in the interstitial fluids, as well as the hypoxia and the acidic pH characteristic of the atherosclerotic plaques and malignant tumors.

(33) and call for more complex *in vitro* studies exploiting the modern multicellular-type organoid cultures to meet the current challenges of the microenvironmental plasticity of immune/inflammatory cells, such as the macrophages (34). The recent advances in the knowledge of the complex macrophage diversity, however, also raise important questions about the distinct roles of macrophages of fetal or postnatal origins and their proliferative capacities in the inflammatory microenvironment of an atherosclerotic plaque and a malignant tumor. Here, we will much discuss the roles of M1 and M2 macrophages which represent the two extreme states of phenotypic macrophage polarization. This apparent lack of sophistication regarding the phenotypic diversity and plasticity of macrophages derives from the fact that most of the cell culture studies have been performed by using these *in vitro* generated phenotypes, which hardly find their pure counterparts in the complex tissue environments *in vivo* (35, 36). Despite the plasticity of macrophages, which allows a dynamic modulation as a continuous phenotype, the M1/M2 dichotomy still persists and serves the studies in which the role of macrophages in atherosclerosis and cancer are examined (21, 32).

Based on the current knowledge about the ontogeny and functions of the various macrophage subsets recently achieved by applying novel technologies in mice models and humans, this review aims to compare the relative significance of macrophages and their lipid-loading capacity on the progression of atherosclerosis and cancer. At this point, we need to denote that the traditional view of a "foam cell" has been used to describe the cholesteryl ester-loaded cells present in atherosclerotic lesions given that their abundant cytoplasmic lipid droplets result in a bubbly or "foamy" appearance under the microscope. There is extensive literature on the macrophage foam cells generated during atherosclerosis progression and, accordingly, this term has been specifically used over the years as referring to the cholesterol-loaded cells present in the plaques. Lack of specific immunohistochemistry markers for human monocyte-derived macrophages, smooth muscle cells, and dendritic cells has made it challenging to identify the various subpopulations of cells and their corresponding lipid-laden forms in atherosclerotic lesions (37). Despite it having been reported that vascular smooth muscle cells and dendritic cells also can take up cholesterol-derived from intimal LDL particles and so turn into cholesterol-loaded foam cells, macrophages are considered the primary source of foam cells in atherosclerosis (38–40). More recently, also lipid-laden TAMs have been detected in tumors, however, their lipid cargo appears to be much smaller than that in the macrophage foam cells present in atherosclerotic lesions. Moreover, the accumulated lipids are triglycerides, glycerophospholipids, and sphingomyelins, rather than cholesteryl esters. Based on the above considerations on the conventional terminology, we have applied the term "foamy" only for the macrophages present in atherosclerotic lesions, but not for those present in the malignant tumors, which have been termed "lipid-laden macrophages."

In this respect, it is also important to highlight that the story of macrophages and foam cells in atherosclerosis was initiated more than 100 years ago with the classical studies of the Russian pathologist Nikolai Anitschkow (41). Therefore, cholesterol-loaded macrophage foam cells were very early recognized as the root cause of atherosclerosis and they have been a persistent and central focus of research in this field. In contrast, the research on macrophages and cancer is much younger, moreover, the potential (perhaps relatively less relevant) role of lipid-laden

macrophages in malignant tumors has called the attention of cancer biologists only recently. By revising the recent discoveries on macrophage biology in atherosclerosis and cancer, we hope to disseminate a piece of challenging interdisciplinary information on this particular topic in two diseases, which are the leading causes of death worldwide.

MACROPHAGES IN ATHEROGENESIS: ONTOGENY, CHOLESTEROL LOADING, POLARIZATION, AND FUNCTIONAL PHENOTYPES

Macrophages are the major immune cell population in the atherosclerotic lesion which contribute to the initiation and progression of atherosclerosis through their diverse roles in cholesterol metabolism and inflammation (42). They are the first inflammatory cells to invade atherosclerotic lesions and the main component of atherosclerotic plaques (13). Macrophages that accumulate in atherosclerotic plaques appear to have a diminished capacity to migrate, which contributes to the failure to resolve inflammation and to the progression of these lesions to more advanced plaques (14). For a long period, they were considered to mainly originate from bone marrow- or spleen-derived monocytes, which once in circulation can infiltrate the arterial intima. Monocytes recruited to atherosclerotic lesions are technically identified as $Ly6C^{high}$ cells that originate from both medullary and extramedullary hematopoiesis. The practical use of the $Ly6C^{high}$, principal marker of mouse monocytes, is based on similar features in the expression pattern of certain molecules that the cluster of differentiation $(CD)14^{++}CD16^{-}$ human classical and most abundant monocyte population shares with the $Ly6C^{hi}$ mouse monocytes (43). More recently, with the increased availability of avant-garde technologies, highly diverse cellular communities of macrophages have been detected in advanced human atherosclerotic plaques including a population of tissue macrophages that originates during the embryonic development. Using genetic fate-mapping approaches, it has been shown that arterial macrophages arise embryonically from C-X3-C motif chemokine receptor 1 $(Cx3cr1)^{+}$ precursors and postnatally from bone marrow-derived monocytes that colonize the tissue immediately after birth (44). Thus, arterial macrophages appeared to be early originated from yolk sac-derived erythromyeloid precursors and one additional wave of blood-derived monocytes shortly after birth (45, 46).

Upon atherosclerosis development, the resident macrophages embryonically originated are replaced by or accompanied by recruited monocyte-derived macrophages that adopt a resident-like macrophage phenotype (3). According to studies in mice, the population of yolk sac erythro-myeloid progenitors substantially contributes to the adventitial macrophage population and gives rise to a defined cluster of resident immune cells with homeostatic functions which then declines in numbers during aging and is not replenished by bone marrow-derived macrophages (47). In line with this report, only a minor part of the aortic resident macrophages in adult mice was found to be embryonically derived and they were mainly located in the adventitial layer, whereas the majority of the macrophages which infiltrate the artery around birth arose from monocyte progenitors, thereafter adopting self-renewing capacity (48). The embryonically originated macrophages express high levels of the hyaluronan receptor LYVE-1, which in the adventitia induces collagen degradation by smooth muscle cells, and thereby prevents collagen deposition and arterial stiffness (47, 49).

Whether of bone marrow or embryonic origin, tissue-resident macrophages can closely resemble each other, including the capacity to renew via proliferation (6). Importantly, regardless of their origin, the proliferation of resident macrophages drives the expansion of the atherosclerotic plaque (14). It was recently found that prolonged hypercholesterolemia in the low-density lipoprotein receptor-deficient (*Ldlr-/-)* mouse model led to a complete loss of the resident-derived lipid-laden foam cells, as they were ultimately replaced entirely by recruited blood monocytes, indicating the key role of monocyte recruitment to sustain macrophage proliferation and to allow the expansion of multiple generations of macrophages during plaque progression (48).

Plasma lipoproteins also cross the endothelial barrier into the arterial intima where they are involved in the regulation of macrophage cholesterol balance. Formation of the atherosclerotic lesion in the arterial intima is characterized by accumulation of low-density lipoprotein (LDL)-derived cholesterol in macrophages with the ensuing generation of foam cells, and is associated with chronic inflammatory responses (50). In the intima, LDL particles interact with a dense extracellular matrix network rich in proteoglycans, collagen, and elastin. Particularly, the interaction with proteoglycans initiates LDL retention in the intima (51) and facilitates various types of modifications of LDL particles, which, increase their proatherogenic roles. The non-regulated uptake of modified LDL particles by the CD36 and the SRA1 scavenger receptors in macrophages enables the intracellular accumulation of the cholesterol contained in them (13, 14). Intracellularly, the cholesteryl esters are first hydrolyzed in lysosomes, and then re-esterified in the cytoplasmic compartment of the macrophages where they form microscopically visible cholesteryl ester droplets typical of foam cells, which, again, are the hallmarks of atherosclerotic lesions (52).

In contrast to LDL, the cardioprotective effects of high-density lipoproteins (HDL) are attributed to their ability to enter the arterial intima where they stimulate cholesterol efflux from macrophages, which is mechanistically linked to the HDL anti-inflammatory functions (53). Abundant experimental evidence supports the anti-inflammatory role of cholesterol efflux, which is exemplified by the increase in inflammatory responses in the ATP-binding cassete transporter (ABC)A1/ABCG1-deficient macrophages. It is also known that HDL and other compounds (as cyclodextrins) can produce anti-inflammatory actions by a variety of mechanisms, most of them based on their cholesterol efflux capacities (54). In this context, we have shown that various specific anti-inflammatory mechanisms induced by apoA-I, the main apolipoprotein of HDL, require the intactness of its C-terminal domain, which is critical to bind with high affinity to human coronary artery endothelial cells (55).

Cholesterol efflux can significantly compensate for the excessive influx of LDL-derived cholesterol to the foam cells and stimulate the anti-atherosclerotic pathway known as reverse cholesterol transport (RCT) (56). Thus, disruption of the endothelial barrier by vasoactive compounds in naturally high-HDL murine models *in vivo* has enhanced the passage of HDL into the interstitial fluid of the skin and, thereby, increased the rate of cholesterol transfer from subcutaneously located macrophage foam cells to feces (macrophage-RCT) (57). The most relevant mechanisms of cholesterol efflux involve the ABCA1 and G1, which upon interaction with lipid-poor and mature HDL, respectively, trigger a cascade of events associated with the release of cholesterol and phospholipids from the cell surface (58). Both ABC efflux transporters are overexpressed in cholesterol-loaded macrophages as a result of activation of liver X receptor (LXR)/retinoid X receptor (RXR)–mediated gene transcription (59, 60). Of note, by disrupting specialized cholesterol and sphingomyelin-rich lipid rafts of the macrophage plasma membrane that serve as platforms for inflammatory signaling pathways, cholesterol efflux mediated by the ABC transporters is associated with anti-inflammatory effects and supports the proper functioning of macrophage immune responses (61). ABCA1 in macrophages also functions as an anti-inflammatory signaling receptor through activation of signal transducer and activator of transcription factor (STAT)3, an effect that is independent of the induction of cholesterol efflux (62). Indeed, a recent transcriptome analysis of advanced human atherosclerotic plaques obtained during carotid endarterectomy indicated that macrophages were found in distinct populations with diverse activation patterns and the most anti-inflammatory foam cell–like cluster was characterized by the expression of ABC cholesterol efflux transporters and other lipid-related genes whose expression was most likely driven by intracellular cholesterol accumulation (31).

Although normal veins and arteries have been found not to express ABCA1 mRNA, in the setting of atherosclerosis widespread expression was observed in macrophages within the lesions (63). However, further studies in human endarterectomy specimens revealed that the ABCA1 protein is markedly reduced in the advanced atherosclerotic lesions, thereby suggesting that a failure to translate ABCA1 mRNA into ABCA1 protein, or, alternatively, increased degradation of the ABCA1 protein may occur in the advanced plaques (64, 65). Recently, a novel transcellular movement of cholesterol from cultured macrophage foam cells to adjacent smooth muscle cells has been described to occur even in the absence of HDL (66). An intriguing question remains whether macrophage foam cells within an atherosclerotic plaque could unload at least some of their surplus cholesterol onto adjacent smooth muscle cells. However, the transfer of cholesterol to intimal smooth muscle cells could enhance their conversion into macrophage-like foam cells, and thereby contribute to the pathogenesis of an atherosclerotic plaque (67).

All cell types present in atherosclerotic plaques, including endothelial cells, smooth muscle cells, lymphocytes, and macrophages, undergo apoptosis, and, importantly, apoptotic cell death has been shown to occur in macrophage-rich regions of the plaques. In early lesions, the apoptotic macrophages can be rapidly cleared by adjacent macrophages via a phagocytotic process known as efferocytosis. However, efferocytosis is impaired in advanced atherosclerotic plaques, a defect that is partly attributed to oxidative stress and cytoplasmic saturation with indigestible material (68). A deficient efferocytosis contributes to the formation of the necrotic core, which promotes plaque disruption, particularly by thinning the fibrous cap separating the core from the arterial lumen (19). Progression of the atherosclerotic lesion is also accelerated by degradation of components of the extracellular matrix, such as collagen and elastin in the fibrous cap, by different elastolytic and proteolytic enzymes secreted locally by macrophages and other intimal cells. These enzymes include several matrix metalloproteinases (MMPs) and cysteine proteases secreted by macrophages (17, 18). All these macrophage-dependent effects contribute to the progression of the atherosclerotic lesion, and also render the plaque more vulnerable to rupture with ensuing acute atherothrombotic complications, such as acute myocardial infarction. Moreover, in the deep hypoxic areas of atherosclerotic plaques, intraplaque neoangiogenesis takes place. Indeed, the severity of tissue hypoxia correlates with the presence of macrophages and the expression of the hypoxia-inducible factor (HIF) and the vascular endothelial growth factor (VEGF) in the advanced human atherosclerotic lesions (20). Ruptures of the fragile microvessels generate intraplaque microhemorrhages and further weaken the plaque (**Table 1**).

In the arterial intima, the macrophages adopt different functional programs in response to various polarizing signals. Among them, the colony-stimulating factors GM-CSF and M-CSF can generate disparate proatherogenic and proinflammatory macrophage phenotypes. Notably, immunostained human coronary arteries showed that macrophages with similar antigen expression as induced *in vitro* by M-CSF, i.e., the M2-like macrophage phenotype, were predominant within human atherosclerotic lesions (69). Interestingly, the distribution of macrophage subtypes is not uniform in human atherosclerotic plaques, being M1 macrophages located at the rupture-prone shoulders of mature plaques while the M2 macrophages are away from the lipid core (70). Because GM-CSF and M-CSF are soluble glycoproteins widely expressed in the arterial intima (71) and the formation of cholesterol-loaded macrophage foam cells is intrinsically related to atherogenesis, we recently investigated the effect of cholesterol loading on the expression of key atheroinflammatory genes in cultured human monocyte-derived macrophages differentiated by either CSF (72). We found that, as compared to M1, the M2 macrophage subtype expressed higher levels of CD36 and SRA1 receptors and were particularly prone to foam cell formation. Moreover, the expression of ABCG1 and C-C Motif Chemokine Ligand (CCL)2 in the M2 subtype was markedly lower and higher, respectively. Since the cholesterol efflux transporter ABCG1 also displays anti-inflammatory effects (53) and CCL2 is an early component of the proinflammatory response in atherosclerosis (73), these data indicated that polarization with M-CSF induces proinflammatory traits in macrophages. Interestingly, cholesterol loading of the M2 polarized macrophages strongly

suppressed their proinflammatory features as indicated by 60-fold upregulation of ABCG1 and 2-fold downregulation of CCL2 (72). The finding that cholesterol loading can override the inflammatory profile of M2 polarized macrophages by reprogramming the gene expression levels of both ABCG1 and CCL2 toward an anti-inflammatory phenotype strongly suggests that, in terms of the local atheroinflammatory component of atherogenesis, macrophage foam cell formation may be considered an anti-atherogenic event (72), a concept also supported by other reports (74–77).

Interestingly, a mechanistic link between cholesterol accumulation and suppression of inflammation in macrophages has been suggested due to a regulated accumulation of desmosterol in cells, which is the last intermediate in the pathway of cholesterol biosynthesis (74). A regulated increase of desmosterol underlies the activation of LXR target genes, such as ABCA1 and ABCG1, and suppression of the genes responsible for inflammatory responses, thereby disclosing a mechanistic link between cholesterol accumulation and suppression of macrophage inflammation. Yet, although cholesterol loading reduces the expression of inflammatory genes, the net result could lead to an attenuated inflammatory profile, rather than to an actual anti-inflammatory phenotype of the foam cells. Moreover, the anti-inflammatory mechanisms associated with cholesterol-loading (74) likely appear to operate in macrophages during the initial stages of the development of atherosclerotic lesions. It is not known whether the pathways for the generation of desmosterol or its intracellular distribution are impaired in the end-stage lesional macrophages of advanced atherosclerotic lesions. The further acquisition of a proinflammatory phenotype during advanced atherosclerosis could also depend on extrinsic proinflammatory stimuli within the artery wall. These could include inflammatory mediators derived from endothelial cells or other types of cells in the arterial intima, increased free cholesterol (crystals) deposited within the extracellular matrix, uptake of extracellular cholesterol crystals, and/or exposure to the debris generated by dying cells.

MACROPHAGES IN TUMOR DEVELOPMENT: ONTOGENY, POLARIZATION, PRO- AND ANTI-TUMORAL MACROPHAGES

Abundant macrophage populations are found in the stromal compartment of solid tumors in virtually all types of malignancy (78). Similar to atherosclerosis, circulating monocytes can give rise to tumor-associated macrophages (TAMs), which play critical roles at all stages of tumor progression. Despite the dogma that recruitment of monocytes from the periphery by chemotaxis is the exclusive source of TAMs, it is now known that embryonic-derived TAMs are also present and that they participate in tumor development (28, 79). Moreover, recent evidence shows that at least in certain tumors, tissue-specific embryonically derived resident macrophages infiltrate tumor tissues and, thus, represent a significant input source of TAMs (80). Moreover, the heterogeneous origin of TAMs has been demonstrated in murine pancreatic ductal adenocarcinoma models by identifying that both inflammatory Ly6C^{high} monocytes and tissue-resident macrophages of embryonic origin are sources of TAMs (81). Moreover, the TAMs of different origins demonstrate distinct phenotypes and divergent functionality, i.e., whereas monocyte-derived TAMs are more potent at sampling tumor antigens, embryonically derived TAMs display higher expression of pro-fibrotic factors (81). The dynamic changes in the ontogeny of TAMs during tumor development were also documented in a breast cancer mouse model, in which it was found that mammary tumor growth induced an overall loss of resident macrophages with a concomitant increase in newly arrived monocyte-derived TAMs (82).

Neoplastic cells in solid tumors maintain intricate interactions with their surrounding stroma composed of blood-derived cells including macrophages (up to 50%), T cells, granulocytes, and mast cells, as well as peripheral fibroblasts and epithelial cells (16, 83). Moreover, the primary tumor cells secrete a variety of chemokines, cytokines, and other factors that promote the mobilization and recruitment of various types of blood cells, notably, monocytes, which become TAMs within the tumor microenvironment (16). TAMs are, overall, involved in many activities associated with tumor growth and progression including inflammation, immune regulation, angiogenesis, invasion, and metastasis (15). The important role of TAMs in tumorigenesis is supported by the fact that TAM numbers have been identified to be an independent prognostic factor in several types of cancer, such as in lung cancer, breast cancer, and lymphomas (84). Moreover, a depletion of TAMs has translated into marked clinical benefit in cancer patients, such as in those affected by a diffuse-type giant cell tumor (85). There is also some evidence pointing out that TAMs can mediate resistance of tumor cells to chemotherapy or radiotherapy by activating STAT3 in the tumor cells, which, again, enhances the proliferation and survival of malignant cells even during treatment with various chemotherapeutics (25) (**Table 1**).

Tumor cells secrete factors that prime immune cells, once in the tumor microenvironment, to gain a tumor-supportive phenotype (86). Accordingly, TAMs can become polarized upon receiving signals from the particular microenvironment they reside in and thereby create inflammatory conditions that facilitate the survival and proliferation of cancer cells (21, 87). The recruitment and differentiation progress of TAMs are also related to local anoxia, inflammation, and high levels of lactic acid (16). TAMs are also thought to affect tumor invasion and stromal cell migration through the extracellular matrix, i.e., by deposition of various types of collagen and breakdown of these components via secretion of proteolytic enzymes such as matrix MMPs, serine proteases, and cathepsins (88). However, the interactions between TAMs and cancer cells are still poorly defined, potentially due to different populations of TAMs analyzed in multiple tumor settings. Thus, there are conflicting pieces of evidence about the role of TAMs heterogeneity regarding their pro- and anti-tumoral activities (22). Given the high plasticity of macrophages, the diverse activities of TAMs may also relate to the existence of distinct subpopulations of TAMs, which are associated with different intratumoral microenvironments

(21). As such, many unanswered questions and paradoxical evidence exist regarding the microenvironmental conditions that determine the differentiation of TAMs, resulting in opposed activities. It has been shown that macrophage polarization toward tumor-promoting phenotypes is not exclusively the result of dysfunctional tissue homeostasis, but instead of a more active process driven by reciprocal interactions with both malignant and stromal cells in the tumor, including the effect of a dysregulated tissue architecture in tumors caused by cell deaths (88). Cell-to-cell contacts among TAMs, cancer cells, and other activated stromal cells can be also of great significance in determining the phenotype and functionality of TAMs within a tumor. However, although the TAMs do not become polarized by their location *per se*, the distribution pattern of macrophages between the tumor nest and the tumor stroma, rather than the total number of TAMs, has been reported to be a better independent prognostic factor for the overall survival in gastric cancer patients (89).

Tumors can also secrete the key macrophage growth factors GM-CSF and M-CSF (22–24), and, accordingly, they can act in an autocrine manner driving the proliferation of TAMs. Based on the expression of specific markers, TAMs can be mainly classified into the anti-tumoral M1 phenotype (classically activated state) and the pro-tumoral M2 phenotype (alternatively activated state). TAMs generally have functional properties associated with an M2-like polarization caused by tumor-derived lactic acid or by secretion of immunosuppressive cytokines from different types of cells in the tumor microenvironment (90, 91), which also highlights the role of the macrophage distribution pattern within the tumor tissue. Thus, TAM populations consist of M2 and a small fraction of M1 cells. Overall, whereas the M1 phenotype is associated with intrinsic phagocytosis and enhanced antitumor inflammatory reactions, M2 exerts a repertoire of tumor-promoting capabilities involving immunosuppression, angiogenesis, and neovascularization, as well as stromal activation and remodeling of the extracellular matrix (21). No direct link has been shown between the ontogeny of TAMs and their pro- or anti-tumoral profile. However, a depletion of TAMs induced by myeloablative chemotherapy has been followed by a transient and massive wave of bone marrow-derived monocytes which contributed to the phagocytosis of cancer cells suggesting that such TAMs can be potent effectors of an anti-tumoral response (28). Moreover, macrophages may also act as effector cells by eliminating tumor cells, particularly via induction of antibody-dependent phagocytosis by monoclonal antibodies during cancer therapy (29). Therefore, a dynamic balance appears to exist between the negative (25) and positive (22, 73) effects of TAMs during the course of a given cancer therapy.

Since the M2-like TAMs are considered to exert pro-tumoral activities and the M1-like TAMs can be regarded as anti-tumoral macrophages, a higher M1/M2 ratio in cancer tissue usually signifies a favorable outcome, whereas a lower M1/M2 ratio often indicates poor prognosis in cancer patients (92). Yet, transcriptome data have reported that TAMs actually express overlapping M1 and M2 characteristics, which may be also derived from a dynamic switch from M1- to M2-like TAM phenotype during tumor progression (22). In this context, depending on the type of tumor and the experimental model, the blockade of M-CSF signaling has in most cases attenuated cancer progression, a finding with potentially high clinical relevance for the use of the M-CSF receptor inhibitors as cancer therapeutics (22). Indeed, inhibition of M-CSF by a specific antibody or chemical inhibitors has been shown to significantly suppress tumor angiogenesis and lymphangiogenesis (93).

In tumors, also the cytokines CCL2, CCL11, CCL16, and CCL21 are major determinants of macrophage infiltration and angiogenesis (16). TAMs also produce CCL2, which primarily contributes to the recruitment of macrophages in tumors (16, 94). Research in mouse models and humans has shown that high levels of tumor-derived CCL2 correlate with an increased number of TAMs in the tumor tissue, and also with a poor cancer prognosis (93). Downregulation of CCL2 expression could therefore be considered a promising target by preventing the cancerous tissue from further collecting TAMs (95). In this context, it would be interesting to investigate whether the expression of CCL2 in TAMs is upregulated by M-CSF, as observed in human macrophage foam cells *in vitro* (72). If so, M-CSF inhibitors might be of further value in their clinical use.

EXTRACELLULAR MICROENVIRONMENTS WITHIN AN ATHEROMA AND A TUMOR: SOLUTES DERIVED FROM THE BLOOD AND THE LOCAL CELLS

The vascular endothelium is a semipermeable barrier that regulates the composition of interstitial fluids by an ultrafiltration process, which applies particularly to the various lipoproteins as the largest solutes in the blood. Depending on the needs, the vascular permeability is dynamically regulated to maintain tissue homeostasis, yet, oxidative stress and hypoxia can challenge the normal endothelial permeability (96). In chronic inflammatory diseases such as atherosclerosis and cancer, a cocktail of inflammatory mediators can disrupt the organization of the endothelial junctions leading to their opening and significant loss of the endothelial barrier function (97), among them also the mast cell-derived (98) and macrophage-derived histamine (99). It was reported that the vasoactive substance P may induce gaps in the endothelial junctions of endothelial cells in vessels of the rat trachea that range from 100 to 400 nm (vs. 5–8 nm in basal blood vessels) (100). In this regard, both the endothelium lining of an atherosclerotic plaque and the tumor vasculature possess leaky capillary gaps (101, 102), which facilitates extravasation of plasma lipids that can influence lipid metabolism in the various populations of tissue-resident macrophages.

An enhanced vascular permeability facilitates the passage of plasma lipoproteins like LDL (22–29 nm particle size range) across such dysfunctional endothelial monolayer. Accordingly, in hypercholesterolemia, the transendothelial entry of high levels of circulating proatherogenic cholesterol-laden LDL particles into the arterial wall will increase. Within the subendothelial intima, the LDL particles are retained, become modified, e.g., oxidized, lipolyzed, or proteolyzed, are recognized by scavenger receptors

and are ingested by the macrophages (26). A fraction of the modified LDL particles form aggregates or cholesterol crystals and are taken up by macrophages by means of fluid-phase pinocytosis processes (103, 104). Whichever is the LDL uptake mechanism by macrophages, foam cell formation typically ensues. Finally, inflammatory activation of the endothelial cells in atherosclerosis-prone areas of the arteries where hemodynamic forces induce endothelial cell dysfunction, also facilitates the transendothelial migration of immune cells into the intima and, thereby, accelerates vascular inflammation (105–107).

Cancer develops in a complex tumor microenvironment where the malignant cells and its stroma, including endothelial cells, pericytes, fibroblasts, immune cells, and the extracellular matrix coexist during tumor evolution (108). Regarding cancer progression, disruption of the endothelial barrier by tumor-derived secreted factors, such as VEGF and CCL2, is a critical step in cancer cell extravasation (109). Thus, the weakening of the endothelial junctions facilitates cancer cells to cross the endothelial barrier and colonize other tissues. In this particular instance, atherosclerotic tissue and tumor tissue are at least partly mirror images of each other regarding disease progression: the dysfunctional endothelial barrier of an atherosclerotic lesion allows entry of circulating inflammatory cells into the developing lesion, while a disrupted endothelial barrier in tumor tissue may open the gates to the exit of tumor cells. Regarding atherosclerotic lesions, no significant exit of cells has been observed, albeit some studies have provided evidence of egress of lesional macrophages or macrophage foam cells back into the circulation or to the lymphatic vessels during regression of the lesions (26, 27). Of interest, macrophage efflux from inflammatory sites was shown to occur by proteolytic shedding of the soluble integrin-β2 followed by its binding to the ICAM-1, which blocks its adhesion capacity and enables macrophages to leave the site of inflammation and also limits further leukocyte infiltration (110).

The proper functionality of key metabolic processes mediated by cytoplasmic enzymes and cell membrane receptors operate at pH optimum near 7.3 (111). Notably, both atherosclerosis and cancer are distinguished by anaerobic metabolism and acidosis, where the low pH of the interstitial fluid is regarded as an important denominator. An acidic extracellular pH is found in various inflammatory sites such as various joint diseases and in atherosclerotic lesions, where local hypoxia and acidosis can affect the ongoing immune response (112, 113). In the intimal fluid of advanced carotid plaques, pH values below 6.0 have been reported, and such low pH values were suggested to be a sign of plaque vulnerability (114). Indeed, acidity enhances the proteolytic, lipolytic, and oxidative modifications of LDL, and strongly increases their affinity for extracellular proteoglycans in the arterial intima and also for the pericellular proteoglycans on macrophage surfaces, so favoring both extracellular and intracellular accumulation of cholesterol in atherogenesis (112). Interestingly, a mechanistic switch in the uptake of modified-LDL from scavenger receptor-mediated mechanism to non-specific fluid-phase pinocytosis is likely to occur at acidic pH (115, 116). Regarding the effect of the extracellular pH on the ability of macrophages to release cholesterol, we have found that sole incubation in acidic culture media (down to pH 5.5) reduced ABCA1 mRNA and protein expression in human macrophage foam cells and, thereby impaired their cholesterol efflux capacity (117). In line with this finding, ABCA1 protein has been reported to be markedly reduced in advanced human carotid atherosclerotic lesions, where the intimal fluid most likely has turned acidic (64). A low extracellular pH also decreases the ACAT-dependent cholesterol esterification in cultured human macrophages and results in intracellular accumulation of unesterified (or "free") cholesterol (118), which could eventually lead to apoptotic cell death.

Also within the core of solid tumors, the pH of extracellular fluid may be as low as 5.2 (119). Tumor acidosis can significantly affect the phenotypic characteristics of macrophages. A recent report found that clear renal cancer cells secreted parathyroid-hormone-related protein that promoted the perinephric adipose tissue browning, which in turn enhanced the release of lactate and tumor growth (120). The accumulation of lactate released by cancer cells into the tumor microenvironment can function as an intrinsic inflammatory mediator that increases the production of the inflammatory cytokine interleukin IL17A by macrophages, so promoting chronic inflammation (121). Lactate also stimulates the macrophage receptor G protein-coupled receptor (GPR) 132 in TAMs, promoting the development of an M2-like phenotype that enables migration and invasion of tumor cells (122). Moreover, when the impact of a low pH as an independent entity from lactate was dissected, human macrophages incubated under polarizing conditions in an acidic medium of pH 6.8 acquired a functional state similar to the pro-tumoral phenotype often ascribed to TAMs, suggesting that sole acidosis is capable to dictate the pro-tumoral functionality of macrophages (123). Furthermore, modulation of the macrophage phenotype by acidity also occurred in a model of prostate cancer *in vivo* and acted as a significant driver of tumor progression (123).

The acidic microenvironments of an atherosclerotic lesion and a tumor also activate secreted lysosomal enzymes with an optimum pH within the acidic range. Therefore, the increased activity of various cysteine cathepsins such as D, F, S, and K secreted by macrophage foam cells in atherosclerotic lesions (112), and the cathepsins B and S secreted by TAMs, e.g., in breast cancer tissue (124), may, respectively, modulate the progression of atherosclerosis and cancer by local proteolytic degradation of the extracellular matrix (17, 18). Activated cysteine proteases can also contribute to deplete the small lipid-poor preβ-migrating HDL particles (125), which are abundant in human interstitial fluids (126). Such proteolytic loss of preβ-HDL in the acidic milieu of the intima, by compromising the cholesterol efflux capacity of the intimal fluid, would further favor the generation and maintenance of cholesterol-loaded macrophage foam cells (127). Regarding cancer, the significance of a compromised cholesterol efflux from TAMs is still unclear (see the following section), however, the cathepsin-rich TAMs were found to be potent suppressors of Taxol-induced tumor cell death thereby blunting the chemotherapeutic response (124).

Finally, in contrast to other tissues in which the concentration of LDL particles is only one tenth of that in the circulation, in the arterial intima their concentration equals that in the circulation (128). The uniquely high concentration of LDL in

the intimal extracellular fluid prevails because the intimal space lacks lymphatic capillaries, and is a closed space separated from the medial layer of the arterial wall by a largely impermeable internal elastic lamina (129). Efficient lymphatic lipoprotein drainage could prevent the continuous cholesterol accumulation and the subsequent lesion development in the arterial intima. However, the arterial intima lacks lymphatic capillaries, and they appear only in very advanced lesions (130). By promoting an abundant macrophage uptake of LDL-derived cholesterol and formation of the intimal foam cells, such distinctive extracellular microenvironment could explain the significant differences in lipid composition of the lipid droplets in these cells relative to those reported in TAMs. In addition, because of the uniquely high levels of LDL in the intima, acidification of the intimal fluid may also have major effects on the retention, modification, and ensuing uptake of LDL by intimal macrophages. Thus, in the intimal fluid of an advanced atherosclerotic lesion, a dual effect of a low pH and high concentrations of LDL exists, which would favor the increased formation of cholesterol-loaded macrophages. While the acidity of the intimal fluid favors the intracellular cholesterol accumulation in macrophages, the extreme high concentrations of LDL in the extracellular matrix of the intima is sufficient *per se* to transform resident macrophages into foam cells. In contrast, mere acidification of the interstitial fluid in the absence of LDL excess, as occurs in the tumor milieu, does not induce cholesterol accumulation in TAMs, as will be described in the next section.

LIPID-LADEN TAMs ARE NOT CHOLESTEROL-LOADED FOAM CELLS

In contrast to the vast information on the cholesterol-laden macrophage foam cells typical of atherosclerosis, the type of accumulated lipids, their potential origins, and the physiopathological role of the lipid cargo in TAMs remains to be fully elucidated. Instead, several studies have rather investigated lipid metabolism in cancer cells and the sources of extracellular lipids available for these cells. Yet, because cancer cells and TAMs coexist and are embedded in the same interstitial fluid, the extracellular lipids identified in the tumor microenvironment would be available also for the neighboring TAMs.

Cancer cells can activate adipocytes and other stromal cells to lipolyze their triglyceride storage, which results in release of fatty acids (FA) into the extracellular space, from where FA are taken by cancer cells via numerous transporters (131). Moreover, several blood components can cross the leaky endothelium of a tumor, among them albumin-bound FA, and very low density lipoprotein (VLDL) and LDL particles, which can release FA by the local actions of lipoprotein lipase and secreted phospholipase A2, thereby enhancing the FA pool of the tumor microenvironment (132). In this respect, a recent clinical study reported that high levels of free FA in serum were associated with an increased risk for six types of cancer (133). A FA-enriched intratumoral milieu would facilitate FA uptake by TAMs *via* phagocytosis mediated by the scavenger receptor CD36, resulting in the formation of cytoplasmic lipid droplets and generating lipid-laden TAMs. Interestingly, the lipid droplet-dependent FA metabolism was shown to induce the immunosuppressive phenotype of TAMs, which suggested that targeting lipid droplets by chemical inhibitors could be potentially used as a novel anti-tumor strategy (134).

Only a few lipidomic analyses have been carried out in cancer tissues, and this lack of data particularly applies to TAMs. Moreover, some conflicting results could be attributed to the specific cancer models used in the reported studies. A recent study *in vitro* found that macrophages from both human and murine tumor tissues were enriched with lipids due to increased lipid uptake (135). TAMs expressed elevated levels of CD36, accumulated lipids, and used FA oxidation instead of glycolysis for energy. As compared with macrophages isolated from normal tissues, neutral lipids were accumulated in lipid droplets in TAMs, as revealed by the fluorescent lipid dye BODIPY (135). In a model of gastric cancer, lipidomic analysis of TAMs generated in the presence of lipid-containing tumor explant supernatants revealed high levels of triglycerides without changes in the levels of cholesteryl esters (136). Another lipidomic study of TAMs cocultured with human papillary thyroid carcinoma cells found that tumor cells can stimulate lipid biosynthesis in the TAMs, which enriched their levels of intracellular lipids, being glycerophospholipids and sphingomyelins the most highly upregulated lipids (137). Therefore, it appears, overall, that lipid droplets in TAMs accumulate mainly triglycerides with variable amounts of glycerophospholipids and sphingomyelins.

Regarding the similarities and differences between the neutral lipid content in the cytoplasmic lipid droplets of macrophage foam cells in human atherosclerotic lesions and tumor tissues, we wish to further denote that a dynamic overlap may exist. Thus, it was found that the macrophage foam cells isolated from human aortic atherosclerotic lesions are able, when exposed to hypoxia, to store in their neutral lipid droplets, in addition to cholesteryl esters, also significant amounts of triglycerides (138). Because unmodified, i.e., native LDL particles, can be taken up by macrophages via fluid-phase pinocytosis without an involvement of lipoprotein receptors (139) and this process appears to be enhanced in acidic microenvironments (115, 116), it is plausible to expect that it would facilitate the uptake of native LDL also by TAMs. However, in contrast to the LDL-enriched extracellular fluid of an atherosclerotic lesion, the LDL levels must be much lower in a well-vascularized tumor tissue due to the abundant presence of lymph capillaries. As a consequence, the contribution of LDL to the generation of lipid-laden TAMs appears to be minute. Thus, stimulation of the fluid-phase pinocytosis in macrophages by the low pH of the intratumoral environment would rather stimulate FA uptake and ensuing accumulation of triglycerides and glycerophospholipids in the lipid droplets, as it has been observed in TAMs (136, 137). In analogy to the strong association between the formation of cholesteryl ester-filled macrophage foam cells and atherosclerosis progression, the formation of neutral lipid droplets in TAMs has been found to correlate with various types of cancer (84), and more recently with the human colorectal cancer progression (134).

While it is obvious that lipid accumulation in TAMs can induce profound effects on their functional polarization (131), how such lipid-induced macrophage reprogramming can specifically affect tumor development is still unclear. Thus, various reports have indicated that the accumulated lipids can polarize TAMs to gain either a pro-tumoral activity or an immunosuppressive phenotype. In a model of gastric tumor-bearing mice it was found that TAMs accumulating high lipid levels were associated with M2-like profiling, which can display pro-tumoral activity (136). Another metabolome study reported a metabolic shift in lipid-laden TAMs increasing the production of proinflammatory cytokines and reactive oxygen species (ROS), which contributed to their pro-tumoral functions (137). In contrast, another report conducted in colorectal cancer patients found that the accumulation of lipid droplets polarized bone marrow-derived myeloid cells into an immunosuppressive phenotype of TAMs (134). Mechanistically, the immunosuppressive phenotype found in TAMs was controlled by long-chain FA metabolism, specifically, unsaturated FA added to the culture medium (134). These data indicated that, in addition to the well-known cytokine signaling effects in modulating macrophage phenotype, lipid droplets are capable to modulate the immunosuppressive capacity of TAMs in the tumor microenvironment. Thus, lipid droplets may become effective targets for chemical inhibitors to block *in vitro* polarization of TAMs and potentially tumor growth *in vivo*, as well.

The activity of ABC transporters can profoundly affect the organization and activation states of lipid domains in the plasma membrane, which can affect the functionality of the cells in many ways (140). Because actively replicating cancer cells have a high demand for cholesterol, it follows that loss of the ABCA1-dependent cholesterol efflux in these cells may promote carcinogenesis. Indeed, ABCA1 downregulation has been observed in prostate cancers (141), and suppression of *ABCA1* expression by oncogenic mutations or loss-of-function mutation has been linked to an accumulation of mitochondrial cholesterol and malignant cell transformation (142). Recent studies indicate that, in contrast to cancer cells, increasing the content of cholesterol in TAMs may exert an inhibitory effect on tumor development. Thus, it was reported in a mouse model of bladder cancer and melanoma that *Abcg1*–/– deficiency shifts the macrophage phenotype toward an M1-like tumoricidal phenotype and also inhibits tumor growth, which was associated with the accumulation of cholesterol in the macrophages (143). Another work in an ovarian cancer model showed that genetic deletion of ABC transporters in TAMs reverts their tumor-promoting functions (144). This study further indicated that cancer cells can scavenge membrane cholesterol from TAMs resulting in the reprogramming of TAMs toward an immunosuppressive and tumor-promoting (M2) phenotype (144). In line with this report, a very recent transcriptome study in human lung tumor tissues found that, although the tumors themselves were cholesterol-rich, the TAMs were depleted of cholesterol and overexpressed *ABCA1* and *ABCG1* (145). Overall, the current evidence points out that cancer cells use TAMs as a source of cholesterol and this is associated with the upregulation of ABC cholesterol efflux transporters in the TAMs. Yet, the mechanisms by which the expression and activity of the key efflux transporters are coordinately upregulated were not disclosed in any of the referred studies. These findings highlight the notion that modulation of cholesterol metabolism in TAMs can change their function, and thereby exert profound effects on tumor growth. Furthermore, these novel data indicate that the macrophage functions primed by the ABC-mediated cholesterol efflux could lead to opposite pathophysiological effects in different cellular microenvironments, i.e., protecting from atherosclerosis but promoting cancer.

CONCLUDING REMARKS

Tissue-resident macrophages are central drivers in the generation of an atherosclerotic lesion and also act as important auxiliary immune cells in tumor development. Because macrophages show a high degree of plasticity, both systemic factors and the local microenvironment in atherosclerotic lesions and tumors may contribute to macrophage polarization by inducing transcriptional and functional reprogramming in these cells. It is conceivable that the different microenvironments within a single atherosclerotic lesion or a malignant tumor are capable of inducing phenotypically different macrophage subsets. Moreover, the microenvironments in atherosclerotic lesions and malignant tumors play primary roles by inducing lipid-loading of the macrophages, which is followed by alterations in their intracellular metabolism and phenotypic characteristics. Such plasticity allows the macrophages to variously influence the course of the disease. In this scenario, the dynamic interactions between the macrophages and their neighboring cells, be they malignant or non-malignant, are of paramount importance.

Strikingly, the macrophages are ontogenically heterogeneous and both bone marrow- and embryonic-derived macrophages have been identified in the aortic intima and various tumor types. These different subsets of macrophages may have different impacts on the progression of both diseases. However, since tissue-resident macrophage expansion appears to be a pathological factor in both atherosclerosis and cancer, blockade of monocyte recruitment and the subsequent concomitant increase of the monocyte-attracting protein CCL2 into the diseased tissue, would at least partially contribute to mitigating the disease progression. A question that remains unanswered is whether the macrophage origin or the tissue environment is the main driver of the functionality of the macrophage, or, whether the complex interplay between both factors is critical. A summary of the ontogeny and phenotypic features of the tissue-residing macrophage populations in an atherosclerotic plaque and a malignant solid tumor is given in **Table 2**.

Because of the extreme plasticity of the macrophages, their phenotype in any tissue can be considered as a continuous variable. However, M2-polarized macrophages appear to be the predominant subpopulation both in atherosclerotic lesions and in malignant tumors. Although lipid-laden macrophages are present in both diseases, the lipid droplets in macrophage foam cells from the atherosclerotic intima are rich in cholesteryl esters,

TABLE 2 | Ontogeny and phenotypic features of the macrophage populations in atherosclerotic plaques and malignant solid tumors.

Macrophages	Atherosclerotic plaques	Malignant solid tumors
Ontogenic origin	Myeloid and embryonic (3, 44, 45, 47, 48)	Myeloid and embryonic (28, 79–81)
Properties of myeloid populations	Critical in driving expansion of the plaque beyond early time points and exacerbation of the evolving plaques (48)	Regulation of tumor immunity (81) Shaping of the tumor expanding microenvironment (28)
Properties of embryonic populations	Homeostatic and metabolic regulation of the arterial wall *via* high expression of the hyaluronan receptor LYVE-1 in the adventitia (47, 49)	Pro-fibrotic transcriptional profile (81)
Polarization into M1- and M2-like phenotypes*	M2-like subpopulation predominates (69)	M2-like subpopulation predominates (90, 91)
Properties of the M1-like macrophages	Proinflammatory actions (32) Predominate in progressing atherosclerotic lesions where they promote calcium deposition in the necrotic core (microcalcification), which may lead to plaque rupture (70)	Anti-tumoral actions (21) Express proinflammatory cytokines (IL1, IL6, and TNF alpha) and MHC molecules implicated in killing tumor cells (15)
Properties of the M2- like macrophages	Anti-inflammatory actions (32, 70) High foam cell-forming capacity (69, 72) Dominate in regressing plaques where they promote macrocalcification, which tends to stabilize the plaques. They also scavenge apoptotic cells and cell debris, and thereby improving lesion repair and healing (70)	Pro-tumoral actions (21) Stimulate angiogenesis and metastasis (15, 21) Suppress immune response as a result of secretion of TGF-beta or IL-10 (15)
Production of CCL2	Yes (73)	Yes (16, 94)
Production of cysteine cathepsins	Cathepsins D, F, S, and K (112)	Cathepsins B and S (124)
Expression and function of the ABC cholesterol efflux transporters	Increased gene expression of *ABCA1* and *ABCG1* in macrophage foam cells (59, 60) Anti-atherosclerotic effect and induction of macrophage-RCT (53, 56, 61)	Increased gene expression of *ABCA1* and *ABCG1* in TAMs (145) Immunosuppressive and pro-tumoral effect in a model of ovarian cancer (144)
Accumulation of cytoplasmic lipid droplets and lipidomic analysis	Filled with abundant lipid droplets, which give macrophages a "foamy" appearance. The lipid droplets contain cholesteryl esters and in hypoxic lesion areas, they may contain also triglycerides (52, 138)	Moderate tendency to accumulate lipid droplets. Macrophage lipids mainly consist of triglycerides, and also of variable amounts of glycerophospholipids and sphingomyelins (135–137)

The information provided in the right column includes only selected illustrative examples of malignant tumors. Note that each malignant tumor tissue is likely to have its unique character.
**Given the high plasticity of macrophages, they dynamically switch their in vivo gene expression in response to the polarizing signals present in their respective microenvironments, rather than forming terminally differentiated phenotypes during the progression of either disease.*

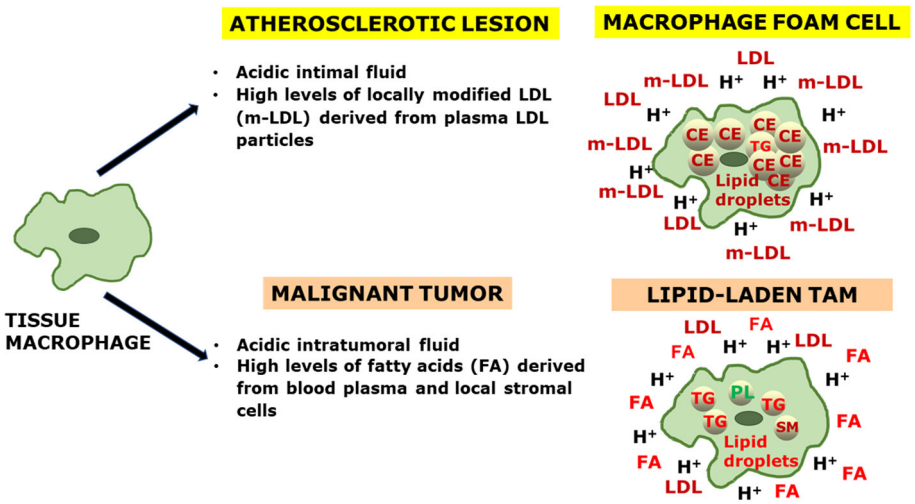

FIGURE 1 | An integrative view of the generation of lipid-laden macrophages in atherosclerosis and cancer. Tissue macrophages (LEFT) are exposed to characteristic microenvironmental conditions present in the extracellular fluids of an atherosclerotic lesion and a malignant tumor (CENTER), which influence the respective lipid cargo of the macrophage foam cells and lipid-laden tumor-associated macrophages (TAMs) (RIGHT). In the extracellular fluid: LDL, low-density lipoprotein; m-LDL, modified low-density lipoprotein; FA, fatty acid; H+, proton. In the intracellular space: CE, cholesteryl ester; TG, triglyceride; PL, phospholipid; SM, sphingomyelin.

while those in TAMs appear to accumulate triglycerides, and variable amounts of glycerophospholipids and sphingomyelins. Independently of the lipid type, lipid loading is followed by changes in cell signaling molecules as well as in gene expression profile, which then modify the metabolic programming of the lipid-laden macrophages. **Figure 1** summarizes the characteristic extracellular conditions and ensuing phenotypic features of lipid-laden macrophages in the atherosclerotic lesion and in tumors.

Finally, in contrast to the classical paradigm that lipid-laden macrophages are culprits of chronic inflammation in atherosclerotic plaques, we and others have reported that foamy macrophages may be less inflammatory than their non-foamy counterparts. More recently, in the context of cancer, it was found that the accumulation of lipids in TAMs can elicit an immunosuppressive macrophage phenotype. Regarding the effect on disease progression, we can surmise that, at least in the initial stages of atherosclerosis, the conversion of proinflammatory macrophages into macrophage foam cells with an anti-inflammatory phenotype would slow down the speed of atherogenesis, while conversion of TAMs into lipid-laden TAMs with an immunosuppressive phenotype would promote the progression of cancer. Overall, more complete knowledge of the physiopathological role of lipid-laden macrophages is needed, and this challenge particularly applies to tumor development. Advances in this emergent field of research will solidify novel therapeutic strategies of targeting different subsets of tissue-resident macrophages and their lipid-laden counterparts as promising tools in the fight against atherosclerosis and cancer—-but cautiously recognizing their fundamental differences as disease-modifying cellular components in these two diseases.

AUTHOR CONTRIBUTIONS

ML-R, PK, JE-G, and JL: conceptualization and writing-review and editing. ML-R: writing-original draft preparation. PK and JE-G: funding acquisition. All authors contributed to the article and approved the submitted version.

FUNDING

Wihuri Research Institute was maintained by the Jenny and Antti Wihuri Foundation. This work was partly funded by the Instituto de Salud Carlos III and FEDER Una manera de hacer Europa grant PI1900136 (JE-G), and Pulsus Foundation (ML-R). CIBERDEM is an Instituto de Salud Carlos III project.

REFERENCES

1. Sreejit G, Fleetwood AJ, Murphy AJ, Nagareddy PR. Origins and diversity of macrophages in health and disease. *Clin Transl Immunol.* (2020) 9:e1222. doi: 10.1002/cti2.1222
2. Epelman S, Lavine KJ, Randolph GJ. Origin and functions of tissue macrophages. *Immunity.* (2014) 41:21–35. doi: 10.1016/j.immuni.2014.06.013
3. Willemsen L, de Winther MP. Macrophage subsets in atherosclerosis as defined by single-cell technologies. *J Pathol.* (2020) 250:705–14. doi: 10.1002/path.5392
4. Gerhardt T, Ley K. Monocyte trafficking across the vessel wall. *Cardiovasc Res.* (2015) 107:321–30. doi: 10.1093/cvr/cvv147
5. Harjunpaa H, Llort Asens M, Guenther C, Fagerholm SC. Cell adhesion molecules and their roles and regulation in the immune and tumor microenvironment. *Front Immunol.* (2019) 10:1078. doi: 10.3389/fimmu.2019.01078
6. Randolph GJ. Tissue macrophages break dogma. *Nat Rev Immunol.* (2021) 21:625. doi: 10.1038/s41577-021-00620-0
7. Lapenna A, De Palma M, Lewis CE. Perivascular macrophages in health and disease. *Nat Rev Immunol.* (2018) 18:689–702. doi: 10.1038/s41577-018-0056-9
8. Guerrini V, Gennaro ML. Foam cells: One size doesn't fit all. *Trends Immunol.* (2019) 40:1163–79. doi: 10.1016/j.it.2019.10.002
9. Cassetta L, Cassol E, Poli G. Macrophage polarization in health and disease. *Scientific World Journal.* (2011) 11:2391–402. doi: 10.1100/2011/213962
10. Biswas SK, Mantovani A. Orchestration of metabolism by macrophages. *Cell Metab.* (2012) 15:432–37. doi: 10.1016/j.cmet.2011.11.013
11. Lacey DC, Achuthan A, Fleetwood AJ, Dinh H, Roiniotis J, Scholz GM, et al. Defining GM-CSF- and macrophage-CSF-dependent macrophage responses by *in vitro* models. *J Immunol.* (2012) 188:5752–65. doi: 10.4049/jimmunol.1103426
12. Pittet MJ, Swirski FK. Monocytes link atherosclerosis and cancer. *Eur J Immunol.* (2011) 41:2519–22. doi: 10.1002/eji.201141727
13. Gui T, Shimokado A, Sun Y, Akasaka T, Muragaki Y. Diverse roles of macrophages in atherosclerosis: from inflammatory biology to biomarker discovery. *Media Inflamm.* (2012) 2012:693083. doi: 10.1155/2012/693083
14. Moore KJ, Sheedy FJ, Fisher EA. Macrophages in atherosclerosis: a dynamic balance. *Nat Rev Immunol.* (2013) 13:709–21. doi: 10.1038/nri3520
15. Poh AR, Ernst M. Targeting macrophages in cancer: from bench to bedside. *Front Oncol.* (2018) 8:49. doi: 10.3389/fonc.2018.00049
16. Zhou J, Tang Z, Gao S, Li C, Feng Y, Zhou X. Tumor-associated macrophages: recent insights and therapies. *Front Oncol.* (2020) 10:188. doi: 10.3389/fonc.2020.00188
17. Lindstedt KA, Leskinen MJ, Kovanen PT. Proteolysis of the pericellular matrix: a novel element determining cell survival and death in the pathogenesis of plaque erosion and rupture. *Arterioscler Thromb Vasc Biol.* (2004) 24:1350–8. doi: 10.1161/01.ATV.0000135322.78008.55
18. Dollery CM, Libby P. Atherosclerosis and proteinase activation. *Cardiovasc Res.* (2006) 69:625–35. doi: 10.1016/j.cardiores.2005.11.003
19. Tabas I. Macrophage death and defective inflammation resolution in atherosclerosis. *Nat Rev Immunol.* (2010) 10:36–46. doi: 10.1038/nri2675
20. Sluimer JC, Gasc JM, van Wanroij JL, Kisters N, Groeneweg M, Sollewijn Gelpke MD, et al. Hypoxia, hypoxia-inducible transcription factor, and macrophages in human atherosclerotic plaques are correlated with intraplaque angiogenesis. *J Am Coll Cardiol.* (2008) 51:1258–65. doi: 10.1016/j.jacc.2007.12.025
21. Liu J, Geng X, Hou J, Wu G. New insights into M1/M2 macrophages: key modulators in cancer progression. *Cancer Cell Int.* (2021) 21:389. doi: 10.1186/s12935-021-02089-2
22. Laoui D, Van Overmeire E, De Baetselier P, Van Ginderachter JA, Raes G. Functional relationship between tumor-associated macrophages and macrophage colony-stimulating factor as contributors to cancer progression. *Front Immunol.* (2014) 5:489. doi: 10.3389/fimmu.2014.00489
23. Nebiker CA, Han J, Eppenberger-Castori S, Iezzi G, Hirt C, Amicarella F, et al. GM-CSF production by tumor cells is associated with improved survival in colorectal cancer. *Clin Cancer Res.* (2014) 20:3094–106. doi: 10.1158/1078-0432.CCR-13-2774

24. Mancino AT, Klimberg VS, Yamamoto M, Manolagas SC, Abe E. Breast cancer increases osteoclastogenesis by secreting M-CSF and upregulating RANKL in stromal cells. *J Surg Res.* (2001) 100:18–24. doi: 10.1006/jsre.2001.6204
25. Duan Z, Luo Y. Targeting macrophages in cancer immunotherapy. *Signal Transduct Target Ther.* (2021) 6:127. doi: 10.1038/s41392-021-00506-6
26. Back M, Yurdagul A, Tabas I, Oorni K, Kovanen PT. Inflammation and its resolution in atherosclerosis: mediators and therapeutic opportunities. *Nat Rev Cardiol.* (2019) 16:389–406. doi: 10.1038/s41569-019-0169-2
27. Schumski A, Winter C, Doring Y, Soehnlein O. The ins and outs of myeloid cells in atherosclerosis. *J Innate Immun.* (2018) 10:479–86. doi: 10.1159/000488091
28. Laviron M, Boissonnas A. Ontogeny of tumor-associated macrophages. *Front Immunol.* (2019) 10:1799. doi: 10.3389/fimmu.2019.01799
29. Gul N, van Egmond M. Antibody-dependent phagocytosis of tumor cells by macrophages: a potent effector mechanism of monoclonal antibody therapy of cancer. *Cancer Res.* (2015) 75:5008–13. doi: 10.1158/0008-5472.CAN-15-1330
30. Jinnouchi H, Guo L, Sakamoto A, Torii S, Sato Y, Cornelissen A, et al. Diversity of macrophage phenotypes and responses in atherosclerosis. *Cell Mol Life Sci.* (2020) 77:1919–32. doi: 10.1007/s00018-019-03371-3
31. Depuydt MAC, Prange KHM, Slenders L, Ord T, Elbersen D, Boltjes A, et al. Microanatomy of the human atherosclerotic plaque by single-cell transcriptomics. *Circ Res.* (2020) 127:1437–55. doi: 10.1161/CIRCRESAHA.120.316770
32. Lin P, Ji HH, Li YJ, Guo SD. Macrophage plasticity and atherosclerosis therapy. *Front Mol Biosci.* (2021) 8:679797. doi: 10.3389/fmolb.2021.679797
33. Dagogo-Jack I, Shaw AT. Tumour heterogeneity and resistance to cancer therapies. *Nat Rev Clin Oncol.* (2018) 15:81–94. doi: 10.1038/nrclinonc.2017.166
34. Fiorini E, Veghini L, Corbo V. Modeling cell communication in cancer with organoids: making the complex simple. *Front Cell Dev Biol.* (2020) 8:166. doi: 10.3389/fcell.2020.00166
35. Rojas J, Salazar J, Martinez MS, Palmar J, Bautista J, Chavez-Castillo M, et al. Macrophage heterogeneity and plasticity: impact of macrophage biomarkers on atherosclerosis. *Scientifica (Cairo).* (2015) 2015:851252. doi: 10.1155/2015/851252
36. Orecchioni M, Ghosheh Y, Pramod AB, Ley K. Macrophage polarization: different gene signatures in M1(LPS+) vs. classically and M2(LPS-) vs. alternatively activated macrophages. *Front Immunol.* (2019) 10:1084. doi: 10.3389/fimmu.2019.01084
37. Owsiany KM, Alencar GF, Owens GK. Revealing the origins of foam cells in atherosclerotic lesions. *Arterioscler Thromb Vasc Biol.* (2019) 39:836–8. doi: 10.1161/ATVBAHA.119.312557
38. Moore KJ, Tabas I. Macrophages in the pathogenesis of atherosclerosis. *Cell.* (2011) 145:341–55. doi: 10.1016/j.cell.2011.04.005
39. Allahverdian S, Pannu PS, Francis GA. Contribution of monocyte-derived macrophages and smooth muscle cells to arterial foam cell formation. *Cardiovasc Res.* (2012) 95:165–72. doi: 10.1093/cvr/cvs094
40. Subramanian M, Tabas I. Dendritic cells in atherosclerosis. *Semin Immunopathol.* (2014) 36:93–102. doi: 10.1007/s00281-013-0400-x
41. Steinberg D. In celebration of the 100th anniversary of the lipid hypothesis of atherosclerosis. *J Lipid Res.* (2013) 54:2946–9. doi: 10.1194/jlr.R043414
42. Mallat Z. Macrophages. *Arterioscler Thromb Vasc Biol.* (2014) 34:2509–19. doi: 10.1161/ATVBAHA.114.304794
43. Kratofil RM, Kubes P, Deniset JF. Monocyte conversion during inflammation and injury. *Arterioscler Thromb Vasc Biol.* (2017) 37:35–42. doi: 10.1161/ATVBAHA.116.308198
44. Ensan S, Li A, Besla R, Degousee N, Cosme J, Roufaiel M, et al. Self-renewing resident arterial macrophages arise from embryonic CX3CR1(+) precursors and circulating monocytes immediately after birth. *Nat Immunol.* (2016) 17:159–68. doi: 10.1038/ni.3343
45. Honold L, Nahrendorf M. Resident and monocyte-derived macrophages in cardiovascular disease. *Circ Res.* (2018) 122:113–27. doi: 10.1161/CIRCRESAHA.117.311071
46. Swirski FK, Robbins CS, Nahrendorf M. Development and function of arterial and cardiac macrophages. *Trends Immunol.* (2016) 37:32–40. doi: 10.1016/j.it.2015.11.004
47. Weinberger T, Esfandyari D, Messerer D, Percin G, Schleifer C, Thaler R, et al. Ontogeny of arterial macrophages defines their functions in homeostasis and inflammation. *Nat Commun.* (2020) 11:4549. doi: 10.1038/s41467-020-18287-x
48. Williams JW, Zaitsev K, Kim KW, Ivanov S, Saunders BT, Schrank PR, et al. Limited proliferation capacity of aortic intima resident macrophages requires monocyte recruitment for atherosclerotic plaque progression. *Nat Immunol.* (2020) 21:1194–204. doi: 10.1038/s41590-020-0768-4
49. Lim HY, Lim SY, Tan CK, Thiam CH, Goh CC, Carbajo D, et al. Hyaluronan receptor LYVE-1-expressing macrophages maintain arterial tone through hyaluronan-mediated regulation of smooth muscle cell collagen. *Immunity.* (2018) 49:326–41.e327. doi: 10.1016/j.immuni.2018.06.008
50. Sorci-Thomas MG, Thomas MJ. Microdomains, inflammation, and atherosclerosis. *Circ Res.* (2016) 118:679–91. doi: 10.1161/CIRCRESAHA.115.306246
51. Williams KJ, Tabas I. The response-to-retention hypothesis of early atherogenesis. *Arterioscler Thromb Vasc Biol.* (1995) 15:551–61. doi: 10.1161/01.ATV.15.5.551
52. Brown MS, Goldstein JL. Lipoprotein metabolism in the macrophage: implications for cholesterol deposition in atherosclerosis. *Annu Rev Biochem.* (1983) 52:223–61. doi: 10.1146/annurev.bi.52.070183.001255
53. Yvan-Charvet L, Wang N, Tall AR. Role of HDL, ABCA1, and ABCG1 transporters in cholesterol efflux and immune responses. *Arterioscler Thromb Vasc Biol.* (2010) 30:139–43. doi: 10.1161/ATVBAHA.108.179283
54. Groenen AG, Halmos B, Tall AR, Westerterp M. Cholesterol efflux pathways, inflammation, and atherosclerosis. *Crit Rev Biochem Mol Biol.* (2021) 56:426–39. doi: 10.1080/10409238.2021.1925217
55. Nguyen SD, Maaninka K, Lappalainen J, Nurmi K, Metso J, Oorni K, et al. Carboxyl-terminal cleavage of apolipoprotein A-I by human mast cell chymase impairs its anti-inflammatory properties. *Arterioscler Thromb Vasc Biol.* (2016) 36:274–84. doi: 10.1161/ATVBAHA.115.306827
56. Lee-Rueckert M, Escola-Gil JC, Kovanen PT. HDL functionality in reverse cholesterol transport–Challenges in translating data emerging from mouse models to human disease. *Biochim Biophys Acta.* (2016) 1861:566–83. doi: 10.1016/j.bbalip.2016.03.004
57. Kareinen I, Cedo L, Silvennoinen R, Laurila PP, Jauhiainen M, Julve J, et al. Enhanced vascular permeability facilitates entry of plasma HDL and promotes macrophage-reverse cholesterol transport from skin in mice. *J Lipid Res.* (2015) 56:241–53. doi: 10.1194/jlr.M050948
58. Phillips MC. Molecular mechanisms of cellular cholesterol efflux. *J Biol Chem.* (2014) 289:24020–9. doi: 10.1074/jbc.R114.583658
59. Tall AR, Costet P, Wang N. Regulation and mechanisms of macrophage cholesterol efflux. *J Clin Invest.* (2002) 110:899–904. doi: 10.1172/JCI0216391
60. Klucken J, Buchler C, Orso E, Kaminski WE, Porsch-Ozcurumez M, Liebisch G, et al. ABCG1 (ABC8), the human homolog of the Drosophila white gene, is a regulator of macrophage cholesterol and phospholipid transport. *Proc Natl Acad Sci USA.* (2000) 97:817–22. doi: 10.1073/pnas.97.2.817
61. Tall AR, Yvan-Charvet L, Terasaka N, Pagler T, Wang N. HDL, ABC transporters, and cholesterol efflux: implications for the treatment of atherosclerosis. *Cell Metab.* (2008) 7:365–75. doi: 10.1016/j.cmet.2008.03.001
62. Tang C, Houston BA, Storey C, LeBoeuf RC. Both STAT3 activation and cholesterol efflux contribute to the anti-inflammatory effect of apoA-I/ABCA1 interaction in macrophages. *J Lipid Res.* (2016) 57:848–57. doi: 10.1194/jlr.M065797
63. Lawn RM, Wade DP, Couse TL, Wilcox JN. Localization of human ATP-binding cassette transporter 1 (ABC1) in normal and atherosclerotic tissues. *Arterioscler Thromb Vasc Biol.* (2001) 21:378–85. doi: 10.1161/01.ATV.21.3.378
64. Albrecht C, Soumian S, Amey JS, Sardini A, Higgins CF, Davies AH, et al. ABCA1 expression in carotid atherosclerotic plaques. *Stroke.* (2004) 35:2801–6. doi: 10.1161/01.STR.0000147036.07307.93
65. Liu HF, Cui KF, Wang JP, Zhang M, Guo YP, Li XY, et al. Significance of ABCA1 in human carotid atherosclerotic plaques. *Exp Ther Med.* (2012) 4:297–302. doi: 10.3892/etm.2012.576
66. He C, Jiang H, Song W, Riezman H, Tontonoz P, Weston TA, et al. Cultured macrophages transfer surplus cholesterol into adjacent cells in the absence

of serum or high-density lipoproteins. *Proc Natl Acad Sci USA.* (2020) 117:10476–83. doi: 10.1073/pnas.1922879117
67. Shankman LS, Gomez D, Cherepanova OA, Salmon M, Alencar GF, Haskins RM, et al. KLF4-dependent phenotypic modulation of smooth muscle cells has a key role in atherosclerotic plaque pathogenesis. *Nat Med.* (2015) 21:628–37. doi: 10.1038/nm.3866
68. Schrijvers DM, De Meyer GR, Kockx MM, Herman AG, Martinet W. Phagocytosis of apoptotic cells by macrophages is impaired in atherosclerosis. *Arterioscler Thromb Vasc Biol.* (2005) 25:1256–61. doi: 10.1161/01.ATV.0000166517.18801.a7
69. Waldo SW, Li Y, Buono C, Zhao B, Billings EM, Chang J, et al. Heterogeneity of human macrophages in culture and in atherosclerotic plaques. *Am J Pathol.* (2008) 172:1112–26. doi: 10.2353/ajpath.2008.070513
70. Liu N, Zhang B, Sun Y, Song W. Macrophage origin, phenotypic diversity, and modulatory signaling pathways in the atherosclerotic plaque microenvironment. *Vessel Plus.* (2021) 5:43. doi: 10.20517/2574-1209.2021.25
71. Di Gregoli K, Johnson JL. Role of colony-stimulating factors in atherosclerosis. *Curr Opin Lipidol.* (2012) 23:412–21. doi: 10.1097/MOL.0b013e328357ca6e
72. Lappalainen J, Yeung N, Nguyen SD, Jauhiainen M, Kovanen PT, Lee-Rueckert M. Cholesterol loading suppresses the atheroinflammatory gene polarization of human macrophages induced by colony stimulating factors. *Sci Rep.* (2021) 11:4923. doi: 10.1038/s41598-021-84249-y
73. Deshmane SL, Kremlev S, Amini S, Sawaya BE. Monocyte chemoattractant protein-1 (MCP-1): an overview. *J Interferon Cytokine Res.* (2009) 29:313–26. doi: 10.1089/jir.2008.0027
74. Spann NJ, Garmire LX, McDonald JG, Myers DS, Milne SB, Shibata N, et al. Regulated accumulation of desmosterol integrates macrophage lipid metabolism and inflammatory responses. *Cell.* (2012) 151:138–52. doi: 10.1016/j.cell.2012.06.054
75. da Silva RF, Lappalainen J, Lee-Rueckert M, Kovanen PT. Conversion of human M-CSF macrophages into foam cells reduces their proinflammatory responses to classical M1-polarizing activation. *Atherosclerosis.* (2016) 248:170–8. doi: 10.1016/j.atherosclerosis.2016.03.012
76. Kim K, Shim D, Lee JS, Zaitsev K, Williams JW, Kim KW, et al. Transcriptome analysis reveals nonfoamy rather than foamy plaque macrophages are proinflammatory in atherosclerotic murine models. *Circ Res.* (2018) 123:1127–42. doi: 10.1161/CIRCRESAHA.118.312804
77. Baardman J, Verberk SGS, Prange KHM, van Weeghel M, van der Velden S, Ryan DG, et al. A defective pentose phosphate pathway reduces inflammatory macrophage responses during hypercholesterolemia. *Cell Rep.* (2018) 25:2044–52.e2045. doi: 10.1016/j.celrep.2018.10.092
78. Lewis CE, Pollard JW. Distinct role of macrophages in different tumor microenvironments. *Cancer Res.* (2006) 66:605–12. doi: 10.1158/0008-5472.CAN-05-4005
79. Wu K, Lin K, Li X, Yuan X, Xu P, Ni P, et al. Redefining tumor-associated macrophage subpopulations and functions in the tumor microenvironment. *Front Immunol.* (2020) 11:1731. doi: 10.3389/fimmu.2020.01731
80. Pan Y, Yu Y, Wang X, Zhang T. Tumor-associated macrophages in tumor immunity. *Front Immunol.* (2020) 11:583084. doi: 10.3389/fimmu.2020.583084
81. Zhu Y, Herndon JM, Sojka DK, Kim KW, Knolhoff BL, Zuo C, et al. Tissue-resident macrophages in pancreatic ductal adenocarcinoma originate from embryonic hematopoiesis and promote tumor progression. *Immunity.* (2017) 47:323–38.e326. doi: 10.1016/j.immuni.2017.07.014
82. Franklin RA, Liao W, Sarkar A, Kim MV, Bivona MR, Liu K, et al. The cellular and molecular origin of tumor-associated macrophages. *Science.* (2014) 344:921–5. doi: 10.1126/science.1252510
83. Azizi E, Carr AJ, Plitas G, Cornish AE, Konopacki C, Prabhakaran S, et al. Single-cell map of diverse immune phenotypes in the breast tumor microenvironment. *Cell.* (2018) 174:1293–308.e1236. doi: 10.1016/j.cell.2018.05.060
84. Guo Q, Jin Z, Yuan Y, Liu R, Xu T, Wei H, et al. New mechanisms of tumor-associated macrophages on promoting tumor progression: recent research advances and potential targets for tumor immunotherapy. *J Immunol Res.* (2016) 2016:9720912. doi: 10.1155/2016/9720912
85. Ries CH, Cannarile MA, Hoves S, Benz J, Wartha K, Runza V, et al. Targeting tumor-associated macrophages with anti-CSF-1R antibody reveals a strategy for cancer therapy. *Cancer Cell.* (2014) 25:846–59. doi: 10.1016/j.ccr.2014.05.016
86. Zou W. Immunosuppressive networks in the tumour environment and their therapeutic relevance. *Nat Rev Cancer.* (2005) 5:263–74. doi: 10.1038/nrc1586
87. Rabold K, Netea MG, Adema GJ, Netea-Maier RT. Cellular metabolism of tumor-associated macrophages - functional impact and consequences. *FEBS Lett.* (2017) 591:3022–41. doi: 10.1002/1873-3468.12771
88. Ruffell B, Affara NI, Coussens LM. Differential macrophage programming in the tumor microenvironment. *Trends Immunol.* (2012) 33:119–26. doi: 10.1016/j.it.2011.12.001
89. Liu JY, Peng CW, Yang GF, Hu WQ, Yang XJ, Huang CQ, et al. Distribution pattern of tumor associated macrophages predicts the prognosis of gastric cancer. *Oncotarget.* (2017) 8:92757–69. doi: 10.18632/oncotarget.21575
90. Nielsen SR, Schmid MC. Macrophages as key drivers of cancer progression and metastasis. *Mediators Inflamm.* (2017) 2017:9624760. doi: 10.1155/2017/9624760
91. Sica A, Schioppa T, Mantovani A, Allavena P. Tumour-associated macrophages are a distinct M2 polarised population promoting tumour progression: potential targets of anti-cancer therapy. *Eur J Cancer.* (2006) 42:717–27. doi: 10.1016/j.ejca.2006.01.003
92. Zheng X, Weigert A, Reu S, Guenther S, Mansouri S, Bassaly B, et al. Spatial density and distribution of tumor-associated macrophages predict survival in non-small cell lung carcinoma. *Cancer Res.* (2020) 80:4414–25. doi: 10.1158/0008-5472.CAN-20-0069
93. Sawa-Wejksza K, Kandefer-Szerszen M. Tumor-associated macrophages as target for antitumor therapy. *Arch Immunol Ther Exp (Warsz).* (2018) 66:97–111. doi: 10.1007/s00005-017-0480-8
94. Mantovani A, Savino B, Locati M, Zammataro L, Allavena P, Bonecchi R. The chemokine system in cancer biology and therapy. *Cytokine Growth Factor Rev.* (2010) 21:27–39. doi: 10.1016/j.cytogfr.2009.11.007
95. Li R, Wen A, Lin J. Pro-inflammatory cytokines in the formation of the pre-metastatic niche. *Cancers (Basel).* (2020) 12:3752. doi: 10.3390/cancers12123752
96. Chistiakov DA, Orekhov AN, Bobryshev YV. Endothelial barrier and its abnormalities in cardiovascular disease. *Front Physiol.* (2015) 6:365. doi: 10.3389/fphys.2015.00365
97. Mehta D, Malik AB. Signaling mechanisms regulating endothelial permeability. *Physiol Rev.* (2006) 86:279–367. doi: 10.1152/physrev.00012.2005
98. Kovanen PT. Mast cells as potential accelerators of human atherosclerosis-from early to late lesions. *Int J Mol Sci.* (2019) 20:4479. doi: 10.3390/ijms20184479
99. Rozenberg I, Sluka SH, Rohrer L, Hofmann J, Becher B, Akhmedov A, et al. Histamine H1 receptor promotes atherosclerotic lesion formation by increasing vascular permeability for low-density lipoproteins. *Arterioscler Thromb Vasc Biol.* (2010) 30:923–30. doi: 10.1161/ATVBAHA.109.201079
100. McDonald DM, Thurston G, Baluk P. Endothelial gaps as sites for plasma leakage in inflammation. *Microcirculation.* (1999) 6:7–22. doi: 10.1080/713773924
101. Lobatto ME, Fuster V, Fayad ZA, Mulder WJ. Perspectives and opportunities for nanomedicine in the management of atherosclerosis. *Nat Rev Drug Discov.* (2011) 10:835–52. doi: 10.1038/nrd3578
102. Hu G, Guo M, Xu J, Wu F, Fan J, Huang Q, et al. Nanoparticles targeting macrophages as potential clinical therapeutic agents against cancer and inflammation. *Front Immunol.* (2019) 10:1998. doi: 10.3389/fimmu.2019.01998
103. Oorni K, Kovanen PT. Aggregation susceptibility of low-density lipoproteins-a novel modifiable biomarker of cardiovascular risk. *J Clin Med.* (2021) 10:1769. doi: 10.3390/jcm10081769
104. Lehti S, Nguyen SD, Belevich I, Vihinen H, Heikkila HM, Soliymani R, et al. Extracellular lipids accumulate in human carotid arteries as distinct three-dimensional structures and have proinflammatory properties. *Am J Pathol.* (2018) 188:525–38. doi: 10.1016/j.ajpath.2017.09.019
105. Pentikainen MO, Oorni K, Ala-Korpela M, Kovanen PT. Modified LDL - trigger of atherosclerosis and inflammation in the arterial

intima. *J Intern Med.* (2000) 247:359–70. doi: 10.1046/j.1365-2796.2000.00655.x
106. Weber C, Noels H. Atherosclerosis: current pathogenesis and therapeutic options. *Nat Med.* (2011) 17:1410–22. doi: 10.1038/nm.2538
107. Lee DY, Chiu JJ. Atherosclerosis and flow: roles of epigenetic modulation in vascular endothelium. *J Biomed Sci.* (2019) 26:56. doi: 10.1186/s12929-019-0551-8
108. Quail DF, Joyce JA. Microenvironmental regulation of tumor progression and metastasis. *Nat Med.* (2013) 19:1423–37. doi: 10.1038/nm.3394
109. Garcia-Roman J, Zentella-Dehesa A. Vascular permeability changes involved in tumor metastasis. *Cancer Lett.* (2013) 335:259–69. doi: 10.1016/j.canlet.2013.03.005
110. Gomez IG, Tang J, Wilson CL, Yan W, Heinecke JW, Harlan JM, et al. Metalloproteinase-mediated Shedding of Integrin beta2 promotes macrophage efflux from inflammatory sites. *J Biol Chem.* (2012) 287:4581–9. doi: 10.1074/jbc.M111.321182
111. Persi E, Duran-Frigola M, Damaghi M, Roush WR, Aloy P, Cleveland JL, et al. Systems analysis of intracellular pH vulnerabilities for cancer therapy. *Nat Commun.* (2018) 9:2997. doi: 10.1038/s41467-018-05261-x
112. Oorni K, Rajamaki K, Nguyen SD, Lahdesmaki K, Plihtari R, Lee-Rueckert M, et al. Acidification of the intimal fluid: the perfect storm for atherogenesis. *J Lipid Res.* (2015) 56:203–14. doi: 10.1194/jlr.R050252
113. Farr M, Garvey K, Bold AM, Kendall MJ, Bacon PA. Significance of the hydrogen ion concentration in synovial fluid in rheumatoid arthritis. *Clin Exp Rheumatol.* (1985) 3:99–104.
114. Naghavi M, John R, Naguib S, Siadaty MS, Grasu R, Kurian KC, et al. pH Heterogeneity of human and rabbit atherosclerotic plaques; a new insight into detection of vulnerable plaque. *Atherosclerosis.* (2002) 164:27–35. doi: 10.1016/S0021-9150(02)00018-7
115. Vermeulen M, Giordano M, Trevani AS, Sedlik C, Gamberale R, Fernandez-Calotti P, et al. Acidosis improves uptake of antigens and MHC class I-restricted presentation by dendritic cells. *J Immunol.* (2004) 172:3196–204. doi: 10.4049/jimmunol.172.5.3196
116. Kong X, Tang X, Du W, Tong J, Yan Y, Zheng F, et al. Extracellular acidosis modulates the endocytosis and maturation of macrophages. *Cell Immunol.* (2013) 281:44–50. doi: 10.1016/j.cellimm.2012.12.009
117. Lee-Rueckert M, Lappalainen J, Leinonen H, Pihlajamaa T, Jauhiainen M, Kovanen PT. Acidic extracellular environments strongly impair ABCA1-mediated cholesterol efflux from human macrophage foam cells. *Arterioscler Thromb Vasc Biol.* (2010) 30:1766–72. doi: 10.1161/ATVBAHA.110.211276
118. Lee-Rueckert M, Lappalainen J, Leinonen H, Plihtari R, Nordstrom T, Akerman K, et al. Acidic extracellular pH promotes accumulation of free cholesterol in human monocyte-derived macrophages via inhibition of ACAT1 activity. *Atherosclerosis.* (2020) 312:1–7. doi: 10.1016/j.atherosclerosis.2020.08.011
119. Jahde E, Rajewsky MF. Tumor-selective modification of cellular microenvironment *in vivo*: effect of glucose infusion on the pH in normal and malignant rat tissues. *Cancer Res.* (1982) 42:1505–12.
120. Wei G, Sun H, Dong K, Hu L, Wang Q, Zhuang Q, et al. The thermogenic activity of adjacent adipocytes fuels the progression of ccRCC and compromises anti-tumor therapeutic efficacy. *Cell Metab.* (2021) 33:2021–39.e8. doi: 10.1016/j.cmet.2021.08.012
121. Yabu M, Shime H, Hara H, Saito T, Matsumoto M, Seya T, et al. IL-23-dependent and -independent enhancement pathways of IL-17A production by lactic acid. *Int Immunol.* (2011) 23:29–41. doi: 10.1093/intimm/dxq455
122. Chen P, Zuo H, Xiong H, Kolar MJ, Chu Q, Saghatelian A, et al. Gpr132 sensing of lactate mediates tumor-macrophage interplay to promote breast cancer metastasis. *Proc Natl Acad Sci USA.* (2017) 114:580–5. doi: 10.1073/pnas.1614035114
123. El-Kenawi A, Gatenbee C, Robertson-Tessi M, Bravo R, Dhillon J, Balagurunathan Y, et al. Acidity promotes tumour progression by altering macrophage phenotype in prostate cancer. *Br J Cancer.* (2019) 121:556–66. doi: 10.1038/s41416-019-0542-2
124. Shree T, Olson OC, Elie BT, Kester JC, Garfall AL, Simpson K, et al. Macrophages and cathepsin proteases blunt chemotherapeutic response in breast cancer. *Genes Dev.* (2011) 25:2465–79. doi: 10.1101/gad.180331.111
125. Lindstedt L, Lee M, Oorni K, Bromme D, Kovanen PT. Cathepsins F and S block HDL3-induced cholesterol efflux from macrophage foam cells. *Biochem Biophys Res Commun.* (2003) 312:1019–24. doi: 10.1016/j.bbrc.2003.11.020
126. Miller NE, Olszewski WL, Hattori H, Miller IP, Kujiraoka T, Oka T, et al. Lipoprotein remodeling generates lipid-poor apolipoprotein A-I particles in human interstitial fluid. *Am J Physiol Endocrinol Metab.* (2013) 304:E321–8. doi: 10.1152/ajpendo.00324.2012
127. Lee-Rueckert M, Kovanen PT. Extracellular modifications of HDL *in vivo* and the emerging concept of proteolytic inactivation of prebeta-HDL. *Curr Opin Lipidol.* (2011) 22:394–402. doi: 10.1097/MOL.0b013e32834a3d24
128. Smith EB. Molecular interactions in human atherosclerotic plaques. *Am J Pathol.* (1977) 86:665–74.
129. Eliska O, Eliskova M, Miller AJ. The absence of lymphatics in normal and atherosclerotic coronary arteries in man: a morphologic study. *Lymphology.* (2006) 39:76–83.
130. Kholova I, Dragneva G, Cermakova P, Laidinen S, Kaskenpaa N, Hazes T, et al. Lymphatic vasculature is increased in heart valves, ischaemic and inflamed hearts and in cholesterol-rich and calcified atherosclerotic lesions. *Eur J Clin Invest.* (2011) 41:487–97. doi: 10.1111/j.1365-2362.2010.02431.x
131. Corn KC, Windham MA, Rafat M. Lipids in the tumor microenvironment: From cancer progression to treatment. *Prog Lipid Res.* (2020) 80:101055. doi: 10.1016/j.plipres.2020.101055
132. Nagarajan SR, Butler LM, Hoy AJ. The diversity and breadth of cancer cell fatty acid metabolism. *Cancer Metab.* (2021) 9:2. doi: 10.1186/s40170-020-00237-2
133. Zhang L, Han L, He J, Lv J, Pan R, Lv T. A high serum-free fatty acid level is associated with cancer. *J Cancer Res Clin Oncol.* (2020) 146:705–10. doi: 10.1007/s00432-019-03095-8
134. Wu H, Han Y, Rodriguez Sillke Y, Deng H, Siddiqui S, Treese C, et al. Lipid droplet-dependent fatty acid metabolism controls the immune suppressive phenotype of tumor-associated macrophages. *EMBO Mol Med.* (2019) 11:e10698. doi: 10.15252/emmm.201910698
135. Su P, Wang Q, Bi E, Ma X, Liu L, Yang M, et al. Enhanced lipid accumulation and metabolism are required for the differentiation and activation of tumor-associated macrophages. *Cancer Res.* (2020) 80:1438–50. doi: 10.1158/0008-5472.CAN-19-2994
136. Luo Q, Zheng N, Jiang L, Wang T, Zhang P, Liu Y, et al. Lipid accumulation in macrophages confers protumorigenic polarization and immunity in gastric cancer. *Cancer Sci.* (2020) 111:4000–11. doi: 10.1111/cas.14616
137. Rabold K, Aschenbrenner A, Thiele C, Boahen CK, Schiltmans A, Smit JWA, et al. Enhanced lipid biosynthesis in human tumor-induced macrophages contributes to their protumoral characteristics. *J Immunother Cancer.* (2020) 8:638. doi: 10.1136/jitc-2020-000638
138. Bostrom P, Magnusson B, Svensson PA, Wiklund O, Boren J, Carlsson LM, et al. Hypoxia converts human macrophages into triglyceride-loaded foam cells. *Arterioscler Thromb Vasc Biol.* (2006) 26:1871–6. doi: 10.1161/01.ATV.0000229665.78997.0b
139. Kruth HS. Receptor-independent fluid-phase pinocytosis mechanisms for induction of foam cell formation with native low-density lipoprotein particles. *Curr Opin Lipidol.* (2011) 22:386–93. doi: 10.1097/MOL.0b013e32834adadb
140. Wu A, Wojtowicz K, Savary S, Hamon Y, Trombik T. Do ABC transporters regulate plasma membrane organization? *Cell Mol Biol Lett.* (2020) 25:37. doi: 10.1186/s11658-020-00224-x
141. Lee BH, Taylor MG, Robinet P, Smith JD, Schweitzer J, Sehayek E, et al. Dysregulation of cholesterol homeostasis in human prostate cancer through loss of ABCA1. *Cancer Res.* (2013) 73:1211–8. doi: 10.1158/0008-5472.CAN-12-3128
142. Smith B, Land H. Anticancer activity of the cholesterol exporter ABCA1 gene. *Cell Rep.* (2012) 2:580–90. doi: 10.1016/j.celrep.2012.08.011

143. Sag D, Cekic C, Wu R, Linden J, Hedrick CC. The cholesterol transporter ABCG1 links cholesterol homeostasis and tumour immunity. *Nat Commun.* (2015) 6:6354. doi: 10.1038/ncomms7354
144. Goossens P, Rodriguez-Vita J, Etzerodt A, Masse M, Rastoin O, Gouirand V, et al. Membrane cholesterol efflux drives tumor-associated macrophage reprogramming and tumor progression. *Cell Metab.* (2019) 29:1376–89.e1374. doi: 10.1016/j.cmet.2019.02.016
145. Hoppstadter J, Dembek A, Horing M, Schymik HS, Dahlem C, Sultan A, et al. Dysregulation of cholesterol homeostasis in human lung cancer tissue and tumour-associated macrophages. *EBioMedicine.* (2021) 72:103578. doi: 10.1016/j.ebiom.2021.103578

Conflict of Interest: The authors declare that the research was conducted in the absence of any commercial or financial relationships that could be construed as a potential conflict of interest.

Publisher's Note: All claims expressed in this article are solely those of the authors and do not necessarily represent those of their affiliated organizations, or those of the publisher, the editors and the reviewers. Any product that may be evaluated in this article, or claim that may be made by its manufacturer, is not guaranteed or endorsed by the publisher.

Copyright © 2022 Lee-Rueckert, Lappalainen, Kovanen and Escola-Gil. This is an open-access article distributed under the terms of the Creative Commons Attribution License (CC BY). The use, distribution or reproduction in other forums is permitted, provided the original author(s) and the copyright owner(s) are credited and that the original publication in this journal is cited, in accordance with accepted academic practice. No use, distribution or reproduction is permitted which does not comply with these terms.

frontiers in Cardiovascular Medicine

REVIEW
published: 18 February 2022
doi: 10.3389/fcvm.2022.763516

Proprotein Convertase Subtilisin/Kexin Type 9 and Inflammation: An Updated Review

*Na-Qiong Wu, Hui-Wei Shi and Jian-Jun Li**

State Key Laboratory of Cardiovascular Diseases, Cardiometabolic Center, National Center for Cardiovascular Diseases, Fu Wai Hospital, Chinese Academy of Medical Sciences and Peking Union Medical College, Beijing, China

The function of Proprotein Convertase Subtilisin/Kexin Type 9 (PCSK9), a novel plasma protein, has mainly been involved in cholesterol metabolism in the liver, while, more interestingly, recent data have shown that PCSK9 also took part in the modulation of inflammation, which appeared to be another explanation for the reduction of cardiovascular risk by PCSK9 inhibition besides its significant effect on lowering lower-density lipoprotein cholesterol (LDL-C) concentration. Overall, a series of previous studies suggested an association of PCSK9 with inflammation. Firstly, PCSK9 is able to induce the secretion of proinflammatory cytokines in macrophages and in other various tissues and elevated serum PCSK9 levels could be observed in pro-inflammatory conditions, such as sepsis, acute coronary syndrome (ACS). Secondly, detailed signaling pathway studies indicated that PCSK9 positively regulated toll-like receptor 4 expression and inflammatory cytokines expression followed by nuclear factor-kappa B (NF-kB) activation, together with apoptosis and autophagy progression. Besides, PCSK9 enhanced and interacted with scavenger receptors (SRs) of inflammatory mediators like lectin-like oxidized-LDL receptor-1 (LOX-1) to promote inflammatory response. Additionally, several studies also suggested that the role of PCSK9 in atherogenesis was intertwined with inflammation and the interacting effect shown between PCSK9 and LOX-1 was involved in the inflammatory response of atherosclerosis. Finally, emerging clinical trials indicated that PCSK9 inhibitors could reduce more events in patients with ACS accompanied by increased inflammatory status, which might be involved in its attenuating impact on arterial plaque. Hence, further understanding of the relationship between PCSK9 and inflammation would be necessary to help prevent and manage the atherosclerotic cardiovascular disease (ASCVD) clinically. This review article will update the recent advances in the link of PCSK9 with inflammation.

Keywords: PCSK9 (proprotein convertase subtilisin kexin type 9), inflammation, ASCVD, TLR4 (toll-like receptor 4), LOX-1

OPEN ACCESS

Edited by:
Wen Dai,
Versiti Blood Research Institute, United States

Reviewed by:
Josep Julve, Institut de Recerca de l'Hospital de la Santa Creu i Sant Pau, Spain
Aldo Grefhorst, Amsterdam University Medical Center, Netherlands
Robert Kiss, McGill University, Canada
Xiaobo Wang, Columbia University, United States

****Correspondence:***
Jian-Jun Li
lijianjun938@126.com

Specialty section:
This article was submitted to Lipids in Cardiovascular Disease, a section of the journal Frontiers in Cardiovascular Medicine

Received: *24 August 2021*
Accepted: *18 January 2022*
Published: *18 February 2022*

Citation:
Wu N-Q, Shi H-W and Li J-J (2022) Proprotein Convertase Subtilisin/Kexin Type 9 and Inflammation: An Updated Review. Front. Cardiovasc. Med. 9:763516. doi: 10.3389/fcvm.2022.763516

INTRODUCTION

Atherosclerotic cardiovascular disease (ASCVD) is a primary cause of morbidity and mortality around the world, which is definitely associated with multiple risk factors. Among them, the inflammation is the principal mechanism for the development of ASCVD except for lipid disorder. A large number of studies have demonstrated that chronic inflammatory response induced by

substantial inherent or acquired risk factors exerts a significant effect on the initiation and development of atherosclerosis and the resulting plaque rupture and erosion, then it contributes to systemic repercussions of atherosclerosis-related cardiovascular diseases (CVD) (1). Besides, the interaction of risk factors such as lipid and inflammation has also been considered to play an important role in ASCVD. Interestingly, emerging data have shown that proprotein convertase subtilisin/kexin type 9 (PCSK9), an key protein of lipid metabolism, is involved in the production of both inflammatory cytokines and atherosclerosis plaque (2–7).

PCSK9 is primarily biosynthesized in the hepatocytes, then reaches the basolateral surface of the hepatocyte and binds low density lipoprotein receptor (LDLR) in an autocrine effect. Subsequently, the complex composed of LDL-C, LDLR, and PCSK9 is internalized into hepatocytes and undergoes endocytosis and lysosomal degradation, thereby reducing LDLR on the cell membrane and raising LDL-C levels (8). In addition of liver, PCSK9 is also expressed in many other tissues including small intestine, lung, kidney, pancreas and brain. Emerging studies have also found that PCSK9 is highly expressed in vascular endothelial cells (EC), smooth muscle cells (SMC) and macrophages (9), subsequently exerting local effects on vascular homeostasis and atherosclerotic plaques (10). Additionally, the detection of PCSK9 provides a new target for the management of hypercholesterolemia and the reduction of cardiovascular risk. Thus, the understandings of the physiology of PCSK9 have helped to broaden our knowledge in PCSK9 and PCSK9 inhibitors. Basically, although the mediation of up-regulation of LDLR accounts for the main effect of PCSK9 inhibitors, there is growing evidence supporting that PCSK9 may have a pleiotropy. One of these effects might be associated with inflammatory modulation in the development of ASCVD independent of LDLR regulation.

In this review, we generalized the biological characteristics of PCSK9 and mainly focused on updated evidence of the relation of PCSK9 to inflammation, in order that we could stress the clinical significance of the interaction between PCSK9 and inflammation.

PCSK9 AND INFLAMMATION: OBSERVATIONAL COHORT EVIDENCE

Several previous studies examined the relation of PCSK9 to inflammation using cross-sectional observations. These studies mainly evaluated the correlation between plasma PCSK9 concentrations and a number of key inflammatory markers, including white blood cells (WBCs), fibrinogen, and high-sensitivity C-reactive protein (hs-CRP) (**Table 1**). For example, a small sample size study in Chinese patients with angiography-proven coronary artery disease (CAD) has shown that the increase of plasma PCSK9 level was associated with the elevation in white blood cell counts (WBCC), fibrinogen and high-sensitivity C-reactive protein (hs-CRP) (11). As is well-known, the WBCC is a traditional marker of inflammation and either inflammation or PCSK9 was considerably connected with atherosclerosis in populations with different levels of baseline risks. Interestingly, in a single-center study of stable CAD patients naïve to lipid-lowering therapy (6), both univariate and multivariate regression analyses showed that plasma PCSK9 levels were positively associated with WBCC subgroup, lymphocyte count and neutrophils count, while the molecular mechanism by which WBCC was associated with plasma PCSK9 levels was still unclear. Meanwhile, a cross-sectional study in stable CAD patients has revealed that circulating PCSK9 levels were positively correlated with fibrinogen levels but unrelated to some potential confounders such as lipid spectrometry and hs-CRP (2). Otherwise, a recent study indicated that PCSK9 was not induced in artificial human inflammation and was not correlated with inflammatory response in ten healthy volunteers stimulated by endotoxin (lipopolysaccharide, LPS) (12). It seemed that the study did not support the notion that PCSK9 could trigger an inflammatory response in human study.

CRP, a kind of acute phase mediator, is considered to be a systemic inflammatory biomarker of sensitivity but of no specificity. The elevation in plasma hs-CRP concentration has also been considered to be the risk factor of atherosclerosis (17). Observational studies have revealed that plasma CRP levels were a powerful predictor for cardiovascular (CV) risk and logarithmically correlated with CAD risk (18). Recently, Pradhan et al. assessed the residual risk of inflammation in 9,738 patients who had received both statins and bococizumab in the Studies of PCSK9 Inhibition and the Reduction of Vascular Events (SPIRE)-1 and SPIRE-2 cardiovascular outcomes trial. They evaluated residual risk according to on-treatment levels of hsCRP(hsCRP$_{OT}$) recorded 14 weeks after drug initiation. The data indicated that increased hsCRP$_{OT}$ remained as an important predictor of cardiovascular risk in CAD patients receiving statins and PCSK9 inhibitors (19). This study suggested that although the maximum reduction in LDL-C was achieved, regulating inflammation provided additional opportunities to reduce cardiovascular risk, which was named as residual inflammatory risk.

Furthermore, in patients with stable CAD, PCSK9 levels were significantly positively correlated with hs-CRP levels (2). Recently, in a large prospective multi-center study conducted in patients with acute coronary syndrome (ACS), patients with higher levels of circulating PCSK9 suffered a higher degree of acute phase inflammation assessed by hs-CRP levels (7). Similarly, a prospective case-control study in CAD patients naïve to lipid-lowering therapy showed a significantly positive correlation between PCSK9 levels and the incidence and severity of CAD (11), and the effect of PCSK9 on CAD is primarily mediated by the increased atherogenic lipids and inflammatory markers. Hence, these studies have shown that PCSK9 is associated with the occurrence of inflammation in the occurrence and development of CAD, suggesting that inhibition of PCSK9 may have a therapeutic effect on atherosclerotic inflammation and CAD. However, although there was no doubt that increased plasma PCSK9 concentrations were in association with elevated inflammatory biomarkers, whether PCSK9 is causal trigger for inflammation might need to be further confirmed.

TABLE 1 | Correlation of plasma PCSK9 levels with inflammatory markers in patients with ASCVD.

References	Features of clinical study	Inflammatory markers	Univariable analysis (*r*, *P*-value)	Multivariable analysis (β, *P*-value)
Li et al. (6)	Single-center, cross-sectional study (251 stable CAD patients)	WBCC	0.167, $P = 0.008$	0.186, $P < 0.01$
Zhang et al. (2)	Cross-sectional study (219 stable CAD patients)	Fibrinogen Hs-CRP	0.211, $P = 0.002$ 0.153, $P = 0.023$	0.168, – 0.011, –
Gencer et al. (7)	Multi-center prospective cohort study (2,168 ACS patients)	Hs-CRP	0.077, $P = 0.006$	–, – –, –
Li et al. (11)	Prospective study (552 CAD patients)	WBCC Fibrinogen	0.077, $P = 0.004$ 0.181, $P < 0.001$	–, – –, –
Heinzl et al. (12)	Prospective, single-blinded, placebo-controlled cross-over study (10 healthy nonsmoking male receiving LPS or placebo)	IL-6 CRP PCSK9 PCSK9 and IL-6	$P = 0.018$ (RM-ANOVA) $P < 0.001$(–) $P = 0.44$(–) $P = 0.358$	–, – –, – –, – –, –

TABLE 2 | Experimental studies about the impact of PCSK9 on atherosclerotic plaques formation.

References	Model	Treatment	Impact on systemic inflammation	Impact on vascular inflammation
Giunzioni et al. (10)	$ApoE^{-/-}$ recipient mice	hPCSK9	Raised Infiltration of Ly6C(hi) inflammatory monocytes (+32%)	–
Tavori et al. (13)	$LDLR^{-/-}$ or $apoE^{-/-}$ mice overexpressing human PCSK9 (Hpcsk9) model	hPCSK9	–	1. Increased atherosclerotic lesion size and composition independent of lipids and lipoprotein changes 2. Increased accumulation of PCSK9 in the arterial wall
Ferri et al. (5)	$PCSK9^{-/-}$ mice model	Deletion of PCSK9 gene	–	1. Attenuated neointimal plaque formation 2. Higher SMCs accumulation
Sun et al. (14)	Atherosclerosis-prone mouse model	Deletion of PCSK9 gene	–	1. Reduced atherogenesis 2. Decreased expression of adhesion molecules, ICAM-1, MCP-1, and MCP-3 by ECs
Kühnast et al. (15)	APOE*3Leiden.CETP mice	Alirocumab	Decreased pro-inflammatory Ly6Chi monocytes	1. Attenuated vascular inflammation and necrotic core formation 2. Improved plaque stability 3. Reduced expression of ICAM-1 in ECs
Landlinger et al. (16)	APOE*3Leiden.CETP mice	Anti-PCSK9 vaccine	Decreased serum levels of MCSF-1 and VEGF-A	1. Reduced plaque number and size 2. Decreased plasma level of ICAM-1 in ECs

PCSK9 AND INFLAMMATION: BASIC INVESTIGATIONS IN ATHEROSCLEROSIS

Although the relation of PCSK9 to the formation of atherosclerotic plaque is unclear, several basic studies showed that PCSK9 might be involved in the development of atherosclerotic plaque through inflammation-mediated process.

It is well-known that ASCVD is an inflammatory process. A previous study using multilocal positron emission tomography- magnetic resonance imaging suggested an arterial inflammation in patients with sub-clinical atherosclerosis, so it convincingly revealed an inflammatory state in the early stages of atherosclerosis (20). Chronic inflammation, along with other factors such as high blood pressure, diabetes and smoking, has become the ultimate critical pathway leading to the development and progression of ASCVD. Data also showed that the activation of endothelium could lead to the secretion of surface molecules which were subsequently adsorbed into inflammatory cells, following monocytes' and macrophages' migration across the endothelium and accumulation beneath the intima. Subsequently, these cells release cytokines and produce a pro-inflammatory environment during activation. With time going by, Lectin-like OXLDL Receptor-1 (LOX-1) combines with circulating oxidized LDL (ox-LDL) on vascular smooth muscle cells (VSMCs) and monocytes/macrophages and enters the vascular stroma, then it results in the formation of foam cells (21, 22). In addition, ischemic myocardium is characterized by the release of pro-inflammatory cytokines into the blood, which causes a violent inflammatory response. In patients with myocardial ischemia, especially in the acute

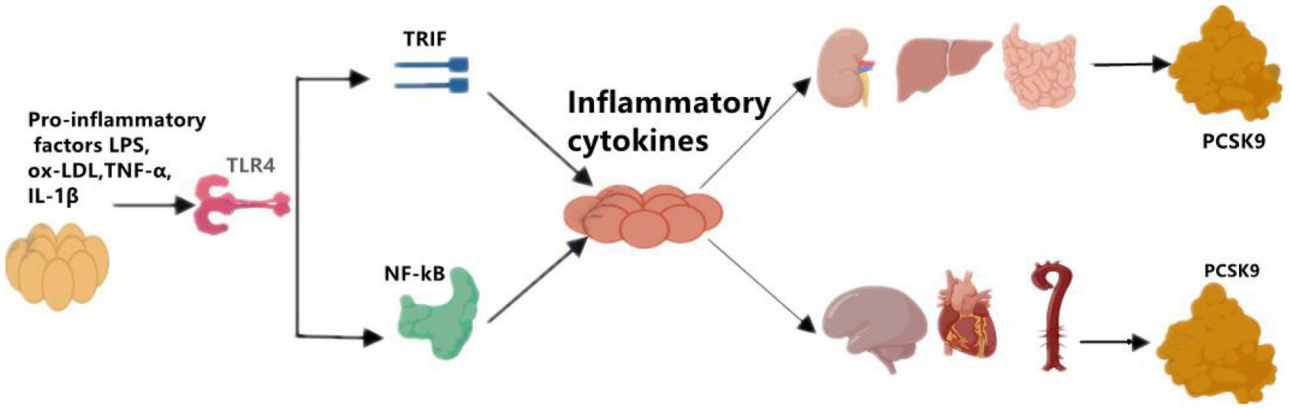

FIGURE 1 | The regulation of on PCSK9 secretion. Pro-inflammatory factors, such as LPS, ox-LDL, TNF-α, and IL-1β induces the expression of PCSK9 in main sources for PCSK9 such as liver, kidney, small intestine, and in brain, heart, artery as well. LPS, lipopolysaccharide; oxLDL, oxidized low-density lipoprotein; TNF-α, tumor necrosis factor alpha; IL-1β, interleukin 1β; TLR4, toll-like receptor 4; NF-kB, nuclear factor kappa-light-chain-enhancer of activated B cells; PCSK9, proprotein convertase subtilisin/kexin Type 9.

phase, pro-inflammatory biological factors such as hsCRP, tumor necrosis factor-α (TNF-α), interleukin-6 (IL-6), and interleukin-1β (IL-1β) were significantly increased (23).

Although the primary sources of PCSK9 are hepatocytes, other cells in extrahepatic tissues such as the brain, heart, kidney, small intestine, and blood vessels can also produce PCSK9 that is secreted into the circulation (**Figure 1**). Epicardial adipose tissue (EAT) could also be a source of PCSK9 and EAT inflammation was correlated with local PCSK9 expression (24). The expression of PCSK9 in vascular endothelial cells (EC) and VSMCs is mainly regulated by proinflammatory stimulation such as ox-LDL, TNF-α, IL-1β, and LPS (25). Studies have shown that plasma levels of PCSK9 were associated with circulating LDL-C as well as some other risk factors for coronary diseases, and that high levels of PCSK9 have been found in patients suffering systemic inflammatory response syndrome (SIRS) and sepsis (26). Moreover, The European Collaborative Project on Inflammation and Vascular Wall Remodeling in Atherosclerosis-Intravascular Ultrasound (ATHEROREMO-IVUS) study showed that serum PCSK9 levels were in relation to the absolute volume of inflammatory plaque and necrotic core tissue (27). In previous studies, Almontashiri et al. observed that elevated serum PCSK9 levels were presented in patients with acute myocardial infarction and myocardial ischemia, especially in those newly diagnosed (28). In their studies, a significant association of serum PCSK9 levels with pro-inflammatory cytokines IL-6, IL-1β, TNF, MCSF (macrophage colony-stimulating factor) and hs-CRP was found (28). Experimental data showed that in the vascular injury model of $PCSK9^{-/-}$ mouse, the loss of PCSK9 was linked to the reduction of neointima formation in atherosclerotic plaques (5). Other experimental studies about the impact of PCSK9 on atherosclerotic plaques formation were shown in **Table 2**.

Notably, PCSK9 can regulate LDLR expression locally in neighboring cells including arterial monocytes/macrophages (29). PCSK9 overexpression could result in increased size of atherosclerotic plaques, the phenomenon of which had not been observed in $LDLR^{-/-}$ mice, suggesting that the role of PCSK9 in atherosclerotic development was related to LDLR (10). In an investigation elucidating the direct pro-atherogenic role of PCSK9 in atherosclerosis, firstly, WT mice expressing null (KO) level of PCSK9 accumulated 4-fold less aortic cholesteryl esters (CE) than WT mice, whereas mice expressing high (Tg) levels of PCSK9 exhibited high CE and severe aortic lesions. In addition, apoE-deficient mice that expressed null (KO/e) levels of PCSK9 showed a 39% reduction in aortic CE accumulation compared to those expressing normal (WT/e) levels of PCSK9, while Tg/e mice showed a 137% increase. Finally, LDLR-deficient mice expressing null (KO/L) and high (Tg/L) levels of PCSK9 exhibited similar levels of plasma cholesterol and CE accumulation to WT/L, suggesting that PCSK9 modulated atherosclerosis mainly via the LDLR (30).

Obviously, these studies have confirmed that PCSK9 enhances the infiltration of inflammatory monocytes into the vessel wall by virtue of the interaction of PCSK9-LDLR in plaques, which thus directly promotes the formation of inflammatory atherosclerotic plaques. In addition of LDLR, other members of the LDLR superfamily such as LRP5 may also be a target of PCSK9. A study focusing on primary cultures of inflammatory cells including monocytes and macrophages found that LRP5 and LDLR acted through different mechanisms. Since for one, no variation in LDLR expression levels existed in control cells but did in LRP5-silenced cells and LRP5 was not regulated by lipoprotein receptor modulator SREBP-2, for another, in PCSK9-silenced macrophages, LDLR expression increased significantly after agLDL loading but LRP5 levels didn't alter. The study also observed that PCSK9 binds LRP5 at the perinuclear area of human macrophages and the two form a complex located in the cytoplasm of macrophages, and this interaction was involved in lipid uptaking in macrophages. In addition, LRP5-silenced macrophages showed a reduced release of PCSK9, demonstrating that LRP5 participates in the release of PCSK9. Further, in macrophages silenced for both LRP5 and PCSK9, reduction in CE accumulation was observed. Moreover, in PCSK9 silenced-macrophages, decreased TLR4 protein levels

and rescued increase in TNFα and IL-1β showed, revealing a role of PCSK9 in macrophage inflammation associated to the TLR4/NFκB pathway (31).

Meanwhile, a clinical study indicated that elevated serum levels of PCSK9 were associated with new plaque formation even after adjusting LDL-C levels and other traditional risk factors (3). Therefore, the pro-atherosclerotic effect of PCSK9 was not only related to the disturbance of lipid metabolism but also intertwined with PCSK9-stimulated plaque inflammation, which was further supported in ApoE$^{-/-}$ or LDLR$^{-/-}$ transgenic mice that overexpressed human PCSK9 (10). This study might provide additional evidence of the local effect of PCSK9 on inflammatory plaques, indicating the direct role of PCSK9 in atherosclerotic plaques. That is, PCSK9 expressed from bone-marrow derived macrophages could directly and locally accentuate vascular inflammation by changing the composition of lesion, but not by changing the lesion size and serum cholesterol level (10). Interestingly, *in vitro* studies have also confirmed the association of PCSK9 with monocyte-mediated plaque inflammation, suggesting that local PCSK9 production by VSMCs could inhibit C-C chemokine receptor type 2(CCR2)-dependent chemotaxis of monocytes in plaques, thereby enhancing their sustaining expression in the atherosclerotic environment (32). In addition, pro-inflammatory leucocytes played a critical role in atherosclerotic development and at the same time regulated the composition of atheroma lesion while no significant changes in cholesterol levels and lesion size were observed (33). Thus, these findings demonstrated that through altering plaque composition and accelerating inflammatory monocytes infiltration and differentiation in plaques, PCSK9 could directly promote atherosclerotic inflammation independently of cholesterol regulation, which indirectly supported the notion that PCSK9 inhibitors can improve clinical outcomes through not only lipid dependent but also lipid independent pathways.

PCSK9 AND INFLAMMATION: POTENTIAL SIGNALING PATHWAYS

Although PCSK9 has been considered as a trigger for the expression of pro-inflammatory cytokines, the detailed mechanism it involves remains to be summarized. There appeared two associated signaling pathways involved in the positive regulation of PCSK9 to inflammatory cytokines expression and atherosclerotic lesions formation.

Firstly, the Toll-like receptor 4(TLR4)/nuclear factor-kappa B (NF-*k*B) signaling pathway has been found to be the main pathway that mediates PCSK9-induced expression of pro-inflammatory cytokine (34), and plays an indispensable role in the initiation and development of atherosclerotic lesions by inducing vascular inflammation (35). TLR4 stimulates the activation of NF-kB transcription factor, which is obligated to producing many pro-inflammatory genes, including TNF-α, IL-6, interleukin(IL)-1, and macrophage chemotactic protein 1 (MCP-1) (36). Primarily functioning through regulating inflammatory response, NF-*k*B is a Redox sensitive transcription factor which can be activated by a variety of stimuli, including oxidized LDL (ox-LDL), reactive oxygen species (ROS), Toll-like receptor (TLR), cytokines, and bacterial products such as LPS. *In vitro* studies in RAW264.7 macrophages stimulated by ox-LDL also identified the involvement of the TLR4/NF-*k*B signaling pathway in PCSK9-mediated inflammation. According to their study, up-regulation and down-regulation of PCSK9, respectively, increased and decreased ox-LDL-induced expression of pro-inflammatory cytokines including TNF-α, IL-1β and MCP-1. This outcome is related to the up-regulation of TLR4 expression triggered by ox-LDL, followed by nuclear translocation of NF-*k*B (34). Basically, PCSK9 is most likely to increase the expression of pro-inflammatory cytokines through combining with the C-terminal domain of TLR4, resulting in increased TLR4 expression as well as activated TLR4/NF-*k*B signaling pathway (34).

The effects of PCSK9 on TLR4/NF-kB regulated inflammation has also been verified in a study with LPS-induced sepsis model, in which LPS could induce inflammatory response by virtue of increased PCSK9 (37). The interaction of LPS and PCSK9 may be explained by previous facts. LPS could induce TLR4 and trigger NF-kB signaling pathway, at the same time it up-regulates PCSK9, then leads to systemic inflammation (38), which might indicate that the pro-inflammatory effect of PCSK9 may be intermediated, at least in proportion, by targeting the activation of the TLR4/NF-kB pathway (38). Another previous study also showed that PCSK9 over-expression could increase plasma IL-6 concentration, while knockout of PCSK9 could decrease plasma IL-6 levels and attenuate organ inflammatory response in the mouse septicemia model (39). Similar results were also reported by another study on PCSK9 knockout mice. In their study, data showed an attenuated impact on LPS-induced inflammation and decreased plasma levels of pro-inflammatory cytokines such as tumor necrosis factor-α (TNF-α), IL-6, MCP-1, and macrophage inflammatory protein 2(MIP-2) (40). Results from a human study further supported that patients with septic shock who carried the PCSK9 loss-of-function (LOF) allele had lower serum levels of pro-inflammatory cytokines compared with patients with the gain-of-function (GOF) allele (40). These findings indicated an association of PCSK9 with inflammation in LPS-induced sepsis model, suggesting that PCSK9 would play a role of pro-inflammatory mediator. Moreover, in the study we have discussed at the beginning of this paragraph, down-regulation of PCSK9 inhibitor Farnesoid X receptor and peroxisome proliferation-activated receptor alpha (PPARα) transcription factor could increase PCSK9 expression, resulting in a decrease in liver LDLR expression and an increase in plasma LDL-C (37) (**Figure 2**).

Next, the activation of the PCSK9-LOX-1 axis has also been demonstrated to participate in PCSK9-mediated inflammatory response. During the formation of atherosclerotic plaque, circulating oxidized LDL (ox-LDL) is bound to scavenger receptors (SRs) of inflammatory mediators like LOX-1 locating on the surface of endothelial cells (ECs) (22). As a well-recognized mediator of inflammation and atherosclerosis (21, 41, 42), LOX-1 is the principal receptor for ox-LDL on ECs and VSMCs, and is expressed when macrophages, SMCs, and fibroblasts are exposed to ox-LDL, angiotensin II, or

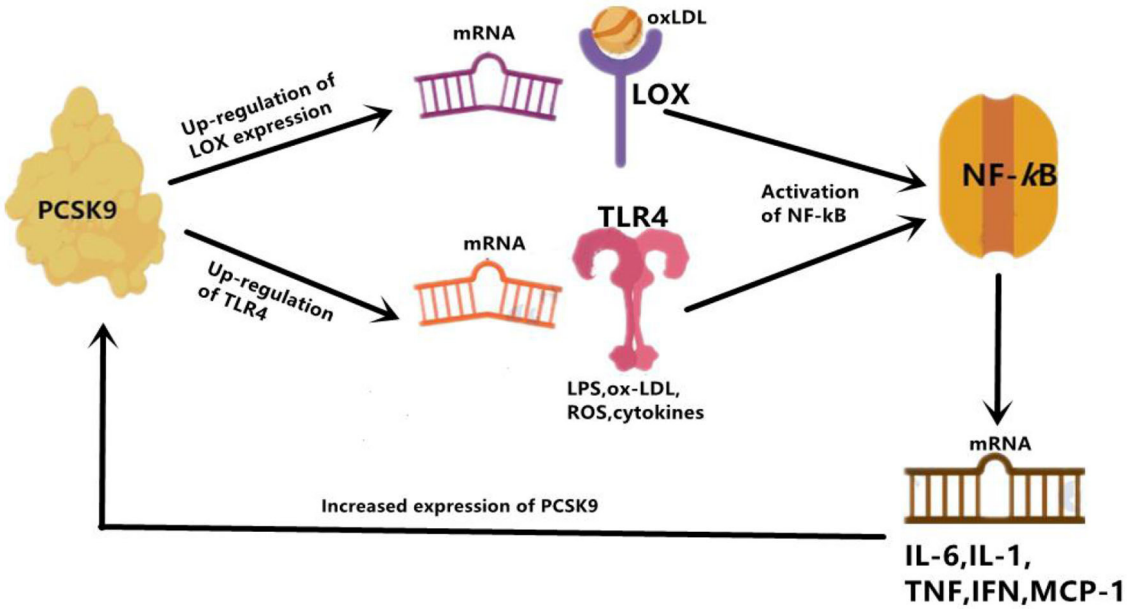

FIGURE 2 | PCSK9 mediate inflammation through enhancing expression of TLR4 and LOX. LOX can mainly increase uptake of ox-LDL, and TLR4 increase uptake of LPS. Then activation of NF-kB follows. Overall, activated NF-kB up-regulates expression of inflammatory cytokines, such as IL-6, IL-1, TNF-α, IFN- γ, and MCP-1. IL-1, interleukin 1; IL-6, interleukin 6; IFN-γ, interferon gamma; MCP-1, monocyte chemoattractant protein 1.

proinflammatory cytokines. Studies have shown that there is a positive feedback between PCSK9 and LOX-1 in VSMCs. The activation of LOX-1 stimulates the expression of PCSK9 (25), and in contrast, PCSK9 promotes the expression of LOX-1 and the uptake of ox-LDL, which triggers a pro-inflammatory state. Additionally, pathological studies did suggest that LOX-1 and PCSK9 were co-expressed in atherosclerotic plaques, indicting that PCSK9 and LOX-1 may interact with each other in the inflammatory microenvironment (25). Notably, LOX-1 is highly expressed in growing plaques and ruptured plaques (41) and also in ischemic heart, leading to inflammation and cardiomyocyte apoptosis (43). And also, acting as a primary NF-kB activator, ox-LDL induces inflammatory response in EC and macrophages and enhances the expression of PCSK9 (44). In contrast, down-regulation of PCSK9 could reduce ox-LDL-induced inflammatory response accompanied by reduction in pro-inflammatory cytokines including IL-1α, IL-6, and TNF-α (44). Laboratory studies on LOX-1 gene deletion and LDLR knockout mice have shown a significant reduction in atherosclerosis progression (45), which might be in relation to a critical reduction in the accumulation of inflammatory cells in the vessel wall. On the contrary, LOX-1 overexpression in ECs could accentuate plaque formation and atherosclerotic progression (46).

The interplay between PCSK9 and LOX-1 may also be explained by the regulation of mitochondrial ROS (mtROS) and NF-kB (47). Interestingly, VSMC-originated PCSK9 was shown to induce the damage of mitochondrial DNA, the fragments of which could promote mtROS-mediated expression of PCSK9/LOX-1 (48). Both *in vitro* and *in vivo* studies showed that changes in ROS production and fluid shear force would activate the PCSK9-LOX-1 axis (47). Mechanically, the regulation of fluid shear stress on PCSK9 expression was mediated by Nicotinamide Adenine Dinucleotide Phosphate (NADPH) oxidase-dependent ROS production in VSMCs and ECs of human and mouse aorta (47). Meanwhile, evidence showed that the two-way crossover linking ROS production and PCSK9 expression may be mediated by the NADPH oxidase system in aortic tissue under inflammatory state, thereby regulating the deposition of LDL and ox-LDL in atherosclerotic areas (49). In general, under low shear stress conditions, such as in the inflammatory state, PCSK9 could enhance inflammatory response in atherosclerotic lesion through activation of the ROS/NF-kB/LOX-1/oxLDL axis in VSMCs.

In summary, PCSK9 up-regulates the expression of TLR4 and LOX-1, both of which further activates NF-kB and induces the expression of inflammatory cytokines. Thus, TLR4/NF-kB axis and PCSK9/LOX-1/NF-kB axis are the two mainly involved signaling pathways mediating the PCSK9-induced pro-inflammatory conditions.

PCSK9 INHIBITORS AND INFLAMMATION: CLINICAL AND EXPERIMENTAL OBSERVATIONS

Both experimental results and clinical trials indicated the repressive role of PCSK9 inhibition on vascular inflammation and subsequent development of atherosclerosis.

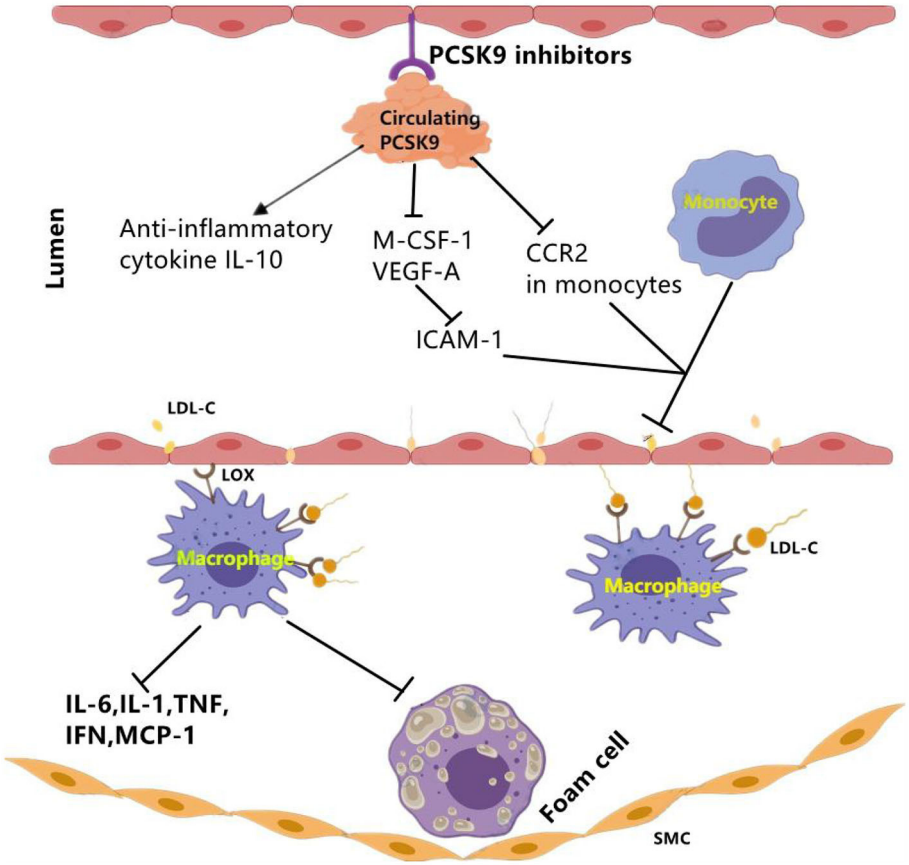

FIGURE 3 | The effect of PCSK9 inhibition on vascular inflammation. PCSK9 inhibition could decrease the expression of main markers of vascular inflammation including M-CSF-1 and VEGF-A which leads to reduced ICAM-1 expression in endothelial cells and reduced infiltration of monocytes into the subendothelial layer. Moveover, PCSK9 inhibition reduces CCR2 expression and the inhibition of monocyte migration. Besides pro-inflammatory mediators, PCSK9 inhibitors may function through elevating anti-inflammatory cytokines such as IL-10. CCR2, C–C chemokine receptor Type 2; ICAM-1, intercellular adhesion molecule 1; LDL-C, low-density lipoprotein cholesterol; LOX-1, lectin-like oxidized LDL receptor-1; MCSF-1, major histocompatibility complex; oxLDL, oxidized low-density lipoprotein; SMCs, smooth muscle cells; VEGF-A, vascular endothelial growth factor A. The signal "→"indicates "promotes," "⊣"indicates "inhibits".

PCSK9 antagonists could be achieved by active vaccination which binds to PCSK9 and inhibits its interaction with LDLR. In APOE*3 Leiden.cholesteryl ester transfer protein (CETP) mice study (16), data showed that PCSK9 AT04A vaccine could exert immunosuppression to circulating PCSK9, and reduce the plasma cholesterol levels by 53% (16), and decrease the concentrations of macrophage colony stimulating factor 1(M-CSF-1), vascular endothelial growth factor A(VEGF-A). Then, reduced plasma levels of M-CSF-1 and VEGF-A led to decreased expression of intracellular adhesion molecule-1 (ICAM-1) in endothelial cells, thereby reducing recruitment and adhesion of monocytes to the vascular endothelium (16) (**Figure 3**). Moreover, a decrease in the number and size of atherosclerotic plaques was also observed in AT04A-inoculated mice (16). Besides, in a prospective, observational, multicenter trial involving 21 consecutive patients with stable CVD, researchers evaluated arterial inflammation using 18F-fluoro-2-deoxy-D-glucose.

(FDG) positron emission tomography/computed tomography (PET/CT). They found that long-term administration of PCSK9 inhibitor significantly improved arterial inflammation, and that in index vessel, target-to-background ratio (TBR) detected by PET/CT significantly decreased by 0.92 (95% CI: 0.56, 1.28, $P < 0.001$) (50).

In addition of clinical data, there was also experimental data from an *in vivo* study using ApoE *3Leiden.CETP mice. This study found that alirocumab reduced endothelial expression of ICAM-1 and Ly6C^{hi} monocytes (Ly6C^{hi} monocytes are the precursors of proinflammatory M1 macrophages, and they would progress into pro-inflammatory M1 macrophages) (15). The results also showed the decrease of other markers for vascular inflammation including T cell abundance in the aortic root region, necrotic content in macrophages, cholesterol division in arterial plaques as well (15). Briefly, alirocumab can significantly improve morphology and stability of lesion in mouse models of atherosclerosis (15).

In addition of intracellular accumulation of lipids in monocytes, a clinical study carried out in patients with Familial hypercholesterolemia (FH) also observed that PCSK9 inhibition decreased chemokine receptor Type-2(CCR2) expression

TABLE 3 | Percentage changes of hsCRP and LDL-C after PCSK9 inhibition agents treatments.

clinical study	PCSK9 inhibition agents	Hs-CRP (mg/L)			LDL-C (mg/dL)		
		Baseline	Post	Percentage change	Baseline	Post	Percentage change
FOURIER (52)	Evolocumab	1.7	1.4	0% vs. placebo	92.0	30.0	−59% vs. placebo
ODYSSEY COMBOII (54)	Alirocumab	3.58	3.51	−2% vs. baseline	108.0	53.3	−49.5% vs. baseline
ODYSSEY OUTCOMES (55)	Alirocumab	1.6	NA	NA	87.0	53.0	−54.7% vs. placebo
Single-Center study (53)	Evolocumab	1.81	2.46	+35.9% vs. baseline	118.0	64.0	−45.7% vs. baseline
Post-hoc analysis of the SPIRE trials (19)	Bococizumab	1.88	1.84	+6.6% vs. placebo	96.5	34.7	−60.5% vs. placebo

which correlated with diminished trans-endothelial migratory capability of monocytes (51). Meanwhile, reduction in TNF-α levels and elevation in anti-inflammatory cytokine IL-10 were also revealed (51). Further evidence from clinical trials showed an anti-inflammatory role of evolocumab, alirocumab, and bococizumab in patients with stable CAD patients (19, 52) and patients living with HIVs (PLWH) and People With Dyslipidemia (53) (**Table 3**).

All these studies indicated that systemic and vascular inflammation and the development of atherosclerosis were ameliorated by PCSK9 inhibitors. However, PCSK9 inhibitors failed to affect the level of hs-CRP in some studies.

Results of *post-hoc* analysis of the SPIRE trials of bococizumab (19) showed that plasma levels of hs-CRP measured 14 weeks after drug initiation did not decrease as expected (+6.6%), while circulating LDL-C markedly reduced by 60.5%. In a placebo-controlled, double-blind study, 14 weeks of alirocumab treatment resulted in a robust reduction in arterial wall inflammation and marked LDL-C–lowering in high CV risk patients, but no changes were observed in the plasma inflammatory markers (56). Besides, in a randomized, double-blind, and dose-ranging phase 2 Study conducted in patients with CHD, PCSK9 inhibitor RG7652 treatment led to a significant dose-dependent decrease in LDL-C level, but failed to bring in significant reductions in circulating systemic markers such as hs CRP, IL-6, and TNF-α (57). More convincingly, a meta-analysis of randomized controlled trials assessing the impact of PCSK9 inhibitors also concluded that there was no significant impact on circulating level of hs-CRP (13).

PCSK9 AND INFLAMMATION: CONCLUSION

As is well-known, ASCVD is a leading cause of mortality in the world and lipid metabolic disorder and inflammation are two principal triggers for the development of ASCVD. PCSK9 as an emerging novel target for LDL-C catabolism has widely been well-recognized since discovery via parallel molecular biology and clinical genetics studies in 2003. Following studies to characterize PCSK9 has shed new light on its multiple effects of cardiovascular system. One of them is the interaction between PCSK9 and inflammation.

The pro-inflammatory role of PCSK9 in atherosclerosis progression has been confirmed both by experimental evidence and clinical data. Animal models confirmed that PCSK9 gene expression could affect serum levels of systemic inflammatory cytokines such as IFN-c, TNF-a, IL-6, and MCP-1. Observations in recent years from clinical studies found that in patients with ACS and CAD, elevated plasma levels of PCSK9 were independently linked to major systemic inflammatory markers including WBCs, hs-CRP, and fibrinogen. At the same time, there still are abundant experimental and clinical data investigating the consequences of PCSK9 inhibition on systemic and vascular inflammation. Atherosclerosis models exhibited that PCSK9 inhibition restrains atherosclerotic progression and improves plaque morphology. Clinical data showed that alirocumab therapy exerted local anti-inflammatory effect through decreasing the expression of CCR2 and anti-inflammatory cytokines. These discoveries regarding the relation of PCSK9 to inflammation have refreshed our understandings of the PCSK9 and PCSK9 inhibitors, which may help to promote a new era of cardiovascular disease prevention.

As a consequence, further studies may be needed to be carried out to explore the direct anti-inflammatory effect of PCSK9 inhibitors irrespective of LDL-C reduction. Exploring the connections of PCSK9 inhibition, amelioration of inflammation, and CV risk reduction by virtue of investigations from future studies and *post-hoc* analyses of long-term clinical trials are also of necessity.

AUTHOR CONTRIBUTIONS

J-JL was the originator, supervisor of the project, and conducted elaborate polishment on the paper. N-QW and H-WS collected and analyzed relevant literature, then completed the writing of the first draft of the paper. All authors read and agree with the final manuscript.

FUNDING

This study was partly supported by Capital Health Development Fund (201614035) and Chinese Academy of Medical Sciences Innovation Fund for Medical Sciences (2016-I2M-1-011) awarded to J-JL.

REFERENCES

1. Ruparelia N, Chai JT, Fisher EA, Choudhury RP. Inflammatory processes in cardiovascular disease: a route to targeted therapies. *Nat Rev Cardiol.* (2017) 14:133–44. doi: 10.1038/nrcardio.2016.185
2. Zhang Y, Zhu CG, Xu RX, Li S, Guo YL, Sun J, et al. Relation of circulating PCSK9 concentration to fibrinogen in patients with stable coronary artery disease. *J Clin Lipidol.* (2014) 8:494–500. doi: 10.1016/j.jacl.2014.07.001
3. Xie W, Liu J, Wang W, Wang M, Qi Y, Zhao F, et al. Association between plasma PCSK9 levels and 10-year progression of carotid atherosclerosis beyond LDL-C: a cohort study. *Int J Cardiol.* (2016) 215:293–8. doi: 10.1016/j.ijcard.2016.04.103
4. Pirillo A, Norata GD, Catapano AL. LOX-1, OxLDL, and atherosclerosis. *Mediators Inflamm.* (2013) 2013:152786. doi: 10.1155/2013/152786
5. Ferri N, Marchiano S, Tibolla G, Baetta R, Dhyani A, Ruscica M, et al. PCSK9 knock-out mice are protected from neointimal formation in response to perivascular carotid collar placement. *Atherosclerosis.* (2016) 253:214–24. doi: 10.1016/j.atherosclerosis.2016.07.910
6. Li S, Guo YL, Xu RX, Zhang Y, Zhu CG, Sun J, et al. Association of plasma PCSK9 levels with white blood cell count and its subsets in patients with stable coronary artery disease. *Atherosclerosis.* (2014) 234:441–5. doi: 10.1016/j.atherosclerosis.2014.04.001
7. Gencer B, Montecucco F, Nanchen D, Carbone F, Klingenberg R, Vuilleumier N, et al. Prognostic value of PCSK9 levels in patients with acute coronary syndromes. *Eur Heart J.* (2016) 37:546–53. doi: 10.1093/eurheartj/ehv637
8. Shapiro MD, Fazio S. PCSK9 and atherosclerosis - lipids and beyond. *J Atheroscler Thromb.* (2017) 24:462–72. doi: 10.5551/jat.RV17003
9. Sun HL, Wu YR, Song FF, Gan J, Huang LY, Zhang L, et al. Role of PCSK9 in the development of mouse periodontitis before and after treatment: a double-edged sword. *J Infect Dis.* (2018) 217:667–80. doi: 10.1093/infdis/jix574
10. Giunzioni I, Tavori H, Covarrubias R, Major AS, Ding L, Zhang Y, et al. Local effects of human PCSK9 on the atherosclerotic lesion. *J Pathol.* (2016) 238:52–62. doi: 10.1002/path.4630
11. Li S, Zhang Y, Xu RX, Guo YL, Zhu CG, Wu NQ, et al. Proprotein convertase subtilisin-kexin type 9 as a biomarker for the severity of coronary artery disease. *Ann Med.* (2015) 47:386–93. doi: 10.3109/07853890.2015.1042908
12. Heinzl MW, Resl M, Klammer C, Egger M, Dieplinger B, Clodi M. Proprotein convertase subtilisin/kexin type 9 (PCSK9) is not induced in artificial human inflammation and is not correlated with inflammatory response. *Infect Immun.* (2020) 88:piie00842–19. doi: 10.1128/IAI.00842-19
13. Tavori H, Giunzioni I, Predazzi IM, Plubell D, Shivinsky A, Miles J, et al. Human PCSK9 promotes hepatic lipogenesis and atherosclerosis development via apoE- and LDLR-mediated mechanisms. *Cardiovasc Res.* (2016) 110:268–78. doi: 10.1093/cvr/cvw053
14. Sun H, Krauss RM, Chang JT, Teng BB. PCSK9 deficiency reduces atherosclerosis, apolipoprotein B secretion, and endothelial dysfunction. *J Lipid Res.* (2018) 59:207–23. doi: 10.1194/jlr.M078360
15. Kuhnast S, van der Hoorn JW, Pieterman EJ, van den Hoek AM, Sasiela WJ, Gusarova V, et al. Alirocumab inhibits atherosclerosis, improves the plaque morphology, and enhances the effects of a statin. *J Lipid Res.* (2014) 55:2103–12. doi: 10.1194/jlr.M051326
16. Landlinger C, Pouwer MG, Juno C, van der Hoorn JWA, Pieterman EJ, Jukema JW, et al. The AT04A vaccine against proprotein convertase subtilisin/kexin type 9 reduces total cholesterol, vascular inflammation, and atherosclerosis in APOE*3Leiden.CETP mice. *Eur Heart J.* (2017) 38:2499–507. doi: 10.1093/eurheartj/ehx260
17. Jialal I, Devaraj S, Venugopal SK. C-reactive protein: risk marker or mediator in atherothrombosis? *Hypertension.* (2004) 44:6–11. doi: 10.1161/01.HYP.0000130484.20501.df
18. Emerging Risk Factors C, Kaptoge S, Di Angelantonio E, Lowe G, Pepys MB, Thompson SG, et al. C-reactive protein concentration and risk of coronary heart disease, stroke, and mortality: an individual participant meta-analysis. *Lancet.* (2010) 375:132–40. doi: 10.1016/S0140-6736(09)61717-7
19. Pradhan AD, Aday AW, Rose LM, Ridker PM. Residual inflammatory risk on treatment with PCSK9 inhibition and statin therapy. *Circulation.* (2018) 138:141–9. doi: 10.1161/CIRCULATIONAHA.118.034645
20. Fernandez-Friera L, Fuster V, Lopez-Melgar B, Oliva B, Sanchez-Gonzalez J, Macias A, et al. Vascular inflammation in subclinical atherosclerosis detected by hybrid PET/MRI. *J Am Coll Cardiol.* (2019) 73:1371–82. doi: 10.1016/j.jacc.2018.12.075
21. Hossain E, Ota A, Karnan S, Takahashi M, Mannan SB, Konishi H, et al. Lipopolysaccharide augments the uptake of oxidized LDL by up-regulating lectin-like oxidized LDL receptor-1 in macrophages. *Mol Cell Biochem.* (2015) 400:29–40. doi: 10.1007/s11010-014-2259-0
22. Steinberg D. Low density lipoprotein oxidation and its pathobiological significance. *J Biol Chem.* (1997) 272:20963–6. doi: 10.1074/jbc.272.34.20963
23. Koenig W. High-sensitivity C-reactive protein and atherosclerotic disease: from improved risk prediction to risk-guided therapy. *Int J Cardiol.* (2013) 168:5126–34. doi: 10.1016/j.ijcard.2013.07.113
24. Dozio E, Ruscica M, Vianello E, Macchi C, Sitzia C, Schmitz G, et al. PCSK9 expression in epicardial adipose tissue: molecular association with local tissue inflammation. *Mediators Inflamm.* (2020) 2020:1348913. doi: 10.1155/2020/1348913
25. Ding Z, Liu S, Wang X, Deng X, Fan Y, Shahanawaz J, et al. Cross-talk between LOX-1 and PCSK9 in vascular tissues. *Cardiovasc Res.* (2015) 107:556–67. doi: 10.1093/cvr/cvv178
26. Boyd JH, Fjell CD, Russell JA, Sirounis D, Cirstea MS, Walley KR. Increased Plasma PCSK9 levels are associated with reduced endotoxin clearance and the development of acute organ failures during sepsis. *J Innate Immun.* (2016) 8:211–20. doi: 10.1159/000442976
27. Cheng JM, Oemrawsingh RM, Garcia-Garcia HM, Boersma E, van Geuns RJ, Serruys PW, et al. PCSK9 in relation to coronary plaque inflammation: results of the ATHEROREMO-IVUS study. *Atherosclerosis.* (2016) 248:117–22. doi: 10.1016/j.atherosclerosis.2016.03.010
28. Almontashiri NA, Vilmundarson RO, Ghasemzadeh N, Dandona S, Roberts R, Quyyumi AA, et al. Plasma PCSK9 levels are elevated with acute myocardial infarction in two independent retrospective angiographic studies. *PLoS ONE.* (2014) 9:e106294. doi: 10.1371/journal.pone.0106294
29. Ferri N, Tibolla G, Pirillo A, Cipollone F, Mezzetti A, Pacia S, et al. Proprotein convertase subtilisin kexin type 9 (PCSK9) secreted by cultured smooth muscle cells reduces macrophages LDLR levels. *Atherosclerosis.* (2012) 220:381–6. doi: 10.1016/j.atherosclerosis.2011.11.026
30. Denis M, Marcinkiewicz J, Zaid A, Gauthier D, Poirier S, Lazure C, et al. Gene inactivation of proprotein convertase subtilisin/kexin type 9 reduces atherosclerosis in mice. *Circulation.* (2012) 125:894–901. doi: 10.1161/CIRCULATIONAHA.111.057406
31. Badimon L, Luquero A, Crespo J, Peña E, Borrell-Pages M. PCSK9 and LRP5 in macrophage lipid internalization and inflammation. *Cardiovasc Res.* (2021) 117:2054–68. doi: 10.1093/cvr/cvaa254
32. Grune J, Meyborg H, Bezhaeva T, Kappert K, Hillmeister P, Kintscher U, et al. PCSK9 regulates the chemokine receptor CCR2 on monocytes. *Biochem Biophys Res Commun.* (2017) 485:312–8. doi: 10.1016/j.bbrc.2017.02.085
33. Guo J, Bot I, de Nooijer R, Hoffman SJ, Stroup GB, Biessen EA, et al. Leucocyte cathepsin K affects atherosclerotic lesion composition and bone mineral density in low-density lipoprotein receptor deficient mice. *Cardiovasc Res.* (2009) 81:278–85. doi: 10.1093/cvr/cvn311
34. Tang ZH, Peng J, Ren Z, Yang J, Li TT, Li TH, et al. New role of PCSK9 in atherosclerotic inflammation promotion involving the TLR4/NF-kappaB pathway. *Atherosclerosis.* (2017) 262:113–22. doi: 10.1016/j.atherosclerosis.2017.04.023
35. Tang YL, Jiang JH, Wang S, Liu Z, Tang XQ, Peng J, et al. TLR4/NF-kappaB signaling contributes to chronic unpredictable mild stress-induced atherosclerosis in ApoE-/- mice. *PLoS ONE.* (2015) 10:e0123685. doi: 10.1371/journal.pone.0123685
36. de Winther MP, Kanters E, Kraal G, Hofker MH. Nuclear factor kappaB signaling in atherogenesis. *Arterioscler Thromb Vasc Biol.* (2005) 25:904–914. doi: 10.1161/01.ATV.0000160340.72641.87
37. Feingold KR, Moser AH, Shigenaga JK, Patzek SM, Grunfeld C. Inflammation stimulates the expression of PCSK9. *Biochem Biophys Res Commun.* (2008) 374:341–4. doi: 10.1016/j.bbrc.2008.07.023
38. Kawai T, Akira S. Signaling to NF-kappaB by Toll-like receptors. *Trends Mol Med.* (2007) 13:460–9. doi: 10.1016/j.molmed.2007.09.002
39. Dwivedi DJ, Grin PM, Khan M, Prat A, Zhou J, Fox-Robichaud AE, et al. Differential expression of PCSK9 modulates infection, inflammation, and coagulation in a murine model of sepsis. *Shock.* (2016) 46:672–80. doi: 10.1097/SHK.0000000000000682

40. Walley KR, Thain KR, Russell JA, Reilly MP, Meyer NJ, Ferguson JF, et al. PCSK9 is a critical regulator of the innate immune response and septic shock outcome. *Sci Transl Med.* (2014) 6:258ra143. doi: 10.1126/scitranslmed.3008782
41. Akhmedov A, Rozenberg I, Paneni F, Camici GG, Shi Y, Doerries C, et al. Endothelial overexpression of LOX-1 increases plaque formation and promotes atherosclerosis *in vivo*. *Eur Heart J.* (2014) 35:2839–48. doi: 10.1093/eurheartj/eht532
42. Pothineni NVK, Karathanasis SK, Ding Z, Arulandu A, Varughese KI, Mehta JL. LOX-1 in atherosclerosis and myocardial ischemia: biology, genetics, and modulation. *J Am Coll Cardiol.* (2017) 69:2759–68. doi: 10.1016/j.jacc.2017.04.010
43. Mehta JL, Sanada N, Hu CP, Chen J, Dandapat A, Sugawara F, et al. Deletion of LOX-1 reduces atherogenesis in LDLR knockout mice fed high cholesterol diet. *Circ Res.* (2007) 100:1634–42. doi: 10.1161/CIRCRESAHA.107.149724
44. Tang Z, Jiang L, Peng J, Ren Z, Wei D, Wu C, et al. PCSK9 siRNA suppresses the inflammatory response induced by oxLDL through inhibition of NF-kappaB activation in THP-1-derived macrophages. *Int J Mol Med.* (2012) 30:931–8. doi: 10.3892/ijmm.2012.1072
45. Li DY, Chen HJ, Staples ED, Ozaki K, Annex B, Singh BK, et al. Oxidized low-density lipoprotein receptor LOX-1 and apoptosis in human atherosclerotic lesions. *J Cardiovasc Pharmacol Ther.* (2002) 7:147–53. doi: 10.1177/107424840200700304
46. Liu S, Deng X, Zhang P, Wang X, Fan Y, Zhou S, et al. Blood flow patterns regulate PCSK9 secretion via MyD88-mediated pro-inflammatory cytokines. *Cardiovasc Res.* (2020) 116:1721–32. doi: 10.1093/cvr/cvz262
47. Ding Z, Liu S, Wang X, Deng X, Fan Y, Sun C, et al. Hemodynamic shear stress via ROS modulates PCSK9 expression in human vascular endothelial and smooth muscle cells and along the mouse aorta. *Antioxid Redox Signal.* (2015) 22:760–71. doi: 10.1089/ars.2014.6054
48. Ding Z, Liu S, Wang X, Mathur P, Dai Y, Theus S, et al. Cross-Talk between PCSK9 and damaged mtDNA in vascular smooth muscle cells: role in apoptosis. *Antioxid Redox Signal.* (2016) 25:997–1008. doi: 10.1089/ars.2016.6631
49. Brandes RP, Kreuzer J. Vascular NADPH oxidases: molecular mechanisms of activation. *Cardiovasc Res.* (2005) 65:16–27. doi: 10.1016/j.cardiores.2004.08.007
50. Vlachopoulos C, Koutagiar I, Skoumas I, Terentes-Printzios D, Zacharis E, Kolovou G, et al. Long-Term administration of proprotein convertase subtilisin/kexin type 9 inhibitors reduces arterial FDG uptake. *JACC Cardiovasc Imaging.* (2019) 12:2573–4. doi: 10.1016/j.jcmg.2019.09.024
51. Bernelot Moens SJ, Neele AE, Kroon J, van der Valk FM, Van den Bossche J, Hoeksema MA, et al. PCSK9 monoclonal antibodies reverse the pro-inflammatory profile of monocytes in familial hypercholesterolaemia. *Eur Heart J.* (2017) 38:1584–93. doi: 10.1093/eurheartj/ehx002
52. Bohula EA, Giugliano RP, Leiter LA, Verma S, Park JG, Sever PS, et al. Inflammatory and cholesterol risk in the FOURIER trial. *Circulation.* (2018) 138:131–140. doi: 10.1161/CIRCULATIONAHA.118.034032
53. Leucker TM, Gerstenblith G, Schär M, Brown TT, Jones SR, Afework Y, et al. Evolocumab, a PCSK9-monoclonal antibody, rapidly reverses coronary artery endothelial dysfunction in people living with HIV and people with dyslipidemia. *J Am Heart Assoc.* (2020) 9:e016263. doi: 10.1161/JAHA.120.016263
54. Cannon CP, Cariou B, Blom D, McKenney JM, Lorenzato C, Pordy R, et al. Efficacy and safety of alirocumab in high cardiovascular risk patients with inadequately controlled hypercholesterolaemia on maximally tolerated doses of statins: the ODYSSEY COMBO II randomized controlled trial. *Eur Heart J.* (2015) 36:1186–94. doi: 10.1093/eurheartj/ehv028
55. Steg PG, Szarek M, Bhatt DL, Bittner VA, Brégeault MF, Dalby AJ, et al. Effect of alirocumab on mortality after acute coronary syndromes. *Circulation.* (2019) 140:103–12. doi: 10.1161/CIRCULATIONAHA.118.038840
56. Hoogeveen RM, Opstal TSJ, Kaiser Y, Stiekema LCA, Kroon J, Knol RJJ, et al. PCSK9 antibody alirocumab attenuates arterial wall inflammation without changes in circulating inflammatory markers. *JACC Cardiovasc Imaging.* (2019) 12:2571–3. doi: 10.1016/j.jcmg.2019.06.022
57. Baruch A, Mosesova S, Davis JD, Budha N, Vilimovskij A, Kahn R, et al. Effects of RG7652, a monoclonal antibody against PCSK9, on LDL-C, LDL-C subfractions, and inflammatory biomarkers in patients at high risk of or with established coronary heart disease (from the phase 2 EQUATOR study). *Am J Cardiol.* (2017) 119:1576–83. doi: 10.1016/j.amjcard.2017.02.020

Conflict of Interest: The authors declare that the research was conducted in the absence of any commercial or financial relationships that could be construed as a potential conflict of interest.

Publisher's Note: All claims expressed in this article are solely those of the authors and do not necessarily represent those of their affiliated organizations, or those of the publisher, the editors and the reviewers. Any product that may be evaluated in this article, or claim that may be made by its manufacturer, is not guaranteed or endorsed by the publisher.

Copyright © 2022 Wu, Shi and Li. This is an open-access article distributed under the terms of the Creative Commons Attribution License (CC BY). The use, distribution or reproduction in other forums is permitted, provided the original author(s) and the copyright owner(s) are credited and that the original publication in this journal is cited, in accordance with accepted academic practice. No use, distribution or reproduction is permitted which does not comply with these terms.

frontiers in Cardiovascular Medicine

ORIGINAL RESEARCH
published: 21 March 2022
doi: 10.3389/fcvm.2022.825310

High Density Lipoprotein Reduces Blood Pressure and Protects Spontaneously Hypertensive Rats Against Myocardial Ischemia-Reperfusion Injury in an SR-BI Dependent Manner

Aishah Al-Jarallah[1]* *and Fawzi Babiker*[2]

[1] Department of Biochemistry, Faculty of Medicine, Kuwait University, Kuwait City, Kuwait, [2] Department of Physiology, Faculty of Medicine, Kuwait University, Kuwait City, Kuwait

Background: Hypertension is a key risk factor in the development of cardiovascular diseases. Elevation in blood pressure alters high density lipoprotein (HDL) function and composition. The exact role of HDL in cardiovascular complications observed in hypertension is however not clearly understood. HDL protected against myocardial ischemia/reperfusion (I/R) injury in normotensive rats. Nonetheless, it's not clear if restoration of HDL function and/or composition protects against myocardial I/R injury in spontaneously hypertensive rats (SHR).

Objectives: In this study we tested the effect of HDL treatment on I/R injury in Wistar Kyoto rats (WKY) and SHR and investigated the possible underlying mechanism(s).

Methods: HDL (900 ng/kg/min) or vehicle were continuously administered to 11-week old WKY and SHR for 1 week (chronic treatment). Blood pressure was measured before and after treatment. Hearts were subjected to I/R injury using a modified Langendorff system. Another set of rats were treated with HDL administered at reperfusion (acute treatment) in the presence or absence of scavenger receptor class B type-I (SR-BI) blocking antibody. Cardiac hemodynamics were computed and cardiac enzyme release and infarct size were measured. Total cholesterol (TC) and HDL-cholesterol (HDL-C) were enzymatically assayed. Markers of autophagy and inflammation were detected by immunoblotting and ELISA, respectively.

Results: HDL treatment did not increase TC or HDL-C levels in SHR or WKY, yet it significantly ($P < 0.01$) reduced systolic and diastolic blood pressure in SHR. Chronic and acute HDL treatment significantly ($P < 0.05$) protected WKY and SHR against myocardial I/R injury. Chronic HDL treatment was significantly ($P < 0.05$) more protective in SHR whereas acute HDL treatment induced significantly ($P < 0.05$) greater protection in WKY. The extent of HDL induced protection was proportional to the expression levels of cardiac SR-BI and blockage of SR-BI completely abolished HDL mediated protection in SHR. Chronic HDL treatment significantly ($P < 0.05$) reduced markers of autophagy and inflammation in hypertensive rats.

OPEN ACCESS

Edited by:
Jue Zhang,
Versiti Blood Research Institute, United States

Reviewed by:
Minqi Huang,
Marshall University, United States

***Correspondence:**
Aishah Al-Jarallah
aishah.aljarallah@ku.edu.kw

Specialty section:
This article was submitted to Lipids in Cardiovascular Disease, a section of the journal Frontiers in Cardiovascular Medicine

Received: *30 November 2021*
Accepted: *12 January 2022*
Published: *21 March 2022*

Citation:
Al-Jarallah A and Babiker F (2022) High Density Lipoprotein Reduces Blood Pressure and Protects Spontaneously Hypertensive Rats Against Myocardial Ischemia-Reperfusion Injury in an SR-BI Dependent Manner. Front. Cardiovasc. Med. 9:825310. doi: 10.3389/fcvm.2022.825310

Conclusions: We demonstrate a novel anti-hypertensive and a cardioprotective effect of HDL against myocardial I/R injury in SHR, the magnitude of which is directly related to the expression levels of cardiac SR-BI. Mechanistically, chronic HDL treatment protected SHR hearts by reducing autophagy and inflammation.

Keywords: high density lipoprotein, ischemia reperfusion injury, cardiac protection, hypertension, autophagy, inflammation

INTRODUCTION

Hypertension is a leading cause of premature deaths. In 2015, elevated systolic blood pressure (SBP) claimed the lives of 8.5 million individuals worldwide (1–3). It represents an ever growing health condition that imposes a huge financial burden on the economy of the affected countries. The number of hypertensive individuals doubled from 1990 to 2019 to be 652 million males and 626 million females (2) and the cost of hypertension per country has been estimated to be several dozen billion Int$ (3). In addition, hypertension is a major risk factor of cardiovascular diseases (CVD), whereby increased blood pressure attributes to 47% of coronary heart disease (CHD) cases (4, 5). Moreover, blood pressure lowering is an effective strategy in reducing blood pressure related deaths (6–9). Control randomized clinical trials demonstrated that patients at high cardiovascular risk or patients with established CVD benefit from blood pressure lowering treatments whether they were normotensive or hypertensive (6–11). In addition an inverse relationship exists between HDL levels and the risk of CHD (12–16). Low HDL cholesterol (HDL-C) and hypertension are symptoms of metabolic syndrome and both are important predictors of acute myocardial infarction (17). HDL-C levels are inversely associated with the risk of hypertension (18, 19) and a combination of high-normal blood pressure with low HDL-C was associated with increased mortality (20). Reduced HDL-C levels and impaired HDL synthesis and turnover were reported in patients with mild hypertension (21). Furthermore, increased blood pressure eliminated the protective effects of HDL against CHD and stroke (9). HDL function and composition were altered by hypertension and anti-hypertensive drugs. Reduced contents of HDL phospholipids and changed phospholipid composition represented as a lower ratio of phosphatidylcholine and higher relative levels of lysophosphatidylcholine, sphingomyelin and phosphatidylethanolamine were reported in patients with hypertension (22). The exact relationship between HDL and hypertension is however not clearly understood.

Deteriorated cardiac functions (23–26) and enhanced cardiac autophagy (27–29) were reported in experimental models of hypertension. Compared to normotensive controls, hearts from experimental models of hypertension were resistant to protection induced by ischemic post-conditioning (30–32), erythropoietin (33), helium (34), and short-term infusion of captopril (35). *In vivo* and *ex vivo* administration of HDL or HDL components protected rodent hearts from ischemia reperfusion (I/R) injury (36). Acting on cardiomyocytes, endothelial cells and leukocytes, HDL induced cardioprotection involved simultaneous inhibition of the damaging effects of I/R injury and activation of internal protective responses including the activation of the reperfusion injury salvage (RISK) (37) and the survivor activating factor enhancement (SAFE) pathways and subsequent inhibition of mitochondrial permeability transition pore (mPTP) opening (38). In addition, HDL stimulated the release of vasoactive (37) and cardioprotective compounds (39). Nonetheless it's not clear if HDL can protect hearts from hypertensive rodents against myocardial I/R injury. We therefore sought to test the effect of HDL on I/R injury in normotensive, Wistar Koyoto rats (WKY), and spontaneously hypertensive rats (SHR) and examine the involvement of autophagy and inflammation as possible mechanisms of HDL mediated effects. We demonstrate that HDL treatment reduces SBP and diastolic blood pressure (DBP) in SHR. Chronic and acute HDL treatments protected WKY and SHR against myocardial I/R injury yet, to different extents. Chronic HDL treatment induced greater protection in SHR, while acute HDL treatment was more protective in WKY. Interestingly the magnitude of HDL protection in WKY and SHR was proportional to the expression levels of cardiac SR-BI in these rats. HDL was more protective against myocardial I/R injury in rats expressing greater levels of cardiac SR-BI. Blockage of SR-BI completely abrogated HDL mediated protection against I/R injury in SHR. HDL treatment reduced autophagy markers beclin, microtubule-associated protein 1 light chain 3 (LC-3) B and autophagy regulated gene (Atg)-12 and tumor necroses factor-α (TNF-α) levels in SHR suggesting that HDL mediated cardiac protection in hypertensive rats involves simultaneous attenuation of multiple detrimental pathways including autophagy and inflammation. Our data emphasize a multifaceted role of HDL in protecting hypertensive rats against myocardial I/R injury by virtue of its systemic (blood pressure lowering) and/or local (attenuation of inflammation and autophagy) effects.

MATERIALS AND METHODS

Materials

All materials were purchased from Sigma Aldrich (Munich, Germany) unless stated otherwise.

Animals and Instrumentation

In experiments testing the effect of chronic HDL treatment on I/R injury, 11-week old male WKY (334 ± 29 g) and SHR (282 ± 20 g) were used. Animals were kept under internationally accepted conditions in the Animal Resource Center, Faculty of Medicine, Kuwait University and had free access to food

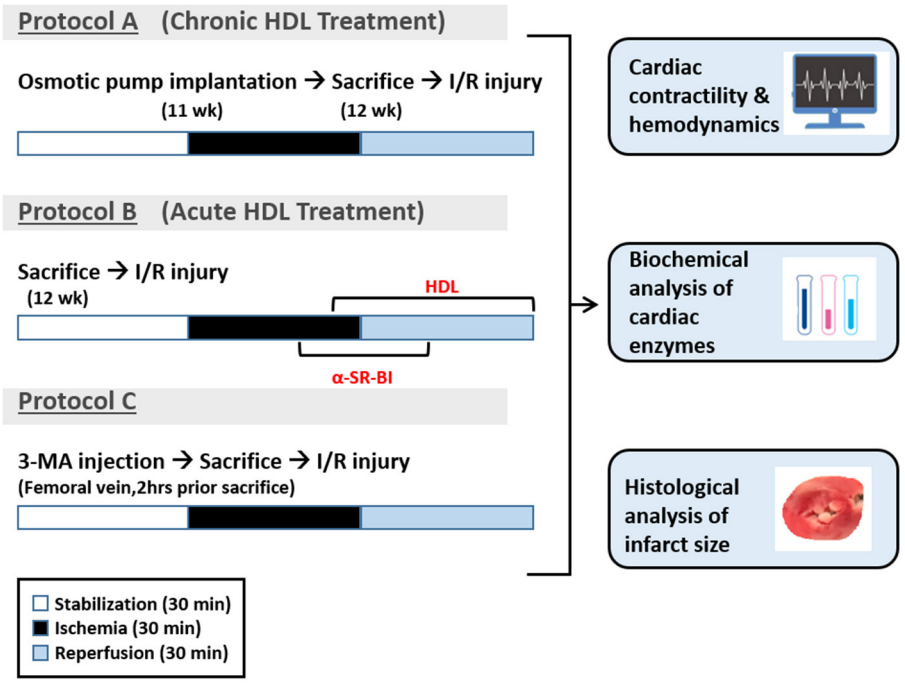

FIGURE 1 | Experimental protocols used in the study. Eleven week old WKY and SHR were implanted with vehicle control or HDL containing osmotic pumps. One week later, rats were sacrificed and subjected to ischemia/reperfusion injury (I/R) with 30 min of stabilization followed by 30 min of ischemia and 30 min of reperfusion (protocol A). A group of untreated WKY and SHR were sacrificed and subjected to I/R injury. SR-BI blocking antibody was administered at 20 min of ischemia. Ten minutes later, hearts were perfused with HDL (400 μg) in the presence of SR-BI blocking antibody for the remaining of the 30 min the reperfusion period (protocol B). Another group of untreated WKY and SHR were injected with 3-MA (30 mg/Kg) into the femoral vein. Two hours later, rats were sacrificed and subjected to 30 min of ischemia followed by 30 min of reperfusion (protocol C).

and water. All procedures that involved rats were approved by the Health Sciences Research Ethics Committee. The rats were divided into four groups (n = 12 rats per group): (1) WKY-vehicle; (2) WKY-HDL; (3) SHR-vehicle; (4) SHR-HDL. HDL (900 ng protein/kg/min) or phosphate-buffered saline (PBS) (as a vehicle) were continuously administered using Alzet osmotic minipumps implanted subcutaneously into the back of the rats. This dosage was selected based on previously reported data by Lin et al. (40). One week later, rats were sacrificed, plasma samples were collected and cardiac response to I/R injury was examined. Blood pressure was measured prior and post-implantation or at week 12 in non-implanted rats using CODA High Throughput System with 4 activated channels (41). SBP ≥160 mmHg was used as a cutoff value for hypertension. Rats that did not reach the cutoff value were excluded from the study. In experiments testing the effects of acute HDL treatment and the involvement of SR-BI, 12-week old WKY and SHR (n = 30) were used. Finally, a distinct cohort of 12-week old WKY and SHR (n = 22) was set to test the effect of 3-methyladenine (3-MA).

Heart cannulation and perfusion was performed as described previously (42). Briefly, isolated hearts were perfused retrogradely with freshly prepared Krebs-Hensleit buffer, pH 7.35–7.45 at 37.0 ± 0.5°C and gassed with CO_2 (5%) and O_2 (95%). Regional ischemia was induced by occluding left anterior descending (LAD) coronary artery for 30 min. The success of ischemia induction was evaluated online at the onset of ischemia by the immediate drop in the coronary flow. Two rats were excluded from the study because of left ventricular (LV) fibrillation. Preload was kept constant at 6 mmHg under basal controlled conditions and perfusion pressure (PP) at 50 mmHg throughout the experimental procedure in all protocols. The perfusion pressure was measured downstream from a branch of the aortic cannula using a "statham pressure transducer" (P23 Db). Constant PP was ensured electronically by means of the perfusion assembly ["Module PPCM type 671 (Hugo Sachs Elektronik- Harvard ApparatusGmbH, Germany")], an effective system for the accurate adjustment of PP between 5 and 150 mmHg with ±1 mmHg accuracy level.

Study Protocol and Study Groups

All hearts were subjected to 30 min of ischemia produced by LAD coronary artery occlusion. The LAD coronary artery was encircled by a snare at ∼0.5 cm below the atrioventricular groove, and a small rigid plastic tube was positioned between the heart and the snare to ensure complete occlusion of the coronary artery. Hearts were then reperfused for 30 min without any additions to the perfusion buffer (**Figure 1**, protocol A). In experiments testing the involvement of SR-BI in HDL mediated

cardiac protection, hearts isolated from WKY and SHR were infused with SR-BI blocking antibody (Novus Biologicals, CO, USA, NB400-113, 1:100) during the last 10 min of ischemia, then perfused with or without HDL (acute treatment, 400 μg protein) in the presence of the antibody for the remaining 30 min of the reperfusion period, using a total volume of 150 ml of the perfusion buffer (**Figure 1**, protocol B). The role of autophagy in I/R injury was tested by the administration of 3-MA (30 mg/Kg) into the femoral vein 2 h prior to sacrifice followed by 30 min of ischemia and 30 min of reperfusion without any additions to the perfusion buffer (**Figure 1**, protocol C).

Data Collection and Processing

LV function was evaluated by the assessment of LV end diastolic pressure (LVEDP) and LV developed pressure (DPmax), cardiac contractility was monitored by heart contractility index values (±dP/dt), while coronary-vascular dynamics were evaluated by the assessment of the coronary flow (CF) and coronary vascular resistance (CVR). Cardiovascular functions were measured as previously described (42). Briefly, a water-filled latex balloon was placed and secured in the LV cavity. The balloon was attached to a pressure transducer and a "DC-Bridge amplifier (DC-BA)" with a pressure module (DC-BA type 660, Hugo-Sachs Electronik, Germany) and interfaced to a personal computer for on-line monitoring of DPmax. LV developed pressure was derived from online acquisition of LV end systolic pressure (LVESP) using Max-Min module (Number MMM type 668, Hugo Sachs Elektronik-Harvard ApparatusGmbH, Germany) which has the ability to convert the output from DC bridge amplifier to DPmax by subtracting LVEDP from the LVESP.

Coronary flow was continuously measured using an electromagnetic flow probe attached to the inflow of the aortic cannula interfaced to a personal computer. The continuous monitoring of the CF in ml/min was digitally monitored using software developed specifically for this purpose and was manually verified by the timed collection of coronary effluent. The CVR and hemodynamics data were determined every 10 s using an on-line data acquisition program (Isoheart software V 1.524-S, Hugo-Sachs Electronik, Germany). By the end of each experiment, hearts were weighed then snap frozen in liquid nitrogen then stored in −80°C. The tibia was isolated and its length was measured with ruler and the heart weight was expressed relative to the tibia length.

Evaluation of Cardiac Injury by Measurements of Infarct Size and Cardiac Enzyme Levels

The infarct size was determined by triphenyltetrazolium chloride (TTC) staining as described previously (32). Each heart was sliced into 4–5 pieces along the long axis. The slices were then incubated for 15 min in 1% TTC solution in isotonic phosphate buffer (pH 7.4) at 37°C and fixed in 4% formaldehyde. Images were taken using a Samsung camera. Red and pale unstained areas of every slice were indicated manually on the image using Leica ImageJ (Image J, Wayne Rasb and National Institute of Health, USA). The percentage infarct area was calculated relative to total LV area. Cardiomyocyte injury was evaluated by measuring creatine kinase (CK), or troponin release in the coronary effluent during the reperfusion period as previously described (43). Briefly, CK was measured using a CK specific kit (catalog # 442635, Beckman Coulter, CA, USA) with an analytical range of 5–1,200 IU/L and ran using UniCel® DXC 800 Synchron Access Clinical Systems (Beckman Coulter, CA, USA). Troponin was measured using troponin specific kit (catalog # B52699, Beckman Coulter, CA, USA) with a quantification limit of 5.6 pg/ml at 10% CV and ran using UniCel® DXI 800 Access Immunoassay System (Beckman Coulter, CA, USA).

Immunoblotting

Heart homogenates were prepared using a buffer containing 0.2× PBS, 0.1 % triton-X 100, 1× phosphatase inhibitor and 1× protease inhibitor cocktail then centrifuged at 14,000 rpm in a bench top minicentrifuge for 10 min at 4°C. Membrane fractions were prepared by homogenizing hearts on ice for 3 min in 20 mM Tris-HCl, pH 7.5 containing 2 mM $MgCl_2$, 0.25 M sucrose, and 1× protease inhibitors. Homogenates were centrifuged at 3,000 × g for 10 min at 4°C and supernatants were subjected to another centrifugation step at 100,000 × g for 1 h at 4°C. The pellet was suspended in 50 mM Tris-HCl, pH 7.5 containing 1× protease inhibitors cocktail and 0.1% sodium dodecyle sulfate. Protein concentration from total homogenates and membrane fractions was measured using the BCA-protein determination kit (Themoscientific, Ottawa, Ontario, CA) and samples were aliquoted and stored at −80°C for further analysis. After boiling, samples (50 μg protein) were subjected to SDS-PAGE and PVDF membranes were immunoblotted with anti-beclin-1, LC3B, Atg-3, Atg-5, Atg-7, Atg-12 (Cell Signaling, MA, USA), or anti-SR-BI (Abcam, MA, USA) overnight, followed by HRP-conjugated donkey anti-rabbit antibody (Jackson ImmunoResearch, PA, USA). Bands were detected using Super Signal Western Pico chemiluminescence Substrate (Thermoscientific, Ottawa, Ontario, CA) and quantified using Biorad gel doc RX System (BioRad, CA, USA).

Measurements of Plasma Cholesterol

Plasma total cholesterol (TC) and HDL cholesterol (HDL-C) were measured enzymatically using commercially available kit (Abcam, MA, USA) following the manufacturer instructions.

Measurements of TNF-α and IL-6 Levels

Total heart homogenates were assayed suing TNF-α and IL-6 ELISA kits (Thermosceinfic, Ottawa, Ontario, CA) according to manufacturer instructions.

Statistical Analysis

Multiple comparisons were evaluated using two-way analysis of variance (ANOVA). In cases of statistical significance, the *post-hoc* analysis using LSD test was performed (SPSS). Student's *T*-Test was used to assess the significance in molecular experiments (Microsoft Excel). Data were considered statistically significant at $P < 0.05$. Data are presented as mean ± standard error of the mean (SEM) of "*n*" number of experiments.

TABLE 1 | Blood pressure measurements of WKY and SHR treated with or without HDL.

	Control				HDL			
	Pre-implantation		Post-implantation		Pre-implantation		Post-implantation	
	SBP	DBP	SBP	DBP	SBP	DBP	SBP	DBP
WKY								
Mean ± SEM (mmHg)	115 ± 2	72 ± 1.9	107 ± 4	70 ± 3.5	130 ± 3	88 ± 2.5	124 ± 6.8	83 ± 6
SHR								
Mean ± SEM (mmHg)	174 ± 4.5$^{\#}$	120 ± 6$^{\#}$	169 ± 6	117 ± 6	169 ± 4$^{\#}$	111 ± 5$^{\#}$	136 ± 4.4$^{*\$}$	85 ± 4$^{*\$}$

$^{\#}P < 0.01$ *vs. WKY.*
$^{*}P < 0.01$ *vs. pre-implantation.*
$^{\$}P < 0.01$ *vs. control SHR.*

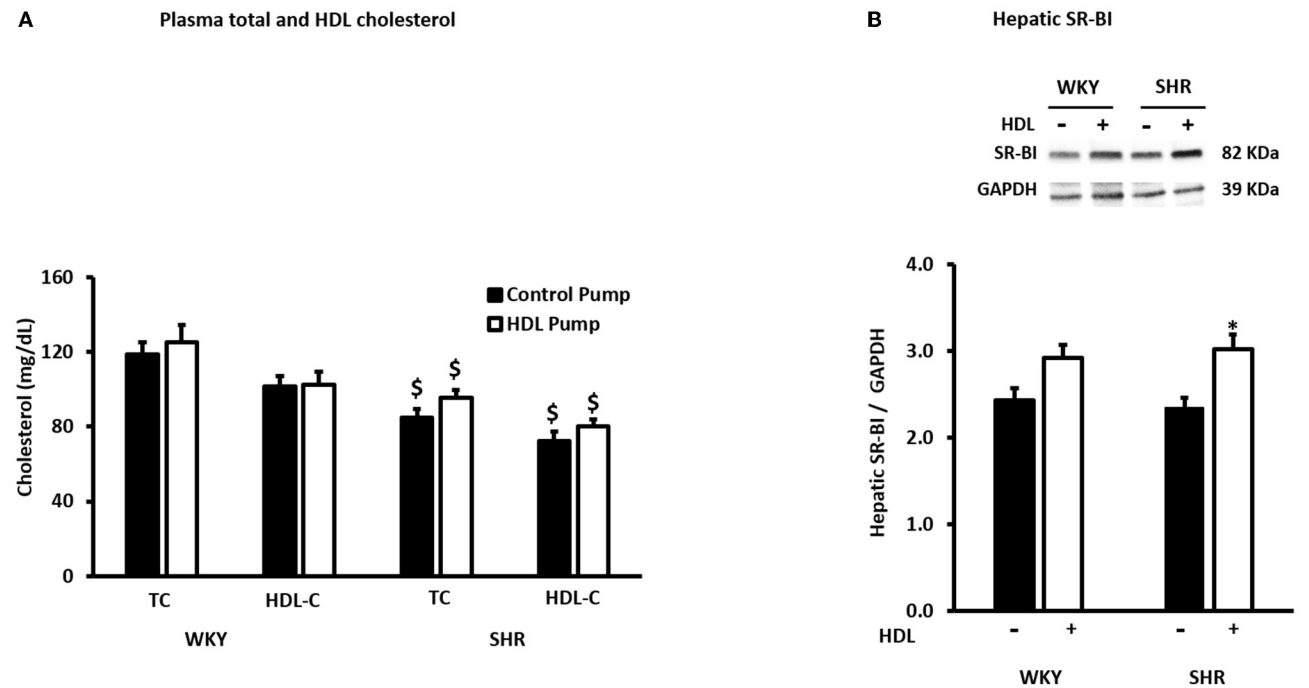

FIGURE 2 | Effects of HDL treatment on plasma cholesterol and hepatic SR-BI expression in WKY and SHR. Plasma total and HDL cholesterol levels **(A)** and hepatic SR-BI expression **(B)** in WKY and SHR treated with or without HDL. Data are mean ± SEM, $^{\$}P < 0.05$ vs. the same parameter and treatment group in WKY, $n =$ 7–10, $^{*}P < 0.05$ vs. untreated animals of the same genotype, $n = 5$–6.

RESULTS

Effects of HDL Treatment on Blood Pressure and Plasma Cholesterol Levels

SHR exhibited significantly higher ($P < 0.01$) SBP and DBP than WKY (**Table 1**). HDL treatment significantly ($P < 0.01$) reduced SBP and DBP in SHR by 20% and 23% relative to preimplantation levels, respectively, and by 20% (SBP) and 27% (DBP) relative to SHR implanted with the vehicle pump (**Table 1**). SBP and DBP in HDL-treated SHR were not significantly ($P > 0.05$) different from WKY (**Table 1**). HDL treatment did not have a significant ($P > 0.05$) effect on heart to tibia length ratio in WKY or SHR (**Supplementary Figure 1**). Finally, SHR demonstrated significantly ($P < 0.05$) lower total cholesterol and HDL-C than WKY and HDL treatment did not significantly ($P > 0.05$) alter plasma total cholesterol or HDL-C in SHR or WKY (**Figure 2A**). The lack of increase in HDL-C in HDL treated rats maybe explained by the trend toward an increase (in WKY) and the statistically significant ($P < 0.05$) increase (SHR) in hepatic SR-BI protein levels (**Figure 2B**) suggesting enhanced clearance of HDL in HDL treated rats.

HDL Protects WKY and SHR Against Myocardial I/R Injury to Different Extents

Hearts from WKY and SHR treated with or without HDL were isolated and subjected to I/R injury *ex-vivo*. Cardiac contractility and hemodynamics were recorded and the extent of ischemic damage was assessed by cardiac enzyme release

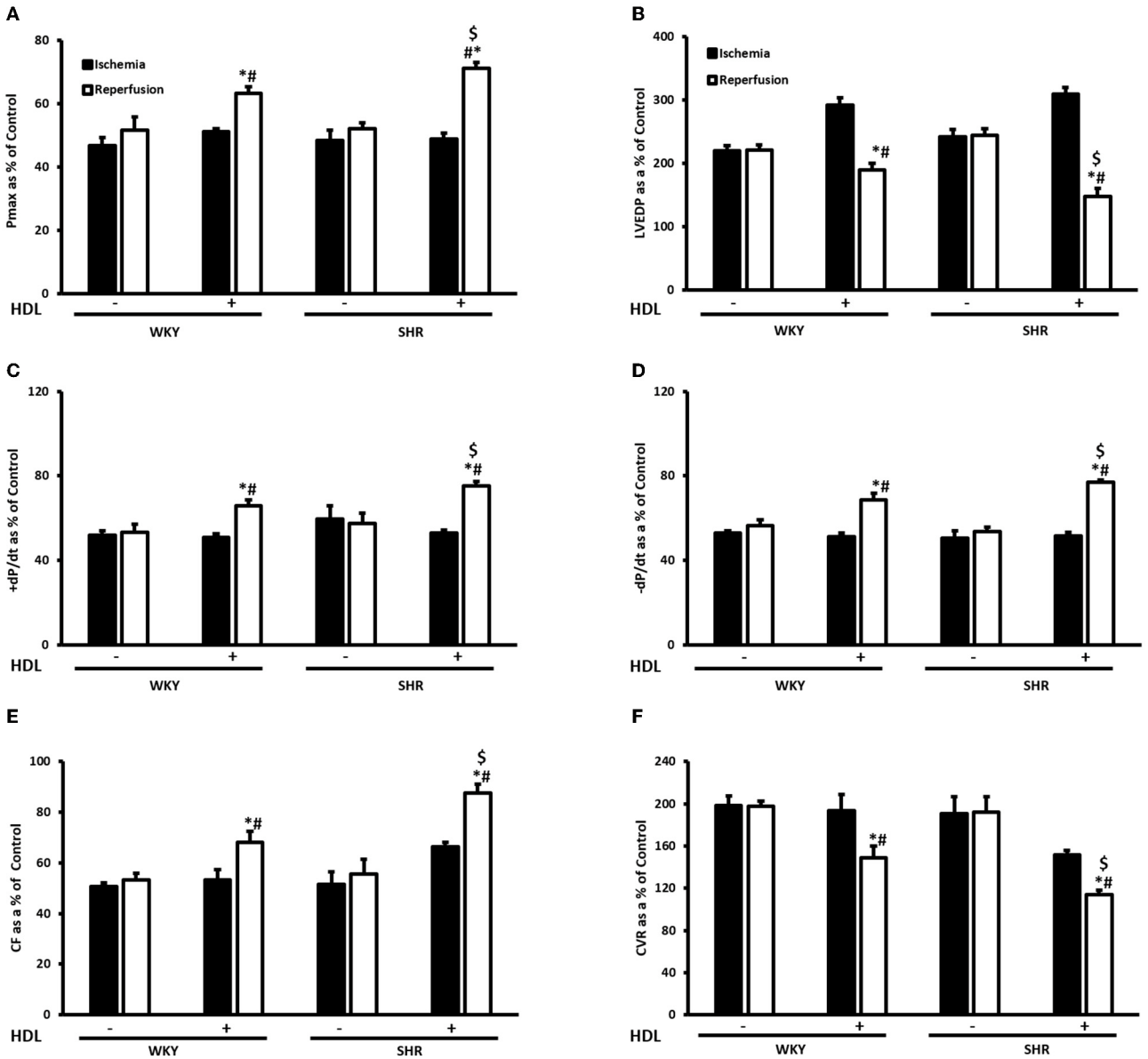

FIGURE 3 | Effect of chronic HDL treatment on I/R injury in WKY and SHR. Post-ischemic recovery parameters of cardiac functions including DPmax **(A)**, LVEDP **(B)**, cardiac contractility **(C,D)**, CF **(E)**, and CVR **(F)**. Data were computed at 30 min of reperfusion and expressed as means ± SEM. DPmax, maximum developed pressure; LVEDP, left ventricular end diastolic pressure; CF, coronary flow; CVR, coronary vascular resistance. $^{*}P < 0.5$ compared to ischemic period, $^{\#}P < 0.5$ compared to control pump, $^{\$}P < 0.05$ vs. HDL treated WKY, $n = 6$–10 rats per group.

and measurements of infarct size. Hearts from normotensive rats treated with HDL (chronic treatment) demonstrated significant ($P < 0.05$) improvements in DPmax and LV pressure (**Figures 3A,B**), cardiac contractility (**Figures 3C,D**) and cardiac hemodynamics (**Figures 3E,F**) during reperfusion compared to ischemic period and relative to untreated controls. Similarly, chronic HDL treatment of SHR significantly ($P < 0.05$) improved DPmax, LV pressure, cardiac hemodynamics, and contractility relative to the ischemic period and relative to SHR controls (**Figures 3A–F**). HDL however, demonstrated significantly ($P < 0.05$) enhanced protection on cardiac contractility and hemodynamics in SHR relative to WKY (**Figures 3A–F**). Moreover, measurements of cardiac enzymes revealed significantly ($P < 0.05$) higher levels of CK in control SHR relative to control WKY during periods of ischemia and reperfusion (**Table 2**), possibly suggesting enhanced susceptibility of hearts from SHR to cardiac damage. Chronic HDL treatment significantly reduced ($P < 0.05$) CK release in WKY and SHR by 46% and 69%, respectively (**Table 2**). In addition, chronic HDL treatment significantly ($P < 0.05$) reduced infarct size in WKY and SHR (**Figure 4**). Collectively this data suggest that chronic, *in vivo*, HDL treatment protects WKY and

TABLE 2 | Effect of chronic HDL treatment on creatine kinase release in response to I/R injury.

	CK (IU/L)			
	Control		HDL	
	Ischemia	Reperfusion	Ischemia	Reperfusion
WKY	3.5 ± 0.54	3.2 ± 1.1	6.2 ±1.8	3.3 ±1.1
SHR	10.5 ± 2.5$^{\$}$	27.76 ± 0.5$^{\#\$}$	12.3 ± 3.1	3.8 ± 0.8$^{\#*}$

$^{\$}P < 0.05$ *vs. WKY.*
$^{\#}P < 0.05$ *vs. ischemia.*
$^{*}P < 0.05$ *vs. untreated controls.*

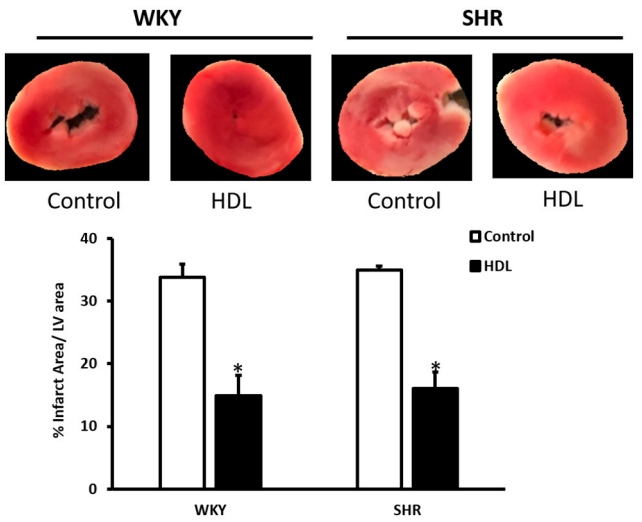

FIGURE 4 | HDL treatment reduces infarct size in WKY and SHR. WKY and SHR rats were treated with or without HDL and subjected to I/R injury *ex-vivo*. Infarct size was quantified in TTC stained sections. Data are expressed as means ± SEM, $^{*}P < 0.01$, $n = 3$–5 per treatment.

SHR against I/R injury. The extent of HDL-mediated protection however, appears to be different between normotensive and hypertensive rats. The observed differences in HDL mediated cardiac protection may possibly suggest differences in HDL signaling between WKY and SHR.

HDL Requires SR-BI for Protection Against Myocardial I/R Injury

We have tested the involvement of the HDL receptor, SR-BI in HDL mediated cardiac protection in WKY and SHR using SR-BI blocking antibody (**Figure 5**). In these experiments HDL was administered at reperfusion (acute treatment) in the presence or absence of SR-BI blocking antibody. HDL administration at reperfusion significantly ($P < 0.05$) improved cardiac contractility and hemodynamics in WKY and SHR (**Figures 5A–F**). HDL however, was more protective in WKY than SHR when administered at reperfusion as indicated by the significant ($P < 0.05$) increase in DPmax (**Figure 5A**), ±dp/dt (**Figures 5C,D**) and CF (**Figure 5E**) and the significant ($P < 0.05$) decrease in CVR (**Figure 5F**).

Furthermore, the administration of HDL at reperfusion in the presence of SR-BI blocking antibody significantly ($P < 0.05$) increased DPmax, cardiac contractility (+dP/dt and –dP/dt) and CF (**Figures 5A,C–E**) and significantly ($P < 0.05$) reduced LVEDP and CVR relative to ischemia and relative to untreated controls in WKY (**Figures 5B,F**). Moreover, HDL treatment in the presence of SR-BI blocking antibody in WKY, significantly ($P < 0.05$) increased DPmax and CVR (**Figures 5A,F**) and significantly ($P < 0.05$) reduced LVEDP, CF relative to HDL-treated rats (**Figures 5B,E**). This suggests blockage of SR-BI did not abolish HDL induced cardiac protection in WKY, rather it reduced it. In SHR however, HDL treatment in the presence of SR-BI blocking antibody did not result in any significant improvements in cardiac contractility, hemodynamics or ventricular pressure relative to ischemia or relative to the untreated controls (**Figures 5A–F**), suggesting the absolute requirement of SR-BI in HDL mediated cardiac protection in SHR.

Together, this data suggest that while SR-BI plays an indispensable role in mediating HDL induced cardiac protection in SHR, this however, does not seem to be the case in normotensive rats. In WKY HDL remained protective, albeit to a lesser extent than HDL alone, in the presence of SR-BI blocking antibody. The residual HDL mediated cardiac protection in WKY in the presence of SR-BI blocking antibody, possibly suggests the presence of alternative or additional pathways or mechanisms by which HDL protects against cardiac I/R injury. Interestingly, the magnitude of HDL induced cardiac protection in WKY and SHR varied between the chronic and acute treatments. In chronic treatment HDL was more protective in SHR (**Figure 3**), however in the acute treatment, HDL was more protective in WKY (**Figure 5**). The finding that SR-BI is required for HDL mediated cardiac protection in WKY and SHR may implicate differences in SR-BI mediated signaling in HDL induced protection against myocardial I/R injury.

We have therefore examined the expression levels of SR-BI in WKY and SHR subjected to chronic or acute HDL treatment (**Figure 6**). There was no significant difference in basal SR-BI protein levels in total heart homogenates from WKY and SHR (**Figure 6A**). Nonetheless, WKY expressed significantly ($P < 0.01$) higher levels of cardiac SR-BI than SHR in membrane fractions (**Figure 6B**) suggesting differences in SR-BI localization between WKY and SHR. Finally, total heart homogenates from WKY and SHR treated *in vivo* (chronically) with or without HDL were examined (**Figure 6C**). Significantly ($P < 0.05$) higher levels of cardiac SR-BI were detected in vehicle treated SHR compared to vehicle treated WKY. Chronic HDL treatment significantly ($P < 0.05$) increased cardiac SR-BI expression in SHR (**Figure 6**). These changes in receptor expression levels in response to HDL were not however observed in WKY. Collectively this data suggest the possibility that the observed differences in the magnitude of HDL induced protection between WKY and SHR in response to chronic or acute treatment could be attributed to differences in SR-BI expression levels. HDL induced greater protection against I/R injury in hearts expressing greater levels of SR-BI.

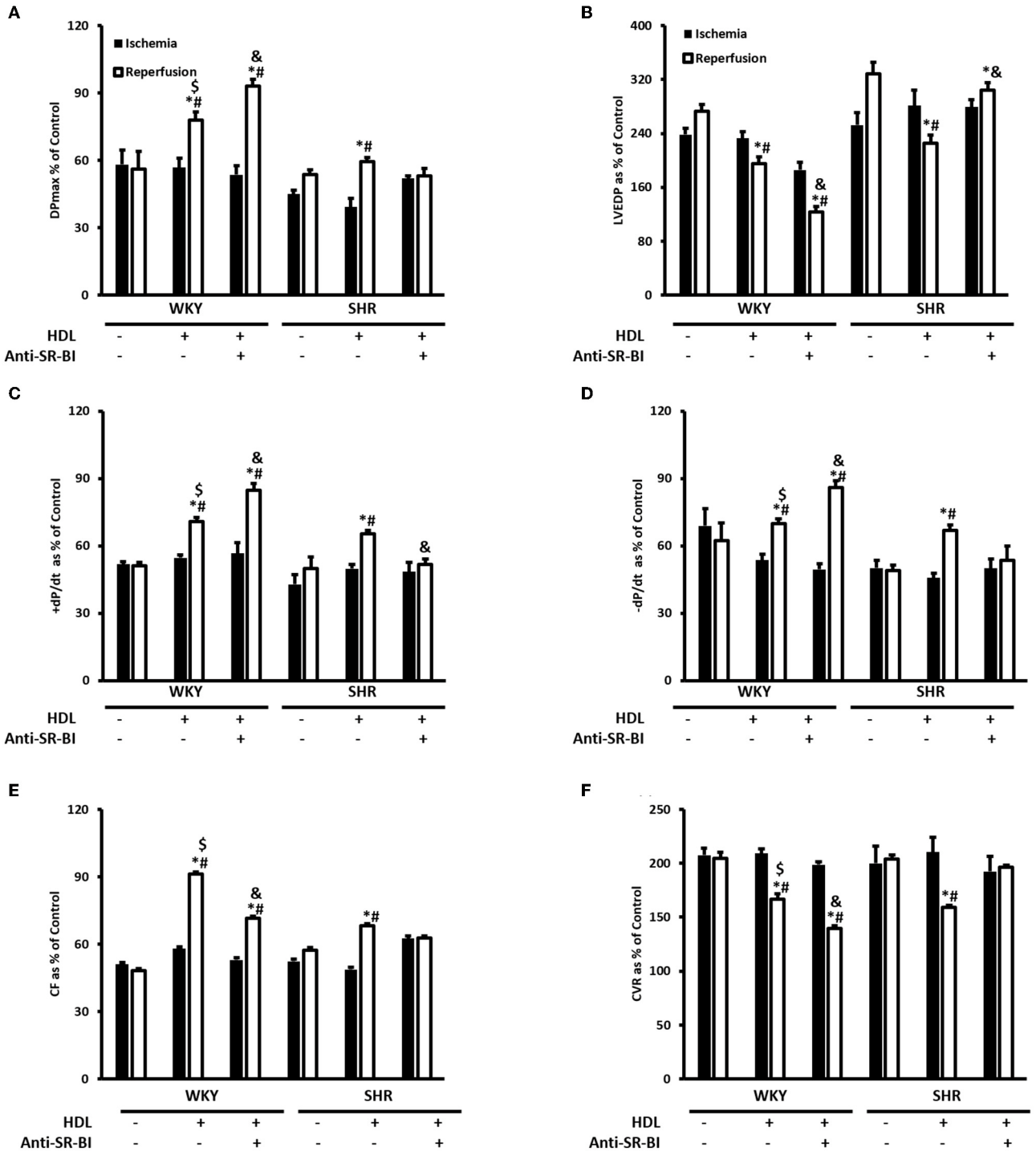

FIGURE 5 | The role of SR-BI in HDL mediated cardiac protection against I/R injury in WKY and SHR. Post-ischemic recovery parameters of cardiac functions including DPmax **(A)**, LVEDP **(B)**, cardiac contractility **(C,D)**, coronary hemodynamics **(E,F)**. Data were computed with no addition control, with HDL (400 μg) administered at reperfusion (acute treatment) in the presence or absence of SR-BI blocking antibody and expressed as means ± SEM. DPmax, maximum developed pressure; LVEDP, left ventricular end diastolic pressure; CF, coronary flow; CVR, coronary vascular resistance; $^{*}P < 0.5$ compared to ischemic period. $^{\#}P < 0.5$ compared to no addition control, $^{\$}P < 0.05$ relative to HDL treated SHR, $^{\&}P < 0.05$ vs. HDL treatment of the same genotype, $n = 3$–8 rats per group.

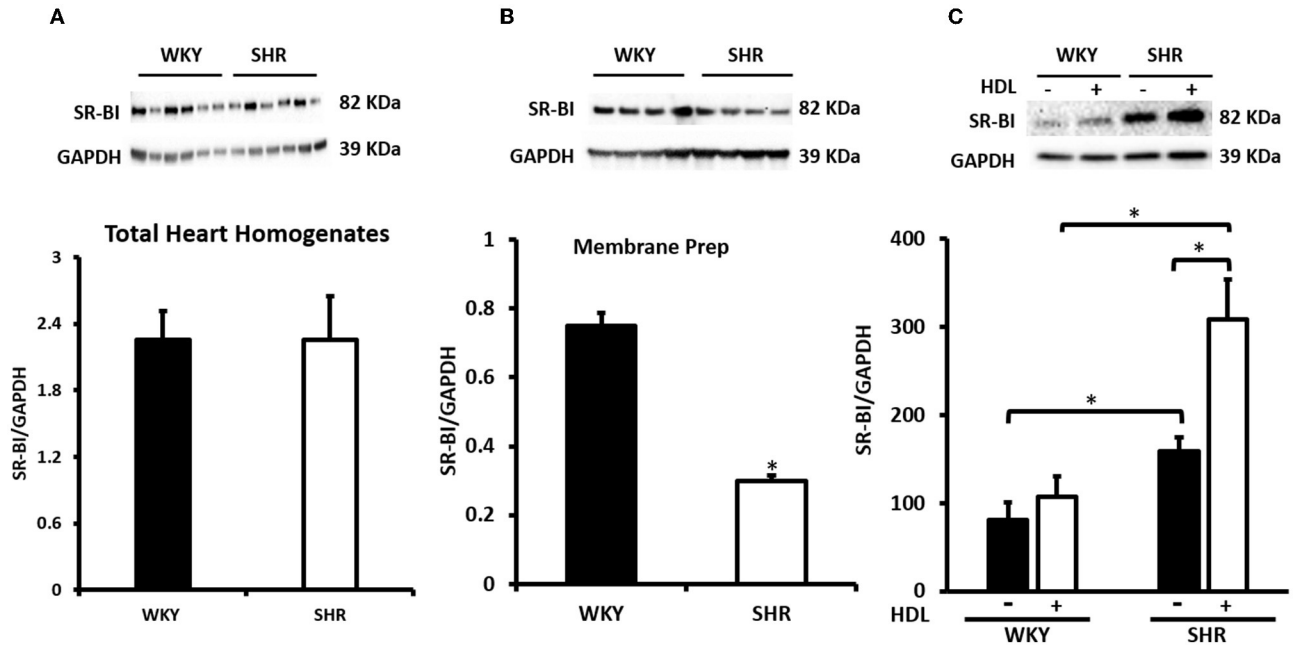

FIGURE 6 | Cardiac SR-BI Expression in WKY and SHR. Total heart homogenates **(A)** and membrane preparations **(B)** from WKY and SHR and total heart homogenates from WKY and SHR implanted with vehicle or HDL containing osmotic pumps **(C)** were subjected to immunoblotting against SR-BI and GAPDH as a loading control. Data are expressed as means ± SEM, $^*P < 0.05$, $n = 5$–6 rats per group.

HDL Attenuates Autophagy and Inflammation in SHR

We have tested the involvement of autophagy in mediating I/R injury in WKY and SHR using autophagy inhibitor 3-MA. Administration of 3-MA *in vivo* significantly ($P < 0.05$) improved cardiac hemodynamics and cardiac contractility in WKY during reperfusion relative to ischemia and relative to untreated controls (**Figures 7A–F**). Treatment of SHR with 3-MA however, did not result in any significant improvements in the tested parameters at reperfusion compared to ischemia or relative to untreated controls (**Figures 7A–F**). Consistent with parameters of cardiac physiology, 3-MA treatment significantly ($P < 0.05$) reduced troponin levels in WKY but not in SHR (**Table 3**). Moreover, 3-MA treatment significantly ($P < 0.001$) reduced the infarct size in WKY but not SHR (**Figure 8**). This suggests that blockage of autophagy protects WKY against I/R injury, yet it's not sufficient to induce protection in SHR. Protection against myocardial I/R injury in SHR may possibly require the simultaneous activation of multiple cardioprotective effects.

We have then investigated the involvement of autophagy in the observed cardioprotective effects of HDL in heart homogenates from WKY and SHR treated with or without HDL. HDL treatment significantly ($P < 0.05$) reduced protein levels of autophagy markers beclin, by 43%, LC3B, by 57%, and Atg-12, by 81.5%, in SHR but not WKY (**Figure 9**). The expression of other autophagy markers including Atg-3, Atg-5, and Atg-7 was not however significantly altered upon HDL treatment in WKY or SHR (**Figure 9**). This suggests that HDL reduced autophagy might be a mechanism by which HDL protects against I/R injury in SHR. Furthermore, HDL treatment significantly ($P < 0.05$) reduced TNF-α levels, by about 20%, in SHR but not in WKY (**Figure 10A**). Nonetheless, HDL treatment did not have a significant effect on IL-6 levels in WKY or SHR (**Figure 10B**). Together these data suggest that treatment with HDL protects WKY and SHR against ischemic damage, yet distinct protection mechanisms appear to exist in WKY and SHR.

DISCUSSION

Hypertension impairs cardiac function (23–26) and alters HDL structure and function (9, 22). HDL protects against I/R injury *in vivo* and *ex vivo*, reviewed in (36). The exact role of HDL in hypertension is however not clearly understood. We have therefore tested the effect HDL on cardiac I/R injury and investigated the possible underlying mechanism(s) in SHR. We demonstrate that HDL treatment reduces SBP and DBP in SHR and protects against cardiac I/R injury in normotensive and hypertensive rats. HDL induced cardiac protection was SR-BI-dependent. Interestingly, the magnitude of HDL mediated protection against I/R injury in WKY and SHR was proportional to the expression levels of cardiac SR-BI. Chronic HDL treatment enhanced cardiac SR-BI expression in SHR and resulted in greater protection against I/R injury in these rats. Chronic HDL treatment reduced cardiac autophagy markers and TNF-α levels in SHR. Our data suggest that in addition to HDL-mediated reduction in SBP and DBP, HDL attenuation of autophagy and inflammation are potential mechanisms by which HDL treatment induces cardiac protection in SHR (**Figure 11**).

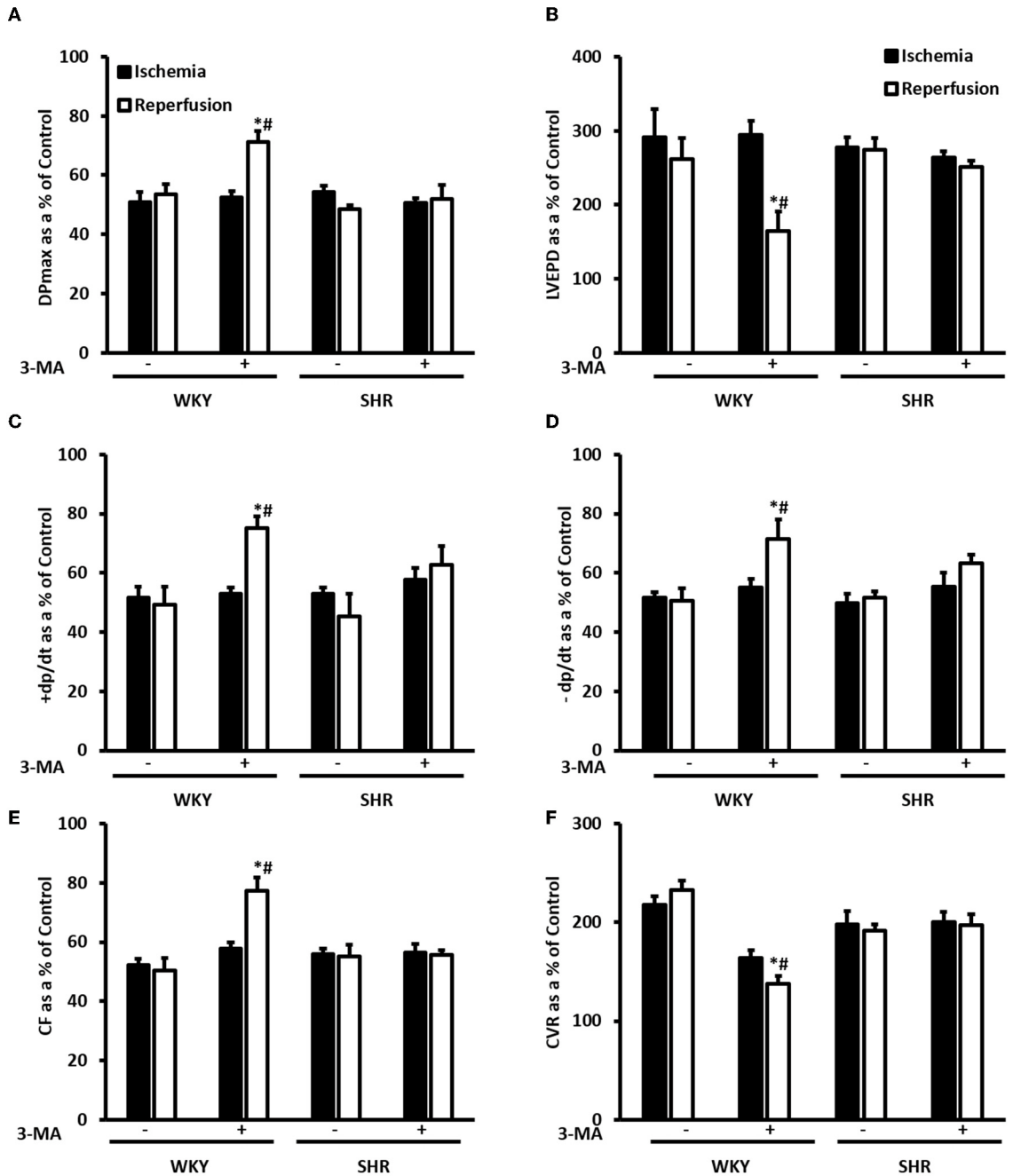

FIGURE 7 | Treatment with 3-MA protects WKY but not SHR against I/R injury. Post-ischemic recovery parameters of cardiac functions including DPmax **(A)**, LVEDP **(B)**, coronary hemodynamics **(C,D)**, cardiac contractility **(E,F)**. Data were computed with no addition control, with 3-MA (30 mg/Kg) administered into the femoral vein 2 h prior to sacrifice. Data are expressed as means ± SEM. DPmax, maximum developed pressure; LVEDP, left ventricular end diastolic pressure; CF, coronary flow; CVR, coronary vascular resistance; 3-MA, 3-methyladenine; $^{*}P < 0.5$ compared to ischemic period. $^{\#}P < 0.5$ compared to no addition control, $n = 4$–7.

Studies in experimental animals have unanimously shown that HDL protects against cardiac I/R injury in the isolated hearts and *in vivo* (37–39, 44–47). Hearts from hypertensive rodents however, appear to be resistant to cardiac protection induced by multiple agents proven to be protective in normotensive controls (30–34). We have therefore tested if HDL treatment can protect against cardiac I/R injury in the well-established model of hypertension, SHR. Interestingly, HDL infusion at (900 ng/kg/min) for a week significantly reduced SBP and DBP in SHR, however, blood pressure of HDL infused SHR remained significantly higher than untreated WKY. Furthermore, HDL treatment did not change heart to tibia length ratio in WKY

TABLE 3 | Effect of blockage of autophagy on troponin release in WKY and SHR.

	Troponin (ng/ml)			
	Control		3-MA	
	Ischemia	Reperfusion	Ischemia	Reperfusion
WKY	0.3 ± 0.1	0.49 ± 0.1	0.62 ± 0.1	0.37 ± 0.042*
SHR	0.16 ± 0.02	0.25 ± 0.1	0.15 ± 0.038	0.42 ± 0.1*

*$P < 0.05$ vs. ischemia.

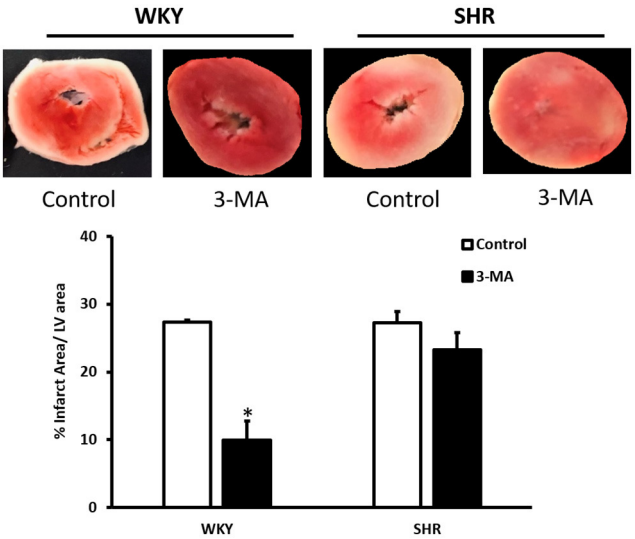

FIGURE 8 | Effect of 3-MA on infarct size in WKY and SHR. TTC staining of heart section from WKY and SHR treated with vehicle control or 3-MA 2 h prior to sacrifice and subjected to I/R injury *ex-vivo*. Data are means ± SEM, *$P <$ 0.001, $n = 3$–8 rats per group.

or SHR. HDL induced reduction in blood pressure appears to be specific to SHR and was not observed in WKY. A lack of an effect of HDL infusion on blood pressure and heart weight in normotensive controls is consistent with previously reported data (40). HDL mediated reduction in blood pressure in hypertensive rats (**Table 1**) could be due to reduction in cardiac contractility and cardiac output (48). Alternatively, HDL could enhance nitric oxide production and reduce vascular resistance (49–51). Moreover, HDL could interact reciprocally with the renin-angiotensin system and reduce blood pressure (52, 53). The exact mechanism of blood pressure lowering effect of HDL however, remains to be investigated. Unlike continuous administration of total HDL (our findings), intermittent intravenous administration of reconstituted HDL (rHDL) did not have any significant effects on SBP or cardiac functions in SHR (54). The lack of a blood pressure lowering and cardioprotective effects in response to intermittent rHDL infusion could be attributed to the type, dose, duration or mode of HDL administration.

Furthermore, our data suggest that chronic HDL infusion does not alter plasma total or HDL cholesterol levels in WKY and SHR, possibly suggesting enhanced clearance in response to HDL infusion. Studies involving deletion (55) or overexpression (56) of hepatic SR-BI demonstrated a key role of the receptor in mediating the selective uptake of HDL associated lipids. Overexpression of hepatic SR-BI resulted in a substantial decrease in plasma HDL cholesterol simultaneously with a significant increase in bile cholesterol indicating a role of hepatic SR-BI in RCT (57). Changes in hepatic SR-BI expression levels has been linked to changes in HDL composition (58, 59). Our finding that hepatic SR-BI protein levels are increased in HDL- treated SHR presumably suggests enhanced HDL clearance and supports the maintenance of homeostatic steady state levels of HDL cholesterol. Nonetheless, changes in HDL composition and/or function in response to increased SR-BI expression cannot be excluded (60, 61).

We further demonstrated that chronic HDL treatment protected WKY and, to a greater extent, SHR against cardiac I/R injury. Chronic HDL treatment improved LV pressure, cardiac contractility and hemodynamics at reperfusion relative to ischemia and relative to controls in SHR. Furthermore, chronic HDL treatment reduced cardiac enzyme release and infarct size in SHR. Our finding that HDL treatment protects against myocardial I/R injury in normotensive rats is consistent with previously reported data (37, 39). Nonetheless, to our knowledge, this is the first report that demonstrates a blood pressure lowering and a cardioprotective effect of HDL in hypertensive rodents.

HDL mediated cardiac protection in SHR could be due to the restoration of HDL function and/or composition upon infusion. Alternatively, it could be due to enhanced HDL mediated signaling or both. HDL mediated cardiac protection *via* signaling through SR-BI (62). In WKY, SR-BI blocking antibody significantly reduced but did not completely block the cardioprotective effects of HDL (**Figure 5**). In SHR however, SR-BI blockage was detrimental. This suggests that in addition to SR-BI, other cardioprotective pathways could also be involved in WKY; the nature of which, however, remains to be investigated. S1P receptor 3 (S1PR3) has been directly implicated in mediating the cardioprotective effects of HDL in an *in vivo* mouse model of myocardial infarction (37). Combined blockage of SR-BI and potential protective pathway(s), possibly S1PR3, may completely abrogate HDL-induced cardiac protection in WKY. The absolute requirement of SR-BI in HDL mediated cardiac protection and the enhanced cardioprotective effects in response to chronic HDL treatment in SHR led us to hypothesize that the enhanced cardiac protection in HDL treated SHR could perhaps be due to enhanced SR-BI expression in these rats. We observed increased cardiac SR-BI expression in SHR in response to chronic treatment with HDL (**Figure 6C**), consistent with the enhanced protection observed in these rats relative to the normotensive controls (**Figure 3**). In agreement with these findings, normotensive rats expressed significantly higher levels of cardiac SR-BI in membrane fractions (**Figure 6B**) but not in total heart homogenates (**Figure 6A**) and demonstrated an enhanced response to HDL (acute treatment) relative to

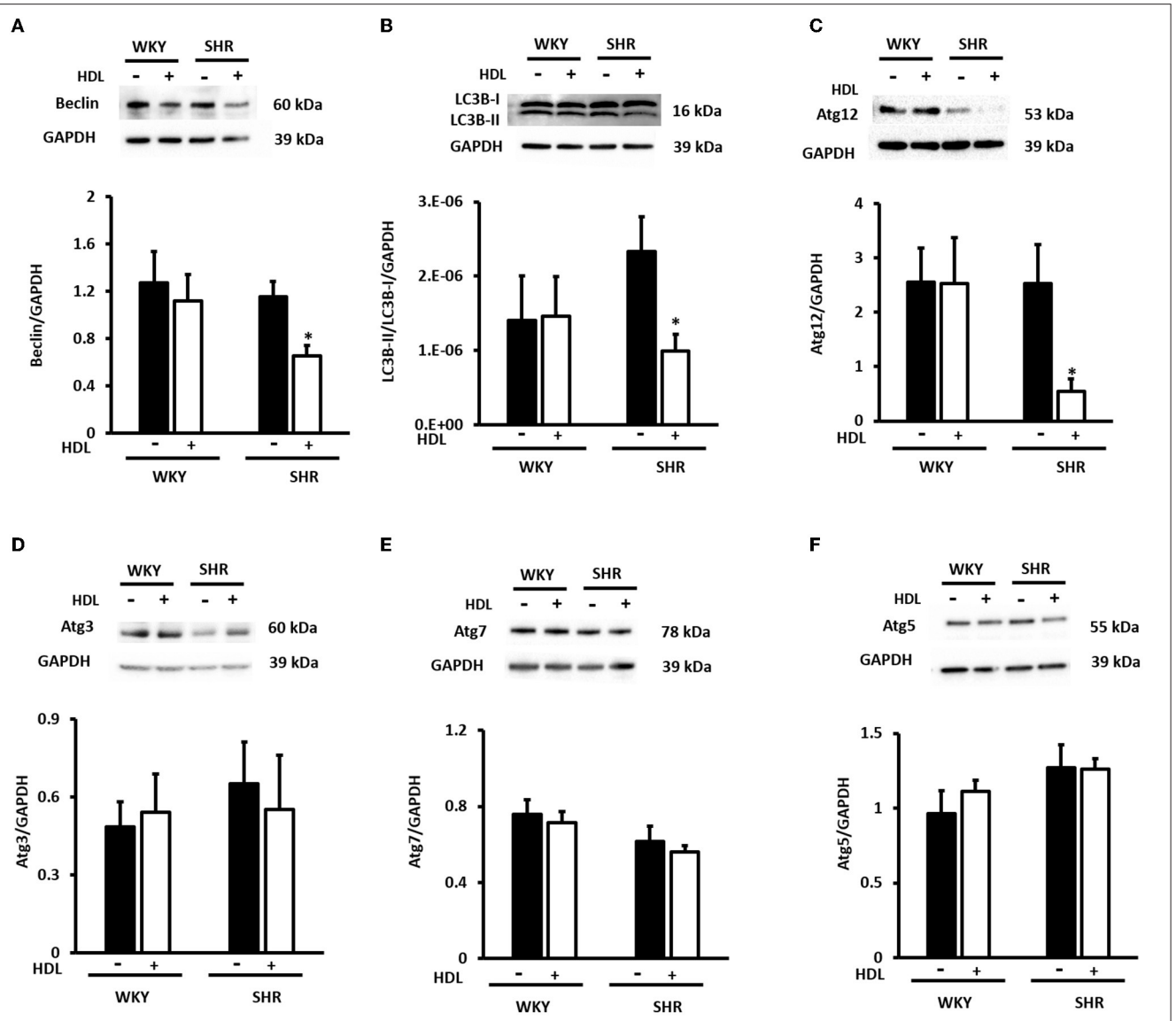

FIGURE 9 | Effect of chronic HDL treatment on the expression of autophagy regulated genes in WKY and SHR. Total heart homogenates were subjected to immunoblotting against beclin, LC3B, Atg-12, Atg-3, Atg-7, Atg-5, and GAPDH as a loading control. Representative images of the relative expression of beclin **(A)**, LC3B-I and II **(B)**, Atg-12 **(C)** Atg-3 **(D)**, Atg-7 **(E)**, and Atg-5 **(F)** in WKY and SHR treated with or without HDL. Data are means ± SEM, $^*P < 0.05$, $n = 3$–8 rats per group.

hypertensive rats (**Figure 5**). These data not only suggest that SR-BI mediates the protective actions of HDL but it also provide a proof of principle that the magnitude of HDL induced protection is proportional to SR-BI protein levels. Enhanced HDL induced protection is observed in rats expressing greater levels of cardiac SR-BI. Our data further, shed light on differences in cardiac SR-BI localization between WKY and SHR. Despite the fact that no significant differences were observed in SR-BI expression in total heart homogenates from WKY and SHR, significantly greater levels of cardiac SR-BI were localized in the membrane fractions of WKY, implicating enhanced HDL-SR-BI interaction, augmented SR-BI mediated signaling and exacerbated cardiac protection in response to HDL. Moreover, our data highlight the novel upregulation of cardiac SR-BI in response to surgical stress in SHR, revealing a previously undiscovered role of cardiac SR-BI in hypertensive rats subjected to a stress response. The significance of these finding, however, awaits further investigation. Enhanced expression of SR-BI, specifically in the infarcted area, has recently been reported in rats subjected to myocardial infarction induced by left coronary ligation, plausibly suggesting a role of SR-BI in myocardial repair (63). At a cellular level, SR-BI mediated the cardioprotective effects of HDL against

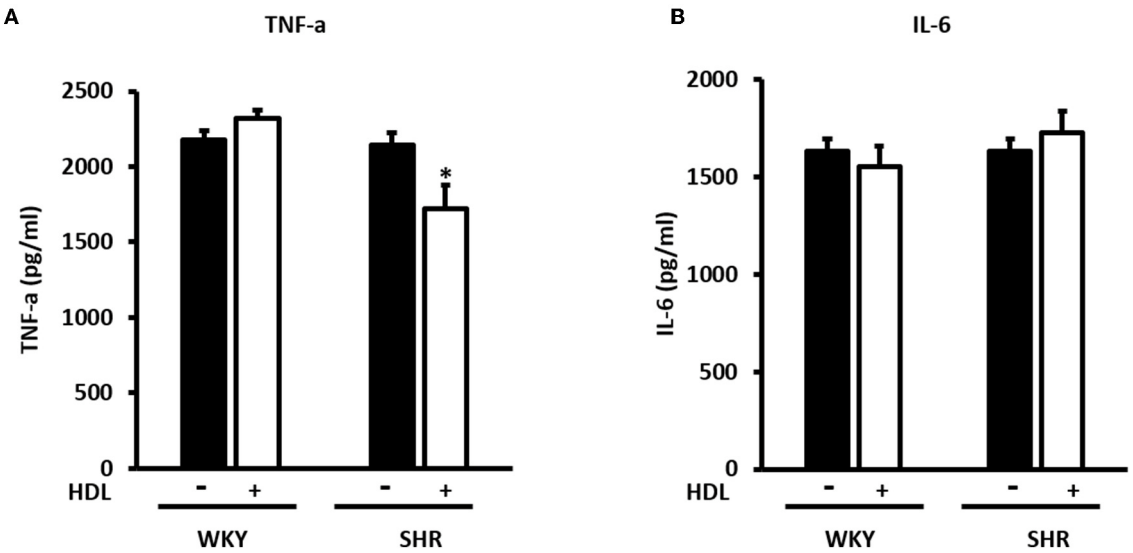

FIGURE 10 | Effect of chronic HDL treatment on inflammatory markers in WKY and SHR. The levels of TNF-α **(A)** and IL-6 **(B)** from hearts treated (chronically) with or without HDL and subjected to I/R injury. Data are means ± SEM, $^*P < 0.05$, $n = 5$–8 rats per group.

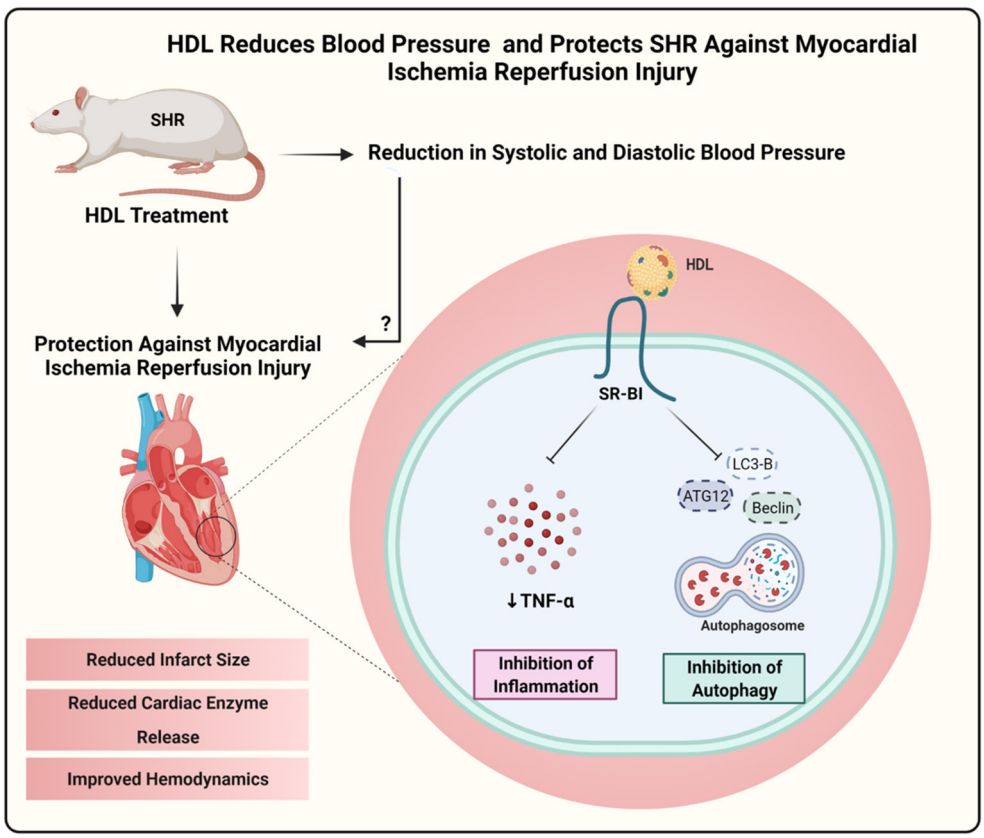

FIGURE 11 | Proposed mechanism of HDL mediated cardiac protection in SHR. Chronic, *in vivo* treatment with HDL reduced blood pressure and protected SHR against myocardial I/R injury. HDL induced cardiac protection required SR-BI and involved attenuation of autophagy and inflammation. Created with Biorender.com.

necrosis induced by oxygen and glucose deprivation in neonatal mouse and human cardiomyocytes (64). A remarkable role of hepatic SR-BI in correcting cardiac dysfunction has recently been reported in SR-BI KO mice overexpressing hepatic SR-BI (65). Hepatocyte specific transfer of the gene encoding SR-BI restored HDL metabolism and abrogated the detrimental effects on cardiac structure and function in mice lacking SR-BI and subjected to transverse aortic constriction (65). Therefore, in addition to enhanced expression of cardiac SR-BI upon HDL treatment, a role of hepatic SR-BI in HDL mediated protection against cardiac I/R injury in SHR cannot be excluded, at least in part *via* the modulation of HDL metabolism in these rats.

The role of autophagy in cardiac I/R injury appears to be controversial and a double edged sword function of autophagy has been proposed (66, 67). We report that treatment with autophagy inhibitor, 3-MA, protects hearts from normotensive but not hypertensive rats against I/R injury. In line with other reports (68, 69), our data suggest a detrimental role of autophagy in mediating I/R injury and blockage of autophagy is protective, at least, in WKY. The lack of cardiac protection in response to autophagy inhibition in SHR may suggest enhanced deteriorations and impairments in these hearts that blockage of a single pathway, autophagy, is not sufficient to induce protection. Consistent with these findings, SHR were resistant to cardiac protection induced by helium, erythropoietin and captopril (33–35).

HDL inhibited mechanical stress induced cardiac hypertrophy and autophagy in cultured cardiomyocytes and *in vivo*, *via* the downregulation of cardiac angiotensin receptor 1 and signaling *via* the PI3K/Akt pathway (70). Furthermore, HDL inhibited autophagic responses in endothelial cells treated with oxLDL (71). On contrary, glycated HDL increased the expression of autophagic proteins beclin, LC3B and Atg-5 in macrophages (72). Our data indicate that chronic HDL treatment reduces the expression levels of autophagy markers, beclin, LC3B and Atg-12 in SHR hearts subjected to I/R injury. Nevertheless, this was not observed in WKY treated with HDL. This suggests that HDL mediated reduction is autophagy might be one protective mechanism by which HDL treatment protects against cardiac I/R injury in hypertensive rats. We further report that chronic HDL treatment reduces cardiac TNF-α levels in SHR. This however, was not observed in WKY. Reciprocal interaction between autophagy and proinflammatory cytokines has been reported. TNF-α treatment was shown to enhance autophagy (73), while 3-MA mediated inhibition of autophagy upregulated TNF-α and IL-6 levels in immortalized bone marrow derived macrophages (74). Our findings indicate that chronic HDL treatment induces cardiac protection in SHR *via* multiple mechanisms, including attenuation of autophagy and inflammation. It remains to be tested however whether HDL attenuates autophagy *via* its anti-inflammatory effects or reduces inflammation by virtue of its effects on autophagy. However, while HDL was protective in WKY, HDL mediated reduction in autophagy and inflammation does not seem to play a significant role in normotensive rats, treated with HDL at least under these experimental conditions. Alternative protection mechanisms may operate in WKY, nonetheless the effects of HDL on inflammation and autophagy in WKY cannot be completely excluded. HDL attenuation of inflammation and autophagy could be involved in HDL mediated protection in WKY however, it might operate at different kinetics and involve markers other than what we used in this study.

The strengths of this study include reporting a novel anti-hypertensive effect of HDL in SHR. In addition, this study elucidated an interesting role of cardiac SR-BI in HDL-mediated protection against I/R injury in normotensive and hypertensive rats whereby the magnitude of HDL induced cardiac protection was directly proportional to the expression levels of cardiac SR-BI. Furthermore, our study unraveled differences in the mechanism(s) by which HDL protected against myocardial injury in WKY and SHR. Nonetheless, our study has some limitations related to the dose, duration and timing of the HDL treatment. It's not clear if HDL administration to younger, perhaps 4 week old, SHR can prevent the development of hypertension or if higher doses of HDL or longer periods of administration will result in further reduction in BP. Male SHR exhibited significantly higher SBP values ($P < 0.05$) at 12-week of age and thereafter than female SHR (75). We demonstrate that HDL treatment reduces SBP and protects against myocardial I/R injury in male SHR. Nonetheless, it not clear if HDL is equally protective in female SHR. Moreover, the study did not investigate if HDL effects will permanently last or be temporarily effective during the treatment period. Flow up studies are required to address these limitations and further investigate the molecular mechanisms of HDL induced cardiac protection.

In conclusion this study shed light on a novel role of HDL in hypertension. HDL treatment reduced blood pressure and protected hypertensive rats against cardiac I/R injury. We demonstrate that chronic HDL treatment reduces blood pressure in SHR and protects against cardiac I/R injury. HDL induced protection appears to involve signaling *via* SR-BI and attenuation of cardiac autophagy and inflammation.

DATA AVAILABILITY STATEMENT

The original contributions presented in the study are included in the article/**Supplementary Material**, further inquiries can be directed to the corresponding author/s.

ETHICS STATEMENT

The animal study was reviewed and approved by Health Sciences Research Ethics Committee Kuwait University.

AUTHOR CONTRIBUTIONS

AA-J obtained the funding for the study and drafted the manuscript. AA-J and FB designed and supervised conducting the experiments, analyzed the data, edited and revised the manuscript. Both authors contributed to the article and approved the submitted version.

FUNDING

This project was funded by the Research Administration at Kuwait University. Grant No. MB03/16.

ACKNOWLEDGMENTS

We thank Mona Rostum, Lilly Verges, Emain Faid, Anju Devass, and Esraa Aly for their technical support.

SUPPLEMENTARY MATERIAL

The Supplementary Material for this article can be found online at: https://www.frontiersin.org/articles/10.3389/fcvm.2022.825310/full#supplementary-material

Supplementary Figure 1 | Heart to tibia length ratios. Herat weights of WKY and SHR rats implanted with vehicle or HDL containing pumps were expressed relative to tibia lengths. Data are mean ± SEM, $n = 7–10$ rats per group.

REFERENCES

1. Zhou B, Perel P, Mensah GA, Ezzati M. Global epidemiology, health burden and effective interventions for elevated blood pressure and hypertension. *Nat Rev Cardiol.* (2021) 18:785–802. doi: 10.1038/s41569-021-00559-8
2. Collaboration NCDRF. Worldwide trends in hypertension prevalence and progress in treatment and control from 1990 to 2019: a pooled analysis of 1201 population-representative studies with 104 million participants. *Lancet.* (2021) 398:957–80. doi: 10.1016/S0140-6736(21)01330-1
3. Wierzejska E, Giernas B, Lipiak A, Karasiewicz M, Cofta M, Staszewski R, et al. global perspective on the costs of hypertension: a systematic review. *Arch Med Sci.* (2020) 16:1078–91. doi: 10.5114/aoms.2020.92689
4. Lawes CM, Vander Hoorn S, Rodgers A, International Society of H. Global burden of blood-pressure-related disease, 2001. *Lancet.* (2008) 371:1513–8. doi: 10.1016/S0140-6736(08)60655-8
5. Lawes CM, Bennett DA, Lewington S, Rodgers A. Blood pressure and coronary heart disease: a review of the evidence. *Semin Vasc Med.* (2002) 2:355–68. doi: 10.1055/s-2002-36765
6. Fox KM, EURopean trial On reduction of cardiac events with Perindopril in stable coronary Artery disease Investigators. Efficacy of perindopril in reduction of cardiovascular events among patients with stable coronary artery disease: randomised, double-blind, placebo-controlled, multicentre trial (the EUROPA study). *Lancet.* (2003) 362:782–8. doi: 10.1016/S0140-6736(03)14286-9
7. Patel A, Group AC, MacMahon S, Chalmers J, Neal B, Woodward M, et al. Effects of a fixed combination of perindopril and indapamide on macrovascular and microvascular outcomes in patients with type 2 diabetes mellitus (the ADVANCE trial): a randomised controlled trial. *Lancet.* (2007) 370:829–40. doi: 10.1016/S0140-6736(07)61303-8
8. Yusuf S, Sleight P, Pogue J, Bosch J, Davies R, Dagenais G. Effects of an angiotensin-converting-enzyme inhibitor, ramipril, on cardiovascular events in high-risk patients. The heart outcomes prevention evaluation study investigators. *N Engl J Med.* (2000) 342:145–53. doi: 10.1056/NEJM200001203420301
9. Hamad A, Salameh M, Mahmoud H, Singh J, Zaghmout M, Ward L. Relation of high levels of high-density lipoprotein cholesterol to coronary artery disease and systemic hypertension. *Am J Cardiol.* (2001) 88:899–901. doi: 10.1016/S0002-9149(01)01902-6
10. Turnbull F, Blood Pressure Lowering Treatment Trialists C. Effects of different blood-pressure-lowering regimens on major cardiovascular events: results of prospectively-designed overviews of randomised trials. *Lancet.* (2003) 362:1527–35. doi: 10.1016/S0140-6736(03)14739-3
11. Group PC. Randomised trial of a perindopril-based blood-pressure-lowering regimen among 6,105 individuals with previous stroke or transient ischaemic attack. *Lancet.* (2001) 358:1033–41. doi: 10.1016/S0140-6736(01)06178-5
12. Assmann G, Schulte H, von Eckardstein A, Huang Y. High-density lipoprotein cholesterol as a predictor of coronary heart disease risk. The PROCAM experience and pathophysiological implications for reverse cholesterol transport. *Atherosclerosis.* (1996) 124:S11–20. doi: 10.1016/0021-9150(96)05852-2
13. Barr DP, Russ EM, Eder HA. Protein-lipid relationships in human plasma. II. In atherosclerosis and related conditions. *Am J Med.* (1951) 11:480–93. doi: 10.1016/0002-9343(51)90183-0
14. Boyd GS, Oliver MF. The circulating lipids and lipoproteins in coronary artery disease. *Postgrad Med J.* (1957) 32:2–6; passim. doi: 10.1136/pgmj.33.375.2
15. Brown MS, Goldstein JL. Lipoprotein metabolism in the macrophage: implications for cholesterol deposition in atherosclerosis. *Annu Rev Biochem.* (1983) 52:223–61. doi: 10.1146/annurev.bi.52.070183.001255
16. Gordon DJ, Rifkind BM. High-density lipoprotein–the clinical implications of recent studies. *N Engl J Med.* (1989) 321:1311–6. doi: 10.1056/NEJM198911093211907
17. Oyama N, Sakuma I, Kishimoto N, Saijo Y, Sakai H, Urasawa K, et al. Low HDL-cholesterol, hypertension and impaired glucose tolerance as predictors of acute myocardial infarction in northern area of Japan. *Hokkaido Igaku Zasshi.* (2006) 81:25–30.
18. Kunutsor SK, Kieneker LM, Bakker SJL, James RW, Dullaart RPF. The inverse association of HDL-cholesterol with future risk of hypertension is not modified by its antioxidant constituent, paraoxonase-1: the PREVEND prospective cohort study. *Atherosclerosis.* (2017) 263:219–26. doi: 10.1016/j.atherosclerosis.2017.06.353
19. Hwang YC, Fujimoto WY, Kahn SE, Leonetti DL, Boyko EJ. Higher high density lipoprotein 2 (HDL2) to total HDL cholesterol ratio is associated with a lower risk for incident hypertension. *Diabetes Metab J.* (2019) 43:114–22. doi: 10.4093/dmj.2018.0053
20. Kim NH, Cho HJ, Kim YJ, Cho MJ, Choi HY, Eun CR, et al. Combined effect of high-normal blood pressure and low HDL cholesterol on mortality in an elderly Korean population: the South-West Seoul (SWS) study. *Am J Hypertens.* (2011) 24:918–23. doi: 10.1038/ajh.2011.78
21. Sheu WH, Swislocki AL, Hoffman BB, Reaven GM, Chen YD. Effect of prazosin treatment on HDL kinetics in patients with hypertension. *Am J Hypertens.* (1990) 3:761–8. doi: 10.1093/ajh/3.10.761
22. Ozerova IN, Perova NV, Shchel'tsyna NV, Mamedov MN. Parameters of high-density lipoproteins in patients with arterial hypertension in combination with other components of metabolic syndrome. *Bull Exp Biol Med.* (2007) 143:320–2. doi: 10.1007/s10517-007-0100-4
23. Ledvenyiova-Farkasova V, Bernatova I, Balis P, Puzserova A, Bartekova M, Gablovsky I, et al. Effect of crowding stress on tolerance to ischemia-reperfusion injury in young male and female hypertensive rats: molecular mechanisms. *Can J Physiol Pharmacol.* (2015) 93:793–802. doi: 10.1139/cjpp-2015-0026
24. Norton GR, Veliotes DG, Osadchii O, Woodiwiss AJ, Thomas DP. Susceptibility to systolic dysfunction in the myocardium from chronically infarcted spontaneously hypertensive rats. *Am J Physiol Heart Circ Physiol.* (2008) 294:H372–8. doi: 10.1152/ajpheart.01024.2007
25. Itoh T, Abe K, Tokumura M, Hirono S, Haruna M, Ibii N. Cardiac mechanical dysfunction induced by ischemia-reperfusion in perfused heart isolated from stroke-prone spontaneously hypertensive rats. *Clin Exp Hyperten.* (2004) 26:485–98. doi: 10.1081/CEH-200031822
26. Golden AL, Bright JM, Pohost GM, Pike MM. Ischemic dysfunction and impaired recovery in hypertensive hypertrophied hearts is associated with exaggerated intracellular sodium accumulation. *Am J Hyperten.* (1994) 7:745–54. doi: 10.1093/ajh/7.8.745
27. McMillan EM, Pare MF, Baechler BL, Graham DA, Rush JW, Quadrilatero J. Autophagic signaling and proteolytic enzyme activity in cardiac and skeletal muscle of spontaneously hypertensive rats following chronic aerobic exercise. *PLoS ONE.* (2015) 10:e0119382. doi: 10.1371/journal.pone.0119382
28. Bloemberg D, McDonald E, Dulay D, Quadrilatero J. Autophagy is altered in skeletal and cardiac muscle of spontaneously hypertensive rats. *Acta Physiol.* (2014) 210:381–91. doi: 10.1111/apha.12178

29. Boluyt MO, O'Neill L, Meredith AL, Bing OH, Brooks WW, Conrad CH, et al. Alterations in cardiac gene expression during the transition from stable hypertrophy to heart failure. Marked upregulation of genes encoding extracellular matrix components. *Circ Res.* (1994) 75:23–32. doi: 10.1161/01.RES.75.1.23
30. Wagner C, Ebner B, Tillack D, Strasser RH, Weinbrenner C. Cardioprotection by ischemic postconditioning is abrogated in hypertrophied myocardium of spontaneously hypertensive rats. *J Cardiovasc Pharmacol.* (2013) 61:35–41. doi: 10.1097/FJC.0b013e3182760c4d
31. Ebrahim Z, Yellon DM, Baxter GF. Ischemic preconditioning is lost in aging hypertensive rat heart: independent effects of aging and longstanding hypertension. *Exp Gerontol.* (2007) 42:807–14. doi: 10.1016/j.exger.2007.04.005
32. Babiker F, Al-Jarallah A, Al-Awadi M. Effects of cardiac hypertrophy, diabetes, aging, and pregnancy on the cardioprotective effects of postconditioning in male and female rats. *Cardiol Res Pract.* (2019) 2019:3403959. doi: 10.1155/2019/3403959
33. Yano T, Miki T, Tanno M, Kuno A, Itoh T, Takada A, et al. Hypertensive hypertrophied myocardium is vulnerable to infarction and refractory to erythropoietin-induced protection. *Hypertension.* (2011) 57:110–5. doi: 10.1161/HYPERTENSIONAHA.110.158469
34. Oei GT, Huhn R, Heinen A, Hollmann MW, Schlack WS, Preckel B, et al. Helium-induced cardioprotection of healthy and hypertensive rat myocardium *in vivo*. *Eur J Pharmacol.* (2012) 684:125–31. doi: 10.1016/j.ejphar.2012.03.045
35. Penna C, Tullio F, Moro F, Folino A, Merlino A, Pagliaro P. Effects of a protocol of ischemic postconditioning and/or captopril in hearts of normotensive and hypertensive rats. *Basic Res Cardiol.* (2010) 105:181–92. doi: 10.1007/s00395-009-0075-6
36. Sposito AC, Carmo HR, Barreto J, Sun L, Carvalho LSF, Feinstein SB, et al. HDL-targeted therapies during myocardial infarction. *Cardiovasc Drugs Ther.* (2019) 33:371–81. doi: 10.1007/s10557-019-06865-1
37. Theilmeier G, Schmidt C, Herrmann J, Keul P, Schafers M, Herrgott I, et al. High-density lipoproteins and their constituent, sphingosine-1-phosphate, directly protect the heart against ischemia/reperfusion injury *in vivo via* the S1P3 lysophospholipid receptor. *Circulation.* (2006) 114:1403–9. doi: 10.1161/CIRCULATIONAHA.105.607135
38. Frias MA, Pedretti S, Hacking D, Somers S, Lacerda L, Opie LH, et al. HDL protects against ischemia reperfusion injury by preserving mitochondrial integrity. *Atherosclerosis.* (2013) 228:110–6. doi: 10.1016/j.atherosclerosis.2013.02.003
39. Calabresi L, Rossoni G, Gomaraschi M, Sisto F, Berti F, Franceschini G. High-density lipoproteins protect isolated rat hearts from ischemia-reperfusion injury by reducing cardiac tumor necrosis factor-alpha content and enhancing prostaglandin release. *Circ Res.* (2003) 92:330–7. doi: 10.1161/01.RES.0000054201.60308.1A
40. Lin L, Gong H, Ge J, Jiang G, Zhou N, Li L, et al. High density lipoprotein downregulates angiotensin II type 1 receptor and inhibits angiotensin II-induced cardiac hypertrophy. *Biochem Biophys Res Commun.* (2011) 404:28–33. doi: 10.1016/j.bbrc.2010.11.037
41. Geenen IL, Kolk FF, Molin DG, Wagenaar A, Compeer MG, Tordoir JH, et al. Nitric oxide resistance reduces arteriovenous fistula maturation in chronic kidney disease in rats. *PLoS ONE.* (2016) 11:e0146212. doi: 10.1371/journal.pone.0146212
42. Babiker FA, Joseph S, Juggi J. The protective effects of 17beta-estradiol against ischemia-reperfusion injury and its effect on pacing postconditioning protection to the heart. *J Physiol Biochem.* (2014) 70:151–62. doi: 10.1007/s13105-013-0289-9
43. Babiker F, Al-Jarallah A, Joseph S. The Interplay between the renin angiotensin system and pacing postconditioning induced cardiac protection. *PLoS ONE.* (2016) 11:e0165777. doi: 10.1371/journal.pone.0165777
44. Gu SS, Shi N, Wu MP. The protective effect of ApolipoproteinA-I on myocardial ischemia-reperfusion injury in rats. *Life Sci.* (2007) 81:702–9. doi: 10.1016/j.lfs.2007.06.021
45. Marchesi M, Booth EA, Davis T, Bisgaier CL, Lucchesi BR. Apolipoprotein A-IMilano and 1-palmitoyl-2-oleoyl phosphatidylcholine complex (ETC-216) protects the *in vivo* rabbit heart from regional ischemia-reperfusion injury. *J Pharmacol Exp Ther.* (2004) 311:1023–31. doi: 10.1124/jpet.104.070789
46. Morel S, Frias MA, Rosker C, James RW, Rohr S, Kwak BR. The natural cardioprotective particle HDL modulates connexin43 gap junction channels. *Cardiovasc Res.* (2012) 93:41–9. doi: 10.1093/cvr/cvr257
47. Rossoni G, Gomaraschi M, Berti F, Sirtori CR, Franceschini G, Calabresi L. Synthetic high-density lipoproteins exert cardioprotective effects in myocardial ischemia/reperfusion injury. *J Pharmacol Exp Ther.* (2004) 308:79–84. doi: 10.1124/jpet.103.057141
48. Horio T, Miyazato J, Kamide K, Takiuchi S, Kawano Y. Influence of low high-density lipoprotein cholesterol on left ventricular hypertrophy and diastolic function in essential hypertension. *Am J Hypertens.* (2003) 16:938–44. doi: 10.1016/S0895-7061(03)01015-X
49. Kuvin JT, Ramet ME, Patel AR, Pandian NG, Mendelsohn ME, Karas RH, et al. novel mechanism for the beneficial vascular effects of high-density lipoprotein cholesterol: enhanced vasorelaxation and increased endothelial nitric oxide synthase expression. *Am Heart J.* (2002) 144:165–72. doi: 10.1067/mhj.2002.123145
50. Shaul PW, Mineo C. HDL action on the vascular wall: is the answer NO? *J Clin Invest.* (2004) 113:509–13. doi: 10.1172/JCI200421072
51. Nofer JR, van der Giet M, Tolle M, Wolinska I, von Wnuck Lipinski K, Baba HA, et al. HDL induces NO-dependent vasorelaxation *via* the lysophospholipid receptor S1P3. *J Clin Invest.* (2004) 113:569–81. doi: 10.1172/JCI200418004
52. Yu X, Murao K, Imachi H, Cao WM, Li J, Matsumoto K, et al. Regulation of scavenger receptor class BI gene expression by angiotensin II in vascular endothelial cells. *Hypertension.* (2007) 49:1378–84. doi: 10.1161/HYPERTENSIONAHA.106.082479
53. Putnam K, Shoemaker R, Yiannikouris F, Cassis LA. The renin-angiotensin system: a target of and contributor to dyslipidemias, altered glucose homeostasis, and hypertension of the metabolic syndrome. *Am J Physiol Heart Circ Physiol.* (2012) 302:H1219–30. doi: 10.1152/ajpheart.00796.2011
54. Imaizumi S, Kiya Y, Miura S, Zhang B, Matsuo Y, Uehara Y, et al. Pharmacological intervention using reconstituted high-density lipoprotein changes in the lipid profile in spontaneously hypersensitive rats. *Clin Exp Hypertens.* (2010) 32:202–8. doi: 10.3109/10641960903265196
55. Varban ML, Rinninger F, Wang N, Fairchild-Huntress V, Dunmore JH, Fang Q, et al. Targeted mutation reveals a central role for SR-BI in hepatic selective uptake of high density lipoprotein cholesterol. *Proc Natl Acad Sci USA.* (1998) 95:4619–24. doi: 10.1073/pnas.95.8.4619
56. Sehayek E, Ono JG, Shefer S, Nguyen LB, Wang N, Batta AK, et al. Biliary cholesterol excretion: a novel mechanism that regulates dietary cholesterol absorption. *Proc Natl Acad Sci USA.* (1998) 95:10194–9. doi: 10.1073/pnas.95.17.10194
57. Kozarsky KF, Donahee MH, Rigotti A, Iqbal SN, Edelman ER, Krieger M. Overexpression of the HDL receptor SR-BI alters plasma HDL and bile cholesterol levels. *Nature.* (1997) 387:414–7. doi: 10.1038/387414a0
58. Trigatti B, Rayburn H, Vinals M, Braun A, Miettinen H, Penman M, et al. Influence of the high density lipoprotein receptor SR-BI on reproductive and cardiovascular pathophysiology. *Proc Natl Acad Sci USA.* (1999) 96:9322–7. doi: 10.1073/pnas.96.16.9322
59. Lee JY, Badeau RM, Mulya A, Boudyguina E, Gebre AK, Smith TL, et al. Functional LCAT deficiency in human apolipoprotein A-I transgenic, SR-BI knockout mice. *J Lipid Res.* (2007) 48:1052–61. doi: 10.1194/jlr.M600417-JLR200
60. Sposito AC, de Lima-Junior JC, Moura FA, Barreto J, Bonilha I, Santana M, et al. Reciprocal multifaceted interaction between HDL (high-density lipoprotein) and myocardial infarction. *Arterioscler Thromb Vasc Biol.* (2019) 39:1550–64. doi: 10.1161/ATVBAHA.119.312880
61. Trigatti BL, Krieger M, Rigotti A. Influence of the HDL receptor SR-BI on lipoprotein metabolism and atherosclerosis. *Arterioscler Thromb Vasc Biol.* (2003) 23:1732–8. doi: 10.1161/01.ATV.0000091363.28501.84
62. Durham KK, Chathely KM, Mak KC, Momen A, Thomas CT, Zhao YY, et al. HDL protects against doxorubicin-induced cardiotoxicity in a scavenger receptor class B type 1-, PI3K-, and Akt-dependent manner. *Am J Physiol Heart Circ Physiol.* (2018) 314:H31–44. doi: 10.1152/ajpheart.00521.2016
63. de Lima AD, Guido MC, Tavares ER, Carvalho PO, Marques AF, de Melo MDT, et al. The expression of lipoprotein receptors is increased in the

infarcted area after myocardial infarction induced in rats with cardiac dysfunction. *Lipids.* (2018) 53:177–87. doi: 10.1002/lipd.12014
64. Durham KK, Chathely KM, Trigatti BL. High-density lipoprotein protects cardiomyocytes against necrosis induced by oxygen and glucose deprivation through SR-B1, PI3K, and AKT1 and 2. *Biochem J.* (2018) 475:1253–65. doi: 10.1042/BCJ20170703
65. Muthuramu I, Amin R, Aboumsallem JP, Mishra M, Robinson EL, De Geest B. Hepatocyte-specific SR-BI gene transfer corrects cardiac dysfunction in scarb1-deficient mice and improves pressure overload-induced cardiomyopathy. *Arterioscler Thromb Vasc Biol.* (2018) 38:2028–40. doi: 10.1161/ATVBAHA.118.310946
66. Ma S, Wang Y, Chen Y, Cao F. The role of the autophagy in myocardial ischemia/reperfusion injury. *Biochim Biophys Acta.* (2015) 1852:271–6. doi: 10.1016/j.bbadis.2014.05.010
67. Cao DJ, Gillette TG, Hill JA. Cardiomyocyte autophagy: remodeling, repairing, and reconstructing the heart. *Curr Hypertens Rep.* (2009) 11:406–11. doi: 10.1007/s11906-009-0070-1
68. Jin Y, Wang H, Cui X, Jin Y, Xu Z. Role of autophagy in myocardial reperfusion injury. *Front Biosci (Elite Ed).* (2010) 2:1147–53. doi: 10.2741/e174
69. Valentim L, Laurence KM, Townsend PA, Carroll CJ, Soond S, Scarabelli TM, et al. Urocortin inhibits Beclin1-mediated autophagic cell death in cardiac myocytes exposed to ischaemia/reperfusion injury. *J Mol Cell Cardiol.* (2006) 40:846–52. doi: 10.1016/j.yjmcc.2006.03.428
70. Lin L, Liu X, Xu J, Weng L, Ren J, Ge J, et al. High-density lipoprotein inhibits mechanical stress-induced cardiomyocyte autophagy and cardiac hypertrophy through angiotensin II type 1 receptor-mediated PI3K/Akt pathway. *J Cell Mol Med.* (2015) 19:1929–38. doi: 10.1111/jcmm.12567
71. Muller C, Salvayre R, Negre-Salvayre A, Vindis C. HDLs inhibit endoplasmic reticulum stress and autophagic response induced by oxidized LDLs. *Cell Death Differ.* (2011) 18:817–28. doi: 10.1038/cdd.2010.149
72. Tian H, Li Y, Kang P, Wang Z, Yue F, Jiao P, et al. Endoplasmic reticulum stress-dependent autophagy inhibits glycated high-density lipoprotein-induced macrophage apoptosis by inhibiting CHOP pathway. *J Cell Mol Med.* (2019) 23:2954–69. doi: 10.1111/jcmm.14203
73. Harris J, Keane J. How tumour necrosis factor blockers interfere with tuberculosis immunity. *Clin Exp Immunol.* (2010) 161:1–9. doi: 10.1111/j.1365-2249.2010.04146.x
74. Harris J, Hartman M, Roche C, Zeng SG, O'Shea A, Sharp FA, et al. Autophagy controls IL-1beta secretion by targeting pro-IL-1beta for degradation. *J Biol Chem.* (2011) 286:9587–97. doi: 10.1074/jbc.M110.202911
75. Reckelhoff JF, Zhang H, Granger JP. Testosterone exacerbates hypertension and reduces pressure-natriuresis in male spontaneously hypertensive rats. *Hypertension.* (1998) 31:435–9. doi: 10.1161/01.HYP.31.1.435

Conflict of Interest: The authors declare that the research was conducted in the absence of any commercial or financial relationships that could be construed as a potential conflict of interest.

Publisher's Note: All claims expressed in this article are solely those of the authors and do not necessarily represent those of their affiliated organizations, or those of the publisher, the editors and the reviewers. Any product that may be evaluated in this article, or claim that may be made by its manufacturer, is not guaranteed or endorsed by the publisher.

Copyright © 2022 Al-Jarallah and Babiker. This is an open-access article distributed under the terms of the Creative Commons Attribution License (CC BY). The use, distribution or reproduction in other forums is permitted, provided the original author(s) and the copyright owner(s) are credited and that the original publication in this journal is cited, in accordance with accepted academic practice. No use, distribution or reproduction is permitted which does not comply with these terms.

frontiers | Frontiers in Cardiovascular Medicine

ORIGINAL RESEARCH
published: 19 April 2022
doi: 10.3389/fcvm.2022.797154

Quantitative Lipidomic Analysis of Takotsubo Syndrome Patients' Serum

Srikanth Karnati[1], Gulcan Guntas[2], Ranjithkumar Rajendran[3], Sergey Shityakov[4], Marcus Höring[5], Gerhard Liebisch[5], Djuro Kosanovic[6], Süleyman Ergün[1], Michiaki Nagai[7] and Carola Y. Förster[8]**

[1] University of Würzburg, Institute of Anatomy and Cell Biology, Würzburg, Germany, [2] Department of Biochemistry, Medical Faculty, Atilim University, Ankara, Turkey, [3] Experimental Neurology, Department of Neurology, Justus Liebig University, Giessen, Germany, [4] Infochemistry Scientific Center, Laboratory of Chemoinformatics, ITMO University, Saint-Petersburg, Russia, [5] Institute of Clinical Chemistry and Laboratory Medicine, University Hospital of Regensburg, Regensburg, Germany, [6] Department of Pulmonology, I. M. Sechenov First Moscow State Medical University (Sechenov University), Moscow, Russia, [7] Hiroshima City Asa Hospital, Department of Cardiology, Hiroshima, Japan, [8] University of Würzburg, Department of Anaesthesiology, Intensive Care, Emergency and Pain Medicine, Würzburg, Germany

OPEN ACCESS

Edited by:
Wen Dai,
Versiti Blood Research Institute, United States

Reviewed by:
Ganesh V. Halade, University of South Florida, United States
Dawn Scantlebury, The University of the West Indies, Barbados
Hernan Mejia-Renteria, Hospital Clínico San Carlos, Spain

***Correspondence:**
Srikanth Karnati
Srikanth.karnati@uni-wuerzburg.de
Carola Y. Förster
Foerster_C@ukw.de

Specialty section:
This article was submitted to Lipids in Cardiovascular Disease, a section of the journal Frontiers in Cardiovascular Medicine

Received: *18 October 2021*
Accepted: *09 March 2022*
Published: *19 April 2022*

Citation:
Karnati S, Guntas G, Rajendran R, Shityakov S, Höring M, Liebisch G, Kosanovic D, Ergün S, Nagai M and Förster CY (2022) Quantitative Lipidomic Analysis of Takotsubo Syndrome Patients' Serum. Front. Cardiovasc. Med. 9:797154. doi: 10.3389/fcvm.2022.797154

Takotsubo syndrome (TTS), also known as the transient left ventricular apical ballooning syndrome, is in contemporary times known as novel acute cardiac syndrome. It is characterized by transient left ventricular apical akinesis and hyperkinesis of the basal left ventricular portions. Although the precise etiology of TTS is unknown, events like the sudden release of stress hormones, such as the catecholamines and the increased inflammatory status might be plausible causes leading to the cardiovascular pathologies. Recent studies have highlighted that an imbalance in lipid accumulation might promote a deviant immune response as observed in TTS. However, there is no information on comprehensive profiling of serum lipids of TTS patients. Therefore, we investigated a detailed quantitative lipid analysis of TTS patients using ES-MSI. Our results showed significant differences in the majority of lipid species composition in the TTS patients compared to the control group. Furthermore, the computational analyses presented was able to link the altered lipids to the pro-inflammatory cytokines and disseminate possible mechanistic pathways involving TNFα and IL-6. Taken together, our study provides an extensive quantitative lipidome of TTS patients, which may provide a valuable Pre-diagnostic tool. This would facilitate the elucidation of the underlying mechanisms of the disease and to prevent the development of TTS in the future.

Keywords: TTS, inflammation, lipids, TNF-α, IL6, PIK3R1, NF-kappa-B, phosphatidylinositol

INTRODUCTION

Takotsubo syndrome (TTS), also known as broken heart syndrome, stress induced cardiomyopathy, and Takotsubo cardiomyopathy, is an acute cardiac syndrome with rapid onset of chest pain and dyspnea (1–6). TTS is often triggered by physical and emotional stress and is characterized by a transient and reversible severe left ventricular dysfunction which typically recovers spontaneously within hours to weeks (7). The prevalence of TTS has been reported to be ∼2–3% of all patients with clinical appearance of acute coronary syndrome (ACS) (8). TTS is a remarkably like ACS with almost the same clinical presentations and ST elevations; therefore, differential diagnosis is critically important in the emergency department.

Despite the pathogenesis of TTS not being fully understood, several pathophysiological mechanisms have been suggested. These could include the following: myocardial ischemia, left ventricular outlet obstruction, increased circulating and myocardial catecholamine levels with myocardial toxicity, endothelial dysfunction, epinephrine-induced switch in signal trafficking, and autonomics nervous system dysfunction with cardiac sympathetic activation including over stimulation of beta receptors (4, 7, 9, 10).

The predominant pattern of TTS is widespread dyskinesia in the apical segments and hyperkinesia in the basal segment of left ventricle (LV) with apical ballooning (9, 11). It is suggested that local differences in adrenergic receptors may be the explanation of this involvement in the LV (11). Experimental studies have shown that the LV in canine has β2-adrenoceptors (β2-AR) that are expressed much more in the apical than in the basal segments (11, 12). Feola et al. also corroborated this hypothesis with a myocardial PET study showing decreased coronary flow reserve and impaired metabolism in the apical segments during the acute phase of TTS (13).

Several studies have shown that adrenergic overstimulation is strongly associated with the pathogenesis of TTS, but the mechanism remains unclear (7–9, 12, 14). The acute phase of TTS is characterized by supraphysiological levels of circulating and cardiac catecholamine (15) which operate as positive inotropic and chronotropic effects on the heart and regulate the myocardial lipid metabolism (7, 14, 16). The heart provides energy from the utilization of lipids. It uptakes lipid by protein transporters and secretes its own ApoB lipoproteins to excrete excess lipids. Excessive plasma catecholamine levels can lead to the disruption of the myocardial lipid metabolism in the heart (14).

Lipids have an important role in cellular energy storage, structure, and signaling. In addition to being a component of membranes, lipids play an essential role in the immune response by regulating signaling complexes in the cellular membrane (17). Recent studies have indicated that lipid metabolic disorders can cause various human diseases (17, 18). The human plasma lipid profile of TTS is so far poorly understood. A detailed lipid analysis of TTS patients could provide a valuable development to elucidate the underlying mechanisms of the disease.

In the current study, a total lipid profiling was performed including the measurement of 140 glycerophospholipids (GP), 44 sphingolipids (SL), 20 sterols (ST), and 58 glycerolipids (GL) in the control, acute TTS, and subacute TTS groups. To our knowledge, this study is the first to measure such an extensive quantitative lipidome analysis in TTS to date. The aim of our study was to investigate the underlying pathophysiological mechanism of TTS in relation to lipid metabolism and to relate it to the pro-inflammatory processes described to be prevalent in this syndrome.

MATERIALS AND METHODS

Materials

All chemicals were purchased from Sigma-Aldrich (Deisenhofen, Germany) unless otherwise mentioned. Phospholipid standards were obtained from the Avanti Polar Lipids (Alabaster, AL, USA), standards of cholesterol and cholesteryl esters with purity >95% obtained from Sigma (Taufkirchen, Germany). High purity cholesterol-(25, 26, 26, 26, 27, 27, 27-d7) was purchased from Cambridge Isotope Laboratories (Andover, MA, USA). HPLC grade solvents methanol and chloroform were obtained from Merck (Darmstadt, Germany). Analytical grade ammonium acetate and acetyl chloride were obtained from Sigma-Aldrich (Buchs, Switzerland). All other reagents used were of high purity and analytical grade.

TABLE 1 | Baseline demographic and vascular risk factors.

	Acute TTS ($n = 4$)	Subacute TTS ($n = 5$)	Control ($n = 6$)	*p*-value
Age (yrs)	76	88	80	$p = 0.21$
Female (%)	50	100	100	$p = 0.052$
Smoking (%)	50	0	0	$p = 0.052$
Hypertension (%)	50	40	67	$p = 0.69$
Lipid disorder (%)	25	20	67	$p = 0.25$
Diabetes mellitus (%)	0	0	17	$p = 0.47$

Data are presented as the median or as percentages. p-value comparison across three groups using an Kruskal-Wallis test for qualitative variables.

Ethics Approval and Consent to Participate

The study protocol was approved by the Hiroshima City Asa Hospital Research Committee (01-3-3), Hiroshima, Japan and was conducted in accordance with the principles stated in the Declaration of Helsinki. All participants provided informed written consent. From July 2019 to September 2019, 9 patients with hospitalized TTS and 6 healthy controls were registered consecutively at Hiroshima City Asa Hospital. While all eligible subjects were included in this analysis, none of the TTS patients and healthy controls were died during hospitalization". In the Kruskall Wallis test, there were no significant difference in the age (median age 83 vs. 80 yrs, $p = 0.48$) and female percentage (78 vs. 100%, $p = 0.23$) between the group with TTS and control.

Human Patient Serum

All human blood from patients providing informed written consent was sampled using S-Monovette collection tubes (Sarstedt). We collected blood samples of 15 pseudonymized patients which were subsequently divided into 3 different groups: control ($n = 6$), patients with acute TTS (first 2 weeks after onset, $n = 4$), patients with subacute TTS (2–6 weeks after onset, $n = 5$). The healthy controls did not present with altered coronary arteries in the coronary angiography diagnostics, while minor cardiovascular or endocrinological diseases were accepted (e.g.,: arterial hypertension, diabetes mellitus). Patient's baseline demographic and vascular risk factors characteristics are summarized in **Table 1**. All patients were diagnosed according to the InterTAK Diagnostic Criteria (19) as was described below:

For serum preparation, all the blood was drawn from subjects in using S-Monovette collection tubes (Sarstedt) and incubated at room temperature for 60 min. Then, the blood samples were centrifuged at 1,500 × g for 15 min, the serum was isolated,

immediately frozen and stored at −80°C until the extraction. All the methods used in this study were performed in accordance with the relevant guidelines and regulations. Serum samples were quantified and analyzed individually.

Lipid Extraction and Sample Preparation

Fresh snap-frozen serum samples were transported to University hospital Würzburg in dry ice. Serum samples were quantified and 5 µl of each subject were used for extraction, and lipids were extracted according to the procedure described by Bligh and Dyer (20). The following lipid species were added as internal standards: PC 14:0/14:0, PC 22:0/22:0, PE 14:0/14:0, PE 20:0/20:0 (di-phytanoyl)c, PS 14:0/14:0, PS 20:0/20:0 (di-phytanoyl), PI 17:0/17:0, LPC 13:0, LPC 19:0, LPE 13:0, Cer d18:1/14:0, Cer d18:1/17:0, D7-FC, CE 17:0, CE 22:0, TG 51:0, TG 57:0, DG 28:0 and DG 40:0. Chloroform phase was recovered by a pipetting robot (Tecan Genesis RSP 150) and vacuum dried. The residues were dissolved in either in 10 mM ammonium acetate in methanol/chloroform (3:1, v/v) (for low mass resolution tandem mass spectrometry) or chloroform/methanol/2-propanol (1:2:4 v/v/v) with 7.5 mM ammonium formate (for high resolution mass spectrometry). In the present study, we analyzed the following lipids: PC, PC O, LPC, PE, PE P, PI, SM, Cer, HexCer, CE, DG, and TG **(Figure 1A)**.

Mass Spectrometric Analysis of Lipids

The analysis of lipids was performed by direct flow injection analysis (FIA) using a triple quadrupole mass spectrometer (FIA-MS/MS; QQQ triple quadrupole) and a hybrid quadrupole-Orbitrap mass spectrometer (FIA-FTMS; high mass resolution).

FIA-MS/MS (QQQ) was performed in positive ion mode using the analytical setup and strategy described previously (21). A fragment ion of m/z 184 was used for lysophosphatidylcholine (LPC) (22). The following neutral losses were applied: Phosphatidylethanolamine (PE) 141, phosphatidylserine (PS) 185, phosphatidylglycerol (PG) 189 and phosphatidylinositol (PI) 277 (23). PE-based plasmalogens (PE P) were analyzed according to the principles described by Zemski-Berry (24). Sphingosine based ceramides (Cer) and hexosylceramides (HexCer) were analyzed using a fragment ion of m/z 264 (25). Quantification was achieved by calibration lines generated by addition of naturally occurring lipid species to the respective sample matrix. Calibration lines were generated for the following naturally occurring species: PC 34:1, 36:2, 38:4, 40:0 and PC O-16:0/20:4; SM 18:1;O2/16:0, 18:1, 18:0; LPC 16:0, 18:1, 18:0; PE 34:1, 36:2, 38:4, 40:6 and PE P-16:0/20:4; PS 34:1, 36:2, 38:4, 40:6; Cer 18:1;O2/16:0, 18:0, 20:0, 24:1, 24:0; FC, CE 16:0, 18:2, 18:1, 18:0.

The Fourier Transform Mass Spectrometry (FIA-FTMS) setup is described in detail in Höring et al. (26). Triglycerides (TG), diglycerides (DG) and cholesteryl ester (CE) were recorded in positive ion mode FTMS in range m/z 500–1,000 for 1 min with a maximum injection time (IT) of 200 ms, an automated gain control (AGC) of 1*106, three microscans and a target resolution of 140,000 (at m/z 200). Phosphatidylcholine (PC), sphingomyelin (SM) were measured in range m/z 520–960. Multiplexed acquisition (MSX) was used for, the [M+NH4]+ of free cholesterol (FC) (m/z 404.39) and D7-cholesterol (m/z 411.43) 0.5 min acquisition time, with a normalized collision energy of 10%, an IT of 100 ms, AGC of 1*105, isolation window of 1 Da, and a target resolution of 140,000 (27). Data processing details were described in Höring et al. (26) using the ALEX software (28) which includes peak assignment and intensity picking. The extracted data were exported to Microsoft Excel 2016 and further processed by self-programmed Macros. FIA-FTMS quantification was performed by multiplication of the spiked IS amount with analyte-to-IS ratio.

Lipid species were annotated according to the latest proposal for shorthand notation of lipid structures that are derived from mass spectrometry (29). For QQQ glycerophospholipid species annotation was based on the assumption of even numbered carbon chains only. SM species annotation is based on the assumption that a sphingoid base with two hydroxyl groups is present. Final quantities of lipid species and total lipid (sum of analysed lipid species) were calculated and expressed in nanomoles per milliliter of serum samples.

Statistics

All data are expressed as mean ± standard deviation (SD) from control ($n = 6$), acute TTS ($n = 4$), and subacute TTS ($n = 5$) groups. Two-way analysis of variance (ANOVA) was calculated using GraphPad Prism 9.1.0 (GraphPad Software, California, USA) and statistical comparisons between the groups were performed by Tukey's multiple comparisons Post-test using the same software. Graphs were prepared using the same GraphPad Prism 9.1.0 software. A p-value of 0.05 or lower was considered as significant. Significance is indicated as * $P \leq 0.05$, ** $P \leq 0.01$, *** $P \leq 0.001$, **** $P \leq 0.0001$.

Computational Methods

The Cytoscape v.3.7.1 software was used to search for the specific pathways and networks of analyzed lipids in humans (30). In particular, we implemented the search mode by lipid IDs. These were taken from the ChEBI (Chemical Entities of Biological Interest) server as a freely available dictionary of molecular entities focused on "small" chemical compounds various databases. Those including IMEx, UntAct, MINT, UniProt, BioGrid, iRefIndex, tfact2gene, bhf-ucl, HPIDd, mentha, EBI-GOA-nonIntAct, Reactome-FIs, MPIDB, MatrixBD, and MBIInfo and were screened to find relevant protein-lipid pathways associated with the proinflammatory cytokines, such as IL-6 and TNF-alpha (31).

RESULTS

Overview of the Quantitative Serum Lipidome

In this study, the serum lipid profiles of 262 individual lipid species and cholesterol were determined with lipidomics from serum samples in controls ($n = 6$), acute TTS ($n = 4$), and subacute TTS ($n = 5$). The 262 individual lipid species consists of 140 glycerophospholipids (28 PC, 14 PC O, 16 LPC, 25 PE, 39 PE P, and 18 PI), 44 sphingolipids (21 SM, 11 Cer, and 12 HexCer), 20 sterols (20 CE), and 58 glycerolipids (12 DG and 46 TG). An

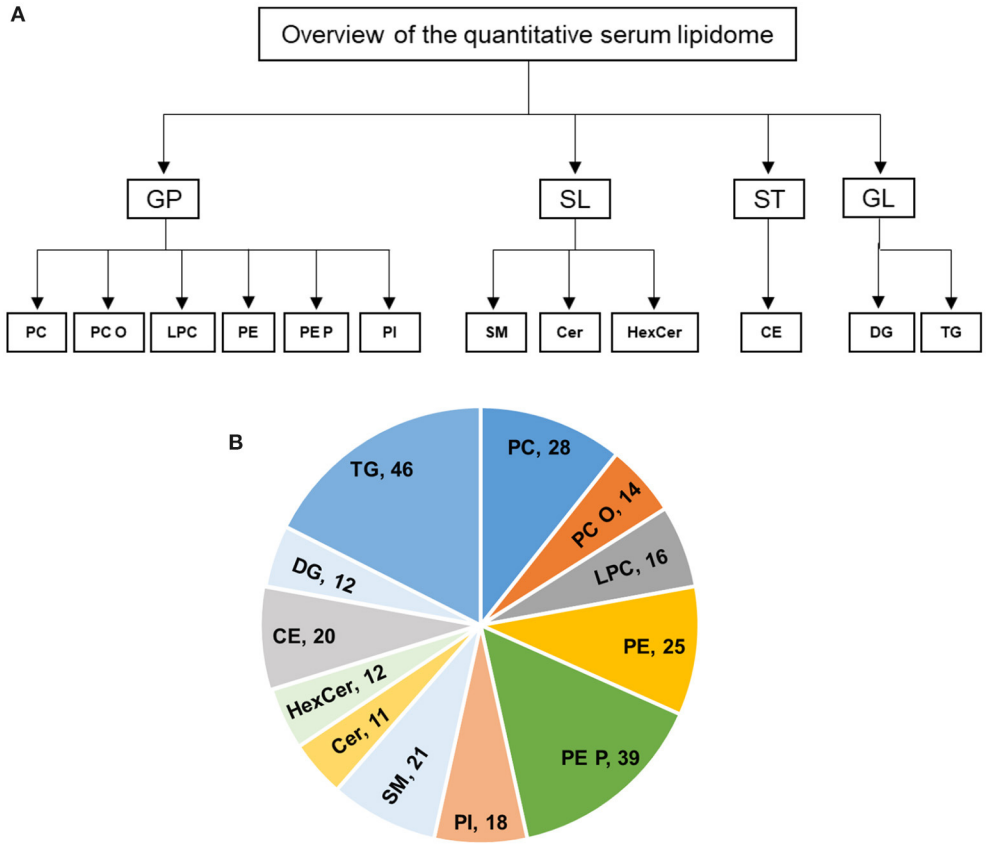

FIGURE 1 | (A,B) Overview of the quantitative lipidomic analyses of study groups by mass spectrometry. The numbers represent number of lipid species quantified for lipid class.

overview of the total lipid analysis of the study groups is shown in **Figures 1A,B**.

Individual Lipid Species Analysis Between Three Study Groups

The current study evaluated the individual lipid alterations in acute and subacute TTS patients and controls. Statistically significant differences in lipid compositions in the TTS patients were observed compared to the control group. These differences of individual lipid species were shown to be generally lower in acute TTS as compared to the control and subacute groups.

Glycerophospholipids Species

Phosphatidylcholine (PC). In total, 28 PC species with different chain length and degree of unsaturation were analyzed in the acute TTS, subacute TTS, and control groups. Their compositions (15 PC species) are represented in **Figure 2**.

The polyunsaturated specie PC 38:4 was slightly decreased in the acute TTS group, as compared to the control group ($P < 0.05$) **(Figure 2)**.

Ether-phosphatidylcholine (PC O). There was a statistical difference between the acute TTS and the subacute TTS in PC O-36:3 ($P < 0.01$), no significant difference was observed between all three groups in other PC O species ($P > 0.05$) **(Figure 3)**.

Lysophosphatidylcholine (LPC). Of the 16 total LPC species analyzed, 7 LPC species were showed in the **Figure 4**, only one was significantly different, and the remaining LPC species did not reveal any differences **(Figure 4)**. The LPC 18:1 showed slightly increased levels in the subacute TTS patients than those in the controls ($P < 0.05$).

Phosphatidylethanolamine (PE). We analyzed 25 individual lipid species of PE and 16 species compositions in all three groups is depicted in **Figure 5**. The most notably increased PE species were the long chain polyunsaturated species included PE 38:4 and PE 38:6. PE 38:4 and PE 36:4 significantly reduced in the acute TTS group in comparison to the controls ($P < 0.05$, $P < 0.05$, respectively). Remaining PE species did not represent any statistical difference in all groups.

Phosphatidylethanolamine based plasmalogens (PE P). The individual composition of 39 species of PE P were analyzed and 13 species were depicted in **Figure 6**. The PE P-18:0/18:1 and PE P-18:0/20:4 had a significantly decreased serum levels in the acute TTS patients compared to the control group. The PE P-18:0/22:6 showed a significant decreased in the subacute TTS patients compared to the control group.

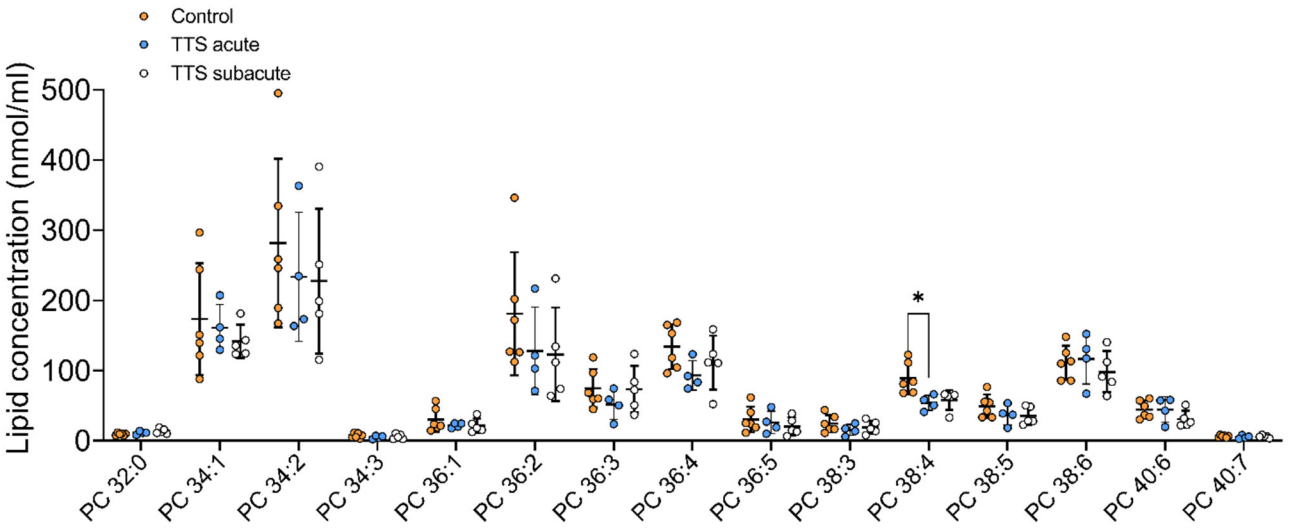

FIGURE 2 | Composition of individual phosphatidylcholine (PC) lipid species in the acute TTS, subacute TTS, and control groups. Values are represented as nmol/ml of serum. Values are mean ± SD, *P*-value: $^{*}P < 0.05$. Where significance is not mentioned, values are considered as being not significant. PC; Phosphatidylcholine, TTS, Takotsubo syndrome.

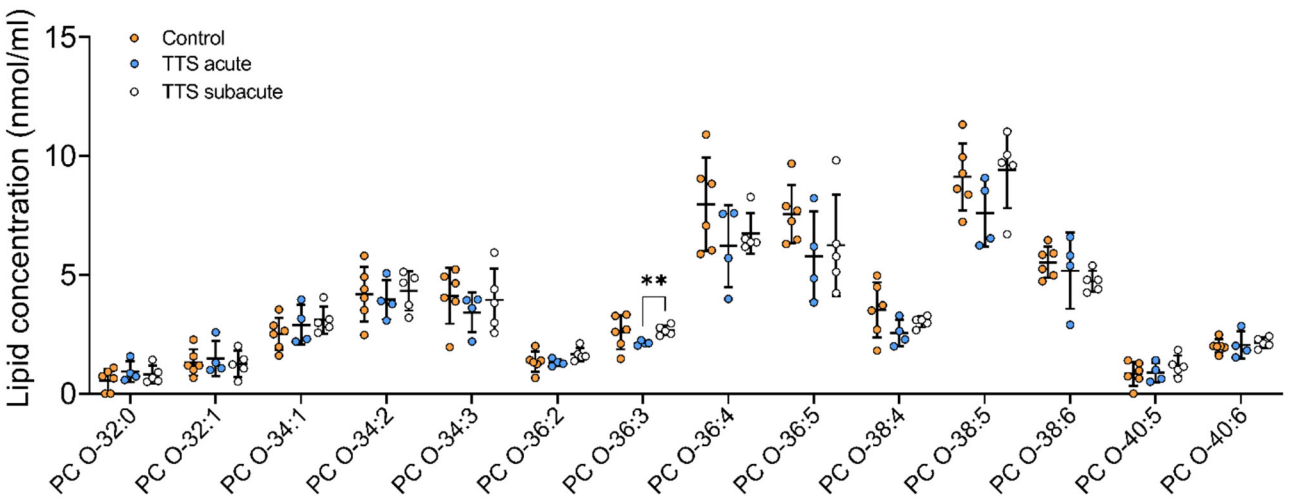

FIGURE 3 | Composition of individual PC O lipid species in the acute TTS, subacute TTS, and control groups. Values are represented as nmol/ml. Values are mean ± SD, *P*-value: $^{**}P < 0.01$. Where significance is not mentioned, values are considered as being not significant. PC O, Ether-phosphatidylcholine; TTS, Takotsubo syndrome.

Phosphatidylinositol (PI). We analyzed 18 individual lipid species of PI and 12 species composition is displayed in **Supplementary Figure 1**. PI lipid species did not indicate any statistical differences in all three groups.

Sphingolipid Species

Sphingomyelin (SM). In total, 21 different SM species were analyzed and 13 species in the three groups are shown in **Supplementary Figure 2**. There was no significant difference in SM species in all three groups.

Ceramide (Cer) and Hexosylceramide (HexCer). A total of 11 Cer and 12 HexCer species were analyzed, and their compositions are shown in **Supplementary Figure 3** and **Figure 7**, respectively. There was no significant difference in Cer species between all three groups.

HexCer 18:1; O2/23:0 was significant reduced in subacute TTS group when compared to the control group. Remaining species of HexCer did not show any statistically differences in the all three groups **(Figure 7)**.

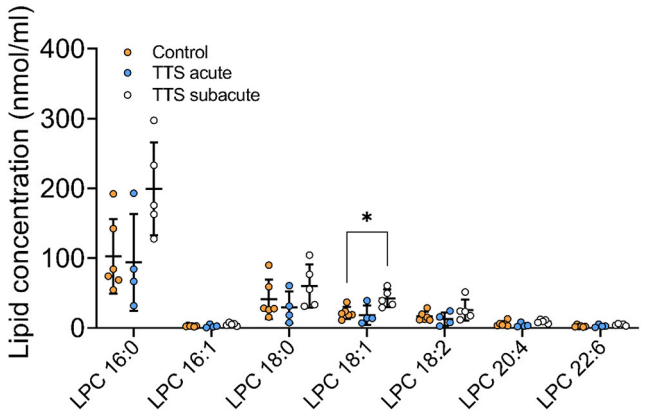

FIGURE 4 | Composition of individual LPC lipid species in the acute TTS, subacute TTS, and control groups. Values are represented as nmol/ml. Values are mean ± SD, *P*-value: $^*P < 0.05$. Where significance is not mentioned, values are considered as being not significant. LPC, Lysophosphatidylcholine; TTS, Takotsubo syndrome.

Sterol Species

Cholesteryl esters (CE). We analyzed 20 CE species along with their compositions **(Supplementary Figure 4)**. There was not observed any statistical difference in the CE species.

Glycerolipid Species

Diacylglycerol (DG) and Triacylglycerol (TG) species. Individual 12 DG were analyzed, and 8 species were displayed in **Figures 8** and 46 TG species were analyzed and 14 species compositions are depicted in **Supplementary Figure 5**.

DG 34:1 showed a slight decrease in the acute TTS group as compared to the subacute group. Interestingly, there was no significant difference between the acute TTS and control groups in DG species. There was not observed any statistical differences in the TG species between the all groups.

Computational Analysis

The Cytoscape algorithm was able to reconstitute a detailed molecular pathway linked to IL-6 and TNF-α for the two lipids (phosphatidylinositol and phosphatidylcholine) used in the study. Both lipids were present in the complete human protein-lipid network comprising 14,277 nodes and 37,778 edges **(Figure 9A)**. This network was processed to reduce the number of interacting nodes (1,272) and edges (2,545) by using the first directed (incoming and outgoing) neighbors of analyzed nodes **(Figure 9B)**. Finally, the two separate networks were produced for each lipid using the first directed and undirected neighbors of analyzed nodes **(Figures 9C,D)**. In particular, a detailed molecular pathway was only predicted for phosphatidylinositol indirectly linked to the proinflammatory cytokines through NF-kappa-B, such as phosphatidylinositol–PIK3R1–SIR2 like protein1–NF-kappa-B p65 subunit–IL6/TNF-α **(Figure 9C)**.

DISCUSSION

In the current study, we have analyzed serum lipidomic profiling of TTS patients and controls. The data obtained from these analyses demonstrate for the first time a distinct composition and quantity of serum lipids of TTS patients as compared to the controls. We analyzed 262 lipid species which consist of GP, SL, ST and GL species. We observed lower levels of individual lipid species other than lysoglycerophospholipids (LGPLs) in acute TTS compared to the control and subacute TTS groups. The LPCs were significantly elevated in the subacute TTS patients compared to the acute TTS and control group.

TTS is an acute cardiac syndrome with akinesia of the LV and apical ballooning (9, 12, 32). Although adrenergic overstimulation is associated with initiating TTS, the underlying pathophysiological mechanisms are not clearly understood. To better understand the disease mechanism of TTS, identification of molecular biomarkers has great importance. It has been suggested that akinetic/dyskinetic segments of the heart may decrease the lipid and glucose uptake and lead to metabolic perturbations in acute TTS (14, 33). Lipids are the essential structural components of cardiomyocyte plasma and organelle membranes and have critical roles in cellular functions, including energy storage and signal transduction (34). The metabolism of lipid is indicated in several human diseases such as CVD, respiratory disease, diabetes, and Alzheimer's disease (18, 35, 36). The normal heart regulates uptake and oxidation of fatty acids to sustain membrane biosynthesis and lipid signaling (37, 38). Since fats are the primary sources for cardiac energy, lipids have a critical role in the heart. Lipidomic profiling enables us to quantify the composition of individual lipids and molecular species that reveal metabolic variation in the structure. Although lipid alterations have been demonstrated in a limited number of studies in TTS (14, 39–41), the potential role of lipid metabolism in the pathology of TTS remains unclear. Therefore, lipidomics profiling could provide valuable information regarding the pathophysiology of TTS disease. Our work is the first comprehensive investigation into lipidome analysis using electrospray ionization-tandem mass spectrometry (ESI-MS/MS) in TTS patients.

The GPs are the main molecules for the backbone of cellular membranes and are involved in cellular signal transduction (42, 43). We analyzed composition ratio of 140 GPs and found that 8 GPs species were present significantly altered in serum from patients with TTS, including 1 PC, 1 PC O, 1 LPC, 2 PE, and 3 PE P. The long chain and polyunsaturated PC 38:4 was slightly decreased in the acute TTS group when compared to the control group **(Figure 2)**. Our results were compatible with the research of Shao et al. (14), which is one of the very limited published studies on TTS and GPs. In this research, they created a stress induced cardiomyopathy (SIC) model with isoprenaline injection in mice. Consistent with our results, they found low PC levels in the plasma of the mice and SIC patients. In addition, they detected severe lipid accumulation and downregulations of ApoB gene expression in the myocardium in ISO-treated mice and SIC patients which may explain these results. It is suggested that catecholamine-induced akinetic/dyskinetic segments of the

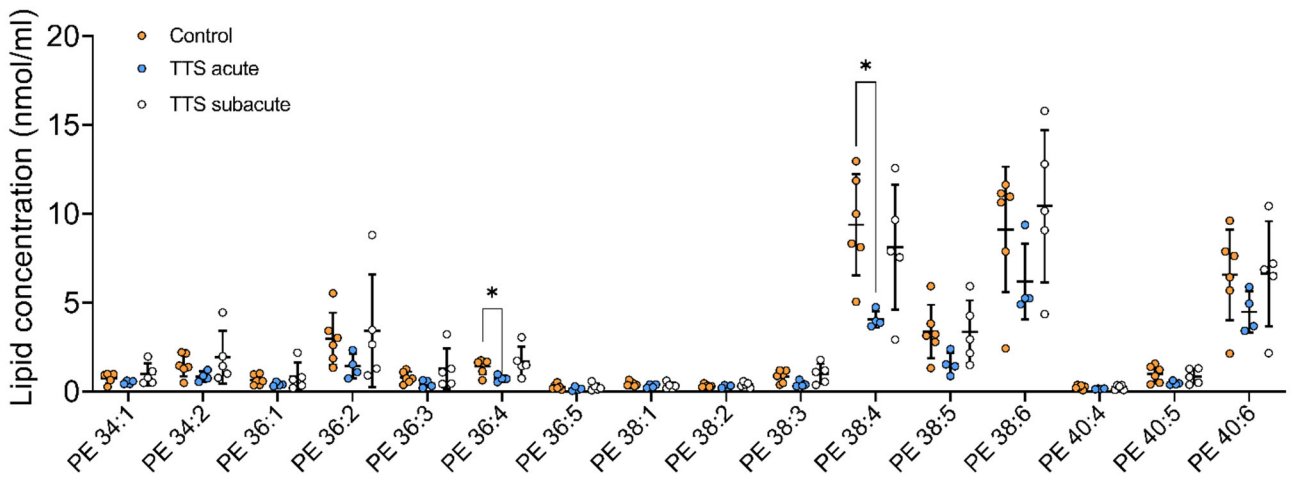

FIGURE 5 | Composition of individual PE lipid species in the acute TTS, subacute TTS, and control groups. Values are represented as nmol/ml. Values are mean ± SD, *P*-value: $^{*}P < 0.05$. Where significance is not mentioned, values are considered as being not significant. PE, Phosphatidylethanolamine; TTS, Takotsubo syndrome.

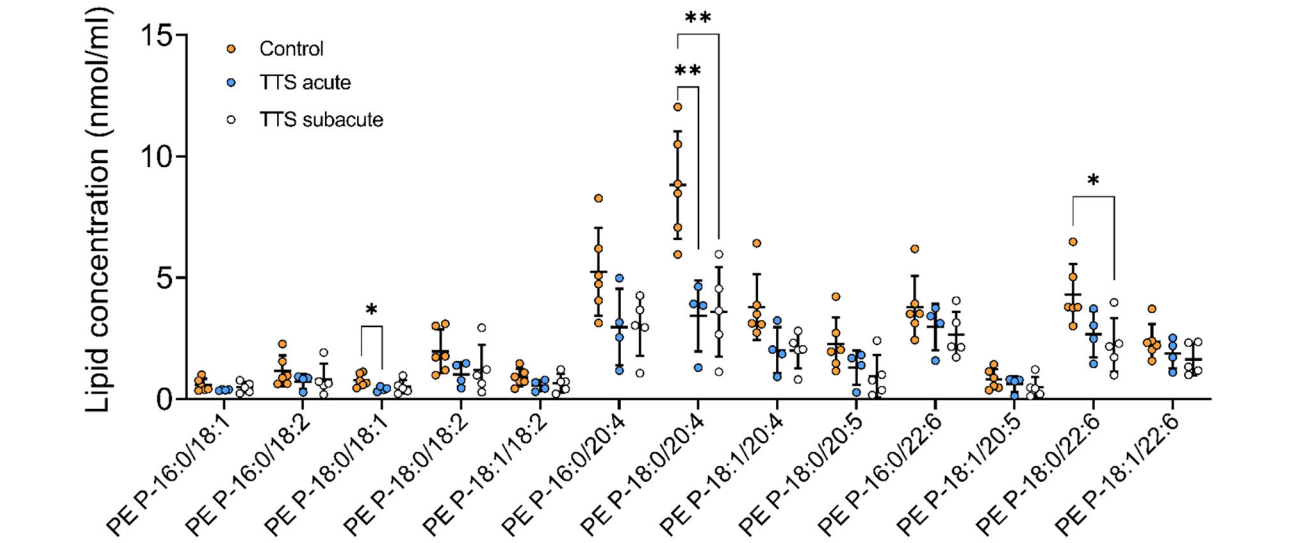

FIGURE 6 | Composition of individual PE P lipid species in the acute TTS, subacute TTS, and control groups. Values are represented as nmol/ml. Values are mean ± SD, *P*-value: $^{**}P < 0.01$, $^{*}P < 0.05$. Where significance is not mentioned, values are considered as being not significant. PE P, PE based plasmalogen; TTS, Takotsubo syndrome.

heart and impaired coronary blood flow reduced lipid uptake capacity during the acute phase of TTS (11, 13, 14, 41). It has been speculated that the increased myocardial lipid burden impairs efficient cardiac lipid export by ApoB, and therefore lower circulating lipid levels are seen in patients with TTS (14, 41). A further lipidomic study performed in the serum of dilated cardiomyopathy patients indicated significantly lower levels of TGs and PCs in line with our study (44). We detected statistically decrease in the PC 38:4, whereas Sysi-Aho and colleagues (44) found significant decrease in PC 38:2/38:5. These results showed that the number and species of altering GP species differs among different type of the disease. The functional importance and the role of altered differences and its mechanism should be clarified in further studies.

Lysoglycerophospholipids (LGPLs) are lacking one FA moiety in their structures. The main Lyso-GPLs are lysophosphatidylcholine (LPC), lysophosphatidic acid (LPA), lysophosphatidylinositol (LPI), and lysophosphatidylethanolamine (LPE) (18, 45). LGPLs have a similar effect to inflammatory lipids that modulates proliferation and apoptosis of endothelial cells in several diseases (18, 46, 47). In our study, we found that LPC 18:1 was significantly increased in the subacute TTS serum in comparison to the controls **(Figure 4)**. This result showed the opposite of our PC results.

The LPC is derived from PC, respectively in lipoproteins or from cell membranes *via* phospholipase A2 (18, 42). It is reported that LPC is elevated in inflammation-associated diseases and exerts its inflammatory effects *via* NF-kB, T-lymphocytes, monocytes, and neutrophils (47). Inflammation has been implicated as one of the various mechanisms involved in the pathogenesis of TTS (48). Active inflammation was displayed in human Post-mortem hearts and experimental models of TTS (9, 48). In our study, we found significantly higher levels of LPC in TTS patients that provide supportive evidence of inflammatory process in TTS.

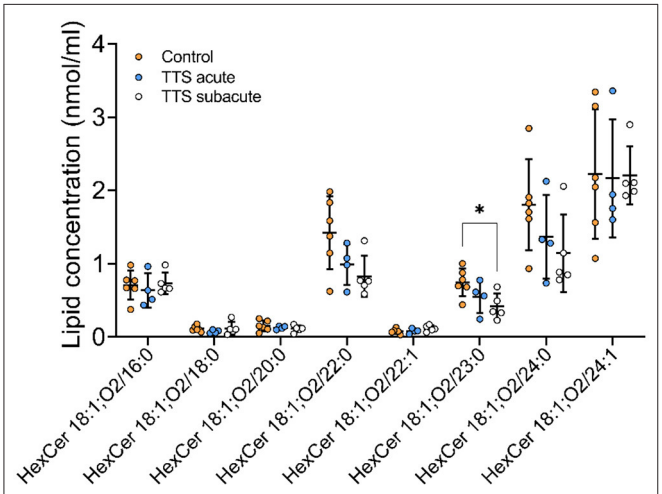

FIGURE 7 | Composition of individual HexCer lipid species in the acute TTS, subacute TTS, and control groups. Values are represented as nmol/ml. Values are mean ± SD, *P*-value: $^*P < 0.05$. Where significance is not mentioned, values are considered as being not significant. HexCer, Hexosylceramide; TTS, Takotsubo syndrome.

Lipid metabolism is essential for maintenance of normal function and structure of the heart (49). Indeed, the importance of cardiac lipid metabolism has been further emphasized by the recent publication in which we provide translational evidence that cardiac glycosphingolipids are required to maintain β-adrenergic signalling and contractile capacity in cardiomyocytes and to preserve normal heart function (50). It was found that LPC is important for normal function. LPC is a major phospholipid component in cell membranes accounting for 40% of total phospholipids in the heart tissue (34, 51, 52). Because of its amphiphilic property, LPC is readily incorporated into the lipid bilayers of the cell membrane, changing the physicochemical property of the cell membrane and thereby affecting the receptors, enzymes, and ion channels embedded in the membrane (53). LPC is also involved in the regulation of intracellular pH (54). Thus, we suggest that the disrupted lipid metabolism is very important risk for trigging TTS. However, we could not conclude the causality because the analysis in this study was cross-sectional manner.

Plasmalogens are a subclass of GPs that have a number of cellular functions, including neurochemical effects, cellular signaling, and functioning as scavengers in cellular membrane (55, 56). Deficiency of plasmalogens plays a role in cardiac failure, obesity, inflammation, and cancer (18, 56). In the current study, 3 PE-based plasmalogen (PE P) and 1 ether-phosphatidylcholine (PC O) significantly decreased in TTS in comparison to the controls. Membranes of myocardial cells, especially the sarcoplasmic reticulum, contain high amounts of PC and PE plasmalogens with arachidonic acid in the sn-2 position (56). In eicosanoid biosynthesis, plasmalogens act

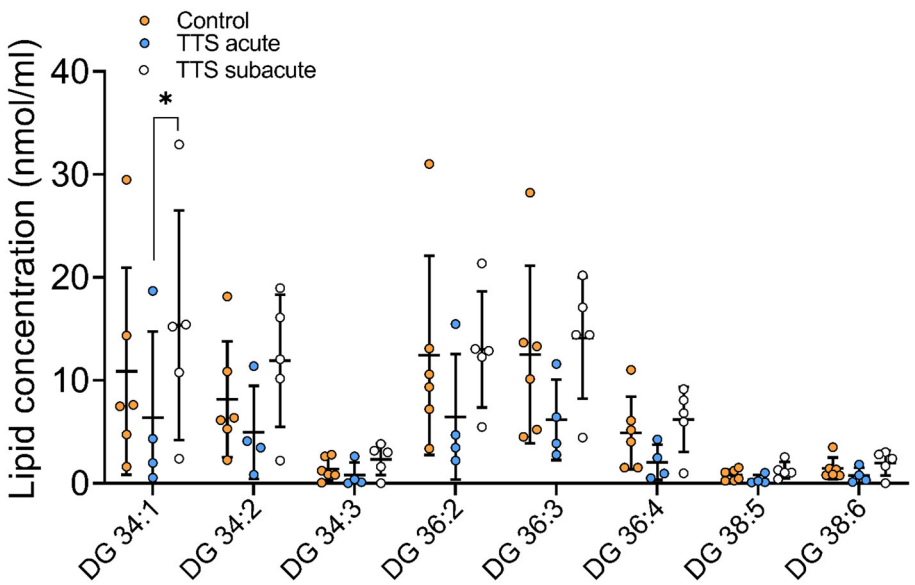

FIGURE 8 | Composition of individual DG lipid species in the acute TTS, subacute TTS, and control groups. Values are represented as nmol/ml. Values are mean ± SD, *P*-value: $^*P < 0.05$. Where significance is not mentioned, values are considered as being not significant. DG, Diacylglycerol; TTS, Takotsubo syndrome.

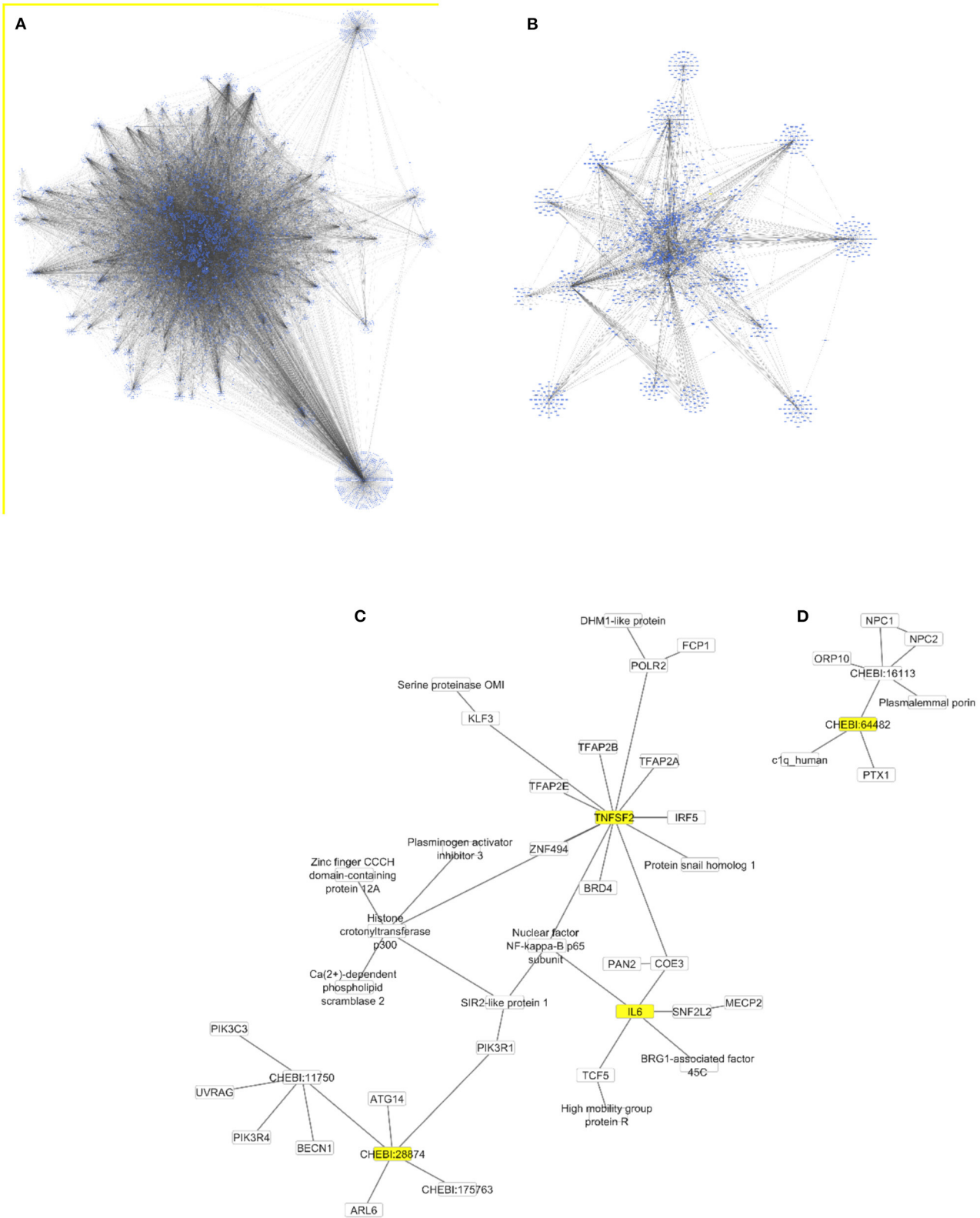

FIGURE 9 | Protein-lipid networks linked to the proinflammatory cytokines [IL6 and TNF-α (TNFSF2)] as complete **(A)**, using the first directed **(B)** and undirected **(C,D)** neighbors to phosphatidylinositol (CHEBI:28874) and phosphatidylcholine (CHEBI:64482) as nodes colored in yellow. All networks are displayed using the yFiles organic layout.

as a reservoir for PUFAs as they contain arachidonic (20:4), docosapentaenoic (22:5n−6) and docosahexanoic (DHA-22:6) acids in the sn-2 position (32, 34). In our study, we detected PE P-18:0/18:1, PE P-18:0/20:4, and PE P-18:0/22:6 species, which enriched with arachidonic acid, were significantly decreased in acute TTS and subacute TTS patients as compared to the control group. We think that the antioxidant properties of plasmalogens may have led to these results. It is reported that overstimulation of adrenoceptors leads to myocellular hypoxia in TTS (7, 14). In addition to decreased coronary flow in TTS, accumulation of lipid droplets in cardiomyocytes may lead to lipid oxidation in the myocardium. These metabolic alterations can cause oxidative changes in membrane phospholipids and disrupt the integrity of cell membranes (57). As expected under such oxidative conditions plasmalogens are decreased and functioning as an antioxidant.

As far as we know, the relationship between TTS and plasmalogen has not been evaluated. On the other hand, similar to our results, studies in coronary stenosis patients (56), and hypertensive patients showed decreased plasma ether lipids in serum. Pietilainen et al. reported that increased levels of LPCs, and decreased level in ether phospholipids suggested a link between plasmalogens and oxidative stress in human obesity (58). Based on the above results and the literature, our study supports the view that inflammation may play a role in TTS, which was also demonstrated by Wilson et al. (48).

We detected 44 sphingolipids (SLs) in serum samples and observed that 6 of them indicated statistical differences in TTS patients when compared to the controls. Perturbation in SLs plasma and tissue levels have been shown to increase the risk of cardiovascular disease (59, 60). It is reported that circulating Cer 18:1; O2/24:1, and Cer 18:1; O2/24:0 are associated with the risk of the incidence of major adverse cardiovascular events in healthy people (61). In the context of cardiomyopathy, increased ceramide levels or changes in ceramide compositions have been suggested to be toxic (62). The increased levels of SM and Cer were displayed in different type of cardiomyopathies (59, 62). To date, no sphingolipids studies have been associated with TTS in patient's serum. Our study performed from serum of TTS patients and the controls and in contrast to above studies, we detected a reduced level of HexCer in patients of TTS. First, these alterations could be due to the differences between different cardiac diseases. Second, research showed that impaired myocardial perfusion and overexpression of catecholamine can disturb myocardial lipid metabolism (14, 41). It was suggested that suppression of myocardial ApoB expression may prevent the export of the accumulated lipids and lead to a reduction of circulating lipids. More lipidomic studies are needed to understand the roles of sphingolipids in TTS.

We also analyzed 78 types of CE, DG, and TG species. Neutral lipids characterize a group of hydrophobic molecules and include TGs, DGs, cholesterol and its esters in mammals (18, 63). CEs, TGs and DGs are thought to be involved in several diseases including cardiovascular diseases, ischemic stroke, hypertension and dyslipidemia (18). In the current study, the extended chain and monounsaturated DG lipid specie was remarkably reduced in the acute TTS patients in comparison to the subacute TTS patients. Long-chain fatty acid (LCFA) is the main sources of cardiomyocytes. TGs are hydrolyzed by adipose triglyceride lipase and released LCFAs which are oxidized in mitochondria to produce ATPs for cardiac energy (64). LCFAs are released on demand and delivered to the heart *via* the circulation and paracrine and used as energy substrates (64). In normal circumstances, the stress-induced increase in cardiac energy demand can be compensated from hydrolyzing TGs. In contrast, in TTS patients, excessive catecholamine-mediated myocardial segmental akinesia reduces lipid uptake and leads to lipid accumulation in the heart (9, 14, 64). Further studies are required to investigate the meaning of alterations in the composition of these individual lipid species.

Our study provides a comprehensive quantitative lipidome analysis which may play an important role in the pathogenesis and management of TTS. Moreover, the reported use of computational methods allowed for a reconstitution of a detailed molecular pathway linking IL-6 and TNF-α for the two lipids (phosphatidylinositol and phosphatidylcholine). Besides lipidomic profiling in TTS, uncovering an intriguing diversity of targetable mechanisms can be exploited to prevent primary or recurrent TTS in the future. Inflammation and lipid signaling are intertwined modulators of homeostasis and immunity. Emerging studies indicate that in addition to the extensively studied eicosanoids and inositol phospholipids, many other lipid species act positively and negatively regulate inflammatory responses (65). Our computational analyses of the lipidomic profile in TTS points to a molecular pathway linked to IL-6 and TNF-α, the pro-inflammatory cytokines characteristically elevated in TTS patients (15) for the two lipids (phosphatidylinositol and phosphatidylcholine). This mechanism largely depends on the phosphatidylinositol 3-kinase regulatory subunit alpha (PIK3R1), which was previously observed mediating TNF-induced NF-kappa-B activation (66). In turn, IL-6 could induce phosphatidylinositol 3-kinase and nitric oxide-dependent protection and preserves mitochondrial function in cardiomyocytes (67). On the other hand, the long-term IL6 signaling or an over-production of IL6R protein could potentially lead to cardiovascular diseases followed by heart failure (68).

Takotsubo cardiomyopathy has already cardiac biomarkers, such as the NT-proBNP (N-terminal B-type natriuretic peptide)/myoglobin and NT-proBNP/troponin T ratios for the diagnosis of acute coronary syndromes and stress-induced cardiomyopathy (61). Based on the computational analysis of the TTS lipidomic profiles, the identified lipids can be connected to the atrial natriuretic factor *via* phosphatidylinositol- and phosphatidylcholine-dependent phospholipases C (62). Moreover, the natriuretic peptide-C receptor was also determined to induce the attenuation of adenylyl cyclase signaling, which activates the phosphatidylinositol turnover in vascular smooth muscle cells (63). However, further investigation is needed to clarify the effect of the TTS lipidomic profiles on the NT-proBNP/myoglobin and NT-proBNP/troponin T concentrations in order to develop novel lipid-dependent biomarker ratios for TTS.

LIMITATIONS OF STUDY

Our study revealed that lipidomic profiling in TTS patients was significantly different from controls. Further research is required to elucidate the significance of altered lipid compositions and quantity in acute TTS and subacute TTS in relation to ACS.

CONCLUSION

Our study revealed a detailed overview of lipid classes and absolute quantitative information on the individual lipid species and their distribution pattern from the blood of TTS patients using high-throughput tandem mass spectrometry. Our investigation links lipid and inflammation biology; the computational pathway and network analyses draw attention to an intriguing diversity of targetable mechanisms potentially relevant to prevent primary or recurrent TTS in the future.

DATA AVAILABILITY STATEMENT

The original contributions presented in the study are included in the article/**Supplementary Material**, further inquiries can be directed to the corresponding authors.

ETHICS STATEMENT

The studies involving human participants were reviewed and approved by Hiroshima City Asa Hospital Research Committee (01-3-3), Hiroshima, Japan. The patients/participants provided their written informed consent to participate in this study.

AUTHOR CONTRIBUTIONS

SK, RR, and DK: data analysis and visualization. SK, GG, RR, and CYF: writing–review and editing draft. SS and CYF: computational analyses. MH and GL: lipid analysis. MN and SE: sample collection and validation. SK: supervision. SK and CYF: designed and conducted. All authors read the study and approved the manuscript for publication.

FUNDING

We are grateful to Stiftung Forschung hilft and DFG 515/5-1 for the research grant to CYF.

ACKNOWLEDGMENTS

We thank Dr. A. Brack University of Würzburg, Department of Anaesthesiology, Intensive Care, Emergency and Pain Medicine, Würzburg, Germany for patient blood sampling, and Elisabeth Wilken for excellent technical assistance. Special thanks are extended to Mr. Todd Axel Johnsen from the Infochemistry Scientific Centre, ITMO University for his assistance in editing and proofreading the manuscript.

SUPPLEMENTARY MATERIAL

The Supplementary Material for this article can be found online at: https://www.frontiersin.org/articles/10.3389/fcvm.2022.797154/full#supplementary-material

REFERENCES

1. Akashi YJ, Nef HM, Lyon AR. Epidemiology and pathophysiology of Takotsubo syndrome. *Nat Rev Cardiol.* (2015) 12:387–97. doi: 10.1038/nrcardio.2015.39
2. Nagai M, Forster CY, Dote K. Right insular cortex atrophy in Takotsubo syndrome: a possible pathogenesis of increased sympathetic nervous system activity? *Clin Res Cardiol.* (2021) 110:601–2. doi: 10.1007/s00392-020-01665-2
3. Nagai M, Kobayashi Y, Kobatake H, Dote K, Kato M, Oda N, et al. Happy heart syndrome: a case of Takotsubo syndrome with left internal carotid artery occlusion. *Clin Auton Res.* (2020) 30:347–50. doi: 10.1007/s10286-020-00696-z
4. Osawa A, Nagai M, Dote K, Kato M, Oda N, Kunita E, et al. A mid-ventricular variant of Takotsubo syndrome: was it triggered by insular cortex damage? *ESC Heart Fail.* (2021) 8:3408–12. doi: 10.1002/ehf2.13397
5. Redfors B, Shao Y, Omerovic E. Stress-induced cardiomyopathy (Takotsubo)–broken heart and mind? *Vasc Health Risk Manag.* (2013) 9:149–54. doi: 10.2147/VHRM.S40163
6. Yoshikawa T. Takotsubo cardiomyopathy, a new concept of cardiomyopathy: clinical features and pathophysiology. *Int J Cardiol.* (2015) 182:297–303. doi: 10.1016/j.ijcard.2014.12.116
7. Pelliccia F, Kaski JC, Crea F, Camici PG. Pathophysiology of Takotsubo Syndrome. *Circulation.* (2017) 135:2426–41. doi: 10.1161/CIRCULATIONAHA.116.027121
8. Redfors B, Vedad R, Angeras O, Ramunddal T, Petursson P, Haraldsson I, et al. Mortality in takotsubo syndrome is similar to mortality in myocardial infarction - a report from the SWEDEHEART registry. *Int J Cardiol.* (2015) 185:282–9. doi: 10.1016/j.ijcard.2015.03.162
9. Oras J, Redfors B, Ali A, Lundgren J, Sihlbom C, Thorsell A, et al. Anaesthetic-induced cardioprotection in an experimental model of the Takotsubo syndrome - isoflurane vs. propofol. *Acta Anaesthesiol Scand.* (2017) 61:309–21. doi: 10.1111/aas.12857
10. S YH, Tornvall P. Epidemiology, pathogenesis, and management of takotsubo syndrome. *Clin Auton Res.* (2018) 28:53–65. doi: 10.1007/s10286-017-0465-z
11. Ancona F, Bertoldi LF, Ruggieri F, Cerri M, Magnoni M, Beretta L, et al. Takotsubo cardiomyopathy and neurogenic stunned myocardium: similar albeit different. *Eur Heart J.* (2016) 37:2830–2. doi: 10.1093/eurheartj/ehw035
12. Paur H, Wright PT, Sikkel MB, Tranter MH, Mansfield C, O'Gara P, et al. High levels of circulating epinephrine trigger apical cardiodepression in a beta2-adrenergic receptor/Gi-dependent manner: a new model of Takotsubo cardiomyopathy. *Circulation.* (2012) 126:697–706. doi: 10.1161/CIRCULATIONAHA.112.111591
13. Feola M, Chauvie S, Rosso GL, Biggi A, Ribichini F, Bobbio M. Reversible impairment of coronary flow reserve in takotsubo cardiomyopathy: a myocardial PET study. *J Nucl Cardiol.* (2008) 15:811–7. doi: 10.1007/BF03007363
14. Shao Y, Redfors B, Stahlman M, Tang MS, Miljanovic A, Mollmann H, et al. A mouse model reveals an important role for catecholamine-induced lipotoxicity in the pathogenesis of stress-induced cardiomyopathy. *Eur J Heart Fail.* (2013) 15:9–22. doi: 10.1093/eurjhf/hfs161
15. Ittner C, Burek M, Stork S, Nagai M, Forster CY. Increased catecholamine levels and inflammatory mediators alter barrier properties of brain microvascular endothelial cells *in vitro*. *Front Cardiovasc Med.* (2020) 7:73. doi: 10.3389/fcvm.2020.00073
16. Jocken JW, Blaak EE. Catecholamine-induced lipolysis in adipose tissue and skeletal muscle in obesity. *Physiol Behav.* (2008) 94:219–30. doi: 10.1016/j.physbeh.2008.01.002

17. Zhao YY, Cheng XL, Lin RC. Lipidomics applications for discovering biomarkers of diseases in clinical chemistry. *Int Rev Cell Mol Biol.* (2014) 313:1–26. doi: 10.1016/B978-0-12-800177-6.00001-3
18. Wang R, Li B, Lam SM, Shui G. Integration of lipidomics and metabolomics for in-depth understanding of cellular mechanism and disease progression. *J Genet Genomics.* (2020) 47:69–83. doi: 10.1016/j.jgg.2019.11.009
19. Ghadri JR, Wittstein IS, Prasad A, Sharkey S, Dote K, Akashi YJ, et al. International expert consensus document on Takotsubo syndrome (Part I): clinical characteristics, diagnostic criteria, and pathophysiology. *Eur Heart J.* (2018) 39:2032–46. doi: 10.1093/eurheartj/ehy076
20. Bligh EG, Dyer WJ. A rapid method of total lipid extraction and purification. *Can J Biochem Physiol.* (1959) 37:911–7. doi: 10.1139/o59-099
21. Liebisch G, Lieser B, Rathenberg J, Drobnik W, Schmitz G. High-throughput quantification of phosphatidylcholine and sphingomyelin by electrospray ionization tandem mass spectrometry coupled with isotope correction algorithm. *Biochim Biophys Acta.* (2004) 1686:108–17. doi: 10.1016/j.bbalip.2004.09.003
22. Liebisch G, Drobnik W, Lieser B, Schmitz G. High-throughput quantification of lysophosphatidylcholine by electrospray ionization tandem mass spectrometry. *Clin Chem.* (2002) 48:2217–24. doi: 10.1093/clinchem/48.12.2217
23. Matyash V, Liebisch G, Kurzchalia TV, Shevchenko A, Schwudke D. Lipid extraction by methyl-tert-butyl ether for high-throughput lipidomics. *J Lipid Res.* (2008) 49:1137–46. doi: 10.1194/jlr.D700041-JLR200
24. Zemski Berry KA, Murphy RC. Electrospray ionization tandem mass spectrometry of glycerophosphoethanolamine plasmalogen phospholipids. *J Am Soc Mass Spectrom.* (2004) 15:1499–508. doi: 10.1016/j.jasms.2004.07.009
25. Liebisch G, Drobnik W, Reil M, Trumbach B, Arnecke R, Olgemoller B, et al. Quantitative measurement of different ceramide species from crude cellular extracts by electrospray ionization tandem mass spectrometry (ESI-MS/MS). *J Lipid Res.* (1999) 40:1539–46. doi: 10.1016/S0022-2275(20)33398-8
26. Horing M, Ejsing CS, Krautbauer S, Ertl VM, Burkhardt R, Liebisch G. Accurate quantification of lipid species affected by isobaric overlap in Fourier-transform mass spectrometry. *J Lipid Res.* (2021) 62:100050. doi: 10.1016/j.jlr.2021.100050
27. Horing M, Ejsing CS, Hermansson M, Liebisch G. Quantification of cholesterol and cholesteryl ester by direct flow injection high-resolution fourier transform mass spectrometry utilizing species-specific response factors. *Anal Chem.* (2019) 91:3459–66. doi: 10.1021/acs.analchem.8b05013
28. Husen P, Tarasov K, Katafiasz M, Sokol E, Vogt J, Baumgart J, et al. Analysis of lipid experiments (ALEX): a software framework for analysis of high-resolution shotgun lipidomics data. *PLoS One.* (2013) 8:e79736. doi: 10.1371/journal.pone.0079736
29. Liebisch G, Fahy E, Aoki J, Dennis EA, Durand T, Ejsing CS, et al. Update on LIPID MAPS classification, nomenclature, and shorthand notation for MS-derived lipid structures. *J Lipid Res.* (2020) 61:1539–55. doi: 10.1194/jlr.S120001025
30. Shannon P, Markiel A, Ozier O, Baliga NS, Wang JT, Ramage D, et al. Cytoscape: a software environment for integrated models of biomolecular interaction networks. *Genome Res.* (2003) 13:2498–504. doi: 10.1101/gr.1239303
31. Degtyarenko K, Hastings J, de Matos P, Ennis M. ChEBI: an open bioinformatics and cheminformatics resource. *Curr Protoc Bioinformatics.* (2009). doi: 10.1002/0471250953.bi1409s26
32. Scally C, Abbas H, Ahearn T, Srinivasan J, Mezincescu A, Rudd A, et al. Myocardial and systemic inflammation in acute stress-induced (Takotsubo) cardiomyopathy. *Circulation.* (2019) 139:1581–92. doi: 10.1161/CIRCULATIONAHA.118.037975
33. Kurowski V, Kaiser A, von Hof K, Killermann DP, Mayer B, Hartmann F, et al. Apical and midventricular transient left ventricular dysfunction syndrome (tako-tsubo cardiomyopathy): frequency, mechanisms, and prognosis. *Chest.* (2007) 132:809–16. doi: 10.1378/chest.07-0608
34. Tomczyk MM, Dolinsky VW. The cardiac lipidome in models of cardiovascular disease. *Metabolites.* (2020) 10:254. doi: 10.3390/metabo10060254
35. Lam SM, Wang Z, Li J, Huang X, Shui G. Sequestration of polyunsaturated fatty acids in membrane phospholipids of Caenorhabditis elegans dauer larva attenuates eicosanoid biosynthesis for prolonged survival. *Redox Biol.* (2017) 12:967–77. doi: 10.1016/j.redox.2017.05.002
36. Wang S, Tang K, Lu Y, Tian Z, Huang Z, Wang M, et al. Revealing the role of glycerophospholipid metabolism in asthma through plasma lipidomics. *Clin Chim Acta.* (2021) 513:34–42. doi: 10.1016/j.cca.2020.11.026
37. Dong S, Zhang R, Liang Y, Shi J, Li J, Shang F, et al. Changes of myocardial lipidomics profiling in a rat model of diabetic cardiomyopathy using UPLC/Q-TOF/MS analysis. *Diabetol Metab Syndr.* (2017) 9:56. doi: 10.1186/s13098-017-0249-6
38. Ma Y, Li J. Metabolic shifts during aging and pathology. *Compr Physiol.* (2015) 5:667–86. doi: 10.1002/cphy.c140041
39. Gaddam S, Nimmagadda KC, Nagrani T, Naqi M, Wetz RV, Weiserbs KF, et al. Serum lipoprotein levels in takotsubo cardiomyopathy vs. myocardial infarction. *Int Arch Med.* (2011) 4:14. doi: 10.1186/1755-7682-4-14
40. Ibrahim T, Nekolla SG, Langwieser N, Rischpler C, Groha P, Laugwitz KL, et al. Simultaneous positron emission tomography/magnetic resonance imaging identifies sustained regional abnormalities in cardiac metabolism and function in stress-induced transient midventricular ballooning syndrome: a variant of Takotsubo cardiomyopathy. *Circulation.* (2012) 126:e324–6. doi: 10.1161/CIRCULATIONAHA.112.134346
41. Kurisu S, Inoue I, Kawagoe T, Ishihara M, Shimatani Y, Nishioka K, et al. Myocardial perfusion and fatty acid metabolism in patients with tako-tsubo-like left ventricular dysfunction. *J Am Coll Cardiol.* (2003) 41:743–8. doi: 10.1016/S0735-1097(02)02924-8
42. Han X. Lipidomics for studying metabolism. *Nat Rev Endocrinol.* (2016) 12:668–79. doi: 10.1038/nrendo.2016.98
43. Yan F, Wen Z, Wang R, Luo W, Du Y, Wang W, et al. Identification of the lipid biomarkers from plasma in idiopathic pulmonary fibrosis by Lipidomics. *BMC Pulm Med.* (2017) 17:174. doi: 10.1186/s12890-017-0513-4
44. Sysi-Aho M, Koikkalainen J, Seppanen-Laakso T, Kaartinen M, Kuusisto J, Peuhkurinen K, et al. Serum lipidomics meets cardiac magnetic resonance imaging: profiling of subjects at risk of dilated cardiomyopathy. *PLoS One.* (2011) 6:e15744. doi: 10.1371/journal.pone.0015744
45. Uphoff A, Hermansson M, Haimi P, Somerharju P. Analysis of complex lipidomes. *Med Appl Mass Spect.* (2008) 223–49. doi: 10.1016/B978-044451980-1.50013-6
46. Shi Q, Jin S, Xiang X, Tian J, Huang R, Li S, et al. The metabolic change in serum lysoglycerophospholipids intervened by triterpenoid saponins from Kuding tea on hyperlipidemic mice. *Food Funct.* (2019) 10:7782–92. doi: 10.1039/C9FO02142F
47. Zeng C, Wen B, Hou G, Lei L, Mei Z, Jia X, et al. Lipidomics profiling reveals the role of glycerophospholipid metabolism in psoriasis. *Gigascience.* (2017) 6:1–11. doi: 10.1093/gigascience/gix087
48. Wilson HM, Cheyne L, Brown PAJ, Kerr K, Hannah A, Srinivasan J, et al. Characterization of the myocardial inflammatory response in acute stress-induced (Takotsubo) cardiomyopathy. *JACC Basic Transl Sci.* (2018) 3:766–78. doi: 10.1016/j.jacbts.2018.08.006
49. Schulze PC, Drosatos K, Goldberg IJ. Lipid use and misuse by the heart. *Circ Res.* (2016) 118:1736–51. doi: 10.1161/CIRCRESAHA.116.306842
50. Andersson L, Cinato M, Mardani I, Miljanovic A, Arif M, Koh A, et al. Glucosylceramide synthase deficiency in the heart compromises beta1-adrenergic receptor trafficking. *Eur Heart J.* (2021) 42:4481–92. doi: 10.1093/eurheartj/ehab412
51. Law SH, Chan ML, Marathe GK, Parveen F, Chen CH, Ke LY. An updated review of lysophosphatidylcholine metabolism in human diseases. *Int J Mol Sci.* (2019) 20:1149. doi: 10.3390/ijms20051149
52. Pradas I, Huynh K, Cabre R, Ayala V, Meikle PJ, Jove M, et al. Lipidomics reveals a tissue-specific fingerprint. *Front Physiol.* (2018) 9:1165. doi: 10.3389/fphys.2018.01165
53. Hashizume H, Chen M, Ma H, Hoque N, Hara A, Yazawa K, et al. Lysophosphatidylcholine: a possible modulator of ischemic injury in the heart. In: Abiko Y, Karmazyn M, editors. *Protection Against Ischemia/Reperfusion Damage of the Heart*. Tokyo: Springer Japan (1998). p. 75–87. doi: 10.1007/978-4-431-68482-4_6
54. Yamaguchi S, Tamagawa M, Nakajima N, Nakaya H. Selective impairment of HCO3—dependent pHi regulation by lysophosphatidylcholine

in guinea pig ventricular myocardium. *Cardiovasc Res.* (1998) 37:179–86. doi: 10.1016/S0008-6363(97)00203-4
55. Karnati S, Garikapati V, Liebisch G, van Veldhoven PP, Spengler B, Schmitz G, et al. Quantitative lipidomic analysis of mouse lung during postnatal development by electrospray ionization tandem mass spectrometry. *PLoS One.* (2018) 13:e0203464. doi: 10.1371/journal.pone.0203464
56. Wallner S, Schmitz G. Plasmalogens the neglected regulatory and scavenging lipid species. *Chem Phys Lipids.* (2011) 164:573–89. doi: 10.1016/j.chemphyslip.2011.06.008
57. Brites P, Waterham HR, Wanders RJ. Functions and biosynthesis of plasmalogens in health and disease. *Biochim Biophys Acta.* (2004) 1636:219–31. doi: 10.1016/j.bbalip.2003.12.010
58. Pietilainen KH, Sysi-Aho M, Rissanen A, Seppanen-Laakso T, Yki-Jarvinen H, Kaprio J, et al. Acquired obesity is associated with changes in the serum lipidomic profile independent of genetic effects–a monozygotic twin study. *PLoS One.* (2007) 2:e218. doi: 10.1371/journal.pone.0000218
59. Hannun YA, Obeid LM. Sphingolipids and their metabolism in physiology and disease. *Nat Rev Mol Cell Biol.* (2018) 19:175–91. doi: 10.1038/nrm.2017.107
60. Tham YK, Bernardo BC, Huynh K, Ooi JYY, Gao XM, Kiriazis H, et al. Lipidomic profiles of the heart and circulation in response to exercise versus cardiac pathology: a resource of potential biomarkers and drug targets. *Cell Rep.* (2018) 24:2757–72. doi: 10.1016/j.celrep.2018.08.017
61. Havulinna AS, Sysi-Aho M, Hilvo M, Kauhanen D, Hurme R, Ekroos K, et al. Circulating ceramides predict cardiovascular outcomes in the population-based FINRISK 2002 Cohort. *Arterioscler Thromb Vasc Biol.* (2016) 36:2424–30. doi: 10.1161/ATVBAHA.116.307497
62. Kovilakath A, Cowart LA. Sphingolipid mediators of myocardial pathology. *J Lipid Atheroscler.* (2020) 9:23–49. doi: 10.12997/jla.2020.9.1.23
63. Quehenberger O, Armando AM, Brown AH, Milne SB, Myers DS, Merrill AH, et al. Lipidomics reveals a remarkable diversity of lipids in human plasma. *J Lipid Res.* (2010) 51:3299–305. doi: 10.1194/jlr.M009449
64. Hirano K-i, Shimizu K, Ikeda Y, Shirakami Y, Nagasaka H. Energy failure hypothesis for Takotsubo cardiomyopathy. *Ann Nucl Cardiol.* (2017) 3:105–9. doi: 10.17996/anc.17-00003
65. Weber C, Noels H. Atherosclerosis: current pathogenesis and therapeutic options. *Nat Med.* (2011) 17:1410–22. doi: 10.1038/nm.2538
66. Reddy SA, Huang JH, Liao WS. Phosphatidylinositol 3-kinase as a mediator of TNF-induced NF-kappa B activation. *J Immunol.* (2000) 164:1355–63. doi: 10.4049/jimmunol.164.3.1355
67. Smart N, Mojet MH, Latchman DS, Marber MS, Duchen MR, Heads RJ. IL-6 induces PI 3-kinase and nitric oxide-dependent protection and preserves mitochondrial function in cardiomyocytes. *Cardiovasc Res.* (2006) 69:164–77. doi: 10.1016/j.cardiores.2005.08.017
68. Fontes JA, Rose NR, Cihakova D. The varying faces of IL-6: From cardiac protection to cardiac failure. *Cytokine.* (2015) 74:62–8. doi: 10.1016/j.cyto.2014.12.024

Conflict of Interest: The authors declare that the research was conducted in the absence of any commercial or financial relationships that could be construed as a potential conflict of interest.

Publisher's Note: All claims expressed in this article are solely those of the authors and do not necessarily represent those of their affiliated organizations, or those of the publisher, the editors and the reviewers. Any product that may be evaluated in this article, or claim that may be made by its manufacturer, is not guaranteed or endorsed by the publisher.

Copyright © 2022 Karnati, Guntas, Rajendran, Shityakov, Höring, Liebisch, Kosanovic, Ergün, Nagai and Förster. This is an open-access article distributed under the terms of the Creative Commons Attribution License (CC BY). The use, distribution or reproduction in other forums is permitted, provided the original author(s) and the copyright owner(s) are credited and that the original publication in this journal is cited, in accordance with accepted academic practice. No use, distribution or reproduction is permitted which does not comply with these terms.

frontiers | Frontiers in Cardiovascular Medicine

ORIGINAL RESEARCH
published: 18 May 2022
doi: 10.3389/fcvm.2022.792717

Plasma Membrane Localization of CD36 Requires Vimentin Phosphorylation; A Mechanism by Which Macrophage Vimentin Promotes Atherosclerosis

Seo Yeon Kim[1†], Se-Jin Jeong[2], Ji-Hae Park[1], Wonkyoung Cho[1], Young-Ho Ahn[1], Youn-Hee Choi[3], Goo Taeg Oh[2], Roy L. Silverstein[4] and Young Mi Park[1]*

[1] Department of Molecular Medicine, College of Medicine, Ewha Womans University, Seoul, South Korea, [2] Department of Life Sciences, Immune and Vascular Cell Network Research Center, National Creative Initiatives, Ewha Womans University, Seoul, South Korea, [3] Department of Physiology, College of Medicine, Ewha Womans University, Seoul, South Korea, [4] Department of Medicine, Medical College of Wisconsin, Milwaukee, WI, United States

OPEN ACCESS

Edited by:
Chieko Mineo,
University of Texas Southwestern Medical Center, United States

Reviewed by:
Robert Kiss,
McGill University, Canada
Linzhang Huang,
Fudan University, China

***Correspondence:**
Young Mi Park
parkym@ewha.ac.kr

†Present address:
Seo Yeon Kim
Department of Pediatrics, Asan Medical Center Children's Hospital, Ulsan University College of Medicine, Seoul, South Korea

Specialty section:
This article was submitted to Lipids in Cardiovascular Disease, a section of the journal Frontiers in Cardiovascular Medicine

Received: 11 October 2021
Accepted: 04 April 2022
Published: 18 May 2022

Citation:
Kim SY, Jeong S-J, Park J-H, Cho W, Ahn Y-H, Choi Y-H, Oh GT, Silverstein RL and Park YM (2022) Plasma Membrane Localization of CD36 Requires Vimentin Phosphorylation; A Mechanism by Which Macrophage Vimentin Promotes Atherosclerosis. Front. Cardiovasc. Med. 9:792717. doi: 10.3389/fcvm.2022.792717

Vimentin is a type III intermediate filament protein expressed in cells of mesenchymal origin. Vimentin has been thought to function mainly as a structural protein and roles of vimentin in other cellular processes have not been extensively studied. Our current study aims to reveal functions of vimentin in macrophage foam cell formation, the critical stage of atherosclerosis. We demonstrated that *vimentin* null ($Vim^{-/-}$) mouse peritoneal macrophages take up less oxidized LDL (oxLDL) than *vimentin* wild type ($Vim^{+/+}$) macrophages. Despite less uptake of oxLDL in $Vim^{-/-}$ macrophages, $Vim^{+/+}$ and $Vim^{-/-}$ macrophages did not show difference in expression of CD36 known to mediate oxLDL uptake. However, CD36 localized in plasma membrane was 50% less in $Vim^{-/-}$ macrophages than in $Vim^{+/+}$ macrophages. OxLDL/CD36 interaction induced protein kinase A (PKA)-mediated vimentin (Ser72) phosphorylation. $Cd36^{-/-}$ macrophages did not exhibit vimentin phosphorylation (Ser72) in response to oxLDL. Experiments using phospho-mimetic mutation of vimentin revealed that macrophages with aspartate-substituted vimentin (V72D) showed more oxLDL uptake and membrane CD36. *LDL receptor* null ($Ldlr^{-/-}$) mice reconstituted with $Vim^{-/-}$ bone marrow fed a western diet for 15 weeks showed 43% less atherosclerotic lesion formation than $Ldlr^{-/-}$ mice with $Vim^{+/+}$ bone marrow. In addition, $Apoe^{-/-}Vim^{-/-}$ (double null) mice fed a western diet for 15 weeks also showed 57% less atherosclerotic lesion formation than $Apoe^{-/-}$and $Vim^{+/+}$mice. We concluded that oxLDL via CD36 induces PKA-mediated phosphorylation of vimentin (Ser72) and phosphorylated vimentin (Ser72) directs CD36 trafficking to plasma membrane in macrophages. This study reveals a function of vimentin in CD36 trafficking and macrophage foam cell formation and may guide to establish a new strategy for the treatment of atherosclerosis.

Keywords: vimentin, atherosclerosis, CD36, macrophage, intracellular trafficking

INTRODUCTION

CD36 is an 88 kDa plasma membrane glycoprotein and one of the major scavenger receptors expressed in various cell types including macrophages, microvascular endothelial cells and adipocytes. CD36 involves in many biological activities through binding to variety of ligands including modified low density lipoprotein (LDL), lipopolysaccharides of bacterial cell wall, and thrombospondin-1. In particular, CD36 binding to oxidized LDL (oxLDL) mediates uptake of oxLDL and leads to macrophage foam cell formation, the initial critical stage of atherosclerosis (1). *Ex vivo* experiments demonstrate that 60–70% of macrophage foam cell formation is induced by CD36-mediated oxLDL uptake (2). Although foam cell formation is a critical stage of atherosclerosis, the molecular mechanism by which macrophages uptake oxLDL has not been clearly defined. OxLDL/CD36 interaction provokes signals through activation of Lyn/MAPKK4/JNK2 in macrophages (3). Several studies elucidate that CD36-mediated oxLDL uptake mechanism is independent of caveloae, clathrin, and actin cytoskeleton but dependent on dynamin (4). It has been reported that the C-terminal six amino acids of the CD36 cytoplasmic tail are critical for binding and endocytosis of OxLDL (5). Therefore, elucidating the mechanism of oxLDL uptake via CD36 is warranted.

Vimentin is a 55 kDa protein, composing the major type III intermediate filament in cells of mesenchymal origin such as macrophages and adipocytes (6). Vimentin composes cytoskeletal networks from nuclear periphery to the cell membrane and functions in distribution of cellular organelles (7), cell migration and cell adhesion (8, 9). In clinical medicine, vimentin is commonly used for a marker for epithelial to mesenchymal transition (EMT) of cancer cells (10). Recent studies reported that vimentin is a component of lipid droplets in adipocytes (11) and influences lipid stability during adipocyte differentiation (12). However, the mechanism has not been fully elucidated. Vimentin plays a role in endocytosis of certain virus (13) and metal ion in fibroblast (14). Nevertheless, there have been few studies for the role of vimentin in functions other than cellular structure maintenance.

Vimentin has a highly conserved alpha helix domain and is capped on each end by amino-, carboxyl domain (15, 16). Two vimentin monomers form a coiled-coil structure and associate other homodimer to produce soluble tetramer that is a longitudinal unit of vimentin filament (17). Vimentin phosphorylation regulates the structure of vimentin, inducing formation of intermediate filaments or disassembly into vimentin monomers. It also changes affinity of vimentin to its binding partners. Vimentin has phosphorylation sites that are modulated by 10 kinases including PKC, PKA, and Cdk1 (18, 19). Phosphorylation-mediated regulation of vimentin has been well studied in cytokinesis. Cdk1 phosphorylates Ser55 on vimentin, leading to depolymerization of vimentin filament from prometaphase to metaphase (20, 21). Ser38 and Ser72 on vimentin are phosphorylated by PKA and lead to disassembly of vimentin filaments in fibroblast. However, the function of phospho-vimentin (Ser72) in macrophages has not been studied.

Atherosclerosis is an important underlying pathology of cardiovascular disease, which is currently the leading cause of mortality worldwide (22). Therefore, verifying the mechanism of macrophage foam cell formation should guide to develop a new strategy for the treatment of atherosclerosis (23–28).

A recently published paper written by Haversen et al. showed that loss of vimentin increased macrophage surface CD36 expression *in vitro*, however, reduced atherosclerosis in two animal models including LDL receptor null ($LDLR^{-/-}$) mice reconstituted with vimentin null ($Vim^{-/-}$) bone marrow and $Vim^{-/-}$ mouse injected with PCSK9 gain-of-function virus (29).

In the current study, we performed experiments to evaluate how vimentin deficiency affects macrophage foam cell formation and atherosclerosis. Our current study reveals that vimentin plays a role in CD36 trafficking to plasma membrane and contributes to macrophage foam cell formation. In addition to *in vitro* experiments, our *in vivo* experiments using *vimentin* null ($Vim^{-/-}$) bone marrow transplantation into hypercholesterolemic mice confirmed the atherosclerosis-promoting effect of vimentin. Regarding the functions of CD36 in various biological activities including immunity and anti-angiogenesis, the mechanism of CD36 trafficking may guide ways to modulate the cellular processes mediated by CD36.

MATERIALS AND METHODS

Regent

Oil red O (ORO), 1,10-dioctadecyl-3,3,30,30-tetramethylindocarbocyanine perchlorate (DiI) and human AB serum were obtained from Sigma (Sigma, United States). The intracellular cholesterol assay kit was from Cayman (Cayman Chemical Co, United States). Antibodies for CD36, Vimentin, tubulin, EEA1 and beta-actin were obtained from Abcam (Abcam, United States). Antibodies for SRA1 conjugated with APC and control antibody were manufactured by Bioyrt (Bioryt, United States). Antibodies for CD36 conjugated with APC and suitable control antibody were from Bio-Rad (Bio-Rad, United States). Sucrose, dextrose, SDS were obtained from Ducefa (Ducefa, Germany). Antibodies for rabbit IgG, IgM were purchased from bethyl chemisty (bethyl, United States). Antibody for p-PKAα/β/γ cat (Thr 198) was from Santa Cruz Biotechnology (sc-32968) (Santa Cruz, United States).

Mouse Protocol

Pathogen-free, male C57BL/6 mice, 6–8 week old were purchased from Orient Bio (Orient Bio, South Korea). *Vimentin* null ($Vim^{-/-}$) mice on a 129 background were provided by Dr. John E. Eriksson (Åbo Akademi University, Finland) and seven times backcrossed to C57Bl/6. *LDL receptor* null ($LDLr^{-/-}$) mice were provided by Dr. Goo Taeg Oh (Ewha Womans University, Seoul, South Korea). In all experiments, age-matched (7–10 weeks old) male mice were used. The Institutional Animal Care and Use Committee (IACUC) of Ewha Womans University College of Medicine approved the experimental protocol (IACUC approval No. ESM-12-0198).

Bone Marrow Transplantation and Atherosclerosis Analysis

LDLr$^{-/-}$mice were reconstituted with bone marrow from *Vim*$^{+/+}$ mice ($n = 11$) and *Vim*$^{-/-}$ mice ($n = 10$). To induce bone marrow aplasia, *LDLr*$^{-/-}$mice (male, age 6 weeks) were exposed to a single dose of 13 Gy (0.28 Gy/min, 200 kV, 4 mA) x-ray (total body irradiation) with a 4 mm aluminum filter, 1 day before the transplantation. Bone marrow cell suspensions were isolated by flushing the femurs and tibias from either male *Vim*$^{+/+}$ or *Vim*$^{-/-}$ mice with phosphate-buffered saline. Irradiated recipients received 1.5×10^7 bone marrow cells by intravenous injection into the tail vein. After 4 weeks, reconstituted *Ldlr*$^{-/-}$ mice were fed a western diet for 15 weeks.

We generated *Apoe*$^{-/-}$ *Vim* $^{-/-}$ (double null) mice by crossing the *Apoe*$^{-/-}$ and *Vim* $^{-/-}$ mouse strains. *Apoe*$^{-/-}$ *Vim* $^{-/-}$ mice and *Apoe*$^{-/-}$ *Vim*$^{+/+}$ mice were fed a western diet for 15 weeks.

Western diet-fed mice were euthanized and perfused with cold 0.01 mol/L PBS through left ventricle. Aortae were dissected from the proximal ascending aorta to the bifurcation of iliac artery and fixed in 4% buffered paraformaldehyde for 24 h. After fixation, the aortae were split longitudinally and pinned open for surface lesion measurements with 0.5% Oil-Red O staining. For aortic sinus analysis, heart was embedded in optimal cutting temperature compound (OCT), and snap-frozen in liquid nitrogen. Serial 7-μm cryosections of the aortic sinus were cut using a Leica CM1950 cryostat. Four or more frozen section slides for aortic sinus were made per mouse. Cryosections were fixed in 4% buffered paraformaldehyde and stained in 0.5% Oil Red O for 25 min. Quantitative analysis of atherosclerotic lesions was performed using the Axiovision release 4.4 software (Carl Zeiss, Germany) program.

Low Density Lipoprotein Preparation and Oxidation

LDL was obtained from human plasma via density gradient ultracentrifugation (30). Oxidized LDL (oxLDL) was generated by dialysis of LDL with 5μM $CuSO_4$ in PBS for 6 h at 37°C. To terminate oxidation of LDL, LDL was dialyzed with 100 μ M EDTA in PBS.

In addition to $CuSO_4$-oxLDL, we generated oxLDL modified by myeloperoxidase (MPO) and used in several experiments as **Figure 1D**. LDL prepared from human plasma by density gradient ultracentrifugation was oxidatively modified by incubation in a buffer containing 50 mM sodium phosphate (pH 7.0) and 100 μM diethylene triamine pentaacetate (DTPA) with 30 nM MPO, 100 μg of glucose, glucose oxidase at 20 ng/ml (grade II; Boehringer Mannheim Biochemicals, Penzberg, Germany), and 0.5 mM $NaNO_2$ at 37°C for 8 h (oxLDL) (31). The oxidation reaction was terminated by the addition of 40 μM butylated hydroxyl-toluene and 300 nM catalase to the reaction mixture.

Cell Culture

Peritoneal macrophages were collected by peritoneal lavage of mice 4 days after intraperitoneal injection of 4% thioglycolate (1 ml). Mice were euthanized with CO_2 before harvesting macrophages. Cells were cultured in RPMI containing 10% fetal bovine serum and 1% penicillin-streptomycin. Media was changed to serum-free RPMI for treatment with oxLDL or other chemicals.

Primary bone marrow-derived macrophages (BMDMs) were collected from *Vim* $^{-/-}$ mice and wild type mice as described previously (32). Briefly, BMDMs were differentiated from murine bone marrow myeloid stem cells and cultured for 7 days with DMEM supplemented with 10% L929 supernatant containing 10% fetal bovine serum (FBS), 1 mM sodium pyruvate, 1% penicillin-streptomycin and 5 × 10–5M 2-mercaptoethanol at 37°C and 5% CO_2.

SW13 cells were purchased from ATCC (ATCC, United States) and incubated following their protocol.

Oil Red O Staining

ORO staining was performed using murine peritoneal macrophages plated in 12-well plate as described previously (33). Cells were incubated with or without 50μg/ml of oxLDL for 18 h. Then macrophages were fixed in 4% paraformaldehyde in PBS for 20 min at room temperature. To stain the intracellular lipids, Cells were washed with PBS twice and treated with 60% isopropanol for 5 min and ORO solution (diluted 2:3 of H2O:0.3% ORO in isopropanol) for 15 min. After rinsing with distilled water, cells were examined microscopically.

We added 500 μl of isopropanol onto the ORO-stained macrophages to extract the ORO incorporated into the intracellular lipids. The amount of the ORO flowing out from the macrophages was measured by using spectrophotometry (absorbance at 510 nm).

Western Blotting

Cells were lysed in buffer containing 1% triton X-100, 20 mM Tris-HCl (pH 7.5), 150 mM NaCl, 1 mM EDTA, 1 mM EGTA and protease inhibitor cocktail (Roche, Germany) and phosphatase inhibitors (10 mM phenylmethylsulfonyl fluoride/PMSF, 1% sodium pyrophosphate, 10 mM sodium fluoride, and 2 mM sodium vanadate). The lysates were separated by SDS-PAGE, transferred to PVDF membrane (Millipore), and analyzed by immunoblotting. Membranes were probed with antibodies for vimentin, CD36, phospho-vimentin (Ser72), and phospho-vimentin (Ser38). Antibodies for β-actin and GAPDH were used for normalization. Band intensities were quantified using Image J program (U. S. National Institutes of Health, United States).

Flow Cytometry

Cells were incubated in 6 well plates with appropriate media containing 10% FBS. After rinsing twice with PBS, cells were harvested gently with scrapers and moved to round bottom glass tubes. After centrifuge at 1,000 × g in glass tubes, cells were incubated with 5% BSA for 30 min at 4°C and then incubated with APC-conjugated anti-CD36 antibody (Bio legend, United States), FITC-conjugated anti-MSR1 antibody or isotype control (Bio legend, United States) diluted in PBS containing 5% BSA for 1 h at 4°C. After three washes with PBS, cells were analyzed by flow cytometry.

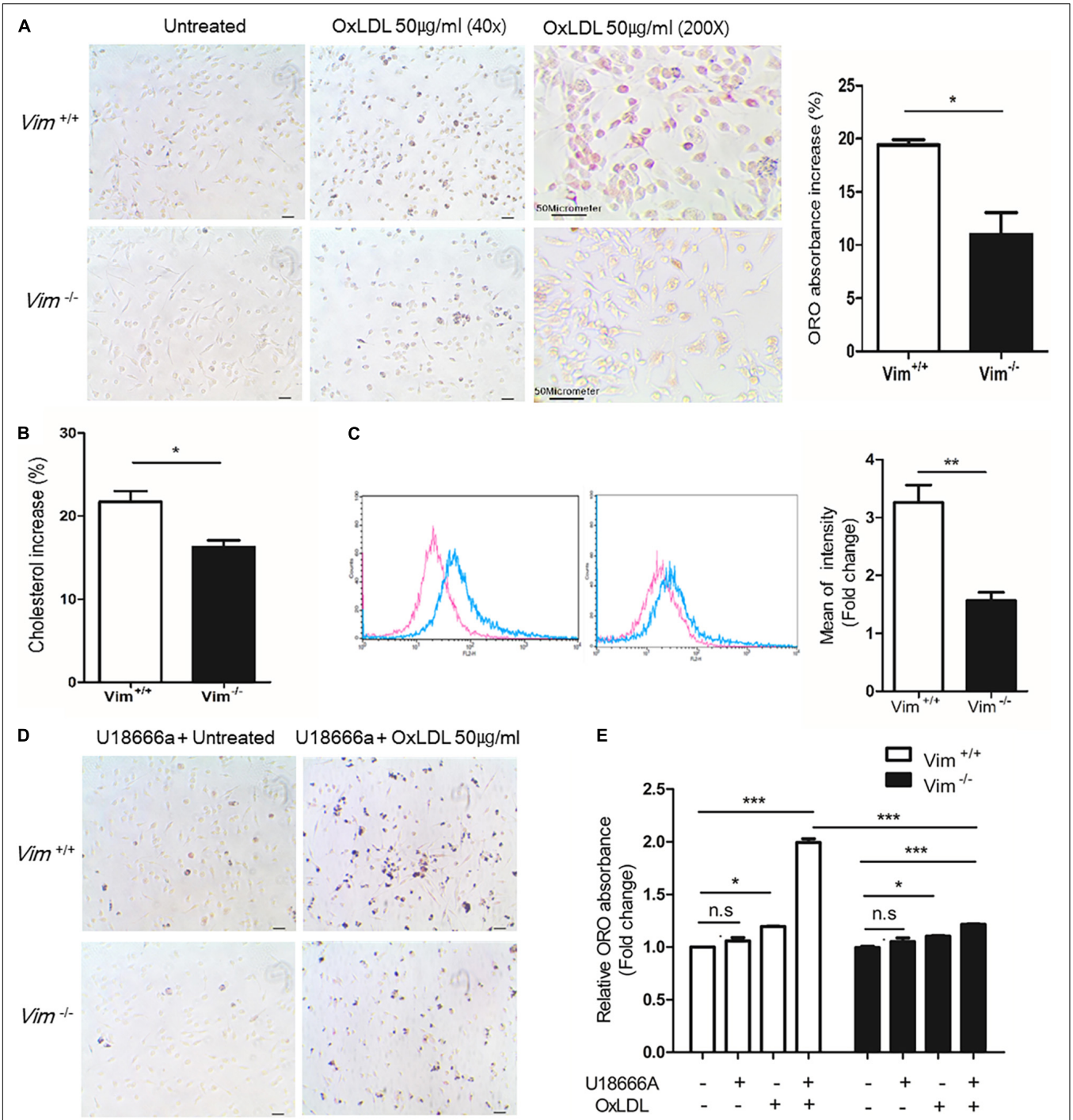

FIGURE 1 | *Vim*$^{-/-}$ murine peritoneal macrophages exhibit less foam cell formation and less uptake of oxLDL than *Vim*$^{+/+}$ macrophages. **(A)** Left, Representative images of ORO staining of *Vim*$^{+/+}$ mouse macrophages and *Vim*$^{-/-}$ mouse macrophages. Both macrophages were incubated with or without oxLDL (50 μg/ml) for 18 h. Right: the absorbance of ORO eluted from macrophages in **(A)**. The absorbance increases induced by oxLDL treatment were compared between *Vim*$^{+/+}$ and *Vim*$^{-/-}$ macrophages. **(B)** Increases of Intracellular cholesterol concentration in *Vim*$^{+/+}$ mouse macrophages and *Vim*$^{-/-}$ mouse macrophages were compared after incubation with oxLDL 50 μg/ml for 18 h. **(C)** Left, Flow cytometry. *Vim*$^{+/+}$ mouse macrophages and *Vim*$^{-/-}$ mouse macrophages were pretreated with non-labeled oxLDL for 30 min, and then exposed to oxLDL complexed with DiI (DiI-oxLDL, 50 μg/ml) for 5 min and fixed with 4% paraformaldehyde. The fluorescence intensities of these cells were measured using flow cytometry. Red line; without oxLDL, Blue line; with oxLDL. Right graph: Geometric mean fluorescence intensities were compared between *Vim*$^{+/+}$ and *Vim*$^{-/-}$ macrophages incubated with oxLDL. The bar graph of comparison was generated from 3 times of separate experiments. **(D)** Representative images of ORO staining of *Vim*$^{+/+}$ and *Vim*$^{-/-}$ mouse macrophages. Both macrophages were pre-incubated with U18666a (NPC inhibitor, 10 nM) for 90 min and then incubated with or without oxLDL (50 μg/ml) for 18 h. **(E)** Relative ratio of absorbance of eluted ORO in **(A,D)**. The ORO was extracted using isopropanol and the absorbance representing intracellular lipids was detected at 540 nm. (*$p < 0.05$, **$p < 0.01$, ***$p < 0.001$. The graph shows mean ± SEM for triplicated determinants of 3 separate experiments).

Immunoprecipitation

Cells were lysed with RIPA buffer (1% triton x-100, 0.1% sodium dodecyl sulfate, 0.5% deoxycholate, 50 mM Tris-HCl (pH 7.5), 150 mM NaCl) and protease inhibitor cocktail. The protein concentrations of the lysates were quantified by BCA method and appreciate amounts of lysates were pre-incubated with Protein A or Protein A/G plus bead (Santa cruz, United States) for 2 h. The supernatant containing 350 mg protein was incubated with 2 μg of anti-CD36 antibody or anti-vimentin antibody overnight at 4°C. Protein A or Protein A/G plus beads were added to the lysates for 4 h. Beads were extensively washed, boiled in laemmli buffer (Bio-rad, United States) and the bead-bound material was analyzed by immunoblotting for CD36, vimentin or PKA.

1,10-Dioctadecyl-3,3,30,30-Tetramethylindocarbocyanine Perchlorate Oxidized LDL Uptake Assay

OxLDL was complexed with DiI as described previously. OxLDL (500 μg/ml) was mixed with 10 μg/ml of DiI in DMSO at 37°C for 16 h. DiI-OxLDL solution was dialyzed in PBS. Macrophages were cultured in 6 well plates and then incubated with oxLDL (50 μg/ml) at 37°C for 30 min. Cells were treated with DiI-oxLDL 50 μg/ml for 5 min, fixed in 4% paraformaldehyde in PBS and washed with PBS. Cells were collected by scrapping and spinned at 1,000 g for cell debris removal. DiI-OxLDL taken up by macrophages was measured using flow cytometry.

Intracellular Cholesterol Concentration Measurement

Intracellular cholesterol was measured using a cholesterol fluorometric assay kit (Cayman). $Vim^{+/+}$ macrophages and $Vim^{-/-}$ macrophages were cultured in 6 well plates with or without oxLDL (50 μg /ml) and cells were washed twice with PBS after 18 h. Assay buffer including 0.5% triton X-100 was added onto the cells. The cell lysates were centrifuged at 13,000 × g for 30 min at 4°C. The supernatants were used for the cholesterol measurement. The value of intracellular cholesterol was normalized by comparison to the protein concentration of the sample.

RNA Isolation and Real Time PCR

Total RNA was extracted from macrophages using Trizol reagent (Invitrogen, United States) according to the manufacturer's instruction. We used iScript cDNA synthesis kit (Bio-rad, United States) to synthesize cDNA. Quantitative real-time reverse transcriptase PCR (qRT-PCR) was performed with Power SYBR Green PCR Master Mix (Applied Biosystems, United States) and an ABI Real-Time PCR thermocycler. RNAs were analyzed by qRT-PCR with following primers (5′-CCC AGA GCA AAA AGC GAC TC-3′ and 5′- GGT CAT CAT CAC TTT GGT CCT TG-3′ for ABCA1, 5′-CAA GAC CCT TTT GAA AGG GAT CTC-3′ and 5′-GCC AGA ATA TTC ATG AGT GTG GAC-3′ for ABCG1, 5′-GGC TGC TGT TTG CTG CG-3′ and 5′-GCT GCT TGA TGA GGG AGG G-3′ for SR-B1, 5′-GAT CGG AAC TGT GGG CTC AT-3' and 5′-GGT TCC TTC TTC AAG GAC AAC TTC-3' for CD36, 5′-AAA GAA GAA CAA GCG CAC GTG G-3' and 5′-GAG CAC CAG GTG GAC CAG TTT G-3' for SR-A1, and 5′-TCC ATG ACA ACT TTG GCA TTG-3' and 5′- TCA CGC CAC AGC TTT CCA-3' for GAPDH.) GAPDH was used for internal control.

Vector Construction

All plasmids were produced using standard cloning techniques. Vimentin sequence was cloned into pAcGFP-Hyro-N1 vector for imaging. pLVX-puro vector were used for mutagenesis. These vectors were provided by Dr. Youngho Ahn (Ewha Womans University, Seoul, South Korea). Vimentin construct was amplified by PCR with following primers (VIM -HindIII-F: GTCA AA GCT TCG ATG TCC ACC AGG TCC, GTG TC, VIM -HindIII-R: GTCA AA GC TTA TTC AAG GTC ATC GTG ATG CTG, VIM -EcoRI-Flag-F: GTCA GAATTC GCCACC ATG GAT TAC AAG GAT GAC GAC GAT AAG ATG TCC ACC AGG TCC GTG TC, VIM -EcoRI-R: GTCA GAATTC TTA TTC AAG GTC ATC GTG ATG CTG) in reactions as follows; denaturation at 94°C for 5 min, followed by 30 cycles of denaturation at 94°C for 2 min, annealing at 59°C for 1 min, and extension at 72°C for 2 min. A final elongation step was carried out at 72°C for 10 min.

For site-directed mutagenesis, we used polymerase chain reaction (PCR) with oligonucleotide mutation primers and the template vimentin cDNA. The primers for site-directed mutagenesis are VIM -S72A-F: GCC GTG CGC CTG CGG GCC AGC GTG CCC GGG GTG, VIM -S72A-R: CAC CCC GGG CAC GCT GGC CCG CAG GCG CAC GGC, VIM -S72D-F: GCC GTG CGC CTG CGG GAC AGC GTG CCC GGG GTG, VIM -S72D-R: CAC CCC GGG CAC GCT GTC CCG CAG GCG CAC GGC. The mutation sites were confirmed by sequencing by Cosmo Genetech.

Lentivirus-Mediated Transfection

Genetically modified lentiviruses were produced by transient transfection of 293T cells with Plvx -VIM, Plvx -V72A, Plvx -V72D, Plvx-puro, PAX2 packaging plasmid (containing gag and pol gene of HIV) and MDG2 envelop plasmid (containing vesicular stomatitis viral glycoprotein expressing vector) using Lipofectamine 2000 reagents (Thermo Fisher Scientific, United States).

A293T cells were seeded onto 6 well plates at 50∼70% confluence 1 day before the transfection. Transfection mixture containing 6 μg target vector, 5 μg PAX2, 3 μg MDG2, and 10 μg/ml Lipofectamine was added to the A293T cells. The media was collected after 24 h, filtered through a 45 μm pore filter and added to the recipient cells. To enhance the transfection efficiency, virus-containing media was mixed with polybrene 5 μg/ml (Millipore). We performed second transfection repeating the same procedure 24 h after the first transfection to promote viral incorporation.

Immunocytochemistry and Immunohistochemistry

Cells grown on glass coverslips were fixed with 4% formaldehyde in ice-cold PBS for 20 min and then 0.1% triton X-100

in ice-cold PBS for 5 min. Cells were incubated with 5% BSA in PBS for 1 h to reduce non-specific signals and then incubated with primary antibodies diluted in PBS containing 5% BSA for 16 h at 4°C. After 3 washes with PBS, cells were incubated with appropriate fluorescent dye-conjugated secondary antibodies for 1 h and washed with PBS. Then nuclei were stained with DAPI-containing mounting solution (Vector laboratories, United States). Fluorescently stained cells were examined under a Zeiss confocal microscope and analyzed by Zeiss imaging processor.

Aortic sinus tissues were embedded in optimal cutting temperature compound (SAKURA Tissue-Tek, United States) for frozen section and snap frozen at –80°C. These frozen tissues were sectioned on a cryostat, transferred to slides and then dried to preserve morphology. Sections were dried for 5 min at room temperature and were fixed by pre-cold acetone for 15 min. The following process was equal to immunocytochemistry.

Early-Endosome Fraction Assay

Mouse peritoneal macrophages were incubated with oxLDL (50 μg /ml) for 10 min. After the designated time point, cells were washed twice with RPMI followed by the application of 0.5 ml of homogenization buffer [250 mM sucrose, 1 mM EDTA, 1 mM phenylmethylsulfonyl fluoride (PMSF)], in which cells were gently detached using a cell scraper, lysed, and further processed for examination by a sucrose flotation assay. Specifically, after centrifugation (1,000 × g), the post-nuclear supernatant was collected and adjusted to a concentration of 25% sucrose and 1 mM EDTA in 1 ml total volume. In 1 ml increments, 2.4 ml of 45% sucrose was transferred to the bottom of a SW41Ti tube and successively overlaid with 5.2 ml of 35% sucrose, 3.9 ml of 25% sucrose, and 1 ml of post-nuclear supernatant in 25% sucrose. These fractions were further analyzed using endosomal markers, CD36 and vimentin.

Thiobarbituric Acid Reactive Substance Assay

Lipid peroxidation of LDL was measured by Thiobarbituric Acid Reactive Substance (TBARS) formation. Briefly, LDL and oxLDL were incubated with ice cold 10% Trichloroacetic acid to precipitate protein for 15 min on ice. And centrifuge samples 2,200 × g for 15 min at 4°C. Place supernatant into new labeled tube and add equal volume of 0.67% (w/v) Thiobarbituric Acid (TBA). Incubate in a boiling water bath for 10 min and record absorbance at 532 nm.

Statistical Analysis

Data are expressed as mean ± standard error of the mean (SEM). Student's *t*-test was used for comparisons between two sample means. ANOVA test was used to compare three or more groups. We also used non-parametric Kruskal–Wallis test for post-comparison hoc test. A *p*-value less than 0.05 were considered statistically significant. All experiments were repeated at least 3 times independently and all the measurements were done three times for a set. Analyses were performed using GraphPad Prism Software (GraphPad Software).

RESULTS

Vim$^{-/-}$ Murine Peritoneal Macrophages Exhibit Less Uptake of Oxidized LDL Than *Vim*$^{+/+}$ Macrophages

To determine if vimentin plays a role in macrophage foam cell formation, we performed ORO staining with *Vim*$^{+/+}$ and *Vim*$^{-/-}$ murine peritoneal macrophages incubated with oxLDL for 18 h (**Figure 1A**). We extracted ORO from the ORO-stained macrophages and measured the absorbance to quantify the amount of intracellular lipids. The ORO incorporated in the *Vim*$^{-/-}$ macrophages was 10% less than that in the *Vim*$^{+/+}$ macrophages (**Figure 1A**). In accordance, the increment of intracellular cholesterol after the oxLDL treatment which was measured by cholesterol oxidase assay was 6% less in *Vim*$^{-/-}$ macrophages than in *Vim*$^{+/+}$ macrophages (**Figure 1B**). These data indicate that vimentin deletion reduces macrophage foam cell formation.

Previous reports revealed that vimentin functions in uptake of virus and metal ion such as zinc (13, 14, 34). To evaluate roles of vimentin in lipid uptake, peritoneal macrophages from *Vim*$^{-/-}$ and *Vim*$^{+/+}$ mice were treated with oxLDL complexed with diI (DiI-oxLDL) for 5 min and fixed with 4% paraformaldehyde. Our data from flow cytometry showed that the mean fluorescence intensity of macrophages representing DiI-oxLDL uptake was 50% less in *Vim*$^{-/-}$ macrophages than in *Vim*$^{+/+}$ macrophages (**Figure 1C**).

To clarify in which stage of oxLDL-internalization vimentin functions, we treated macrophages with U18666a (10 nM), Niemann-Pick C1 (NPC-1) inhibitor, to block the later process of endocytosis, especially the transport of LDL-derived cholesterol from lysosomes to endoplasmic reticulum (35). *Vim*$^{+/+}$ and *Vim*$^{-/-}$ mouse peritoneal macrophages were pre-incubated with U18666a (10 nM) for 90 min, incubated with or without oxLDL (50 μg/ml) for 18 h and stained with ORO (**Figure 1D**). The absorbance of ORO eluted from *Vim*$^{-/-}$ macrophages was 1.3 fold increased after the oxLDL treatment while *Vim*$^{+/+}$ macrophages showed 2.0 fold-increase after the oxLDL treatment (**Figure 1E**). The result suggested that less intracellular lipids in *Vim*$^{-/-}$ macrophages were not caused by increased trafficking of free cholesterol from late endosome/lysosomes to other cellular compartments, but is caused by diminished uptake of lipoproteins.

Plasma Membrane CD36 Was Less in *Vim*$^{-/-}$ Macrophages Than in *Vim*$^{+/+}$ Macrophages

Macrophages express various receptors including CD36 and scavenger receptor-A (SR-A) to uptake oxLDL. ABCA1 and ABCG1 mediate cholesterol efflux to apolipoprotein A1 and high density lipoprotein (36–38). Dysregulation of uptake and efflux of lipids leads to foam cell formation. We performed western blot analyses and quantitative real time PCR (RT-PCR) for receptors known to regulate cholesterol influx and efflux. Quantitative RT-PCR results showed no significant

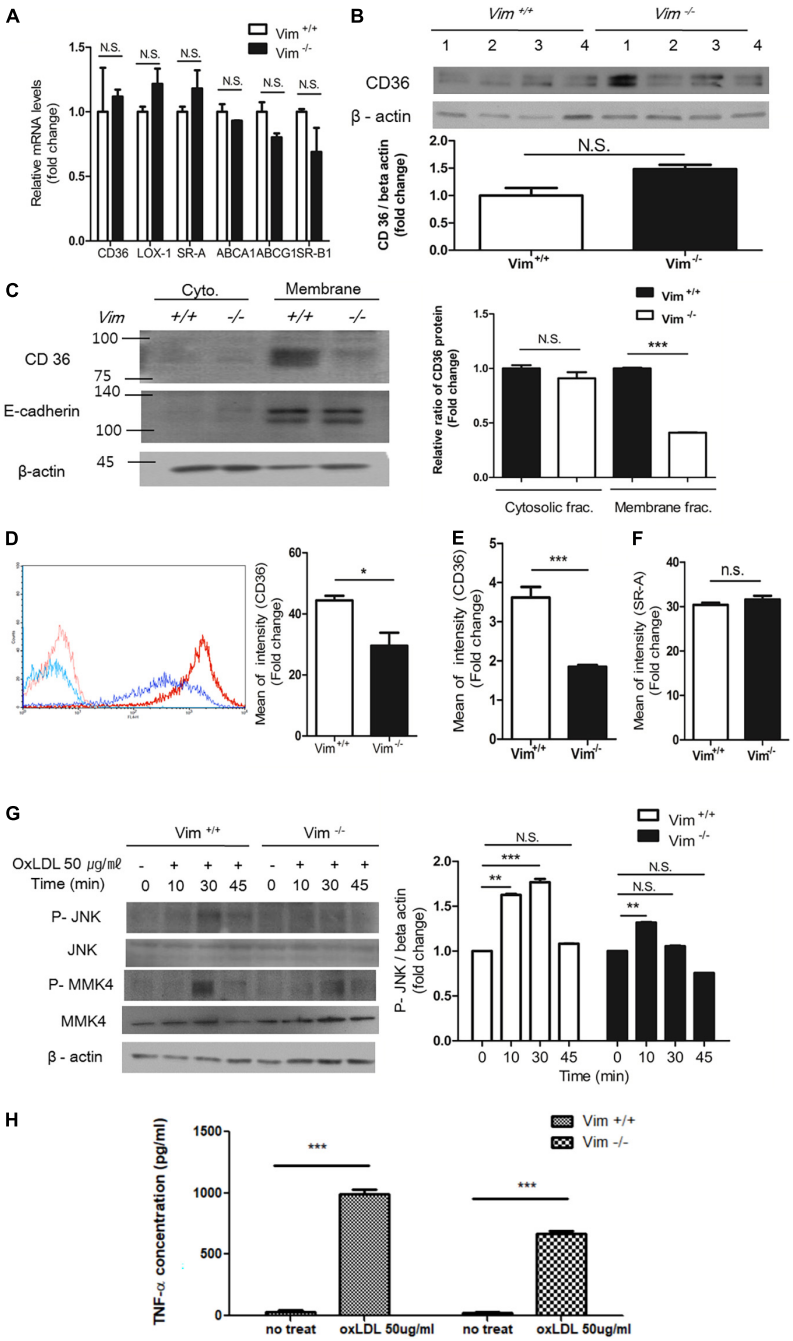

FIGURE 2 | Plasma membrane CD36 in *Vim*$^{-/-}$ macrophages was less than in *Vim* $^{+/+}$ macrophages. **(A)** Quantitative real-time PCR was performed with RNAs from *Vim* $^{+/+}$ and *Vim*$^{-/-}$ murine peritoneal macrophages. GAPDH was used as the internal control. **(B)** Western blot analysis for CD36 was performed using lysates of *Vim* $^{+/+}$ (n = 4) and *Vim*$^{-/-}$ (n = 4) murine peritoneal macrophages. Each lysates were harvested from different mice. Beta actin was used as the internal control. **(C)** Western blot analysis for CD36 was performed using fractionated lysates of *Vim* $^{+/+}$ and *Vim*$^{-/-}$ murine peritoneal macrophages. E-cadherin was used as the marker for plasma membrane fraction and GAPDH was used as the marker for cytosolic fraction. **(D)** Left, The representative flow cytometry data of *Vim* $^{+/+}$ murine peritoneal macrophages and *Vim*$^{-/-}$ murine peritoneal macrophages with APC conjugated monoclonal antibody specific for CD36. Both cell types were incubated with either IgG control (*Vim* $^{+/+}$: pink, *Vim*$^{-/-}$: light blue) or with CD36 antibody (*Vim* $^{+/+}$: red, *Vim*$^{-/-}$: dark blue). Right, Comparison of fluorescence intensities representing cell surface-localized CD36 between *Vim* $^{+/+}$ and *Vim*$^{-/-}$ murine peritoneal macrophages. **(E)** Flow cytometry. Comparison of fluorescence intensities representing cell surface-localized CD36 between *Vim* $^{+/+}$ and *Vim*$^{-/-}$ murine bone marrow-derived macrophages (BMDM). **(F)** Flow cytometry. Comparison of fluorescence intensities representing cell surface-localized SR-A between *Vim* $^{+/+}$ and *Vim*$^{-/-}$ murine peritoneal macrophages. **(G)** Western blot analysis for phospho-JNK, phospho-MMK4 and beta actin using lysates of *Vim* $^{+/+}$ and *Vim*$^{-/-}$ murine peritoneal macrophages. Cells were incubated with oxLDL (50 μg/ml) for indicated times. Beta actin was used as the internal control. *$p < 0.05$, **$p < 0.01$, ***$p < 0.001$. The graph shows mean ± SEM for triplicated determinants of the experiments. **(H)** *Vim*$^{+/+}$ and *Vim*$^{-/-}$ macrophages were treated with or without oxLDL (50 μg/ml) and TNF-α released by the macrophages in the media was measured by ELISA. ***$p < 0.001$.

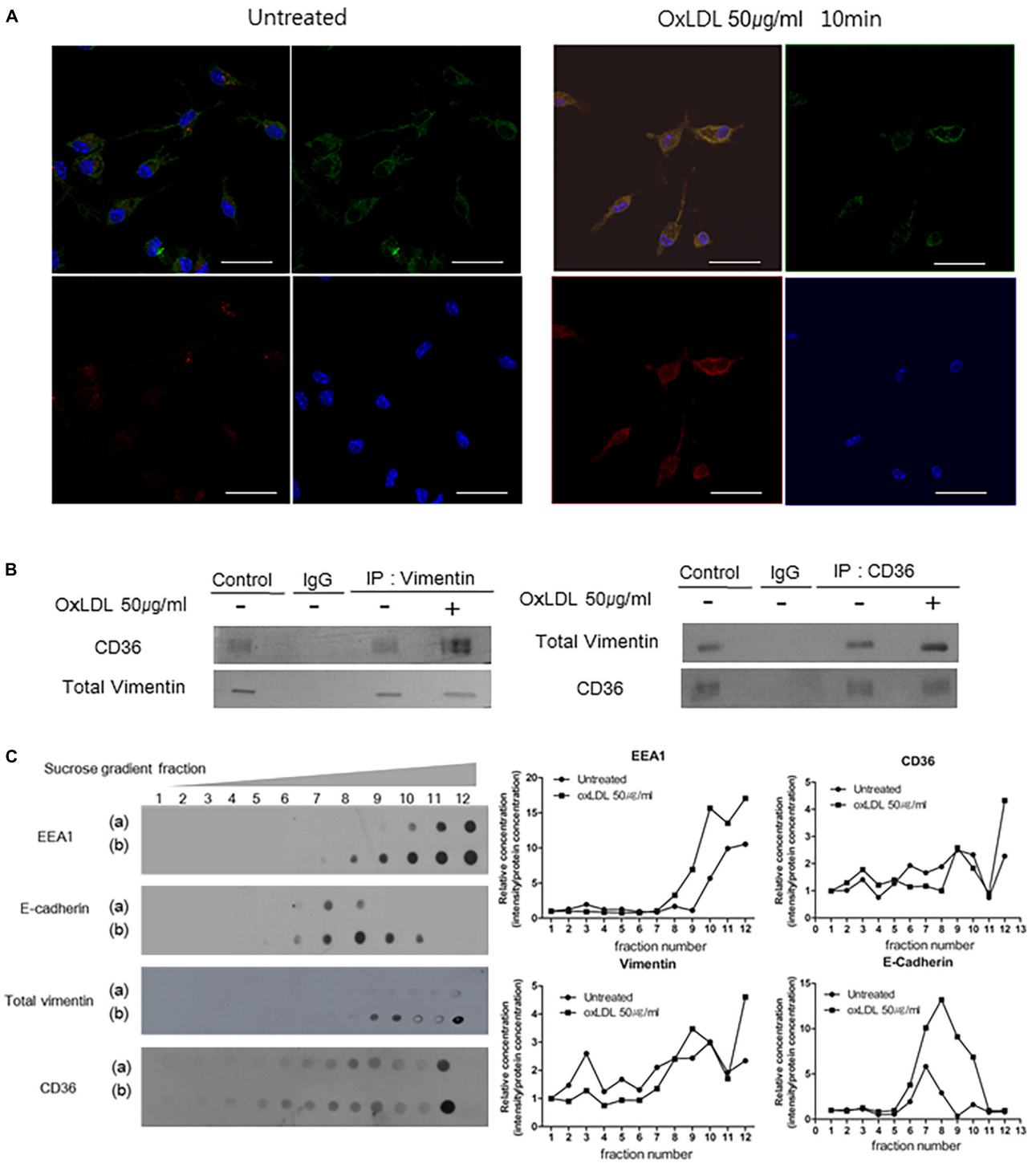

FIGURE 3 | OxLDL induces CD36-Vimentin colocalization in early endosome. **(A)** Representative immunocytochemistry images of wild type macrophages incubated with or without oxLDL (50 μg/ml) for 10 min. Cells were stained with a rabbit polyclonal antibody to CD36 (Dylight 594; Red) and a mouse monoclonal antibody to vimentin (Alexa 488; Green). Scale Bars represent 20 μm. **(B)** *Vim* $^{+/+}$ mouse peritoneal macrophages were treated with or without oxLDL (50 μg/ml) for 10 min and immunoprecipitated with indicated antibodies. The precipitants were analyzed by western blot with antibodies against vimentin and CD36. **(C)** Sucrose gradient early endosome fraction test. Wild type macrophages were incubated with or without oxLDL (50 μg/ml) for 10 min and homogenized. The lysates were added to 15∼40% sucrose gradient column and centrifuged. (a) oxLDL-untreated and (b) oxLDL-treated macrophage lysates. Immunoblot analyses for indicated proteins.

difference in expressions of CD36, LOX-1, SR-A, ABCA1, ABCG1, and SR-B1 between $Vim^{+/+}$ and $Vim^{-/-}$ mouse macrophages (**Figure 2A**). The western blot showed that CD36 protein levels were not different between $Vim^{+/+}$ and $Vim^{-/-}$ macrophages (**Figure 2B**).

However, plasma membrane-localized CD36 was significantly different between $Vim^{+/+}$ and $Vim^{-/-}$ macrophages. Subcellular fractionation and western blots using the cytoplasmic and membrane fractions of macrophage lysates revealed that plasma membrane-localized CD36 in $Vim^{-/-}$ mouse peritoneal macrophages was 60% less than in $Vim^{+/+}$ mouse peritoneal macrophages (**Figure 2C**). In accordance, flow cytometry showed that $Vim^{-/-}$ macrophages exhibited less cell surface-localized CD36 than $Vim^{+/+}$ mouse peritoneal macrophages (**Figure 2D**). Bone marrow-derived macrophages (BMDM) from $Vim^{-/-}$ mice also showed 50% less cell surface-localized CD36 than BMDM from $Vim^{+/+}$ mice in our flow cytometry data (**Figure 2E**). However, cell surface-localized SR-A measured by flow cytometry did not show difference between $Vim^{+/+}$ and $Vim^{-/-}$ mouse peritoneal macrophages (**Figure 2F**).

OxLDL via CD36 activates c-Jun N-terminal kinase (JNK) 1/2 through MKK4 in macrophages (3). OxLDL treatment induced phosphorylation of MKK4 and JNK 1/2 in $Vim^{+/+}$ macrophages, however, $Vim^{-/-}$ macrophages showed diminished responses to oxLDL (**Figure 2G**).

It has been reported that OxLDL/CD36 interaction induces release of cytokines including TNF-α (39). We measured TNF-α production in response to oxLDL in $Vim^{+/+}$ and $Vim^{-/-}$ macrophages. $Vim^{+/+}$ macrophage secreted 1.47 fold more TNF-α than $Vim^{-/-}$ macrophages (**Figure 2H**).

The results revealed that vimentin deletion decreases oxLDL/CD36-provoked signaling via less CD36 trafficking to plasma membrane.

Oxidized LDL Induces Vimentin–CD36 Colocalization in Macrophages

Since we have found decreases in oxLDL uptake and CD36 trafficking that are attributed to vimentin deficiency, we tested if vimentin and CD36 are physically associated. The immunostaining showed that CD36 and vimentin are co-localized. The co-localization of vimentin and CD36, especially near the plasma membrane, was increased within 10 min after the oxLDL treatment compared with oxLDL-untreated macrophages (**Figure 3A**). Moreover, immunoprecipitaion assay results indicated that oxLDL increased association between vimentin and CD36 (**Figure 3B**).

We isolated endosomal fractions using sucrose gradient fractionation. Early endosomes were labeled by early endosome marker EEA1 and are in the 10th, 11th, and 12th fractions. There were CD36 and vimentin in early endosome fractions. In addition, the amounts of CD36 and vimentin in the early endosome fractions were increased when the cells were treated with oxLDL (50 μg/ml) (**Figure 3C**).

Overall, these results reveal that oxLDL promotes colocalization of CD36 and vimentin.

Oxidized LDL/CD36 Interaction Induces Vimentin Phosphorylation at Serine 72 and Induces Disassembly of Vimentin Filaments

The major regulatory mechanism of vimentin is site-specific phosphorylation (18). We found that oxLDL induced phosphorylation of serine72 (ser72) in a dose-dependent manner (**Figures 4A,B**). OxLDL induced more vimentin phosphorylation (Ser72) than native LDL (**Supplementary Figure 1**). However, serine38 of vimentin was not affected by oxLDL (**Figure 4A**). Subcellular fractionation study showed that phosphorylated vimentin was increased in response to oxLDL both in the cytosolic and the membrane fractions of macrophages (**Figure 4C**). Vimentin phosphorylation (Ser72) by oxLDL was dependent on CD36. Western blot showed that oxLDL induced vimentin phosphorylation (Ser72) in macrophages from wild type mice while vimentin phosphorylation (Ser72) was not induced by oxLDL in macrophages from CD36 null mice (**Figure 4D**).

Vimentin phosphorylation at Ser72 is known to impair the assembly of vimentin intermediate filaments during mitosis in fibroblasts (18). To demonstrate the effect of vimentin phosphorylation (Ser72) in macrophages, we separated macrophage lysates into soluble/insoluble fractions based on solubility in triton X-100. In the soluble fraction which contains monomeric vimentin, vimentin was increased after the oxLDL treatment. In accordance, the level of vimentin in insoluble, filamentous fraction was decreased after the oxLDL treatment (**Figure 4E**).

Protein Kinase A Mediates Vimentin Phosphorylation (Ser72) Induced by Oxidized LDL

To identify the specific kinase that phosphorylates vimentin in response to oxLDL, we blocked various kinases using inhibitors as staurosporine, IPA-3, LY294002 and H-89. We found that H-89, a specific inhibitor for Protein Kinase A (PKA) (40), reduced oxLDL-induced vimentin phosphorylation (Ser72). We also found that oxLDL induced phosphorylation of PKA (PKA α/β/γ-c, Thr198) (**Figure 5A**). In accordance, H-89-treated wild type macrophages internalized 50% less DiI-oxLDL than H-89-untreated macrophages (**Figure 5B**).

BMDMs transfected with PKA-specific siRNA showed less oxLDL-induced phosphorylation of vimentin (Ser72) than control siRNA-transfected cells (**Figure 5C**). However, BMDMs transfected with siRNA against protein kinase C (PKC) which is also known to phosphorylate vimentin (41) did not show changes in oxLDL-induced vimentin phosphorylation (Ser72) (**Figure 5D**). To see if PKA is physically associated with vimentin, we performed immunoprecipitaion using anti-vimentin antibody and immunoblotting with anti-PKA antibody. The result showed that oxLDL treatment for 5 min induced association between PKA and vimentin (**Figure 5E**).

These data demonstrated that PKA is activated by oxLDL and mediates vimentin phosphorylation (Ser72).

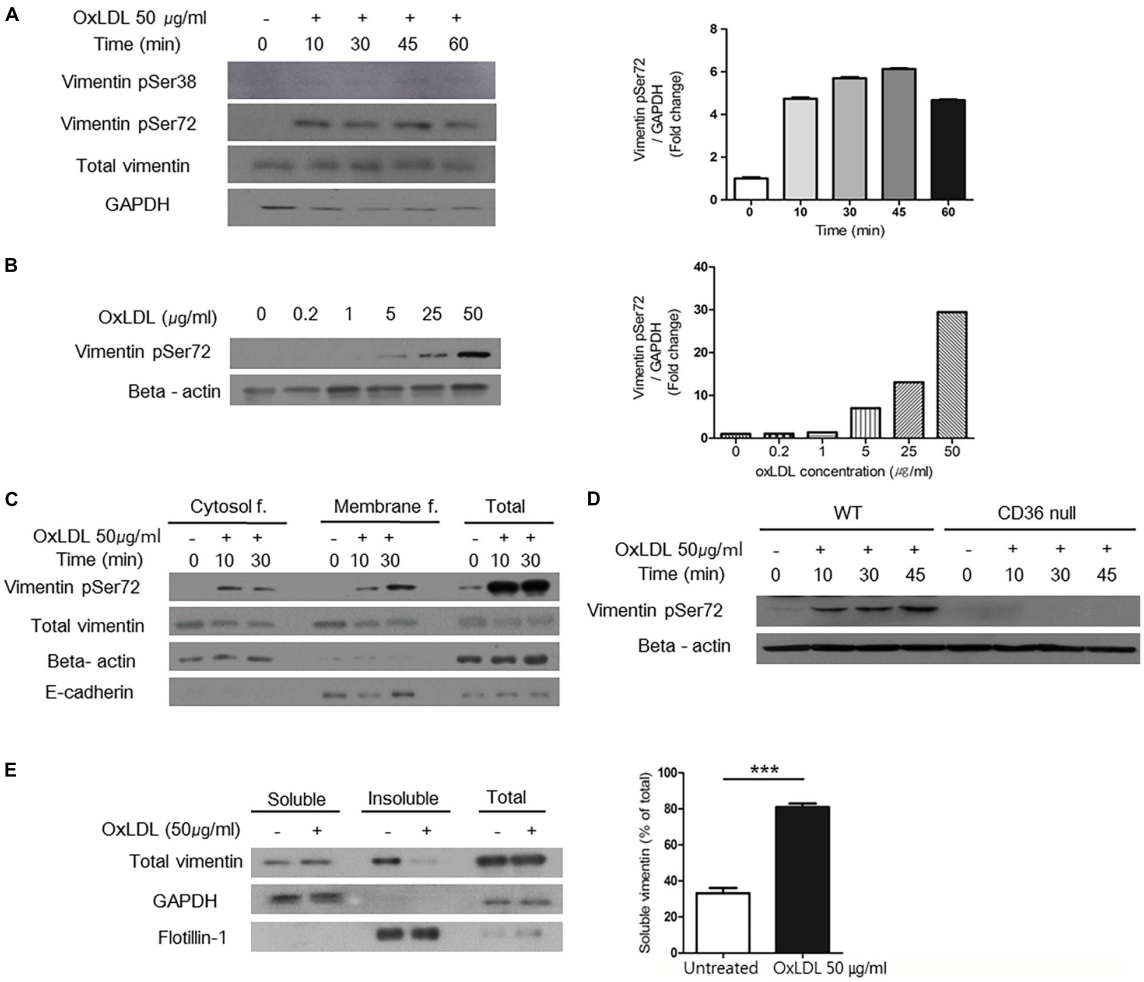

FIGURE 4 | OxLDL-induced vimentin (Ser72) phosphorylation depended on CD36 and led to disassembly of vimentin filaments. **(A)** Western blots for phosphorylated vimentin (Ser72) and phosphorylated vimentin (Ser38) using cell lysates of wild type murine peritoneal macrophages. Cells were treated with oxLDL (50 μg/ml) for indicated times. **(B)** Western blot for phosphorylated vimentin (Ser72) using cell lysates of wild type murine peritoneal macrophages. Cells were treated with various concentrations of oxLDL for 10 min. **(C)** Wild type murine peritoneal macrophages were incubated with OxLDL (50 μg/ml) for indicated times. Cytosolic and membrane fractions were separated using buffer-based protocol. E-cadherin was used as a marker for plasma membrane fraction and beta actin was used as a marker for cytosolic fraction. **(D)** Wild type and CD36 null murine peritoneal macrophages were incubated with myeloperoxidase (MPO)-modified LDL (oxLDL, 50 μg/ml) for indicated times. The lysates were analyzed by western blot for phosphorylated vimentin (Ser72). **(E)** Macrophages were treated with oxLDL (50 μg/ml) for 10 min. Cytosolic fraction is divided based on the solubility in triton X-100. Western blot for vimentin was done. GAPDH was used as a marker for soluble fraction and flotilin-1 was used as a marker for insoluble fraction. $^{***}p < 0.001$. The graph shows mean ± SEM for triplicated determinants of the experiments.

Vimentin (Ser72) Phosphorylation Induced by Oxidized LDL Regulates Membrane Localization of CD36 and Is Necessary for Uptake of Oxidized LDL

To evaluate the role of phosphorylated vimentin (Ser72), we generated Ser72-to-Asp phospho-mimicking mutant (V72D) and Ser72-to-Ala (V72A) non-phospho-mimicking mutant using site-directed mutagenesis. $Vim^{-/-}$ BMDM showed 40% less DiI-oxLDL uptake than $Vim^{+/+}$ BMDM and $Vim^{-/-}$ BMDM that restored vimentin expression showed increased uptake of oxLDL. $Vim^{-/-}$ BMDM transfected with V72D showed 1.3 and 2.0-fold higher rates of DiI-oxLDL uptake than vimentin or V72A-transfected macrophages, respectively (**Figure 6A**).

The site-directed mutagenesis experiments were repeated using SW13 cells, renal epithelial cell line not expressing vimentin. SW13 cells transfected with phospho-mimicking mutant (V72D) showed 1.4 fold increased uptake of DiI-oxLDL compared with SW13 cells with wild type vimentin (**Figure 6B**).

Since $Vim^{-/-}$ mouse macrophages showed less CD36 in plasma membrane than $Vim^{+/+}$ mouse macrophages, we hypothesized that vimentin phosphorylation may influence CD36 trafficking from cytosol to membrane. To prove the hypothesis, we stained plasma membrane CD36 with fluorescently labeled anti-CD36 antibody and performed flow cytometry to measure the fluorescence intensities that represent the amount of CD36 localized in plasma membrane. CD36 localized in plasma membrane was 2.0 fold more in

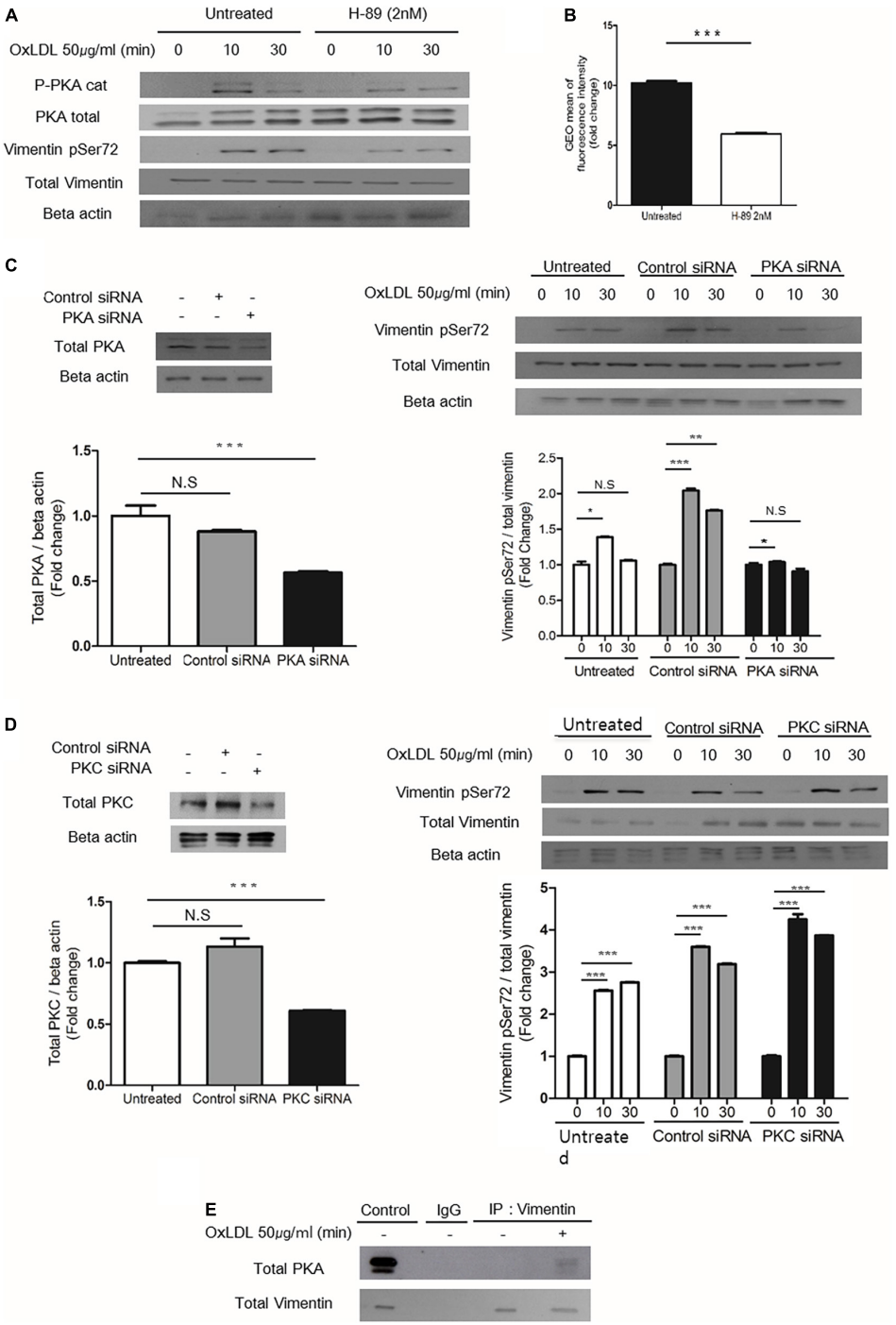

FIGURE 5 | PKA mediates oxLDL-induced vimentin (Ser72) phosphorylation. **(A)** Wild type murine peritoneal macrophages pretreated with H-89(2 nM), a specific PKA inhibitor were incubated with oxLDL (50 μg/ml) for indicated times. The lysates were analyzed by immunoblot for phosphorylated vimentin (Ser72) and total vimentin. Beta actin was used for internal control. **(B)** Flow cytometry data. BMDMs were pretreated with or without H-89 (2 nM) and then exposed to DiI- oxLDL (50 μg/ml) for 5 min. The fluorescence intensities of these cells were measured. **(C)** Left, Western blot analysis for PKA was performed using cell lysates of wild type murine BMDM transfected with control siRNA or siRNA against PKA. Cells were lysed 24 h after the siRNA treatment and analyzed by immunoblot for PKA. Right: Wild type murine BMDMs were transfected with control siRNA or siRNA against PKA and incubated with oxLDL (50 μg/ml) for indicated times and analyzed by western blot. **(D)** Left: Western blot analysis for PKC was performed using cell lysates of wild type murine BMDM transfected with control siRNA or siRNA against PKC. Cells were lysed 24 h after the siRNA treatment and analyzed by immunoblotting to confirm the suppression of PKC expression. Right: Wild type murine BMDMs were transfected with control siRNA or siRNA against PKC and incubated with oxLDL (50 μg/ml) for indicated times and analyzed by western blot. **(E)** *Vim* $^{+/+}$ murine peritoneal macrophages were treated with or without oxLDL (50 μg/ml) for 10 min and immunoprecipitated with anti-vimentin antibody. The precipitants were analyzed by western blot for PKA. $^{*}p < 0.05$, $^{**}p < 0.01$, $^{***}p < 0.001$.

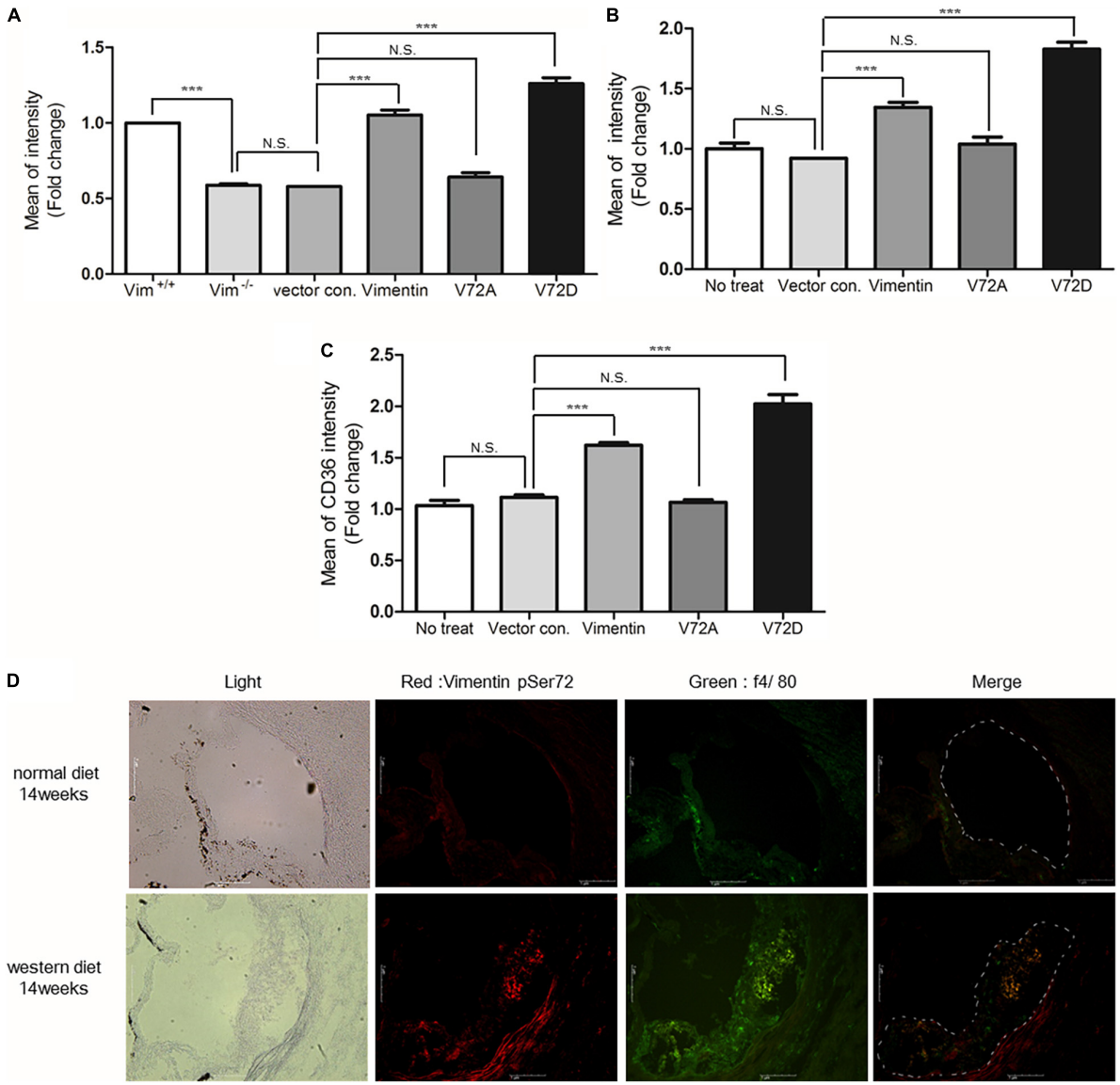

FIGURE 6 | Vimentin (Ser72) phosphorylation induced by oxLDL is required for the uptake of oxLDL. **(A)** Flow cytometry. Fluorescence intensities of dil-oxLDL-treated *Vim*$^{-/-}$ BMDM. Cells were transfected with vectors for vimentin or vimentin mutants. **(B)** Flow cytometry. Geometric mean fluorescence intensities of dil-oxLDL-treated SW13 cells. Cells were transfected with vectors for vimentin or vimentin mutants. **(C)** Measurement of membrane CD36. *Vim*$^{-/-}$ BMDM were transfected with vimentin or mutant vimentin vectors. Stabilized macrophages were stained with APC conjugated anti-CD36 antibody and analyzed using flow cytometry. **(D)** The representative immunohistochemistry images of aortic sinuses *of Ldlr*$^{-/-}$ mice fed a normal diet for 14 weeks or western diet for 14 weeks. Both samples were stained with antibody against phosphorylated vimentin (Ser72) (Dylight 594; Red) and antibody against f4/80 (Alexa 488; Green), a macrophage marker. Scale bars represent 1 μm. N.S. not significant, ***$p < 0.001$.

the macrophages with V72D compared with macrophages with V72A (**Figure 6C**). These data suggest that vimentin (Ser72) phosphorylation promotes translocation of CD36 to plasma membrane.

To evaluate if atherosclerotic arterial lesion has higher levels of phosphorylated vimentin (Ser72) in macrophages, we performed immunostaining of cross-sections of the aortic sinuses of *Ldlr* $^{-/-}$ mice fed a normal chow diet and *Ldlr* $^{-/-}$ mice fed a western diet for 14 weeks. The result showed that macrophages in the atherosclerotic plaque of the western diet-fed mice had higher levels of phosphorylated vimentin (Ser72) compared with macrophages in the aortic sinuses of the chow-diet fed mice (**Figure 6D**).

Deletion of Vimentin in Macrophages Reduces Atherosclerotic Lesion Development in *Ldlr*$^{-/-}$ Mice

To investigate whether deletion of vimentin in macrophages affects the formation of atherosclerotic lesions, we transplanted

bone marrow from $Vim^{+/+}$ and $Vim^{-/-}$ mice to $Ldlr^{-/-}$ mice and placed these mice on a western diet for 15 weeks. En face aortae with ORO staining showed that $Ldlr^{-/-}$ mice with $Vim^{-/-}$ bone marrow had less atherosclerotic lesion than $Ldlr^{-/-}$ mice with $Vim^{+/+}$ bone marrow (13.13 4.42% vs. 7.464 1.95%, p-value = 0.0019, **Figure 7A**). The cross sections of the aortic sinuses stained with ORO also showed that atherosclerotic plaques are smaller in $Ldlr^{-/-}$ mice with $Vim^{-/-}$ bone marrow than in $Ldlr^{-/-}$ mice with $Vim^{+/+}$ bone marrow (**Figure 7B**). Macrophage counts obtained from F4/80 staining of the cross sections showed that $Ldlr^{-/-}$ mice with $Vim^{-/-}$ bone marrow had 60% less macrophage number in the atherosclerotic plaque area compared to $Ldlr^{-/-}$ mice with $Vim^{+/+}$ bone marrow (**Figure 7C**).

Blood VLDL/LDL and total cholesterol concentrations of these two groups of mice were not different, however, the HDL concentrations of $Ldlr^{-/-}$ mice with $Vim^{-/-}$ bone marrow were 20% less than $Ldlr^{-/-}$ mice with $Vim^{+/+}$ bone marrow (**Figure 7D**). The body weight of $Ldlr^{-/-}$ mice with $Vim^{-/-}$ bone marrow and $Ldlr^{-/-}$ mice with $Vim^{+/+}$ bone marrow were not significantly different (**Figure 7E**).

These data suggest that macrophage vimentin contributes to the development of atherosclerosis.

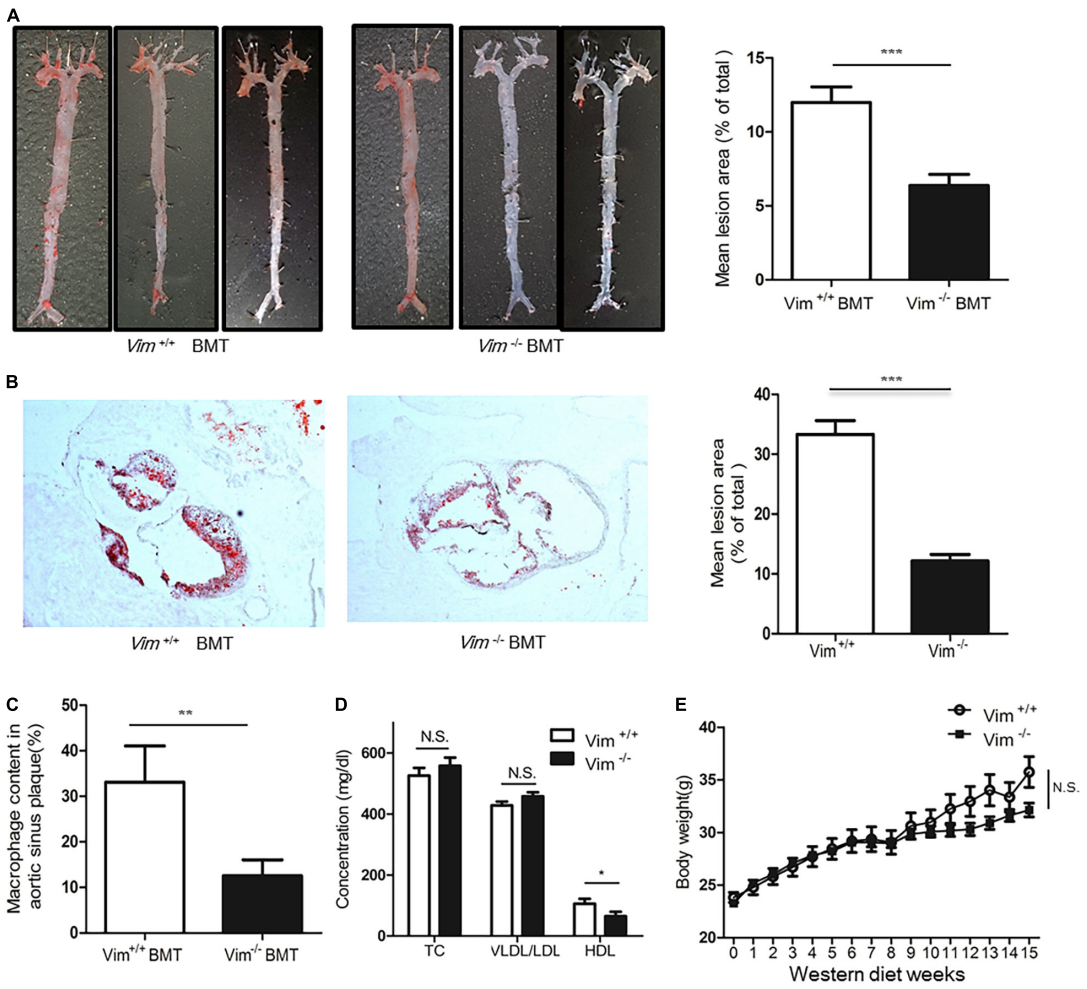

FIGURE 7 | Loss of vimentin in macrophages reduces atherosclerotic lesion in $Ldlr^{-/-}$ mice. Lethally irradiated $Ldlr^{-/-}$ mice were reconstituted with bone marrow from $Vim^{+/+}$ mice (n = 11) and $Vim^{-/-}$ mice (n = 10). After 4 weeks, reconstituted $Ldlr^{-/-}$ mice were fed a western diet for 15 weeks. **(A)** Left: Representative en face aortae stained with ORO of $Ldlr^{-/-}$ mice transplanted with $Vim^{+/+}$ and $Vim^{-/-}$ bone marrow. Right: Quantification of percent lesion area in the en face preparations of aortae. Bars indicate mean ± SEM; mice with $Vim^{+/+}$ bone marrow (n = 11) and mice with $Vim^{-/-}$ bone marrow (n = 10). **(B)** Left: Representative cross sections of aortic sinuses stained with ORO, of mice transplanted with $Vim^{+/+}$ and $Vim^{-/-}$ bone marrow. Right: Quantification of ORO (+) lesion area percentage of the cross sections of the aortic sinuses of mice with $Vim^{+/+}$ bone marrow and $Vim^{-/-}$ bone marrow. Bars indicate mean ± SEM; $Ldlr^{-/-}$ mice with $Vim^{+/+}$ bone marrow (n = 11) and $Vim^{-/-}$ bone marrow (n = 10). **(C)** Histomorphometric measurements of staining with F4/80, a specific marker of macrophages are shown in bar graphs. Bars indicate mean ± SEM; $Ldlr^{-/-}$ mice with $Vim^{+/+}$ bone marrow (n = 11) and $Vim^{-/-}$ bone marrow (n = 10). **(D)** Blood lipid profile of the $Ldlr^{-/-}$ mice with $Vim^{+/+}$ bone marrow (n = 11) and $Vim^{-/-}$ bone marrow (n = 10) in **(A)**. TC; Total cholesterol, Bars indicate mean ± SD. **(E)** Body weight changes of the $Ldlr^{-/-}$ mice with $Vim^{+/+}$ bone marrow (n = 11) and $Vim^{-/-}$ bone marrow (n = 10) during the western diet period. Bars indicate mean ± SEM. $^{*}p < 0.05$, $^{**}p < 0.01$, $^{***}p < 0.001$.

We generated *Apoe*$^{-/-}$ *Vim* $^{-/-}$ mice and fed a high fat diet for 15 weeks. Atherosclerotic lesions of aortae were analyzed by ORO staining of the en face bloc. *Apoe*$^{-/-}$ *Vim* $^{-/-}$ mice showed 57% less atherosclerotic lesions in the aortae than *Apoe*$^{-/-}$ *Vim*$^{+/+}$mice. The cross sections of the aortic sinuses stained with ORO also showed that atherosclerotic plaques are smaller in *Apoe*$^{-/-}$ *Vim* $^{-/-}$ mice than *Apoe*$^{-/-}$ *Vim*$^{+/+}$mice (**Supplementary Figure 2**).

We concluded that vimentin promotes atherosclerosis in hypercholesterolemic mice.

DISCUSSION

Vimentin, the most abundant intermediate filament protein in mesenchymal cells, is well known as a structural protein that supports distribution of intracellular organelles. Vimentin attaches to endoplasmic reticulum, mitochondria and nucleus (41). Several groups made *Vim*$^{-/-}$ transgenic mice to evaluate the role of vimentin *in vivo*, but *Vim*$^{-/-}$ mice did not show a specific phenotype, which has caused limited number of studies for the role of vimentin (42). Vimentin is used as a marker of mesenchymal cells and thus used to assess epithelial-mesenchymal transition (EMT) in malignancy. Recent studies have found several physiological roles of vimentin related to endocytosis. Fay and Panté reported that vimentin is required for parvovirus infection in which vimentin mediates endosomal trafficking of viral particle (13). Sarria et al.'s found that vimentin-lacking adrenal cells and normal adrenal cells have the same ability to internalize LDLs but have different abilities in storing LDLs. They suggested that vimentin plays a role in transport of LDL-derived cholesterol from lysosomes to mitochondria, the site for esterification of cholesterol in adrenal cells (43). Heid et al.'s found that vimentin is one of the lipid droplet components in adipocytes based on the proteomic analyses of the components of lipid droplets in adipocytes (44).

We demonstrated that *Vim*$^{-/-}$ mouse peritoneal macrophages uptake less oxLDL than *Vim*$^{+/+}$ mouse peritoneal macrophages, which was proven by DiI-oxLDL uptake assay and oil-red O staining of macrophages incubated with oxLDL (**Figure 1**).

To clarify which stage of lipid uptake was affected by vimentin, we used U18666A, a specific inhibitor for NPC-1 (Niemann-Pick disease, type C1) (45). NPC-1 is a membrane protein that has a role in intracellular transport of cholesterol from late endosomes to post-lysosomal destinations (46). Blocking NPC-1 protein halts the movement of cholesterol after the late endosome formation. Therefore, we could assess the oxLDL uptake or the early endosome formation distinguished from late endosome. The difference in oxLDL uptake between *Vim* $^{+/+}$ and *Vim* $^{-/-}$ mouse peritoneal macrophages was increased after blocking NPC-1. Therefore, we concluded that vimentin functions in foam cell formation via mediating uptake of oxLDL in macrophages.

We found that CD36 localized in plasma membrane was 50% less in *Vim*$^{-/-}$ macrophages than in *Vim* $^{+/+}$ macrophage. Despite less uptake of oxLDL in *Vim* $^{-/-}$ macrophages, there was no difference in the amount of CD36 proteins in whole cell lysates between *Vim* $^{+/+}$ and *Vim* $^{-/-}$ macrophages. We showed that vimentin–CD36 co-localization was increased by oxLDL in macrophages using various techniques including immunoprecipitaion, immunostaining, and sucrose gradient early endosomal fraction assay.

Vimentin has a central alpha-helical domain and capped on each end by non-helical domain. Two vimentin monomers form a coil-coil dimer, which forms the basis for the filamentous vimentin and this process is known to be regulated by phosphorylation of vimentin. We found that oxLDL/CD36 interaction induced vimentin (Ser72) phosphorylation via PKA (**Figure 1**). We observed that phospho-mimetic of vimentin (Ser72) increased oxLDL uptake and membrane CD36 localization. In summary, our studies revealed that oxLDL/CD36 interaction induces phosphorylation of vimentin (Ser72) and phospho-vimentin (Ser72) promotes CD36 trafficking to the plasma membrane.

CD36 mediates various cellular activities including fatty acid transport, engulfing virus-infected cells and oxLDL uptake (47). Macrophage CD36 expression is known to be promoted by its ligand, oxLDL, which is called "eat me signal." CD36 transcription is induced by oxLDL via activation of peroxisome proliferator-activated receptor γ (PPARγ) (48). Both 9- hydroxyoctadecadienoic acid (9-HODE) and 13-HODE in oxLDL serve as endogenous PPAR γ ligands. To reduce foam cell formation and treat atherosclerosis, there have been various efforts to reduce CD36 expression. Those includes usage of drugs such as α-tocopherol and tamoxifen. However, no drugs have achieved enough efficacy in clinical settings (49). Therefore, modulating functions of vimentin may be one way to inhibit macrophage foam cell formation. Regarding our finding, oxLDL increases uptake of itself in macrophages via two ways; one is increase of CD36 transcription and the other is increase of membrane trafficking of CD36.

Recently, Haversen et al. reported that vimentin deficiency increased membrane-localized CD36, resulting in increased uptake of oxLDL (29), which is an opposite observation to our finding. However, animal experiment using *Vim*$^{-/-}$ bone marrow transplantation in their study showed the same finding to ours that *LDLR*$^{-/-}$ mice reconstituted with *Vim*$^{-/-}$ bone marrow had less atherosclerotic lesions than *LDLR*$^{-/-}$ mice with *Vim*$^{+/+}$ bone marrow. Contrary findings in cellular experiments may have been caused by different experimental settings. Peritoneal macrophages and BMDMs are known to be phenotypically distinct and differ in expression of M1/M2 markers and lipid metabolism genes (50). Differences in methods to achieve BMDMs could contribute to different responses of the cells. We differentiated murine bone marrow myeloid stem cells into BMDMs by culturing in DMEM supplemented with 10% L929 supernatant and 10% fetal bovine serum (FBS) for 7 days. Harversen et al. used high-glucose DMEM supplemented with 10% whole supernatant of cell line CMG14-12 as a source of mouse M-CSF.

To clarify the differences in baseline CD36 expression between BMDM and peritoneal macrophages, we measured cell surface CD36 in both types of cells. FACS analysis using anti-CD36 antibody showed that 3.02 times higher intensity was measured in peritoneal macrophages (**Supplementary Figure 3**). Peritoneal

macrophages released more TNF-α in response to oxLDL and MCP-1 than BMDM (**Supplementary Figure 4**).

Although baseline expressions of CD36 and other molecules are different between BMDM and peritoneal macrophages, in our current study, we attained consistent results that vimentin deficiency reduces expression of cell surface CD36 and thus reduces uptake of oxLDL in both BMDM and peritoneal macrophags (**Figures 2D,E**). We also conducted site-specific mutagenesis study using BMDM (**Figure 6**). As in the experiment using peritoneal macrophages from $Vim^{-/-}$ and $Vim^{+/+}$ mice (**Figure 1**), BMDM from $Vim^{-/-}$ mice showed 40% less oxLDL uptake than BMDM from $Vim^{+/+}$ mice or $Vim^{-/-}$ BMDM that restored vimentin expression (**Figure 6A**) and also showed less expression of plasma membrane CD36 (**Figure 6C**).

Another report revealing that the inhibitory effect of tetrahydroxystilbene glucoside on macrophage foam cell formation is driven by reduction of vimentin (51) also supports our observation. In a different study of ours, we also showed that membrane-localized CD36 in $Vim^{-/-}$ adipocytes was 41∼58% less than in control $Vim^{+/+}$ adipocytes and thus fatty acid uptake of $Vim^{-/-}$ adipocytes was 27% less than $Vim^{+/+}$ adipocytes (52).

We measured LDLR expression in peritoneal macrophages from $Vim^{+/+}$ and $Vim^{-/-}$ mice. The expression of LDLR was 1.37 fold higher in $Vim^{-/-}$ macrophages (**Supplementary Figure 5**).

Differences in oxLDL preparations could attribute to the disparity among *in vitro* studies. We generated $CuSO_4$-oxLDL and measured oxidation degree of the $CuSO_4$-oxLDL by TBARS assay (thiobarbituric acid reactive substance assay). Our oxLDL was 8–10 nmol TBARS/mg protein MDA equivalents which could be classified as mildly oxidized LDL (**Supplementary Figure 6**). It has been reported that mildly oxidized LDL is chemically different from unmodified LDL and has more affinity to CD36 than the other scavenger receptors including scavenger receptor-A (53). We also used myeloperoxidase (MPO)-modified LDL in our assay to evaluate effect of CD36 in oxLDL-induced vimentin (Ser72) phosphorylation (**Figure 4D**). MPO is physiological oxidizing reagent in the human body and thus MPO-modified LDL should be closer to the endogenously oxidized LDL. We achieved consistent results from the assays using $CuSO_4$-oxLDL and MPO-modified LDL.

A recent study by Wang et al. revealed that palmitoylation of CD36 by DHHC4 and DHHC5 is required for its plasma membrane localization and fatty acid uptake activity (54). It is possible that phospho-vimentin may affect palmitoylation of CD36 via modulating activities of palmitoyl-acyltransferase like DHHC4 and DHHC5. The question we should solve is whether CD36 increase in plasma membrane is derived from achieving stability of membrane-localized CD36 or it is from increased dynamic trafficking (fast receptor recycling via increased dynamic assembly and disassembly of vimentin intermediate filament). This question is on our venue of on-going research.

In summary, our current study demonstrated that vimentin-deficient macrophages uptake less oxLDL via decreased membrane localization of CD36 and thus CD36-deficiency in macrophages reduces development of atherosclerosis. We suggest underlying mechanisms that oxLDL/CD36 interaction-induced vimentin (Ser72) phosphorylation leads to disassembly of vimentin filament and vimentin mediates membrane trafficking of CD36 and receptor-mediated endocytosis of CD36. Our study suggests a new therapeutic strategy for the treatment of atherosclerosis by revealing a new function of vimentin in macrophages. It may also suggest ways to regulate CD36 trafficking and modulate functions of CD36 in various biological activities including fatty acid transport in adipocytes, immunity, and anti-angiogenesis.

DATA AVAILABILITY STATEMENT

The original contributions presented in the study are included in the article/**Supplementary Material**, further inquiries can be directed to the corresponding author/s.

ETHICS STATEMENT

The animal study was reviewed and approved by Institutional Animal Care and Use Committee (IACUC) of Ewha Womans University College of Medicine.

AUTHOR CONTRIBUTIONS

SK designed and performed the work. S-JJ, J-HP, and WC contributed to the acquisition and analysis of the work. Y-HA and Y-HC designed the work. GO and RS contributed to interpretation of the work. YP designed and analyzed the work. All authors contributed to the article and approved the submitted version.

FUNDING

This work was supported by the National Research Foundation of Korea (NRF) grant funded by the Korean government (MSIT) (No. NRF-2016R1D1A1B01012964) and was partly supported by the Health Fellowship Foundation.

ACKNOWLEDGMENTS

We gratefully acknowledge Eun-Sook Kang in the Department of Laboratory Medicine and Genetics, Samsung Medical Center, Sungkyunkwan University School of Medicine for her support in preparing LDL. The current study includes a part of SK's Ph.D. thesis.

SUPPLEMENTARY MATERIAL

The Supplementary Material for this article can be found online at: https://www.frontiersin.org/articles/10.3389/fcvm.2022.792717/full#supplementary-material

REFERENCES

1. Silverstein RL, Febbraio M. Cd36 and atherosclerosis. *Curr Opin Lipidol.* (2000) 11:483–91.
2. Podrez EA, Febbraio M, Sheibani N, Schmitt D, Silverstein RL, Hajjar DP, et al. Macrophage scavenger receptor cd36 is the major receptor for ldl modified by monocyte-generated reactive nitrogen species. *J Clin Invest.* (2000) 105:1095–108. doi: 10.1172/JCI8574
3. Rahaman SO, Lennon DJ, Febbraio M, Podrez EA, Hazen SL, Silverstein RL. A cd36-dependent signaling cascade is necessary for macrophage foam cell formation. *Cell Metab.* (2006) 4:211–21. doi: 10.1016/j.cmet.2006.06.007
4. Sun B, Boyanovsky BB, Connelly MA, Shridas P, van der Westhuyzen DR, Webb NR. Distinct mechanisms for oxldl uptake and cellular trafficking by class b scavenger receptors cd36 and sr-bi. *J Lipid Res.* (2007) 48:2560–70. doi: 10.1194/jlr.M700163-JLR200
5. Malaud E, Hourton D, Giroux LM, Ninio E, Buckland R, McGregor JL. The terminal six amino-acids of the carboxy cytoplasmic tail of cd36 contain a functional domain implicated in the binding and capture of oxidized low-density lipoprotein. *Biochem J.* (2002) 364:507–15. doi: 10.1042/BJ20011373
6. Minin AA, Moldaver MV. Intermediate vimentin filaments and their role in intracellular organelle distribution. *Biochemistry (Moscow).* (2009) 73:1453–66. doi: 10.1134/s0006297908130063
7. Styers ML, Salazar G, Love R, Peden AA, Kowalczyk AP, Faundez V. The endo-lysosomal sorting machinery interacts with the intermediate filament cytoskeleton. *Mol Biol Cell.* (2004) 15:5369–82. doi: 10.1091/mbc.e04-03-0272
8. Eckes B, Dogic D, Colucci-Guyon E, Wang N, Maniotis A, Ingber D, et al. Impaired mechanical stability, migration and contractile capacity in vimentin-deficient fibroblasts. *J Cell Sci.* (1998) 111:1897–907. doi: 10.1242/jcs.111.13.1897
9. Kim H, Nakamura F, Lee W, Hong C, Perez-Sala D, McCulloch CA. Regulation of cell adhesion to collagen via beta1 integrins is dependent on interactions of filamin a with vimentin and protein kinase c epsilon. *Exp Cell Res.* (2010) 316:1829–44. doi: 10.1016/j.yexcr.2010.02.007
10. Mendez MG, Kojima S-I, Goldman RD. Vimentin induces changes in cell shape, motility, and adhesion during the epithelial to mesenchymal transition. *FASEB J.* (2010) 24:1838–51. doi: 10.1096/fj.09-151639
11. Franke WW, Hergt M, Grund C. Rearrangement of the vimentin cytoskeleton during adipose conversion: formation of an intermediate filament cage around lipid globules. *Cell.* (1987) 49:131–41. doi: 10.1016/0092-8674(87)90763-x
12. Lieber JG, Evans RM. Disruption of the vimentin intermediate filament system during adipose conversion of 3t3-l1 cells inhibits lipid droplet accumulation. *J Cell Sci.* (1996) 109(Pt 13):3047–58. doi: 10.1242/jcs.109.13.3047
13. Fay N, Panté N. The intermediate filament network protein, vimentin, is required for parvoviral infection. *Virology.* (2013) 444:181–90. doi: 10.1016/j.virol.2013.06.009
14. Pérez-Sala D, Oeste CL, Martínez AE, Carrasco MJ, Garzón B, Cañada FJ. Vimentin filament organization and stress sensing depend on its single cysteine residue and zinc binding. *Nat Commun.* (2015) 6:7287. doi: 10.1038/ncomms8287
15. Fuchs E, Weber K. Intermediate filaments: structure, dynamics, function, and disease. *Annu Rev Biochem.* (1994) 63:345–82. doi: 10.1146/annurev.bi.63.070194.002021
16. Herrmann H, Strelkov SV, Burkhard P, Aebi U. Intermediate filaments: primary determinants of cell architecture and plasticity. *J Clin Invest.* (2009) 119:1772–83. doi: 10.1172/JCI38214
17. Parry DA, Strelkov SV, Burkhard P, Aebi U, Herrmann H. Towards a molecular description of intermediate filament structure and assembly. *Exp Cell Res.* (2007) 313:2204–16. doi: 10.1016/j.yexcr.2007.04.009
18. Eriksson JE, He T, Trejo-Skalli AV, Härmälä-Braskén A-S, Hellman J, Chou Y-H, et al. Specific in vivo phosphorylation sites determine the assembly dynamics of vimentin intermediate filaments. *J Cell Sci.* (2004) 117:919–32. doi: 10.1242/jcs.00906
19. Tsujimura K, Ogawara M, Takeuchi Y, Imajoh-Ohmi S, Ha MH, Inagaki M. Visualization and function of vimentin phosphorylation by cdc2 kinase during mitosis. *J Biol Chem.* (1994) 269:31097–106. doi: 10.1016/s0021-9258(18)47395-4
20. Yamaguchi T, Goto H, Yokoyama T, Sillje H, Hanisch A, Uldschmid A, et al. Phosphorylation by cdk1 induces plk1-mediated vimentin phosphorylation during mitosis. *J Cell Biol.* (2005) 171:431–6. doi: 10.1083/jcb.200504091
21. Ivaska J, Vuoriluoto K, Huovinen T, Izawa I, Inagaki M, Parker PJ. Pkcepsilon-mediated phosphorylation of vimentin controls integrin recycling and motility. *EMBO J.* (2005) 24:3834–45. doi: 10.1038/sj.emboj.7600847
22. Barquera S, Pedroza-Tobias A, Medina C, Hernandez-Barrera L, Bibbins-Domingo K, Lozano R, et al. Global overview of the epidemiology of atherosclerotic cardiovascular disease. *Arch Med Res.* (2015) 46:328–38. doi: 10.1016/j.arcmed.2015.06.006
23. Libby P. Inflammation in atherosclerosis. *Nature.* (2002) 420:868–74.
24. Stary HC, Chandler AB, Glagov S, Guyton JR, Insull W Jr., Rosenfeld ME, et al. A definition of initial, fatty streak, and intermediate lesions of atherosclerosis. A report from the committee on vascular lesions of the council on arteriosclerosis, american heart association. *Circulation.* (1994) 89:2462–78. doi: 10.1161/01.cir.89.5.2462
25. Kleemann R, Zadelaar S, Kooistra T. Cytokines and atherosclerosis: a comprehensive review of studies in mice. *Cardiovasc Res.* (2008) 79:360–76. doi: 10.1093/cvr/cvn120
26. Febbraio M, Podrez EA, Smith JD, Hajjar DP, Hazen SL, Hoff HF, et al. Targeted disruption of the class b scavenger receptor cd36 protects against atherosclerotic lesion development in mice. *J Clin Invest.* (2000) 105:1049–56. doi: 10.1172/JCI9259
27. de Winther MP, Hofker MH. Scavenging new insights into atherogenesis. *J Clin Invest.* (2000) 105:1039–41. doi: 10.1172/JCI9919
28. Glass CK, Witztum JL. Atherosclerosis. The road ahead. *Cell.* (2001) 104:503–16.
29. Haversen L, Sundelin JP, Mardinoglu A, Rutberg M, Ståhlman M, Wilhelmsson U, et al. Vimentin deficiency in macrophages induces increased oxidative stress and vascular inflammation but attenuates atherosclerosis in mice. *Sci Rep.* (2018) 8:16973. doi: 10.1038/s41598-018-34659-2
30. Hatch FT. Practical methods for plasma lipoprotein analysis. *Adv Lipid Res.* (1968) 6:1–68. doi: 10.1016/b978-1-4831-9942-9.50008-5
31. Podrez EA, Schmitt D, Hoff HF, Hazen SL. Myeloperoxidase-generated reactive nitrogen species convert LDL into an atherogenic form in vitro. *J Clin Invest.* (1999) 103:1547–60. doi: 10.1172/JCI5549
32. Gilchrist M, Thorsson V, Li B, Rust AG, Korb M, Kennedy K, et al. Systems biology approaches identify atf3 as a negative regulator of toll-like receptor 4. *Nature.* (2006) 441:173–8. doi: 10.1038/nature04768
33. Xu S, Huang Y, Xie Y, Lan T, Le K, Chen J, et al. Evaluation of foam cell formation in cultured macrophages: an improved method with oil red o staining and dii-oxldl uptake. *Cytotechnology.* (2010) 62:473–81. doi: 10.1007/s10616-010-9290-0
34. Teo CSH, Chu JJH. Cellular vimentin regulates construction of dengue virus replication complexes through interaction with ns4a protein. *J Virol.* (2014) 88:1897–913. doi: 10.1128/JVI.01249-13
35. Lu F, Liang Q, Abi-Mosleh L, Das A, De Brabander JK, Goldstein JL, et al. Identification of npc1 as the target of u18666a, an Inhibitor of lysosomal cholesterol export and ebola infection. *Elife.* (2015) 4:e12177. doi: 10.7554/eLife.12177
36. Ye D, Lammers B, Zhao Y, Meurs I, Van Berkel TJ, Van Eck M. Atp-binding cassette transporters a1 and g1, hdl metabolism, cholesterol efflux, and inflammation: important targets for the treatment of atherosclerosis. *Curr Drug Targets.* (2011) 12:647–60. doi: 10.2174/138945011795378522
37. Soumian S, Albrecht C, Davies AH, Gibbs RG. Abca1 and atherosclerosis. *Vasc Med.* (2005) 10:109–19.
38. Sliverstein RL, Li W, Park YM, Rahaman SO. Mechanisms of cell signaling by the scavenger receptor CD36: implication in atherosclerosis and thrombosis. *Trans Am Clin Climatol Assoc.* (2010) 121:206–20.
39. Park YM. CD36, a scavenger receptor implicated in atherosclerosis. *Exp Mol Med.* (2014) 46:e99. doi: 10.1038/emm.2014.38
40. Song J, Cheon SY, Lee WT, Park KA, Lee JE. Pka inhibitor h89 (n-[2-p-bromocinnamylamino-ethyl]-5-isoquinolinesulfonamide) attenuates synaptic dysfunction and neuronal cell death following ischemic injury. *Neural Plast.* (2015) 2015:374520. doi: 10.1155/2015/374520
41. Katsumoto T, Mitsushima A, Kurimura T. The role of the vimentin intermediate filaments in rat 3y1 cells elucidated by immunoelectron microscopy and computer-graphic reconstruction. *Biol Cell.* (1990) 68:139–46. doi: 10.1016/0248-4900(90)90299-i
42. Colucci-Guyon E, Portier MM, Dunia I, Paulin D, Pournin S, Babinet C. Mice lacking vimentin develop and reproduce without an obvious phenotype. *Cell.* (1994) 79:679–94. doi: 10.1016/0092-8674(94)90553-3

43. Sarria AJ, Panini SR, Evans RM. A functional role for vimentin intermediate filaments in the metabolism of lipoprotein-derived cholesterol in human sw-13 cells. *J Biol Chem.* (1992) 267:19455–63. doi: 10.1016/s0021-9258(18)41797-8
44. Heid H, Rickelt S, Zimbelmann R, Winter S, Schumacher H, Dorflinger Y, et al. On the formation of lipid droplets in human adipocytes: the organization of the perilipin-vimentin cortex. *PLoS One.* (2014) 9:e90386. doi: 10.1371/journal.pone.0090386
45. Sugimoto Y, Ninomiya H, Ohsaki Y, Higaki K, Davies JP, Ioannou YA, et al. Accumulation of cholera toxin and gm1 ganglioside in the early endosome of niemann–pick c1-deficient cells. *Proc Natl Acad Sci U S A.* (2001) 98:12391–6. doi: 10.1073/pnas.221181998
46. Carstea ED, Morris JA, Coleman KG, Loftus SK, Zhang D, Cummings C, et al. Niemann-pick c1 disease gene: homology to mediators of cholesterol homeostasis. *Science.* (1997) 277:228–31. doi: 10.1126/science.277.5323.228
47. Han J, Hajjar DP, Febbraio M, Nicholson AC. Native and modified low density lipoproteins increase the functional expression of the macrophage class b scavenger receptor, cd36. *J Biol Chem.* (1997) 272:21654–9. doi: 10.1074/jbc.272.34.21654
48. Nagy L, Tontonoz P, Alvarez JG, Chen H, Evans RM. Oxidized LDL regulates macrophage gene expression through ligand activation of PPAR-gamma. *Cell.* (1998) 93:229–40. doi: 10.1016/s0092-8674(00)81574-3
49. Yu M, Jiang M, Chen Y, Zhang S, Zhang W, Yang X, et al. Inhibition of macrophage cd36 expression and cellular oxidized low density lipoprotein (oxLDL) accumulation by tamoxifen: a peroxisome proliferator-activated receptor (PPAR)-γ-dependent mechanism. *J Biol Chem.* (2016) 291:16977–89. doi: 10.1074/jbc.M116.740092
50. Bisgaard LS, Mogensen CK, Rosendahl A, Cucak H, Nielsen LB, Rasmussen SE, et al. Bone marrow-derived and peritoneal macrophages have different inflammatory response to oxLDL and M1/M2 marker expression – implications for atherosclerosis research. *Sci Rep.* (2016) 6:35234. doi: 10.1038/srep35234
51. Yao W, Huang L, Sun Q, Yang L, Tang L, Meng G, et al. The inhibition of macrophage foam cell formation by tetrahydroxystilbene glucoside is driven by suppressing vimentin cytoskeleton. *Biomed Pharmacother.* (2016) 83:1132–40. doi: 10.1016/j.biopha.2016.08.032
52. Kim SY, Kim I, Cho W, Oh GT, Park YM. Vimentin deficiency prevents high-fat diet-induced obesity and insulin resistance in mice. *Diabetes Metab J.* (2020) 45:97–108. doi: 10.4093/dmj.2019.0198
53. Endeman G, Stanton LW, Madden KS, Bryant CM, White RT, Protter AA. CD36 is a receptor for oxidized low density lipoprotein. *J Biol Chem.* (1993) 268:11811–6. doi: 10.1016/s0021-9258(19)50272-1
54. Wang J, Hao J-W, Wang X, Guo H, Sun H-H, Lai X-Y, et al. DHHC4 and DHHC5 facilitate fatty acid uptake by palmitoylating and targeting CD36 to the plasma membrane. *Cell Rep.* (2019) 26:209–21.e205. doi: 10.1016/j.celrep.2018.12.022

Conflict of Interest: The authors declare that the research was conducted in the absence of any commercial or financial relationships that could be construed as a potential conflict of interest.

Publisher's Note: All claims expressed in this article are solely those of the authors and do not necessarily represent those of their affiliated organizations, or those of the publisher, the editors and the reviewers. Any product that may be evaluated in this article, or claim that may be made by its manufacturer, is not guaranteed or endorsed by the publisher.

Copyright © 2022 Kim, Jeong, Park, Cho, Ahn, Choi, Oh, Silverstein and Park. This is an open-access article distributed under the terms of the Creative Commons Attribution License (CC BY). The use, distribution or reproduction in other forums is permitted, provided the original author(s) and the copyright owner(s) are credited and that the original publication in this journal is cited, in accordance with accepted academic practice. No use, distribution or reproduction is permitted which does not comply with these terms.

Advantages of publishing in Frontiers

OPEN ACCESS
Articles are free to read for greatest visibility and readership

FAST PUBLICATION
Around 90 days from submission to decision

HIGH QUALITY PEER-REVIEW
Rigorous, collaborative, and constructive peer-review

TRANSPARENT PEER-REVIEW
Editors and reviewers acknowledged by name on published articles

Frontiers
Avenue du Tribunal-Fédéral 34
1005 Lausanne | Switzerland

Visit us: www.frontiersin.org
Contact us: frontiersin.org/about/contact

REPRODUCIBILITY OF RESEARCH
Support open data and methods to enhance research reproducibility

DIGITAL PUBLISHING
Articles designed for optimal readership across devices

FOLLOW US
@frontiersin

IMPACT METRICS
Advanced article metrics track visibility across digital media

EXTENSIVE PROMOTION
Marketing and promotion of impactful research

LOOP RESEARCH NETWORK
Our network increases your article's readership